EL METODO DEL ELEMENTO FINITO EN LA INGENIERIA MECANICA 1982

DIRECTORIO DE PROFESORES

1 DR. JORGE ANGELES ALVAREZ
SUBJEFE DEL AREA DE INGENIERIA ELECTROMECANICA
DIVISION DE ESTUDIOS DE POSGRADO
FACULTAD DE INGENIERIA, UNAM
CIUDAD UNIVERSITARIA
MEXICO 20, D.F.
TEL: 550.52.15 ext. 4482 ó 4477

2 DR. PORFIRIO BALLESTEROS BAROCIO
PROFESOR DE MEDIO TIEMPO
AREA DE INGENIERIA ELECTROMECANICA
DIVISION DE ESTUDIOS DE POSGRADO
FACULTAD DE INGENIERIA, UNAM
CIUDAD UNIVERSITARIA
MEXICO 20, D.F.
TEL: 550.52.15 ext. 4498

3 ING. ERNESTO MARTIN DEL CAMPO VAZQUEZ

...2

EVALUACIÓN DEL PERSONAL DOCENTE

EVALUACION DEL PERSONAL DOCENTE

CURSO: El Método del Elemento Finito en la Ingeniería Mecánica.

FECHA: Del 12 al 16 de Abril, 1982.

CONFERENCISTA	DOMINIO DEL TEMA	EFICIENCIA EN EL USO DE AYUDAS AUDIOVISUALES	MANTENIMIENTO DEL INTERES. (COMUNICACION CON LOS ASISTENTES, AMENIDAD, FACILIDAD DE EXPRESION).	PUNTUALIDAD	
1. Dr. Víctor Hugo Muciño Quintero					
2. Dr. Porfirio Ballesteros Barocio					
3. Dr. Nicholas J. Salamon					
4. Dr. Jorge Angeles Alvarez					
5. Ing. Enrique Martín del Campo Vázquez					
6.					
7.					
8.					
9.					

ESCALA DE EVALUACION: 1 a 10

EVALUACION DE LA LICENCIA

EVALUACION DEL CURSO

	CONCEPTO	EVALUACION
1.	APLICACION INMEDIATA DE LOS CONCEPTOS EXPUESTOS	
2.	CLARIDAD CON QUE SE EXPUSIERON LOS TEMAS	
3.	GRADO DE ACTUALIZACION LOGRADO CON EL CURSO	
4.	CUMPLIMIENTO DE LOS OBJETIVOS DEL CURSO	
5.	CONTINUIDAD EN LOS TEMAS DEL CURSO	
6.	CALIDAD DE LAS NOTAS DEL CURSO	
7.	GRADO DE MOTIVACION LOGRADO CON EL CURSO	

ESCALA DE EVALUACION DE 1 A 10

1. ¿Qué le pareció el ambiente en la División de Educación Continua?

MUY AGRADABLE	AGRADABLE	DESAGRADABLE

2. Medio de comunicación por el que se enteró del curso:

PERIODICO EXCELSIOR ANUNCIO TITULADO DI VISION DE EDUCACIÓN CONTINUA	PERIODICO NOVEDADES ANUNCIO TITULADO DI VISION DE EDUCACIÓN CONTINUA	FOLLETO DEL CURSO

CARTEL MENSUAL	RADIO UNIVERSIDAD	COMUNICACION CARTA, TELEFONO, VERBAL, ETC.

REVISTAS TECNICAS	FOLLETO ANUAL	CARTELERA UNAM "LOS UNIVERSITARIOS HOY"	GACETA UNAM

3. Medio de transporte utilizado para venir al Palacio de Minería:

AUTOMOVIL PARTICULAR	METRO	OTRO MEDIO

4. ¿Qué cambios haría usted en el programa para tratar de perfeccionar el curso?

_____

_____

_____

5. ¿Recomendaría el curso a otras personas?

SI	NO

6. ¿Qué cursos le gustaría que ofreciera la División de Educación Continua?

7. La coordinación académica fue:

EXCELENTE	BUENA	REGULAR	MALA

8. Si está interesado en tomar algún curso intensivo ¿Cuál es el horario más conveniente para usted?

LUNES A VIERNES DE 9 A 13 H. Y DE 14 A 18 H. (CON COMIDAS)	LUNES A VIERNES DE 17 A 21 H.	LUNES, MIERCOLES Y VIERNES DE 18 A 21 H.	MARTES Y JUEVES DE 18 A 21 H.

VIERNES DE 17 A 21 H. SABADOS DE 9 A 14 H.	VIERNES DE 17 A 21 H. SABADOS DE 9 A 13 Y DE 14 a 18 H.	O T R O

9. ¿Qué servicios adicionales desearía que tuviese la División de Educación Continua, para los asistentes?

10. Otras sugerencias:

EL METODO DEL ELEMENTO FINITO EN LA INGENIERIA MECANICA

Fecha	Tema	Horario	Profesor
Abril 12	Introducción	9 a 13:30 h	Dr. Jorge Angeles Alvarez
	Introducción y conceptos fundamentales del método del elemento finito y repaso del algebra de matrices.		
	Comida	1:30 a 15 h	
	Ecuaciones de Equilibrio	15 a 18:30 h	Dr. Porfirio Ballesteros Barocio
	Ecuaciones de equilibrio, condiciones a la frontera y repaso de teoría de la elasticidad.		
Abril 13	Modelación	9 a 13:30 h	Dr. Víctor Hugo Muciño Quintero
	Modelación matemática con elementos finitos, problemas de campo con valores iniciales y formulación variacional.		
	Comida	13:30 a 15 h	
	Librería de Elementos	15 a 18:30 h	Dr. Nicholas J. Salamon
	Tipos de elementos para la representación de sistemas mecánicos y estructurales		
Abril 14	Paquetes Computacionales	9 a 11 a.m. 11:30 a 13:30	Dr. Porfirio Ballesteros Dr. Nicholas J. Salamon
	Estructura general de paquetes computacionales de elementos finitos para su aplicación a problemas reales.		

EL METODO DEL ELEMENTO FINITO EN LA INGENIERIA MECANICA

Fecha	Tema	Horario	Profesor
Abril 14	Comida	13:30 a 15 h	
	Aplicaciones: Análisis Estático	15 a 18:30 h	Dr. Jorge Angeles Alvarez
	Aplicaciones del método del elemento finito para el análisis estático de estructuras y elementos de máquinas.		
Abril 15	Aplicaciones: Análisis Dinámico	9 a 13:30 h 15 a 18:30 h	Dr. Nicholas J. Salamon Dr. Mihir Sen.
	Aplicaciones del método del elemento finito para el análisis dinámico de estructuras y sistemas mecánicos.		
	Aplicaciones Avanzadas		
	Aplicaciones avanzadas del método del elemento finito al análisis de problemas no-lineales tales como plasticidad, contacto, deformaciones grandes, no-linealidades de material, etc.		
Abril 16	Taller de Aplicaciones	9 a 13:30 h	Dr. Víctor Hugo Muciño Quintero
	Introducción y descripción del paquete "SAP IV" para su uso en la computadora		
	Comida	13:30 a 15 H	
	Utilización del Programa SAP IV	15 a 18:30 h.	Dr. Víctor Hugo Muciño Quintero
	Solución de problemas propuestos por los asistentes.		Ing. Enrique Martín del Campo Vazquez.

DIVISION DE EDUCACION CONTINUA
FACULTAD DE INGENIERIA U.N.A.M.

EL METODO DEL ELEMENTO FINITO EN LA INGENIERIA MECANICA

INTRODUCCION Y CONCEPTOS FUNDAMENTALES

DR. JORGE ANGELES ALVAREZ

ABRIL, 1982

1.1 Introducción

En terminos generales, el método del elemento finito (MEF) es un medio para obtener una aproximación a la solución de un problema que requiere la integración de un sistema de ecuaciones diferenciales, provisto de ciertas condiciones que definen completamente el problema y, de ahí, su solución. En el más sencillo de los casos, la ecuación diferencial es ordinaria y lineal ; pero puede contener derivadas de orden arbitrario y condiciones de frontera dadas, que involucren combinaciones arbitrarias de la función buscada y sus derivadas. Si se denota como y la función buscada, que constituye la solución al problema en cuestión, y como x, la variable independiente, este problema adopta la forma : "Resolver la ecuación diferencial ordinaria

$$f\,(x,\ y,\ y',\ y'',\ \ldots,\ y^{(i)},\ \ldots,\ y^{(n)}) = 0 \qquad (1.1)$$

sujeta a las condiciones de frontera

$$\begin{aligned} &g_1(y_{10},\ y_{11},\ \ldots,\ y_{1n}) = 0 \\ &\quad\vdots \\ &g_m(y_{m0},\ y_{m1},\ \ldots,\ y_{mn}) = 0" \end{aligned} \qquad (1.2)$$

donde y_{ij} es el valor que adquiere la derivada de orden j de y con respecto a x, en la i^{a} ecuación del conjunto (1.2). Al introducir un cambio de variables se puede transformar la ec (1.1) en un sistema de n ecuaciones de primer orden. En efecto, sean

$$\begin{aligned} y_1(x) &= y(x) \\ y_2(x) &= y'(x) \\ &\vdots \\ y_i(x) &= y^{(i-1)}(x) \\ &\vdots \\ y_n(x) &= y^{(n-1)}(x) \end{aligned} \qquad (1.3)$$

La ec (1.1) toma entonces la forma

$$\begin{aligned} y_1'(x) &= y_2(x) \\ y_2'(x) &= y_3(x) \\ &\vdots \\ y_{n-1}'(x) &= y_n(x) \\ f(x, y_1, y_2, \ldots, y_n, y_n') &= 0 \end{aligned} \qquad (1.4)$$

En general, las variables y_i tienen un significado físico inmediato, por lo que permiten visualizar mejor el problema.

Ejemplo 1.1.1 Análisis estático de una viga en voladizo (Fig 1)

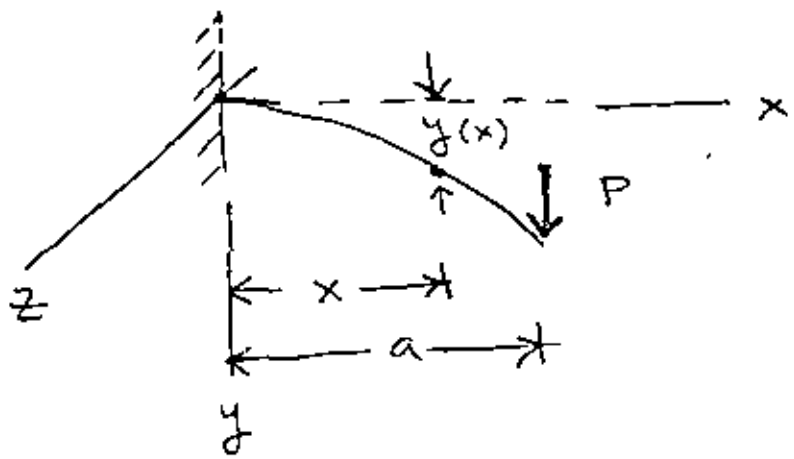

Fig 1 Viga en voladizo

La deflexión y(x) se obtiene integrando la ecuación [1]:

$$E I y''(x) = M(x) \qquad (1.5)$$

donde E es el módulo elástico del material de la viga, I es el momento de inercia de la sección transversal de la viga con respecto al eje Z (constante) y M(x) es el momento flexionante en el punto

de abscisa x. Este es igual a

$$M(x) = P(a-x) \tag{1.6}$$

Sustituyendo la ec (1.6) en la ec (1.5) se tiene

$$y''(x) - \frac{P}{EI}(a-x) = 0 \tag{1.7}$$

que es una ecuación diferencial ordinaria de 2^{o} orden, de la forma (1.1).

Defínase

$$y'(x) = p(x) \tag{1.8}$$

como la pendiente de la curva $y = y(x)$ en el punto x ; así, la ec (1.7) se transforma en el sistema

$$y'(x) = p(x) \tag{1.9 a}$$

$$p'(x) = \frac{P}{EI}(a-x) \tag{1.9 b}$$

que es un sistema de 2 ecuaciones diferenciales ordinarias de primer orden, de la forma (1.4). Para integrar este sistema se requiere, desde luego, contar con 2 constantes de integración, que se obtienen de las condiciones de frontera

$$y(0) = 0, \quad p(0) = 0 \tag{1.10}$$

Intégrese la ec (1.9 b) con la segunda condición de frontera (1.10). Se obtiene

$$p(x) = \frac{P}{EI}\left(ax - \frac{x^2}{2}\right) + C_1 \tag{1.11}$$

$$p(0) = C_1 = 0 \tag{1.12}$$

Por lo tanto,

$$p(x) = \frac{P}{EI}\left(ax - \frac{x^2}{2}\right) \qquad (1.13)$$

Sustitúyase la ec (1.13) en la ec (1.9 a). Se obtiene

$$y'(x) = \frac{P}{EI}\left(ax - \frac{x^2}{2}\right) \qquad (1.14)$$

Intégrese la ec (1.14) con la primera condición de frontera (1.10). Se obtiene

$$y(x) = \frac{P}{EI}\left(a\frac{x^2}{2} - \frac{x^3}{6}\right) + C_2 \qquad (1.15)$$

$$y(0) = C_2 = 0 \qquad (1.16)$$

Por lo tanto,

$$y(x) = \frac{P}{EI}\left(a\frac{x^2}{2} - \frac{x^3}{6}\right) \qquad \underline{\text{Solución}} \qquad (1.17)$$

El problema anterior se escogió muy simple a propósito. Sin embargo, es representativo de una clase más amplia de problemas que surgen del análisis estático de ganchos, columnas, etc. Se puede complicar si se incluyen otras variables espaciales, como en el caso del análisis estático de placas y cascarones, o bien si se le introduce la variable tiempo, como es el caso del análisis dinámico de vigas, placas y cascarones.

En problemas de mayor complejidad no es posible obtener la solución por simple integración de funciones sencillas, como en el Ejemplo 1.1.1En efecto, las ecuaciones de equilibrio de una placa circular de radio a empotrada, sujeta a una carga transversal q

(Fig 2) son [2] :

$$\Delta \Delta w = \frac{q}{D} \qquad (1.18)$$

sujeta a las condiciones de frontera

$$w = 0, \quad \frac{\partial w}{\partial r} = 0, \text{ en } r = a \qquad (1.19)$$

donde Δ es el operador laplaciano definido en coordenadas cilíndricas como

$$\Delta \equiv \frac{\partial^2}{\partial r^2} + \frac{1}{r}\frac{\partial}{\partial r} + \frac{1}{r^2}\frac{\partial^2}{\partial \theta^2} \qquad (1.20)$$

por lo que

$$\Delta\Delta = \left(\frac{\partial^2}{\partial r^2} + \frac{1}{r}\frac{\partial}{\partial r} + \frac{1}{r^2}\frac{\partial^2}{\partial \theta^2}\right)\left(\frac{\partial^2}{\partial r^2} + \frac{1}{r}\frac{\partial}{\partial r} + \frac{1}{r^2}\frac{\partial^2}{\partial \theta^2}\right) \qquad (1.21)$$

$q = q(r, \theta)$ es la carga que actúa sobre la placa y D es la rigidez a la flexión de la placa, definida como [2, p. 20]:

$$D = \frac{E h^3}{12 (1 - \nu^2)} \qquad (1.22)$$

En la ec (1.22), E es el módulo elástico del material, h es el espesor de la placa y ν es el módulo de Poisson [3] del material.

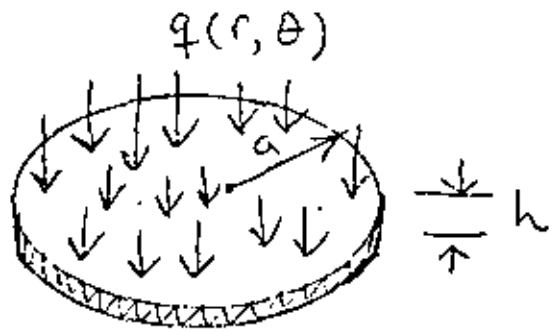

Fig 2 Placa circular cargada lateralmente

El problema representado por la ec (1.18) y las condiciones de frontera (1.19) es mucho más complicado de resolver que el del Ejemplo 1.1.1, como salta a la vista. Sin embargo, ambos problemas se refieren al análisis estático de un elemento estructural de comportamiento lineal (sus ecuaciones diferenciales correspondientes son lineales, es decir, tanto la función buscada como sus derivadas aparecen en esa ecuación elevadas a la primera potencia), sujeto a una carga dada, con condiciones de apoyo bien definidas (condiciones de frontera).

Nótese que los modelos matemáticos (ecuaciones diferenciales y condiciones de frontera) del Ejemplo 1.1.1.y de la Fig 2 involucran una ecuación diferencial, que en el primer caso es ordinaria y en segundo, parcial. En situaciones más complejas, en vez de una ecuación pueden tenerse varias y, además, acopladas. Un conjunto de ecuaciones se dice que es acoplado cuando en cada una de las ecuaciones aparece no una sola incógnita, sino varias. El hecho de haber obtenido ecuaciones diferenciales (espaciales) en los modelos matemáticos anteriores se debe a que se trata del análisis de elementos estructurales que son continuos. Por contraposición, un sistema que contenga elementos concentrados da lugar a modelos matemáticos provistos de ecuaciones algebraicas, esto es, que son de la forma

$$\begin{aligned} f_1(x_1, x_2, \ldots, x_n) &= 0 \\ f_2(x_1, x_2, \ldots, x_n) &= 0 \\ &\vdots \\ f_n(x_1, x_2, \ldots, x_n) &= 0 \end{aligned} \qquad (1.23)$$

En general, el sistema de ecuaciones algebraicas (1.23) es no lineal ; pero con frecuencia los sistemas físicos analizados

presentan un comportamiento lineal y, en este caso, dan lugar a modelos matemáticos del tipo lineal. Un modelo matemático de esta naturaleza contiene un sistema de ecuaciones algebraicas lineales del tipo

$$\begin{aligned} a_{11}x_1 + a_{12}x_2 \quad &\cdots \quad a_{1n}x_n = b_1 \\ a_{21}x_1 + a_{22}x_2 \quad &\cdots \quad a_{2n}x_n = b_2 \\ &\vdots \\ a_{n1}x_1 + a_{n2}x_2 \quad &\cdots \quad a_{nn}x_n = b_n \end{aligned} \tag{1.24}$$

En forma compacta el sistema (1.23) se puede escribir como

$$\underset{\sim}{f}(\underset{\sim}{x}) = \underset{\sim}{0} \tag{1.25}$$

donde

$$\underset{\sim}{f} = \begin{bmatrix} f_1 \\ f_2 \\ \cdot \\ \cdot \\ \cdot \\ f_n \end{bmatrix}, \quad \underset{\sim}{x} = \begin{bmatrix} x_1 \\ x_2 \\ \cdot \\ \cdot \\ \cdot \\ x_n \end{bmatrix}, \quad \underset{\sim}{0} = \begin{bmatrix} 0 \\ 0 \\ \cdot \\ \cdot \\ \cdot \\ 0 \end{bmatrix} \tag{1.26}$$

son vectores de dimensión n, o sea de n componentes. Por su parte, el sistema (1.24) se puede escribir en forma compacta como

$$\underset{\sim}{A}\,\underset{\sim}{x} = \underset{\sim}{b} \tag{1.27}$$

donde

$$\underset{\sim}{A} = \begin{bmatrix} a_{11} & a_{12} \cdots a_{1n} \\ a_{21} & a_{22} \cdots a_{2n} \\ \cdot & \\ \cdot & \\ \cdot & \\ a_{n1} & a_{n2} \cdots a_{nn} \end{bmatrix}, \quad \underset{\sim}{x} = \begin{bmatrix} x_1 \\ x_2 \\ \cdot \\ \cdot \\ \cdot \\ x_n \end{bmatrix}, \quad \underset{\sim}{b} = \begin{bmatrix} b_1 \\ b_2 \\ \cdot \\ \cdot \\ \cdot \\ b_n \end{bmatrix}$$

son una matriz de n x n y dos vectores de dimensión n.

En la mayor parte de este curso se tratará con sistemas lineales por lo que, en general, se llegará a modelos lineales de la forma (1.27).

A continuación se presenta el análisis de un sistema de parámetros concentrados, cuyo análisis estático da lugar a un modelo de la forma de la ec (1.27), donde la matriz $\underset{\sim}{A}$ y los vectores involucrados adquieren un significado físico palpable.

Considérese ahora el sistema compuesto por los tres resortes concentrados de rigideces k_1, k_2 y k_3, cuyos extremos se encuentran fijos (Fig 3). Este puede constituir un modelo muy simplificado de un tramo de una tubería sujeta a cargas axiales que pueden ser producida por cambios en la temperatura del fluido que transporte. El extremo fijo puede representar un anclaje de la tubería. Si se dispone de instrumentos que midan los desplazamientos en los nodos, se puede calcular las cargas que actúan en éstos, suponiendo que se conozcan los valores de la rigidez de los resortes.

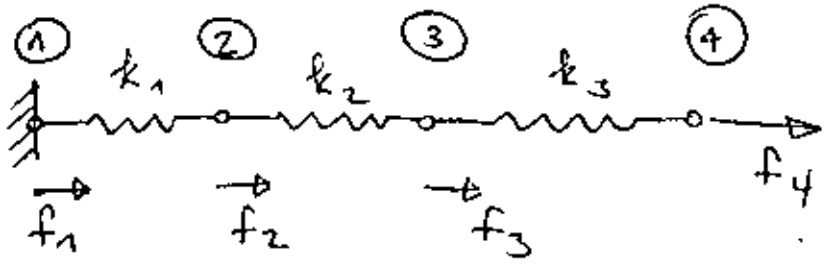

Fig 3 Sistema elástico de doble grado de libertad

El análisis estático del sistema de la Fig 3 se realizará considerando que cada resorte es lineal, esto es, que su comportamiento obedece a la siguiente ecuación constitutiva

$$F = k \Delta u$$

donde F es la fuerza que actúa en cada uno de sus extremos, como lo indica la Fig 4, mientras que k es su rigidez (constante) y Δu, el incremento en su desplazamiento desde una configuración en la que la fuerza en sus extremos es nula y que, por esto, recibe el nombre de configuración "descargada".

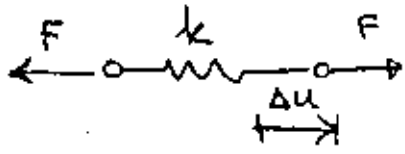

Fig 4 Resorte lineal

En un sistema como el de la Fig 3 se supone que las cargas actúan únicamente en los nodos. Más aún, la carga externa que actúa en el nodo i se representará por f_i, y estará en equilibrio con la carga interna F_i que actúa en el resorte i y con la F'_i, que actúa en el resorte i+1, como se muestra en la Fig 5

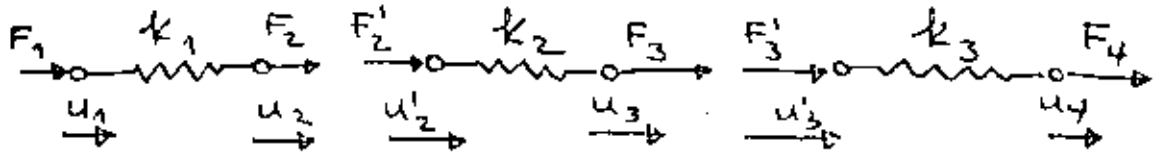

Fig 5 Cargas internas en el sistema elástico de la Fig 3

Además, llámese u_i al desplazamiento del nodo i asociado al resorte i, minetras que u_i' al del nodo i asociado al resorte i + 1. Por compatibilidad, es claro que

$$u_i' = u_i \tag{1.29}$$

Por equilibrio en cada nodo se tiene

$$f_1 = F_1,\ f_2 = F_2 + F_2',\ f_3 = F_3 + F_3',\ f_4 = F_4 \tag{1.30}$$

Un resorte típico, entonces, está sujeto al estado de cargas de la Fig 6

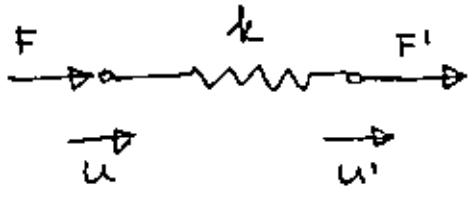

Fig 6 Estado de carga en un resorte lineal

En la Fig 6 se supone que cuando $u = u' = 0$, el resorte se encuentra descargado.

Si se supone que el estado de carga es equivalente a la superposición de dos estados, cada uno de ellos en equilibrio, se tiene la disposición de la Fig 7

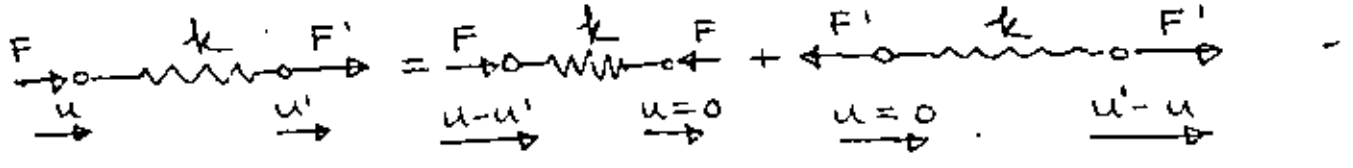

Fig 7 Estado de carga equivalente al de la Fig 6

Para el primer estado de carga del miembro derecho de la ecuación de la Fig 7 se tiene

$$F = k(u - u') \tag{1.31}$$

mientras que para el segundo

$$F' = k(u' - u) \tag{1.32}$$

Las ecs (1.31) y (1.32) se pueden poner en forma matricial como

$$\begin{bmatrix} F \\ F' \end{bmatrix} = \begin{bmatrix} k & -k \\ -k & k \end{bmatrix} \begin{bmatrix} u \\ u' \end{bmatrix} \tag{1.33}$$

que es una relación de la forma

$$\underset{\sim}{F} = \underset{\sim}{K}\,\underset{\sim}{u} \tag{1.34}$$

donde $\underset{\sim}{F}$ y $\underset{\sim}{u}$ son los vectores de fuerza y de desplazamiento, respectivamente, mientras que $\underset{\sim}{K}$ es la matriz de rigidez de cada resorte. Esta también se llama matriz elemental de rigidez para distinguirla de la matriz global de rigidez, que aún está por definirse. Nótese que $\underset{\sim}{K}$ es una matriz simétrica, esto es, que su elemento (1, 2) es igual a su elemento (2, 1). Además, es positiva semidefinida. En la sección de Algebra de Matrices se estudia con más detalle este último concepto ; pero aquí baste con decir que una matriz es positiva semidefinida si la forma cuadrática

$$\phi = \underset{\sim}{u}^T\,\underset{\sim}{K}\,\underset{\sim}{u} \tag{1.35}$$

asociada a ella nunca es negativa, lo cual es el caso de la matriz $\underset{\sim}{K}$ de la ec (1.33). En efecto, desarróllese la forma (1.35). Se tiene

$$\underset{\sim}{u}^T\,\underset{\sim}{K}\,\underset{\sim}{u} = \begin{bmatrix} u, & u' \end{bmatrix} \begin{bmatrix} k(u - u') \\ -k(u - u') \end{bmatrix} = k(u - u')^2 \tag{1.36}$$

que, como se ve de inmediato, nunca es negativa, pues $k > 0$. La forma cuadrática (1.35) es en realidad el doble de la energía elástica de deformación del resorte o energía potencial elástica. Esta energía, en vista de la expresión (1.36), se ha considerado como nula en el estado descargado, o sea, cuando $u = u' = 0$. Nótese, sin embargo, que también se anula esa energía cuando $u = u'$, lo cual corresponde a un desplazamiento de cuerpo rígido del resorte, que claramente, no produce incremento alguno en la energía elástica de deformación del resorte. Fuera de estos casos de energía elástica nula, se observa que ésta es siempre positiva, lo cual establece una correspondencia entre el carácter positivo semidefinido de $\underset{\sim}{K}$ y el carácter físico de la energía elástica de deformación.

Si se representa la energía elástica de deformación del resorte por V, se tiene que

$$V = \frac{1}{2} \underset{\sim}{u}^T \underset{\sim}{K} \underset{\sim}{u} \qquad (1.37)$$

que es una expresión semejante a

$$V = \frac{1}{2} k u^2 \qquad (1.38)$$

como en el caso de un resorte con un extremo fijo, que sufre un desplazamiento $\underset{\sim}{u}$ a partir de su estado descargado. De la ec (1.38) se obtiene

$$\frac{dV}{du} = k u \qquad (1.39)$$

Por analogía, para el caso de la ec (1.37) se tiene

$$\frac{\partial V}{\partial \underset{\sim}{u}} = \underset{\sim}{K} \underset{\sim}{u} \qquad (1.40)$$

que es un vector de dimensión 2. De hecho, es el gradiente de la

energía V con respecto a u. En la sección de Operaciones con Matrices se estudia con más detalle el concepto de gradiente, o sea, de derivada con respecto a un vector. De la ec (1.39) se tiene en seguida que

$$\frac{d^2 V}{d u^2} = k \qquad (1.41)$$

esto es, la rigidez del resorte es la segunda derivada de la energía potencial elástica con respecto al desplazamiento medido desde el estado descargado. Por analogía, se tiene de la ec (1.40),

$$\frac{\partial^2 V}{\partial u^2} = \underset{\sim}{K} \qquad (1.42)$$

esto es, la matriz de rigidez se puede obtener como la matriz Hessiana o sea, de segundas derivadas, de la energía potencial elástica con respecto al desplazamiento medido desde el estado descargado. En realidad, como se verá a continuación, es más fácil obtener esa matriz calculándola como la matriz de segundas derivadas de la energía potencial elástica.

Ejemplo 1.1.2 Análisis estático de un sistema elástico de doble grado de libertad.

Dado un conjunto de desplazamiento u_1, u_2, u_3 y u_4, medidos en los modos (1) a (4) correspondientes, del sistema elástico de la Fig 3, determinar las cargas que actúan en esos nodos.

De las expresiones (1.33) para las fuerzas que actúan en los extremos de cada resorte, y de las ecs (1.30), se tiene

$$\begin{aligned}
f_1 &= k_1(u_1 - u_2) \\
f_2 &= k_1(-u_1 + u_2) + k_2(u_2 - u_3) = -k_1u_1 + (k_1+k_2)u_2 - k_2u_3 \\
f_3 &= k_2(-u_2 + u_3) + k_3(u_3 - u_4) = -k_2u_2 + (k_2+k_3)u_3 - k_3u_4 \\
f_4 &= k_3(-u_3 + u_4)
\end{aligned} \qquad (1.43)$$

Escribiendo las ecs (1.43) en forma matricial se tiene

$$\begin{bmatrix} f_1 \\ f_2 \\ f_3 \\ f_4 \end{bmatrix} = \begin{bmatrix} k_1 & -k_1 & 0 & 0 \\ -k_1 & k_1+k_2 & -k_2 & 0 \\ 0 & -k_2 & k_2+k_3 & -k_3 \\ 0 & 0 & -k_3 & k_3 \end{bmatrix} \begin{bmatrix} u_1 \\ u_2 \\ u_3 \\ u_4 \end{bmatrix} \qquad (1.44)$$

que es una relación de la forma

$$\underset{\sim}{f} = \underset{\sim}{K}\,\underset{\sim}{u} \qquad (1.45)$$

entre la fuerza externa f que actúa en cada modo y el desplazamiento del nodo. En esa relación,

$$\underset{\sim}{f} = \begin{bmatrix} f_1 \\ f_2 \\ f_3 \\ f_4 \end{bmatrix}, \quad \underset{\sim}{u} = \begin{bmatrix} u_1 \\ u_2 \\ u_3 \\ u_4 \end{bmatrix}, \quad \underset{\sim}{K} = \begin{bmatrix} k_1 & k_1 & 0 & 0 \\ -k_1 & k_1+k_2 & -k_2 & 0 \\ 0 & -k_2 & k_2+k_3 & -k_3 \\ 0 & 0 & -k_3 & k_3 \end{bmatrix} \qquad (1.46)$$

donde $\underset{\sim}{K}$ es la <u>matriz global de rigidez</u>. Nótese que esta matriz es simétrica, al igual que la matriz de rigidez de cada resorte. Puede demostrarse, además, que es igualmente <u>positiva semi-definida</u>. La energía potencial elástica del sistema es, por su parte

$$V = \frac{1}{2}\,\underset{\sim}{u}^T\,\underset{\sim}{K}\,\underset{\sim}{u} \qquad (1.47)$$

De la ec (1.44), nótese que, si $u_1 = u_2 = u_3 = u_4$, esto es, si los resortes sufren un desplazamiento de cuerpo rígido, $\underset{\sim}{f} = \underset{\sim}{0}$ y, consecuentemente, $V = 0$, lo cual es acorde con el hecho de que el sistema es insensible a movimientos de cuerpo rígido, esto es, este

tipo de movimientos no induce sobre él incremento alguno en su energía potencial elástica. Por otra parte, de la ec (1.44) se observa además, que la matriz global de rigidez resulta de una superposición de las matrices elementales de rigidez. Finalmente, esta matriz es "bandeada", esto es, sus elementos no nulos se encuentran alojados sobre una "banda" de ancho 3 centrada en su diagonal.

Para efectuar el análisis del sistema de la Fig 3 debe incluirse la condición de frontera $u_1 = 0$. Si se introduce ésta en las expresiones (1.43) se llega a

$$\begin{aligned} f_1 &= -k_1 u_2 \\ f_2 &= (k_1 + k_2)u_2 - k_2 u_3 \\ f_3 &= -k_2 u_2 + (k_2 + k_3)u_3 \\ f_4 &= k_3(-u_3 + u_4) \end{aligned} \qquad (1.48)$$

con lo que se obtiene el valor deseado de las cargas en los nodos.

Por otra parte, la ec (1.44) se pudo haber obtenido imponiendo una condición de <u>minimalidad</u> sobre un <u>funcional</u>. Un funcional no es sino un número real definido sobre un espacio vectorial. En otras palabras, es una función escalar de variable vectorial. Sea

$$U(\underset{\sim}{u}) = V - \underset{\sim}{f}^T \underset{\sim}{u} \qquad (1.49)$$

un funcional que depende del vector de desplazamiento $\underset{\sim}{u}$, cuyo valor no es sino la diferencia entre la energía potencial elástica del sistema, V, y el trabajo desarrollado por las cargas, $\underset{\sim}{f}$. Este funcional alcanza un mínimo en los valores de $\underset{\sim}{u}$ para los cuales se tiene un valor estacionario de U. Del cálculo de funciones de varias variables se sabe que U alcanza un valor estacionario en los puntos en los que su gradiente con respecto a $\underset{\sim}{u}$ se anula, esto es,

donde

$$\frac{\partial U}{\partial \underset{\sim}{u}} = \frac{\partial V}{\partial \underset{\sim}{u}} - \frac{\partial}{\partial \underset{\sim}{u}} \underset{\sim}{f}^{m} \underset{\sim}{u} = \underset{\sim}{0} \qquad (1.50)$$

Pero

$$\frac{\partial V}{\partial \underset{\sim}{u}} = \underset{\sim}{K}\,\underset{\sim}{u} \qquad (1.51)$$

de la ec (1.40). Además, como $\underset{\sim}{f}$ no depende explícitamente de $\underset{\sim}{u}$,

$$\frac{\partial}{\partial \underset{\sim}{u}} \underset{\sim}{f}^{T} \underset{\sim}{u} = \underset{\sim}{f} \qquad (1.52)$$

como se muestra en la Sección de Operaciones con Matrices. Sustituyendo (1.51) y (1.52) en (1.50), se obtiene la ec (1.45) o bien, la (1.44), como se deseaba demostrar. El resultado anterior constituye lo que se llama un "Principio de mínimo" en Mecánica. En realidad, la condición (1.50) es necesaria y suficiente para que U alcance un valor estacionario, que puede ser máximo, mínimo o punto silla. Para que el punto estacionario en cuestión sea mínimo es suficiente que la matriz Hessiana de U con respecto a $\underset{\sim}{u}$ sea positiva semidfinida ; pero, de (1.50),

$$\frac{\partial^2 U}{\partial \underset{\sim}{u}^2} = \underset{\sim}{K} \qquad (1.53)$$

que es efectivamente positiva semidefinida. Sin embargo, en esta parte no se presenta la demostración de la positividad semidefinida de culaquier matriz de rigidez. Baste con decir que ésta proviene del hecho de que la forma cuadrática (1.47) asociada a K representa un incremento en la energía potencial elástica del sistema elástico

en cuestión, desde su posición descargada, el cual no puede ser negativo, independientemente de los valores de los desplazamientos de los nodos, medidos desde esa configuración descargada.

Hasta aquí se han introducido ideas generales asociadas a sistemas físicos compuestos ya sea de elementos de parámetros distribuidos (vigas, placas, cascarones, fluidos), cuyos modelos dan lugar a sistemas de ecuaciones diferenciales, o bien de elementos con parámetros concentrados (resortes, por ejemplo), cuyos modelos dan lugar a ecuaciones algebraicas. Sin embargo, todavía no se ha hablado en concreto del MEF. De hecho, es este método el que establece esta relación, pues permite formular problemas asociados a sistemas continuos o de parámetros distribuidos en forma discreta, esto es, como si se tratara de sistemas con parámetros concentrados. Esto lo consigue el MEF mediante un proceso de <u>discretización</u>, que consiste en hacer depender la solución al problema original continuo de un conjunto <u>discreto</u> de valores. Mediante este proceso se obtiene una <u>aproximación</u> a la solución al problema original, y no un valor exacto de ella. Para ilustrar las ideas anteriores, considérese el mismo problema de determinar las cargas sobre el tramo de tubería de la Fig 3 ; pero ahora supóngase que cada sección i (porción entre nodos) se trata como una barra continua (y no como un resorte concentrado) de longitud a_i, de sección de área A_i y de módulo de elasticidad E_i. Esta consideración puede ser una aproximación a una barra (tubería) de diametro variable, ya sea continuamente o "por saltos", de materia. heterogéneo, esto es, de un material cuyas propiedades no fueran constantes. Se tendría entonces el sistema de la Fig 8

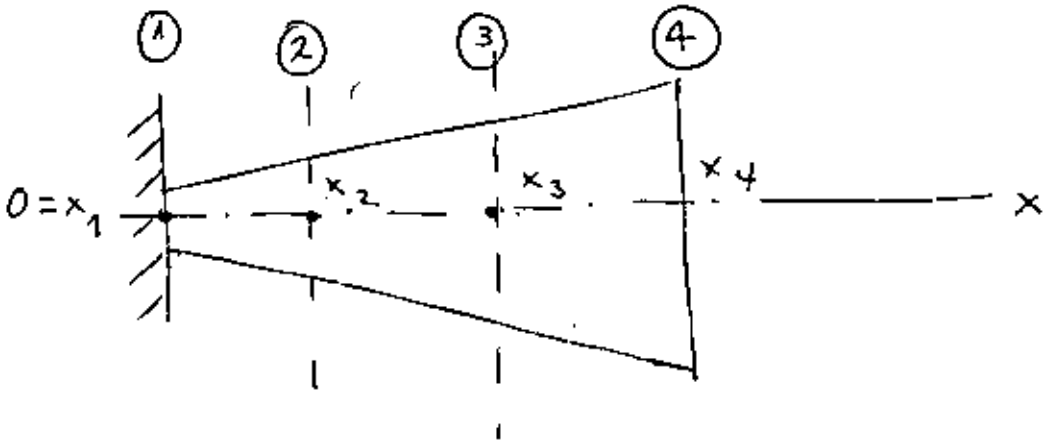

Fig 8 Sistema elástico continuo

Para el análisis de este sistema considérese que cada tramo, entre el nodo i y el i + 1, se puede tratar como una barra de sección de área constante A_i, de longitud a_i y de módulo elástico constante E_i. Más aún, condisérese que el desplazamiento a lo largo de esta barra elemental tiene una distribución lineal, esto es, es de la forma

$$u(x) = a_{0i} + a_{1i}(x - x_i),\ x_i \leq x \leq x_{i+1} \qquad (1.54)$$

Llamando u_i al desplazamiento en el nodo i, la expresión (1.54) debe cumplir con las condiciones de frontera

$$u(x_i) = u_i,\ u(x_{i+1}) = u_{i+1} \qquad (1.55)$$

por lo que se obtiene, como valores de a_{0i} y de a_{1i},

$$a_{0i} = u_i,\ a_{1i} \quad \frac{\Delta u_i}{\Delta x_i} \qquad (1.56)$$

donde

$$\Delta x_i \equiv x_{i+1} - x_i,\ \Delta u_i \equiv u_{i+1} - u_i \qquad (1.57)$$

Entonces, u (x) en $x_i \leq x \leq x_{i+1}$ se puede escribir como un producto escalar (Ver la Sección Algebra de matrices) de dos vectores, en la forma

$$u(x) = \left[1 - \frac{x - x_i}{\Delta x_i},\ \frac{x - x_i}{\Delta x_i}\right] \begin{bmatrix} u_i \\ u_{i+1} \end{bmatrix} \qquad (1.58)$$

La expresión anterior se puede simplificar si se introduce la notación

$$\xi_i \equiv x - x_i$$

La ec (1.58) se transforma, entonces, en

$$u(x) = \left[1 - \frac{\xi_i}{\Delta x_i},\ \frac{\xi_i}{\Delta x_i}\right] \begin{bmatrix} u_i \\ u_{i+1} \end{bmatrix} \qquad (1.59)$$

La deformación en un punto x de la barra, ε, que es la derivada de u con respecto a x [1, p.], se puede obtener derivando con respecto a x la expresión (1.54) :

$$\varepsilon \cong u'(x) = a_{1i} = \frac{\Delta u_i}{\Delta x_i} = \left[-\frac{1}{\Delta x_i},\ \frac{1}{\Delta x_i}\right] \begin{bmatrix} u_i \\ u_{i+1} \end{bmatrix} \qquad (1.60)$$

El esfuerzo queda expresado, entonces, como [1, p.]

$$\sigma \cong E_i \varepsilon = E_i \left[-\frac{1}{\Delta x_i},\ \frac{1}{\Delta x_i}\right] \begin{bmatrix} u_i \\ u_{i+1} \end{bmatrix} \qquad (1.61)$$

La energía potencial elástica V_i almacenada en el tramo comprendido entre los nodos i e i + 1 es, entonces [1, p.]:

$$V_i = \frac{1}{2}\int_{x_i}^{x_{i+1}} \sigma \varepsilon A_i \, dx = \frac{1}{2}\int_{x_i}^{x_{i+1}} E_i \varepsilon^2 A_i \, dx \qquad (1.62)$$

Pero, de las ecs (1.60) y (1.61), en $x_i \leq x \leq x_{i+1}$,

$$\sigma \varepsilon = E_i \left(-\frac{u_i}{\Delta x_i} \quad \frac{u_{i+1}}{\Delta x_i}\right)^2$$

que es independiente de x, al igual que E_i y A_i, por lo que se pueden sacar de la integral, y la expresión para V_i se reduce a

$$V_i = \frac{1}{2} E_i A_i \left(-\frac{u_i}{\Delta x_i} + \frac{u_{i+1}}{\Delta x_i}\right)^2 \int_{x_i}^{x_{i+1}} dx =$$

$$= \frac{1}{2} E_i A_i \left(-\frac{u_i}{\Delta x_i} + \frac{u_{i+1}}{\Delta x_i}\right)^2 \Delta x_i \qquad (1.63)$$

La energía potencial elástica total del sistema es, entonces, simplificando V_i,

$$V = \frac{1}{2}\sum_{1}^{3} V_i = \frac{1}{2}\sum_{1}^{3} \frac{E_i A_i}{\Delta x_i} (- u_i + u_{i+1})^2 \qquad (1.64)$$

Llamando

$$k_i = \frac{E_i A_i}{\Delta x_i} \qquad (1.65)$$

y desarrollando la expresión (1.64), se tiene

$$2V = k_1 (u_2 - u_1)^2 + k_2 (u_3 - u_2)^2 + k_3 (u_4 - u_3)^2 =$$

$$= k_1 u_1^2 - 2 k_1 u_1 u_2 + (k_1 + k_2) u_2^2 - 2 k_2 u_2 u_3 + (k_2 + k_3) u_3^2$$

$$2 k_3 u_3 u_4 + k_3 u_4^2 \qquad (1.66)$$

La matriz de rigidez de cada elemento, es decir, de cada tramo comprendido entre x_i y x_{i+1} se obtiene como

$$\underset{\sim}{K}_i \quad \frac{\partial^2 V_i}{\partial \underset{\sim}{u}_i^2} \qquad (1.67)$$

donde $\underset{\sim}{u}_i$ es el vector $[u_i, u_{i+1}]^T$. Así, de (1.63),

$$\frac{\partial V_i}{\partial \underset{\sim}{u}_i} = \begin{bmatrix} \frac{\partial V_i}{\partial u_i} \\ \frac{\partial V_i}{\partial u_{i+1}} \end{bmatrix} = k_i \begin{bmatrix} - (- u_i + u_{i+1}) \\ (- u_i + u_{i+1}) \end{bmatrix} \qquad (1.68)$$

por lo que

$$\underset{\sim}{K}_i = \frac{\partial^2 v_i}{\partial \underset{\sim}{u}_i^2} = \begin{bmatrix} k_i & -k_i \\ -k_i & k_i \end{bmatrix} \qquad (1.69)$$

y la matriz de rigidez global $\underset{\sim}{K}$ se obtiene como

$$\underset{\sim}{K} = \frac{\partial^2 V}{\partial \underset{\sim}{u}^2}$$

donde $\underset{\sim}{u} = [u_1, u_2, u_3, u_4]^T$. Tomando la primera derivada,

$$\frac{\partial V}{\partial \underset{\sim}{u}} = \begin{bmatrix} \partial V/\partial u_1 \\ \partial V/\partial u_2 \\ \partial V/\partial u_3 \\ \partial V/\partial u_4 \end{bmatrix} = \begin{bmatrix} k_1 (u_1 - u_2) \\ -k_1 u_1 + (k_1 + k_2) u_2 - k_2 u_3 \\ -k_2 u_2 + (k_2 + k_3) u_3 - k_3 u_4 \\ k_3 (-u_3 + u_4) \end{bmatrix}$$

Tomando las derivadas con respecto a $\underset{\sim}{u}$ de la expresión anterior se tiene

$$\underset{\sim}{K} = \frac{\partial^2 V}{\partial \underset{\sim}{u}^2} = \begin{bmatrix} k_1 & -k_1 & 0 & 0 \\ -k_1 & k_1 + k_2 & -k_3 & 0 \\ 0 & -k_2 & k_2 + k_3 & -k_3 \\ 0 & 0 & -k_3 & k_3 \end{bmatrix} \qquad (1.70)$$

Se observa de la expresión (1.69) que la matriz elemental de rigidez del sistema continuo es idéntica a la del sistema discreto, (1.33). Asimismo, de la expresión (1.70) se observa que la matriz

global de rigidez del sistema continuo es idéntica a la del sistema discreto, (1.46). Por otra parte, el comportamiento estático del sistema continuo de la Fig 7 está gobernado por una ecuación diferencial ordinaria provista de condictiones de frontera dadas. Esta se obtiene a continuación. Sea $u = u(x)$ el campo (continuo) de desplazamiento. La deformación unitaria, o gradiente de desplazamiento $\varepsilon(x)$, se obtiene como $\varepsilon(x) = u'(x)$. De la "Ley de Hooke" se obtiene el esfuerzo como $\sigma(x) = E(x)\,\varepsilon(x) = E(x)\,u'(x)$. Por equilibrio estático, $\sigma(x)$ debe ser igual a la carga aplicada en el punto x, $q(x)$, dividida entre el área de la sección en el punto x, $A(x)$, esto es :

$$E(x)\,u'(x) = \frac{q(x)}{A(x)} \qquad (1.71)$$

o bien

$$u'(x) = \frac{q(x)}{E(x)\,A(x)} \qquad (1.72)$$

con la condición de frontera $u(0) = 0$. La obtención de $u(x)$ para el problema formulado en la forma de la ec (1.72) requiere la integración de una función, mientras que, con el método del elemento finito, requiere la solución de un sistema de ecuaciones de la forma

$$\underset{\sim}{K}\,\underset{\sim}{u} = \underset{\sim}{f} \qquad (1.73)$$

donde, si se supone $\underset{\sim}{f}$ conocida, $\underset{\sim}{u}$ se puede calcular por simple inversión de la matriz $\underset{\sim}{K}$, esto es, como

$$\underset{\sim}{u} = \underset{\sim}{K}^{-1}\,\underset{\sim}{f} \qquad (1.74)$$

En la Sección de Métodos Números se verá que en realidad nunca es necesario invertir la matriz $\underset{\sim}{K}$ tal como aparece en (1.74).

Por otra parte, de la expresión (1.70) se puede observar que la matriz $\underset{\sim}{K}$ es singular, pues si $u_1 = u_2 = u_3 = u_4$, $\underset{\sim}{f}$ resulta ser nula. Para que $\underset{\sim}{K}$ tenga una inversa debe introducirse en el problema la condición de frontera $u_1 = 0$.

En suma, el MEF permite llevar la solución de un problema que, en principio requiere la integración de un sistema de ecuaciones diferenciales, a la forma de un problema algebraico, esto es, de un problema que requiere la solución de un sistema de ecuaciones algebraicas. Este sistema, en general, puede ser no lineal. Sin embargo, en una gran clase de problemas el sistema es lineal. El interés por llevar un problema continuo a una forma algebraica estriba en que los sistemas algebraicos, especialmente los lineales, de la forma (1.73), están plenamente estudiados desde el siglo pasado. Más aún, con el advenimiento de las computadoras electrónicas de los años cincuenta, se desarrollaron métodos muy eficaces para resolver estos sistemas, como se verá en la Sección de Métodos Numéricos.

1.2 GENERALIDADES SOBRE MATRICES

Una matriz es una tabla rectangular de números o de símbolos dispuestos en renglones y en columnas. Frecuentemente se le representa limitándola con corchetes. A continuación se representa una matriz de m renglones y n columnas :

$$\underset{(m \times n)}{\underset{\sim}{A}} = \begin{bmatrix} a_{11} & a_{12} & \cdots & a_{1j} & \cdots & a_{1n} \\ a_{21} & a_{22} & \cdots & a_{2j} & \cdots & a_{2n} \\ \vdots & \vdots & & \vdots & & \vdots \\ a_{i1} & \cdots & & a_{ij} & \cdots & a_{in} \\ \vdots & \vdots & & \vdots & & \vdots \\ a_{m1} & \cdots & & a_{mj} & \cdots & a_{mn} \end{bmatrix}$$

Es necesario señalar que siempre se menciona el número de renglones (m) primero. Por consiguiente, $\underset{\sim}{A}$ es una matriz (m x n).

En los siguientes párrafos se hará frecuente mención de matrices o vectores renglón o columna. Suponiendo que m = 1, se tiene

una matriz renglón o un vector renglón

$$\underset{\sim}{A} = \begin{bmatrix} a_{11} & a_{12} & \cdots & a_{ij} & \cdots & a_{1n} \end{bmatrix}$$

Sin embargo, si se supone que n = 1, se obtiene

una matriz columna o un vector columna

$$\underset{\sim}{A} = \begin{bmatrix} a_{11} & a_{21} & \cdots & a_{j1} & \cdots & a_{m1} \end{bmatrix}^T = \begin{bmatrix} a_{11} \\ a_{21} \\ \vdots \\ a_{j1} \\ \vdots \\ a_{m1} \end{bmatrix}$$

Existen matrices especiales que es necesario mencionar.

Matriz diagonal

$$\underset{(4 \times 4)}{\underset{\sim}{A}} = \begin{bmatrix} a_{11} & 0 & 0 & 0 \\ & a_{22} & 0 & 0 \\ & & a_{33} & 0 \\ \text{simétrica} & & & a_{44} \end{bmatrix} \qquad a_{ij} = 0 \text{ si } i \neq j$$

Otra notación sería

$$\underset{\sim}{A} = \text{diag } (a_{11}, a_{22}, a_{33}, a_{44})$$

Matriz identidad

Dicha matriz es un caso especial de arriba. En el caso de una matrix 3 x 3, por ejemplo, se tiene

$$\underset{\sim}{I}_3 = \begin{bmatrix} 1 & 0 & 0 \\ & 1 & 0 \\ \text{sim} & & 1 \end{bmatrix} = \text{diag } (1, 1, 1)$$

Matriz bandeada

Se aplica la denominación "matriz bandeada" cuando todos elementos de una matriz que no son iguales a 0 están colocados alrededor de la diagonal principal. Por ejemplo :

$$\begin{bmatrix} a_{11} & a_{12} & 0 & 0 & . & . & . & 0 & 0 \\ a_{21} & a_{22} & 0 & 0 & . & . & . & 0 & 0 \\ 0 & 0 & a_{33} & a_{34} & . & . & . & 0 & 0 \\ 0 & 0 & a_{43} & a_{44} & . & . & . & 0 & 0 \\ . & . & . & . & . & . & . & . & . \\ 0 & 0 & 0 & 0 & . & . & . & a_{n-1,\,n-1} & a_{n-1,\,n} \\ 0 & 0 & 0 & 0 & . & . & . & a_{n,\,n-1} & a_{nn} \end{bmatrix}$$

Matriz triangular

Se dice de una matriz que es triangular superior (S) o inferior (I) cuando la totalidad de sus elementos situados ya sea arriba o abajo de la diagonal principal es igual a zero.

$$\underset{(n \times n)}{\underset{\sim}{L}} = \begin{bmatrix} a_{11} & 0 & 0 & . & . & 0 \\ a_{21} & a_{22} & 0 & . & . & 0 \\ . & . & . & . & . & . \\ a_{n1} & a_{n2} & . & . & . & a_{nn} \end{bmatrix}$$

Matriz simétrica

En una matriz simétrica, a_{ij} es siempre igual a a_{ji}. En mecánica estructural lineal por ejemplo, todas las matrices de rigidez son simétricas.

Matriz transpuesta

Se obtiene una matriz transpuesta cuando se cambian renglones por columnas, como por ejemplo

$$\underset{(2 \times 3)}{\underset{\sim}{A}} = \begin{bmatrix} a_{11} & a_{12} & a_{13} \\ a_{21} & a_{22} & a_{23} \end{bmatrix}$$

Así, la matriz transpuesta de $\underset{\sim}{A}$, es

$$\underset{(3 \times 2)}{\underset{\sim}{A}^T} = \begin{bmatrix} a_{11} & a_{21} \\ a_{12} & a_{22} \\ a_{13} & a_{23} \end{bmatrix}$$

Además,

$$(\underset{\sim}{A}^T)^T = \underset{\sim}{A}$$

y, en el caso de matrices simétricas,

$$\underset{\sim}{A}^T = \underset{\sim}{A}$$

Subdivisión de matrices

Las matrices muy grandes de, por ejemplo, 5 000 x 5 000 que contienen 25 millones de elementos, tienen necesariamente que subdividirse en matrices más pequeñas, como

$$\left[\begin{array}{cc:c} a_{11} & a_{12} & a_{13} \\ a_{21} & a_{22} & a_{23} \\ \hdashline a_{31} & a_{32} & a_{33} \end{array}\right] = \begin{bmatrix} \underset{\sim}{A}_{11} & \underset{\sim}{A}_{12} \\ \underset{\sim}{A}_{21} & \underset{\sim}{A}_{22} \end{bmatrix}$$

donde

$$\underset{(2 \times 2)}{\underset{\sim}{A}_{11}} = \begin{bmatrix} a_{11} & a_{12} \\ a_{21} & a_{22} \end{bmatrix} \qquad \underset{(2 \times 1)}{\underset{\sim}{A}_{12}} = \begin{bmatrix} a_{13} & a_{23} \end{bmatrix}$$

$$\underset{(1 \times 2)}{\underset{\sim}{A}_{21}} = \begin{bmatrix} a_{31} & a_{32} \end{bmatrix} \qquad \underset{(1 \times 1)}{\underset{\sim}{A}_{22}} = \begin{bmatrix} a_{33} \end{bmatrix}$$

Operaciones con matrices

En el cálculo, es posible procesar matrices de la misma manera en que se procesan normalmente los datos numéricos. Se indican más abajo las definiciones necesarias.

Igualdad de matrices

$$\underset{\sim}{A} = \underset{\sim}{B}$$

significa que, para toda i y toda j, $a_{ij} = b_{ij}$.

Adición y substracción

Si

$$\underset{\sim}{A} + \underset{\sim}{B} = \underset{\sim}{C}$$

entonces

$c_{ij} = a_{ij} + b_{ij}$.

Por consiguiente, en el caso de substracción, se obtiene

$c_{ij} = a_{ij} - b_{ij}$.

Multiplicación de matrices

Si se debe multiplicar una matriz por un factor c, cada elemento debe multiplicarse por c, por ejemplo

$$[c\underset{\sim}{A}] = [ca_{ij}]$$

Cuando se multiplican dos matrices es condición sine qua non que sus dimensiones sean compatibles. Si, por ejemplo, la matriz $\underset{\sim}{A}$ de m x n debe multiplicarse por la matriz $\underset{\sim}{B}$ de p x q, es necesario que $n = p$, esto es, el número de renglones n contenido en $\underset{\sim}{A}$ debe ser igual al número de columnas p contenidas en $\underset{\sim}{B}$. Así,

$$\underset{(m \times n)}{\underset{\sim}{A}} \quad \underset{(p \times q)}{\underset{\sim}{B}} = \underset{(m \times q)}{\underset{\sim}{C}}$$

y

$$c_{ij} = a_{ir}b_{rj} \qquad \begin{matrix} i = 1, 2 \ldots m \; ; \; j = 1, 2 \ldots q \\ r = 1, 2, \ldots ; \; n = p \end{matrix}$$

Otro ejemplo sería

$$\begin{bmatrix} a_{11} & a_{12} & a_{13} \\ a_{21} & a_{22} & a_{23} \end{bmatrix} \begin{bmatrix} b_{11} \\ b_{21} \\ b_{31} \end{bmatrix} =$$

$$= \begin{bmatrix} a_{11}b_{11} + a_{12}b_{21} + a_{13}b_{31} \\ a_{21}b_{11} \quad a_{22}b_{21} \quad a_{23}b_{31} \end{bmatrix}$$

Valores característicos

Dada una matriz cuadrada $\underset{\sim}{A}$ de n x n y un vector $\underset{\sim}{u}$ de dimensión n sobre el que opera $\underset{\sim}{A}$, el producto

$$\underset{\sim}{v} = \underset{\sim}{A}\,\underset{\sim}{u}$$

es un vector también de dimensión n. En general, $\underset{\sim}{v}$ es muy diferente de $\underset{\sim}{u}$. Si, por ejemplo, $\underset{\sim}{v}$ resulta nulo para valores particulares de $\underset{\sim}{u} \neq \underset{\sim}{0}$, se dice que $\underset{\sim}{v}$ es un vector del espacio nulo de A. Por ejemplo, sea

$$\underset{\sim}{A} = \begin{bmatrix} 0 & 1 \\ 0 & 0 \end{bmatrix}$$

Un vector del espacio nulo de A es, claramente,

$$\underset{\sim}{u} = [\,x,\ 0\,]^T = x\,[\,1,\ 0\,]^T$$

Se observa que si se multiplica el vector $\underset{\sim}{w} = [\,1,\ 0\,]^T$ por el escalar x, se obtiene una infinidad de vectores del espacio nulo de $\underset{\sim}{A}$, uno para cada valor que pueda adquirir x. Sin embargo, $\underset{\sim}{w}$ es el único vector de magnitud unitaria que pertenece al espacio nulo de $\underset{\sim}{A}$. Por esto se puede decir que $\underset{\sim}{w}$ es una base normal de este espacio. En general, el espacio nulo de una matriz de n x n tiene una base compuesta por $m \leq n$ vectores. Si estos vectores se seleccionan de magnitud unitaria y mutuamente ortogonales, se dice que la base es ortonormal. Las matrices no singulares tienen un espacio nulo de de dimensión cero, esto es, no existe ningún vector no nulo que sea transformado por ellas en $\underset{\sim}{0}$.

Por otra parte, puede darse el caso que el vector $\underset{\sim}{v} = \underset{\sim}{A}\,\underset{\sim}{u}$ sea linealmente dependiente con $\underset{\sim}{u}$, esto es, que uno resulte de multiplicar

el otro por una constante. En esta discusión se deja fuera el vector $\underset{\sim}{u} = \underset{\sim}{0}$. En estas condiciones, se tiene

$$\underset{\sim}{A}\,\underset{\sim}{u} = \lambda\,\underset{\sim}{u} \qquad (*)$$

donde λ es un escalar, en general, complejo. Nótese que la ecuación anterior se puede escribir en la forma

$$(\underset{\sim}{A} - \lambda\underset{\sim}{I})\underset{\sim}{u} = \underset{\sim}{0}$$

donde $\underset{\sim}{I}$ es la matriz identidad de n x n. Para que $\underset{\sim}{u} \neq \underset{\sim}{0}$ satisfaga la ecuación anterior, debe pertenecer al espacio nulo de $\underset{\sim}{A} - \lambda\underset{\sim}{I}$. Ahora bien, para que $\underset{\sim}{A} - \lambda\underset{\sim}{I}$ tenga un espacio nulo no vacío, esto es, para que existan vectores $\underset{\sim}{u} \neq \underset{\sim}{0}$ tales que $(\underset{\sim}{A} - \lambda\underset{\sim}{I})\underset{\sim}{u} = \underset{\sim}{0}$, $\underset{\sim}{A} - \lambda\underset{\sim}{I}$ debe ser singular. Para que sea singular, su determinante debe anularse, esto es, debe tenerse

$$\det(\underset{\sim}{A} - \lambda\underset{\sim}{I}) = 0$$

Pero el determinante en cuestión, esto es, el miembro izquierdo de la ecuación anterior, es un polinomio de orden n en λ, si $\underset{\sim}{A}$ es de n x n. Llamando $P_n(\lambda)$ a este polinomio, la ecuación anterior es

$$P_n(\lambda) = 0$$

Si $\underset{\sim}{A}$ es una matriz de elementos reales, $P_n(\lambda)$ es un polinomio de coeficientes reales y, por el Teorema Fundamental del Algebra [4], posee n raíces complejas, de las cuales algunas pueden aparecer repetidas. Las n raíces del polinomio $P_n(\lambda)$, llamado polinomio característico de A, reciben el nombre de valores característicos de $\underset{\sim}{A}$. Si cada valor característico de $\underset{\sim}{A}$ se sustituye en la ec (*), se obtiene un conjunto de vectores $\underset{\sim}{u}_i$ correspondientes que se llaman vectores característicos de $\underset{\sim}{A}$. Nótese que si se conoce un vector característico $\underset{\sim}{e}_i$, esto es, si

$$\underset{\sim}{A}\,\underset{\sim}{e}_i = \lambda_i\,\underset{\sim}{e}_i$$

entonces el producto de éste por un escalar (en general, complejo) es otro vector característico de $\underset{\sim}{A}$, lo cual puede comprobarse por sustitución delnuevo vector en la ecuación anterior. Entonces, a cada valor característico λ_i de $\underset{\sim}{A}$ corresponde una infinidad de vectores característicos. Sin embargo, no todos éstos interesan, sino sólo aquéllos que son linealmente independientes. Un conjunto de vectores $\{ \underset{\sim}{v}_1, \underset{\sim}{v}_2, \ldots, \underset{\sim}{v}_m \}$ es linealmente independiente si la combinación lineal

$$\underset{\sim}{1} = c_1 \underset{\sim}{v}_1 + c_2 \underset{\sim}{v}_2 + \cdots + c_m \underset{\sim}{v}_m$$

se anula si, y sólo si, todos y cada uno de los escalares c_i se anulan. De lo contrario, el conjunto es linealmente dependiente.

Ejemplo 1.2.1. Sea la matriz

$$\underset{\sim}{A} = \frac{1}{3} \begin{bmatrix} 2 & 1 & 2 \\ -2 & 2 & 1 \\ -1 & -2 & 2 \end{bmatrix}.$$

Su polinomio característico es

$$P_3(\lambda) = (1 - \lambda)(\lambda^2 - 1)$$

cuyas raíces son

$$\lambda_1 = 1, \lambda_{2,3} = \frac{1}{2} \pm i \frac{\sqrt{3}}{2} = e^{\pm i\pi/3}$$

donde i es la unidad imaginaria $i = \sqrt{-1}$.

El Ejemplo 1.2.1 mostró que la matriz en cuestión tiene dos valores característicos complejos que, como consecuencia del Teorema Fundamental del Algebra, son conjugados. Si la matriz aludid

es simétrica, se puede demostrar [5] que sus valores característicos son reales y sus vectores característicos son mutuamente ortogonales. En consecuencia, una matriz simétrica de n x n siempre puede expresarse con respecto a una base (esto es, un conjunto de n vectores linealmente independientes), que resulta ser su conjunto de vectores característicos, en la que adquiere la forma diagonal.

Ejemplo 1.2.2. Sea la matriz

$$\underset{\sim}{A} = \begin{bmatrix} 0 & 2 \\ 2 & 3 \end{bmatrix}$$

Esta matriz es simétrica y por lo tanto tiene valores característicos reales y vectores característicos ortogonales. En efecto, su polinomio característico es

$$P_2(\lambda) = \det (A - \lambda I) = \det \begin{bmatrix} -\lambda & 2 \\ 2 & 3 - \lambda \end{bmatrix}$$

$$= -\lambda(3 - \lambda) - 4 = \lambda^2 - 3\lambda - 4$$

cuyas raíces son

$$\lambda_1 = -1, \lambda_2 = 4$$

Denótense sus vectores característicos correspondientes por

$$\underset{\sim}{e}_1 = \begin{bmatrix} e_{11} \\ e_{21} \end{bmatrix}, \quad \underset{\sim}{e}_2 = \begin{bmatrix} e_{12} \\ e_{22} \end{bmatrix}$$

Estos se calculan de las relaciones

$$(\underset{\sim}{A} - \lambda_i \underset{\sim}{I})\underset{\sim}{e}_i = \underset{\sim}{0}$$

De ahí

$$(\underset{\sim}{A} - \lambda_1 \underset{\sim}{I})\underset{\sim}{e}_1 = \begin{bmatrix} 1 & 2 \\ 2 & 4 \end{bmatrix} \begin{bmatrix} e_{11} \\ e_{21} \end{bmatrix} = \begin{bmatrix} 0 \\ 0 \end{bmatrix}$$

por lo que

$$e_{11} + 2e_{21} = 0$$

y

$$e_{21} = -\frac{1}{2} e_{11}$$

Imponiendo la condición

$$e_{11}^2 + e_{21}^2 = 1$$

se tiene

$$e_{11}^2 + \frac{1}{4} e_{11}^2 = 1 \Rightarrow e_{11} = \frac{2\sqrt{5}}{5} \Rightarrow e_{21} = -\frac{\sqrt{5}}{5}$$

Análogamente se obtiene

$$e_{12} = \frac{\sqrt{5}}{5}, \quad e_{22} = \frac{2\sqrt{5}}{5}$$

El problema de valores característicos reviste particular importancia en Mecánica. En efecto, la determinación de las frecuencias y los modos maturales de vibración de sistemas mecánicos (Ver, p. , ej. [6]). La determinación de tales modos y frecuencias para sistemas mecánicos de parámetros distribuidos, mediante el MEF conduce a un problema de valores característicos, como se verá posteriormente en este curso.

Formas cuadráticas

El escalar definido por la expresión

$$f = \underset{\sim}{u}^T \underset{\sim}{A}\, \underset{\sim}{u}$$

donde $\underset{\sim}{A}$ es una matriz de $n \times n$ y $\underset{\sim}{u}$, un vector de dimensión n, recibe el nombre de forma cuadrática. Esta forma es equivalente a la forma escalar au^2. De esta última expresión se puede concluir una propiedad interesante de la forma cuadrática f antes definida. Nótese que, si a y u son reales, au^2 es una expresión cuyo signo depende enteramente de a, y no de u. Análogamente, el signo de la forma cuadrática f depende enteramente de $\underset{\sim}{A}$ y no de $\underset{\sim}{u}$, si ambos tienen elementos reales (o bien, si, aunque $\underset{\sim}{A}$ tenga elementos complejos, es idéntica a la matriz obtenida de transponerla y luego tomar el conjugado de cada uno de sus elementos).

Se dice que $\underset{\sim}{A}$ es

- positiva definida, si $f > 0, \forall\ \underset{\sim}{u} \neq \underset{\sim}{0}$ (D 1)
- positiva semidefinida, si $f \geqslant 0, \forall\ \underset{\sim}{u} \neq \underset{\sim}{0}$ (D 2)
- negativa definida, si $f < 0, \forall\ \underset{\sim}{u} \neq \underset{\sim}{0}$ (D 3)
- negativa semidefinida, si $f \leqslant 0, \forall\ \underset{\sim}{u} \neq \underset{\sim}{0}$ (D 4)

De otra forma, $\underset{\sim}{A}$ es de signo indefinido. Las matrices positivas definidas y semidefinidas juegan un papel importante en la Mecánica, pues están asociadas o bien a cantidades intrínsecamente positivas, como la energía cinética de un vehículo en movimiento, o bien a cantidades intrínsecamente no negativas, como la energía potencial almacenada en la suspensión de un vehículo, medida desde su estado descargado.

Nótese que las definiciones (D 1) a (D 4) no proporcionan un medio práctico para determinar si una matriz es positiva definida, por ejemplo, pues según ellas, sería necesario probar el signo de f para todos y cada uno de los valores posibles de $\underset{\sim}{u} \neq \underset{\sim}{0}$. Sin embargo, la caracterización del signo de una matriz se puede conseguir a través de sus valores característicos, según lo siguiente :

Una matriz $\underset{\sim}{A}$ es

- positiva definida, si todos sus valores característicos son positivos,
- positiva semidefinida, si ninguno de sus valores característicos es negativo
- negativa definida, si todos sus valores característicos son negativos
- negativa semidefinida, si ninguno de sus valores característicos es positivo.

Derivadas de funciones de varias variables

Dada la función $g = g(u_1, u_2, \ldots, u_n)$, escrita en forma compacta como $g = g(\underset{\sim}{u})$, se dice que g es una función escalar de variable vectorial. El gradiente de g, representado por ∇g o por $\partial g/\partial \underset{\sim}{u}$, es el vector de dimensión n definido por

$$\nabla g = \frac{\partial g}{\partial \underset{\sim}{u}} = \begin{bmatrix} \partial g/\partial u_1 \\ \partial g/\partial u_2 \\ \vdots \\ \partial g/\partial u_n \end{bmatrix}$$

Sea el conjunto de funciones

$$h_1 = h_1(u_1, u_2, \ldots, u_n)$$
$$h_2 = h_2(u_1, u_2, \ldots, u_n)$$
$$\vdots$$
$$h_m = h_m(u_1, u_2, \ldots, u_n)$$

Este se representa en forma compacta como $\underset{\sim}{h} = \underset{\sim}{h}(\underset{\sim}{u})$, donde, obviamente, $\underset{\sim}{h}$ y $\underset{\sim}{u}$ son vectores de dimensiones m y n, respectivamente. Se dice, entonces, que $\underset{\sim}{h}$ es una función vectorial de argumento vectorial. El gradiente de $\underset{\sim}{h}$, representado por $\nabla \underset{\sim}{h}$ o $\partial \underset{\sim}{h}/\partial \underset{\sim}{u}$, es la matriz de m x n definida por

$$\nabla \underset{\sim}{h} = \frac{\partial \underset{\sim}{h}}{\partial \underset{\sim}{u}} = \begin{bmatrix} h_1/u_1 & h_1/u_2 & \cdots & h_1/u_n \\ h_2/u_1 & h_2/u_2 & \cdots & h_2/u_n \\ \vdots & \vdots & & \vdots \\ h_m/u_1 & h_m/u_2 & & h_m/u_n \end{bmatrix}$$

Si resulta que

$$\underset{\sim}{h} = \nabla g$$

entonces $\underset{\sim}{h}$ es de dimensión $m = n$, donde n es la dimensión de u. Entonces, $\nabla \underset{\sim}{h} = \nabla\nabla g$, es la matriz Hessiana de g y es de $n \times n$.

Volviendo a la función $g = g(\underset{\sim}{u})$, ésta alcanza un valor estacionario en un "punto" $\underset{\sim}{u}_0$ en el que su gradiente se anula. Este valor puede ser un extremo local o un punto silla. Es un extremo local si la matriz Hessiana de g, $\nabla\nabla g$, es de signo semidefinido. De hecho, es un máximo local si $\nabla\nabla g$ es negativa semidefinida, mientras que es un mínimo local si $\nabla\nabla g$ es positiva semidefinida. Si esa matriz Hessiana es de signo indefinido, el punto estacionario en cuestión es un punto silla. El resultado anterior no es más que el resultado ampliamente conocido del cálculo elemental, que se ilustra en la Fig 1.2.1

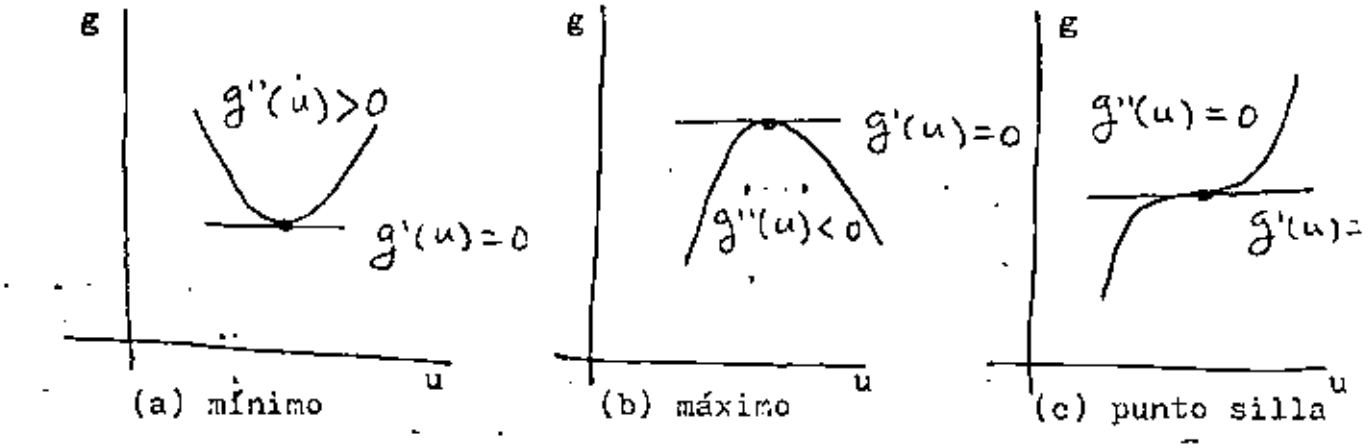

Fig 1.2.1 Puntos estacionarios de una función escalar de argumentos escalar.

1.3 METODOS NUMERICOS

A continuación se presenta un esbozo de los métodos numéricos aplicables al problema

$$\underset{\sim}{A}\,\underset{\sim}{u} = \underset{\sim}{b} \qquad (1.3.1)$$

donde $\underset{\sim}{A}$ es de n x n. Otro problema frecuente en cálculos de elemento finito es él de valores característicos

$$\underset{\sim}{A}\,\underset{\sim}{u} = \lambda\,\underset{\sim}{u} \qquad (1.3.2)$$

Sin embargo, dadas las limitaciones de tiempo de este curso, el segundo problema no será tratado.

Para resolver el problema (1.3.1) existen dos amplias clases de métodos :

- métodos directos
- métodos iterativos.

Estas dos clases de métodos resuelven el sistema (1.3.1), esto es, calculan el valor que deban tener todos los componentes de $\underset{\sim}{u}$, para valores dados de $\underset{\sim}{A}$ y de $\underset{\sim}{b}$, de manera tal que se satisfagan todas las ecuaciones del sistema (1.3.1). Los métodos directos resuelven el problema en cuestión mediante una secuencia de operaciones bien definidas que se aplican una sola vez. Los métodos iterativos resuelven este mismo problema aplicando un ciclo de operaciones reiteradamente, hasta aproximar la solución de manera satisfactoria. Cada ciclo recibe el nombre de iteración.

En este punto es necesario hacer la siguiente observación : en teoría es posible resolver el sistema 1.3.1 mediante un tercer método, llamado "regla de Cramer", en la forma

$$u_i = \frac{\det \underset{\sim}{A}_i}{\det \underset{\sim}{A}}, \quad i = 1, \ldots, n \qquad (1.3.3)$$

En la expresión anterior, $\underset{\sim}{A}_i$ es la matriz que se obtiene sustituyendo la $i^{\underline{a}}$ columna de $\underset{\sim}{A}$ por el vector $\underset{\sim}{b}$. Este método requiere, entonces, el cálculo de $n + 1$ determinantes. En seguida se determina el número de multiplicaciones requerido para calcular un determinante de $n \times n$ y, de ahí, el tiempo de ejecución requerido por la "regla de Cramer". En una computadora digital de alta velocidad una multiplicación consume un tiempo del orden de 10^{-4} segundos, mientras que una suma o una resta, un tiempo de un orden mucho menor; por esta razón, en lo que sigue se considera como "operación", una multiplicación, quedando las sumas y restas sin contabilizarse.

Existen varias formas de calcular un determinante. Aquí se empleará la conocida como <u>expansión por cofactores</u>. Dada una matriz $\underset{\sim}{A}$ de $n \times n$, cuyo elemento (i, j) se representa por a_{ij}, el <u>cofactor</u> de a_{ij} es el producto de $(-1)^{i+j}$ por el determinante de la matriz de $(n-1) \times (n-1)$, obtenida al eliminar de $\underset{\sim}{A}^T$ el $i^{\underline{o}}$ renglón y la $j^{\underline{a}}$ columna. Llámese c_{ij} al cofactor de a_{ij}. Se tiene, entonces,

$$\det \underset{\sim}{A} = a_{i1}c_{i1} + a_{i2}c_{i2} + \cdots + a_{in}c_{in} =$$
$$= a_{1j}c_{1j} + a_{2j}c_{2j} + \cdots + a_{2n}c_{2n}$$

El cálculo del determinante de una matriz de 2×2 se realiza, desde luego, sencillamente como

$$\det \begin{bmatrix} a_{11} & a_{12} \\ a_{21} & a_{22} \end{bmatrix} = a_{11}a_{22} - a_{12}a_{21}$$

que requiere 2 operaciones.

Ahora, para una matriz de 3×3, expandiendo su determinante por cofactores de su primer renglón, se tiene

$$\det \begin{bmatrix} a_{11} & a_{12} & a_{13} \\ a_{21} & a_{22} & a_{23} \\ a_{31} & a_{32} & a_{33} \end{bmatrix} = a_{11}c_{11} + a_{12}c_{12} + a_{13}c_{13}$$

que requiere 3 operaciones. Cada cofactor c_{ij}, que es un determinante de 2 x 2, requiere a su vez 2 operaciones, como se acaba de ver, por lo que el cálculo de este determinante requiere 3 x 2 operaciones. No es difícil demostrar, siguiendo este camino, que el cálculo de un determinante de n x n requiere n! operaciones. En suma, la solución del sistema (1.3.1) mediante la "regla de Cramer" requiere $n!(n+1) = (n+1)!$ operaciones. Suponiendo que el sistema en cuestión contuviera 25 ecuaciones con 25 incógnitas, su solución mediante este método requeriría 26! operaciones, que es un número muy grande, del orden de 10^{27}. Si cada operación requiere 10^{-4} segundos, el total de operaciones requiere, entonces, un tiempo de ejecución de 10^{23} segundos. Para tener una idea de la magnitud de este tiempo, baste decir que, si se admite que el universo tiene una vida de 10^{17} segundos [7], el tiempo requerido para resolver el sistema (1.3.1) con 25 incógnitas utilizando una computadora rápida, es ¡ un millón de veces la vida del universo! Sobra decir que, hasta el momento, ningún ser humano ha resuelto jamás un sistema lineal de 25 ecuaciones con 25 incógnitas utilizando la regla de Cramer. Sin embargo, tratándose de resolver problemas elásticos mediante el MEF, es común llegar a sistemas de ecuaciones de la forma (1.3.1) con mil incógnitas. En lo que sigue se presentan métodos numéricos prácticos utilizados en la solución de tales sistemas.

El método directo empleado actualmente para resolver sistemas como el (1.3.1) es el de eliminación de Gauss. Este método es equivalente al método llamado LU por los angloparlantes (L, de "lower", que quiere decir inferior ; U, de "upper", que quiere decir superior). Este método se ilustra con un ejemplo de 3 ecuaciones con 3 incógnitas

$$\begin{aligned} a_{11}u_1 + a_{12}u_2 + a_{13}u_3 &= b_1 \\ a_{21}u_1 + a_{22}u_2 + a_{23}u_3 &= b_2 \\ a_{31}u_1 + a_{32}u_2 + a_{33}u_3 &= b_3 \end{aligned} \qquad (1.3.4)$$

Divídace ambos miembros de la segunda ecuación entre a_{21} y multiplíqueseles por a_{11}. Procédase, en seguida, con la 3a. ecuación en forma semejante, excepto que, en vez de dividírseles entre a_{21}, divídaseles entre a_{31}. Se tiene, entonces

$$\begin{aligned} a_{11}u_1 + a_{11}\frac{a_{22}}{a_{21}}u_2 + a_{11}\frac{a_{23}}{a_{21}}u_3 &= a_{11}\frac{b_2}{a_{21}} \\ a_{11}u_1 + a_{11}\frac{a_{32}}{a_{31}}u_2 + a_{11}\frac{a_{33}}{a_{31}}u_3 &= a_{11}\frac{b_3}{a_{31}} \end{aligned} \qquad (1.3.5)$$

A continuación, réstese la la ecuación de (1.3.4) de cada una de las ecs (1.3.5). Se tiene

$$\begin{aligned} (a_{11}\frac{a_{22}}{a_{21}} - a_{12})u_2 + (a_{11}\frac{a_{23}}{a_{21}} - a_{13})u_3 &= a_{11}\frac{b_2}{a_{21}} - b_1 \\ (a_{11}\frac{a_{32}}{a_{31}} - a_{12})u_2 + (a_{11}\frac{a_{33}}{a_{31}} - a_{13})u_3 &= a_{11}\frac{b_3}{a_{31}} - b_2 \end{aligned}$$

Por sencillez, escríbase el sistema anterior en la forma

$$\begin{aligned} a'_{22}u_2 + a'_{23}u_3 &= b'_2 \\ a'_{32}u_2 + a'_{33}u_3 &= b'_3 \end{aligned} \qquad (1.3.6)$$

Ahora procédase como con el sistema (1.3.4), esto es, divídase la 2a. ecuación de (1.3.6) entre a'_{32} y multiplíquese por a'_{22}. Se tiene

$$a'_{22}u_2 + a'_{22}\frac{a'_{33}}{a'_{32}}u_3 = a'_{22}\frac{b'_3}{a'_{32}} \qquad (1.3.7)$$

Réstese a continuación la la. ecuación de (1.3.6) de la última ecuación, obteniéndose

$$(a'_{22}\frac{a'_{33}}{a'_{32}} - a'_{23})u_3 = a'_{22}\frac{b'_3}{a'_{32}} - b_2$$

que se puede escribir en forma simplificada como

$$a''_{33}u_3 = b''_3$$

de donde

$$u_3 = \frac{b''_3}{a''_{33}}$$

es el valor de la 3a. incógnita. La segunda se obtiene sustituyendo este valor en la ec (1.3.7), que contiene ahora una sola incógnita, u_2. Esta se obtiene despejándola en la forma

$$u_2 = \frac{1}{a'_{22}} \left(a'_{22} \frac{b'_3}{a'_{32}} - a'_{22} \frac{a'_{33}}{a'_{32}} u_3 \right)$$

Finalmente, sustitúyanse los valores obtenidos de u_2 y u_3 en la la ecuación de (1.3.4). Se obtiene u_1 como

$$u_1 = \frac{1}{a_{11}} (b_1 - a_{12}u_2 - a_{13}u_3)$$

quedando así totalmente resuelto el problema.

El esquema anterior es básicamente el método de eliminación de Gauss. Sin embargo, aplicado tal y como se presentó, puede causar dificultades si alguno de los dividendos es cero, o un número muy pequeño. Para eliminar esta posibilidad, se escogen como dividendos los números más grandes de cada columna de la matriz $\underset{\sim}{A}$, lo cual equivale a reordenarlas. Este proceso es conocido como pivoteo parcial, para distinguirlo del pivoteo total, que consiste en buscar el número más grande no sólo en cada columna, sino también en cada renglón. Si en el proceso resulta que el número más grande es cero, o un número tan pequeño que la máquina lo tome como cero, el método no se puede aplicar, lo cual indica no otra cosa sino que el sistema es singular, esto es, que $\det \underset{\sim}{A} = 0$. En este caso es imposible resolver el sistema, independientemente del método empleado.

Este método se realiza en computadora utilizando el concepto de descomposición LU, que se basa en el Teorema de Descomposición que establece que toda matriz $\underset{\sim}{A}$ de n x n se puede factorizar en el producto de una matriz triangular inferior $\underset{\sim}{L}$ y una triangular superior $\underset{\sim}{U}$. La matriz $\underset{\sim}{L}$ contiene unos en su diagonal y ceros arriba de ella, mientras que la $\underset{\sim}{U}$ contiene, en su diagonal los <u>valores singulares</u> de $\underset{\sim}{A}$, que son las raíces positivas de los valores característicos (positivos todos ellos) de la matriz $\underset{\sim}{A}\,\underset{\sim}{A}^T$ y ceros abajo de su diagonal. $\underset{\sim}{L}$ y $\underset{\sim}{U}$ son, entonces, matrices de la forma

$$L = \begin{bmatrix} 1 & & & & \\ l_{21} & 1 & & & \\ \cdot & \cdot & \cdot & & \\ \cdot & \cdot & & \cdot & \\ \cdot & \cdot & & & \cdot \\ l_{n1} & l_{n2} & \cdots & & 1 \end{bmatrix}, \quad U = \begin{bmatrix} 1 & u_{12} & \cdots & & u_{1n} \\ & 2 & & & 2n \\ & & \cdot & & \cdot \\ & & & \cdot & \cdot \\ & & & & n \end{bmatrix}$$

El Teorema de Descomposición en cuestión establece, entonces, que

$$\underset{\sim}{A} = \underset{\sim}{L}\,\underset{\sim}{U}$$

El sistema (1.3.1) de esta manera adopta la forma

$$\underset{\sim}{L}\,\underset{\sim}{U}\,\underset{\sim}{u} = \underset{\sim}{b} \qquad (1.3.8)$$

Llámese

$$\underset{\sim}{U}\,\underset{\sim}{u} = \underset{\sim}{v} \qquad (1.3.9)$$

Sustituyendo este valor en la ec (1.3.8) se tiene

$$\underset{\sim}{L}\,\underset{\sim}{v} = \underset{\sim}{b} \qquad (1.3.9)$$

que, en forma de componentes, adopta la forma

$$\begin{aligned} v_1 &= b_1 \\ l_{21}v_1 + v_2 &= b_2 \\ &\vdots \\ l_{n1}v_1 + l_{n2}v_2 + \ldots + v_n &= b_n \end{aligned} \qquad (1.3.10)$$

de donde la primera incógnita, v_1, ya está despejada en la primera ecuación. La segunda incógnita se despeja de la 2a.ecuación, en donde se ha sustituido previamente el valor calculado de v_1. Procediendo en forma semejante con el resto de las ecuaciones de (1.3.10) se obtienen todos los componentes del vector $\underset{\sim}{v}$ de (1.3.9). Sustituyendo ahora este vector, ya conocido, en la ec (1.3.9) se tiene el sistema

$$\begin{aligned} \sigma_1 u_1 + u_{12}u_2 + \ldots + u_{1n}u_n &= v_1 \\ \sigma_2 u_2 + \ldots \sigma u_{2n}u_n &= v_2 \\ &\vdots \\ \sigma_{n-1}u_{n-1} + u_{n-1,n}u_n &= v_{n-1} \\ \sigma_n u_n &= v_n \end{aligned} \qquad (1.3.11)$$

De la última ecuación de (1.3.11) se tiene

$$u_n = \frac{\sigma_n}{\sigma_n}$$

Sustituyendo este valor en la penúltima ecuación de (1.3.11) se tiene

$$u_{n-1} = \frac{1}{\sigma_{n-1}} (\sigma_{n-1} - u_{n-1,n}u_n)$$

Procediendo en este orden regresivo con las restantes n - 2 ecuaciones se calculan todos los componentes de $\underset{\sim}{u}$, con lo que queda resuelto el problema.

Este método ha sido realizado en diversos subprogramas de computadora. Los más eficientes son los llamados DECOMP y SOLVE [8]. DECOMP produce la descomposición LU de $\underset{\sim}{A}$, mientras que SOLVE, la solución regresiva de los sistemas triangulares (1.3.10) y (1.3.11).

Una ventaja de estos programas es que, una vez descompuesta la matriz $\underset{\sim}{A}$, se puede resolver una serie de sistemas de la forma

$$\underset{\sim}{A}\,\underset{\sim}{u}_1 = \underset{\sim}{b}_1,\ \underset{\sim}{A}\,\underset{\sim}{u}_2 = \underset{\sim}{b}_2,\ \ldots,\ \underset{\sim}{A}\,\underset{\sim}{u}_m = \underset{\sim}{b}_m \qquad (1.3.12)$$

sin tener que volver a descomponer $\underset{\sim}{A}$, cuya descomposición no depende del miembro derecho de las ecs (1.3.12). Todo lo que tiene que hacer es aplicar m veces la subrutina SOLVE, la que consume la menor part del tiempo total. La mayor parte del tiempo se utiliza en la descomposición de $\underset{\sim}{A}$. Este método requiere un número de operaciones del orden de n^3. Así, para resolver el sistema anteriormente presentado de 25 ecuaciones, con este método se requiere ejecutar $25^3 = 15\,625$ operaciones, lo cual consume en una computadora rápida algo así como 1.6 segundos, que es una cantidad sustancialmente por abajo de la anterior.

El problema de resolver m sistemas de ecuaciones de la forma (1.3.12) en relación con el MEF se presenta en aplicaciones de diseño se ingeniería cuando se desea conocer la distribución del esfuerzo en una misma estructura o en una misma máquina sujeta a diferentes condiciones de carga que se puedan presentar en operación.

Volviendo a las aplicaciones del MEF, la matriz $\underset{\sim}{A}$ viene a ser la matriz global de rigidez que, como ya se vio, tiene propiedades particulares como simetría y positividad definida. Para este tipo de

matrices, el método de Gauss, o LU, se simplifica sustencialmente. La versión simplificada recibe el nombre de método de Cholesky. Ya que la matriz de rigidez es positiva definida, se puede descomponer en la forma

$$\underset{\sim}{K} = \underset{\sim}{G}^T \underset{\sim}{G}$$

donde $\underset{\sim}{G}$ es una matriz triangular superior. Por otra parte, la estructura bandeada de esta matriz aporta ventajas adicionales que redundan en una solución más económica. En efecto, el tiempo de solución de una matriz bandeada de ancho de banda d, es del orden de $n^2 d$. Como normalmente el ancho de banda de una matriz es algunos órdenes de magnitud inferior a su número de renglones y columnas, esto es, $d << n$, la economía de ejecución es evidente. Así, por ejemplo, una matriz de rigidez típica de 5 000 x 5 000 puede tener un ancho de banda de 100. Si se utilizara el método de descomposición LU directamente, se realizarían algo así como 6.25×10^{11} operaciones, muchas de ellas inútiles, pues involucrarían multiplicaciones por cero. Explotando la naturaleza bandeada de la matriz, el número de operaciones requerido sería del orden de 2.5×10^8, es decir, 3 órdenes de magnitud inferior al anterior. Más aún, el orden de numeración de los nodos de una malla de elemento finito afecta enormemente el ancho de banda, d, de la matriz de rigidez. Existe, entonces, un orden de numeración (que no es único) óptimo que proporciona un ancho de banda mínimo. En el mercado se pueden obtener diferentes preprocesadoras que se encargan de proporcionar el ancho de banda mínimo, como el programa BAMIN, desarrollado en la Universidad de Manchester.

Por su parte, los métodos iterativos se basan en el esquema siguiente : descómpóngase la matriz $\underset{\sim}{A}$ en la forma

$$\underset{\sim}{A} = \underset{\sim}{D} - \underset{\sim}{E} - \underset{\sim}{F} \qquad (1.3.13)$$

donde $\underset{\sim}{D}$ es diagonal, mientras que $\underset{\sim}{E}$ y $\underset{\sim}{F}$ son matrices estrictamente triangular inferior y superior, respectivamente, esto es, tienen ceros

en su diagonal. De esta manera, el sistema (1.3.1) se puede escribir como

$$\underset{\sim}{D}\,\underset{\sim}{u} = (\underset{\sim}{E} + \underset{\sim}{F})\underset{\sim}{u} + b \qquad (1.3.14)$$

Dado un valor inicial arbitrario $\underset{\sim}{u}^0$, genérese la secuencia

$$\underset{\sim}{D}\,\underset{\sim}{u}^{k+1} = (\underset{\sim}{E} + \underset{\sim}{F})\underset{\sim}{u}^k + \underset{\sim}{b} \qquad (1.3.15)$$

o bien

$$\underset{\sim}{u}^{k+1} = \underset{\sim}{D}^{-1}(\underset{\sim}{E} + \underset{\sim}{F})\underset{\sim}{u}^k + \underset{\sim}{D}^{-1}\underset{\sim}{b} \qquad (1.3.16)$$

donde $\underset{\sim}{D}$ es invertible si $\underset{\sim}{A}$ lo es. El <u>esquema iterativo</u> (1.3.16) constituye el <u>método de Jacobi</u>, llamándose $\underset{\sim}{D}^{-1}(\underset{\sim}{E} + \underset{\sim}{F})$ matriz de Jacobi. Este esquema tiene la desventaja de que requiere almacenar el valor anterior de $\underset{\sim}{u}^k$ y el actual $\underset{\sim}{u}^{k+1}$. Lo lógico sería utiliza para el cálculo de la $i^{\underline{a}}$ componente de $\underset{\sim}{u}^{k+1}$, u_i^{k+1}, todos los valores actualizados de las componentes anteriores u_1^{k+1}, u_2^{k+1}, ..., u_{i-1}^{k+1}, destruyendo las componentes viejas u_1^k, u_2^k, ..., u_{i-1}^k. De esta suerte, el esquema iterativo (1.3.16) se sustituye por

$$\underset{\sim}{u}^{k+1} = (\underset{\sim}{D} - \underset{\sim}{E})^{-1}\,\underset{\sim}{F}\,\underset{\sim}{u}^k + (\underset{\sim}{D} - \underset{\sim}{E})^{-1}\,\underset{\sim}{b} \qquad (1.3.17)$$

El esquema iterativo (1.3.17) recibe el nombre de <u>método de Gauss-Seidel</u>, mientras que la matriz $(\underset{\sim}{D} - \underset{\sim}{E})^{-1}\,\underset{\sim}{F}$, el de <u>matriz de Gauss-Seidel</u>. Este método posee, además, la ventaja de que con él se aproxima la solución más rapidamente, esto es, <u>converge</u> más rápidamente a la solución. Escríbase los esquemas (1.3.16) y (1.3.17) en la forma

$$\underset{\sim}{u}^{k+1} = \underset{\sim}{J}\,\underset{\sim}{u}^k + \underset{\sim}{D}^{-1}\,\underset{\sim}{b} \qquad (1.3.18)$$

y

$$\underset{\sim}{u}^{k+1} = \underset{\sim}{G}\,\underset{\sim}{u}^k + (\underset{\sim}{D} - \underset{\sim}{E})^{-1}\,\underset{\sim}{b} \qquad (1.3.19)$$

Ahora se determina la evolución del error para cada esquema. Para el de Jacobi, si u^* es la solución, entonces satisface (1.3.18) con $\underset{\sim}{u}^{k+1} = \underset{\sim}{u}^{k} = \underset{\sim}{u}^*$, esto es

$$\underset{\sim}{u}^* = \underset{\sim}{J}\,\underset{\sim}{u}^* + \underset{\sim}{D}^{-1}\,\underset{\sim}{b} \qquad (1.3.20)$$

Llámese $\underset{\sim}{e}^k$ al error $\underset{\sim}{u}^k - \underset{\sim}{u}^*$ en la k a. iteración. Restando (1.3.20) de (1.3.18) se tiene

$$\underset{\sim}{e}^{k+1} = \underset{\sim}{J}\,\underset{\sim}{e}^k \qquad (1.3.21)$$

Del hecho que

$$\underset{\sim}{e}^1 = \underset{\sim}{J}\,\underset{\sim}{e}^0$$
$$\underset{\sim}{e}^2 = \underset{\sim}{J}\,\underset{\sim}{e}^1 = \underset{\sim}{J}^2\,\underset{\sim}{e}^0$$
$$\vdots$$
$$\text{etc.}$$

se concluye que **

$$\underset{\sim}{e}^k = \underset{\sim}{J}^k\,\underset{\sim}{e}^0 \qquad (1.3.22)$$

cuya evolución sólo depende de $\underset{\sim}{J}$. Se dice que $\underset{\sim}{J}$ es convergente si $\lim_{k \to \infty} \underset{\sim}{J}^k = \underset{\sim}{0}$. Así, para $\underset{\sim}{J}$ convergente, $\lim_{k \to \infty} \underset{\sim}{e}^k = \underset{\sim}{0}$. Se observa que $\underset{\sim}{J}$ es convergente cuando se va haciendo más y más pequeña a medida que se le eleva a potencias más altas. Así como un número real de valor absoluto menor que 1 se va haciendo cada vez más pequeño a medida que se le eleva a potencias más altas, una matriz es

---

** En e^k, k es superíndice, mientras que J^k, exponente.

convergente si los valores absolutos de todos sus valores característicos son estrictamente menores que 1. Al máximo valor absoluto de los valores característicos de una matriz A se le llama "radio espectral" y se representa por ρ. Así

$$\rho(\underset{\sim}{A}) = \max_i \{|\lambda_i|\} \tag{1.3.23}$$

Entonces, el esquema iterativo de Jacobi converge si

$$\rho(\underset{\sim}{J}) < 1 \tag{1.3.24}$$

Análogamente, el error del esquema iterativo de Gauss-Seidel (1.3.19) adopta la forma

$$\underset{\sim}{e}^{k+1} = \underset{\sim}{G}^k \underset{\sim}{e}^o \tag{1.3.25}$$

por lo que este esquema converge si

$$\rho(\underset{\sim}{G}) < 1 \tag{1.3.26}$$

Es claro que mientras menor sea el radio espectral de un esquema iterativo su rapidez de convergencia será mayor. Una forma de lograr un radio espectral menor es modificando el esquema iterativo de Gauss-Seidel, introduciendo un factor de sobrerrelajación, ω, mayor que 1. Se obtiene, entonces, el método iterativo de sobrerrelajación sucesiva, cuyo esquema es el siguiente :

$$(\underset{\sim}{D} - \omega\underset{\sim}{E})\underset{\sim}{u}^{k+1} = \left[(1-\omega)\underset{\sim}{D} + \omega\underset{\sim}{F}\right]\underset{\sim}{u}^k + \omega\underset{\sim}{b} \tag{1.3.27}$$

o bien

$$\underset{\sim}{u}^{k+1} = (\underset{\sim}{I} - \omega\underset{\sim}{L})^{-1}\left[(1-\omega)\underset{\sim}{I} + \omega\underset{\sim}{U}\right]\underset{\sim}{u}^k + \omega(\underset{\sim}{I} - \omega\underset{\sim}{L})^{-1}\underset{\sim}{D}^{-1}\underset{\sim}{b} \tag{1.3.28}$$

donde

$$\underset{\sim}{L} \equiv \underset{\sim}{D}^{-1}\,\underset{\sim}{E}, \quad \underset{\sim}{U} \equiv \underset{\sim}{D}^{-1}\,\underset{\sim}{F}$$

La rapidez de convergencia del esquema (1.3.28) depende, entonces sólo del factor de sobrerrelajaciónω. Para cada problema particular existe un valor óptimo de sobrerrelajación que maximiza esa rapidez. Sin embargo, no existe en general, un método para hallar ese factor y normalmente tiene que determinarse experimentando con varios valores.

En toda la discusión anterior se ha considerado que tanto $\underset{\sim}{A}$ como $\underset{\sim}{b}$ se conocen a la perfección. Sin embargo, en la práctica esto no sucede. En efecto, si $\underset{\sim}{A}$ o $\underset{\sim}{b}$ proceden de mediciones, éstas introducen siempre "ruido", esto es, imprecisiones debidas a la imposibilidad de calibrar perfectamente los instrumentos de medición, o bien a errores de apreciación de parte de quienes toman las lecturas. En cálculos relacionados con el MEF, tanto la matriz $\underset{\sim}{A}$ como el vector $\underset{\sim}{b}$ se calculan dentro de la máquina, lo cual introduce errores llamados "de redondeo", esto es, debidos a que cualquier computadora no dispone más que de un conjunto finito de números, que se llaman "de punto flotante". Operaciones entre números de punto flotante, en general, no producen otro número de punto flotante, por lo que el resultado deberá aproximarse a uno de los dos números de punto flotante más próximos al resultado real. Algunas máquinas aproximan por defecto y otras, por exceso ; pero no necesariamente al número de punto flotante más próximo. En seguida se presenta una discusión somera de los errores de redondeo presentes al resolver el problema (1.3.1).

Antes de continuar con la presente discusión se introduce el concepto de norma de vectores y de matrices.

La norma de un vector $\underset{\sim}{v}$ de dimensión n es una generalización del concepto de magnitud. En efecto, la magnitud de un vector da una idea sobre el tamaño de sus componentes considerados globalmente. Esta se define como

$$\| \underset{\sim}{v} \| = (v_1^2 + v_2^2 + \ldots + v_n^2)^{1/2} \qquad (1.3.29)$$

Se observa que esta magnitud nunca es negativa y se anula si, y sólo si $\underset{\sim}{v} = \underset{\sim}{0}$, esto es, si todos y cada uno de los números v_i se anulan. Por otro lado, si cada componente v_i se multiplica por el mismo escalar c, se tiene

$$\| c \underset{\sim}{v} \| = | c | \| \underset{\sim}{v} \| \qquad (1.3.30)$$

y, finalmente, para todo par de vectores $\underset{\sim}{v}$ y $\underset{\sim}{w}$,

$$\| \underset{\sim}{v} + \underset{\sim}{w} \| \leq \| \underset{\sim}{v} \| + \| \underset{\sim}{w} \| \qquad (1.3.31)$$

que no es otra cosa que una condición de existencia del triángulo de lados $\underset{\sim}{v}$, $\underset{\sim}{w}$ y $\underset{\sim}{v} + \underset{\sim}{w}$. Por esto, la última relación, (1.3.31), se llama "desigualdad del triángulo". Generalizando el concepto anterior se tendrá : una norma para un espacio vectorial es un número real que, si $\underset{\sim}{v}$, $\underset{\sim}{w}$ son vectores del espacio,

i) La norma es positiva definida, esto es

$$\| \underset{\sim}{v} \| > \underset{\sim}{0}$$

y se anula si y sólo si $\underset{\sim}{v}$ se anula igualmente.

ii) Es linealmente homogénea : esto es

$$\| c \underset{\sim}{v} \| = | c | \| \underset{\sim}{v} \|$$

iii) Satisface la desigualdad del triángulo, esto es

$$\| \underset{\sim}{v} + \underset{\sim}{w} \| = \| \underset{\sim}{v} \| + \| \underset{\sim}{w} \|$$

Nótese que en la definición anterior no se ha impuesto forma alguna para calcular la norma, como es el caso en la definición (1.3.29). Así, cualquier número real asociado a cada vector del espacio en consideración, que satisfaga las propiedades i) a iii) anteriores es una norma. Ejemplos de normas son los siguientes :

$$\| \underset{\sim}{v} \| = \max_i \{ | v_i | \} \qquad (1.3.32\ a)$$

$$\| \underset{\sim}{v} \| = \sum_i | v_i | \qquad (1.3.32\ b)$$

De éstas dos, la primera es la más fácil y económica de calcular y por eso se emplea mucho en análisis numérico para cálculo de errores.

Por otra parte, ya que la definición anterior de norma no se limita a vectores definidos como arreglos unidimensionales, se puede aplicar a matrices. Una norma de un espacio de matrices, entonces, es una medida del tamaño de las componentes de cada matriz del espacio, consideradas globalmente, de manera que mientras más pequeña sea la norma de una matriz, más próxima estará de la matriz nula. Ejemplos de normas de matrices son

$$\| \underset{\sim}{A} \| = \sqrt{\mathrm{Tr}\ \underset{\sim}{A}\ \underset{\sim}{A}^T} \qquad (1.3.33\ a)$$

$$\| \underset{\sim}{A} \| = \max_j \sum_i | a_{ij} | \qquad (1.3.33\ b)$$

$$\| \underset{\sim}{A} \| = \max_{i,j} | a_{ij} | \qquad (1.3.33\ c)$$

Un concepto primordial en el análisis de error de redondeo en cálculos con matrices es el de <u>condición</u> de una matriz. Dada una matriz $\underset{\sim}{A}$ de n x n, invertible, su condición se define como

$$\mathrm{cond}\ (\underset{\sim}{A}) = \| \underset{\sim}{A} \|\ \| \underset{\sim}{A}^{-1} \| \qquad (1.3.34)$$

Se observa de inmediato que la condición es un número adimensional y se demostrará que es una medida de la amplificación del error de redondeo. Así, un número de condición bajo está próximo a 1, aunque nunca es inferior a la unidad, mientras que uno alto puede ser del orden de 1 000 o mayor aún. Mientras más alta sea la condición de una matriz, más imprecisos serán los resultados de las operaciones en que interviene esta matriz.

Supóngase que se conoce $\underset{\sim}{A}$ a la perfección y pero que $\underset{\sim}{b}$ está contaminado con un error de redondeo $\delta \underset{\sim}{b}$. Así, la ec (1.3.1) es, en realidad

$$\underset{\sim}{A}(\underset{\sim}{u} + \delta \underset{\sim}{u}) = \underset{\sim}{b} + \delta \underset{\sim}{b} \qquad (1.3.35)$$

donde $\delta \underset{\sim}{u}$ es el error de redondeo producido por $\delta \underset{\sim}{b}$. Interesará calcular el error de redondeo en el cálculo de $\underset{\sim}{u}$, en términos del de $\underset{\sim}{b}$, esto es interesa calcular el cociente $\| \delta \underset{\sim}{u} \| / \| \underset{\sim}{u} \|$ en términos de $\| \delta \underset{\sim}{b} \| / \| \underset{\sim}{b} \|$. Ya que la ec (1.3.1) se satisface teóricamente, restándola de la ec (1.3.35) se tiene

$$\underset{\sim}{A} \quad \underset{\sim}{u} = \underset{\sim}{b}$$

o bien

$$\underset{\sim}{u} = \underset{\sim}{A}^{-1} \underset{\sim}{b} \qquad (1.3.36)$$

De una propiedad de las normas se tiene

$$\| \underset{\sim}{A}^{-1} \delta \underset{\sim}{b} \| \leq \| \underset{\sim}{A}^{-1} \| \| \delta \underset{\sim}{b} \| \qquad (1.3.37)$$

que aquí no se demostrará. Basta con decir que esta desigualdad está asociada al producto interno de vectores. En efecto, si $\underset{\sim}{v}$ y $\underset{\sim}{w}$ son dos vectores del mismo espacio (para el cual previamente se ha definido

un producto interno como $\underset{\sim}{v}\cdot\underset{\sim}{w} = v_1w_1 + v_2w_2 + \ldots + v_nw_n$),

$$|\underset{\sim}{v}\cdot\underset{\sim}{w}| = \|\underset{\sim}{v}\|\ \|\underset{\sim}{w}\|\ |\cos(\underset{\sim}{v}, \underset{\sim}{w})|$$

donde $\cos(\underset{\sim}{v}, \underset{\sim}{w})$ es el coseno del ángulo que forman los vectores $\underset{\sim}{v}$ y $\underset{\sim}{w}$. Del hecho de que $|\cos(\underset{\sim}{v}, \underset{\sim}{w})| \leq 1$, la igualdad anterior se tranforma en la desigualdad

$$\|\underset{\sim}{v}\cdot\underset{\sim}{w}\| \leq \|\underset{\sim}{v}\|\ \|\underset{\sim}{w}\|$$

que es una desigualdad conocida como de Schwarz.

Volviendo al sistema (1.3.1), ya que

$$\underset{\sim}{A}\ \underset{\sim}{u} = \underset{\sim}{b}$$

se tiene

$$\|\underset{\sim}{b}\| \leq \|\underset{\sim}{A}\|\ \|\underset{\sim}{u}\| \tag{1.3.38}$$

Aplicando la desigualdad (1.3.37) a la ec (1.3.36), se tiene

$$\|\delta\underset{\sim}{u}\| \leq \|\underset{\sim}{A}^{-1}\|\ \|\delta\underset{\sim}{b}\| \tag{1.3.39}$$

Multiplicando miembro a miembro las desigualdades (1.3.38) y (1.3.39), se tiene

$$\|\delta\underset{\sim}{u}\|\ \|\underset{\sim}{b}\| \leq \|\underset{\sim}{A}\|\ \|\underset{\sim}{A}^{-1}\|\ \|\underset{\sim}{u}\|\ \|\delta\underset{\sim}{b}\|$$

Si $\underset{\sim}{b} \neq \underset{\sim}{0}$, se pueden dividir ambos miembros de la última desigualdad entre $\|\underset{\sim}{u}\|\ \|\underset{\sim}{b}\|$, con lo que se obtiene

$$\frac{\|\delta\underset{\sim}{u}\|}{\|\underset{\sim}{u}\|} \leq \|\underset{\sim}{A}\|\ \|\underset{\sim}{A}^{-1}\| \frac{\|\delta\underset{\sim}{b}\|}{\|\delta\underset{\sim}{b}\|} = \text{cond}(\underset{\sim}{A})\ \frac{\|\delta\underset{\sim}{b}\|}{\|\underset{\sim}{b}\|} \tag{1.3.40}$$

con lo que se demuestra que la condición de una matriz es el facto de amplificación del error de redondeo.

Un resultado semejante se habría obtenido si se hubiera supuesto imprecisión en $\underset{\sim}{A}$, en lugar de $\underset{\sim}{b}$; pero en aras de la brevedad, este análisis ya no se continúa.

Por la importancia que tiene la condición de una matriz, la mayor parte de los programas de elemento finito proporcionan una estimación de este número, ya que un cálculo exacto sería demasiado costoso ; pero también, innecesario. En aplicaciones del MEF a problemas en medios elásticos planos se genera una malla de elementos. Si la malla es triangular, se tendrán elementos de las formas de la Fig 1.3.1

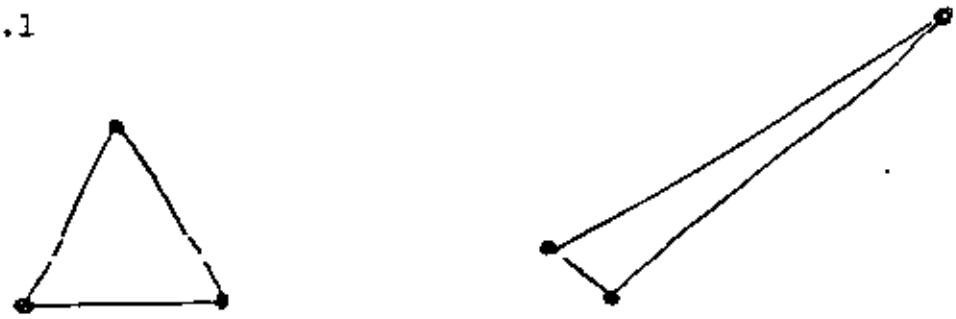

Fig 1.3.1 Elementos finitos

El elemento de la Fig 1.3.1 (a) es casi equilátero, mientras que él de la Fig 1.3.1 (b) es "muy escaleno", esto es, sus lados son de longitudes muy desiguales. Una malla con elementos equiláteros produce una matriz de rigidez de condición baja, mientras que una con elementos muy desbalanceados, como él de la Fig 1.3.1 (b), produce una matriz de rigidez de condición muy alta. Existen preprocesadores que balancean una malla desbalanceada.

Referencias :

1. Byars E.F. y Snyder R.D., Mecánica de Cuerpos Deformables, Tercera Edición, Representaciones y Servicios de Ingeniería, S.A., C. de México, 1978, pp. 274-284

2. Timoshenko S. y Woinowsky-Krieger S., Teoría de Placas y Láminas, Ediciones Urmo, Bilbao, 1970, p. 310

3. Byars E.F. y Snyder R.D., op. cit., pp. 73 y 74

4. Herstein I.N., Algebra Moderna, Editorial Trillas, C. de México, 1974, pp. 210-218

5. Mostow G.D. y Sampson J.H., Algebra Lineal, Mc Graw-Hill de México, S A de C V, 1972

6. Angeles J., "Modelo dinámico de una suspensión para vehículos de transporte masivo", INGENIERIA, Vol. L, No. 2, 1980, pp. 43-51

7. Gamow G., One, Two, Three ... Infinity, Bantam Books, Inc., Nueva York, 1967, p. 14

8. Forsythe G.E., Malcom M.A. y Moler C.B., Computer Methods for Mathematical Computations, Prentice-Hall, Inc., Englewood Cliffs, N.J., 1977

DIVISION DE EDUCACION CONTINUA
FACULTAD DE INGENIERIA U.N.A.M.

EL METODO DEL ELEMENTO FINITO EN LA INGENIERIA MECANICA

ECUACIONES DE EQUILIBRIO

DR. PORFIRIO BALLESTEROS BAROCIO

ABRIL, 1982

1 METODO DE LAS RIGIDECES PARA ANALIZAR ESTRUCTURAS ORTOGONALES PLANAS

1.1 Convención de signos.

La siguiente convención de signos será utilizada en el desarrollo del método de las rigideces y sus aplicaciones en marcos ortogonales planos.

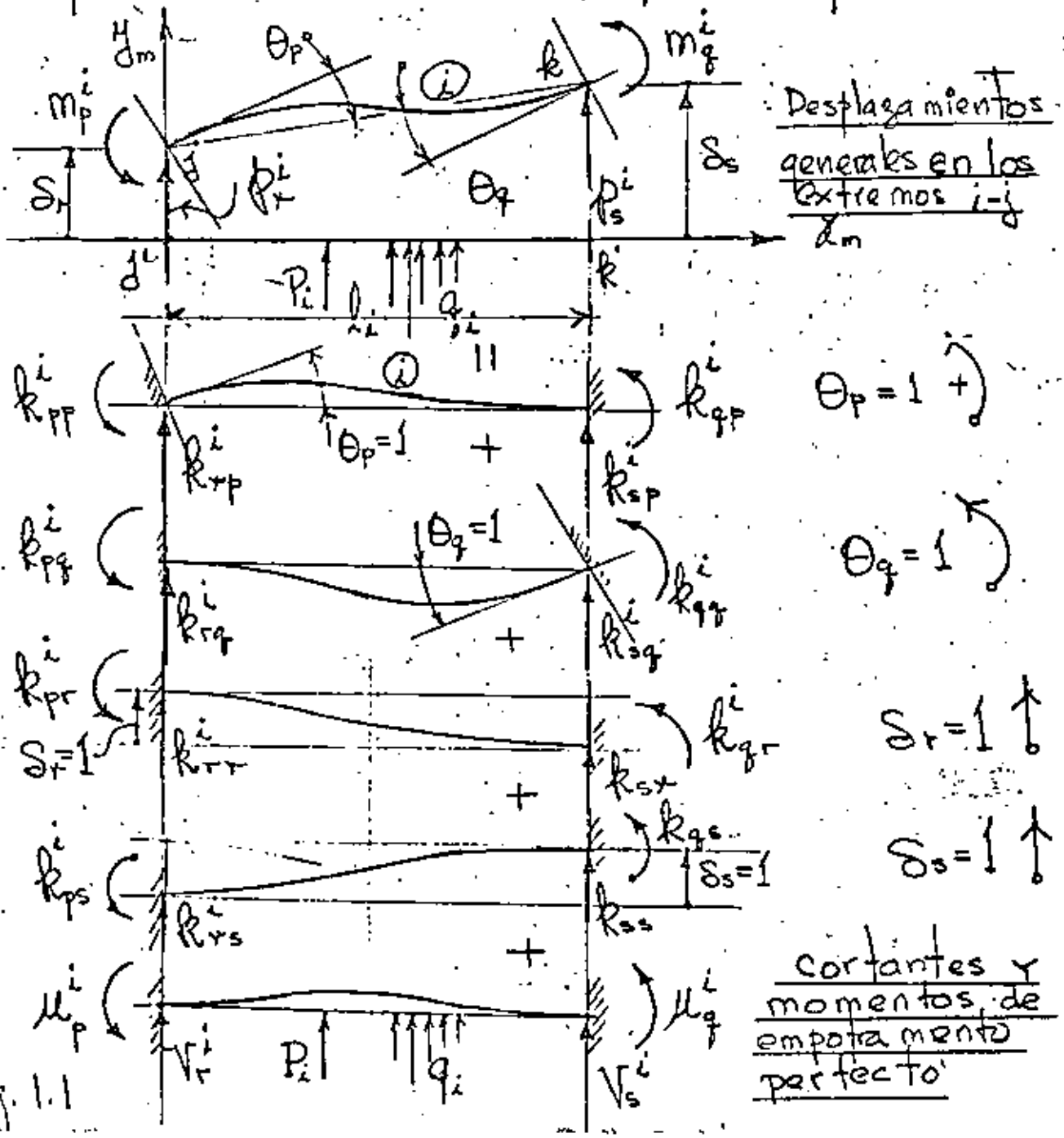

Fig. 1.1

De la Fig. 1.1 aceptando el principio de superposición se tiene:

$$\begin{aligned} m_p^i &= k_{pp}^i \theta_p + k_{pq}^i \theta_q + k_{pr}^i \delta_r + k_{ps}^i \delta_s + \mu_p^i \\ m_q^i &= k_{qp}^i \theta_p + k_{qq}^i \theta_q + k_{qr}^i \delta_r + k_{qs}^i \delta_s + \mu_q^i \\ p_r^i &= k_{rp}^i \theta_p + k_{rq}^i \theta_q + k_{rr}^i \delta_r + k_{rs}^i \delta_s + V_r^i \\ p_s^i &= k_{sp}^i \theta_p + k_{sq}^i \theta_q + k_{sr}^i \delta_r + k_{ss}^i \delta_s + V_s^i \end{aligned} \qquad (1.1)$$

en (1.1) se despreciа el efecto de la carga normal expresando (1.1) matricialmente se tiene

$$\{m\}_i = [k]_i \{\delta\}_i + \{\mu\}_i \qquad (1.2)$$

donde:

$$\{m\}_i = \begin{Bmatrix} m_p \\ m_q \\ p_r \\ p_s \end{Bmatrix}_i ; \quad \{\delta\}_i = \begin{Bmatrix} \theta_p \\ \theta_q \\ \delta_r \\ \delta_s \end{Bmatrix}_i ; \quad \{\mu\}_i = \begin{Bmatrix} \mu_r \\ \mu_q \\ V_r \\ V_s \end{Bmatrix}_i \qquad (1.3)$$

$\{m\}_i$; componentes de acciones sobre barra para mantener equil.

$\{\delta\}_i$; Desplazamientos en los extremos del miembro (i)

$\{\mu\}_i$; Momentos y cortantes de empotamiento perfecto en (i)

$[k]_i$; Matriz de rigidez del miembro (i)., la cual despreciando el efecto de cortante y carga normal, para un miembro de sección constante es:

$$[k]_i = \begin{bmatrix} \frac{4EI}{l} & \frac{2EI}{l} & \frac{6EI}{l^2} & -\frac{6EI}{l^2} \\ \frac{2EI}{l} & \frac{4EI}{l} & \frac{6EI}{l^2} & -\frac{6EI}{l^2} \\ \frac{6EI}{l^2} & \frac{6EI}{l^2} & \frac{12EI}{l^3} & -\frac{12EI}{l^3} \\ -\frac{6EI}{l^2} & -\frac{6EI}{l^2} & -\frac{12EI}{l^3} & -\frac{12EI}{l^3} \end{bmatrix} \begin{matrix} p \\ q \\ r \\ s \end{matrix} \qquad (1.4)$$

$\quad\quad p \quad\quad q \quad\quad r \quad\quad s$

La filosofía básica del método de las rigideces ha sido presentada, antes de aplicarlo a diversos sistemas estructurales su procedimiento conviene organizarlo en un programa sistemático y las ecuaciones básicas del análisis presentarlas en términos generales. Como ejemplo consideraremos el marco siguiente.

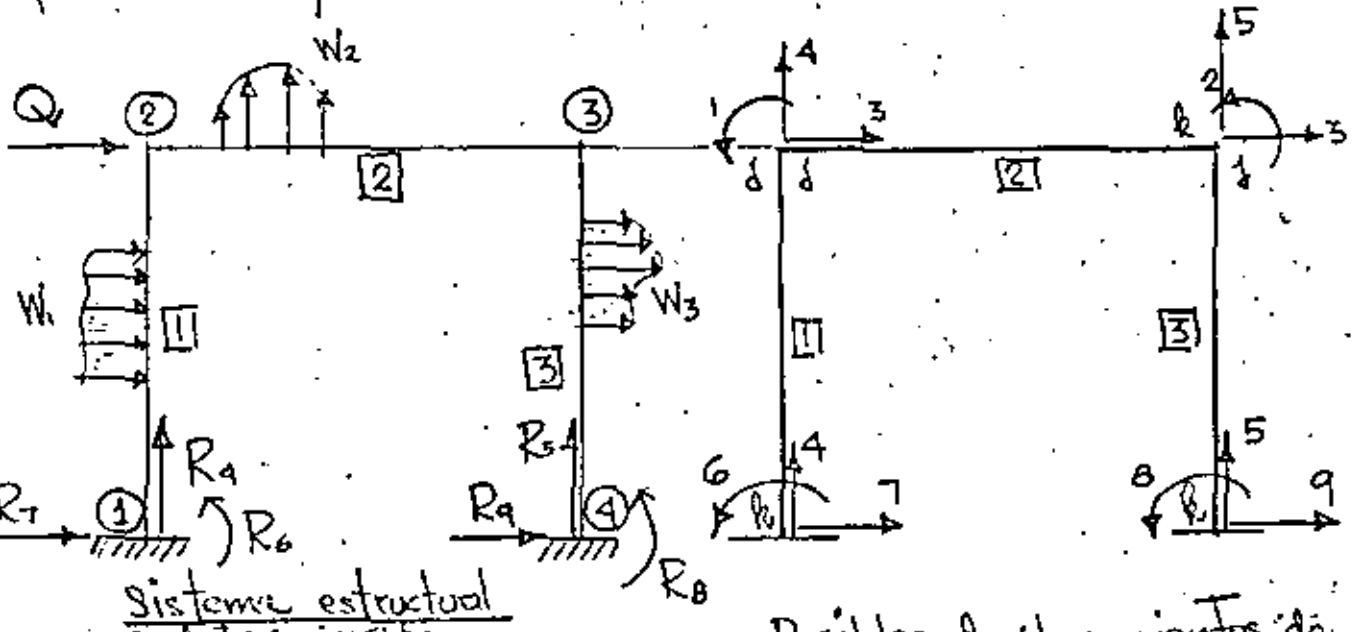

Fig. 1.2

El pórtico de la Fig. 1.2 es indeterminado de tercer grado con θ_1, θ_2 y δ_3, porque las condiciones de apoyo anulan a δ_4, δ_5, θ_6, δ_7, θ_8, δ_9. Como primera etapa consideramos la estructura con los nudos fijos determinando la suma de momentos y cortantes correspondientes S_{mo}.

Aplicando las ecuaciones (1.1) al marco de la Fig. 1.2

Miembro 1

$$\begin{cases} m_1' = k_{11}'\theta_1 + k_{16}'(0) + k_{13}'\delta_3 + k_{17}'(0) + \mu_1' \\ m_6' = k_{61}'\theta_1 + k_{66}'(0) + k_{63}'\delta_3 + k_{67}'(0) + \mu_6' \\ p_3' = k_{31}'\theta_1 + k_{36}'(0) + k_{33}'\delta_3 + k_{37}'(0) + V_3' \\ p_7' = k_{71}'\theta_1 + k_{76}'(0) + k_{73}'\delta_3 + k_{77}'(0) + V_7' \end{cases} \quad (1.5)$$

Miembro 2

$$\begin{cases} m_1^2 = k_{11}^2\theta_1 + k_{12}^2\theta_2 + k_{14}^2(0) + k_{15}^2(0) + \mu_1^2 \\ m_2^2 = k_{21}^2\theta_1 + k_{22}^2\theta_2 + k_{24}^2(0) + k_{25}^2(0) + \mu_2^2 \\ p_4^2 = k_{41}^2\theta_1 + k_{42}^2\theta_2 + k_{44}^2(0) + k_{45}^2(0) + V_4^2 \\ p_5^2 = k_{51}^2\theta_1 + k_{52}^2\theta_2 + k_{54}^2(0) + k_{55}^2(0) + V_5^2 \end{cases} \quad (1.6)$$

Miembro 3

$$\begin{cases} m_2^3 = k_{22}^3\theta_2 + k_{28}^3(0) + k_{23}^3\delta_3 + k_{29}^3(0) + \mu_2^3 \\ m_8^3 = k_{82}^3\theta_2 + k_{88}^3(0) + k_{83}^3\delta_3 + k_8^3(0) + \mu_8^3 \\ p_3^3 = k_{32}^3\theta_2 + k_{38}^3(0) + k_{33}^3\delta_3 + k_{39}^3(0) + V_3^3 \\ p_9^3 = k_{92}^3\theta_2 + k_{98}^3(0) + k_{93}^3\delta_3 + k_{99}^3(0) + V_9^3 \end{cases} \quad (1.7)$$

Como se demostró previamente el análisis de la estructura indeterminada de la Fig. 1.2 puede ser evaluado de

$$[S_{ij}]\{\delta_i\} = \{Q_i\} \qquad (1.8)$$

en el caso de la Fig 1.2, (1.8) es igual a

$$\begin{bmatrix} S_{11} & S_{12} & S_{13} \\ S_{21} & S_{22} & S_{23} \\ S_{31} & S_{41} & S_{51} \end{bmatrix} \begin{Bmatrix} \theta_1 \\ \theta_2 \\ \delta_3 \end{Bmatrix} = \begin{Bmatrix} M'_{21} + M^2_{23} \\ M^2_{32} + M^3_{34} \\ V'_{21} + V^3_{24} - Q \end{Bmatrix} \qquad (1.9)$$

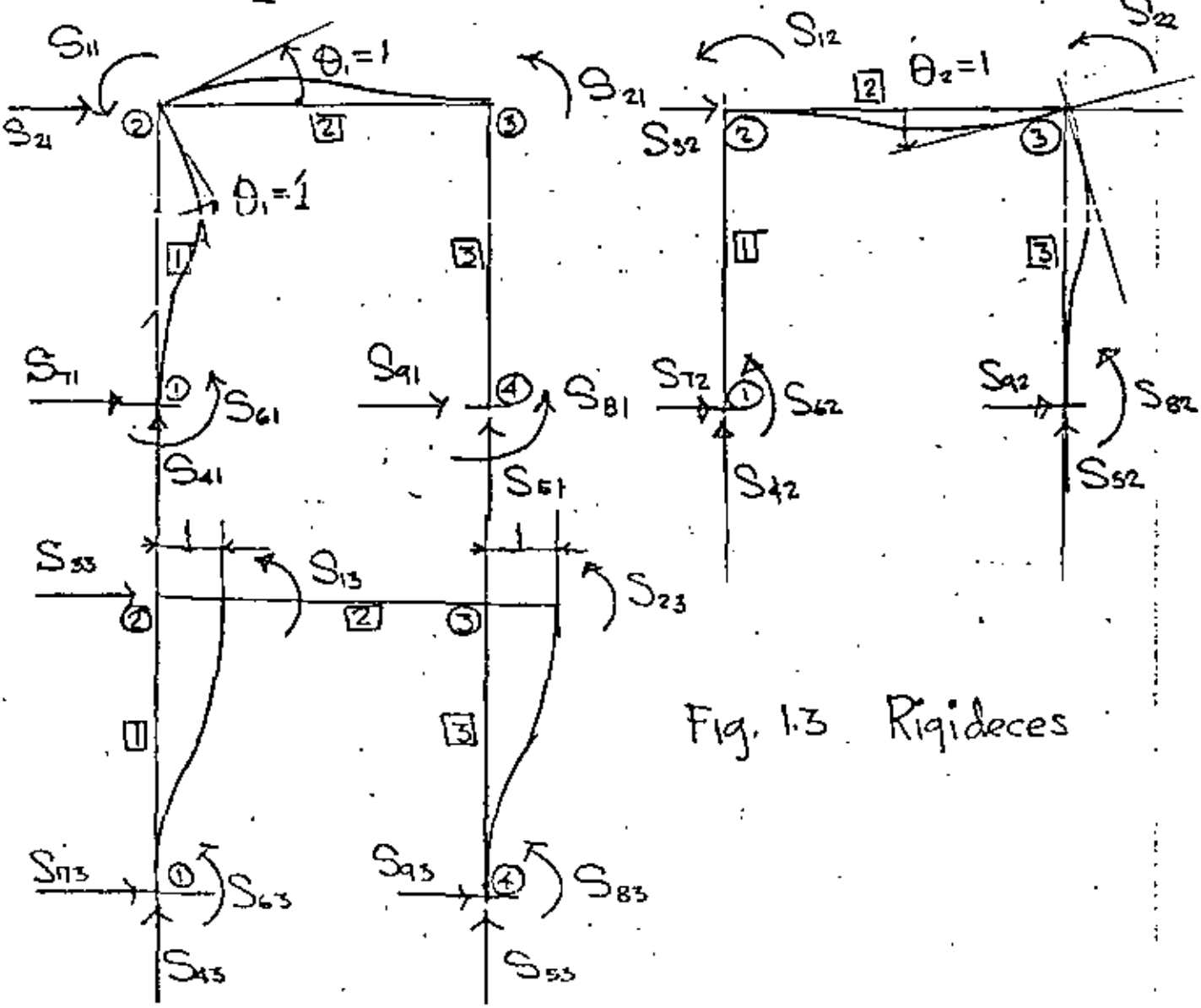

Fig. 1.3 Rigideces

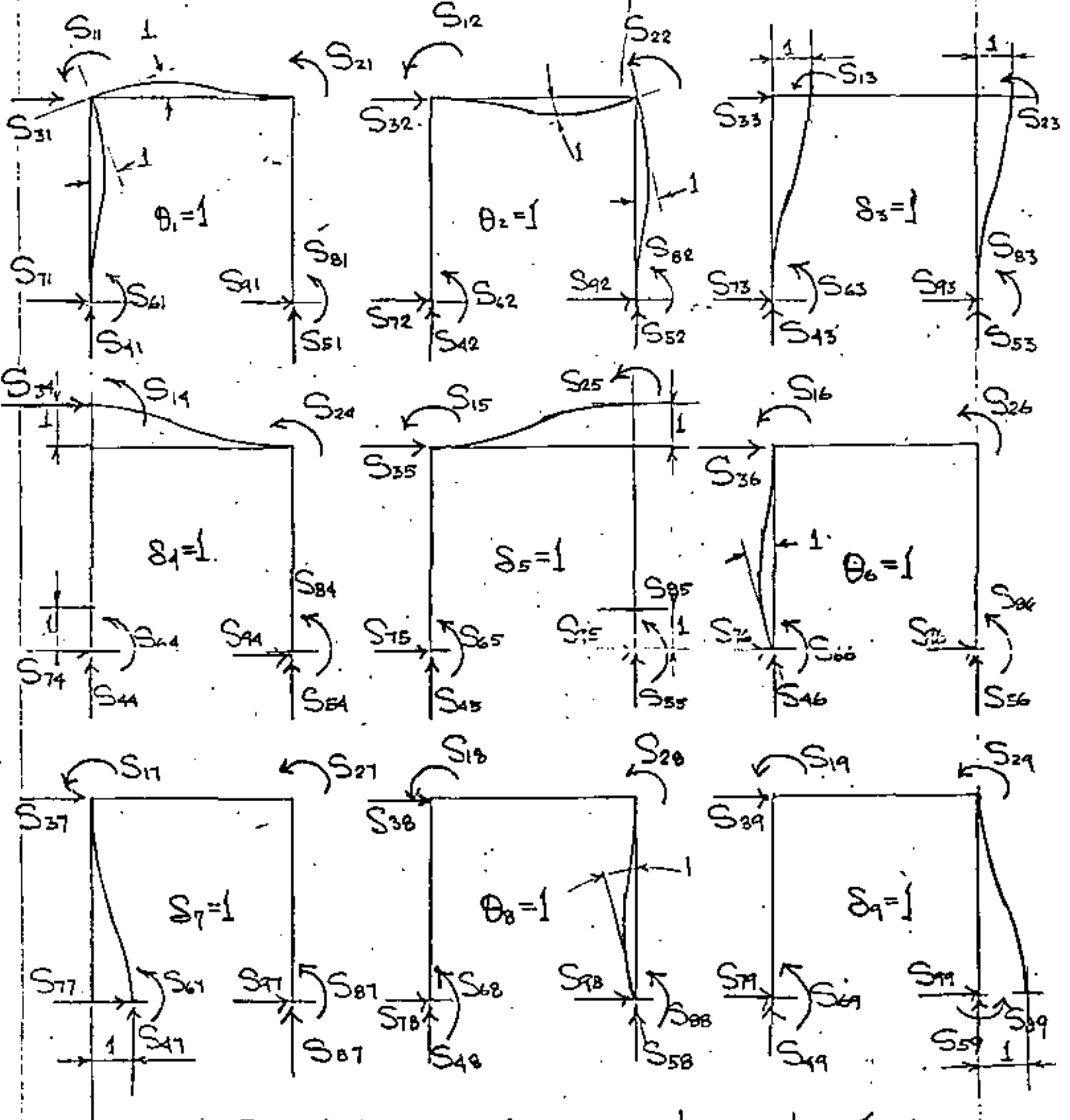

Fig. 1.4 Rigideces considerando todos los posibles grados de libertad despreciando deformaciones axiales (se suponen direcciones positivas)

De la Fig. 1.4 el desarrollo completo de las ecuaciones de superposición incluyendo reacciones es

$$S_{11}\theta_1 + S_{12}\theta_2 + S_{13}\delta_3 + S_{14}\delta_4 + S_{15}\delta_5 + S_{16}\theta_6 + S_{17}\delta_7 + S_{18}\theta_8 + S_{19}\delta_9 + \mu'_{21} + \mu^2_{23} = 0$$

$$S_{21}\theta_1 + S_{22}\theta_2 + S_{23}\delta_3 + S_{24}\delta_4 + S_{25}\delta_5 + S_{26}\theta_6 + S_{27}\delta_7 + S_{28}\theta_8 + S_{29}\delta_9 + \mu^2_{32} + \mu^3_{24} = 0$$

$$S_{31}\theta_1 + S_{32}\theta_2 + S_{33}\delta_3 + S_{34}\delta_4 + S_{35}\delta_5 + S_{36}\theta_6 + S_{37}\delta_7 + S_{38}\theta_8 + S_{39}\delta_9 + V'_{21} + V^3_{21} = Q$$

$$S_{41}\theta_1 + S_{42}\theta_2 + S_{43}\delta_3 + S_{44}\delta_4 + S_{45}\delta_5 + S_{46}\theta_6 + S_{47}\delta_7 + S_{48}\theta_8 + S_{49}\delta_9 + V^2_{23} = R_4 \qquad (1.10)$$

$$S_{51}\theta_1 + S_{52}\theta_2 + S_{53}\delta_3 + S_{54}\delta_4 + S_{55}\delta_5 + S_{56}\theta_6 + S_{57}\delta_7 + S_{58}\theta_8 + S_{59}\delta_9 + V^2_{32} = R_5$$

$$S_{61}\theta_1 + S_{62}\theta_2 + S_{63}\delta_3 + S_{64}\delta_4 + S_{65}\delta_5 + S_{66}\theta_6 + S_{67}\delta_7 + S_{68}\theta_8 + S_{69}\delta_9 + \mu'_{12} = R_6$$

$$S_{71}\theta_1 + S_{72}\theta_2 + S_{73}\delta_3 + S_{74}\delta_4 + S_{75}\delta_5 + S_{76}\theta_6 + S_{77}\delta_7 + S_{78}\theta_8 + S_{79}\delta_9 + V'_{12} = R_7$$

$$S_{81}\theta_1 + S_{82}\theta_2 + S_{83}\delta_3 + S_{84}\delta_4 + S_{85}\delta_5 + S_{86}\theta_6 + S_{87}\delta_7 + S_{88}\theta_8 + S_{89}\delta_9 + \mu^3_{43} = R_8$$

$$S_{91}\theta_1 + S_{92}\theta_2 + S_{93}\delta_3 + S_{94}\delta_4 + S_{95}\delta_5 + S_{96}\theta_6 + S_{97}\delta_7 + S_{98}\theta_8 + S_{99}\delta_9 + V^3_{43} = R_9$$

expresando (1.10) matricialmente se obtiene:

$$\begin{bmatrix} S_{11} & S_{12} & S_{13} & S_{14} & S_{15} & S_{16} & S_{17} & S_{18} & S_{19} \\ S_{21} & S_{22} & S_{23} & S_{24} & S_{25} & S_{26} & S_{27} & S_{28} & S_{29} \\ S_{31} & S_{32} & S_{33} & S_{34} & S_{35} & S_{36} & S_{37} & S_{38} & S_{39} \\ S_{41} & S_{42} & S_{43} & S_{44} & S_{45} & S_{46} & S_{47} & S_{48} & S_{49} \\ S_{51} & S_{52} & S_{53} & S_{54} & S_{55} & S_{56} & S_{57} & S_{58} & S_{59} \\ S_{61} & S_{62} & S_{63} & S_{64} & S_{65} & S_{66} & S_{67} & S_{68} & S_{69} \\ S_{71} & S_{72} & S_{73} & S_{74} & S_{75} & S_{76} & S_{77} & S_{78} & S_{79} \\ S_{81} & S_{82} & S_{83} & S_{84} & S_{85} & S_{86} & S_{87} & S_{88} & S_{89} \\ S_{91} & S_{92} & S_{93} & S_{94} & S_{95} & S_{96} & S_{97} & S_{98} & S_{99} \end{bmatrix} \begin{Bmatrix} \theta_1 \\ \theta_2 \\ \delta_3 \\ \delta_4 \\ \delta_5 \\ \delta_6 \\ \delta_7 \\ \delta_8 \\ \delta_9 \end{Bmatrix} + \begin{Bmatrix} \mu_{21}^1 + \mu_{23}^2 \\ \mu_{32}^2 + \mu_{34}^3 \\ V_{21}^1 + V_{21}^3 \\ V_{23}^2 \\ V_{32}^2 \\ \mu_{12}^1 \\ V_{12}^1 \\ \mu_{43}^3 \\ V_{43}^3 \end{Bmatrix} = \begin{Bmatrix} 0 \\ 0 \\ Q \\ R_4 \\ R_5 \\ R_6 \\ R_7 \\ R_8 \\ R_9 \end{Bmatrix} \quad (1.11)$$

$[S_{kl}]$ $\{\delta\}$ $\{\mu\}$ $\{R\}$

Expresando (1.11) matricialmente con la notación indicada

$$[S_{kl}]\{\delta_i\} + \{\mu\}_k = \{R\} \quad (1.12)$$

El analisis por el método de las rigideces se reduce a evaluar de (1.8) $\{\delta_i\}$ o sea

$$\{\delta_i\} = [S_{ij}]^{-1}\{Q_i\} \quad (1.13)$$

y substituyendo (1.13) en (1.2) se obtiene para cada barra

$$\{m_i\} = [k]_i [S_{ij}]^{-1}\{Q_i\} + \{\mu\}_i \quad (1.14)$$

y las reacciones se obtienen substituyendo (1.13) en (1.12)

$$\{R\} = [S_{kl}][S_{ij}]^{-1}\{Q_i\} + \{\mu\}_k \quad (1.15)$$

2 METODO DE LAS RIGIDECES DE ANALISIS DE ESTRUCTURAS TRIDIMENCIONALES

2.1 ELEMENTO VIGA

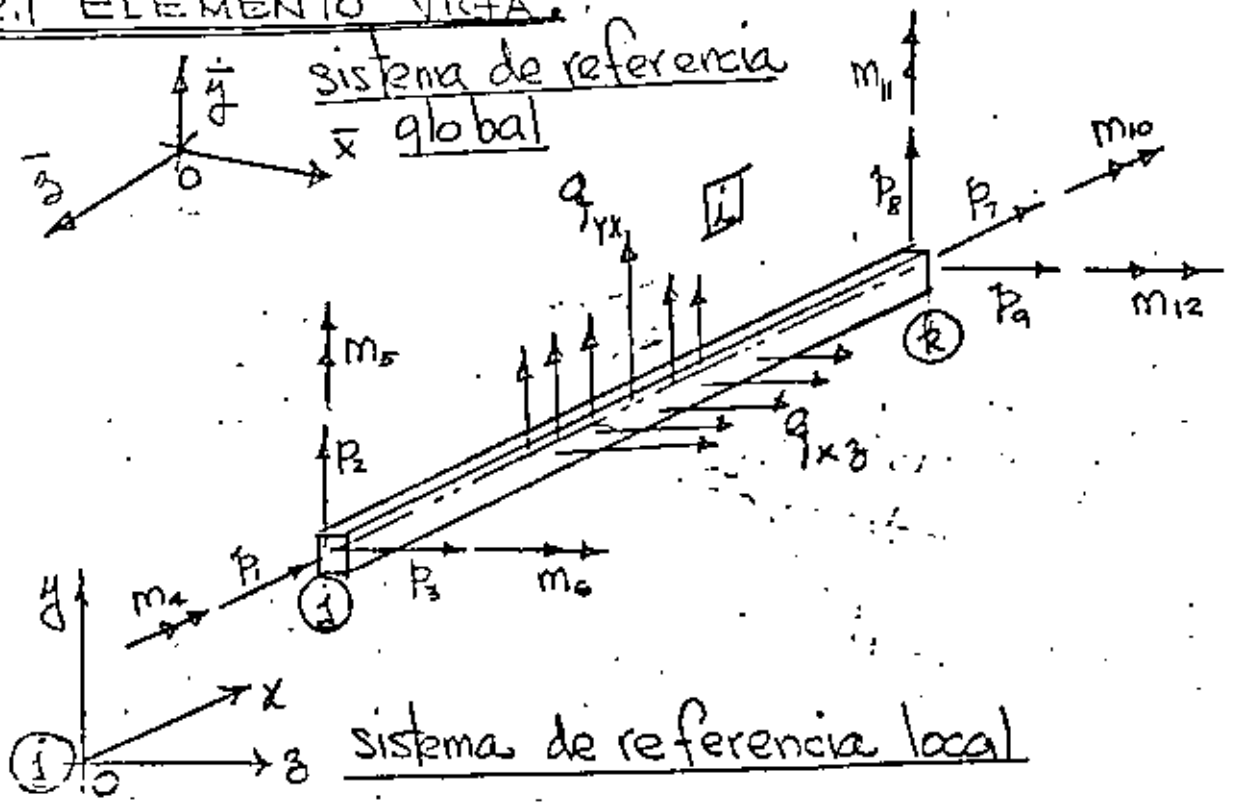

Fig. 2.1 Elemento viga; ejes y, z son centroidales y principales ($Q_y = Q_z = I_{yz} = 0$)

El elemento estructual j-k, se supone una barra capaz de resistir fuerzas axiales, momentos flectores respecto a dos ejes principales en el plano de la sección transversal, y momentos de torsión respecto a su eje centroidal. Las siguientes fuerzas actuan en la viga j k: Fuerzas axiales P_1 y P_7; Fuerzas cortantes P_2, P_3, P_8 y P_9; Momentos flectores m_5, m_6, m_{11} y m_{12}; y Momentos de torsión m_4 y m_{10}. la localización y dirección positiva se muestra en Fig. 2.1

Los desplazamientos correspondientes serán $u_1, u_2, u_3, \ldots, u_{12}$ serán positivos en la dirección positiva de las fuerzas. La posisión del elemento viga j k será especificado por las coordenadas del extremo j y los cosenos directores del eje x (dirección j k) y del eje y con respecto al sistema global $(\bar{x}, \bar{y}, \bar{z})$.

La matriz de rigidez del elemento viga será de 12×12 pero siempre es posible integrarla con submatrices de 2×2 y 4×4. De la teoría de flexión y torsión de vigas las fuerzas p_1 y p_7 dependen solo de sus desplazamientos correspondientes; lo mismo es cierto para los momentos torsionantes m_4 y m_{10}. Sinembargo, para una selección arbitraria de los planos de flexión, los momentos flectores y fuerzas de corte en el plano xy dependerán no solo de sus desplazamiento correspondientes pero también en los desplazamiento correspondientes a las fuerzas en los planos xy. Solamente si los xy y xz coinciden con los ejes principales de la sección transversal puede considerarse la flexion y corte sobre dichos planos independiente una de la otra.

$$\begin{Bmatrix} P_1 \\ P_2 \\ P_3 \\ m_4 \\ m_5 \\ m_6 \\ P_7 \\ P_8 \\ P_9 \\ m_{10} \\ m_{11} \\ m_{12} \end{Bmatrix}_i = \begin{bmatrix} k_{11} & k_{12} & k_{13} & k_{14} & k_{15} & k_{16} & k_{17} & k_{18} & k_{19} & k_{1,10} & k_{1,11} & k_{1,12} \\ k_{21} & k_{22} & k_{23} & k_{24} & k_{25} & k_{26} & k_{27} & k_{28} & k_{19} & k_{2,10} & k_{2,11} & k_{2,12} \\ k_{31} & \cdot & k_{33} & \cdot & \cdot & \cdot & \cdot & \cdot & \cdot & \cdot & \cdot & k_{3,12} \\ k_{41} & \cdot & \cdot & k_{44} & \cdot & \cdot & \cdot & \cdot & \cdot & \cdot & \cdot & k_{4,12} \\ k_{51} & \cdot & \cdot & \cdot & k_{55} & \cdot & \cdot & \cdot & \cdot & \cdot & \cdot & k_{5,12} \\ k_{61} & \cdot & \cdot & \cdot & \cdot & k_{66} & \cdot & \cdot & \cdot & \cdot & \cdot & k_{6,12} \\ k_{71} & \cdot & \cdot & \cdot & \cdot & \cdot & k_{77} & \cdot & \cdot & \cdot & \cdot & k_{7,12} \\ k_{81} & \cdot & \cdot & \cdot & \cdot & \cdot & \cdot & k_{88} & \cdot & \cdot & \cdot & k_{8,12} \\ k_{91} & \cdot & \cdot & \cdot & \cdot & \cdot & \cdot & \cdot & k_{99} & \cdot & \cdot & k_{9,12} \\ k_{10,1} & \cdot & \cdot & \cdot & \cdot & \cdot & \cdot & \cdot & \cdot & k_{10,10} & \cdot & k_{10,12} \\ k_{11,1} & \cdot & \cdot & \cdot & \cdot & \cdot & \cdot & \cdot & \cdot & \cdot & k_{11,11} & k_{11,12} \\ k_{12,1} & \cdot & \cdot & \cdot & \cdot & \cdot & \cdot & \cdot & \cdot & \cdot & \cdot & k_{12,12} \end{bmatrix} \begin{Bmatrix} \delta_1 \\ \delta_2 \\ \delta_3 \\ \theta_4 \\ \theta_5 \\ \theta_6 \\ \delta_7 \\ \delta_8 \\ \delta_9 \\ \theta_{10} \\ \theta_{11} \\ \theta_{12} \end{Bmatrix}_i + \begin{Bmatrix} P_1 \\ P_2 \\ P_3 \\ \mu_4 \\ \mu_5 \\ \mu_6 \\ P_7 \\ P_8 \\ P_9 \\ \mu_{10} \\ \mu_{11} \\ \mu_{12} \end{Bmatrix}_i \qquad (2.1)$$

(Simétrica)

$\{p\}_i$ $\quad [k_{ij}] \quad$ $\{\delta\}_i$ $\quad \{\mu\}_i$

Donde:

$\{p\}$; vector de cargas actuando sobre j k

$[k_{ij}]$; matriz de rigidez de la barra j k

$\{s\}$; vector de desplazamientos nodales

$\{\mu\}$; vector de reacciones de empotramiento perfecto

2.2 Elementos de la matriz de rigidez $[k_{ij}]$.

En el calculo de las rigideces k_{ij} se utiligan los principios energéticos expuestos considerándose la energía elástica de deformación por flexión corte y carga normal.

2.2.1 Fuerzas axiales P_1 y P_7.

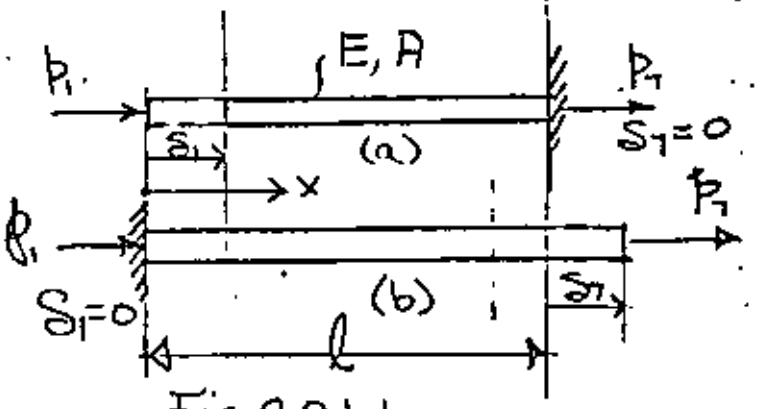

Fig. 2.2.1.1

De la ley de Hooke y la Fig. 2.2.1.2 se obtiene

$$k_{11} = \frac{P_1}{S_1} = \frac{EA}{l} \quad ; \quad k_{71} = -\frac{EA}{l} \qquad (a)$$

$$k_{77} = \frac{P_7}{S_7} = \frac{EA}{l} \quad ; \quad k_{17} = -\frac{EA}{l} \qquad (b)$$

2.2.2 Momentos de torsión m_4 y m_{10}.

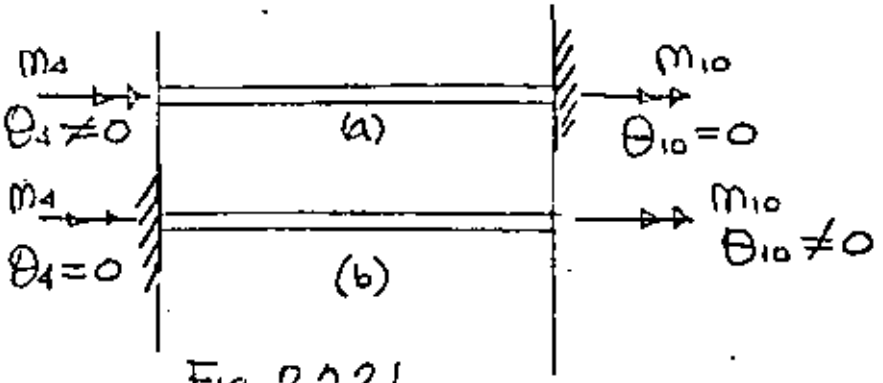

Fig. 2.2.2.1

De la teoría de torsión de barras y la fig. 2.2.2.1 se obtiene

$$k_{4,4} = \frac{m_4}{\theta_4} = \frac{GJ}{\ell} \quad ; \quad k_{10,4} = -\frac{GJ}{\ell} \qquad (a)$$

$$k_{10,10} = \frac{m_{10}}{\theta_{10}} = \frac{GJ}{\ell} \quad ; \quad k_{4,10} = -\frac{GJ}{\ell} \qquad (b)$$

2.2.3 Fuerzas de corte P_2 y P_8.

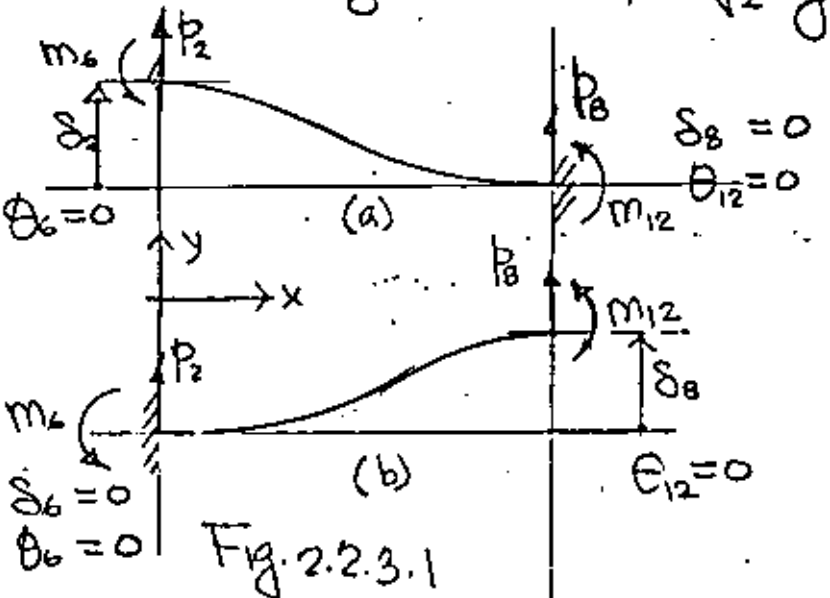

Fig. 2.2.3.1

De la Fig. 2.2.3.1 y los principios energéticos previamente expuestos, conidetando la energía de deformación por flexión y cortante se obtiene.

$$k_{22} = \frac{P_2}{\delta_2} = \frac{12EI_z}{(1+\Phi_Y)l^3} \quad a$$

$$k_{62} = \frac{m_6}{\delta_2} = \frac{6EI_z}{(1+\Phi_Y)l^2} \quad ; \quad k_{26} = \frac{P_2}{\theta_6} = \frac{6EI_z}{(1+\Phi_Y)l^2} \quad b$$

$$k_{82} = \frac{P_8}{\delta_2} = \frac{-12EI_z}{(1+\Phi_Y)l^3} \quad ; \quad k_{28} = \frac{P_2}{\delta_8} = \frac{-12EI_z}{(1+\Phi_Y)l^3} \quad c$$

$$k_{12,2} = \frac{m_{12}}{\delta_2} = \frac{6EI_z}{(1+\Phi_Y)l^2} \quad ; \quad k_{2,12} = \frac{P_2}{\theta_{12}} = \frac{6EI_z}{(1+\Phi_Y)l^2} \quad d$$

$$k_{88} = \frac{P_8}{\delta_8} = \frac{P_2}{\delta_2} = \frac{12EI_z}{(1+\Phi_Y)l^3} \quad (\text{si } EI \text{ es constante}) \quad e$$

$$k_{12,8} = \frac{m_{12}}{\delta_8} = \frac{-6EI_z}{(1+\Phi_Y)l^2} = -\frac{P_2}{\theta_6} = -k_{62} \quad (f)$$

$$k_{8,12} = \frac{P_8}{\theta_{12}} = \frac{-6EI}{(1+\Phi_Y)l^2} \quad (g)$$

2.2.4 Momentos Flectores

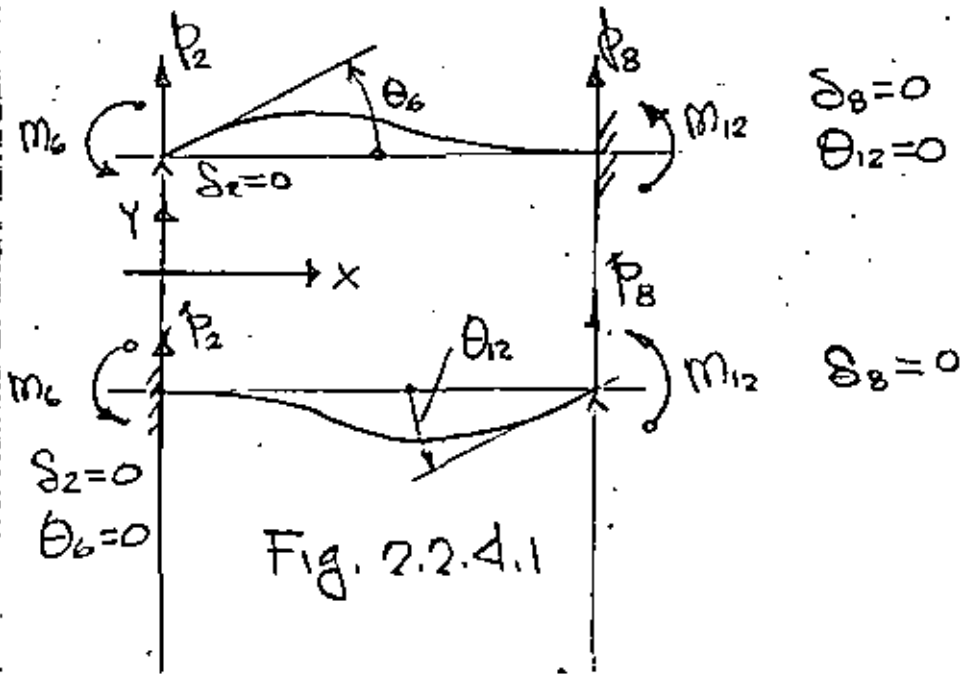

Fig. 2.2.4.1

De la Fig. 2.2.4.1 y los principios energéticos previamente expuestos, considerando la energía de deformación por flexión y corte se obtiene

$$k_{66} = \frac{m_6}{\theta_6} = \frac{(4+\phi_y) EI_3}{(1+\phi_y) l} \quad a$$

$$k_{86} = \frac{p_8}{\theta_6} = -\frac{6EI_3}{(1+\phi_y) l^2} \; ; \; k_{68} = \frac{m_6}{\delta_8} = -\frac{6EI_3}{(1+\phi_y) l^2} \quad b$$

$$k_{12,6} = \frac{m_{12}}{\theta_6} = \frac{(2-\phi_y) EI_3}{(1+\phi_y) l} \; ; \; k_{6,12} = \frac{m_6}{\theta_{12}} = \frac{(2-\phi_y) EI_3}{(1+\phi_y) l} \quad c$$

$$k_{12,12} = \frac{m_{12}}{\theta_{12}} = \frac{(4+\phi_y) EI_3}{(1+\phi_y) l} \quad d$$

$$k_{8,12} = \frac{p_8}{\theta_{12}} = -\frac{6EI_3}{(1+\phi_y) l^2} \; ; \; k_{12,8} = \frac{m_{12}}{\delta_8} = k_{8,12} \quad e$$

$$k_{6,12} = \frac{m_6}{\theta_{12}} = \frac{(2-\phi_y) EI_3}{(1+\phi_y) l} \; ; \; k_{12,6} = \frac{m_{12}}{\theta_6} = k_{6,12} \quad f$$

2.2.5 Fuerzas de corte p_3 y p_9.

Los coeficientes de rigidez relacionados con los desplazamientos δ_3 y δ_9 se obtienen de los resultados previos. Debe observarse, que con la convención de signos adoptada en la Fig 2.1 las direcciones de los momentos flectores positivos en el plano x y son diferentes al plano x 3 : 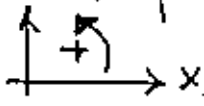 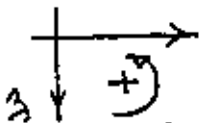 , la convención

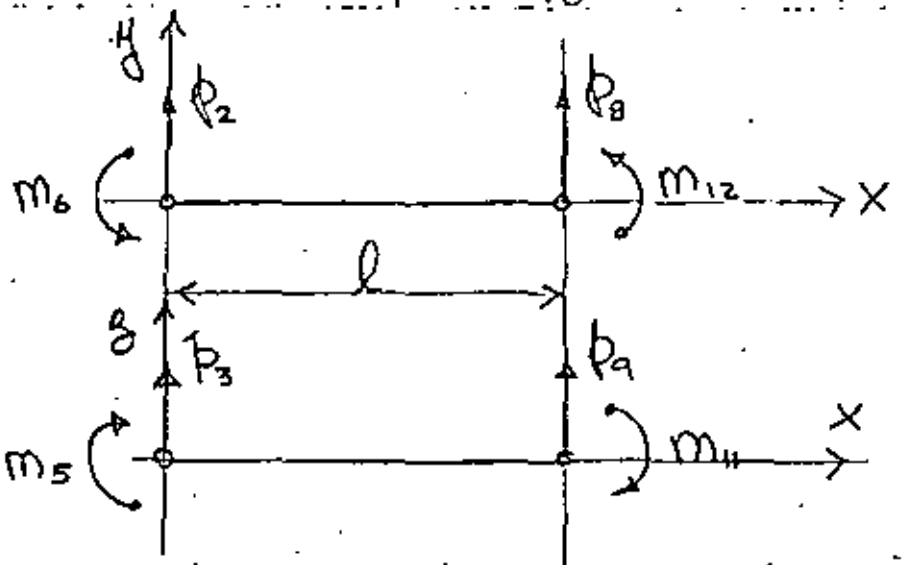

Fig. 2.2.5 Convención de signos para fuerzas de corte y momentos flectores;

de signos se muestra en la Fig. 2.2.5, basado en lo anterior es evidente que

$$k_{33} = \frac{P_3}{\delta_3} = -k_{22} = -\frac{P_2}{\delta_2} \quad a$$

$$k_{53} = \frac{m_5}{\delta_3} = -k_{62} = -\frac{m_6}{\delta_2} \quad b$$

$$k_{93} = \frac{P_9}{\delta_3} = -k_{82} = -\frac{P_8}{\delta_2} \quad c$$

$$k_{11,3} = \frac{m_{11}}{\delta_3} = -k_{12,2} = -\frac{m_{12}}{\delta_2} \quad d$$

$$k_{99} = \frac{P_9}{\delta_9} = -k_{88} = -\frac{P_8}{\delta_8} \quad e$$

$$k_{11,9} = \frac{m_{11}}{\delta_9} = -k_{12,8} = -\frac{m_{12}}{\delta_8} \quad f$$

Debé considerarse en el plano x z a I_1 y ϕ_2 como momento de inercia y parámetro de cortante..

2.2.6 Momentos Flectores m_5 y m_{11}

Aplicando las mismas observaciones de la sección anterior, se obtiene

$$k_{55} = \frac{m_5}{\theta_5} = k_{66} = \frac{m_6}{\theta_6} = \frac{(4+\phi_3)}{1+\phi_3}\frac{EI_z}{l} \quad a$$

$$k_{95} = \frac{P_9}{\theta_5} = -k_{86} = -\frac{\phi_8}{\theta_6} = +\frac{6EI_z}{(1+\phi_3)l} = k_{59} \quad b$$

$$k_{11,5} = \frac{m_{11}}{\theta_5} = k_{12,6} = \frac{m_{12}}{\theta_6} = \frac{(2-\phi_3)EI_z}{(1+\phi_3)l} = k_{5,11} \quad c$$

Substituyendo los valores k_{ij} obtenidas en las subsecciones anteriores se obtiene la matriz de rigidez de la barra jk de la Fig. 2.1 ecuación 2.5. en donde

$$\phi_z = \frac{12EI_3}{GA_{sz}l^2} = 24(1+\nu)\frac{A}{A_{sz}}\left(\frac{r_3}{l}\right)^2 = \frac{12f_zEI_3}{GAl^2}$$
$$\phi_z = \frac{12EI_z}{GA_{sz}l^2} = 24(1+\nu)\frac{A}{A_{sz}}\left(\frac{r_z}{l}\right)^2 = \frac{12f_3EI_z}{GAl^2} \quad (6.3)$$

ν = relación de Poisson, A=área total de la sección, A_{sz} y A_{sz} = áreas efectivas en cortante en direcciones y y 3 resp. r_z y r_3 = radios de giro respecto a y y resp. a x. ϕ_z y ϕ_3 = Parámetros de deformación de corte. Si r_3/l y r_z/l son pequeños comparados con la unidad, como son en elementos flexibles, ambos ϕ_z y ϕ_3 se pueden considerar cero. Los factores de forma son:

$$\therefore f_z = \frac{A}{I_3^2}\int_A\left(\frac{Q_3}{b_3}\right)^2 dA, \quad f_3 = \frac{A}{I_z^2}\int_A\left(\frac{Q_z}{b_z}\right)^2 dA \quad (6.4)$$

DESFI-UNAM | Marzo-19 | P. Ballesteros | 18 | 18

$$[R_{ij}] =$$

	δ_1	δ_2	δ_3	θ_4	θ_5	θ_6	δ_7	δ_8	δ_9	θ_{10}	θ_{11}	θ_{12}
δ_1	$\frac{EA}{l}$											
δ_2	0	$\frac{12EI_z}{l^3(1+\Phi_y)}$										
δ_3	0	0	$\frac{12EI_y}{l^3(1+\Phi_z)}$									
θ_4	0	0	0	$\frac{GJ}{l}$								
θ_5	0	0	$\frac{-6EI_y}{l^2(1+\Phi_z)}$	0	$\frac{(4+\Phi_z)EI_y}{l(1+\Phi_z)}$							
θ_6	0	$\frac{6EI_z}{l^2(1+\Phi_y)}$	0	0	0	$\frac{(4+\Phi_y)EI_z}{l(1+\Phi_y)}$						
δ_7	$\frac{-EA}{l}$	0	0	0	0	0	$\frac{AE}{l}$					
δ_8	0	$\frac{-12EI_z}{l^3(1+\Phi_y)}$	0	0	0	$\frac{-6EI_z}{l^2(1+\Phi_y)}$	0	$\frac{12EI_z}{l^3(1+\Phi_y)}$				
δ_9	0	0	$\frac{-12EI_y}{l^3(1+\Phi_z)}$	0	$\frac{6EI_y}{l^2(1+\Phi_z)}$	0	0	0	$\frac{12EI_y}{l^3(1+\Phi_z)}$			
θ_{10}	0	0	0	$\frac{-GJ}{l}$	0	0	0	0	0	$\frac{GJ}{l}$		
θ_{11}	0	0	$\frac{-6EI_y}{l^2(1+\Phi_z)}$	0	$\frac{(2-\Phi_z)EI_y}{l(1+\Phi_z)}$	0	0	0	$\frac{6EI_y}{l^2(1+\Phi_z)}$	0	$\frac{(4+\Phi_z)EI_y}{l(1+\Phi_z)}$	
θ_{12}	0	$\frac{6EI_z}{l^2(1+\Phi_y)}$	0	0	0	$\frac{(2-\Phi_y)EI_z}{l(1+\Phi_y)}$	0	$\frac{-6EI_z}{l^2(1+\Phi_y)}$	0	0	0	$\frac{(4+\Phi_y)EI_z}{l(1+\Phi_y)}$

(Simetrica)

Para problemas Bi-dimensionales, el elemento viga ik se reduce a seis fuerzas y momentos nodales y seis desplazamientos y rotaciones nodales. Utilizando

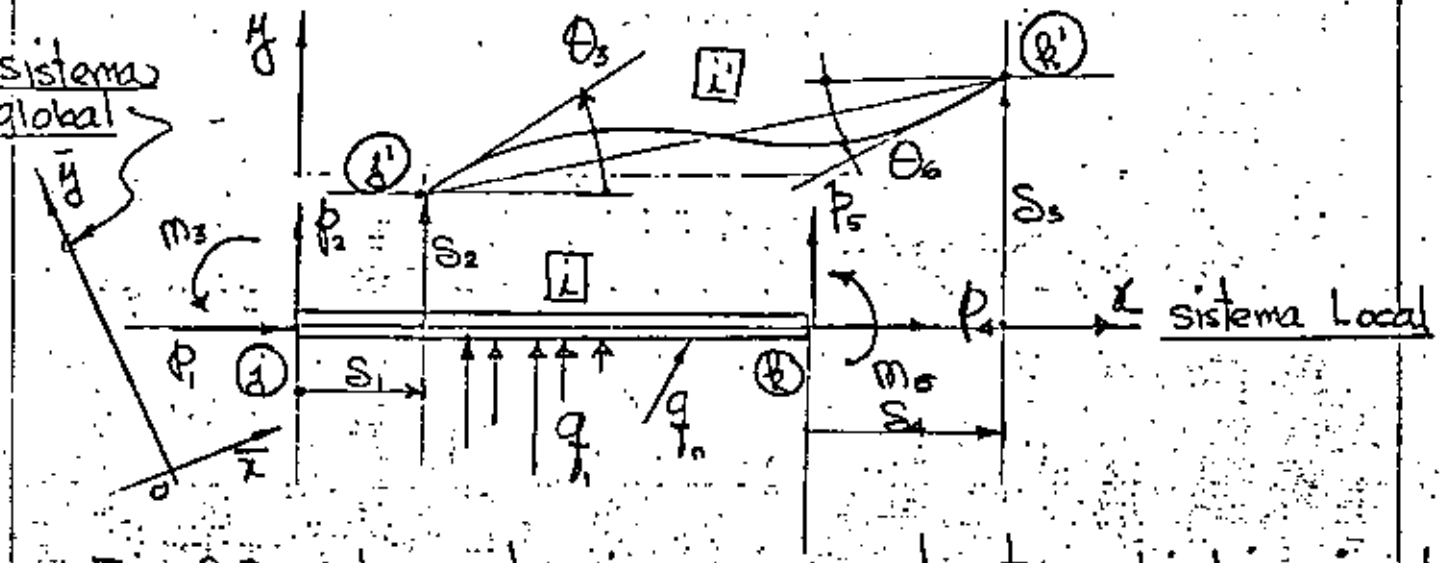

Fig. 2.2 Elemento viga para estructuras bidimensionales

la nomenclatura de la Fig. 2.2 (2.1) queda en

$$\begin{Bmatrix} P_1 \\ P_2 \\ m_3 \\ P_4 \\ P_5 \\ m_6 \end{Bmatrix}_i = \begin{bmatrix} k_{11} & k_{12} & k_{13} & k_{14} & k_{15} & k_{16} \\ k_{21} & & & & & k_{26} \\ & & & & & \\ & & & & & \\ & & & & & \\ k_{61} & & & & & k_{66} \end{bmatrix}_i \begin{Bmatrix} S_1 \\ S_2 \\ \theta_3 \\ S_4 \\ S_5 \\ \theta_6 \end{Bmatrix}_i + \begin{Bmatrix} P_1 \\ P_2 \\ \mu_3 \\ P_4 \\ P_5 \\ \mu_6 \end{Bmatrix}_i \qquad (2.6)$$

o sea:

$$\{P\}_i = [k_{ij}]_i \{S\}_i + \{\mu\}_i \qquad (2.7)$$

De los resultados discutidos previamente la matriz de rigidez de la barra i figura 2.2 queda

$$[k_{ij}]_i = \begin{array}{c} \\ \frac{EA}{l} \\ 0 \\ 0 \\ -\frac{EA}{l} \\ 0 \\ 0 \end{array} \begin{array}{c} \begin{array}{ccccccc} \delta_1 & \delta_2 & \theta_3 & \delta_4 & \delta_5 & \theta_6 & \end{array} \\ \begin{bmatrix} \frac{EA}{l} & & & & & & \\ 0 & \frac{12EI_z}{l^3(1+\Phi_y)} & & & & & \\ 0 & \frac{6EI_z}{l^2(1+\Phi_y)} & \frac{(4+\Phi_z)EI_z}{l(1+\Phi_y)} & & & & \\ -\frac{EA}{l} & 0 & 0 & \frac{EA}{l} & & & \\ 0 & \frac{-12EI_z}{l^3(1+\Phi_y)} & \frac{-6EI_z}{l^2(1+\Phi_y)} & 0 & \frac{12EI_z}{l^3(1+\Phi_y)} & & \\ 0 & \frac{6EI_z}{l^2(1+\Phi_y)} & \frac{(2-\Phi_y)EI_z}{l(1+\Phi_y)} & 0 & \frac{-6EI_z}{l^2(1+\Phi_y)} & \frac{(4+\Phi_y)EI_z}{l(1+\Phi_y)} & \end{bmatrix} \end{array} \begin{array}{c} \\ \delta_1 \\ \delta_2 \\ \theta_3 \\ \delta_4 \\ \delta_5 \\ \theta_6 \end{array} \qquad (2.8)$$

Si las deformaciones por cortante son despreciables esto es, $\Phi_y = 0$, la matriz de rigidez (2.8) se simplifica a

$$[k_{ij}] = \frac{EI_z}{l^3} \begin{array}{c} \\ \frac{Al^2}{I_z} \\ 0 \\ 0 \\ -\frac{Al^2}{I_z} \\ 0 \\ 0 \end{array} \begin{array}{c} \begin{array}{ccccccc} & & & & & & \end{array} \\ \begin{bmatrix} \frac{Al^2}{I_z} & & & & & & \\ 0 & 12 & & & & & \\ 0 & 6l & 4l^2 & & & & \\ -\frac{Al^2}{I_z} & 0 & 0 & \frac{Al^2}{I_z} & & & \\ 0 & -12 & -6l & 0 & 12 & & \\ 0 & 6l & 2l^2 & 0 & -6l & 4l^2 & \end{bmatrix} \end{array} \qquad (2.9)$$

La ecuación matricial relacionando los desplazamientos entre el sistema coordenado local y el global. Puede fácilmente demostrarse para el elemento viga mostrado en Fig. 2.1 es de la forma

$$\begin{Bmatrix} \delta_1 \\ \delta_2 \\ \delta_3 \\ \theta_4 \\ \theta_5 \\ \theta_6 \\ \delta_7 \\ \delta_8 \\ \delta_9 \\ \theta_{10} \\ \theta_{11} \\ \theta_{12} \end{Bmatrix} = \begin{bmatrix} \bar{\lambda}_{ox} & & & & & & & & & & & \\ \bar{\lambda}_{oy} & 0 & 0 & 0 & & & & & & & & \\ \bar{\lambda}_{oz} & & & & & & & & & & & \\ & \bar{\lambda}_{ox} & & & & & & & & & & \\ 0 & \bar{\lambda}_{oy} & 0 & 0 & & & & & & & & \\ & \bar{\lambda}_{oz} & & & & & & & & & & \\ & & & & \bar{\lambda}_{ox} & & & & & & & \\ 0 & 0 & \bar{\lambda}_{oy} & 0 & & & & & & & & \\ & & \bar{\lambda}_{oz} & & & & & & & & & \\ & & & & & \bar{\lambda}_{ox} & & & & & & \\ 0 & 0 & 0 & & \bar{\lambda}_{oy} & & & & & & & \\ & & & & \bar{\lambda}_{oz} & & & & & & & \end{bmatrix} \begin{Bmatrix} \bar{\delta}_1 \\ \bar{\delta}_2 \\ \bar{\delta}_3 \\ \bar{\theta}_4 \\ \bar{\theta}_5 \\ \bar{\theta}_6 \\ \bar{\delta}_7 \\ \bar{\delta}_8 \\ \bar{\delta}_9 \\ \bar{\theta}_{10} \\ \bar{\theta}_{11} \\ \bar{\theta}_{12} \end{Bmatrix} \tag{2.10}$$

$$\{\delta\} \qquad [\lambda] \qquad \{\bar{\delta}\}$$

o sea $$\{\delta\} = [\lambda]\{\bar{\delta}\} \tag{2.11}$$

donde
$$\bar{\lambda}_{ox} = [l_{ox} \; m_{ox} \; n_{ox}]$$
$$\bar{\lambda}_{oy} = [l_{oy} \; m_{oy} \; n_{oy}] \tag{2.12}$$
$$\bar{\lambda}_{oz} = [l_{oz} \; m_{oz} \; n_{oz}]$$

representa las matrices de los cosenos directores

para las direcciones ox, oy y oz, respectivamente, referidas al sistema global $\bar{x}$, $\bar{y}$ y $\bar{z}$, y $\{\bar{\delta}\}$ representa los desplazamientos de la barra [i] respecto al sistema global.

Para problemas bidimensionales la matriz de transformación $[\lambda]$ se reduce a

$$[\lambda] = \begin{bmatrix} l_{ox} & m_{ox} & 0 & 0 & 0 & 0 \\ l_{oy} & m_{oy} & 0 & 0 & 0 & 0 \\ 0 & 0 & 1 & 0 & 0 & 0 \\ 0 & 0 & 0 & l_{ox} & m_{ox} & 0 \\ 0 & 0 & 0 & l_{oy} & m_{oy} & 0 \\ 0 & 0 & 0 & 0 & 0 & 1 \end{bmatrix} \qquad (2.13)$$

El análisis de marcos tridimensionales se puede describir por las mismas ecuaciones básicas usadas en la descripción del análisis de estructuras planas. Considerando el sistema total, el equilibrio estático nodal es definido por la ecuación matricial

$$[S_c]\{\delta_c\} + \{\mu_c\} = \{R_c\} \qquad (2.14)$$

donde:

$[S_c]$ = Matriz de rigidez completa de la estructura.

$[\delta_c]$ = Vector de desplazamientos nodales completo.

$\{\mu_c\}$ = Vector de cargas nodales completo.

$\{R\}$ vector de reacciones de la estructura y de (2.14) se obtiene la ecuación

$$[S_{ui}]\{S_{ii}\} + \{\mu_i\} = 0 \qquad (2.15)$$

de donde se obtiene $\{S_i\}$ y $\{S_c\}$, el que substituyéndolo en (2.14) y (2.1) se obtiene $\{R_c\}$ y $\{P\}_i$ como

$$\{R_c\} = -[S_c][S_{ui}]^{-1}\{\mu_i\} \qquad (2.16)$$

$$\{P\}_i = [k_{ij}]_i [S_{ui}]^{-1}\{\mu_i\} + \{\mu\}_i \quad (i=1,2\ldots,n) \qquad (2.17)$$

Ejemplo: En el sistema estructural de la Fig. 2.3, determine las reacciones nodales $\{P\}_i$ en los extremos de cada miembro y las reacciones originadas por las cargas indicadas.

La estructura tiene miembros prismáticos con las siguientes propiedades:

$$EI_y = EI_z = EI$$
$$GI_x = \frac{EI}{4} \qquad (2.18)$$
$$EA_x = \frac{EI}{4}$$

la estructura es flexible y se puede considerar la ($\phi_y = \phi_z$) deformación por cortante despreciable

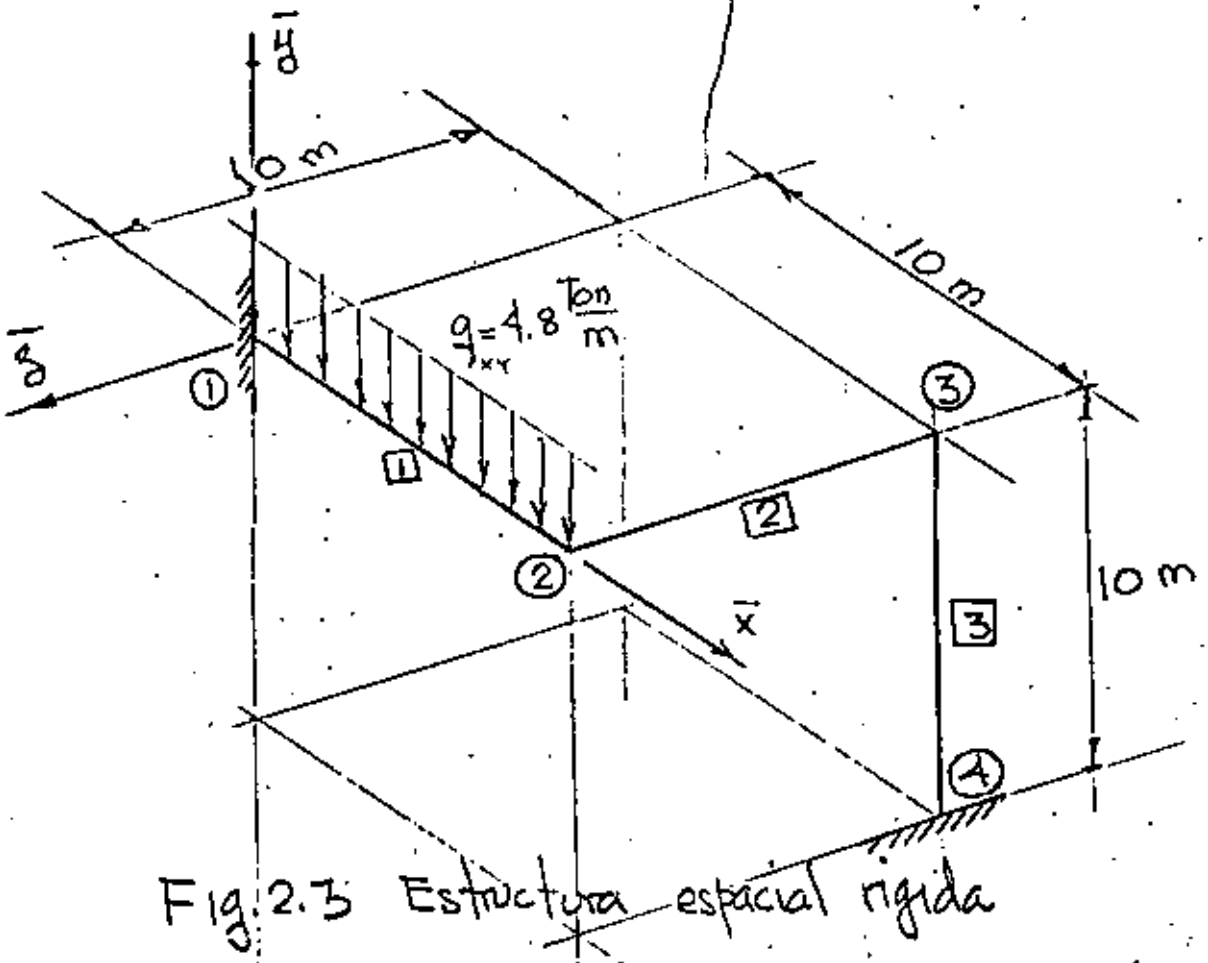

Fig. 2.3 Estructura espacial rígida

Las tablas 2.1 y 2.2 dan la información requerida para cada nodo y miembro

Nodo	$\bar{X}$	$\bar{Y}$	$\bar{Z}$
1	0	0	0
2	10.0	0	0
3	10.0	0	-10.00
4	10.0	-10.00	-10.00

Tabla 2.1 coordenadas nodales en metros.

Barra	Longitud (m)	Nodo j	Nodo k	Cosenos directores -l_ok	Cosenos directores M_ok	Cosenos directores N_ok	TIPO DE TRANSFORMACION	Angulo ψ
1	10.0	1	2	+1	0	0	y-z-x	0
2	10.0	2	3	0	0	-1	y-z-x	0
3	10.0	4	3	0	+1	0	z-y-x	90°

Tabla 2.2 longitudes, cosenos directores y Tipos de Transformación.

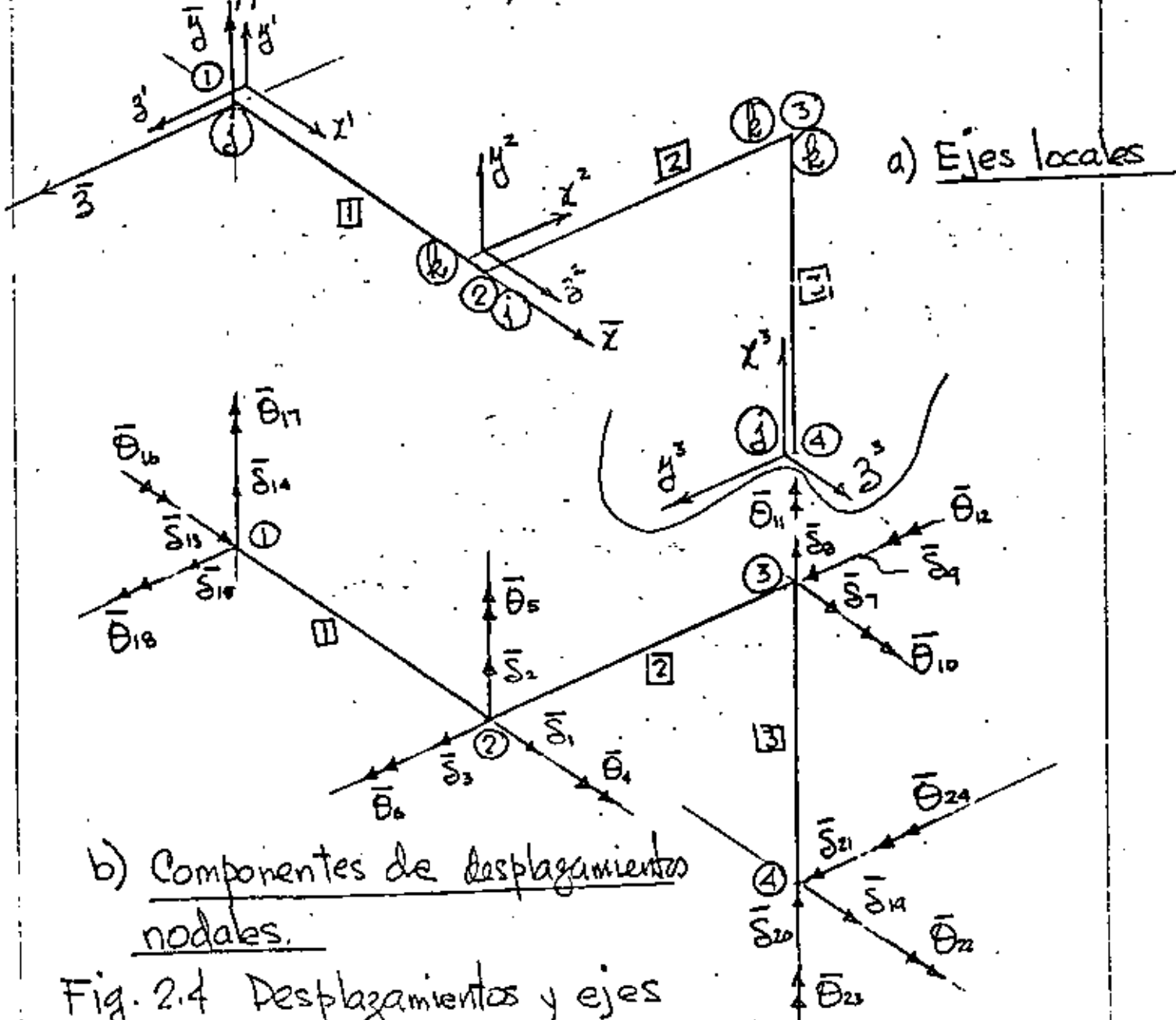

Fig. 2.4 Desplazamientos y ejes

vector columna de desplazamientos nodales $\{\delta_c\}$

$$\{\delta_c\} = \begin{Bmatrix} \delta_1 \\ \delta_2 \\ \delta_3 \\ \theta_4 \\ \theta_5 \\ \theta_6 \\ \delta_7 \\ \delta_8 \\ \delta_9 \\ \theta_{10} \\ \theta_{11} \\ \theta_{12} \\ \delta_{13} \\ \delta_{14} \\ \delta_{15} \\ \theta_{16} \\ \theta_{17} \\ \theta_{18} \\ \delta_{19} \\ \delta_{20} \\ \delta_{21} \\ \theta_{22} \\ \theta_{23} \\ \theta_{24} \end{Bmatrix} = \begin{Bmatrix} \{\delta_u\} \\ \{\delta_r\} \end{Bmatrix} \qquad (2.14)$$

Matriz de rigidiz de cada miembro

Para cada elemento viga, la matriz de rigidez se establece por medio de (2.1) con respecto a los ejes locales; la matriz de transformación se puede establecer por medio de la expresión (2.10); y la matriz de rigideg de miembro transformada, $[\bar{k}_{ij}]_i$ respecto al sistema global se obtiene de

$$[\bar{k}_{ij}]_i = [\lambda]_i^T [k_{ij}]_i [\lambda]_i \qquad (2.20)$$

Miembro [1]

$$[\lambda]_1 = \left[\begin{array}{ccc|ccc|ccc|cc} 1&0&0&0&0&0&0&0&0&0&0 \\ 0&1&0&0&0&0&0&0&0&0&0 \\ 0&0&1&0&0&0&0&0&0&0&0 \\ \hline 0&0&0&1&0&0&0&0&0&0&0 \\ 0&0&0&0&1&0&0&0&0&0&0 \\ 0&0&0&0&0&1&0&0&0&0&0 \\ \hline 0&0&0&0&0&0&1&0&0&0&0 \\ 0&0&0&0&0&0&0&1&0&0&0 \\ 0&0&0&0&0&0&0&0&1&0&0 \\ \hline 0&0&0&0&0&0&0&0&0&1&0 \\ 0&0&0&0&0&0&0&0&0&0&1 \end{array}\right] \equiv [I] \; ; \; [\bar{k}_{ij}]_1 = [I]^T [k_{ij}]_1 [I]$$

$$= [k_{ij}]_1 \qquad (2.21)$$

$$EI \left[\begin{array}{cccccccccccc} 13 & 14 & 15 & 16 & 17 & 18 & 1 & 2 & 3 & 4 & 5 & 6 \\ \hline .025 & 0 & 0 & 0 & 0 & 0 & -.025 & 0 & 0 & 0 & 0 & 0 \\ 0 & .012 & 0 & 0 & 0 & .060 & 0 & -.012 & 0 & 0 & 0 & .060 \\ 0 & 0 & .012 & 0 & -.060 & 0 & 0 & 0 & -.012 & 0 & -.060 & 0 \\ 0 & 0 & 0 & .025 & 0 & 0 & 0 & 0 & 0 & -.025 & 0 & 0 \\ 0 & 0 & -.06 & 0 & 0.4 & 0 & 0 & 0 & .06 & 0 & 0.2 & 0 \\ 0 & .06 & 0 & 0 & 0 & 0.4 & 0 & -.06 & 0 & 0 & 0 & 0.2 \\ -.025 & 0 & 0 & 0 & 0 & 0 & .025 & 0 & 0 & 0 & 0 & 0 \\ 0 & -.012 & 0 & 0 & 0 & -.06 & 0 & .012 & 0 & 0 & 0 & -.06 \\ 0 & 0 & -.012 & 0 & .06 & 0 & 0 & 0 & .012 & 0 & .06 & 0 \\ 0 & 0 & 0 & -.025 & 0 & 0 & 0 & 0 & 0 & .025 & 0 & 0 \\ 0 & 0 & -.06 & 0 & 0.2 & 0 & 0 & 0 & .06 & 0 & .4 & 0 \\ \hline \end{array}\right] \begin{array}{c} 13 \\ 14 \\ 15 \\ 16 \\ 17 \\ 18 \\ 1 \\ 2 \\ 3 \\ 4 \\ 5 \\ 6 \end{array} \qquad (2.22)$$

Miembro [2] De (2.5) se obtiene:

$$[k_{ij}]_2 = EI \begin{bmatrix}
.025 & 0 & 0 & 0 & 0 & 0 & -.025 & 0 & 0 & 0 & 0 & 0 \\
0 & .012 & 0 & 0 & 0 & -.06 & 0 & -.012 & 0 & 0 & 0 & -.06 \\
0 & 0 & .012 & 0 & -.06 & 0 & 0 & 0 & -.012 & 0 & -.06 & 0 \\
0 & 0 & 0 & .025 & 0 & 0 & 0 & 0 & 0 & -.025 & 0 & 0 \\
0 & 0 & -.06 & 0 & 0.4 & 0 & 0 & 0 & .06 & 0 & 0.2 & 0 \\
0 & .06 & 0 & 0 & 0 & 0.4 & 0 & -.06 & 0 & 0 & 0 & 0.2 \\
-.025 & 0 & 0 & 0 & 0 & 0 & .025 & 0 & 0 & 0 & 0 & 0 \\
0 & -.012 & 0 & 0 & 0 & -.06 & 0 & .012 & 0 & 0 & 0 & -.06 \\
0 & 0 & -.012 & 0 & .06 & 0 & 0 & 0 & .012 & 0 & .06 & 0 \\
0 & 0 & 0 & -.025 & 0 & 0 & 0 & 0 & 0 & .025 & 0 & 0 \\
0 & 0 & -.06 & 0 & 0.2 & 0 & 0 & 0 & -.06 & 0 & .4 & 0 \\
0 & .06 & 0 & 0 & 0 & 0.2 & 0 & -.06 & 0 & 0 & 0 & .4
\end{bmatrix} \qquad (2.23)$$

De (2.12); $\bar{\lambda}_{ox_2} = [0\ 0\ -1]_2,\ \bar{\lambda}_{oY_2} = [0\ 1\ 0]_2,\ \bar{\lambda}_{oz_2} = [1\ 0\ 0]_2 \qquad (2.12)_a$

Subst. $(6.12)_a$ en (2.10) se obtiene

$$[\lambda]_2 = \begin{bmatrix}
0 & 0 & -1 & & & & & & & & & \\
0 & 1 & 0 & & & & & & & & & \\
1 & 0 & 0 & & & & & & & & & \\
 & & & 0 & 0 & -1 & & & & & & \\
 & & & 0 & 1 & 0 & & & & & & \\
 & & & 1 & 0 & 0 & & & & & & \\
 & & & & & & 0 & 0 & -1 & & & \\
 & & & & & & 0 & 1 & 0 & & & \\
 & & & & & & 1 & 0 & 0 & & & \\
 & & & & & & & & & 0 & 0 & -1 \\
 & & & & & & & & & 0 & 1 & 0 \\
 & & & & & & & & & 1 & 0 & 0
\end{bmatrix} \qquad (2.24)$$

Subst (2.24) y (2.23) en (2.20) se obtiene

$$[\bar{k}_{ij}]_2 = EI \begin{bmatrix}
.012 & 0 & 0 & 0 & -.06 & 0 & -.012 & 0 & 0 & 0 & -.06 & 0 \\
0 & .012 & 0 & .06 & 0 & 0 & 0 & -.012 & 0 & .06 & 0 & 0 \\
0 & 0 & .025 & 0 & 0 & 0 & 0 & 0 & -.025 & 0 & 0 & 0 \\
0 & .06 & 0 & .4 & 0 & 0 & 0 & -.06 & 0 & 0.2 & 0 & 0 \\
-.06 & 0 & 0 & 0 & 0.4 & 0 & .06 & 0 & 0 & 0 & .2 & 0 \\
0 & 0 & 0 & 0 & 0 & .025 & 0 & 0 & 0 & 0 & 0 & -.025 \\
-.012 & 0 & 0 & 0 & .06 & 0 & .012 & 0 & 0 & 0 & .06 & 0 \\
0 & -.012 & 0 & -.06 & 0 & 0 & 0 & .012 & 0 & -.06 & 0 & 0 \\
0 & 0 & -.025 & 0 & 0 & 0 & 0 & 0 & .025 & 0 & 0 & 0 \\
0 & .06 & 0 & 0.2 & 0 & 0 & 0 & -.06 & 0 & .4 & 0 & 0 \\
-.06 & 0 & 0 & 0 & 0.2 & 0 & .06 & 0 & 0 & 0 & .4 & 0 \\
0 & 0 & 0 & 0 & 0 & -.025 & 0 & 0 & 0 & 0 & 0 & .025
\end{bmatrix} \qquad (2.25)$$

(1 2 3 4 5 6 7 8 9 10 11 12)

Miembro [3], De (2.5) se obtiene la matriz de rigidez. la cual resulta igual a la de los miembros [1] y [2]

$$[k_{ij}]_3 = [k_{ij}]_2 = [k_{ij}]_1 \tag{2.26}$$

De (2.12) se obtiene

$$\overline{\lambda}_{ox_3} = [0\ 1\ 0]_3,\ \overline{\lambda}_{oy_3} = [0\ 0\ 1]_3,\ \overline{\lambda}_{oz_3} = [1\ 0\ 0]_3 \tag{2.27}$$

De (2.27) y (2.10) se obtiene

$$[\lambda]_3 = \begin{bmatrix} 0 & 1 & 0 & & & & & & & & & \\ 0 & 0 & 1 & & & & & & & & & \\ 1 & 0 & 0 & & & & & & & & & \\ & & & 0 & 1 & 0 & & & & & & \\ & & & 0 & 0 & 1 & & & & & & \\ & & & 1 & 0 & 0 & & & & & & \\ & & & & & & 0 & 1 & 0 & & & \\ & & & & & & 0 & 0 & 1 & & & \\ & & & & & & 1 & 0 & 0 & & & \\ & & & & & & & & & 0 & 1 & 0 \\ & & & & & & & & & 0 & 0 & 1 \\ & & & & & & & & & 1 & 0 & 0 \end{bmatrix} \tag{2.28}$$

De (2.20) (2.26) y (2.28) se obtiene

$$[k_{ij}]_3 = E\begin{bmatrix} 19 & 20 & 21 & 22 & 23 & 24 & 7 & 8 & 9 & 10 & 11 & 12 & \\ .012 & 0 & 0 & 0 & 0 & -.06 & -.012 & 0 & 0 & 0 & 0 & -.06 & 19 \\ 0 & .025 & 0 & 0 & 0 & 0 & 0 & -.025 & 0 & 0 & 0 & 0 & 20 \\ 0 & 0 & .012 & .06 & 0 & 0 & 0 & 0 & -.012 & .06 & 0 & 0 & 21 \\ 0 & 0 & .06 & .4 & 0 & 0 & 0 & 0 & -.06 & .2 & 0 & 0 & 22 \\ 0 & 0 & 0 & 0 & .025 & 0 & 0 & 0 & 0 & 0 & -.025 & 0 & 23 \\ -.06 & 0 & 0 & 0 & 0 & .4 & .06 & 0 & 0 & 0 & 0 & .2 & 24 \\ -.012 & 0 & 0 & 0 & 0 & .06 & .012 & 0 & 0 & 0 & 0 & .06 & 7 \\ 0 & -.025 & 0 & 0 & 0 & 0 & 0 & .025 & 0 & 0 & 0 & 0 & 8 \\ 0 & 0 & -.012 & -.06 & 0 & 0 & 0 & 0 & .012 & -.06 & 0 & 0 & 9 \\ 0 & 0 & .06 & .2 & 0 & 0 & 0 & 0 & -.06 & .4 & 0 & 0 & 10 \\ 0 & 0 & 0 & 0 & -.025 & 0 & 0 & 0 & 0 & 0 & .025 & 0 & 11 \\ -.06 & 0 & 0 & 0 & 0 & .2 & .06 & 0 & 0 & 0 & 0 & .4 & 12 \end{bmatrix} \tag{2.29}$$

Matriz de rigideg de la estructura.

La matriz completa de la estructura $[S_c]$ se obtiene sumando los coeficientes de rigideg de miembro dados en las expresiones (2.22), (2.25) y (2.29) con respecto a la identificación de subindices de los elementos se obtiene

$$[S_c] = EI \begin{array}{c} \begin{array}{cccccccccccc} 1 & 2 & 3 & 4 & 5 & 6 & 7 & 8 & 9 & 10 & 11 & 12 \end{array} \\ \left[\begin{array}{cccccccccccc} .037 & 0 & 0 & 0 & -.06 & 0 & -.012 & 0 & 0 & 0 & -.06 & 0 \\ 0 & .024 & 0 & .06 & 0 & -.06 & 0 & -.012 & 0 & .06 & 0 & 0 \\ 0 & 0 & .037 & 0 & .06 & 0 & 0 & 0 & -.025 & 0 & 0 & 0 \\ 0 & .06 & 0 & .425 & 0 & 0 & 0 & -.06 & 0 & 0.2 & 0 & 0 \\ -.06 & 0 & .06 & 0 & 0.8 & 0 & .06 & 0 & 0 & 0 & 0.2 & 0 \\ 0 & -.06 & 0 & 0 & 0 & .425 & 0 & 0 & 0 & 0 & 0 & -.025 \\ -.012 & 0 & 0 & 0 & .06 & 0 & .024 & 0 & 0 & 0 & .06 & .06 \\ 0 & -.012 & 0 & -.06 & 0 & 0 & 0 & .037 & 0 & -.06 & 0 & 0 \\ 0 & 0 & -.025 & 0 & 0 & 0 & 0 & 0 & .037 & -.06 & 0 & 0 \\ 0 & .06 & 0 & 0.2 & 0 & 0 & 0 & -.06 & -.06 & .8 & 0 & 0 \\ -.06 & 0 & 0 & 0 & 0.2 & 0 & .06 & 0 & 0 & 0 & .425 & 0 \\ 0 & 0 & 0 & 0 & 0 & -.025 & .06 & 0 & 0 & 0 & 0 & .425 \\ \hline -.025 & 0 & 0 & 0 & 0 & 0 & 0 & 0 & 0 & 0 & 0 & 0 \\ 0 & -.012 & 0 & 0 & 0 & .06 & 0 & 0 & 0 & 0 & 0 & 0 \\ 0 & 0 & -.012 & 0 & -.06 & 0 & 0 & 0 & 0 & 0 & 0 & 0 \\ 0 & 0 & 0 & -.025 & 0 & 0 & 0 & 0 & 0 & 0 & 0 & 0 \\ 0 & 0 & .06 & 0 & 0.2 & 0 & 0 & 0 & 0 & 0 & 0 & 0 \\ 0 & -.06 & 0 & 0 & 0 & 0.2 & 0 & 0 & 0 & 0 & 0 & 0 \\ 0 & 0 & 0 & 0 & 0 & 0 & -.012 & 0 & 0 & 0 & 0 & -.06 \\ 0 & 0 & 0 & 0 & 0 & 0 & 0 & -.025 & 0 & 0 & 0 & 0 \\ 0 & 0 & 0 & 0 & 0 & 0 & 0 & 0 & -.012 & .06 & 0 & 0 \\ 0 & 0 & 0 & 0 & 0 & 0 & 0 & 0 & -.06 & .2 & 0 & 0 \\ 0 & 0 & 0 & 0 & 0 & 0 & 0 & 0 & 0 & 0 & -.025 & 0 \\ 0 & 0 & 0 & 0 & 0 & 0 & .06 & 0 & 0 & 0 & 0 & .2 \end{array}\right] \begin{array}{c} 1 \\ 2 \\ 3 \\ 4 \\ 5 \\ 6 \\ 7 \\ 8 \\ 9 \\ 10 \\ 11 \\ 12 \\ \\ 13 \\ 14 \\ 15 \\ 16 \\ 17 \\ 18 \\ 19 \\ 20 \\ 21 \\ 22 \\ 23 \\ 24 \end{array} \end{array} = \left[\begin{array}{c} [S_{\mu\mu}] \\ \hline [S_{\nu\mu}] \end{array}\right] \qquad (2.30)$$

De (2.30) se obtiene $[S_{\mu\mu}]^{-1}$

31 31 (2.31)

$\left[\frac{S}{EI}\right] = \frac{1}{EI}$

1	2	3	4	5	6	7	8	9	10	11	12	
38.396	1.266	-6.236	0.001	1.750	0.085	11.279	-0.403	-5.028	-0.503	3.005	-1.578	1
1.266	210.745	-43.160	-21.908	5.487	30.182	-39.151	11.279	-50.707	-13.286	3.124	7.303	2
-6.236	-43.160	102.028	2.421	-11.235	-6.537	50.707	5.028	84.038	9.312	-2.752	-7.543	3
0.001	-21.908	2.421	5.546	-0.346	-3.130	3.124	3.005	2.752	0.688	-0.278	-0.625	4
1.750	5.487	-11.235	-0.346	3.048	0.888	-13.286	-0.503	-9.312	-1.061	0.688	1.928	5
0.085	30.182	-6.537	-3.130	0.888	16.698	-7.303	1.587	-7.543	-1.928	0.625	1.425	6
11.279	-39.151	50.707	3.124	-13.286	-7.303	210.745	1.266	43.160	5.487	-21.908	-30.182	7
-0.403	11.279	5.028	3.005	-0.503	1.587	1.266	38.396	6.236	1.757	0.001	-0.085	8
-5.028	-50.707	84.038	2.752	-9.312	-7.543	43.160	6.236	102.028	11.235	-2.421	-6.537	9
-0.503	-13.286	9.312	0.688	-1.061	-1.928	5.487	1.750	11.235	3.048	-0.346	-0.888	10
3.005	3.124	-2.752	-0.278	0.688	0.625	-21.908	0.001	-2.421	-0.346	5.546	3.130	11
-1.587	7.303	-7.543	-0.625	1.928	1.425	-30.182	-0.085	-6.537	-0.888	3.130	6.698	12

Vector de momentos y reacciones fijas miembro [1]

$$\{\mu\}_1 = \begin{Bmatrix} P_{13} \\ P_{14} \\ P_{15} \\ \mu_{16} \\ \mu_{17} \\ \mu_{18} \\ P_1 \\ P_2 \\ P_3 \\ \mu_4 \\ \mu_5 \\ \mu_6 \end{Bmatrix}_1 = \begin{Bmatrix} 0 \\ 24 \\ 0 \\ 0 \\ 0 \\ 40 \\ 0 \\ 24 \\ 0 \\ 0 \\ 0 \\ -40 \end{Bmatrix}_1 = \{\bar{\mu}\}_1 \qquad (2.32)$$

$$\{\bar{\mu}\}_1 = [\lambda]_1^t \{\mu\}_1 \qquad (2.33)$$

$$\{\mu\}_2 = 0 \quad ; \{\bar{\mu}\}_2 = 0$$

$$\{\mu\}_3 = 0 \quad ; \{\bar{\mu}\}_3 = 0$$

Habiendo definido las cargas nodales en términos de las acciones fijas en los extremos con respecto a los ejes de referencia, se deduce el vector de cargas nodales completo $\{\mu_c\}$, como.

$$\{\mu_c\}_r = \left\{\begin{matrix}\{\mu_{ij}\} \\ \hline \{\mu_{r-}\}\end{matrix}\right\} = \left\{\begin{matrix} 0 \\ -24 \\ 0 \\ 0 \\ 0 \\ 40.0 \\ 0 \\ 0 \\ 0 \\ 0 \\ 0 \\ 0 \\ \hline 0 \\ -24 \\ 0 \\ 0 \\ 0 \\ -40.0 \\ 0 \\ 0 \\ 0 \\ 0 \\ 0 \end{matrix}\right. \begin{matrix} 1 \\ 2 \\ 3 \\ 4 \\ 5 \\ 6 \\ 7 \\ 8 \\ 9 \\ 10 \\ 11 \\ 12 \\ \\ 13 \\ 14 \\ 15 \\ 16 \\ 17 \\ 18 \\ 19 \\ 20 \\ 21 \\ 22 \\ 23 \\ 24 \end{matrix} \quad (2.34)$$

Etiqueta de grados de libertad

Substituyendo (2.31) y (2.34) en (2.15) se obtiene

$$\{\delta_u\} = -[S_{uu}]^{-1}\{H_u\} \tag{2.35}$$

$$\{\bar{\delta}_u\} = \begin{Bmatrix} \bar{\delta}_1 \\ \bar{\delta}_2 \\ \bar{\delta}_3 \\ \bar{\theta}_4 \\ \bar{\theta}_5 \\ \bar{\theta}_6 \\ \bar{\delta}_7 \\ \bar{\delta}_8 \\ \bar{\delta}_9 \\ \bar{\theta}_{10} \\ \bar{\theta}_{11} \\ \bar{\theta}_{12} \end{Bmatrix} = \frac{1}{EI} \begin{Bmatrix} -26.984 \\ -3850.6 \\ 774.36 \\ 400.592 \\ -96.168 \\ -456.448 \\ 647.504 \\ -207.216 \\ 915.248 \\ 241.744 \\ -49.976 \\ -118.272 \end{Bmatrix} \tag{2.36}$$

Los valores de los desplazamientos dados por (2.36) con respecto al sistema global son valores relativos, para obtener los valores se substituye E en ton/m^2 e I en m^4 en (2.36) y se obtiene δ_i en metros y θ en radianes.

Acciones Finales en los extremos.

Habiendo evaluado las componentes de los desplazamiento nodales con respecto al sistema global de referencia por medio de (2.10) se evaluan con respecto a las coordenadas locales de cada barra y las acciones

finales para cada miembro de la estructura se calculan de (2.1)

$$\{P\}_i = [k_{ij}][\lambda]_i\{\bar{S}\}_i + \{\mu\}_i \qquad (2.37)$$

De la Fig. 2.4 se tiene para el ..... miembro [1]

$$\{\bar{S}\}_1 = \begin{Bmatrix} \bar{S}_{13} \\ \bar{S}_{14} \\ \bar{S}_{15} \\ \bar{\theta}_{16} \\ \bar{\theta}_{17} \\ \bar{\theta}_{18} \\ \bar{S}_1 \\ \bar{S}_2 \\ \bar{S}_3 \\ \bar{\theta}_4 \\ \bar{\theta}_5 \\ \bar{\theta}_6 \end{Bmatrix}_1 = \frac{1}{EI} \begin{Bmatrix} 0 \\ 0 \\ 0 \\ 0 \\ 0 \\ 0 \\ -26.964 \\ -3850.6 \\ 774.36 \\ 400.592 \\ -96.168 \\ -456.448 \end{Bmatrix}_1 \qquad (2.38)$$

De (2.21), (2.38), (2.1) y (2.5) se obtiene

$$\{P\}_1 = \begin{Bmatrix} F_1 \\ F_2 \\ P_3 \\ m_4 \\ m_5 \\ m_6 \\ F_7 \\ P_8 \\ F_9 \\ m_{10} \\ m_{11} \\ m_{12} \end{Bmatrix} = \begin{Bmatrix} 0.7 \text{ Ton} \\ 42.8 \text{ Ton} \\ -3.5 \text{ Ton} \\ -10.0 \text{ Ton-m} \\ 27.2 \text{ Ton-m} \\ 179.7 \text{ Ton-m} \\ -0.7 \text{ Ton} \\ 5.2 \text{ Ton} \\ 3.5 \text{ Ton} \\ 10.0 \text{ Ton-m} \\ 8.0 \text{ Ton-m} \\ 8.5 \text{ Ton-m} \end{Bmatrix}$$

(Indices según convención Fig. 2.4)

(2.39)

Miembro [illegible]. $\{\bar{\delta}\}_2 = \{\delta_u\} = [\lambda]_2 \{\bar{\delta}_u\}$ y $\{\bar{M}\}_2 = \{\bar{P}\}$

De [illegible], (2.24) (2.25), (2.1) y (2.5) se obtiene

$$\{P\}_2 = \begin{Bmatrix} P_1 \\ P_2 \\ P_3 \\ m_4 \\ m_5 \\ m_6 \\ P_7 \\ P_8 \\ P_9 \\ m_{10} \\ m_{11} \\ m_{12} \end{Bmatrix} = \begin{Bmatrix} 3.5 \text{ Ton} \\ -5.2 \text{ "} \\ 0.7 \text{ "} \\ 8.5 \text{ Ton-m} \\ -8.0 \text{ "} \\ -10.0 \text{ "} \\ -3.5 \text{ Ton} \\ 5.2 \text{ "} \\ -0.7 \text{ "} \\ -8.5 \text{ Ton-m} \\ 1.2 \text{ "} \\ -41.8 \text{ "} \end{Bmatrix}$$

(Indices según convención Fig. 2.4)

(2.40)

Miembro [3]

$$\{S\}_3 = \begin{Bmatrix} \bar{S}_{19} \\ \bar{S}_{20} \\ \bar{S}_{21} \\ \bar{\Theta}_{22} \\ \bar{\Theta}_{23} \\ \bar{\Theta}_{24} \\ \bar{S}_7 \\ \bar{S}_8 \\ \bar{S}_9 \\ \bar{\Theta}_{10} \\ \bar{\Theta}_{11} \\ \bar{\Theta}_{12} \end{Bmatrix}_3 = \frac{1}{EI} \begin{Bmatrix} 0 \\ 0 \\ 0 \\ 0 \\ 0 \\ 0 \\ 647.504 \\ -207.216 \\ 915.248 \\ 241.744 \\ -49.976 \\ -118.272 \end{Bmatrix}_3 \qquad (2.41)$$

en [3] También $\{\mu\}_3 = 0$, De (2.28), (2.29), (2.1) y (2.5) se obtiene

$$\{P\}_3 = \begin{Bmatrix} P_1 \\ P_2 \\ P_3 \\ m_4 \\ m_5 \\ m_6 \\ P_7 \\ P_8 \\ P_9 \\ m_{10} \\ m_{11} \\ m_{12} \end{Bmatrix}_3 = \begin{Bmatrix} 5.2 \text{ Ton} \\ 3.5 \text{ "} \\ -0.7 \text{ "} \\ 1.2 \text{ Ton-m} \\ 15.2 \text{ "} \\ -6.6 \text{ "} \\ -5.2 \text{ Ton} \\ -3.5 \text{ "} \\ 0.7 \text{ "} \\ -1.2 \text{ Ton-m} \\ -8.5 \text{ "} \\ 41.8 \text{ "} \end{Bmatrix}_3 \qquad (2.42)$$

Reacciones.

Substituyendo las matrices apropiadas en

$$\{R\} = [S_{ru}]\{\delta_u\} - \{u_r\}$$

se obtiene

$$\{R\} = \begin{Bmatrix} R_{13} \\ R_{14} \\ R_{15} \\ R_{16} \\ R_{17} \\ R_{18} \\ R_{19} \\ R_{20} \\ R_{21} \\ R_{22} \\ R_{23} \\ R_{24} \end{Bmatrix} = \begin{Bmatrix} 0.7 \text{ Ton} \\ 42.8 \text{ "} \\ -3.5 \text{ "} \\ -10.0 \text{ Ton-m} \\ 27.2 \text{ Ton-m} \\ 179.7 \text{ "} \\ -0.7 \text{ Ton} \\ 5.2 \text{ "} \\ 8.5 \text{ "} \\ -6.6 \text{ Ton-m} \\ 1.2 \text{ "} \\ 15.2 \text{ "} \end{Bmatrix} \qquad 2.43$$

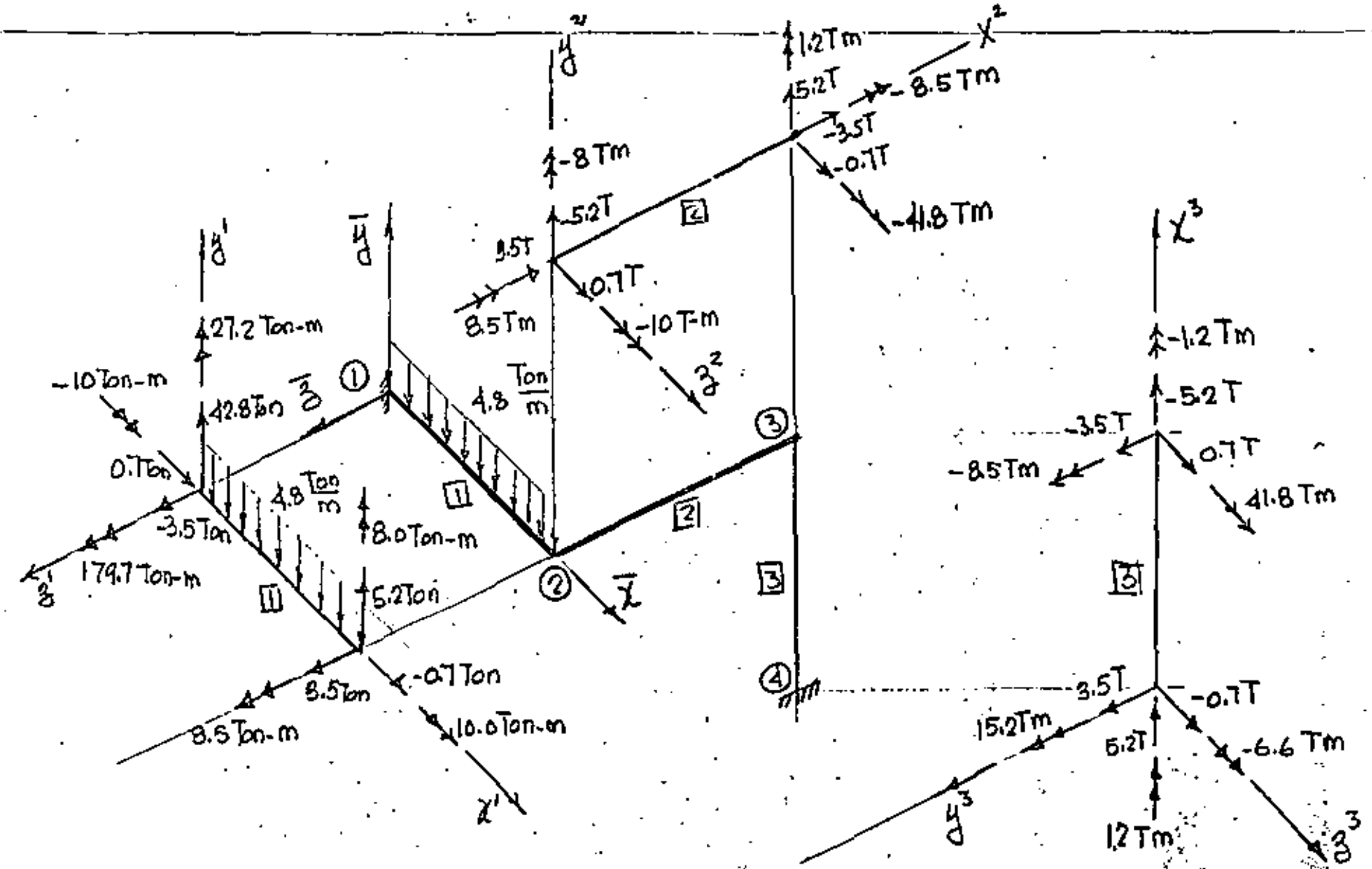

Fig. 2.5 Componentes de acciones finales {P_f} en los extremos j k

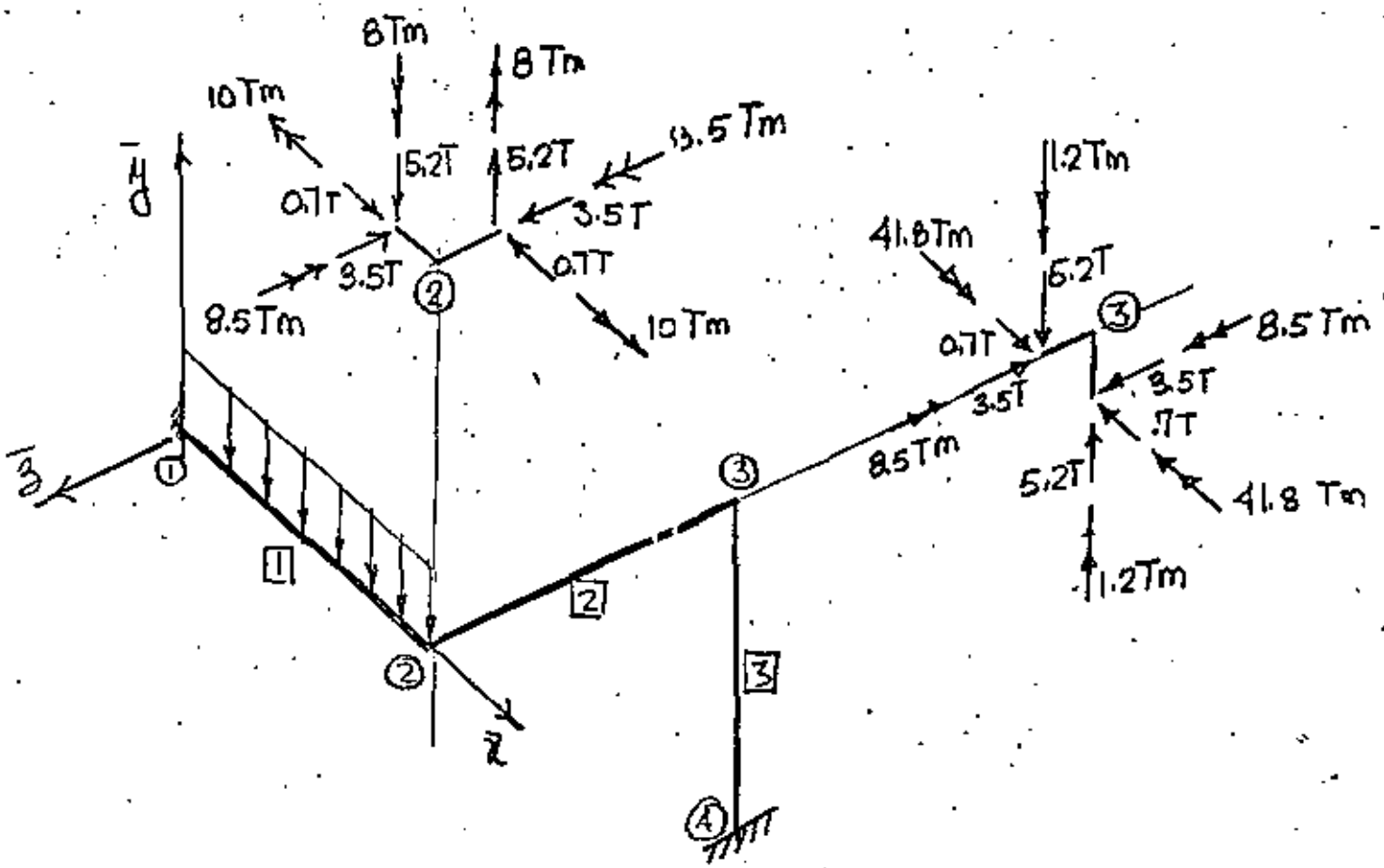

Fig. 2.6 Diagrama de cuerpo libre de los nodos ② y ③

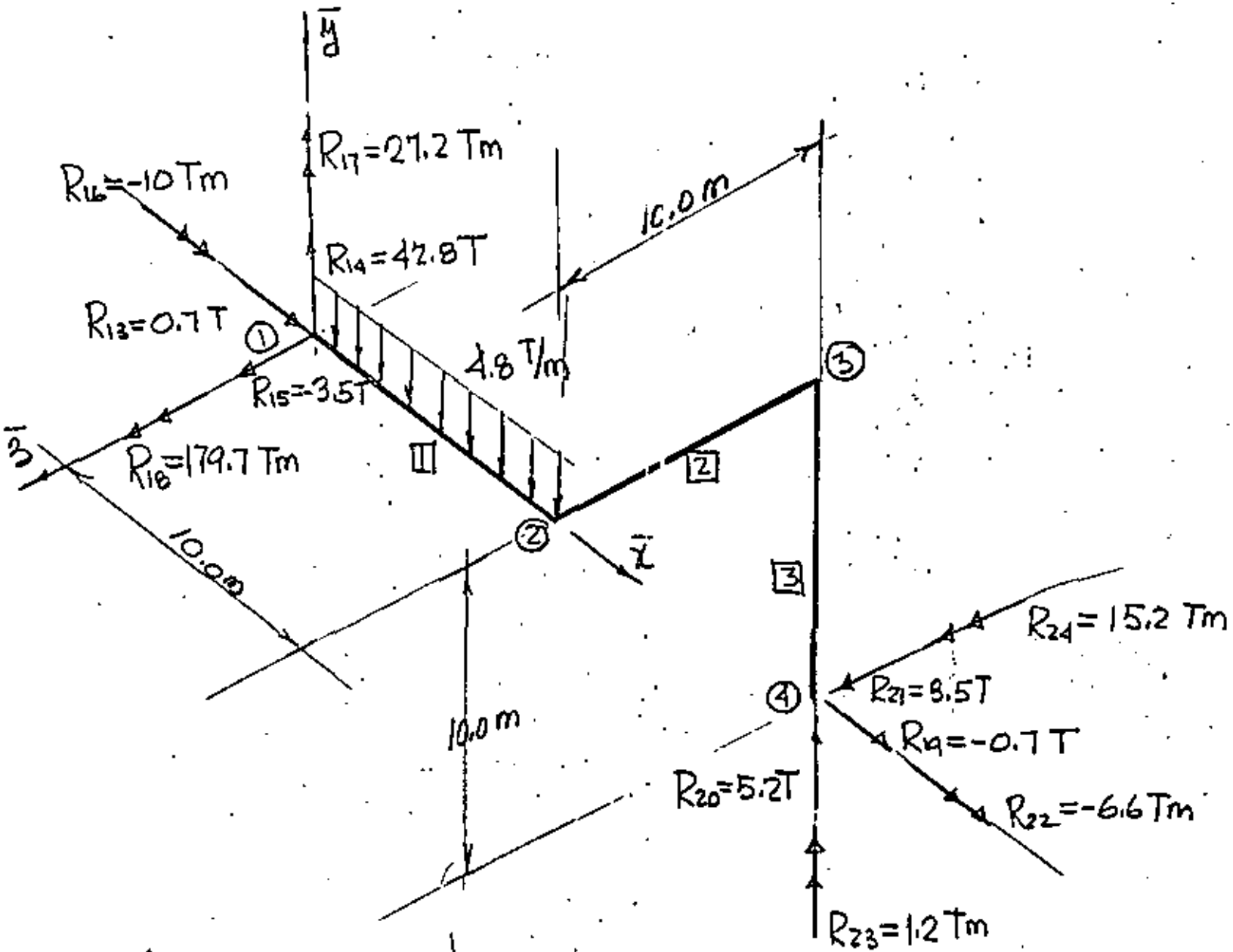

Fig. 2.7 Componentes de las reacciones en los apoyos ① y ④

1.-Introducción.- La naturaleza de las fuerzas que actuan dentro de un cuerpo para equilibrar el efecto de las fuerzas de cuerpo y externas o de superficie, es una de las partes principales del estudio de la mecanica de sólidos. Se aplicará el método de secciones para aislar un elemento diferencial y definir el concepto de esfuerzo.

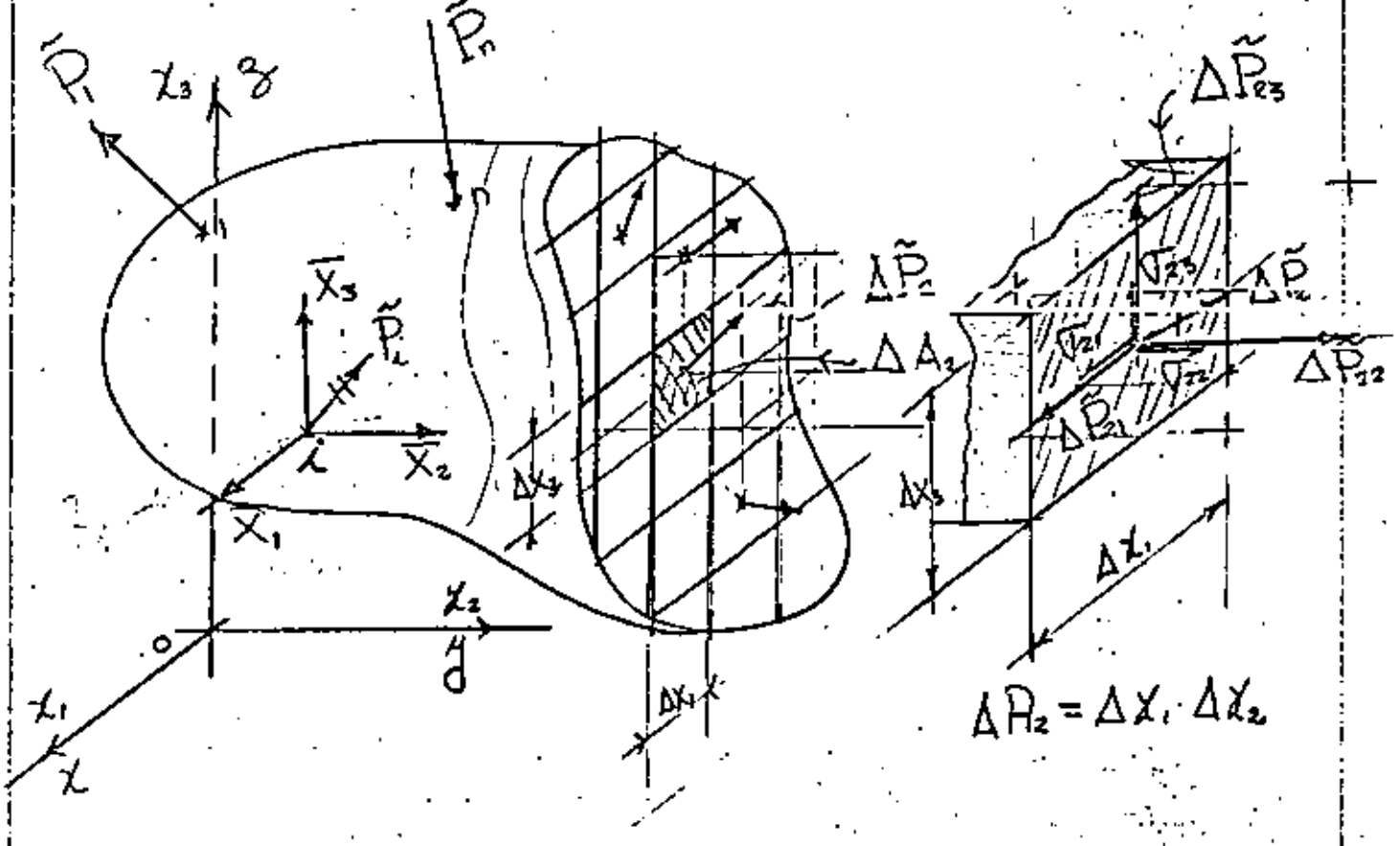

Fig.1 Cuerpo seccionado paralelo al plano x_1, x_3

2.-Definición de esfuerzo.

En general, las fuerzas internas actuando sobre las areas infinitesimales $\Delta x_i \Delta x_j$ del corte, son de

magnitudes y direcciones variables. Fuerzas de naturaleza vectorial y mantienen el equilibrio. En mecánica de sólidos es particularmente significante determinar la intensidad y dirección en distintos puntos a traveg del corte. En general varían de punto a punto en intensidad y dirección. Es usual resolver sus intensidades perpendicular y paralelas a la seccion en consideación. En particular el corte de la Fig.1 es perpendicular al eje χ_1, $\Delta\tilde{P}_2$ es la fuerga resultante que actua sobre $\Delta A_2 = \Delta\chi_1 \Delta\chi_2$, cuyas componentes son: $[\Delta\tilde{P}_{21}\ \Delta\tilde{P}_{22}\ \Delta\tilde{P}_{23}]$, el primer subindice significa que el plano en que actuan es perpedicular al eje χ_2 y el segundo respecto al eje que son paralelos, Puesto que las componentes de fuerza por unidad de area, son correctas solo en el punto, la definición matemática de esfuergo es *

$$\sigma_{21} = \lim_{\Delta A_2 \to 0} \frac{\Delta\tilde{P}_{21}}{\Delta A_2}\ ,\quad \sigma_{22} = \lim_{\Delta A_2 \to 0} \frac{\Delta\tilde{P}_{22}}{\Delta A_2}\ ,\quad \sigma_{23} = \lim_{\Delta A_2 \to 0} \frac{\Delta\tilde{P}_{23}}{\Delta A_2}$$

similarmente los esfuergos actuando en un plano perpendicular a χ_1 son

$$\sigma_{11} = \lim_{\Delta A_1 \to 0} \frac{\Delta\tilde{P}_{11}}{\Delta A_1}\ ,\quad \sigma_{12} = \lim_{\Delta A_1 \to 0} \frac{\Delta\tilde{P}_{12}}{\Delta A_1}\ ,\quad \sigma_{13} = \lim_{\Delta A_1 \to 0} \frac{\Delta\tilde{P}_{13}}{\Delta A_1}\ ,$$

y los esfuergos actuando sobre un plano perpendicular a χ_3 son

$$\sigma_{31} = \lim_{\Delta A_3 \to 0} \frac{\Delta\tilde{P}_{31}}{\Delta A_3}\ ,\quad \sigma_{32} = \lim_{\Delta A_3 \to 0} \frac{\Delta\tilde{P}_{32}}{\Delta A_3}\ ,\quad \sigma_{33} = \lim_{\Delta A_3 \to 0} \frac{\Delta\tilde{P}_{33}}{\Delta A_3}$$

---

* Cuando $\Delta A_i \to 0$, existen preguntas desde el punto de vista atómico en definir esfuergo en esta forma. Sin embargo, un modelo homogeneo para materia molecular no homogenea trabaja bien en problemas de Ingeniería

Se observa que las definiciones de esfuerzo normal y cortante representan la intensidad de una fuerza sobre una area, y sus unidades son de $\left[\frac{F}{L^2}\right]$; en el sistema métrico Kg/cm^2 o ton/cm^2 y en el Ingles lbs/pul^2 o $Kips/pul^2$.

Debe notarse que los esfuerzos multiplicados multiplicado por las areas sobre las cuales actuan nos dan fuerzas, y es la suma de estas fuerzas, y es la suma de estas fuerzas sobre cualquier corte imaginario lo que conserva el equilibrio de un cuerpo

3. Tensor de esfuerzos.

Si, además del diagrama de cuerpo libre de la Fig. 1.1 se hacen pasar tres pares de planos paralelos y separados por distancias infinitesimales, un cubo de dimensiones infinitesimales sera aislado del cuerpo con el origen del sistema local coordenado en el punto de coordenadas $x_i(x_1, x_2, x_3)$. Tal cubo se muestra en la Fig. 3.1

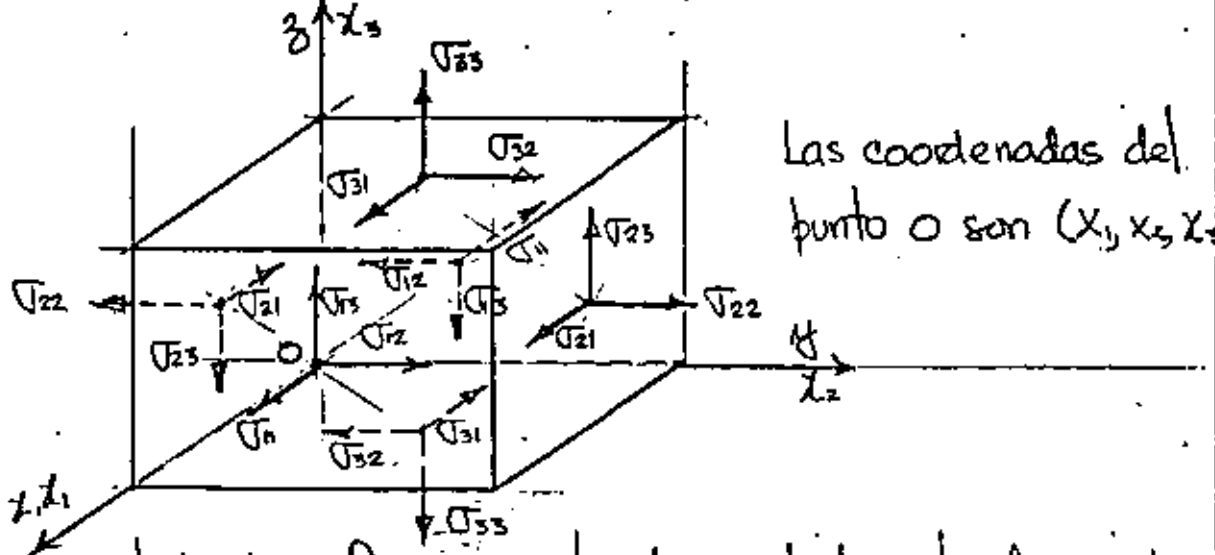

Las coordenadas del punto O son (X_1, X_2, X_3)

Fig. 3.1 Estado de esfuerzos actuando en el elemento dx_i. El sentido indicado es convencionalmente el positivo.

Examinando la Fig. 3.1, se observa que hay tres esfuerzos normales $\sigma_{11}, \sigma_{22}, \sigma_{33}$, y seis esfuerzos cortantes $\sigma_{12}, \sigma_{21}, \sigma_{23}, \sigma_{32}, \sigma_{31}, \sigma_{13}$. El arreglo matricial

$$\underline{\sigma} \equiv [\sigma_{ij}] \equiv [\sigma] = \begin{bmatrix} \sigma_{11} & \sigma_{12} & \sigma_{13} \\ \sigma_{21} & \sigma_{22} & \sigma_{23} \\ \sigma_{31} & \sigma_{32} & \sigma_{33} \end{bmatrix} \qquad (3.1)$$

es la representación del tensor de esfuerzos. Es un tensor de segundo orden referido al espacio Euclidiano tridimensional. Un vector es un tensor de primer orden y un escalar es un tensor de cero orden

4.- Fuerzas de cuerpo y fuerzas de superficie

En el mismo elemento diferencial consideremos el vector de fuerzas de cuerpo por unidad de volumen $\{X_i\}^T = [X_1\ X_2\ X_3]$, y en consideraciones no polares el vector de momentos de cuerpo por unidad de volumen $\{m_i\}^T = [m_1\ m_2\ m_3]$ actuando en el centroide del elemento diferencial como se indica en la Fig. 4.1

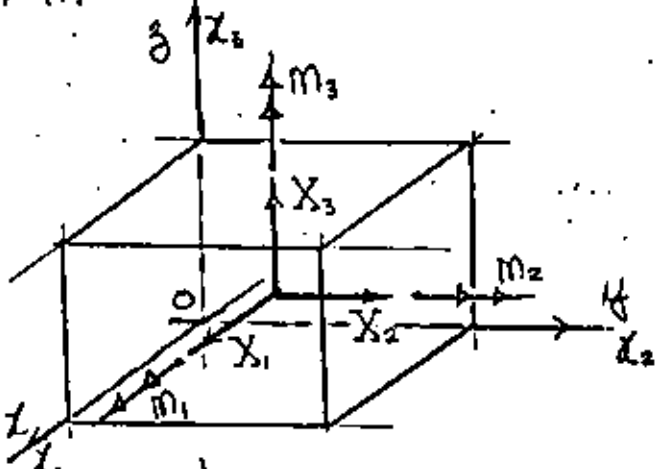

Fig. 4.1 Fuerzas y momentos de cuerpo por unidad de volumen $\{X_i\}$ y $\{m_i\}$ actuando en el centro de gravedad de dx_i.

en donde $X_i = \rho(f_i - a_i)$ (4.1)

donde ρ es la densidad o masa especifica, f_i es la fuerza por unidad de masa en la dirección x_i y a_i es la aceleración del elemento dx_i en la dirección de x_i

2.- Las fuerzas de superficie actuan en la frontera del cuerpo y las tres componentes de $\bar{P}_i$ Fig 1.1 las designaremos por $\{\bar{X}_i\}^T = [\bar{X}_1\ \bar{X}_2\ \bar{X}_3]_i$ sus unidades son fuerza por unidad de area $\left[\frac{F}{L^2}\right]$, Kg/cm² en el sistema métrico y lbs/pul² en el ingles, y en el internacional Newtons/cm². Las unidades de las fuerzas de cuerpo serán $\left[\frac{F}{L^3}\right]$. Las fuerzas de superficie deben satisfacer las condiciones en la frontera [Fig. 5.1] que para el punto i [Fig. 1.1] son

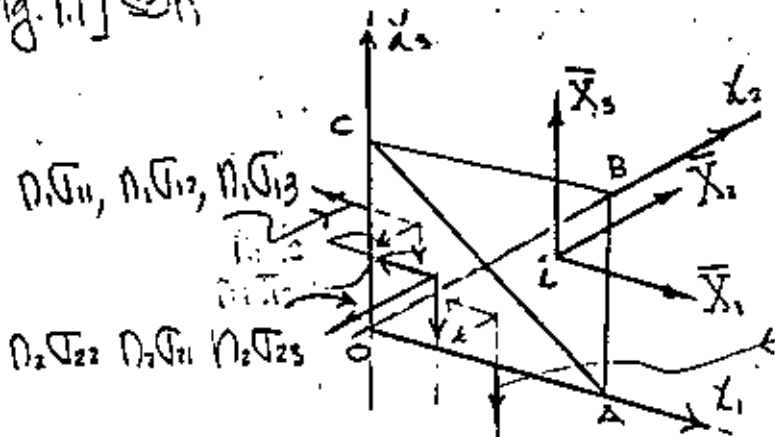

Fig. 5.1 Equilibrio del punto i [Fig. 1.1] en la superficie

Si ABC = unidad, $OBC = \cos\phi = n_1$, $OAC = \cos\beta = n_2$, y $OAB = \cos\gamma = n_3$, donde $\{n_i\}^T = [n_1\ n_2\ n_3]$ son los cosenos directores de la normal al plano ABC, y del equilibrio de OABC se obtiene

$$\begin{bmatrix} \sigma_{11} & \sigma_{21} & \sigma_{31} \\ \sigma_{12} & \sigma_{22} & \sigma_{32} \\ \sigma_{13} & \sigma_{23} & \sigma_{33} \end{bmatrix} \begin{Bmatrix} n_1 \\ n_2 \\ n_3 \end{Bmatrix} = \begin{Bmatrix} \bar{X}_1 \\ \bar{X}_2 \\ \bar{X}_3 \end{Bmatrix} \quad \text{o} \quad [\sigma_{ij}]^T \{n_i\} = \{\bar{X}_i\} \quad (4.1)$$

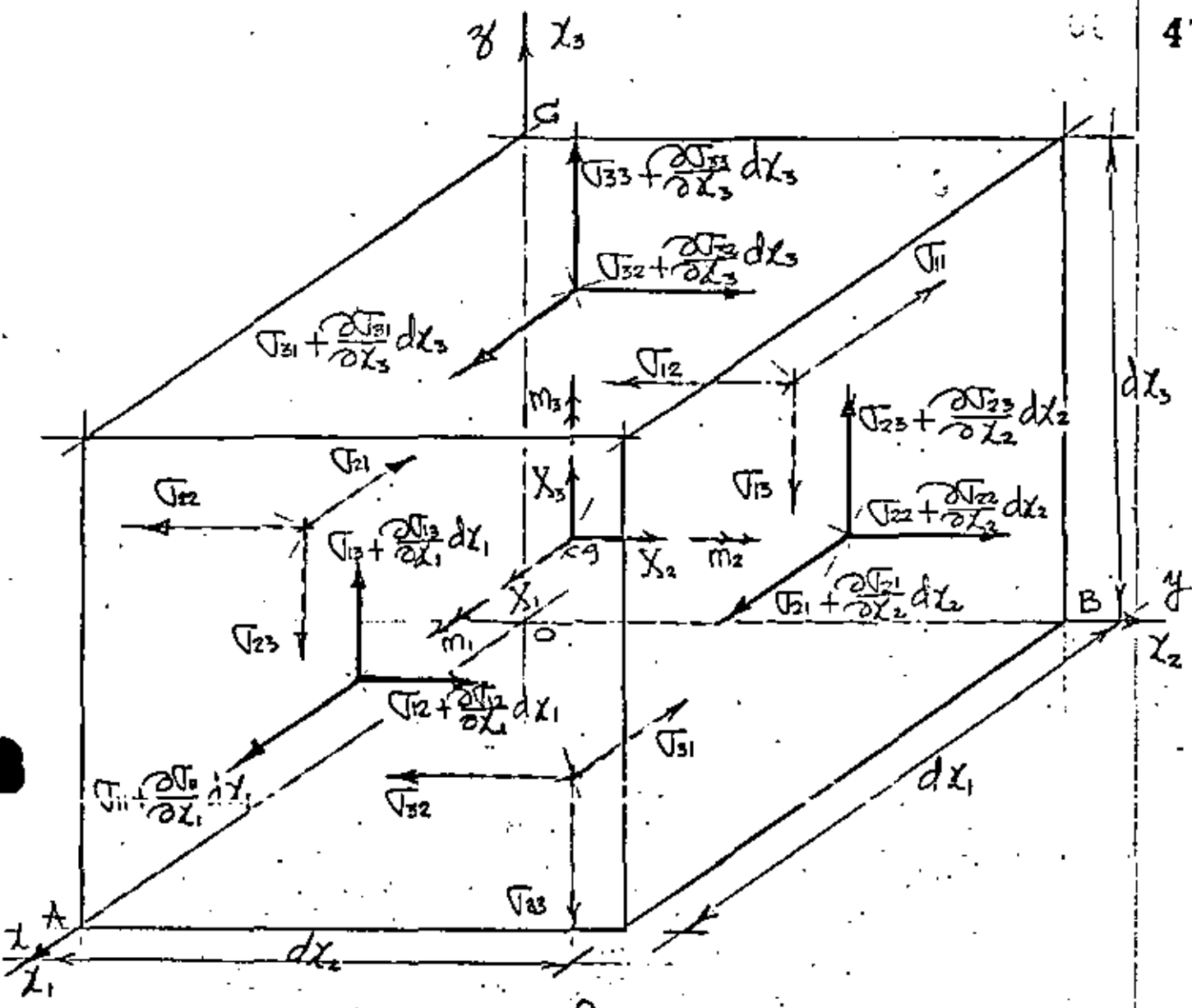

Fig. 5.1. Equilibrio de esfuerzos $[\sigma]$, fuerzas de cuerpo $\{X\}$ y momentos de cuerpo $\{m\}$, en el elemento dx_i

(4.1) es la representación matricial de las condiciones de equilibrio del punto i en la frontera x_i.

5.- Equilibrio del elemento dx_i.

Las seis ecuaciones de equilibrio del elemento de la Fig. 5.1 son

$$\sum F_{x_1}=\sum F_{x_2}=\sum F_{x_3}=\sum M_{x_1}=\sum M_{x_2}=\sum M_{x_3}=0 \qquad (5.1)$$

de $\sum F_{x_1}=0$, en el límite cuando $dx_i \to 0$ se obtiene

$$\left(\sigma_{11}+\frac{\partial \sigma_{11}}{\partial x_1}dx_1\right)dx_2dx_3-\sigma_{11}dx_2dx_3+\left(\sigma_{21}+\frac{\partial \sigma_{21}}{\partial x_2}dx_2\right)dx_1dx_3$$

$$-\sigma_{21}dx_1dx_3+\left(\sigma_{31}+\frac{\partial \sigma_{31}}{\partial x_3}\right)dx_1dx_2-\sigma_{31}dx_1dx_2+X_1dx_1dx_2dx_3=0$$

efectuando operaciones algebráicas se obtiene

$$\frac{\partial \sigma_{11}}{\partial x_1}+\frac{\partial \sigma_{21}}{\partial x_2}+\frac{\partial \sigma_{31}}{\partial x_3}+X_1=0$$

Similar mente de $\sum F_{x_2}=0$, $\frac{\partial \sigma_{12}}{\partial x_1}+\frac{\partial \sigma_{22}}{\partial x_2}+\frac{\partial \sigma_{32}}{\partial x_3}+X_2=0$ (5.2)

de $\sum F_{x_3}=0$, $\frac{\partial \sigma_{13}}{\partial x_1}+\frac{\partial \sigma_{23}}{\partial x_2}+\frac{\partial \sigma_{33}}{\partial x_3}+X_3=0$

De $\sum M_{x_1}=0$, en el límite cuando $dx_i \to 0$, y considerando el eje de momentos paralelo a ox_1 y a traves del centroide del elemento dx_i, y despreciando los diferenciales de segundo orden dx_i^2, se obtiene bajo la convención de signos de la Fig. 5.1 lo siguiente

$$\left(\sigma_{23}+\frac{\partial \sigma_{23}}{\partial x_2}dx_2\right)dx_1dx_3\frac{dx_2}{2}+\sigma_{23}dx_1dx_3\frac{dx_2}{2}$$

$$-\left(\sigma_{32}+\frac{\partial \sigma_{32}}{\partial x_3}dx_3\right)dx_1dx_2\frac{dx_3}{2}-\sigma_{32}dx_1dx_2\frac{dx_3}{2}+m_1dx_1dx_2dx_3=0$$

efectuando operaciones algebraicas se obtiene

$$\sigma_{23}-\sigma_{32}+m_1=0$$

Similarmente de $\sum M_{x_2}=0$, $\sigma_{31}-\sigma_{13}+m_2=0$ (5.3)

y de $\sum M_{x_3}=0$, $\sigma_{12}-\sigma_{21}+m_3=0$

Las ecuaciones (5.2) y (5.3) son las seis ecuaciones de equilibrio en coordenadas rectangulares y en su forma polar, generalmente los momentos de cuerpo $m_i=0$

Expresando (5.2) matricialmente se tiene

$$\left[\frac{\partial}{\partial x_1}\ \frac{\partial}{\partial x_2}\ \frac{\partial}{\partial x_3}\right]\begin{bmatrix}\sigma_{11} & \sigma_{12} & \sigma_{13}\\ \sigma_{21} & \sigma_{22} & \sigma_{23}\\ \sigma_{31} & \sigma_{32} & \sigma_{33}\end{bmatrix}+\begin{Bmatrix}X_1\\ X_2\\ X_3\end{Bmatrix}=0 \qquad (5.4)$$

o

$$\left[\frac{\partial}{\partial x_i}\right]\left[\sigma_{ij}\right]+\{X_i\}=0 \qquad (5.5)$$

Con notación índice (5.2) se representa

$$\sigma_{ij,i}+X_j=0 \qquad (5.6)$$

en donde $\sigma_{ij,i}=\frac{\partial \sigma_{ij}}{\partial x_i}$. Y las ecuaciones (5.3)

$$\sigma_{ij}-\sigma_{ji}+m_k=0 \qquad (5.7)$$

6. Diferentes notaciones del tensor de esfuerzos.

A continuación gráficamente mostraremos las diferentes notaciones que han sido utilizadas para representar las componentes del tensor de esfuerzos.

6.1 Cauchy inicialmente.

$$\begin{bmatrix}A & F & E\\ F & B & D\\ E & D & C\end{bmatrix} \qquad (m_k=0)$$

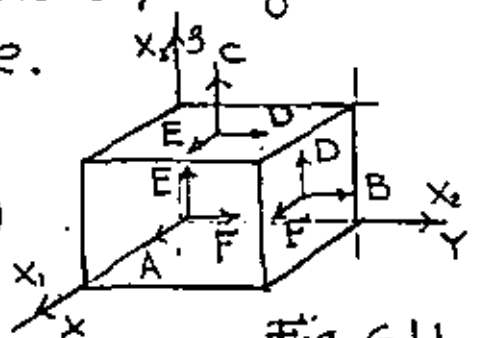

Fig. 6.1.1

6.2 Kelvin.

$$\begin{bmatrix}P & V & T\\ V & Q & S\\ T & S & R\end{bmatrix} \qquad (m_k=0)$$

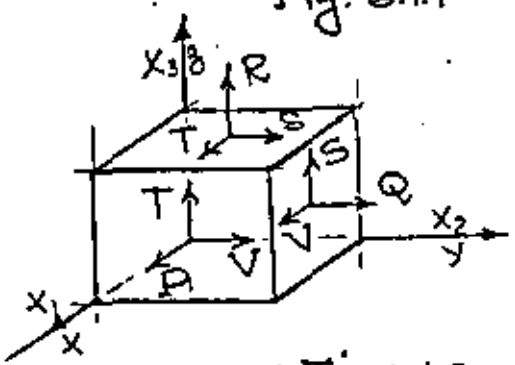

Fig. 6.1.2

6.2 Cauchy posteriormente, Saint-Venant ó Maxwel, introducen por primera vez la notación cartesiana, y

$$\begin{bmatrix} P_{xx} & P_{xy} & P_{xz} \\ P_{yx} & P_{yy} & P_{yz} \\ P_{zx} & P_{zy} & P_{zz} \end{bmatrix} \quad (m_k \neq 0)$$

condiciones polares.

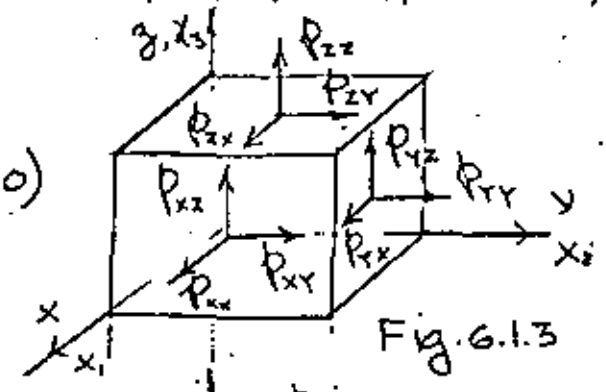

Fig. 6.1.3

6.3 Newman, Kirchhof y Love.

$$\begin{bmatrix} X_x & X_y & X_z \\ Y_x & Y_y & Y_z \\ Z_x & Z_y & Z_z \end{bmatrix} \quad (m_k \neq 0)$$

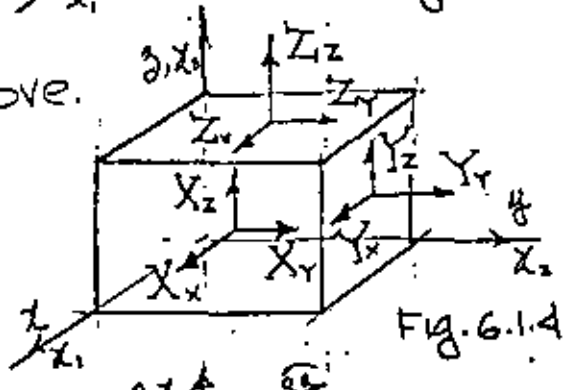

Fig. 6.1.4

6.4 K. Pearson.

$$\begin{bmatrix} \widehat{xx} & \widehat{xy} & \widehat{xz} \\ \widehat{yx} & \widehat{yy} & \widehat{yz} \\ \widehat{zx} & \widehat{zy} & \widehat{zz} \end{bmatrix} \quad (m_k \neq 0)$$

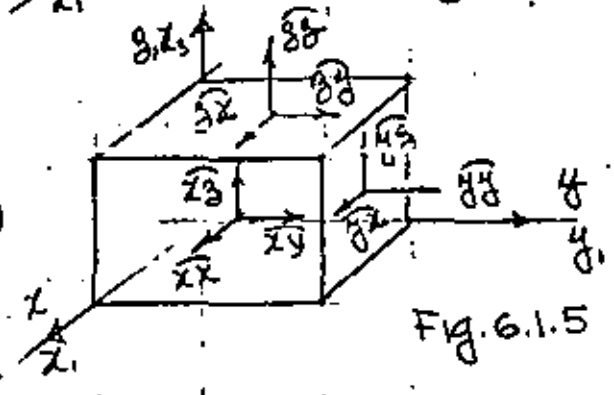

Fig. 6.1.5

6.5 S. Timoshenko y T. Von Karmán introducen la notación de Ingeniería, simplificando la notación cartesiana utilizando solo un subindice en los esfuerzos normales denominándolos por σ, y los tangenciales por τ.

$$\begin{bmatrix} \sigma_x & \tau_{xy} & \tau_{xz} \\ \tau_{yx} & \sigma_y & \tau_{yz} \\ \tau_{zx} & \tau_{zy} & \sigma_z \end{bmatrix} \quad (m_k \neq 0)$$

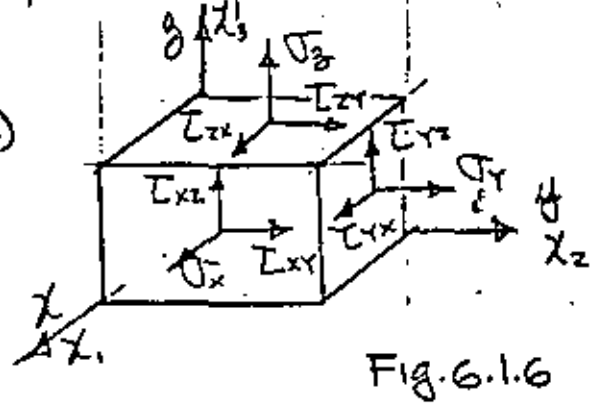

Fig. 6.1.6

6.6 Green, Zerna y autores Rusos introducen notación indice similar a la utiligada previamente 51

$$[T_{ij}] \equiv [\tau_{ij}]$$

6.7 Cleibsch, C. Truesdell y A.C. Eringen, también utiligan la notación indice representando el tensor de esfuergos

$$[t_{ij}]$$

6.8 D.C. Leigh; y L. Malvern, también utiligan notación indice representando el tensor de esfuergos como

$$[T_{ij}]$$

Es importante observar que en la derivación de l... ecuaciones de equilibrio (5.6) y (5.7) las propiedades mecánicas del material no han sido usadas. Lo cual significa que son aplicables a materiales elásticos, plásticos, o viscoelasticos. También es muy importante observar que no hay suficientes ecuaciones de equilibrio para determinar las incógnitas esfuergo, el problema es estáticamente indeterminado.

7. Desplazamiento, deformación.

El analisis de la deformación de un sólido es de importancia paralela al analisis de esfuergos. Requiere la definición precisa de deformación, la cual significa la intensidad del desplazamiento. Un cuerpo sólido sujeto a un cambio de temperatura o a cargas externas.

Por ejemplo, si una muestra es sujeta a una fuerza P como se muesta en la Fig. 7.1, Un cambio de longitud ocurre entre los dos puntos de calibración A y B. Si l_o es la longitud inicial y l la longitud observada bajo la carga P, y el alargamiento $\Delta l = l - l_o$. El

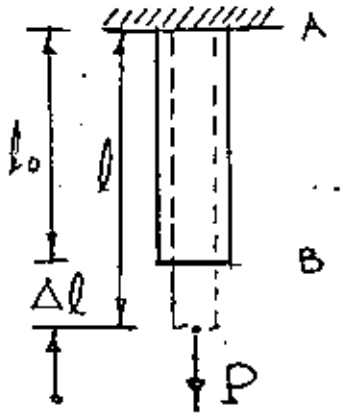

Fig. 7.1 Muestra a tensión.

alargamiento por unidad de longitud ε (epsilon) es

$$\varepsilon = \int_{l_o}^{l} \frac{dl}{l_o} = \frac{l - l_o}{l_o} = \frac{\Delta l}{l_o} \qquad (7.1)$$

el cual es llamado deformación lineal. Es una cantidad adimensional, pero generalmente se mide o se refiere en $\frac{cm}{cm}$ o $\frac{pulg}{pulg}$. Algunas veces se expresa en porciento. La cantidad ε es generalmente muy pequeño. En la mayoría de las aplicaciones de ingeniería tiene un orden máximo de magnitud de 0.001. Cuando las deformaciones son grandes, por ejemplo, en formado de metales, se introduce el la deformación natural que implica una lo variable, dada por

$$\bar{\varepsilon} = \int_{l_o}^{l} \frac{dl}{l} = \ln \frac{l}{l_o} = \ln(1+\varepsilon) \qquad (7.2)$$

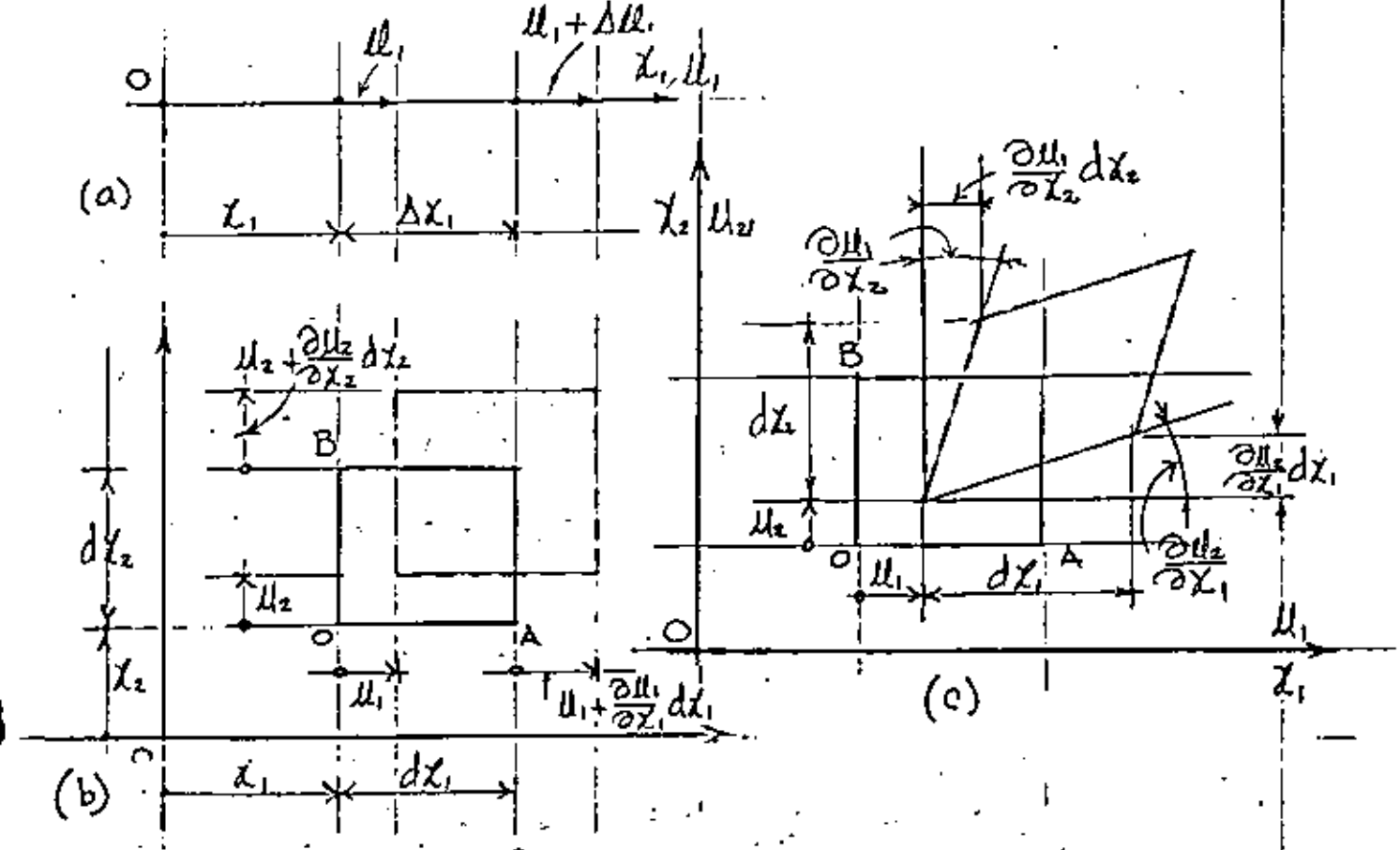

Fig. 7.2 Elementos deformados en posisiones inicial y final

Sea el vector de desplazamientos $\{u_i\}^T = \lfloor u_1\ u_2\ u_3 \rfloor$ en las direcciones x_1 x_2 y x_3 respectivamente, en base a los desplazamientos mostrados en la Fig. 7.2a, la definición de deformación lineal es

$$\varepsilon_{11} = \lim_{\Delta x_1 \to 0} \frac{u_1 + \Delta u_1 - u_1}{\Delta x_1} = \frac{\partial u_1}{\partial x_1} \equiv u_{1,1} \qquad (7.2)$$

Similarmente

$$\varepsilon_{22} = \frac{\partial u_2}{\partial x_2} \equiv u_{2,2}\ , \quad \varepsilon_{33} = \frac{\partial u_3}{\partial x_3} \equiv u_{3,3} \qquad (7.3)$$

el signo positivo significa alargamientos. El elemento también experimenta deformaciones de cortante como

se muestra en la Fig. 7.2c el ángulo recto AOB es reducido por la cantidad $\frac{\partial u_1}{\partial x_2} + \frac{\partial u_2}{\partial x_1}$. Por lo tanto, para pequeños cambios del ángulo, la definición de deformación de cortante asociada con el plano x_1, x_2 es

$$\gamma_{12} = \gamma_{21} = \frac{\partial u_1}{\partial x_2} + \frac{\partial u_2}{\partial x_1} \equiv u_{1,2} + u_{2,1}$$, analogamente con los otros planos, $\gamma_{23} = \gamma_{32} = \frac{\partial u_2}{\partial x_3} + \frac{\partial u_3}{\partial x_2} \equiv u_{3,2} + u_{2,3}$ (7.4)

$$\gamma_{31} = \gamma_{13} = \frac{\partial u_3}{\partial x_1} + \frac{\partial u_1}{\partial x_3} \equiv u_{3,1} + u_{1,3}$$

en el caso que las deformaciones no sean pequeñas, se demuestra facilmente que

$$\varepsilon_{11} = \frac{\partial u_1}{\partial x_1} + \frac{1}{2}\left[\left(\frac{\partial u_1}{\partial x_1}\right)^2 + \left(\frac{\partial u_2}{\partial x_1}\right)^2 + \left(\frac{\partial u_3}{\partial x_3}\right)^2\right]$$

$$\varepsilon_{22} = \frac{\partial u_2}{\partial x_2} + \frac{1}{2}\left[\left(\frac{\partial u_1}{\partial x_2}\right)^2 + \left(\frac{\partial u_2}{\partial x_2}\right)^2 + \left(\frac{\partial u_3}{\partial x_2}\right)^2\right]$$

$$\varepsilon_{33} = \frac{\partial u_3}{\partial x_3} + \frac{1}{2}\left[\left(\frac{\partial u_1}{\partial x_3}\right)^2 + \left(\frac{\partial u_2}{\partial x_3}\right)^2 + \left(\frac{\partial u_3}{\partial x_3}\right)^2\right] \quad (7.5)$$

$$\gamma_{12} = \frac{\partial u_1}{\partial x_2} + \frac{\partial u_2}{\partial x_1} + \frac{\partial u_1}{\partial x_1}\cdot\frac{\partial u_1}{\partial x_2} + \frac{\partial u_2}{\partial x_1}\cdot\frac{\partial u_2}{\partial x_2} + \frac{\partial u_3}{\partial x_1}\cdot\frac{\partial u_3}{\partial x_2}$$

$$\gamma_{23} = \frac{\partial u_2}{\partial x_3} + \frac{\partial u_3}{\partial x_2} + \frac{\partial u_1}{\partial x_2}\cdot\frac{\partial u_1}{\partial x_3} + \frac{\partial u_2}{\partial x_2}\cdot\frac{\partial u_2}{\partial x_3} + \frac{\partial u_3}{\partial x_2}\cdot\frac{\partial u_3}{\partial x_3}$$

$$\gamma_{31} = \frac{\partial u_3}{\partial x_1} + \frac{\partial u_1}{\partial x_3} + \frac{\partial u_1}{\partial x_1}\cdot\frac{\partial u_1}{\partial x_3} + \frac{\partial u_2}{\partial x_1}\cdot\frac{\partial u_2}{\partial x_3} + \frac{\partial u_3}{\partial x_1}\cdot\frac{\partial u_3}{\partial x_3}$$

En las ecuaciones (7.5) aplicables a deformaciones grandes ya se observa la no linearidad en geometría. (7.4) es un caso particular de (7.5) cuando los términos de segundo grado son despreciables respecto a los de primer grado. o sea pequeñas deformaciones. (7.5) en

notación compacta queda:

$$\varepsilon_{11} = u_{1,1} + \frac{1}{2}(u_{1,1}^2 + u_{2,1}^2 + u_{3,1}^2)$$
$$\varepsilon_{22} = u_{2,2} + \frac{1}{2}(u_{1,2}^2 + u_{2,2}^2 + u_{3,2}^2)$$
$$\varepsilon_{33} = u_{3,3} + \frac{1}{2}(u_{1,3}^2 + u_{2,3}^2 + u_{3,3}^2) \qquad (7.6)$$

$$\gamma_{12} = \gamma_{21} = u_{1,2} + u_{2,1} + u_{1,1}u_{1,2} + u_{2,1}u_{2,2} + u_{3,1}u_{3,2}$$
$$\gamma_{23} = \gamma_{32} = u_{2,3} + u_{3,2} + u_{1,2}u_{1,3} + u_{2,2}u_{2,3} + u_{3,2}u_{3,3}$$
$$\gamma_{31} = \gamma_{13} = u_{3,1} + u_{1,3} + u_{1,1}u_{1,3} + u_{2,1}u_{2,3} + u_{3,1}u_{3,3}$$

Examinando las ecuaciones deformación-desplazamiento para pequeñas deformaciones (7.2), (7.3) y (7.4), se observa que son seis ecuaciones que dependen solamente de tres desplazamientos u_1, u_2 y u_3. Por lo tanto las ecuaciones no pueden ser independientes. Por lo tanto seis ecuaciones independientes pueden desarrollarse relacionando a $\varepsilon_{11}, \varepsilon_{22}, \varepsilon_{33}, \gamma_{12}, \gamma_{23}$ y γ_{31}, ecuaciones conocidas como ecuaciones de compatibilidad.

$$\frac{\partial^2\varepsilon_{11}}{\partial x_2^2} + \frac{\partial^2\varepsilon_{22}}{\partial x_1^2} = \frac{\partial^2\gamma_{12}}{\partial x_1 \partial x_2} \quad ; \quad 2\frac{\partial^2\varepsilon_{11}}{\partial x_2 \partial x_3} = \frac{\partial}{\partial x_1}\left(-\frac{\partial\gamma_{23}}{\partial x_1} + \frac{\partial\gamma_{13}}{\partial x_2} + \frac{\partial\gamma_{12}}{\partial x_3}\right)$$
$$\frac{\partial^2\varepsilon_{11}}{\partial x_3^2} + \frac{\partial^2\varepsilon_{33}}{\partial x_1^2} = \frac{\partial^2\gamma_{13}}{\partial x_1 \partial x_3} \quad ; \quad 2\frac{\partial^2\varepsilon_{22}}{\partial x_1 \partial x_3} = \frac{\partial}{\partial x_2}\left(\frac{\partial\gamma_{23}}{\partial x_1} - \frac{\partial\gamma_{13}}{\partial x_2} + \frac{\partial\gamma_{12}}{\partial x_3}\right) \qquad (7.7)$$
$$\frac{\partial^2\varepsilon_{22}}{\partial x_3^2} + \frac{\partial^2\varepsilon_{33}}{\partial x_2^2} = \frac{\partial^2\gamma_{23}}{\partial x_2 \partial x_3} \quad ; \quad 2\frac{\partial^2\varepsilon_{33}}{\partial x_1 \partial x_2} = \frac{\partial}{\partial x_3}\left(\frac{\partial\gamma_{23}}{\partial x_1} + \frac{\partial\gamma_{13}}{\partial x_2} - \frac{\partial\gamma_{12}}{\partial x_3}\right)$$

sustituyendo (7.2), (7.3) y (7.4) en (7.7) se verifican las ecuaciones de compatibilidad de pequeñas deformaciones.

Similarmente a las componentes del Tensor de esfuerzos en las notaciones indice, cartesiana y de ingeniería, se representan las componentes del tensor de deformaciones como

56

$$[\varepsilon_{ij}] \equiv \underline{\underline{\varepsilon}} = \begin{bmatrix} \varepsilon_{11} & \varepsilon_{12} & \varepsilon_{13} \\ \varepsilon_{21} & \varepsilon_{22} & \varepsilon_{23} \\ \varepsilon_{31} & \varepsilon_{32} & \varepsilon_{33} \end{bmatrix} \equiv \begin{bmatrix} \varepsilon_{xx} & \varepsilon_{xy} & \varepsilon_{xz} \\ \varepsilon_{yx} & \varepsilon_{yy} & \varepsilon_{yz} \\ \varepsilon_{zx} & \varepsilon_{zy} & \varepsilon_{zz} \end{bmatrix} \equiv \begin{bmatrix} \varepsilon_x & \frac{\gamma_{xy}}{2} & \frac{\gamma_{xz}}{2} \\ \frac{\gamma_{yx}}{2} & \varepsilon_y & \frac{\gamma_{yz}}{2} \\ \frac{\gamma_{zx}}{2} & \frac{\gamma_{zy}}{2} & \varepsilon_z \end{bmatrix} \qquad (7.8)$$

(índice) (cartesiana) (ingeniería)

en (7.8) fué necesario fué necesario modificar las relaciones de deformación por cortante con el objeto de someter al tensor $\underline{\underline{\varepsilon}}$ enteramente obedecer ciertas leyes de transformación, por lo que $\varepsilon_{ij} = \frac{1}{2}\gamma_{ij}$ para toda $i \neq j$. Analogamente al tensor de esfuerzos $[\sigma_{ij}]$ puede diagonalizarse quedando

$$\begin{bmatrix} \sigma_1 & 0 & 0 \\ 0 & \sigma_2 & 0 \\ 0 & 0 & \sigma_3 \end{bmatrix} \qquad (7.9)$$

8. Ley de Hooke en un estado uniaxial de esfuerzos,

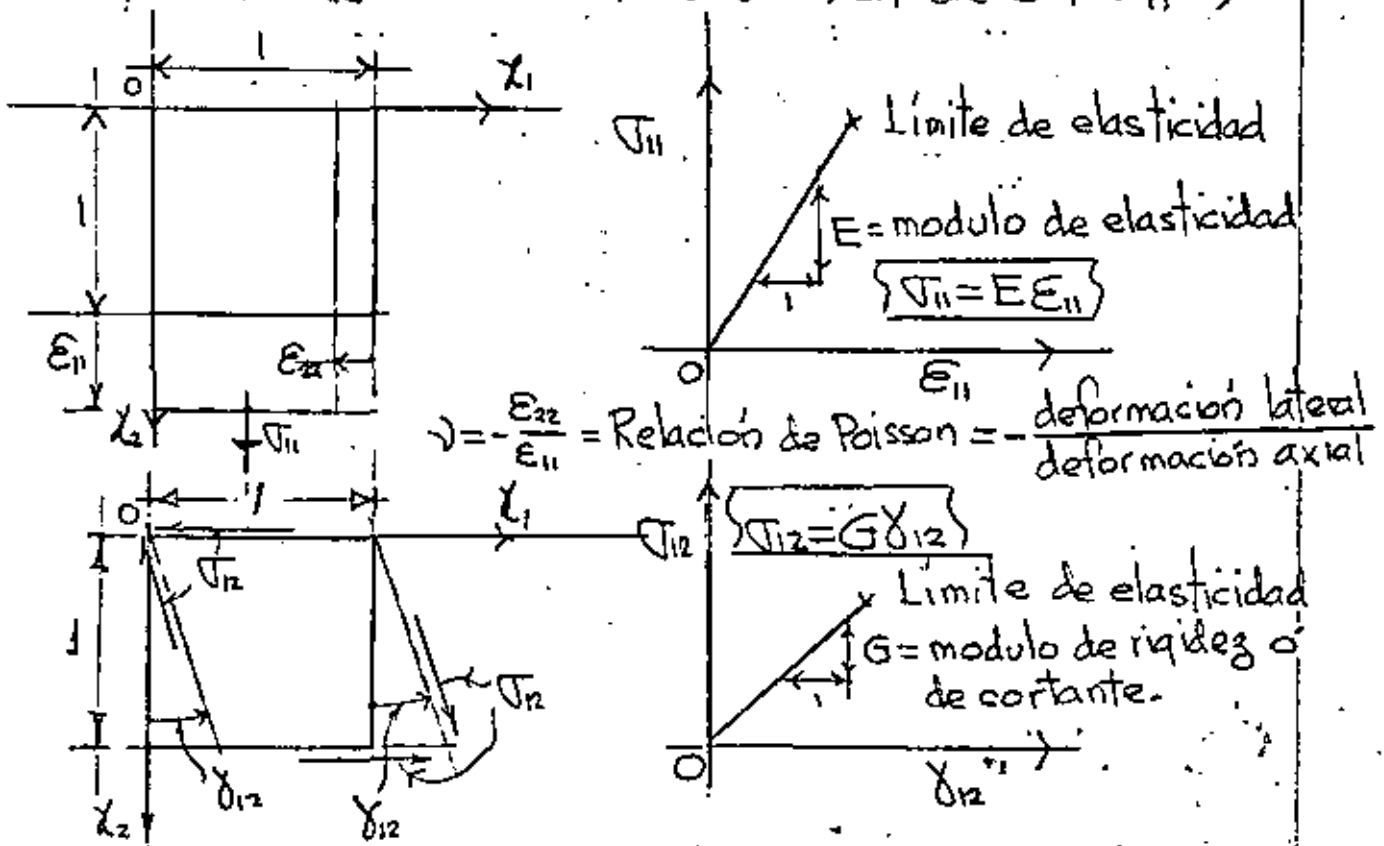

Fig. 8.1 Ley de Hooke en tensión uniaxial σ_{11} y corte puro σ_{12}.

puesto que el sistema es elástico lineal rige el principio de superposición de causas y efectos, por lo tanto en la Fig. 8.2 se considera un estado triaxial llegando a él en tres etapas de carga, etapa 1: actuando σ_{11}, etapa 2: actuando σ_{11} y σ_{22} y etapa 3: actuando σ_{11}, σ_{22} y σ_{33}. Se llega a las siguientes ecuaciones constitutivas

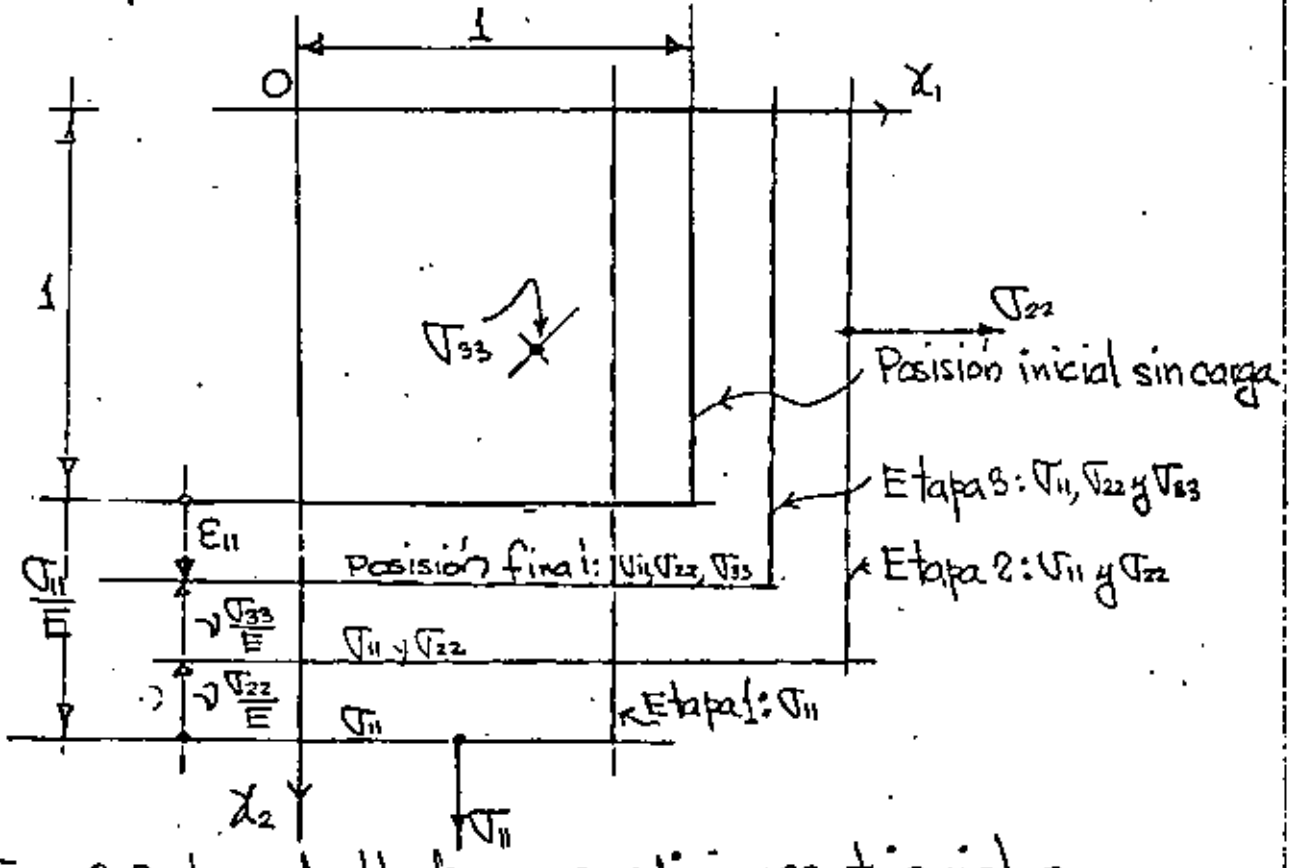

Fig. 8.2 Ley de Hooke en condiciones triaxiales

$$\varepsilon_{11} = \frac{1}{E}\sigma_{11} = \frac{\nu}{E}\sigma_{22} - \frac{\nu}{E}\sigma_{33}$$

$$\varepsilon_{22} = -\frac{\nu}{E}\sigma_{11} + \frac{1}{E}\sigma_{22} - \frac{\nu}{E}\sigma_{33} \qquad (8.1)$$

$$\varepsilon_{33} = -\frac{\nu}{E}\sigma_{11} - \frac{\nu}{E}\sigma_{22} + \frac{1}{E}\sigma_{33}$$

$$\gamma_{12} = \frac{1}{G}\sigma_{12}$$

$$\gamma_{23} = \frac{1}{G}\sigma_{23}$$

$$\gamma_{31} = \frac{1}{G}\sigma_{31}$$

(8.1) representa la ley de Hooke en condiciones triaxiales 58
ó más correctamente las ecuaciones constitutivas para un sólido elástico homogeneo e isotrópico. Las constantes E, G y ν son experimentales y estan relacionadas por

$$G = \frac{E}{2(1+\nu)} \tag{8.2}$$

Substituyendo (8.2) en (8.1) y expresando el resultado matricialmente se obtiene (considerando $\varepsilon_{ij} = \frac{\gamma_{ij}}{2}$ para $i \neq j$)

$$\begin{Bmatrix} \varepsilon_{11} \\ \varepsilon_{22} \\ \varepsilon_{33} \\ \varepsilon_{12} \\ \varepsilon_{23} \\ \varepsilon_{31} \end{Bmatrix} = \frac{1}{E} \begin{bmatrix} 1 & -\nu & -\nu & 0 & 0 & 0 \\ -\nu & 1 & -\nu & 0 & 0 & 0 \\ -\nu & -\nu & 1 & 0 & 0 & 0 \\ 0 & 0 & 0 & 2(1+\nu) & 0 & 0 \\ 0 & 0 & 0 & 0 & 2(1+\nu) & 0 \\ 0 & 0 & 0 & 0 & 0 & 2(1+\nu) \end{bmatrix} \begin{Bmatrix} \sigma_{11} \\ \sigma_{22} \\ \sigma_{33} \\ \sigma_{12} \\ \sigma_{23} \\ \sigma_{31} \end{Bmatrix} \tag{8.3}$$

o

$$\{\varepsilon\} = [C]\{\sigma\} \tag{8.4}$$

despejando $\{\sigma\}$ de (8.4) se obtiene

$$\begin{Bmatrix} \sigma_{11} \\ \sigma_{22} \\ \sigma_{33} \\ \sigma_{12} \\ \sigma_{23} \\ \sigma_{31} \end{Bmatrix} = \frac{E}{(1+\nu)(1-2\nu)} \begin{bmatrix} 1-\nu & \nu & \nu & 0 & 0 & 0 \\ \nu & 1-\nu & \nu & 0 & 0 & 0 \\ \nu & \nu & 1-\nu & 0 & 0 & 0 \\ 0 & 0 & 0 & \frac{1-2\nu}{2} & 0 & 0 \\ 0 & 0 & 0 & 0 & \frac{1-2\nu}{2} & 0 \\ 0 & 0 & 0 & 0 & 0 & \frac{1-2\nu}{2} \end{bmatrix} \begin{Bmatrix} \varepsilon_{11} \\ \varepsilon_{22} \\ \varepsilon_{33} \\ \varepsilon_{12} \\ \varepsilon_{23} \\ \varepsilon_{31} \end{Bmatrix} \tag{8.5}$$

o sea

$$\{\sigma\} = [C]^{-1}\{\varepsilon\} \tag{8.6}$$

Se observa en las ecuaciones anteriores que solo interviene E y ν.

En un medio elástico lineal anisotrópico en las ecuaciones (8.3), aceptando el principio de superposición se expresan

$$\begin{Bmatrix} \varepsilon_{11} \\ \varepsilon_{22} \\ \varepsilon_{33} \\ \varepsilon_{12} \\ \varepsilon_{23} \\ \varepsilon_{31} \end{Bmatrix} = \begin{bmatrix} C_{11} & C_{12} & C_{13} & C_{14} & C_{15} & C_{16} \\ C_{21} & C_{22} & C_{23} & C_{24} & C_{25} & C_{26} \\ C_{31} & C_{32} & C_{33} & C_{34} & C_{35} & C_{36} \\ C_{41} & C_{42} & C_{43} & C_{44} & C_{45} & C_{46} \\ C_{51} & C_{52} & C_{53} & C_{54} & C_{55} & C_{56} \\ C_{61} & C_{62} & C_{63} & C_{64} & C_{65} & C_{66} \end{bmatrix} \begin{Bmatrix} \sigma_{11} \\ \sigma_{22} \\ \sigma_{33} \\ \sigma_{12} \\ \sigma_{23} \\ \sigma_{31} \end{Bmatrix} \qquad (8.7)$$

Las ecuaciones constitutivas (8.7) tienen 36 constantes. Sin embargo a traves de consideraciones energéticas* se demuestra que el numero de constantes es 21 y que $C_{ij} = C_{ji}$ para $i \neq j$, son simétricas respecto a la diagonal principal de (8.7) Todas las constantes C_{ij} deben determinarse experimentalmente: Se supone el material homogéneo, Ejemplos de estos materiales son: concreto, concreto reforzado, madera, plástico reforzado con filamentos, fierro fundido, etc.. Cuando se tienen tres direcciones ortogonales anisotrópicas el material se dice que es ortotrópico, y para estos materiales el número de constantes se reduce solo a nueve constantes independientes.

Haciendo $\lambda = \frac{\nu E}{(1+\nu)(1-2\nu)}$ y considerando (8.2) las

* Sokolnikoff, I.S., "Mathematical Theory of Elasticity", McGraw-Hill, 1956, p. 61.

ecuaciones constitutivas (8.3) con notación índice se escriben* 60

$$\sigma_{ij} = \lambda \delta_{ij} \varepsilon_{kk} + 2G\varepsilon_{ij} \quad (i,j,k = 1,2,3) \tag{8.8}$$

donde, $\delta_{ij} = 1$ para $i=j$, y $\delta_{ij}=0$ para $i \neq j$, y $\varepsilon_{kk} = \varepsilon_{11} + \varepsilon_{22} + \varepsilon_{33} \equiv e$. Desarrollando (8.8) se tiene

$$\begin{aligned}
&\text{para } i=1, j=1, \quad \sigma_{11} = \lambda e + 2G\varepsilon_{11} \equiv \lambda e + 2G\varepsilon_x = \sigma_x \\
&i=2, j=2, \quad \sigma_{22} = \lambda e + 2G\varepsilon_{22} \equiv \lambda e + 2G\varepsilon_y = \sigma_y \\
&i=3, j=3, \quad \sigma_{33} = \lambda e + 2G\varepsilon_{33} \equiv \lambda e + 2G\varepsilon_z = \sigma_z \\
&i=1, j=2, \quad \sigma_{12} = 2G\varepsilon_{12} \equiv 2G\varepsilon_{xy} = G\gamma_{xy} = \tau_{xy} \\
&i=2, j=3, \quad \sigma_{23} = 2G\varepsilon_{23} \equiv 2G\varepsilon_{yz} = G\gamma_{yz} = \tau_{yz} \\
&i=3, j=1, \quad \sigma_{31} = 2G\varepsilon_{31} \equiv 2G\varepsilon_{zx} = G\gamma_{zx} = \tau_{zx}
\end{aligned} \tag{8.9}$$

Si en el sólido existe un incremento de temperatura ΔT, siendo α el coeficiente de expansión térmica las ecuaciones (8.3) quedan

$$\begin{Bmatrix} \varepsilon_{11} \\ \varepsilon_{22} \\ \varepsilon_{33} \\ \varepsilon_{12} \\ \varepsilon_{23} \\ \varepsilon_{31} \end{Bmatrix} = \frac{1}{E} \begin{bmatrix} 1 & -\nu & -\nu & 0 & 0 & 0 \\ -\nu & 1 & -\nu & 0 & 0 & 0 \\ -\nu & -\nu & 1 & 0 & 0 & 0 \\ 0 & 0 & 0 & 2(1+\nu) & 0 & 0 \\ 0 & 0 & 0 & 0 & 2(1+\nu) & 0 \\ 0 & 0 & 0 & 0 & 0 & 2(1+\nu) \end{bmatrix} \begin{Bmatrix} \sigma_{11} \\ \sigma_{22} \\ \sigma_{33} \\ \sigma_{12} \\ \sigma_{23} \\ \sigma_{31} \end{Bmatrix} + \alpha \Delta T \begin{Bmatrix} 1 \\ 1 \\ 1 \\ 0 \\ 0 \\ 0 \end{Bmatrix} \quad (a)$$

*Green, A.E., and W. Zerna: "Theoretical Elasticity", Oxford University Press, Fair Lawn, N.J. 1970.

9. Elasticidad bidimensional.

Utilizando la notación de Timoshenko y Von Karman ó la notación de ingeniería las ecuaciones de equilibrio en un elemento $dx\,dy$ se reducen a

$$\frac{\partial \sigma_x}{\partial x} + \frac{\partial \tau_{xy}}{\partial y} + X = 0 \qquad (9.1)$$

$$\frac{\partial \tau_{xy}}{\partial x} + \frac{\partial \sigma_y}{\partial y} + Y = 0$$

(9.1) matricialmente queda

$$\begin{bmatrix} \frac{\partial}{\partial x} & \frac{\partial}{\partial y} \end{bmatrix} \begin{bmatrix} \sigma_x & \tau_{xy} \\ \tau_{yx} & \sigma_y \end{bmatrix} + \begin{Bmatrix} X \\ Y \end{Bmatrix} = 0 \qquad (9.2)$$

Y las ecuaciones de compatibilidad (7.7) se reducen a

$$\frac{\partial^2 \varepsilon_x}{\partial y^2} + \frac{\partial^2 \varepsilon_y}{\partial x^2} = \frac{\partial^2 \gamma_{xy}}{\partial x \partial y} \qquad (9.3)$$

En la Fig. 6.1 se muestran los dos estados o condiciones de esfuerzos que en este caso se tienen, esfuerzos planos;

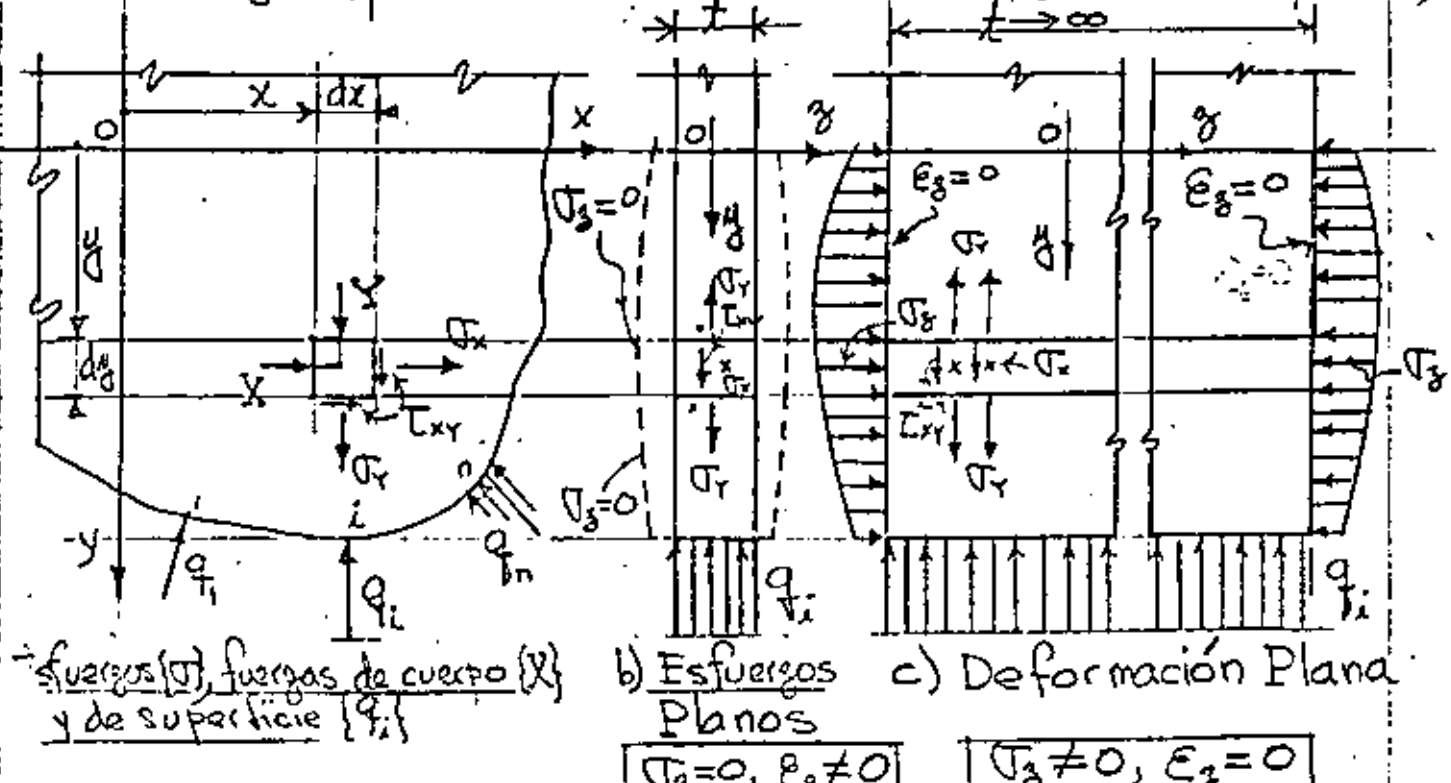

Fig. 6.1. Estados o condiciones de esfuerzos bidimensionales.

caso de una placa de espesor finito t, sin problemas de pandeo que se deforma bajo la acción de $\{X\}$ y $\{q\}$, según la línea punteada indicada en la Fig. 6.1 b, las ecuaciones (8.3), bajo la condición de $\sigma_{33} \equiv \sigma_z = 0$ se reducen a

$$\begin{Bmatrix} \sigma_x \\ \sigma_y \\ \tau_{xy} \end{Bmatrix} = \frac{E}{1-\nu^2} \begin{bmatrix} 1 & \nu & 0 \\ \nu & 1 & 0 \\ 0 & 0 & \frac{1-\nu}{2} \end{bmatrix} \begin{Bmatrix} \varepsilon_x \\ \varepsilon_y \\ \gamma_{xy} \end{Bmatrix} \qquad (9.4)$$

σ_x, σ_y y τ_{xy} son el promedio sobre el espesor pequeño t y son independientes de z. Las componentes γ_{yz} y γ_{zx} se anulan en las superficies, mientas que la componente ε_z es dada por

$$\varepsilon_z = -\frac{\nu}{E}(\sigma_x + \sigma_y) = -\frac{\nu}{1-\nu}(\varepsilon_x + \varepsilon_y) \qquad (9.5)$$

Problemas de cuerpos largos en la dirección longitudinal z cuya geometría y cargas no varían en z se consideran problemas de <u>deformación plana</u> en la Fig. 6.2 se muestran como ejemplos un muro de presa, y una zapata corrida larga,

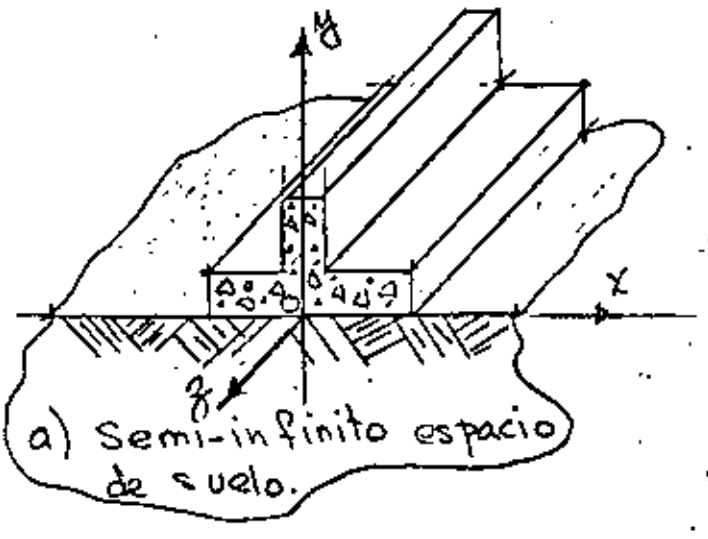

a) Semi-infinito espacio de suelo.

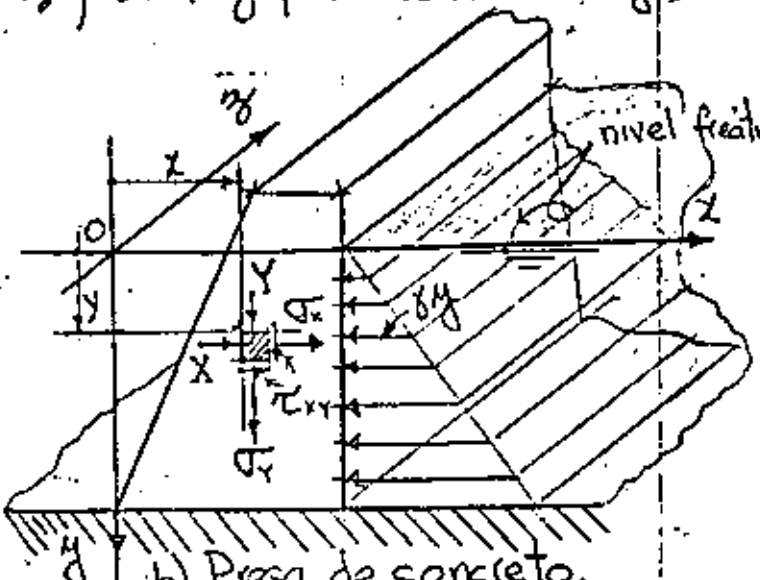

b) Presa de concreto.

Fig. 6.2. Ejemplos de problemas de deformación plana.

en estos casos el desplazamiento $u_3 \equiv w = 0$ por lo tanto $\varepsilon_{33} \equiv \varepsilon_3 = 0$, $\gamma_{yz} = 2\varepsilon_{23} = 0$, y $\gamma_{zx} = 2\varepsilon_{31} = 0$, Las ecuaciones (8.3) se reducen a

$$\begin{Bmatrix} \sigma_x \\ \sigma_y \\ \tau_{xy} \end{Bmatrix} = \frac{E}{(1+\nu)(1-2\nu)} \begin{bmatrix} 1-\nu & \nu & 0 \\ \nu & 1-\nu & 0 \\ 0 & 0 & \frac{1-2\nu}{2} \end{bmatrix} \begin{Bmatrix} \varepsilon_x \\ \varepsilon_y \\ \gamma_{xy} \end{Bmatrix} \qquad (9.6)$$

y el esfuerzo σ_3 se expresa en términos de σ_x y σ_y como

$$\sigma_3 = -\nu(\sigma_x + \sigma_y) \qquad (9.7)$$

Muchos problemas de ingeniería involucran sólidos de revolución (sólidos axisimétricos) sujetos a carga de revolución ó axialmente simétrica, por ejemplo un cilindro circular bajo presión externa uniforme, zapata circular en una masa de suelo semi-infinita como se muestran en la Fig. 6.3

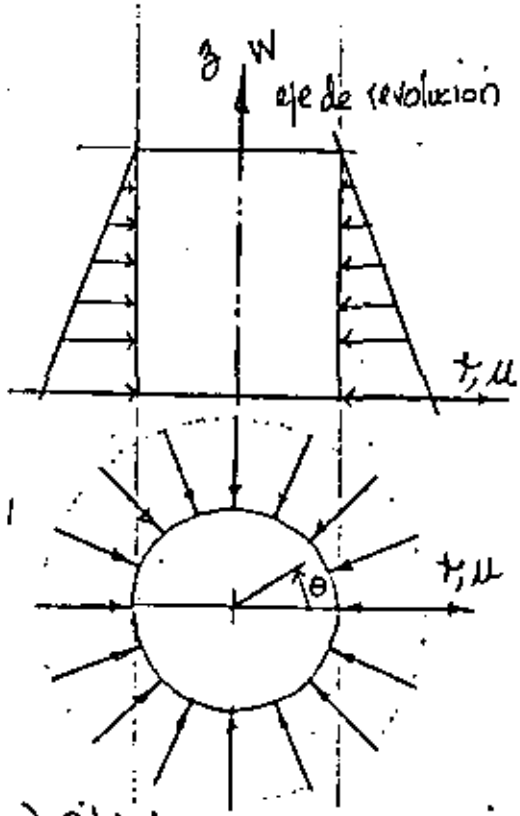

a) Cilindro con carga axisimétrica

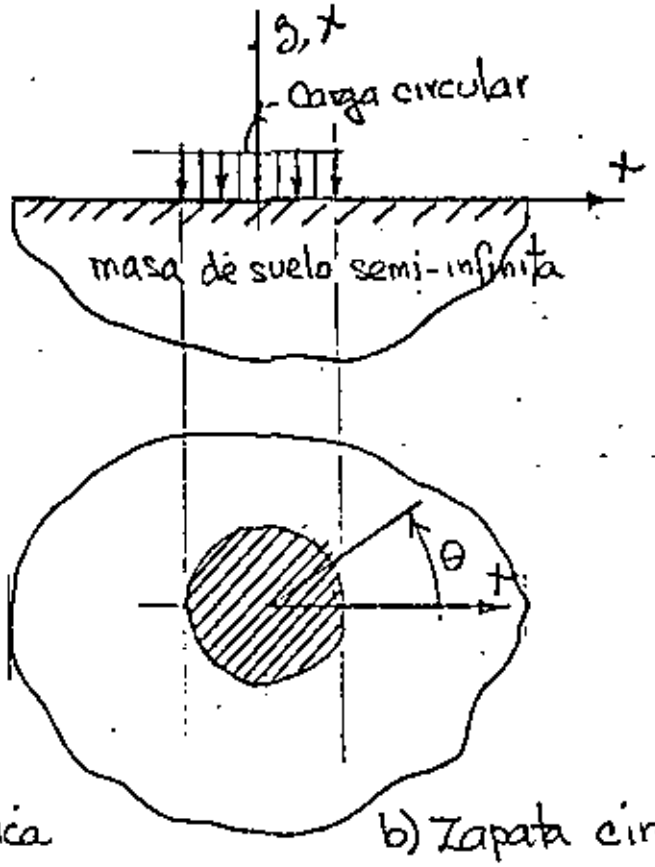

b) Zapata circular

Fig. 6.3 Problemas axisimétricos.

Debido al eje axisimétrico respecto a geometría y cargas, las componentes del esfuerzo son independiente del angulo θ; por lo tanto todas las derivadas respecto a θ se anulan y las componentes v, $\gamma_{r\theta}$, $\gamma_{\theta z}$, $\tau_{r\theta}$, y $\tau_{\theta z}$ son cero. Las componentes de esfuerzo diferente de cero son σ_r, σ_θ, σ_z y τ_{rz}. Las relaciones deformación desplazamiento son, para las deformaciones diferente de cero

$$\varepsilon_r = \frac{\partial u}{\partial r}, \quad \varepsilon_\theta = \frac{u}{r}, \quad \varepsilon_z = \frac{\partial w}{\partial z}, \quad \gamma_{rz} = \frac{\partial u}{\partial z} + \frac{\partial w}{\partial r} \tag{9.8}$$

y la relación constitutiva es

$$\begin{Bmatrix} \sigma_r \\ \sigma_z \\ \sigma_\theta \\ \tau_{rz} \end{Bmatrix} = \frac{E}{(1+\nu)(1-2\nu)} \begin{bmatrix} 1-\nu & \nu & \nu & 0 \\ & 1-\nu & \nu & 0 \\ \text{(simétrica)} & & 1-\nu & 0 \\ & & & \frac{1-2\nu}{2} \end{bmatrix} \begin{Bmatrix} \varepsilon_r \\ \varepsilon_z \\ \varepsilon_\theta \\ \gamma_{rz} \end{Bmatrix} \tag{9.9}$$

despejando de (9.4) $\{\varepsilon\}$, substituyéndolo en la ecuación de compatibilidad (9.3), y eliminando por medio de (9.1) a $\frac{\partial^2 \tau_{xy}}{\partial x \partial y}$ se obtiene

$$\left(\frac{\partial^2}{\partial x^2} + \frac{\partial^2}{\partial y^2}\right)(\sigma_x + \sigma_y) = -(1+\nu)\left(\frac{\partial X}{\partial x} + \frac{\partial Y}{\partial y}\right) \tag{9.10}$$

La ecuación (9.10) junto con las de equilibrio (9.1) son suficientes para la solución del <u>problema de esfuerzo planos</u> $\sigma_z = 0$, de ellas se obtiene $\{\sigma\}^T = [\sigma_x \; \sigma_y \; \tau_{xy}]$.

Similarmente despejando $\{\varepsilon\}$ de (9.6) y substituyéndolo en la ecuación de compatibilidad (9.3), y eliminando por medio de las ecuaciones de equilibrio (9.1) a $\frac{\partial^2 \tau_{xx}}{\partial x \partial y}$ se

obtiene

$$\left(\frac{\partial^2}{\partial x^2}+\frac{\partial^2}{\partial y^2}\right)(\sigma_x+\sigma_y)=-\frac{1}{1-\nu}\left(\frac{\partial X}{\partial x}+\frac{\partial Y}{\partial y}\right) \qquad (9.11)$$

La ecuación (9.11) junto con las de equilibrio (9.1) son suficientes para la solución del problema de deformación plana ($\varepsilon_z=0$), con fuerzas de cuerpo diferente de cero, de ellas se obtiene $\{\sigma\}^T=[\sigma_x\ \sigma_y\ \tau_{xy}]$.

Cuando las fuerzas de cuerpo X es solo función de y; constante ó cero, y cuando la fuerza de cuerpo Y es solo función de x, constante ó cero, las ecuaciones (9.10) y (9.11) para esfuerzos y deformación plana respectivamente, se reducen a una sola que es

$$\left(\frac{\partial^2}{\partial x^2}+\frac{\partial^2}{\partial y^2}\right)(\sigma_x+\sigma_y)=0 \qquad (9.12)$$

Es importante observar que en este caso, en las ecuaciones de equilibrio (9.1), y la de compatibilidad (9.12), modificada por las ecuaciones constitutivas, no intervienen las constantes elásticas del sólido E. y ν. Conclusión de fundamental importancia para el uso de modelos transparentes en Fotoelasticidad. También se concluye en este caso que en ambos estados; de esfuerzo y deformación plano los esfuerzos $\{\sigma\}$ son iguales, solamente las deformaciones $\{\varepsilon\}$ y los desplazamientos $\{u\}$ son diferentes. ∎

Para la solución del problema anterior cuando $\{X\}=0$ Airy, G.B. (Brit. Assoc. Advan. Sci. Rept., 1862) introduce

una función $\phi(x,y)$, llamada función de esfuerzos, en forma tal que

$$\sigma_x = \frac{\partial^2 \phi}{\partial y^2}, \quad \sigma_y = \frac{\partial^2 \phi}{\partial x^2}, \quad \tau_{xy} = -\frac{\partial^2 \phi}{\partial x \partial y} \tag{9.13}$$

(9.13) satisface las ecuaciones de equilibrio (9.1) cuando las fuerzas de cuerpo $\{X\}$ son cero, y substituyéndolas en (9.12) se obtiene

$$\nabla^2 \nabla^2 \phi = \left(\frac{\partial^2}{\partial x^2} + \frac{\partial^2}{\partial y^2}\right)\left(\frac{\partial^2 \phi}{\partial x^2} + \frac{\partial^2 \phi}{\partial y^2}\right) = 0 \tag{9.14}$$

desarrollando el operador bi-laplaciano se obtiene

$$\nabla^4 \phi = \frac{\partial^4 \phi}{\partial x^4} + 2\frac{\partial^4 \phi}{\partial x^2 \partial y^2} + \frac{\partial^4 \phi}{\partial y^4} = 0 \tag{9.15}$$

La ecuación (9.14) se llama bi-armónica o bi-laplaciana y la forma (9.15) gradiente cuarto de ϕ.

Por lo demostrado anteriormente el problema de solución de esfuerzos en medios elásticos lineales homogeneos e isotrópicos bidimensionales se reduce a una solución de (9.15) que satisfaga las condiciones en la frontera bidimensionales que para el punto i son:

$$\bar{X}_i = \sigma_x n_x + \tau_{xy} n_y$$
$$\bar{Y}_i = \tau_{xy} n_x + \sigma_y n_y$$

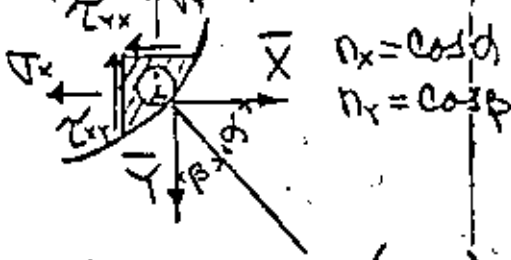

matricial mente:

$$\begin{bmatrix} \sigma_x & \tau_{xy} \\ \tau_{yx} & \sigma_y \end{bmatrix} \begin{Bmatrix} n_x \\ n_y \end{Bmatrix} = \begin{Bmatrix} \bar{X} \\ \bar{Y} \end{Bmatrix} \tag{9.10}$$

Del Teorema de la unicidad* la solución mencionada es úni

* Timoshenko, S. and J.N. Goodier, "Theory of Elasticity", McGraw Hill, 1966.

Si las fuerzas de cuerpo existen, general mente es posible relacionarlas mediante una función potencial $V(x,y)$ en forma tal que

$$X=\frac{\partial V}{\partial x}\ ,\ Y=\frac{\partial V}{\partial y} \tag{9.11}$$

sustituyendo (9.11) en las ecuaciones de equilibrio (9.1) se obtiene

$$\begin{aligned}\frac{\partial}{\partial x}(\sigma_x-V)+\frac{\partial \tau_{xy}}{\partial y}&=0\\ \frac{\partial}{\partial y}(\sigma_y-V)+\frac{\partial \tau_{xy}}{\partial x}&=0\end{aligned} \tag{9.12}$$

en este caso la función de esfuerzos es

$$\sigma_x-V=\frac{\partial^2\phi}{\partial y^2}\ ,\ \sigma_y-V=\frac{\partial^2\phi}{\partial x^2}\ ,\ \tau_{xy}=-\frac{\partial^2\phi}{\partial x\partial y} \tag{9.13}$$

por supuesto (9.13) satisface las ecuaciones de equilibrio (9.1), y sustituyéndola en la ecuación (9.10) la reduce a

$$\nabla^4\phi=-(1+\nu)\left(\frac{\partial^2 V}{\partial x^2}+\frac{\partial^2 V}{\partial y^2}\right)\equiv-(1+\nu)\nabla^2 V \tag{9.14}$$

(9.14) nos resuelve el problema de esfuerzo planos con fuerzas de cuerpo relacionadas por (9.11).

Substituyéndo (9.13) en (9.11) se obtiene

$$\nabla^4\phi=-\frac{1}{1+\nu}\left(\frac{\partial^2 V}{\partial x^2}+\frac{\partial^2 V}{\partial y^2}\right)\equiv-\frac{1}{1+\nu}\nabla^2 V \tag{9.15}$$

10. Ecuaciones de equilibrio en términos de los desplazamientos $\{u\}^T=[u_1\ u_2\ u_3]\equiv[u\ v\ w]$.

Uno de los métodos de solución en problemas de elasticidad lineal, homogenea e isotrópica consiste

en eliminar las componentes de esfuerzos $\{\sigma\}$ de las ecuaciones de equilibrio (5.2) expresando las ecuaciones constitutivas (8.5) en términos de los desplazamientos (7.2), (7.3) y (7.4). Por lo tanto substituyendo (7.2), (7.3) y (7.4) en (8.9) se obtiene 68

$$\begin{aligned}
\sigma_x \equiv \sigma_{11} &= \lambda e + 2G\frac{\partial u}{\partial x} \\
\sigma_y \equiv \sigma_{22} &= \lambda e + 2G\frac{\partial v}{\partial y} \\
\sigma_z \equiv \sigma_{33} &= \lambda e + 2G\frac{\partial w}{\partial z} \\
\tau_{xy} \equiv \sigma_{12} &= G\left(\frac{\partial u}{\partial y} + \frac{\partial v}{\partial x}\right) \\
\tau_{yz} \equiv \sigma_{23} &= G\left(\frac{\partial v}{\partial z} + \frac{\partial w}{\partial y}\right) \\
\tau_{zx} \equiv \sigma_{31} &= G\left(\frac{\partial w}{\partial x} + \frac{\partial u}{\partial z}\right)
\end{aligned} \tag{10.1}$$

donde $e = \varepsilon_{11} + \varepsilon_{22} + \varepsilon_{33} \equiv \varepsilon_x + \varepsilon_y + \varepsilon_z = \frac{\partial u}{\partial x} + \frac{\partial v}{\partial y} + \frac{\partial w}{\partial z}$ (10.2)

Substituyendo (10.1) en las ecuaciones de equilibrio (5.2) se obtiene

$$(\lambda+G)\begin{Bmatrix} \frac{\partial e}{\partial x} \\ \frac{\partial e}{\partial y} \\ \frac{\partial e}{\partial z} \end{Bmatrix} + G\nabla^2\begin{Bmatrix} u \\ v \\ w \end{Bmatrix} + \begin{Bmatrix} X \\ Y \\ Z \end{Bmatrix} = 0 \tag{10.3}$$

donde en este caso el operador diferencial $\nabla^2 = \frac{\partial^2}{\partial x^2} + \frac{\partial^2}{\partial y^2} + \frac{\partial^2}{\partial z^2}$.

En (10.3) cuando las fuerzas de cuerpo $\{X\}$ son cero (10.3) queda

$$(\lambda+G)\begin{Bmatrix} \frac{\partial e}{\partial x} \\ \frac{\partial e}{\partial y} \\ \frac{\partial e}{\partial z} \end{Bmatrix} + G\nabla^2\begin{Bmatrix} u \\ v \\ w \end{Bmatrix} = 0 \tag{10.4}$$

En las ecuaciones (10.4), diferenciando la primera respecto a x, la segunda respecto a y, y la tercera respecto a z, y después sumándolas se obtiene

$$(\lambda+2G)\nabla^2 e = 0 \qquad (10.5)$$

(10.5) significa que la expansión volumétrica unitaria $e = e_x + e_y + e_z$ satisface la ecuación diferencial

$$\nabla^2 e = \frac{\partial^2 e}{\partial x^2} + \frac{\partial^2 e}{\partial y^2} + \frac{\partial^2 e}{\partial z^2} = 0 \qquad (10.6)$$

En la ecuación (10.3) las fuerzas de cuerpo son

$$\begin{aligned} X &= \rho(f_x - a_x) \\ Y &= \rho(f_y - a_y) \\ Z &= \rho(f_z - a_z) \end{aligned} \qquad (10.7)$$

donde f_x, f_y y f_z son las fuerzas por unidad de masa, a_x, a_y y a_z las componentes de la aceleración, y ρ es la densidad ó masa específica. Si en las ecuaciones (10.9) la primera la multiplicamos por el vector unitario $\bar{i}$, la segunda por el vector unitario $\bar{j}$, y la tercera por el vector unitario $\bar{k}$, y las sumamos entre sí se obtiene la expresión vectorial de las ecuaciones (10.9) como

$$(\lambda+G)\,\text{grad div}\,\bar{s} + G\nabla^2\bar{s} + \rho(\bar{f}-\bar{a}) = 0 \qquad (10.8)$$

en donde

$$\begin{aligned} \bar{a} &= \bar{i}a_x + \bar{j}a_y + \bar{k}a_z \\ \bar{f} &= \bar{i}f_x + \bar{j}f_y + \bar{k}f_z \\ \bar{s} &= \bar{i}u + \bar{j}v + \bar{k}w \\ \text{div}\,s = e &= \frac{\partial u}{\partial x} + \frac{\partial v}{\partial y} + \frac{\partial w}{\partial z} \\ \text{grad div}\,\bar{s} &= \bar{i}\frac{\partial e}{\partial x} + \bar{j}\frac{\partial e}{\partial y} + \bar{k}\frac{\partial e}{\partial z} \end{aligned} \qquad (10.9)$$

En la Fig. 2 se tiene lo siguiente
o'n es normal al plano ABC, formando ángulos α, β y γ con respecto a los ejes coordenados x_1, x_2, y x_3 respectivamente, la distancia oo' es igual a r las coordenadas de o' son x_1, x_2, x_3 por lo tanto

$$n_1 = \cos\alpha = \frac{x_1}{r}, \quad n_2 = \cos\beta = \frac{x_2}{r}, \quad n_3 = \cos\gamma = \frac{x_3}{r} \quad (2)$$

donde $\{n_i\} = [n_1\ n_2\ n_3]^T$ es el vector columna de cosenos directores de la normal al plano ABC (o'n // oo'). Si el area ABC es considerada como la unidad, las proyecciones

$$\begin{aligned} n_1 &= \text{area } OBC \\ n_2 &= \text{area } OAC \\ n_3 &= \text{area } OAB \end{aligned} \quad (2)$$

$\bar{S}$ = Esfuerzo resultante actuando sobre el plano ABC
$\{\bar{X}_i\} = [\bar{X}_1\ \bar{X}_2\ \bar{X}_3]^T$; proyecciones de $\bar{S}$ sobre x_i
$\bar{T}_n$ = Proyección de $\bar{S}$ sobre la normal al plano ABC
$\bar{\tau}_n$ = Proyección de $\bar{S}$ sobre el plano ABC.
Del equilibrio del elemento OABC se obtiene

71

$$X_1 = \sigma_{11} n_1 + \sigma_{21} n_2 + \sigma_{31} n_3$$
$$X_2 = \sigma_{12} n_1 + \sigma_{22} n_2 + \sigma_{32} n_3 \quad (3)$$
$$X_3 = \sigma_{13} n_1 + \sigma_{23} n_2 + \sigma_{33} n_3$$

expresando (3) matricialmente se obtiene

$$\begin{Bmatrix} X_1 \\ X_2 \\ X_3 \end{Bmatrix} = \begin{bmatrix} \sigma_{11} & \sigma_{21} & \sigma_{31} \\ \sigma_{12} & \sigma_{22} & \sigma_{32} \\ \sigma_{13} & \sigma_{23} & \sigma_{33} \end{bmatrix} \begin{Bmatrix} n_1 \\ n_2 \\ n_3 \end{Bmatrix} \quad (4)$$

Si no existen momentos de cuerpo, $\sigma_{ij} = \sigma_{ji}$ para $i \neq j$ y $[\sigma_{ij}] = [\sigma_{ij}]^T$ por lo que (4) puede escribirse

$$\begin{Bmatrix} X_1 \\ X_2 \\ X_3 \end{Bmatrix} = \begin{bmatrix} \sigma_{11} & \sigma_{12} & \sigma_{13} \\ \sigma_{21} & \sigma_{22} & \sigma_{23} \\ \sigma_{31} & \sigma_{32} & \sigma_{33} \end{bmatrix} \begin{Bmatrix} n_1 \\ n_2 \\ n_3 \end{Bmatrix} \quad (5)$$

ó $$\{X_i\} = [\sigma_{ij}] \{n_i\} \quad (6)$$

El esfuerzo normal al plano ABC es

$$\sigma_n = X_1 n_1 + X_2 n_2 + X_3 n_3 \quad (7)$$

ó $$\sigma_n = \{X_i\}^T \{n_i\} \quad (8)$$

Substituyendo (5) en (7) se obtiene

$$\sigma_n = \sigma_{11} n_1^2 + \sigma_{22} n_2^2 + \sigma_{33} n_3^2 + 2(\sigma_{12} n_1 n_2 + \sigma_{23} n_2 n_3 + \sigma_{31} n_3 n_1)$$

ó matricialmente de (6) y (8)

$$\sigma_n = \{n_i\}^T [\sigma_{ij}] \{n_i\} \quad (11)$$

72

$$S^2 = X_1^2 + X_2^2 + X_3^2 \quad (11)$$

$$\sigma_n^2 + \tau_n^2 = S^2 \quad (12)$$

Esfuerzos principales. Esfuerzo principal es un valor particular del esfuerzo normal tal que $\tau_n = 0$ por lo tanto

$$\begin{aligned} X_1 &= \sigma_n n_1 \\ X_2 &= \sigma_n n_2 \\ X_3 &= \sigma_n n_3 \end{aligned} \quad (13)$$

De (3) y (15) se obtiene

$$\begin{Bmatrix} \sigma_n l_1 \\ \sigma_n l_2 \\ \sigma_n l_3 \end{Bmatrix} = \begin{bmatrix} \sigma_{11} & \sigma_{12} & \sigma_{13} \\ \sigma_{21} & \sigma_{22} & \sigma_{23} \\ \sigma_{31} & \sigma_{32} & \sigma_{33} \end{bmatrix} \begin{Bmatrix} n_1 \\ n_2 \\ n_3 \end{Bmatrix} \quad (4)$$

De donde

$$\begin{bmatrix} (\sigma_n - \sigma_{11}) & -\sigma_{12} & -\sigma_{13} \\ -\sigma_{21} & (\sigma_n - \sigma_{22}) & -\sigma_{23} \\ -\sigma_{31} & -\sigma_{32} & (\sigma_n - \sigma_{33}) \end{bmatrix} \begin{Bmatrix} n_1 \\ n_2 \\ n_3 \end{Bmatrix} = 0 \quad (15)$$

puesto que $\{n_i\} \neq 0$, entonces el determinante

$$\begin{vmatrix} (\sigma_n - \sigma_{11}) & -\sigma_{12} & -\sigma_{13} \\ -\sigma_{21} & (\sigma_n - \sigma_{22}) & -\sigma_{23} \\ -\sigma_{31} & -\sigma_{32} & \sigma_n - \sigma_{33} \end{vmatrix} = 0. \quad (16)$$

De (16) se obtiene 73

$$\sigma_n^3 - (\sigma_{11}+\sigma_{22}+\sigma_{33})\sigma_n^2 + (\sigma_{11}\sigma_{22}+\sigma_{22}\sigma_{33}+\sigma_{33}\sigma_{11}-\sigma_{12}^2-\sigma_{23}^2-\sigma_{31}^2)\sigma_n$$

$$-(\sigma_{11}\sigma_{22}\sigma_{33}+2\sigma_{12}\sigma_{23}\sigma_{31}-\sigma_{11}\sigma_{23}^2-\sigma_{22}\sigma_{31}^2-\sigma_{33}\sigma_{12}^2)=0 \quad (17)$$

las tres raices de la ecuación (17) nos determinan los valores de los esfuerzos principales σ_1, σ_2 y σ_3 cuyos coeficientes nos representan los invariantes de esfuerzos, dependen de σ_1, σ_2 y σ_3 independientes del sistema de ejes coordenados

$$I_1 = \sigma_{11}+\sigma_{22}+\sigma_{33} \equiv \sigma_1+\sigma_2+\sigma_3$$
$$I_2 = \sigma_{11}\sigma_{22}+\sigma_{22}\sigma_{33}+\sigma_{33}\sigma_{11}-\sigma_{12}^2-\sigma_{23}^2-\sigma_{31}^2 \equiv \sigma_1\sigma_2+\sigma_2\sigma_3+\sigma_3\sigma_1 \quad (18)$$
$$I_3 = \sigma_{11}\sigma_{22}\sigma_{33}+2\sigma_{12}\sigma_{23}\sigma_{31}-\sigma_{11}\sigma_{23}^2-\sigma_{22}\sigma_{13}^2-\sigma_{33}\sigma_{12}^2 \equiv \sigma_1\sigma_2\sigma_3$$

donde I_1, I_2 e I_3 son los invariantes de esfuerzos, otras expresiones de invariantes pueden formarse de (18) por ejemplo (19)

$$2I_1^2-6I_2=(\sigma_{11}-\sigma_{22})^2+(\sigma_{22}-\sigma_{33})^2+(\sigma_{33}-\sigma_{11})^2+6(\sigma_{13}^2+\sigma_{23}^2+\sigma_{31}^2)$$

(19) se usa en la expresión de la energía de deformación, su uso se discutirá posteriormente

Despues de diagonalizar el tensor de esfuerzo $[T_{ij}]$, el elemento de la Fig. 2 se muestra en la Fig. 3, y las ecuaciones de equilibrio (3) quedan:

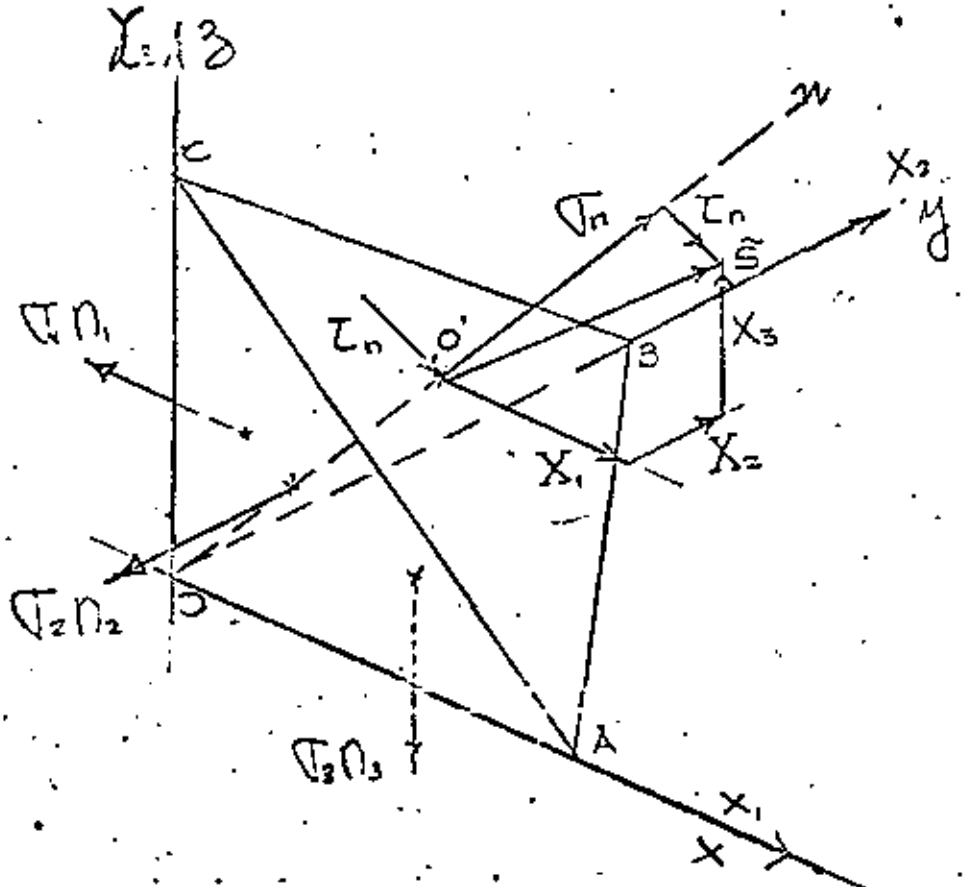

Fig. 3 Componentes del tensor de esfuerzo diagonalizado

$$\begin{Bmatrix} X_1 \\ X_2 \\ X_3 \end{Bmatrix} = \begin{bmatrix} T_1 & 0 & 0 \\ 0 & T_2 & 0 \\ 0 & 0 & T_3 \end{bmatrix} \begin{Bmatrix} n_1 \\ n_2 \\ n_3 \end{Bmatrix} \qquad (20)$$

En (20) las componentes $\{X_i\}$, $\{n_i\}$, $\tilde{S}$, $\tilde{T}_n$, $\tilde{\tau}_n$ son diferentes a las (5) que se muestran en Fig. 2. De aquí se conoce que

$$n_1^2 + n_2^2 + n_3^2 = 1 \qquad (21)$$

Sustituyendo (20) en (21) se obtiene la ecuación

$$\frac{Y_{x1}^2}{\sigma_1^2} + \frac{Y_{x2}^2}{\sigma_2^2} + \frac{X_3^2}{\sigma_3^2} = 1 \qquad (22)$$

la cual representa una superficie elipsoidal en el espacio de esfuerzos σ_i, algunos autores lo denominan elipsoide de Lamé, en la Fig. 4 se muestra su perspectiva isométrica. Para el conjunto

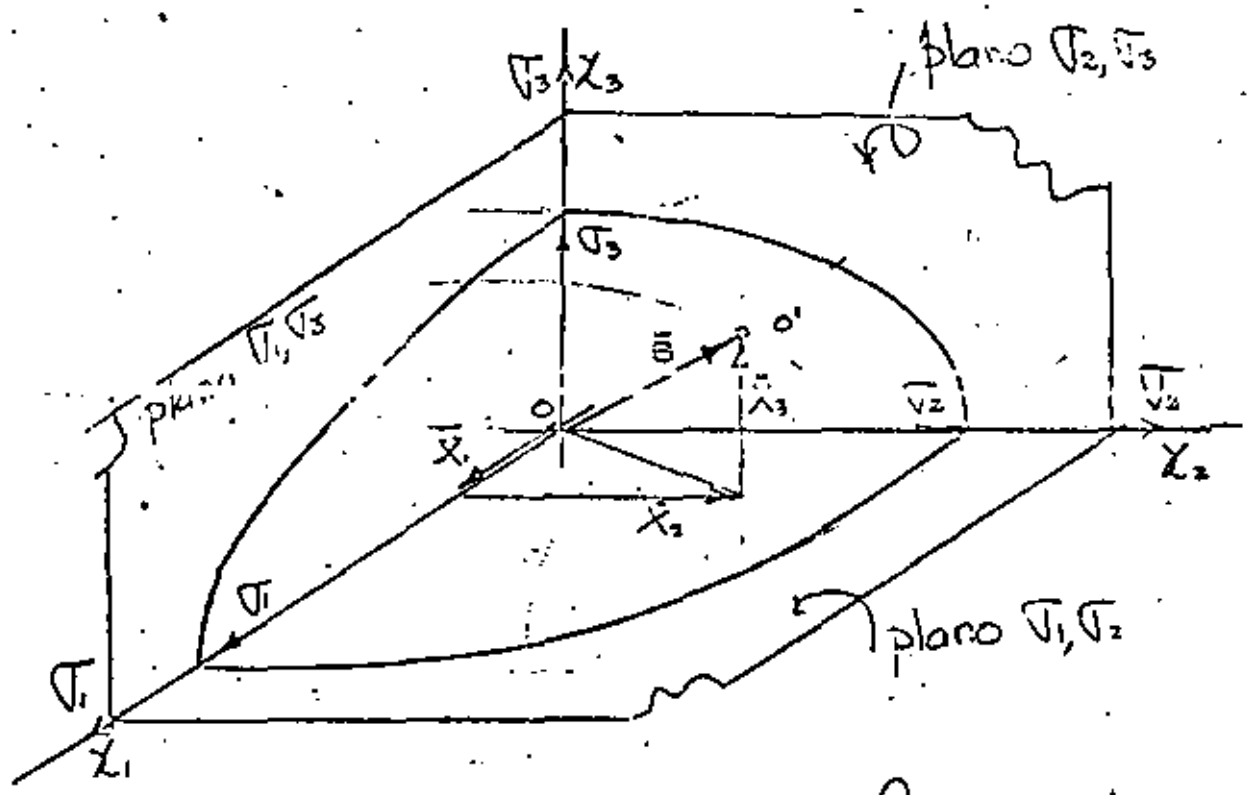

Fig. 4 Elipsoide de Lamé referido al espacio de esfuerzos σ_i, (un octagono).

de planos con cosenos directores $\{n_i\}$ a través de o Fig. 2, le corresponde el conjunto de componentes $\{X_i\}$ los cuales junto con los esfuerzos principales σ_1, σ_2 y σ_3 forman la superficie elipsoidal de la Fig. 4.

De (20), si $\sigma_1=\sigma_2=\sigma_3=\sigma$, la superficie es esférica. si $\sigma_1\neq 0$, $\sigma_2\neq 0$ y $\sigma_3=0$ la superficie es cilíndrica de sección elíptica con eje contenido en el eje σ_3. Si $\sigma_1=\sigma_2$ y $\sigma_3=0$ la superficie es cilíndrica de sección circular con eje contenido en el eje σ_3, Si $\sigma_1\neq 0$ y $\sigma_2=\sigma_3=0$ la superficie son dos planos paralelos al plano $\sigma_2\sigma_3$ a continuación se indican los casos particulares mencionados

$$\begin{bmatrix} T_1 \\ T_2 \\ T_3 \end{bmatrix} = \begin{bmatrix} \sigma & 0 & 0 \\ 0 & \sigma & 0 \\ 0 & 0 & \sigma \end{bmatrix} \quad (23)$$

$$X_1^2+X_2^2+X_3^2=\sigma^2 \quad (24)$$

$\sigma \equiv S$

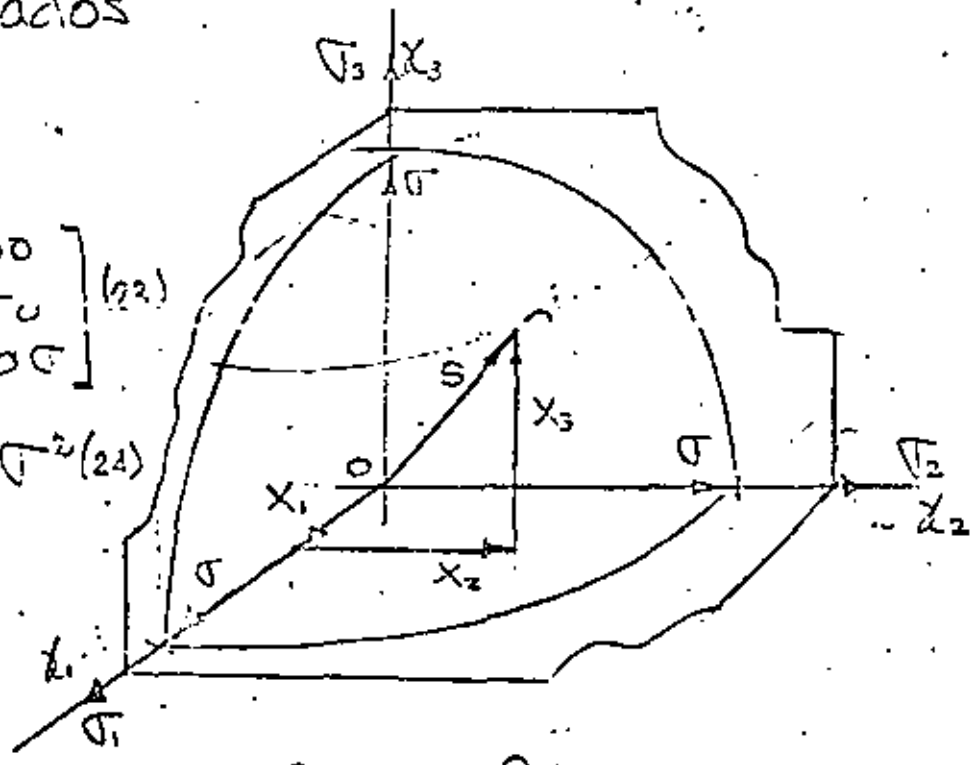

Fig. 5 Superficie esférica, equivalente a una Tensión o compresión uniforme o hidrostática

77

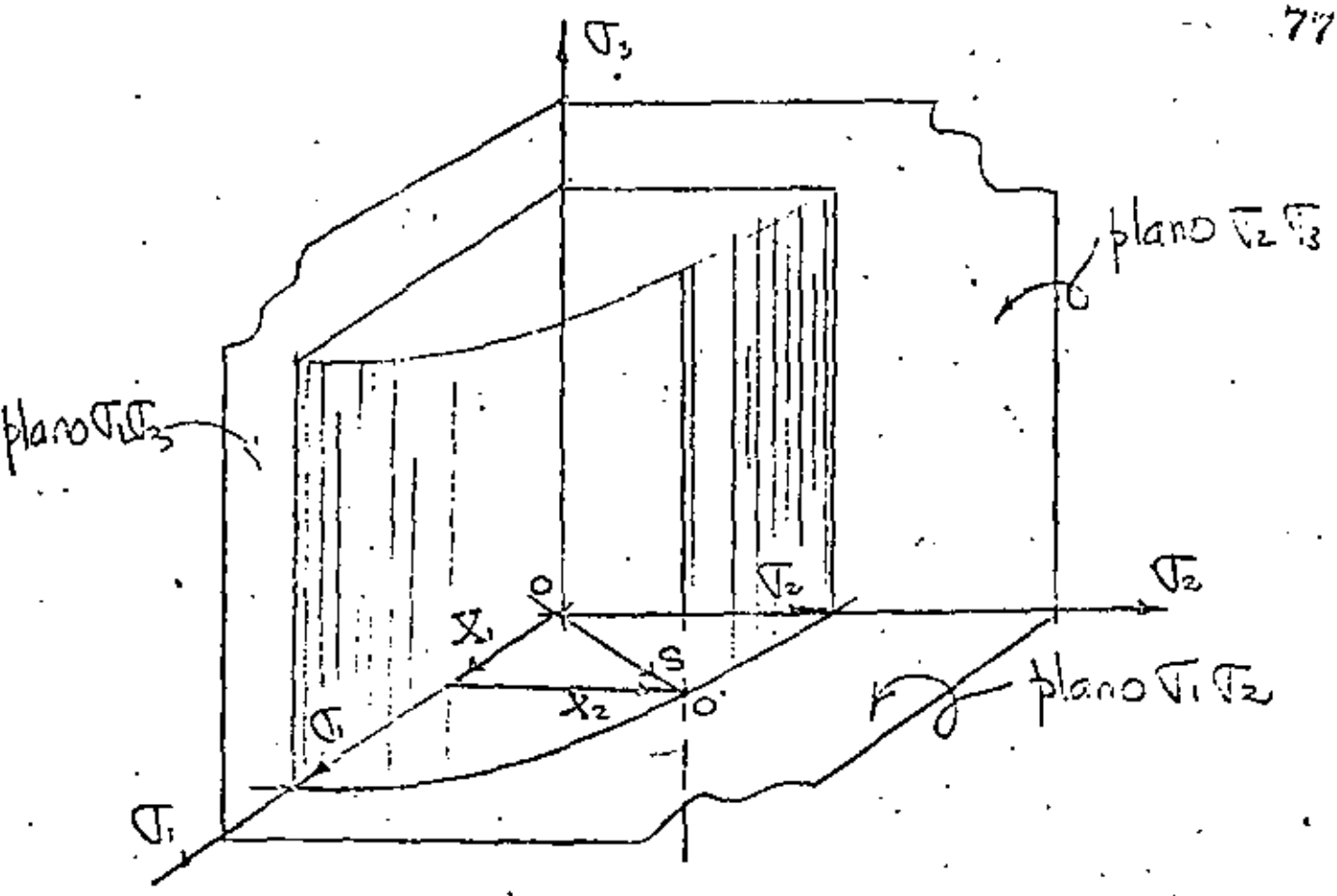

Fig. 6 Superficie cilíndrica de sección elíptica directrices paralelas al eje $o\sigma_3$.

Componentes del tensor de esfuerzos: $[\sigma_{ij}] = \begin{bmatrix} \sigma_1 & 0 & 0 \\ 0 & \sigma_2 & 0 \\ 0 & 0 & 0 \end{bmatrix}$ (65)

Ecuación de la superficie: $\frac{X_1^2}{\sigma_1^2} + \frac{X_2^2}{\sigma_2^2} = 1$ (66)

Como caso particular de de (25) si $\sigma_1 = \sigma_2 = \sigma$ se tiene un cilindro con componentes del tensor de esfuerzos $[\sigma_{ij}] = \begin{bmatrix} \sigma & 0 & 0 \\ 0 & \sigma & 0 \\ 0 & 0 & 0 \end{bmatrix}$ (67)

y ecuación de la superficie

$$X_1^2 + X_2^2 = \sigma^2 \quad (67')$$

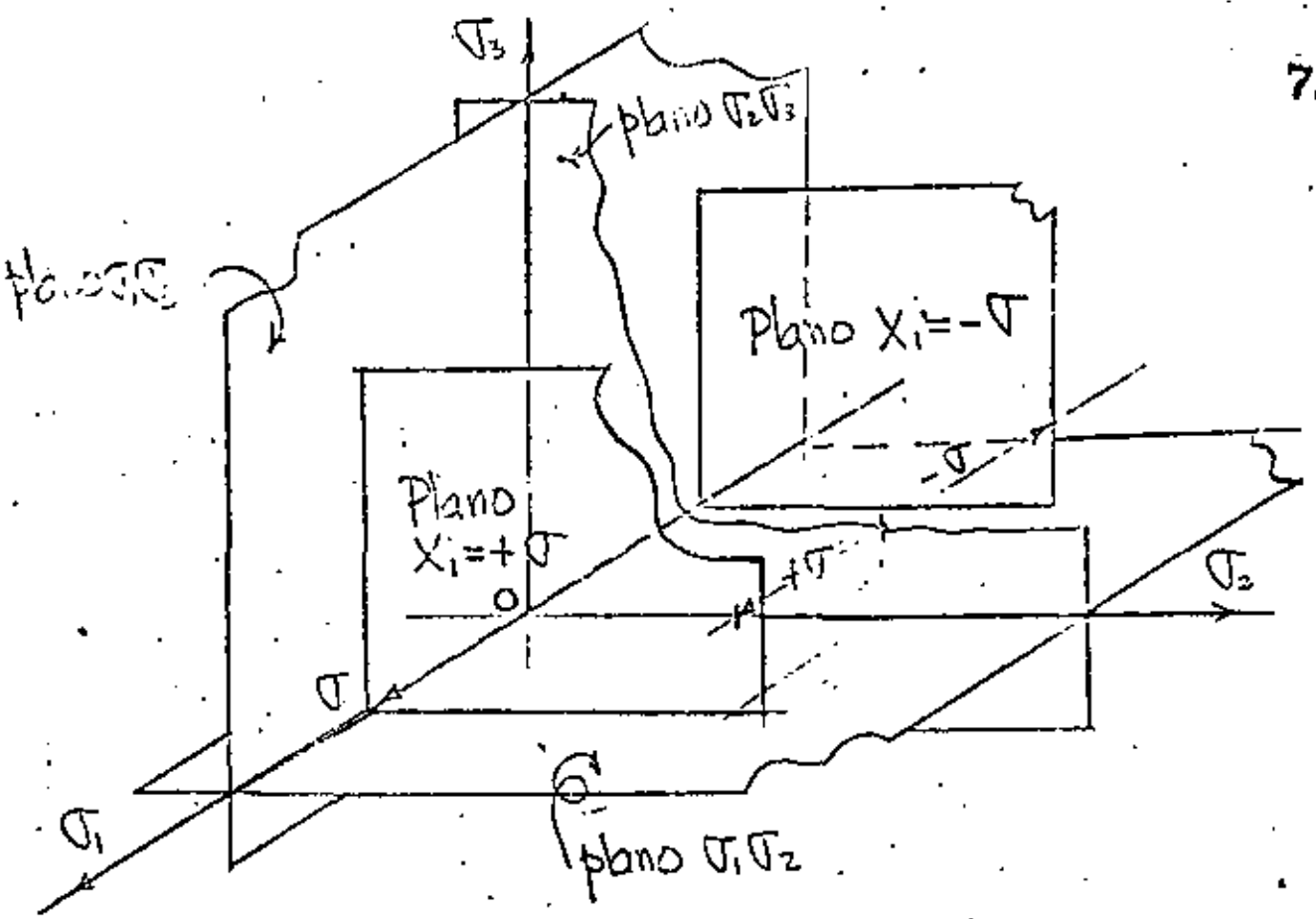

Fig. 6 Superficies planas paralelas al plano $\sigma_2\sigma_3$

Componentes del tensor de esfuerzos:

$$[\sigma_{ij}] = \begin{bmatrix} \sigma & 0 & 0 \\ 0 & 0 & 0 \\ 0 & 0 & 0 \end{bmatrix} \tag{29}$$

Ecuación de la Superficie:

$$X_1 = \pm \sigma \tag{30}$$

La ecuación (21) en el espacio de cosenos directores nos representa una esfera de radio unitario como se muestra en la Fig. 7

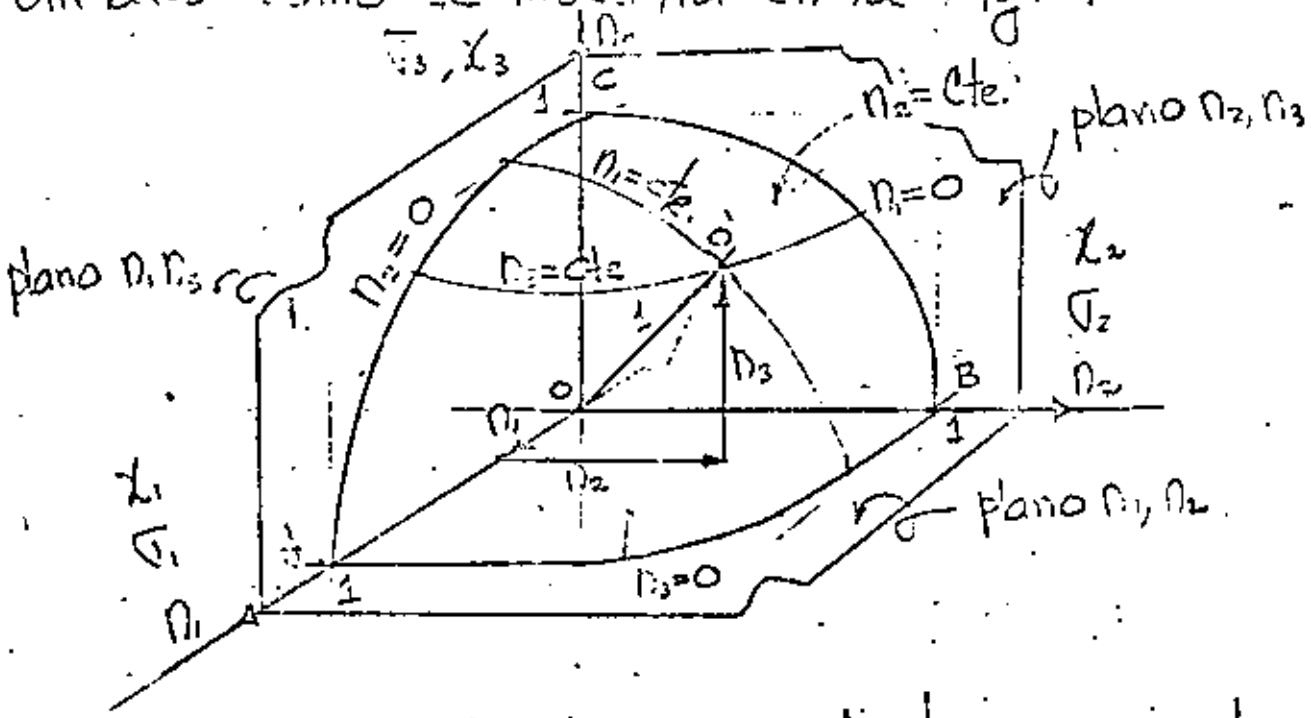

Fig. 7 Espacio de cosenos directores. Un octavo de la esfera de Mohr.

$$\overline{OA} = \overline{OB} = \overline{OC} = \overline{OO'} = 1$$

De la Fig. 3 se observa que substituyendo (20) en (7) se obtiene

$$\sigma_n = \sigma_1 n_1^2 + \sigma_2 n_2^2 + \sigma_3 n_3^2 \qquad (31)$$

Substituyendo (20) y (31) en (11) y (12) se obtiene

$$\tau_n^2 = \sigma_1^2 n_1^2 + \sigma_2^2 n_2^2 + \sigma_3^2 n_3^2 - (\sigma_1 n_1^2 + \sigma_2 n_2^2 + \sigma_3 n_3^2)^2 \qquad (32)$$

de las ecuaciones (31), (32) y (21) se obtiene el siguiente sistema de 3 ecuaciones con 3 incógnitas no lineal en n_1, n_2 y n_3

$$\begin{bmatrix} 1 & 1 & 1 \\ \sigma_1 & \sigma_2 & \sigma_3 \\ f(\sigma_1 n_1^2) & f(\sigma_2 n_2^2) & f(\sigma_3 n_3^2) \end{bmatrix} \begin{Bmatrix} n_1^2 \\ n_2^2 \\ n_3^2 \end{Bmatrix} = \begin{Bmatrix} 1 \\ \sigma_n \\ \tau_n^2 \end{Bmatrix} \quad (33)$$

de (33) se obtiene

$$n_1^2 = \frac{(\sigma_2-\sigma_n)(\sigma_3-\sigma_n)+\tau_n^2}{(\sigma_2-\sigma_1)(\sigma_3-\sigma_1)} \quad (34)$$

$$n_2^2 = \frac{(\sigma_3-\sigma_n)(\sigma_1-\sigma_n)+\tau_n^2}{(\sigma_3-\sigma_2)(\sigma_1-\sigma_2)} \quad (35)$$

$$n_3^2 = \frac{(\sigma_1-\sigma_n)(\sigma_2-\sigma_n)+\tau_n^2}{(\sigma_1-\sigma_3)(\sigma_2-\sigma_3)} \quad (36)$$

De la Fig. 7 considerando n_1 = constante de la ecuación (34) se obtiene

$$n_1^2(\sigma_2-\sigma_1)(\sigma_3-\sigma_1) = (\sigma_2-\sigma_n)(\sigma_3-\sigma_n)+\tau_n^2 \quad (37)$$

efectuando operaciones algebraicas en (37) se obtiene

$$n_1^2(\sigma_2-\sigma_1)(\sigma_3-\sigma_1)+\left(\frac{\sigma_2-\sigma_3}{2}\right)^2 = \left[\sigma_n-\frac{\sigma_2+\sigma_3}{2}\right]^2+\tau_n^2 = \text{Constante}$$

de donde: $Y_1^2 = \left[\sigma_n-\frac{\sigma_2+\sigma_3}{2}\right]^2+\tau_n^2 \equiv (x-a)^2+y^2$ que es la ecuación de un círculo a una distancia $\frac{\sigma_2+\sigma_3}{2}$ del origen por lo tanto el radio σ_1 que haciendo centro en $\frac{\sigma_2+\sigma_3}{2}$ localiza el punto de coordenadas $\sigma_n\tau_n$ en el diagrama de Mohr es

81

$$\tau_1 = \sqrt{n_1^2(\sigma_2-\sigma_1)(\sigma_3-\sigma_1)+\left(\frac{\sigma_2-\sigma_3}{2}\right)^2} \qquad (38)$$

Similarmente suponiendo n_2 = constante de (35) se obtiene

$$\tau_2 = \sqrt{n_2^2(\sigma_3-\sigma_2)(\sigma_1-\sigma_2)+\left(\frac{\sigma_1-\sigma_3}{2}\right)^2} \qquad (39)$$

Similarmente suponiendo n_3 = constante de (36) se obtiene

$$\tau_3 = \sqrt{n_3^2(\sigma_1-\sigma_3)(\sigma_2-\sigma_3)+\left(\frac{\sigma_1-\sigma_2}{2}\right)^2} \qquad (40)$$

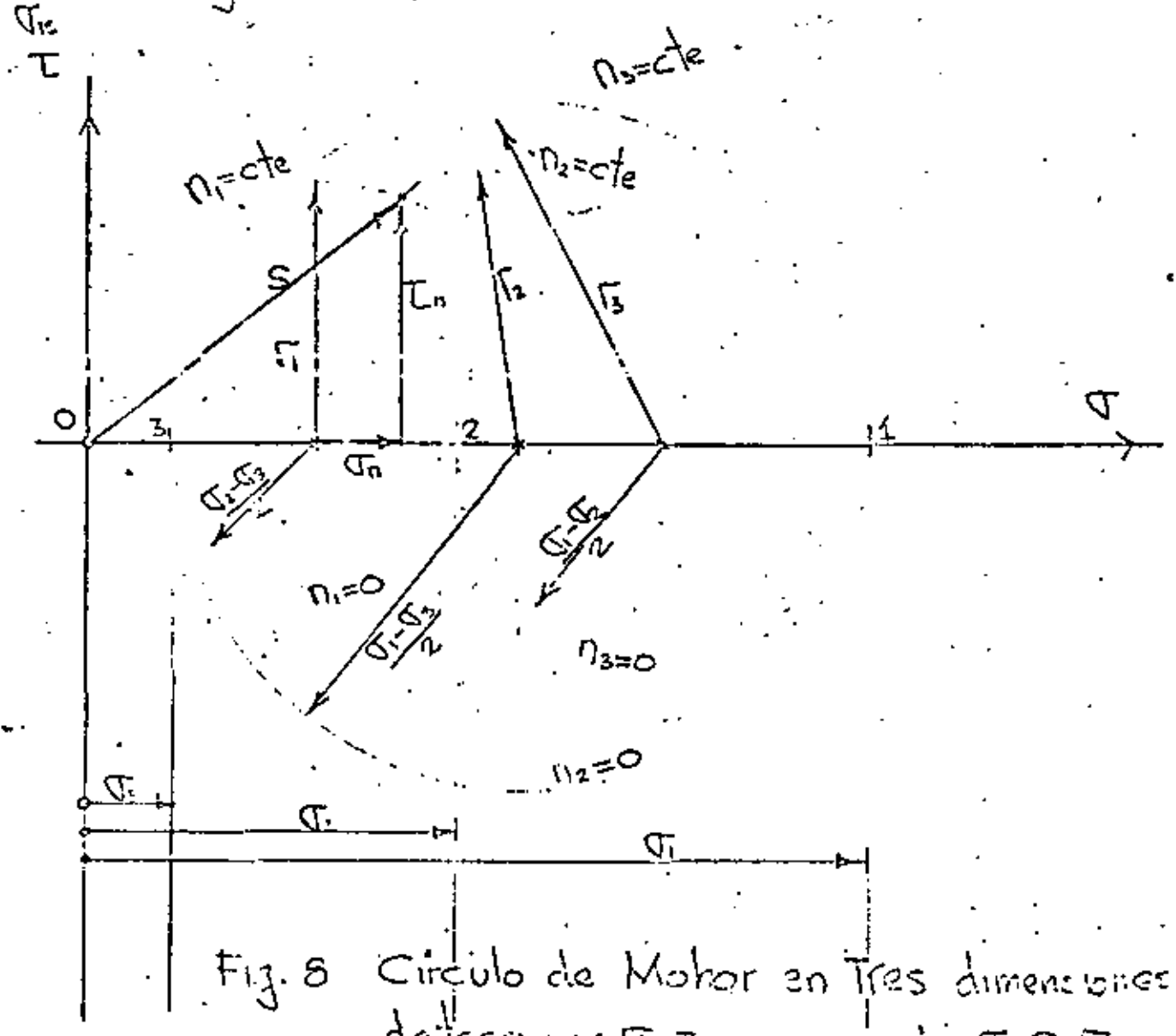

Fig. 8 Círculo de Mohor en Tres dimensiones determinar σ_n, τ_n, conociendo $\sigma_1, \sigma_2, \sigma_3$ y n_1, n_2 y n_3

2- Esfuerzos cortantes máximos, esfuerzo esférico, esfuerzo octaedral

Sean x_1, x_2, x_3 las direcciones principales (Fig. 2) y n_1, n_2, n_3 los cosenos directores de cierto plano ABC, se tiene que

$$\tau_n^2 = S^2 - \sigma_n^2 \quad (41)$$

$$S^2 = \sigma_1^2 n_1^2 + \sigma_2^2 n_2^2 + \sigma_3^2 n_3^2 \quad (42)$$

$$\sigma_n^2 = (\sigma_1 n_1^2 + \sigma_2 n_2^2 + \sigma_3 n_3^2)^2 \quad (43)$$

sustituyendo (43) y (42) en (41) se obtiene

$$\tau_n^2 = \sigma_1^2 n_1^2 + \sigma_2^2 n_2^2 + \sigma_3^2 n_3^2 - (\sigma_1 n_1^2 + \sigma_2 n_2^2 + \sigma_3 n_3^2)^2 \quad (44)$$

Para determinar las direcciones maximas de corte de $n_3^2 = 1 - n_1^2 - n_2^2$ se elimina n_3 de (44) y se determinan

$$\frac{\partial}{\partial n_1}(\tau_n^2) = 0; \quad n_1\left[(\sigma_1 - \sigma_3)n_1^2 + (\sigma_2 - \sigma_3)n_2^2 - \tfrac{1}{2}(\sigma_1 - \sigma_2)\right] = 0 \quad (45)$$

$$\frac{\partial}{\partial n_2}(\tau_n^2) = 0; \quad n_2\left[(\sigma_1 - \sigma_3)n_1^2 + (\sigma_2 - \sigma_3)n_2^2 - \tfrac{1}{2}(\sigma_2 - \sigma_3)\right] = 0 \quad (46)$$

las soluciones de (45) y (46) que hacen τ_n máximo:

Si $n_2 = 0$ $\quad n_1 = \sqrt{\frac{1}{2}}$ $\quad n_3 = \sqrt{\frac{1}{2}}$

" $n_1 = 0$ $\quad n_2 = \sqrt{\frac{1}{2}}$ $\quad n_3 = \sqrt{\frac{1}{2}}$ y similarmente

" $n_3 = 0$ $\quad n_1 = \sqrt{\frac{1}{2}}$ $\quad n_2 = \sqrt{\frac{1}{2}}$

se repiten los calculos en (44) se elimina n_1 y despues n_2, Conviene observar que en (45) y (46)

no hay soluciones de n_1 y n_2 que sean ambos diferentes de cero, porque las expresiones dentro del paréntesis no pueden anularse.

	n_1	n_2	n_3	n_1	n_2	n_3
n_1	0	0	± 1	0	$\pm\sqrt{\frac{1}{2}}$	$\pm\sqrt{\frac{1}{2}}$
n_2	0	± 1	0	$\pm\sqrt{\frac{1}{2}}$	0	$\pm\sqrt{\frac{1}{2}}$
n_3	± 1	0	0	$\pm\sqrt{\frac{1}{2}}$	$\pm\sqrt{\frac{1}{2}}$	0
	Esf. Principales $\tau_n = 0$			Cortantes máximos		

Tabla 1 Cosenos directores

Repitiendo los calculos en (44), eliminado n_1 y determinando n_2 y n_3 tal que τ_n sea máximo y después n_2 y determinando n_1 y n_3 tal que τ_n sea máximo se obtienen los valores

$$(\tau_{max})_1 = \tau_1 = \pm \frac{1}{2}(\sigma_2 - \sigma_3)$$
$$(\tau_{max})_2 = \tau_2 = \pm \frac{1}{2}(\sigma_1 - \sigma_3) \qquad (47)$$
$$(\tau_{max})_3 = \tau_3 = \pm \frac{1}{2}(\sigma_1 - \sigma_2)$$

de (47) y (32) se puede expresar τ_n en la siguiente forma

$$\tau_n^2 = 4(n_1^2 n_2^2 \tau_3^2 + n_2^2 n_3^2 \tau_1^2 + n_1^2 n_3^2 \tau_2^2) \qquad (48)$$

Las 3 primeras columnas de la Tabla 1 dan las direcciones de los planos coordenados de las direcciones principales, para ellos $\tau_n = 0$ y (32) es un mínimo, las tres columnas restantes dan planos a través de un eje principal bisectando los otros dos direcciones de esfuerzos principales, sustituyendo los valores de Tabla 1 en (32)

se obtienen los valores de los esfuerzos cortantes máximos (47), los lados del octaedro mostrado en la Fig 9 son las direcciones principales de cortante, y las direcciones χ_1 χ_2 y χ_3 son la direcciones

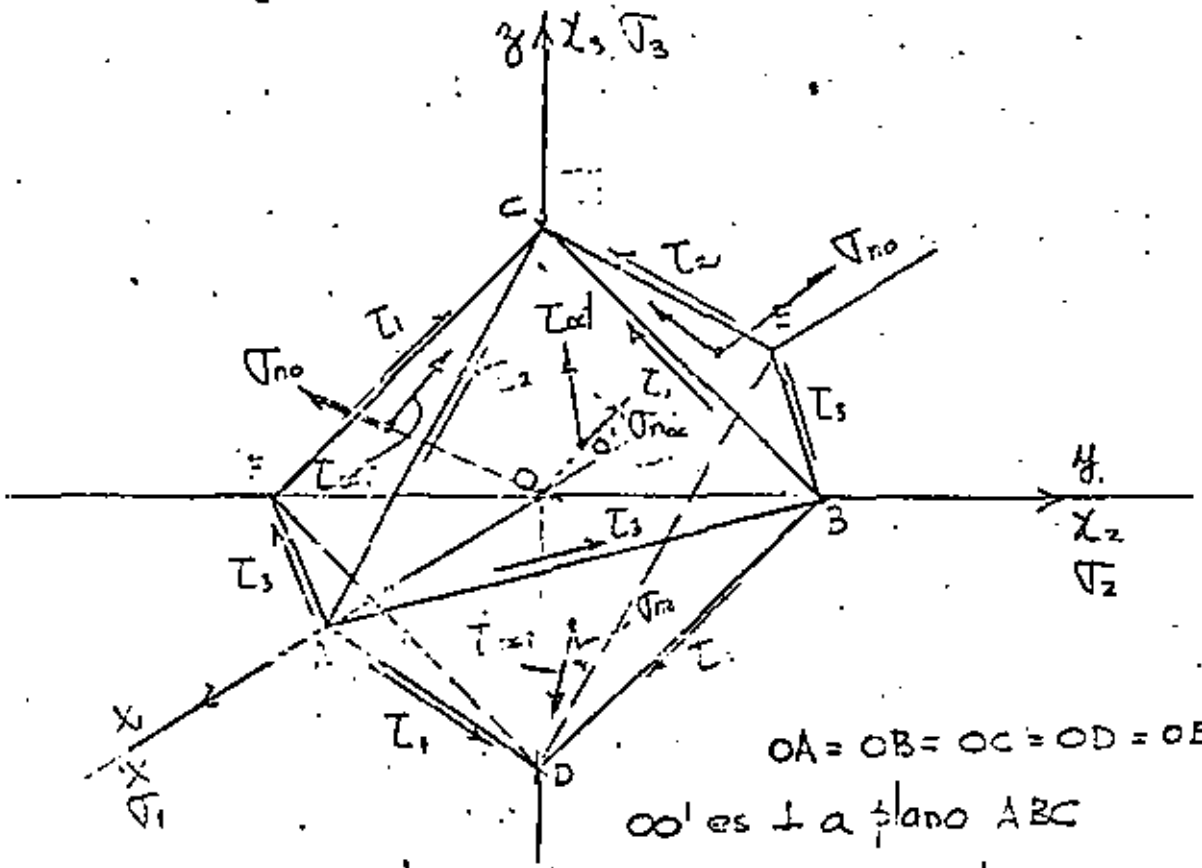

Fig. 9 octaedro regular cuyos lados son las direcciones de esfuerzo cortante máximo.

principales σ_1, σ_2 y σ_3, la normal al tetaedro OABC tiene cosenos directores $n_1 = n_2 = n_3 = \frac{1}{\sqrt{3}}$ $(\alpha = \beta = \gamma = 54.76°)$ y (31) el esfuerzo normal es igual a

$$\sigma_{no} = \frac{1}{3}(\sigma_1 + \sigma_2 + \sigma_3) \qquad (48)$$

a) se denomina esfuerzo medio, esférico o hidrostático, el esfuerzo de corte correspondiente de (44) es

$$\tau_{oct}^2 = \frac{1}{3}(\sigma_1^2 + \sigma_2^2 + \sigma_3^2) - \frac{1}{9}(\sigma_1 + \sigma_2 + \sigma_3)^2 = \frac{1}{9}\left[(\sigma_1 - \sigma_2)^2 + (\sigma_2 - \sigma_3)^2 + (\sigma_3 - \sigma_1)^2\right]$$

$$\tau_{oct} = \frac{1}{3}\sqrt{\left[(\sigma_1-\sigma_2)^2+(\sigma_2-\sigma_3)^2+(\sigma_3-\sigma_1)^2\right]} \qquad (49)$$

de (48) y (49) se obtiene

$$\tau_{oct} = \sqrt{\frac{1}{3}\left[(\sigma_1-\sigma_n)^2+(\sigma_2-\sigma_n)^2+(\sigma_3-\sigma_n)^2\right]} \qquad (50)$$

al esfuerzo de corte dado por (49) y (50) es llamado esfuerzo octaedral de corte, porque la cara donde actua es la cara ABC del octaedro regular de la Fig. 9 que tiene vertices en los ejes coordenados, se usa frecuentemente en Teoría de Plasticidad

TEORIAS DE FALLA

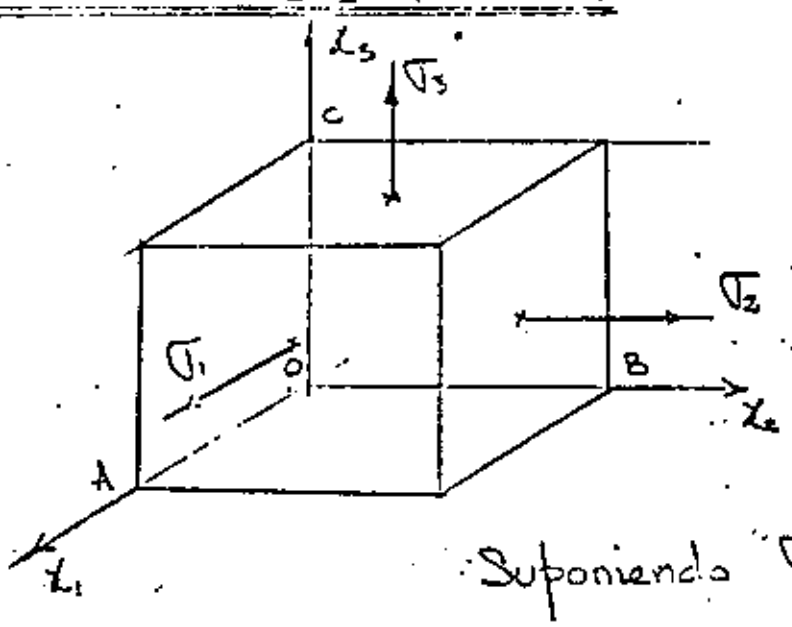

Suponiendo $\sigma_1 > \sigma_2 > \sigma_3$

Fig. 10

En la Fig. 1, después de diagonalizar las componentes del tensor de esfuerzo, se tiene

$$[\bar{\sigma}_{ij}] = \begin{bmatrix} \sigma_1 & 0 & 0 \\ 0 & \sigma_2 & 0 \\ 0 & 0 & \sigma_3 \end{bmatrix} \qquad (51)$$

se trata de obtener la superficie $f(\sigma_1 \sigma_2 \sigma_3) = 0$ en la cual el medio entra a falla plástica, a continuación se presenta el diagrama idealizado esfuerzo deformación en condiciones uniaxiales

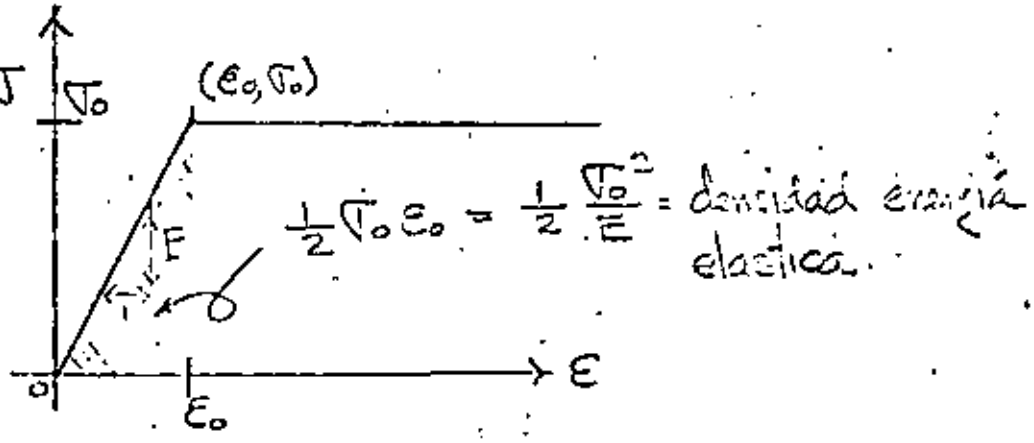

a) Teoría del Máximo esfuerzo (Rankine) 87

Se supone que $\sigma_1 = \sigma_0'$ o $\sigma_3 = \sigma_0'$

σ_0' esfuerzo de fluencia en tensión

σ_0'' " " " " compresión

ó σ_0' y σ_0'' pueden ser dos esfuerzos de fluencia en dos direcciones perpendiculares, suponiendo un estado plano de esfuerzos $\sigma_3 = 0$ y que $\sigma_1 = \sigma_2 = \sigma_0$ se obtiene el diagrama de esfuerzos de la Fig. 12

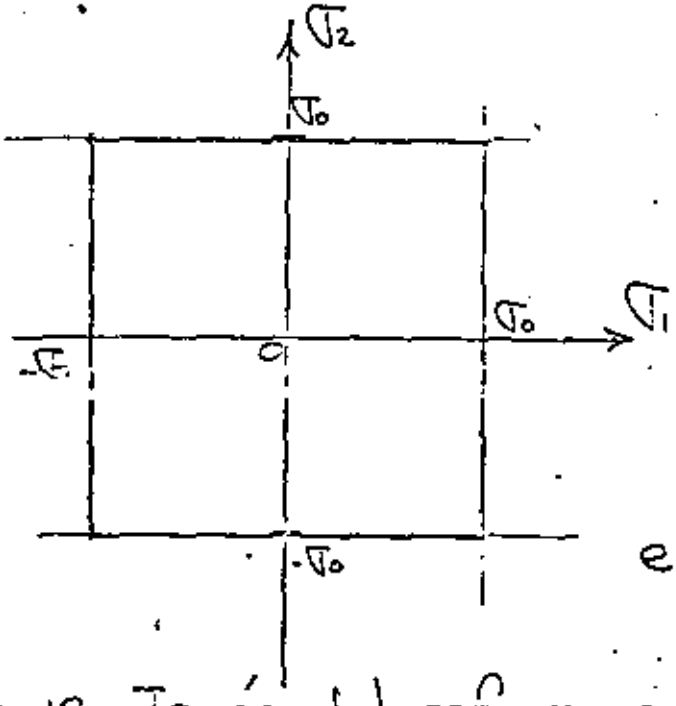

Planos de falla

$\sigma_1 = \pm \sigma_0$

$\sigma_2 = \pm \sigma_0$

$\sigma_3 = \pm \sigma_0$

Superficie cubica en el espacio de esfuerzos

Fig. 12 Teoría del esfuerzo máximo en esfuerzos planos.

b) Teoría de la deformación máxima (Saint-Venant)

Condición triaxial de esfuerzos que alcanza la deformación de fluencia ε_0.

$$\varepsilon_0 = \frac{\sigma_0}{E} = \frac{1}{E}\left[\sigma_1 - \nu(\sigma_2 + \sigma_3)\right] \qquad (52)$$

de (52) la superficie de esfuerzo referida al

espacio de esfuerzos. $\sigma_1, \sigma_2, \sigma_3$ es

$$f_I(\sigma_1 \sigma_2 \sigma_3) = (\sigma_1 - \sigma_0) - \nu(\sigma_2 + \sigma_3) = 0 \qquad (53)$$

en (53) suponiendo $\sigma_3 = 0$ y para $\sigma_1 = \sigma_2 = \sigma$ (esfuerzos planos) se obtiene para $\nu = 0.3$

$$\sigma_0 = (1-\nu)\sigma$$

$$\sigma = \frac{1}{1-\nu}\sigma_0 = \frac{1}{1-0.3}\sigma_0 = 1.43\,\sigma_0 \qquad (54)$$

Si $\sigma_1 = -\sigma_2 = \sigma_0$

$$\sigma_0 = (1+\nu)\sigma_0$$

$$\sigma = \frac{1}{1+\nu}\sigma_0 = \frac{1}{1+0.3}\sigma_0 = 0.77\,\sigma_0 \qquad (55)$$

llevando los valores (54) y (55) al plano σ_1, σ_2 del espacio de esfuerzos se obtiene las rectas de falla de la Fig. 13

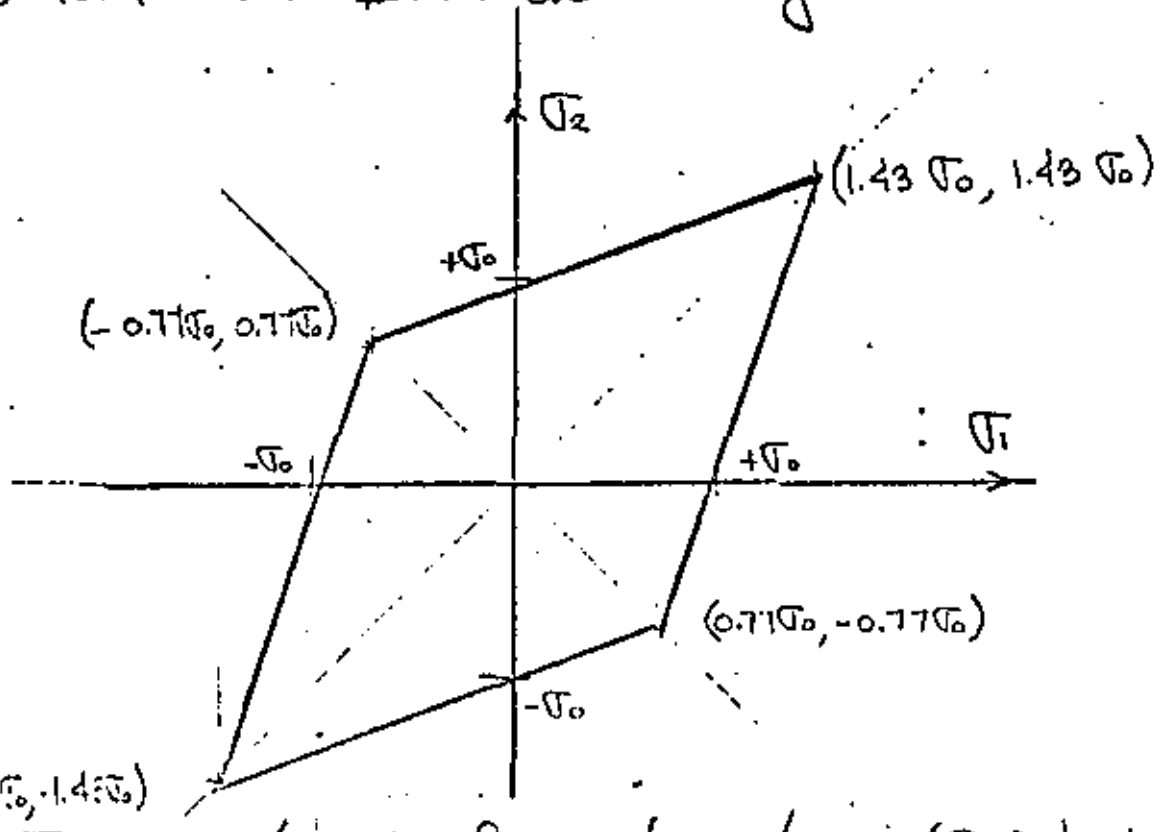

Fig 13 Teoría de deformación máxima (Saint-Venant)

c) Teoría del Esfuerzo Cortante Máximo (Coulomb)

Si $\sigma_1 > \sigma_2 > \sigma_3$ Coulomb establece que la falla se alcanza cuando

$$(\tau_2)_{max} = \frac{\sigma_1 - \sigma_3}{2} = \pm \frac{1}{2}\sigma_0 \qquad (56)$$

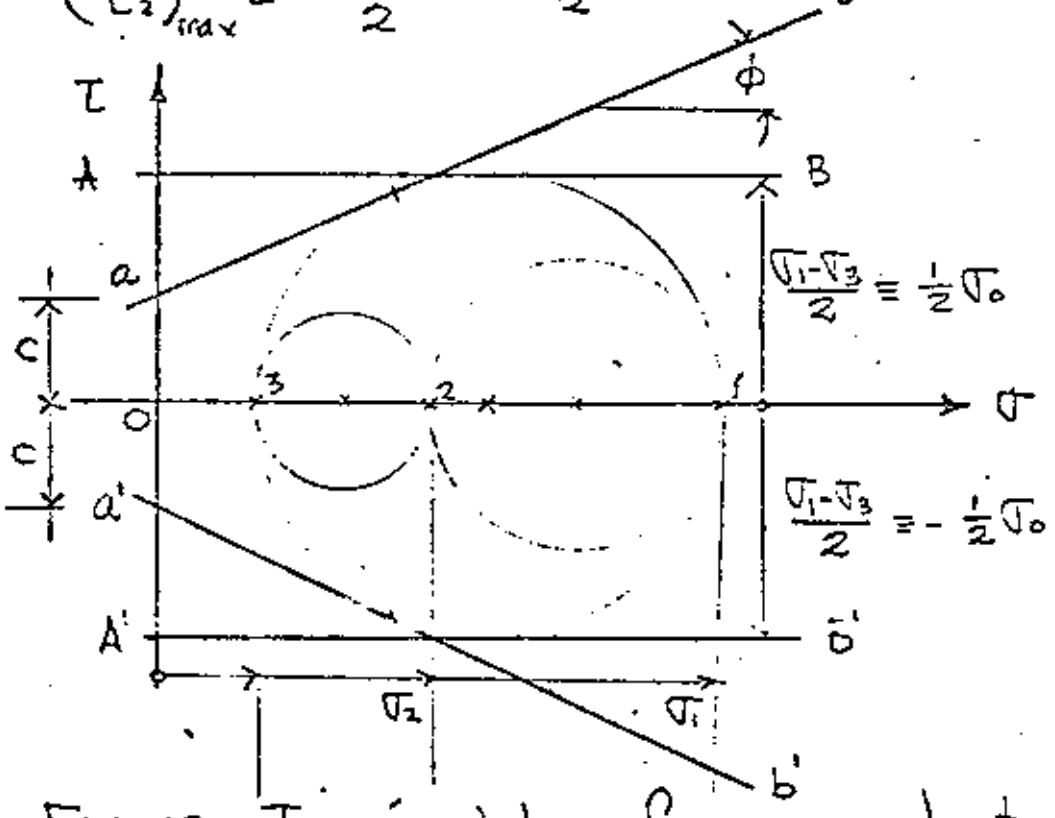

Fig. 13 Teoría del esfuerzo cortante máximo

(56) en el diagrama de Mohor establece como rectas de falla a AB y A'B' en Fig. 13 cuando el ángulo de fricción interna $\phi = 0$, y cuando $\phi > 0$ las rectas de falla son las ab y a'b' cuya ecuación es igual a

$$\tau_{max} = c + \sigma \operatorname{Tan}\phi \qquad (57)$$

c = cohesión o resistencia al esfuerzo cortante puro
ϕ = ángulo de fricción interna
σ = esfuerzo de falla.

c y ϕ son constantes constitutivas experimentales que se pueden obtener mediante una prueba triaxial de ruptura. La ecuación 56 en el plano de esfuerzo $\sigma_1 \sigma_3$ se muestra en la fig. 14

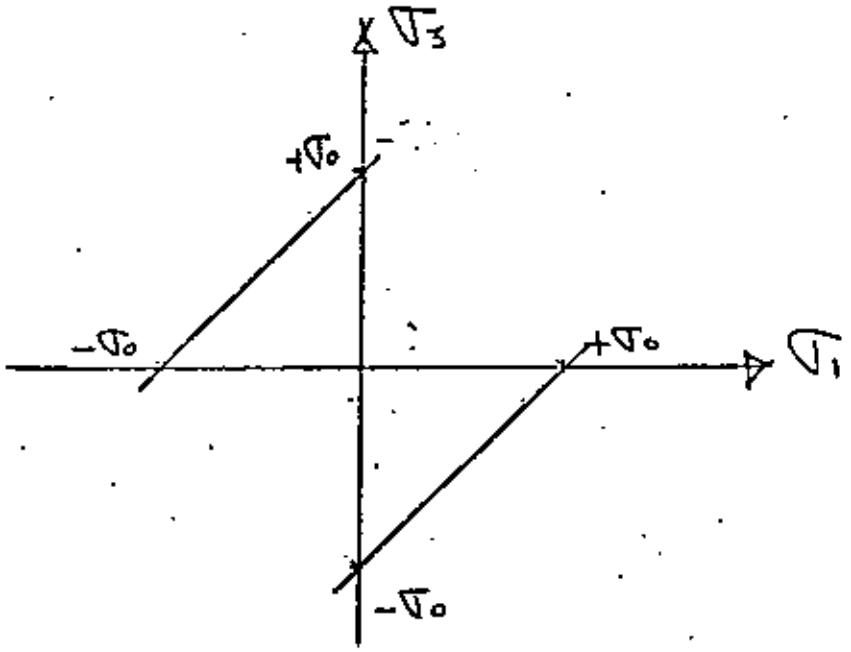

Fig. 14 Teoría del esfuerzo cortante máximo

d) Teoría de la máxima energía de deformación (Beltrami, Haig)

La densidad de energía en un medio elástico lineal viene dada por

$$U_0 = \frac{1}{2E}(\sigma_1^2 + \sigma_2^2 + \sigma_3^2) - \frac{\nu}{E}(\sigma_1\sigma_2 + \sigma_1\sigma_3 + \sigma_2\sigma_3) \quad (58)$$

de la Fig. 11 la densidad de energía hasta el límite elástico σ_0 es

$$U_0 = \frac{1}{2}\frac{\sigma_0^2}{E} \quad (59)$$

de (58) y (59) se obtiene la superficie de falla

$$f(\sigma_i) = \sigma_1^2 + \sigma_2^2 + \sigma_3^2 - 2\nu(\sigma_1\sigma_2 + \sigma_2\sigma_3 + \sigma_3\sigma_1) - \sigma_0^2 = 0 \quad (60)$$

En esfuerzos planos $\sigma_3 = 0$ se obtiene

$$\frac{\sigma_1^2 + \sigma_2^2}{2} - \nu\sigma_1\sigma_2 = \frac{\sigma_0^2}{2} \quad (61)$$

(61) es la ecuación de una elipse la cual en el plano de esfuerzos $\sigma_1\sigma_2$ se muestra en la Fig. 15 para el acero con $\nu = 0.3$, y las

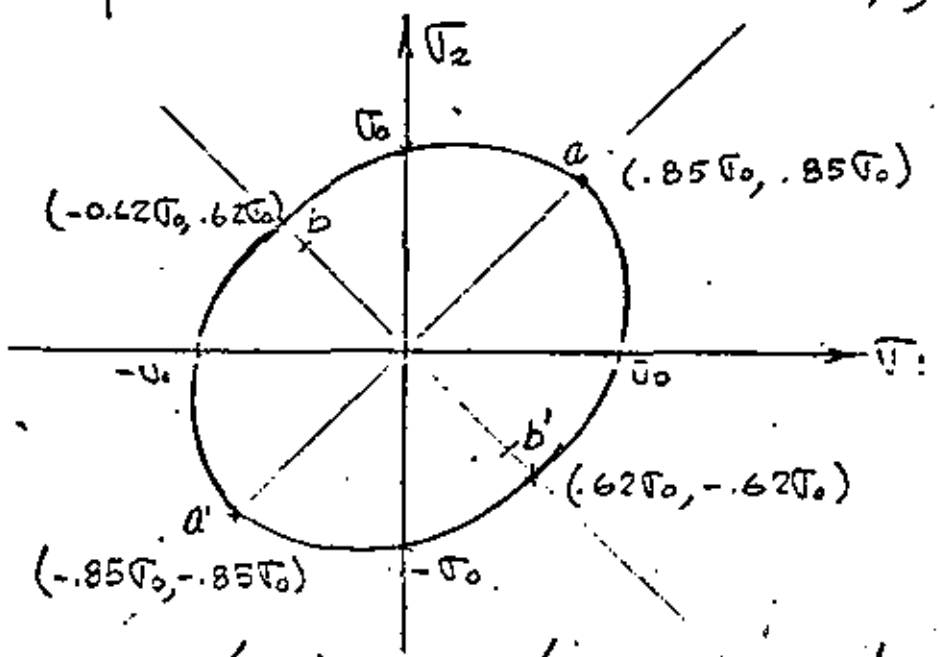

Fig. 15 Teoría de la máxima energía de deformación en el plano $\sigma_1\sigma_2$ para $\nu = 0.3$

Coordenadas de los puntos a, a', b, y b'.

e) Teoría de energía máxima distorsional.
(1856, J.C. Maxwell. M.T. Huber, R.V. Mises, H. Hencky).

Los esfuerzos cortantes máximos actuan sobre el plano octaedral cuyos cosenos directores son

$|n_i| = \left[\frac{1}{\sqrt{3}} \frac{1}{\sqrt{3}} \frac{1}{\sqrt{3}}\right]$, y el esfuerzo normal correspondiente llamado, medio, esférico o hidrostático es

$$p = \frac{1}{3}(\sigma_1 + \sigma_2 + \sigma_3) \qquad (62)$$

la expansión volumétrica por unidad de volumen correspondiente se expresa por

$$e = \varepsilon_1 + \varepsilon_2 + \varepsilon_3 = \frac{2(1-2\nu)}{E} p \qquad (63)$$

la energía por cambio unitario de volumen será

$$U_1 = \frac{1}{2} p e \qquad (64)$$

Substituyendo (62) y (63) en (64) se obtiene

$$U_1 = \frac{1-2\nu}{6E}(\sigma_1 + \sigma_2 + \sigma_3)^2 \qquad (65)$$

en un medio elástico lineal homogeneo e isotrópico la energía de deformación por unidad de volumen es

$$U_0 = \frac{1}{2E}(\sigma_1^2 + \sigma_2^2 + \sigma_3^2) - \frac{\nu}{E}(\sigma_1\sigma_2 + \sigma_2\sigma_3 + \sigma_3\sigma_1) \qquad (66)$$

La densidad de energía desviatonica maxima es

$$\Delta U = U_0 - U_1 \qquad (67)$$

substituyendo (65) y (66) en (67) se obtiene

$$\Delta U = \frac{1+\nu}{6E}\left[(\sigma_1-\sigma_2)^2+(\sigma_1-\sigma_3)^2+(\sigma_2-\sigma_3)^2\right] \quad (68)$$

el valor máximo en (68) sería si $\sigma_2=\sigma_3=0$ y (68) se transforma para $\sigma_1=\sigma_0$ en

$$\Delta U_{max} = \frac{1+\nu}{3E}\sigma_0^2 \quad (69)$$

por lo tanto de (68) y (69) se obtiene cuando $\Delta U = \Delta U_{max}$

$$f(\sigma_i) = (\sigma_1-\sigma_2)^2+(\sigma_1-\sigma_3)^2+(\sigma_2-\sigma_3)^2 - 2\sigma_0^2 = 0 \quad (70)$$

(70) es la ecuación de de un cilindro circular cuyo eje y directrices en el espacio de esfuerzo forma iguales ángulos con los ejes σ_i, la intersección de (70) con el plano $\sigma_1\sigma_2$ se obtiene de (70) para $\sigma_3=0$.

$$(\sigma_1-\sigma_2)^2+\sigma_1^2+\sigma_2^2-2\sigma_0 = 0 \quad (71)$$

(71) y (61) deben ser iguales para $\nu=0.5$ material incompresible (71) representa también una elipse como en la Fig. 15 solo que las coordenadas de a, a', b y b' son para $\nu=0.3$

$a(\sigma_0, \sigma_0)$ $\quad$ $b(-0.577\sigma_0, 0.577\sigma_0)$

$a'(-\sigma_0, -\sigma_0)$ $\quad$ $b'(0.577\sigma_0, -0.577\sigma_0)$

ABCD: Teoría del esfuerzo máximo. (Rankine) 94

EFGH: " deformación máxima. (Saint-Venant)

——— " de máxima energía de deformación. (Beltrami)

– – – – " " " " distorcionante. (Von-Mises)

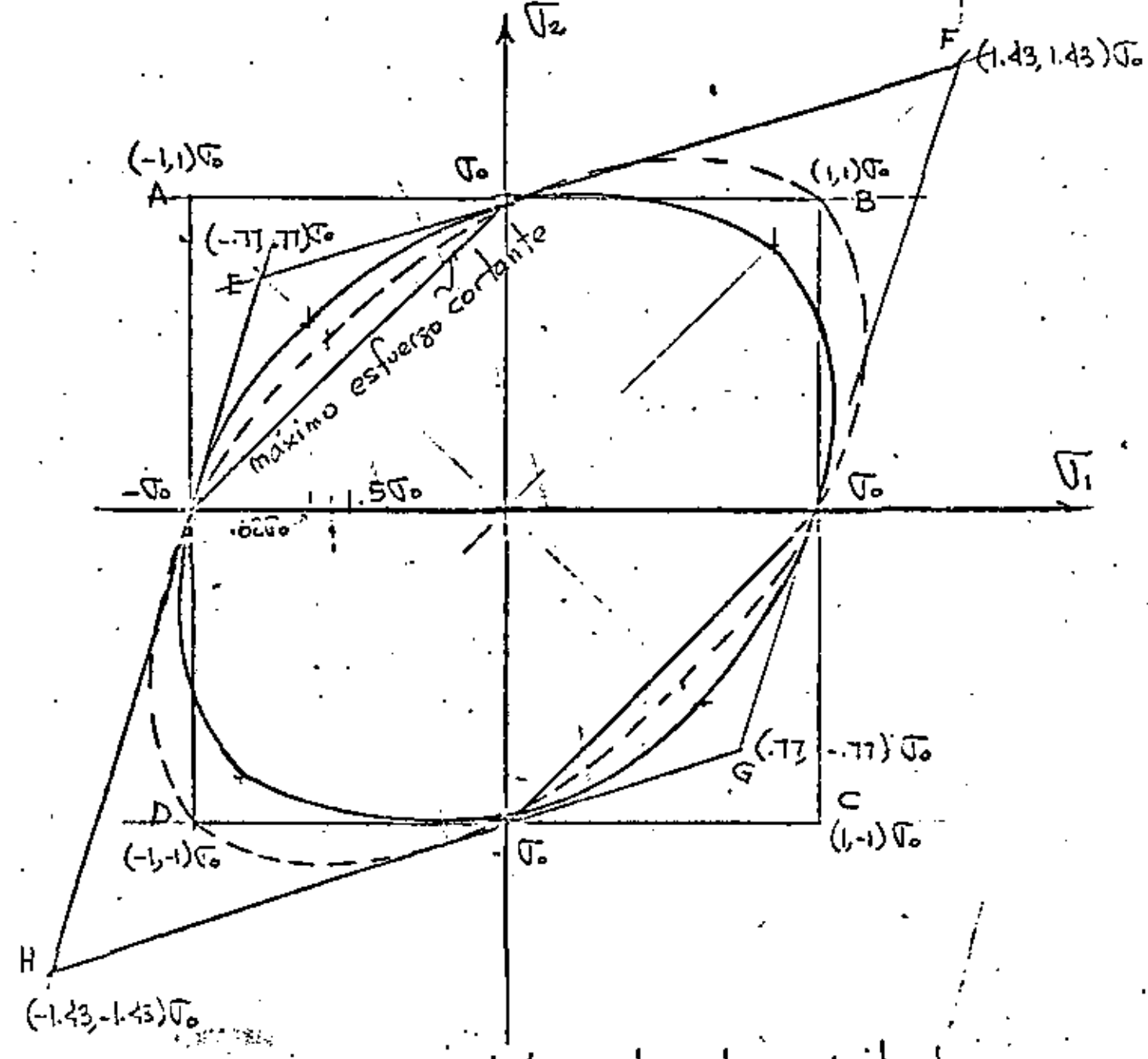

Fig. 16 Comparación entre las distintas Teorías de falla para $\nu = 0.3$, $\phi = 0$

EL METODO DEL ELEMENTO FINITO EN LA INGENIERIA MECANICA

M O D E L A C I O N

DR. VICTOR HUGO HUCIÑO QUINTERO

ABRIL, 1982

El Método del Elemento Finito en la Ingeniería Mecánica

3 MODELACION

3.1 Introducción

El concepto fundamental del método del elemento finito (MEF) consiste en que cualquier función continua en un dominio dado, pueda aproximarse mediante una sucesión de funciones que se definan en una serie de subdominios dentro de los cuales estas funciones son continuas y las cuales se interconectan para aproximar así la función dada (Fig.3.1)

Desde un punto de vista físico, el concepto fundamental del método del elemento finito consiste en que para resolver un sistema que representa una estructura física sujeta a ciertas condiciones físicas, se puede utilizar un modelo aproximado compuesto de una serie de elementos que se interconectan en una serie de puntos llamados nodos (Fig.3.2) y cuyo comportamiento es conocido a través de ciertas ecuaciones preestablecidas y que corresponden a los tipos de elementos usados y al número de nodos en cada uno de ellos.

La solución de las ecuaciones del modelo pueden ser exactas, pero el modelo en sí es una aproximación discreta al sistema físico y la solución de dicho modelo se aproxima a la solución del sistema real. Los antecedentes del método del elemento finito datan de los años 50's cuando surgió del análisis de estructuras aeronáuticas, y ha evolucionado rápidamente hasta expander sus aplicaciones a varios campos de la ingeniería como son la transmisión de calor, la elasticidad, mecánica de fluidos, estructuras, lubricación y otras muchas.

3.2 Formulación de un Problema de Ingeniería

La formulación matemática en problemas de ingeniería generalmente se puede efectuar en dos formas diferentes, la primera considera el comportamiento de una área o volumen infinitecimal del sistema y las ecuaciones correspondientes se formulan en forma diferencial, y como el área o volumen considerado es representativo de toda la región, las mismas ecuaciones son válidas para todo el dominio de esa región. Como ejemplo tenemos la ecuación de Reynolds en la lubricación hidrodinámica de cojinetes (Fig 3.3) la cual es una ecuación diferencial en dos dimensiones que se deriva a partir de un elemento infinetesimal y es de la forma:

$$\frac{1}{R}\frac{\partial}{\partial\theta}\left[h^3\frac{\partial P}{\partial\theta}\right]+\frac{\partial}{\partial z}\left[h^3\frac{\partial P}{\partial z}\right]=6\mu\omega\frac{\partial h}{\partial\theta} \qquad (3.1)$$

en donde h es el espesor de la capa lubricante, θ es la coordenada polar angular, z es la perpendicular al plano (x,y), μ es la viscosidad del lubricante, ω es la velocidad angular de rotación de la flecha y P es la distribución de la presión al rededor y a lo largo del eje z.

En la segunda alternativa se postula un principio que engloba la región entera o dominio dado y consecuentemente es una formulación en forma integral y la solución es generalmente dada por valores extremos de dicha integral. Este método es conocido como el Método Variacional y como ejemplo se tiene el caso de la energía potencial de cuerpos elásticos, en el cual se establece que la configuración del equilibrio estático de una estructura deformable requiere de una energía potencial mínima. Esta energía se refiere al total de la energía de toda la estructura y se obtiene mediante la suma de energías de las partes de la estructura.

De todas las posibles configuraciones que la estructura pueda adoptar, aquella que cada un valor mínimo a la energía potencial nos da la configuración de equilibrio. Esto se conoce como el Principio de la Energía Potencial Mínima.

Resumiendo lo anterior, el procedimiento para desarrollar el análisis de una estructura deformable consiste en establecer un funcional, el cual es el valor de una integral y que tiene la forma

$$\Pi = \int_{x_a}^{x_b} F(x,\eta,\eta')\,dx \qquad (3.2)$$

en donde

$$\eta = \eta(x) \quad , \quad \eta' = \frac{d\eta(x)}{dx} \qquad (3.1)$$

Una vez establecido este funcional se procede a encontrar sus valores extremos, lo cual requiere que su primera variación sea igual a cero, es decir que cumpla con la condición de estacionaridad de una integral mediante:

$$\delta \Pi = 0 \qquad (3.4)$$

Cabe mencionar que encontrar el valor estacionario de una integral es similar a encontrar los valores mínimos o máximos de una función en cálculo diferencial, excepto que al minimizar una función se obtiene un valor de la variable independiente que nos da un mínimo en la función, mientras que al minimizar un funcional se obtiene una función que al integrarse hace el valor de dicha integral mínimo.

Para llevar a cabo lo anterior se puede proceder a discretizar la integral mediante la siguiente ecuación

$$\Pi = \int_{x_a}^{x_b} F(x,\eta,\eta')dx = \int_{x_a}^{x_1} F(x,\eta,\eta')dx + \int_{x_1}^{x_2} F(x,\eta,\eta')dx + \cdots + \int_{x_n}^{x_b} F(x,\eta,\eta')dx \qquad (3.5)$$

O bien:

$$\Pi = \Pi_1 + \Pi_2 + \Pi_3 + \cdots + \Pi_n \qquad (3.6)$$

La integral total π ahora consiste en varias integrales parciales π_i, cada una extendiéndose en los subdominios (x_{i-1}, x_i).

El concepto de discretizar la integral de la ecuación (3.4) puede tener una interpretación física al dividir el dominio de la función en una serie de elementos a los cuales se asigna cada una de las integrales. La ventaja es que ahora es posible usar alguna aproximación polinomial (lineal, parabólica etc.) para la función $Y(x)$ en cada integral, es decir en cada elemento. Esto permite que el valor de cada función integral sea una función de los coeficientes utilizados en el polinomio de dicho elemento. Entonces la integral total π es también una función de los coeficientes polinomiales usados en cada uno de los elementos y la condición de la ecuación 3.2 se satisface si

$$\frac{\partial \Pi}{\partial a_i} = 0 \qquad (i = 1,2,\ldots n) \qquad (3.7)$$

donde las a_i's son el juego completo de coeficientes polinomiales usados en cada elemento.

Al substituir la función $Y(x)$ por una aproximación polinomial $y(x)=a_1x+a_2x^2\ldots$ el problema se reduce a encontrar los coeficientes de los polinomios usados en la aproximación.

Es decir, la solución directa de la ecuación (3.2) sujeta a las condiciones (3.3) puede ser bastante complicada y es necesario aplicar los conceptos de cálculo variacional, sin embargo el problema se puede formular mediante la ecuación (3.5) y al substituir la aproximación polinomial el problema se puede resolver algebráicamente

3.2 Energía Potencial

En la introducción de conceptos fundamentales del método del elemento finito se derivaron unas ecuaciones algebráicas de equilibrio que en forma matricial se pueden expresar como:

$$[K]\{D\} = \{P\} \tag{3.8}$$

Este sistema de ecuaciones representa un modelo matemático cuya interpretación física está directamente relacionada con la definición de un sistema físico el cual consiste de un cuerpo deformable caracterizado por la matriz de propiedades elásticas [k], y por las cargas que actuan sobre el sistema {P} que ocasionan ciertos desplazamientos en dicho cuerpo {D}.

En general, un cuerpo elástico es la composición de una infinidad de partículas las cuales interactuan entre si y producen ciertas respuestas a ciertas perturbaciones y dado a que existe un número infinito de partículas en cada cuerpo no es conveniente describir la respuesta de un sistema elástico en términos de los desplazamientos de cada partícula, más bien se toma un número finito de puntos que puedan caracterizar el comportamiento del sistema.

En ciertos casos es posible formular las ecuaciones de equilibrio en base a relaciones directas de carga y desplazamiento, como es en el caso de resortes lineales, o vigas, pero en otros casos no es tan evidente la relación de carga y deformación y por lo tanto es conveniente usar métodos alternativos para la formulación de las ecuaciones de equilibrio. Uno de estos métodos se basa en la expresión de la energía potencial la cual se define como sigue:

La energía potencial de un cuerpo deformable sujeto a cargas estáticas es igual a la energía interna o de deformación almacenada en el cuerpo deformado menos el trabajo

realizado por las cargas que actuan en el a lo largo de los desplazamientos de los puntos de aplicación de dichas cargas. Esto se puede expresar como sigue

$$V = U - W \tag{3.9}$$

en donde V=Energía potencial
U=Energía de deformación o interna.
W=Trabajo de las cargas aplicadas

Como ejemplo podemos considerar el caso simple de un resorte lineal mostrado en la Fig. 3.4. El desplazamiento D del extremo libre del resorte es ocasionado por la carga P aplicada en ese extremo en tonces la energía potencial se puede expresar como:

$$V = \int_0^D kx\,dx - \int_0^D P\,dx \tag{3.10}$$

En esta expresión, la primera integral representa la energía de deformación y la segunda el trabajo realizado por la carga sobre el resorte de constante K. Al integrar se obtiene:

$$V = \tfrac{1}{2}(kx^2)\Big|_0^D - Px\Big|_0^D = \tfrac{1}{2}kD^2 - PD \tag{3.11}$$

Es decir la expresión de la energía potencial es el valor de una integral y por lo tanto V es un funcional el cual puede ser minimizado, de acuerdo al principio de la energía potencial mínima. Entonces de la ecuación (3.4) se tiene que:

$$\delta V = (kD - P)\delta D \tag{3.12}$$

La cual es consistente con el principio de trabajo virtual y dado que δD es diferente de cero entonces

$$KD - P = 0 \qquad (3.12a)$$

Es decir que el desplazamiento D que resulta en el equilibrio del sistema es tal que:

$$D_e = \frac{P}{K} \qquad (3.12b)$$

Gráficamente la ecuación (3.11) se puede representar por medio de la suma de dos funciones tal como se muestra en la fig 3.5, de tal forma para un potencial mínimo se tiene que el desplazamiento D es aquel que produce el equilibrio.

3.3 Sistemas con Varios Grados de Libertad

Por definición los grados de libertad son aquellas variables que definen completamente y en forma única el estado o configuración de un sistema dado, por ejemplo, el sistema de resorte lineal que se acaba de ver es un sistema con un solo grado de libertad ya que una sola cantidad define el estado del sistema, esa variable es el desplazamiento lineal del extremo del resorte. Si en ese extremo se anexa otro resorte, entonces existen dos grados de libertad y así sucesivamente. Sin embargo la naturaleza de los grados de libertad no es necesariamente la misma, ya que éstos se pueden referir a desplazamientos, rotaciones, temperaturas o también coeficientes de un polinomio que aproximan una función.

Si consideramos un sistema elástico con n grados de libertad el cual está sujeto a ciertas perturbaciones. Entonces la energía potencial total se puede expresar como un función de estos n grados de libertad o sea

$$\Pi_T = \Pi_T(D_1, D_2, D_3 \ldots D_n) \qquad (3.13)$$

entonces la primera variación del potencial con respecto a los grados de libertad se expresa como

$$\delta\Pi_T = \frac{\partial \Pi_T}{\partial D_1}\delta D_1 + \frac{\partial \Pi_T}{\partial D_2}\delta D_2 + \frac{\partial \Pi_T}{\partial D_3}\delta D_3 \ldots + \frac{\partial \Pi}{\partial D_n}\delta D_n \qquad (3.14)$$

la cual debe cumplir con la condición de estacionaridad de la ecuación (3.4), es decir $\delta\Pi = 0$ y por lo tanto:

$$\frac{\partial \Pi}{\partial D_1} = \frac{\partial \Pi}{\partial D_2} = \ldots = \frac{\partial \Pi}{\partial D_n} = 0 \qquad (3.15)$$

De acuerdo con el principio de energía potencial mínima, la ecuación (3.15) define la configuración de equilibrio del sistema.

Un ejemplo de un sistema con dos grado de libertad es el que se muestra en la fig. 3.6 el cual consta de dos resortes lineales empotrados, y una barra rígida ligada los dos resortes con una carga puntal como se muestra. La expresión para la energía potencial se puede escribir ya integrada como:

$$V = \frac{1}{2}K_1D^2 + \frac{1}{2}K_2(D + \theta L)^2 - P(D + \theta a) \qquad (3.16)$$

Al substituir V por Π en la ecuación (3.5) el resultado es:

$$\frac{\partial V}{\partial D} = K_1D + K_2D + K_2\theta L - P = 0 \qquad (3.17)$$

$$\frac{\partial V}{\partial \theta} = K_2LD + K_2L^2\theta - aP = 0 \qquad (3.18)$$

que en forma matricial adquiere la siguiente forma

$$\begin{bmatrix} (k_1+k_2) & k_2 L \\ k_2 L & k_2 L^2 \end{bmatrix} \begin{Bmatrix} D \\ \theta \end{Bmatrix} - \begin{Bmatrix} P \\ aP \end{Bmatrix} = \begin{Bmatrix} 0 \\ 0 \end{Bmatrix} \qquad (3.19)$$

que se pueda reducir a la forma común de las ecuaciones de equilibrio

$$[K]\{x\} = \{F\} \qquad (3.20)$$

En la ecuación 3.19, (F) y (aP) son llamadas las fuerzas generalizadas correspondientes a las coordenadas generalizadas (D) y (θ).

De este ejemplo se puede concluir entonces que la matriz de rigidez [k] es una matriz simétrica es decir $k_{ij}=k_{ji}$ y también que el producto de una fuerza generalizada por su correspondiente coordenada siempre tiene unidades de trabajo.

Si un tercer resorte es anexado al sistema digamos en el punto intermedio de la barra, el sistema se convierte en un sistema estaticamente indeterminado, sin embargo las coordenadas D y θ son aun suficientes para determinar la configuración del sistema y dos ecuaciones de equilibrio son generadas, es decir la indeterminación estática no afecta el procedimiento general basado en la minimización del potencial.

3.4 Formulación General Usando Campos de Desplazamiento

Antes de desarrollar una expresión general para la energía potencial de cuerpos elásticos es conveniente describir el concepto de campo de desplazamiento y aproximaciones.

En muchos sistemas mecánicos la configuración del mismo en un instante dado puede ser expresada en términos de los desplazamientos de ciertos puntos de referencia, los cuales representan un campo de desplazamientos con respecto a un marco de referencia. Por ejemplo el campo de desplazamiento de una barra elastica de sección uniforme con una carga axial Fig.3.7 se puede describir en términos de los desplazamientos en los extremos de la misma en una forma lineal. Es decir el desplazamiento en cualquier punto intermedio de una barra se puede expresar como una función del desplazamiento de los puntos extremo de la misma con una relación de la forma

$$D_x = D_i + \frac{x}{L}(D_j - D_i) \qquad (3.21)$$

Donde Dx es el desplazamienot de un punto en la coordenada x de la barra, L es la longitud original de la barra y D(i,j) es el desplazamiento del extremo (i,j) de la barra.

La ecuación (3.21) puede escribirse en forma matricial como sigue;

$$D_x = \left[\left(1-\frac{x}{L}\right) \quad \left(\frac{x}{L}\right)\right] \begin{Bmatrix} D_i \\ D_j \end{Bmatrix} \qquad (3.22)$$

Si consideramos que la barra representa un elemento con el nodo i en el extremo i y el nodo j en el extremo j y que f es el desplazamiento de un punto cualquiera del elemento entonces la ecuación (3.22) se puede expresar en forma matricial como sigue:

$$\{f\} = [N]\{d\} \qquad (3.23)$$

En el caso de un elemento en dos dimensiones como el mostrado en la Fig.3.8, el vector {d} los desplazamientos en dos dimensiones de los nodos del elemento, entonces la ecuación (3.23) tendría la forma:

$$\{f\} = \begin{Bmatrix} u \\ v \end{Bmatrix} = \begin{bmatrix} N_1 & 0 & N_2 & 0 & N_3 & 0 & N_4 & 0 \\ 0 & N_1 & 0 & N_2 & 0 & N_3 & 0 & N_4 \end{bmatrix} \begin{Bmatrix} u_1 \\ v_1 \\ u_2 \\ v_2 \\ u_3 \\ v_3 \\ u_4 \\ v_4 \end{Bmatrix} \qquad (3.24)$$

en donde:

$$N_1 = \frac{(b-x)(c-y)}{4bc} \quad , \quad N_2 = \frac{(b+x)(c+y)}{4bc}$$

$$N_3 = \frac{(b+x)(c-y)}{4bc} \quad , \quad N_4 = \frac{(b-x)(c+y)}{4bc} \qquad (3.25)$$

$N_{1,2,3,4}$ son llamadas las funciones de "forma" o de interpolación. La descripción del campo de desplazamiento para otros elementos también es posible en base de los desplazamientos nodales, es decir que es posible conocer el desplazamiento absoluto de cualquier punto en un elemento o estructura conociendo el vector de desplazamientos nodales. Por lo tanto la formulación general usando elementos finitos está orientada a obtener la solución de un sistema con un número finito de grados de libertad, en donde los grados de libertad son los desplazamientos independientes de cada nodo y donde dichos desplazamientos pueden ser de traslación o de rotación.

La aproximación a un campo de desplazamiento también se puede hacer en base a un polinomio cuyo grado de libertad sea el mismo que el correspondiente al elemento en cuestión, por ejmplo en el caso de la barra uniforme se puede utilizar un polinomio del tipo:

$$\{f\} = \{u\} = \{a_1 + a_2 x\} \qquad (3.26)$$

$$\{f\} = \begin{bmatrix} 1 & x \end{bmatrix} \begin{Bmatrix} a_1 \\ a_2 \end{Bmatrix} \qquad (3.27)$$

en donde a_1 y a_2 son los coeficientes del polinomio de grado 1, entonces hay dos coeficientes para un elemento que tiene dos grados de libertad.

Los desplazamientos nodales $\{d\}$ se pueden expresar en función de estos coeficientes substituyendo las condiciones de frontera

$$u_{x=0} = u_i$$

$$u_{x=L} = u_j \qquad (3.28)$$

Entonces substituyendo en (3.26) resulta el siguiente sistema:

$$\{d\} = \begin{Bmatrix} u_i \\ u_j \end{Bmatrix} = \begin{bmatrix} 1 & 0 \\ 1 & L \end{bmatrix} \begin{Bmatrix} a_1 \\ a_2 \end{Bmatrix} = [A]\{a\} \qquad (3.29)$$

Despejando $\{a\}$ de (3.29) y substituyendo en (3.27) se tiene

$$\{f\} = \begin{bmatrix} 1 & x \end{bmatrix} [A]^{-1} \{d\} \qquad (3.30)$$

Invirtiendo la matriz $[A]$ y desarrollando el producto en la ecuación (3.30) se obtiene la ecuación (3.22) o sea:

$$\{f\} = \begin{bmatrix} (1 - \frac{x}{L}) & (\frac{x}{L}) \end{bmatrix} \{d\} = [N]\{d\} \qquad (3.31)$$

En el caso de un elemento plano triangular como el mostrado en la Figura3.8, la aproximación se puede hacer en base a las siguientes polinomios:

$$u = a_1 + a_2 x + a_3 y$$

$$v = a_4 + a_5 x + a_6 y \qquad (3.32)$$

Que en forma matricial quedan expresados como

$$\begin{Bmatrix} u \\ v \end{Bmatrix} = \begin{bmatrix} 1 & x & y & 0 & 0 & 0 \\ 0 & 0 & 0 & 1 & x & y \end{bmatrix} \begin{Bmatrix} a_1 \\ a_2 \\ a_3 \\ a_4 \\ a_5 \\ a_6 \end{Bmatrix} \tag{3.33}$$

Tomando las condiciones de frontera se obtiene que para la dirección x

$$\begin{Bmatrix} u_1 \\ u_2 \\ u_3 \end{Bmatrix} = \begin{bmatrix} 1 & x_1 & y_1 \\ 1 & x_2 & y_2 \\ 1 & x_3 & y_3 \end{bmatrix} \begin{Bmatrix} a_1 \\ a_2 \\ a_3 \end{Bmatrix} \tag{3.34}$$

y para la dirección y

$$\begin{Bmatrix} v_1 \\ v_2 \\ v_3 \end{Bmatrix} = \begin{bmatrix} 1 & x_1 & y_1 \\ 1 & x_2 & y_2 \\ 1 & x_3 & y_3 \end{bmatrix} \begin{Bmatrix} a_4 \\ a_5 \\ a_6 \end{Bmatrix} \tag{3.35}$$

de donde

$$\begin{Bmatrix} a_1 \\ a_2 \\ a_3 \end{Bmatrix} = [A]^{-1} \begin{Bmatrix} u_1 \\ u_2 \\ u_3 \end{Bmatrix} \tag{3.36}$$

y

$$\begin{Bmatrix} a_4 \\ a_5 \\ a_6 \end{Bmatrix} = [A]^{-1} \begin{Bmatrix} v_1 \\ v_2 \\ v_3 \end{Bmatrix} \tag{3.37}$$

Substituyendo (3.36) y (3.37) en la ecuación (3.33) se obtiene

$$u = [1 \;\; x \;\; y][A]^{-1}\{u_1 \; u_2 \; u_3\}^T \tag{3.38}$$

$$v = [1 \;\; x \;\; y][A]^{-1}\{v_1 \; v_2 \; v_3\}^T \tag{3.39}$$

y donde

$$[A]^{-1} = \begin{bmatrix} x_2y_3 - x_3y_2 & x_3y_1 - x_1y_3 & x_1y_2 - x_2y_1 \\ y_2 - y_3 & y_3 - y_1 & y_1 - y_2 \\ x_3 - x_2 & x_1 - x_3 & x_2 - x_1 \end{bmatrix} \tag{3.40}$$

Substituyendo (3.40) en (3.38) y (3.39) y reduciendo el sistema resultante se

$$\begin{Bmatrix} u \\ v \end{Bmatrix}_{Triang^{lo}} = \begin{bmatrix} N_1 & 0 & N_2 & 0 & N_3 & 0 \\ 0 & N_1 & 0 & N_2 & 0 & N_3 \end{bmatrix} \begin{Bmatrix} u_1 \\ v_1 \\ u_2 \\ v_2 \\ u_3 \\ v_3 \end{Bmatrix} \tag{3.41}$$

en donde

$$N_1 = \frac{1}{2A}\left[\frac{2A}{3} + (y_2 - y_3)x + (x_3 - x_2)y\right] \tag{3.42}$$

$$N_2 = \frac{1}{2A}\left[\frac{2A}{3} + (y_3 - y_1)x + (x_1 - x_3)y\right] \tag{3.43}$$

$$N_3 = \frac{1}{2A}\left[\frac{2A}{3} + (y_1 - y_2)x + (x_2 - x_1)y\right] \tag{3.44}$$

De la misma manera se puede aproximar el campo de desplazamiento para un elemento cuadrilatero plano de la Fig. 3.7 usando polinomios del tipo:

$$u = a_1 + a_2x + a_3y + a_4xy \tag{3.45}$$

$$v = a_5 + a_6x + a_7y + a_8xy \tag{3.46}$$

Los cuales conducen a un sistema equivalente al dado en las ecuaciones (3.34) y (3.35).

3.25 Expresión General de la Energía Potencial

Podemos considerar ahora el caso general de un cuerpo elástico en el espacio el cual está sujeto a cargas que producen un campo de desplazamientos, deformaciones y esfuerzos tal que en un punto dado de dicho cuerpo y con respecto a un marco de referencia, los vectores de esfuerzos y de deformaciones son:

$$\{\sigma\} = \{\sigma_x \; \sigma_y \; \sigma_z \; \tau_{xy} \; \tau_{yz} \; \tau_{zx}\}^T \tag{3.47}$$

y $$\{\epsilon\} = \{\epsilon_x \ \epsilon_y \ \epsilon_z \ \gamma_{xy} \ \gamma_{yz} \ \gamma_{zx}\}^T \quad (3.48)$$

La relación esfuerzo-deformación puede escribirse como:

$$\{\sigma\} = [E]\{\epsilon\} + \{\sigma_0\} \quad (3.49)$$

en donde $[E]$ es la matriz de propiedades elásticas del material y el vector $\{\sigma_0\}$ es el vector de esfuerzos iniciales (dichos esfuerzos iniciales pueden referirse a los esfuerzos presentes sin la aplicación de las cargas externas, como podrían ser esfuerzos residuales, esfuerzos de ensamble etc.).

La definición de energía interna o de deformación se puede escribir como

$$U_e = \frac{1}{2}\{\epsilon\}^T[E]\{\epsilon\} - \frac{1}{2}\{\epsilon_0\}^T[E]\{\epsilon_0\} \quad (3.50)$$

Esta energía de deformación es originada por ciertas cargas que actuan en el cuerpo las cuales desarrolan un cierto trabajo. Estas fuerzas se pueden clasificar en fuerzas internas o de cuerpo, que en un punto cualquiera tiene la forma:

$$\{\phi\} = \{\phi_x \ \phi_y \ \phi_z\}^T \quad (3.51)$$

y el vector de fuerzas de superficie expresado por:

$$\{F\} = \{F_x \ F_y \ F_z\}^T \quad (3.52)$$

Entonces usando las expresiones (3.49) a la (3.52) y la expresión general de la energía potencial de la siguiente forma

$$\Pi = \int_{vol}\left(\frac{1}{2}\{\epsilon\}^T[E]\{\epsilon\} + \{\epsilon\}^T\{\sigma_0\}\right)dV - \int_{vol}\{f\}^T\{F\}\,dV - \int_{Sup}\{f\}^T\{\phi\}\,dS \quad (3.53)$$

en donde la primera integral representa la energía interna o de deformación, la segunda integral representa el trabajo desarrollado por las fuerzas de cuerpo sobre la estructura y la tercera integral representa el trabajo desarrollado por las fuerzas de superficie sobre el cuerpo. La ecuación (3.53) es una forma más general de la ecuación (3.9).

3.6 Formulación Elemental en Base a la Energía Potencial

El objetivo ahora es formular las ecuaciones que caracterizan un elemento en base a la minimización de la energía potencial usando la expresión general (3.53) y la expresión del campo de desplazamiento $\{f\}=\{u \ v \ w\}$.

Primeramente las deformaciones en un elemento se pueden expresar en terminos de los desplazamientos nodales a través de la siguiente expresión

$$\{\epsilon\} = [B]\{d\} \quad (3.54)$$

en donde $[B]$ es la matriz esfuerzo-deformación que en el caso general de un material elástico isotropico es de la forma

$$[B] = \frac{E}{(1+\nu)(1-2\nu)}\begin{bmatrix} 1-\nu & \nu & \nu & 0 & 0 & 0 \\ \nu & 1-\nu & \nu & 0 & 0 & 0 \\ \nu & \nu & 1-\nu & 0 & 0 & 0 \\ 0 & 0 & 0 & \frac{1-2\nu}{2} & 0 & 0 \\ 0 & 0 & 0 & 0 & \frac{1-2\nu}{2} & 0 \\ 0 & 0 & 0 & 0 & 0 & \frac{1-2\nu}{2} \end{bmatrix} \quad (3.55)$$

Substituyendo las ecuaciones (3.23) y (3.54) en (3.53) la energía potencial puede expresarse como:

$$\Pi_e = \frac{1}{2}\{d\}^T\left(\int_{Vol}[B]^T[E][B]\,dV\right)\{d\} + \{d\}^T\int_{Vol}[B]^T\{G_i\}\,dV$$

$$-\{d\}^T\int_{Vol}[N]^T\{F\}\,dV - \{d\}^T\int_{S_\sigma}[N]^T\{\bar{\Phi}\}\,dS \qquad (3.56)$$

En esta ecuación el subíndice en π_e indica que la energía potencial es de un elemento y por lo tanto el vector $\{d\}$ es el vector de desplazamientos nodales de un elemento solamente, y para una estructura compuesta de varios elementos se tiene que la energía potencial total se expresa como la sumatoria de las energías potenciales de cada uno de los elementos y la energía potencial total queda expresada como:

$$\Pi_T = \frac{1}{2}\{D\}^T\left(\sum_{i}^{m}\int_{Vol}[B]^T[E][B]\,dV\right)\{D\} + \{D\}^T\sum_{i}^{m}\left(\int_{Vol}[B]^T\{G_i\}\,dV\right.$$

$$\left.-\int_{Vol}[N]^T\{F\}\,dV - \int_{S_\sigma}[N]^T\{\bar{\Phi}\}\,dS\right) - \{D\}^T\{P\} \qquad (3.57)$$

Una vez encontrada la expresión general de la energía potencial se procede a encontrar el valor extremo del funcional π_T substituyendo en la ecuación (3.4) lo cual resulta en el sistema de ecuaciones dado por la ecuación (3.7) o

$$\left\{\frac{\partial \Pi_T}{\partial D}\right\} = 0 \qquad (3.58)$$

Entonces al substituir π_p dado por la ecuación (3.57) en la ecuación (3.58) se obtiene el siguiente sistema de ecuaciones de equilibrio.

$$\left(\sum_{i}^{m}\int_{Vol}[B]^T[E][B]\,dV\right)\{D\} = \sum_{i}^{m}\left(-\int_{Vol}[B]^T\{G_i\}\,dV + \int_{Vol}[N]^T\{F\}\,dV\right.$$

$$\left.+\int_{S_\sigma}[N]^T\{\bar{\Phi}\}\,dS\right) + \{P\} \qquad (3.59)$$

La ecuación (3.59) se puede abreviar en tal forma que la sumatoria de las integrales del lado izquierdo de la ecuación (3.59) sea identificada como la "Matriz de Rigidez" y la sumatoria de integrales del lado derecho de la ecuación como vector de cargas generalizadas, entonces la ecuación 3.59 queda

$$[K]\{D\} = \{R\} \qquad (3.60)$$

Ejemplo. Podemos considerar un caso simple en forma general mediante el cual podremos establecer la siguiente secuencia de operaciones

$$\{f\} = \{u\} = [1 \quad x]\{a\} \qquad (3.61)$$

$$\{d\} = \begin{Bmatrix} d_1 \\ d_2 \end{Bmatrix} = \begin{bmatrix} 1 & 0 \\ 1 & L \end{bmatrix}\begin{Bmatrix} a_1 \\ a_2 \end{Bmatrix} = [A]\{a\} \qquad (3.62)$$

$$\{f\} = [1 \quad x][A]^{-1}\{d\} = \left[\left(1-\frac{x}{L}\right) \quad \left(\frac{x}{L}\right)\right]\{d\} = [N]\{d\} \qquad (3.63)$$

$$U = \int_0^L \frac{1}{2} E\,\varepsilon_x^2 A\,dx = \frac{1}{2}\int_0^L \varepsilon_x^T E\,\varepsilon_x A\,dx \qquad (3.64)$$

$$U = \frac{1}{2}\{d\}^T\int_0^L [B]^T E\,[B] A\,dx\,\{B\} \qquad (3.65)$$

$$k_e = \int_0^L [B]^T E [B] A dx = \int_0^L \begin{bmatrix} -\frac{1}{L} \\ \frac{1}{L} \end{bmatrix} E \begin{bmatrix} -\frac{1}{L} & \frac{1}{L} \end{bmatrix} A dx \qquad (3.66)$$

$$k_e = \frac{AE}{L} \begin{bmatrix} 1 & -1 \\ -1 & 1 \end{bmatrix} \equiv \text{Matriz elemental de rigidez} \qquad (3.67)$$

3.7 El Método Rayleigh-Ritz

Podemos considerar un ejemplo unidimensional para describir el método Rayleigh-Ritz como el mostrado en la Fig. 3.9 en donde el área (A) y el módulo elástico (E) son constantes y la carga distribuida (q) son tales que

$$A = E = L = 1 \quad ; \quad q = x \qquad (3.68)$$

Las condiciones de frontera son:

$$u = 0 \quad @ \quad x = 0$$
$$u_{,x} = 0 \quad @ \quad x = L \qquad (3.69)$$

La energía potencial se puede expresar como:

$$\Pi = \int_0^1 \frac{AE}{2} u_{,x}^2 \, dx - \int_0^L u(q\,dx) \qquad (3.70)$$

Sabatituyendo los valores dados en (3.69) y asumiendo que los desplazamientos u son de la forma $u = a_1 x$ entonces

$$\Pi = \frac{1}{2} a_1^2 - \frac{a_1}{3} \qquad (3.71)$$

$$\frac{\partial \Pi}{\partial a_1} = 0 = a_1 - \frac{1}{3} \quad \Rightarrow \quad a_1 = \frac{1}{3} \qquad (3.72)$$

Si se asume ahora que $u = a_1 x + a_2 x^2$, entonces la energía potencial queda como sigue:

$$\Pi = \int_0^1 \frac{1}{2}(a_1 + 2a_2 x)^2 dx - \int_0^1 (a_1 x + a_2 x^2) x \, dx \qquad (3.73)$$

$$\frac{\partial \Pi}{\partial a_1} = \frac{\partial \Pi}{\partial a_2} = 0 \Rightarrow \begin{bmatrix} 1 & 1 \\ 1 & 4/3 \end{bmatrix} \begin{Bmatrix} a_1 \\ a_2 \end{Bmatrix} = \begin{Bmatrix} 1/3 \\ 1/4 \end{Bmatrix} \qquad (3.74)$$

$$\begin{Bmatrix} a_1 \\ a_2 \end{Bmatrix} = \begin{Bmatrix} 7/12 \\ -1/4 \end{Bmatrix} \qquad (3.75)$$

Sumarizando Resultados:

	$u(x=1/4)$	$u(x=1/2)$	$u(x=3/4)$	$u(x=1)$	$\Pi(x=0)$	$\Pi(x=1)$
1 Término	.0833	.1667	.2500	.3333	.3333	.3333
2 Términos	.1302	.2292	.2969	.3333	.5833	.0833
Exacto	.1224	.2292	.3047	.3333	.1000	.0

Si asumimos un polinomio de 3er grado para u(tres términos) obtendríamos la solución exacta porque la solución exacta es cúbica de la forma $u = (3x - x^3)/4$ o sea que el método Rayleigh-Ritz basado en

$$u = a_1 x + a_2 x^2 + a_3 x^3 \qquad (3.76)$$

daría como resultado

$$a_1 = 3/4$$
$$a_2 = 0 \qquad (3.77)$$
$$a_3 = -1/4$$

y si se incluyeran más términos como por ejemplo

$$u = a_0 x + a_1 x^2 + a_3 x^3 + a_4 x^4 + \cdots + a_n x^n \tag{3.78}$$

la solución sería:

$$\begin{aligned} a_1 &= V_2 \\ a_2 &= 0 \\ a_3 &= -V_6 \\ a_4 &= a_5 = \cdots = a_n = 0 \end{aligned} \tag{3.79}$$

3.8 El Método del elemento finito y su relación con R.R

Podemos considerar ahora la barra del ejemplo anterior pero dividida en tres elementos como se muestra en la Fig 3.10. Para cada elemento existe una matriz de forma tal que el campo de desplazamientos en cada elemento se puede expresar como:

$$u_j = [N]_j \begin{Bmatrix} u_i \\ u_k \end{Bmatrix}_j \tag{3.80}$$

y donde $$[N]_j = \begin{bmatrix} \frac{l_j - s}{l_j} & \frac{s}{l_j} \end{bmatrix} \tag{3.81}$$

Las deformaciones son dadas por:

$$\varepsilon_x = u_{,x} \quad y \quad \frac{\partial}{\partial x} = \frac{\partial}{\partial s} \tag{3.82}$$

Usando la ecuación (3.82) en la ecuación (3.80)

$$\varepsilon_x = \frac{\partial}{\partial s}[N]\{d\} = [B]\{d\} \tag{3.83}$$

en donde $$[B] = \frac{\partial}{\partial s}[N] \quad y \quad \{d\} = \begin{Bmatrix} u_i \\ u_j \end{Bmatrix} \tag{3.84}$$

y donde que es un escalar entonces:

$$\varepsilon_x^T \varepsilon_x = \{d\}^T [B]^T [B] \{d\} \tag{3.85}$$

Sustituyendo la ecuación (3.85) en la expresión para la energía de un elemento se obtiene que

$$U_i = \int_0^l \frac{AE}{2} \varepsilon_x^T dx = \frac{1}{2}\{d\}_i^T \int_0^l AE \begin{bmatrix} -V_l \\ V_l \end{bmatrix} [-V_l \quad V_l] ds \{d\} \tag{3.86}$$

la cual se puede expresar en forma compacta como:

$$U_i = \frac{1}{2}\{d\}_i^T [K]_i \{d\}_i \tag{3.87}$$

en donde

$$[K]_i = \int_0^l AE \begin{bmatrix} -V_l \\ V_l \end{bmatrix} [-V_l \quad V_l] ds = \frac{AE}{l} \begin{bmatrix} 1 & -1 \\ -1 & 1 \end{bmatrix} \tag{3.88}$$

Por otra parte el trabajo realizado por la carga es

$$W = \int_0^l q\, u\, ds = \{d\}_i^T \int_0^l [N]^T q\, ds \tag{3.89}$$

y el potencial total de la estructura es

$$\Pi_T = \Pi_1 + \Pi_2 + \Pi_3 \tag{3.90}$$

Suponiendo que para cada elemento las propiedades cumplen con las propiedades de las ecuaciones (3.68) y además

$$\begin{aligned} l &= V_3 \\ q &= x \quad \text{para el elemento 1} \\ q &= \tfrac{1}{3} + s \quad \text{para el elemento 2} \\ q &= \tfrac{2}{3} + s \quad \text{para el elemento 3} \end{aligned} \tag{3.91}$$

Expandiendo los vectores al rango de la estructura se tiene que el vector global es

$$\{D\} = \begin{Bmatrix} u_1 \\ u_2 \\ u_3 \\ u_4 \end{Bmatrix} \tag{3.92}$$

Substituyendo las condiciones (3.91) en (3.90) y expandiendo al rango de la estructura, la energía potencial es:

$$\Pi_T = \frac{1}{2}\{D\}^T\left(\begin{bmatrix} 3 & -3 & 0 & 0 \\ -3 & 3 & 0 & 0 \\ 0 & 0 & 0 & 0 \\ 0 & 0 & 0 & 0 \end{bmatrix} + \begin{bmatrix} 0 & 0 & 0 & 0 \\ 0 & 3 & -3 & 0 \\ 0 & -3 & 3 & 0 \\ 0 & 0 & 0 & 0 \end{bmatrix} + \begin{bmatrix} 0 & 0 & 0 & 0 \\ 0 & 0 & 0 & 0 \\ 0 & 0 & 3 & -3 \\ 0 & 0 & -3 & 3 \end{bmatrix}\right)\{D\}$$

$$-\{D\}^T\left(\frac{1}{54}\begin{Bmatrix} 1 \\ 2 \\ 0 \\ 0 \end{Bmatrix} + \frac{1}{54}\begin{Bmatrix} 0 \\ 4 \\ 5 \\ 0 \end{Bmatrix} + \frac{1}{54}\begin{Bmatrix} 0 \\ 0 \\ 7 \\ 3 \end{Bmatrix}\right) \tag{3.93}$$

Minimizando la energía potencial se obtiene que

$$\left\{\frac{\partial \Pi_T}{\partial D}\right\} = 0 \tag{3.94}$$

la cual resulta en el siguiente sistema de ecuaciones de equilibrio

$$\begin{bmatrix} 3 & -3 & 0 & 0 \\ -3 & 6 & -3 & 0 \\ 0 & -3 & 6 & -3 \\ 0 & 0 & -3 & 3 \end{bmatrix}\begin{Bmatrix} u_1 \\ u_2 \\ u_3 \\ u_4 \end{Bmatrix} = \begin{Bmatrix} 1/54 \\ 6/54 \\ 12/54 \\ 8/54 \end{Bmatrix} \tag{3.95}$$

La Matriz cuadrada del lado izquierdo de esta ecuación es singular debido a que no se han impuesto las condiciones de frontera de la estructura. Esta condición es

$$u_1 = 0 \tag{3.96}$$

Al imponer la condición (3.96) en la ecuación (3.95) se obtiene

$$\begin{bmatrix} 6 & -3 & 0 \\ -3 & 6 & -3 \\ 0 & -3 & 3 \end{bmatrix}\begin{Bmatrix} u_2 \\ u_3 \\ u_4 \end{Bmatrix} = \frac{1}{54}\begin{Bmatrix} 6 \\ 12 \\ 8 \end{Bmatrix} \tag{3.97}$$

de donde se obtiene que u_2=.1605, u_3=.2840 y u_4=.333 los cuales son exactos sin embargo son aproximados en cualquier otro punto, por ejemplo en x=L/2 se tiene

$$u = [N]\{d\}_1 = \begin{bmatrix} \frac{1-x_1}{l} & \frac{x_1}{l} \end{bmatrix}\begin{Bmatrix} u_2 \\ u_3 \end{Bmatrix} \tag{3.98}$$

$$u = \begin{bmatrix} x_2 & x_1 \end{bmatrix}\begin{Bmatrix} .1605 \\ .2840 \end{Bmatrix} = .22\,l \tag{3.99}$$

El valor exacto de u en x=L/2 es de 0.2292. El esfuerzo en el elemento i es $\sigma_i = (E\,u_{,x})_i$ o también

$$\sigma_i = E\,[B]\begin{Bmatrix} u_i \\ u_{i+1} \end{Bmatrix} \tag{3.100}$$

Substituyendo las condiciones (3.91) en (3.100) se obtienen los siguientes resultados:

$\sigma_x = .4215$ Exacto en $x = \frac{L}{6}$

$\sigma_x = .5704$ Exacto en $x = \frac{L}{4}$

$\sigma_x = .1481$ Exacto en $x = \frac{5L}{6}$

Es decir los esfuerzos no son continuos en el modelo y los desplazamientos son más exactos que los esfuerzos como se puede apreciar en la Fig. 3.11.

De estos dos ejemplos se puede concluir que el método clásico de Rayleigh-Ritz (R-R) es aproximado pero más exacto si se utilizan más términos en el polinomio. En el caso de cargas destribuidas el método de R-R puede ser exacto si se usan suficientes términos en el polinomio y la inclusión de más términos no cambia la solución.

Por otro lado usando elementos finitos se llega a resultados exactos si las cargas se localizan en los nodos y es aproximado para el caso de cargas distribuidas pero puede ser bastante cercano al exacto si se usan más elementos.

El método clásico de R-R utiliza un polinomio que se aplica a todo el dominio de la estructura, mientras que el método del elemento finito utiliza un polinomio apra cada elemento.

3.9 Modelación de Sistemas con Elementos Finitos

Existe una variedad muy grande de sistemas mecánicos y estructurales los cuales requieren de una solución la cual no es siempre trivial ni simple de obtener, en tales casos es práctica común hacer una clasificación de efectos significantes y otros que por su naturaleza pueden considerarse insignificantes o ignorables, de tal manera que en general siempre se habla en términos de una solución aproximada a la solución real del sistema o de una solución exacta o aproximada de un modelo aproximado al sistema real.

En la formulación analítica de un sistema, las suposiciones de que algunos efectos son ignorables tienen como objetivo simplificar los procedimientos de cálculo, sin embargo a través del desarrollo de técnicas digitales se han podido mejorar dichos procedimientos, aunque en general siempre es necesario hacer algunas suposiciones respecto a aquellos efectos que pueden ser ignorables o simplemente no dominentes.

La formulación con elementos finitos también requiere de suposiciones lógicas en base a la naturaleza del sistema en cuestión y para tal efecto se han desarrollado una variedad de elemntos cuyas propiedades son representativas de algunos casos específicos de sistemas y así se tienen por ejemplo elementos planos para la simulación de problemas bidimensionales de esfuerzo plano o deformación plana, elementos viga en dos y tres dimensiones, elementos sólidos o de volumen, elementos cascaron y otros varios que tienen propósitos específicos.

En general, el análisis y modelación de un sistema es un proceso que se desarrolla en varias etapas que son:

1. Definición del sistema físico
2. Definición de condiciones de frontera
3. Definición de agentes de perturbación
4. Definición de variables de respuesta
5. Definición de efectos despreciables
6. Desarrollo del modelo analítico o modelo matemático
7. Aplicación sistemática de procedimientos de Cálculo
8. Interpretación de resultados

Cabe mencionar que un entendimiento general del sistema en cuestión es siempre básico e importante pues la definición

del sistema físico, de las condiciones iniciales y de frontera y la definición de agentes perturbadores puede depender de un entendimiento bastante completo del problema que se está analizando ya que una formulación errónea conceptualmente genera resultados que no corresponden al verdadero problema.

En el área de aplicaciones del método del elemento finito se parte de la suposición que el análisis conoce y entiende el problema en cuestión, de tal forma que los puntos del 1 al 5 del proceso de análisis quedan satisfactoriamente establecidos.

En el punto 6, referente al desarrollo del modelo matemático es necesario que las características de los elementos empleados sean compatibles con el comportamiento general del sistema y por compatibilidad se entiende que el conjunto de elementos que componen el sistema sean capaces de reproducir en forma aproximada la respuesta del sistema a las perturbaciones y condiciones a que está sujeto.

Son varios los aspectos que se deben tomar en cuenta para la selección de los elementos apropiados para cada caso, por ejemplo:

- -El número de nodos del elemento
- -El número de grados de libertad
- -Condiciones naturales de frontera del elemento
- -Tipo de cargas admisibles por el elemento
- -Tipo de geometría permitido por el elemento
- -Sistemas de coordenadas permisibles del elemento
- -Limitaciones del tipo de elemento

En la Fig. 3.12 se muestran algunos elementos que en general pueden ser aplicados a la modelación de varios tipos de sistemas y a continuación se presentan algunos casos específicos de aplicaciones a sistemas reales.

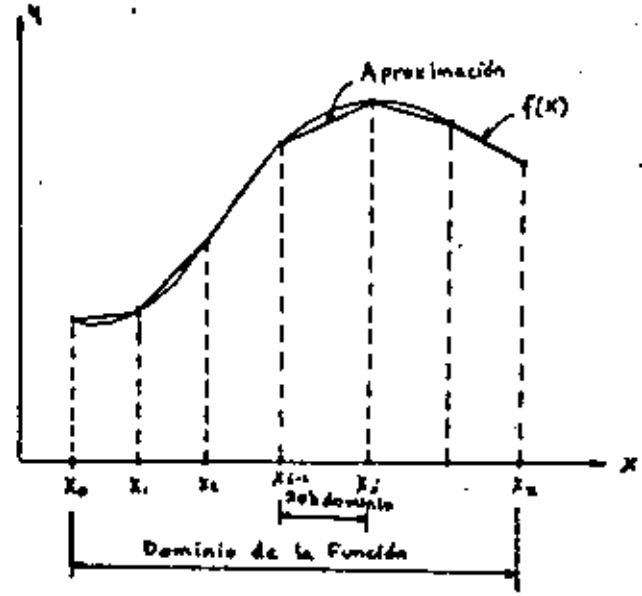

Fig 1. Aproximación de una función continua a través de una serie de funciones lineales conectadas

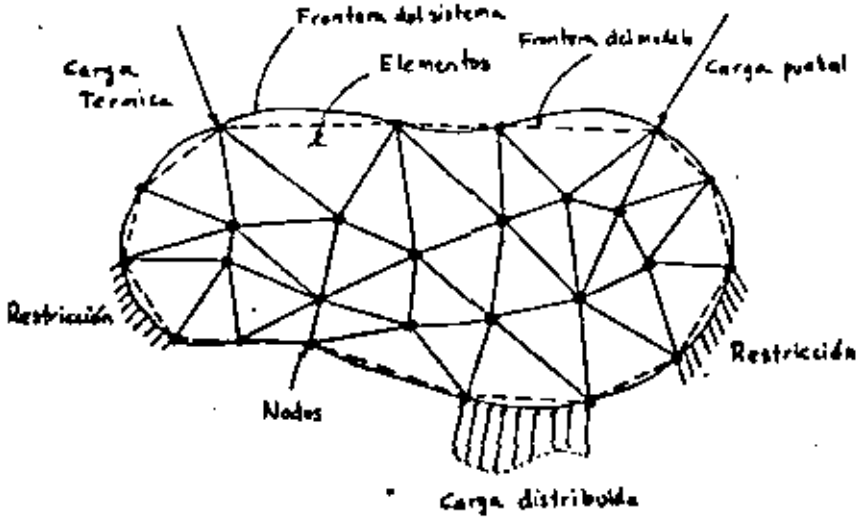

Fig 2. Sistema de un cuerpo deformable sujeto a cargas y restricciones y discretizado con elementos finitos

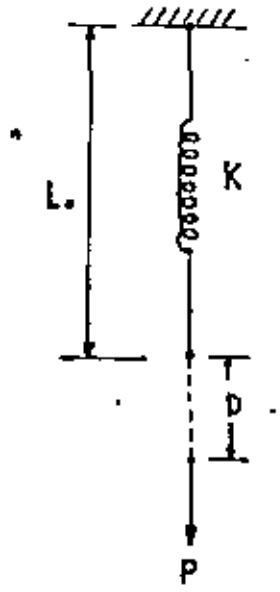

Fig 4. Sistema de resorte lineal con un extremo fijo y otro extremo libre y cargado (1 grado de libertad)

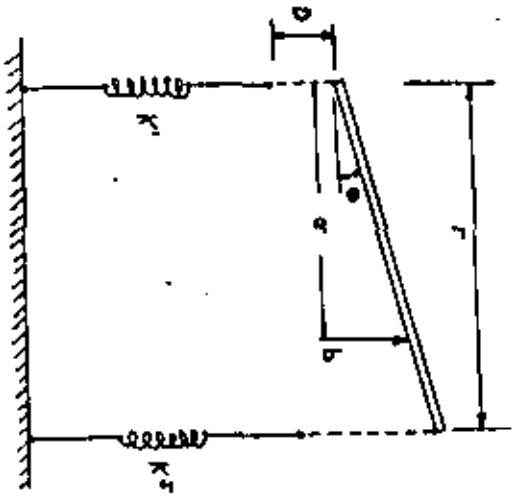

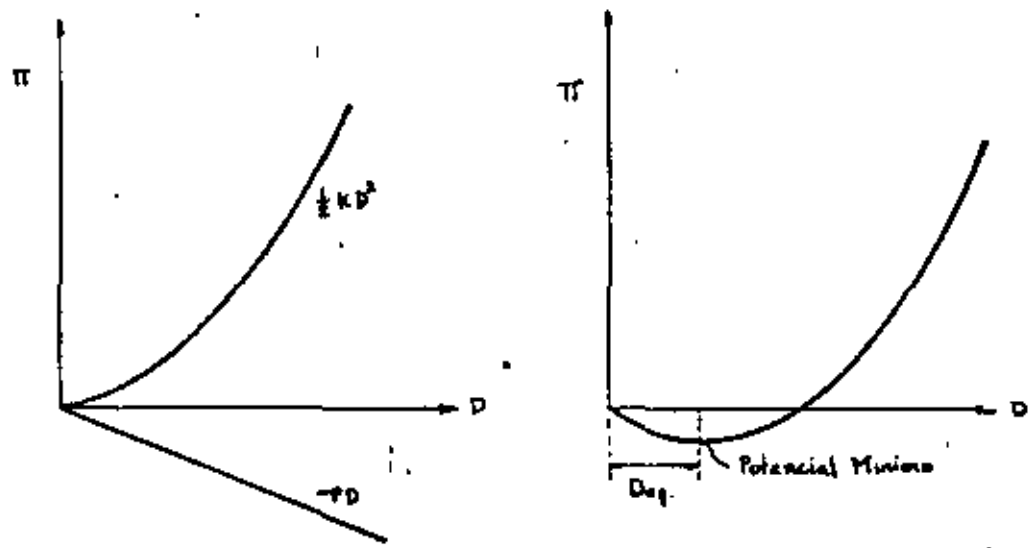

Fig. 5 Energía potencial como función del desplazamiento en el extremo libre de un resorte con constante k y carga P dadas

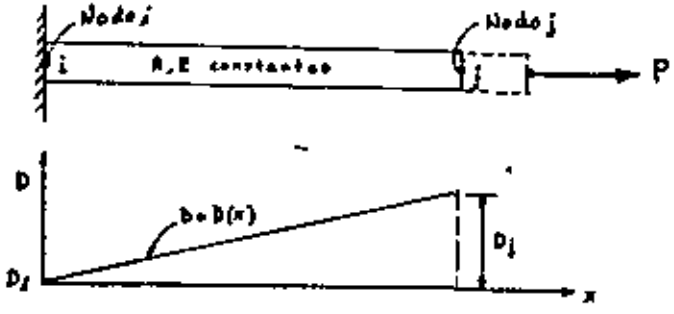

Fig. 7 Campo de desplazamientos en una barra de sección uniforme en terminos de los desplazamientos nodales.

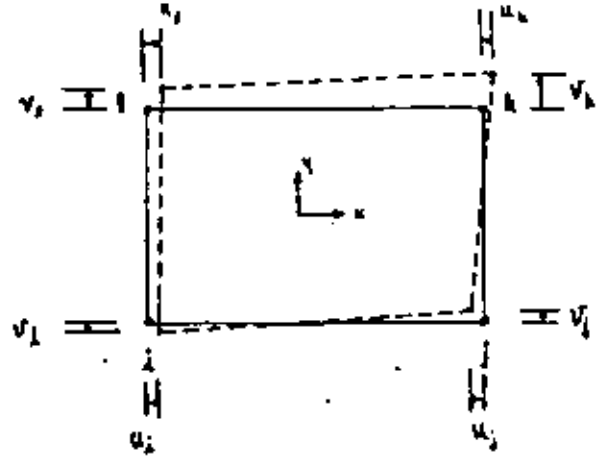

Fig. 8 Elemento cuadrilatero bidimensional, 2 grados de libertad por nodo, 4 nodos o sea 8 g.d.l.

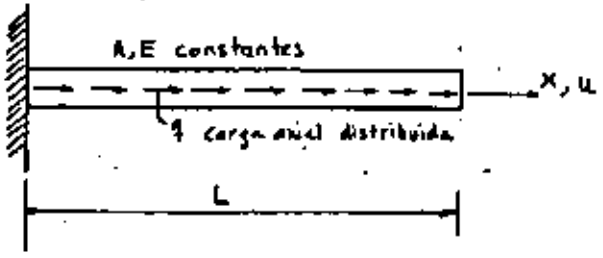

Condiciones de frontera:

Forzada $u=0$ @ $x=0$

Natural $u,x=0$ @ $x=L$

Fig.9 Barra con carga axial distribuida y sección constante

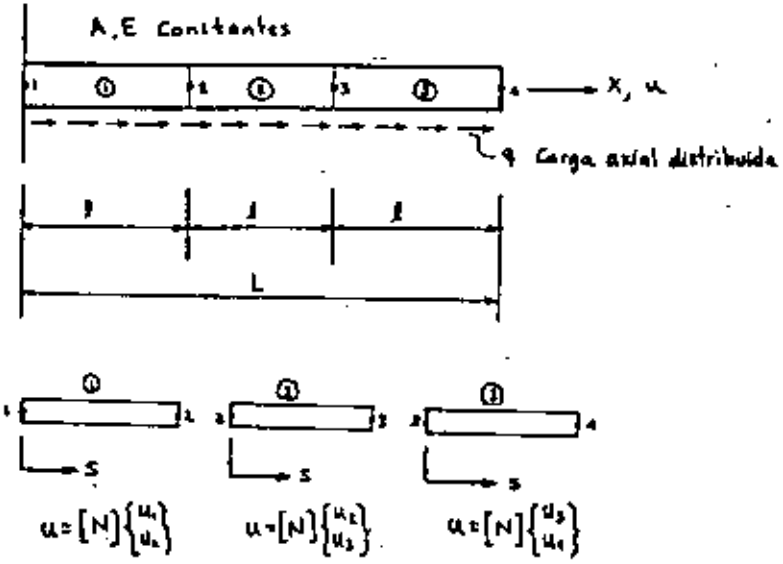

$u=[N]\begin{Bmatrix} u_1 \\ u_2 \end{Bmatrix}$ $u=[N]\begin{Bmatrix} u_2 \\ u_3 \end{Bmatrix}$ $u=[N]\begin{Bmatrix} u_3 \\ u_4 \end{Bmatrix}$

Fig 10. Barra con carga axial distribuida dividida en tres elementos.

Elemento Viga

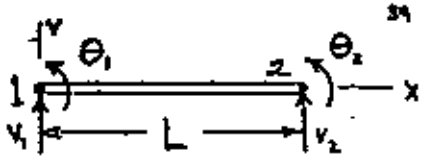

$$v = [N_1 \quad N_2 \quad N_3 \quad N_4] \begin{Bmatrix} v_1 \\ \theta_1 \\ v_2 \\ \theta_2 \end{Bmatrix}, \quad \text{donde}$$

$$N_1 = 1 - \frac{3x^2}{L^2} + \frac{2x^3}{L^3} \qquad N_2 = x - \frac{2x^2}{L} + \frac{x^3}{L^2}$$

$$N_3 = \frac{3x^2}{L^2} - \frac{2x^3}{L^3} \qquad N_4 = -\frac{x^2}{L} + \frac{x^3}{L^2}$$

$$v_{xx} = [B_1 \quad B_2 \quad B_3 \quad B_4] \begin{Bmatrix} v_1 \\ \theta_1 \\ v_2 \\ \theta_2 \end{Bmatrix}, \quad \text{donde}$$

$$B_1 = -\frac{6}{L^2} + \frac{12x}{L^3} \qquad B_2 = -\frac{4}{L} + \frac{6x}{L^2}$$

$$B_3 = \frac{6}{L^2} - \frac{12x}{L^3} \qquad B_4 = -\frac{2}{L} + \frac{6x}{L^2}$$

$$[k] = \int_0^L [B]^T EI [B]\, dx = \frac{EI}{L^3} \begin{bmatrix} 12 & 6L & -12 & 6L \\ 6L & 4L^2 & -6L & 2L^2 \\ -12 & -6L & 12 & -6L \\ 6L & 2L^2 & -6L & 4L^2 \end{bmatrix}$$

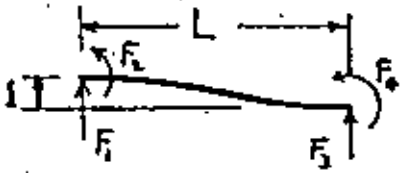

$$\begin{Bmatrix} F_1 \\ F_2 \\ F_3 \\ F_4 \end{Bmatrix} = \begin{Bmatrix} 12EI/L^3 \\ 6EI/L^2 \\ -12EI/L^3 \\ 6EI/L^2 \end{Bmatrix}$$

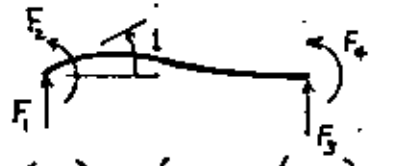

$$\begin{Bmatrix} F_1 \\ F_2 \\ F_3 \\ F_4 \end{Bmatrix} = \begin{Bmatrix} 6EI/L^2 \\ 4EI/L \\ -6EI/L^2 \\ 2EI/L \end{Bmatrix}$$

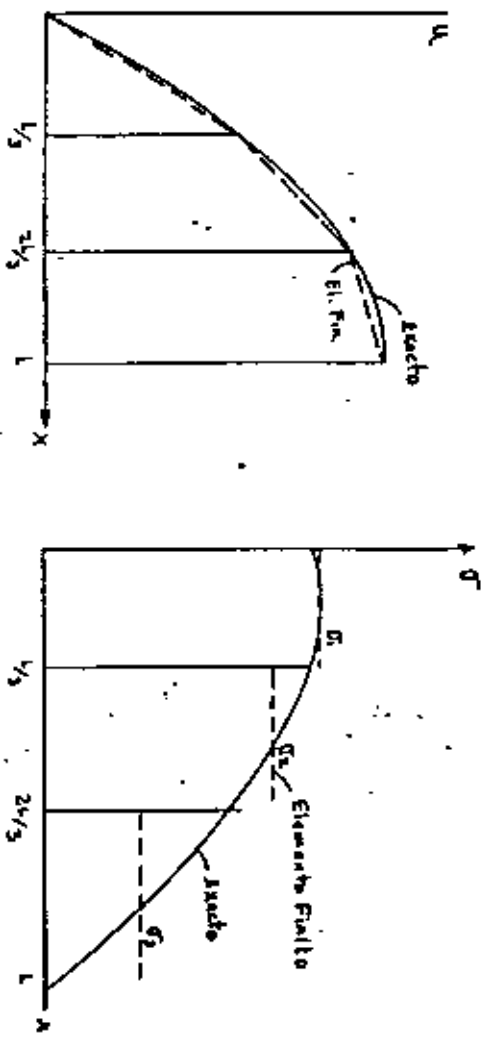

Fig 11 Comparación del método del elemento finito y la solución exacta para el problema de la barra con carga distribuida

Matriz de Rigidez de un elemento cuadrilatero

Ref. Fig. 8

$$[B] = \begin{bmatrix} \frac{\partial}{\partial x} & 0 \\ 0 & \frac{\partial}{\partial y} \\ \frac{\partial}{\partial y} & \frac{\partial}{\partial x} \end{bmatrix} [N]$$

$$\underset{3\times 8}{[B]} = \frac{1}{4bc} \begin{bmatrix} -(c-y) & 0 & (c-y) & 0 & \cdots \\ 0 & -(b-x) & 0 & -(b+x) & \cdots \\ -(b-x) & -(c-y) & -(b+x) & (c-y) & \cdots \end{bmatrix}$$

$$\underset{8\times 8}{[k]} = \int_{-c}^{c}\int_{-b}^{b} \underset{8\times 3}{[B]^T} \underset{3\times 3}{[E]} \underset{3\times 8}{[B]}\, t\, dx\, dy \qquad (a)$$

En donde:

$$[E] = \frac{E}{1-\nu^2} \begin{bmatrix} 1 & \nu & 0 \\ \nu & 1 & 0 \\ 0 & 0 & \frac{1-\nu}{2} \end{bmatrix}$$

ELEMENTOS ISOPARAMETRICOS

Barra en coordenadas rectangulares

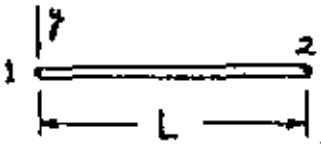

Barra en coordenadas Isoparam.

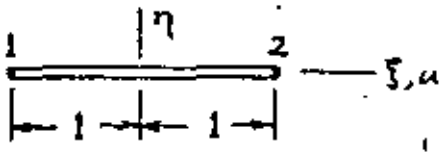

Relaciones: $x = \frac{L}{2}(1+\xi)$ $\quad dx = \frac{L}{2} d\xi = J\, d\xi$

$$\frac{d\xi}{dx} = \frac{2}{L}$$

$$u = \begin{bmatrix} \frac{L-x}{L} & \frac{x}{L} \end{bmatrix} \begin{Bmatrix} u_1 \\ u_2 \end{Bmatrix}$$

$$\epsilon_x = u_{,x} = \begin{bmatrix} -\frac{1}{L} & \frac{1}{L} \end{bmatrix} \begin{Bmatrix} u_1 \\ u_2 \end{Bmatrix}$$

$$= [B] \begin{Bmatrix} u_1 \\ u_2 \end{Bmatrix}$$

$$[k] = \int_0^L AE\, [B]^T [B]\, dx$$

$$[k] = AE \begin{bmatrix} \frac{1}{L^2} & -\frac{1}{L^2} \\ -\frac{1}{L^2} & \frac{1}{L^2} \end{bmatrix} L$$

$$[k] = \frac{AE}{L} \begin{bmatrix} 1 & -1 \\ -1 & 1 \end{bmatrix}$$

$$u = \begin{bmatrix} \frac{1-\xi}{2} & \frac{1+\xi}{2} \end{bmatrix} \begin{Bmatrix} u_1 \\ u_2 \end{Bmatrix}$$

$$\epsilon_x = u_{,x} \frac{d\xi}{dx} = \frac{2}{L} \begin{bmatrix} -\frac{1}{2} & \frac{1}{2} \end{bmatrix} \begin{Bmatrix} u_1 \\ u_2 \end{Bmatrix}$$

$$= [B] \begin{Bmatrix} u_1 \\ u_2 \end{Bmatrix}$$

$$[k] = \int_{-1}^{1} AE\, [B]^T [B]\, J\, d\xi$$

$$[k] = AE \begin{bmatrix} \frac{1}{L^2} & -\frac{1}{L^2} \\ -\frac{1}{L^2} & \frac{1}{L^2} \end{bmatrix} \frac{L}{2} 2$$

$$[k] = \frac{AE}{L} \begin{bmatrix} 1 & -1 \\ -1 & 1 \end{bmatrix}$$

Podemos continuar con este ejemplo un paso mas, este es aumentar un nodo en la barra a la mitad del segmento, entonces:

$$u = \left[\frac{2x^2}{L^2} - \frac{3x}{L} + 1 \;,\; \frac{2x^2}{L^2} - \frac{x}{L} \;,\; -\frac{4x^2}{L^2} + \frac{4x}{L} \right] \begin{Bmatrix} u_1 \\ u_2 \\ u_3 \end{Bmatrix} \qquad \text{(Rectangular)}$$

$$u = \left[\frac{-\xi + \xi^2}{2} \qquad \frac{\xi + \xi^2}{2} \qquad 1 - \xi^2 \right] \begin{Bmatrix} u_1 \\ u_2 \\ u_3 \end{Bmatrix}$$

$$\epsilon_x = \underbrace{\frac{2}{L} \left[\frac{-1 + 2\xi}{2} \qquad \frac{1 + 2\xi}{2} \qquad -2\xi \right]}_{[B]} \begin{Bmatrix} u_1 \\ u_2 \\ u_3 \end{Bmatrix}$$

Entonces en general [B] es una función de las coordenadas naturales, de la misma manera J dependerá de ξ si el nodo 3 no estuviera colocado en el centro.

$$\begin{bmatrix} u \\ v \end{bmatrix} = \begin{bmatrix} N_1 & 0 & N_2 & 0 & N_3 & 0 & N_4 & 0 \\ 0 & N_1 & 0 & N_2 & 0 & N_3 & 0 & N_4 \end{bmatrix} \begin{Bmatrix} u_1 \\ v_1 \\ u_2 \\ \vdots \\ v_4 \end{Bmatrix}$$

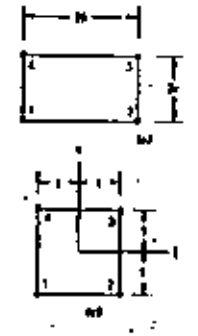

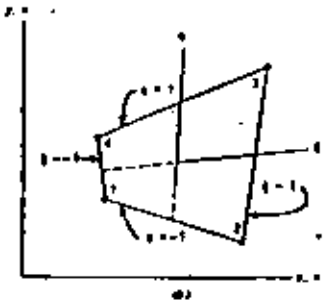

$$x = a_1 + a_2\xi + a_3\eta + a_4\xi\eta$$

$$N_1 = \frac{(1-\xi)(1-\eta)}{4}, \qquad N_2 = \frac{(1+\xi)(1-\eta)}{4}$$

$$N_3 = \frac{(1+\xi)(1+\eta)}{4}, \qquad N_4 = \frac{(1-\xi)(1+\eta)}{4}$$

$$x = \sum_{i=1}^{4} N_i x_i \qquad y = \sum_{i=1}^{4} N_i y_i$$

$$u = \sum_{i=1}^{4} N_i u_i \qquad v = \sum_{i=1}^{4} N_i v_i$$

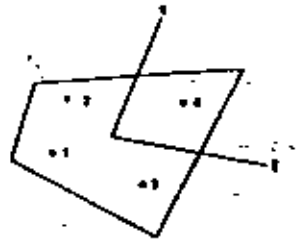

$$I = \int_{-1}^{1}\int_{-1}^{1}\int_{-1}^{1} f(\xi,\eta,\zeta)\,d\xi\,d\eta\,d\zeta = \sum_{i}\sum_{j}\sum_{k} W_i W_j W_k f(\xi_i,\eta_j,\zeta_k) \qquad (8.3.8)$$

Gauss Quadrature Coefficients

No. of Points	Locations	Associated Weights W_i
1	$x_1 = 0.000000000000000000000000000$	2.
2	$x_1, x_2 = \pm 0.577350269189625764509148$	1.
3	$x_1, x_3 = \pm 0.774596669241483377035853$	$\frac{5}{9}$ (= 0.555 ...)
	$x_2 = 0.000000000000000000000000000$	$\frac{8}{9}$ (= 0.888 ...)

SOME ELEMENT TYPES

linear

quadratic

quadratic

linear - quadratic

linear

quadratic

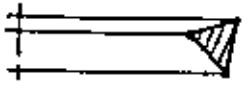

6 d.o.f

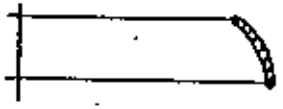

4 d.o.f

elements for axisymmetric solids & thin shells

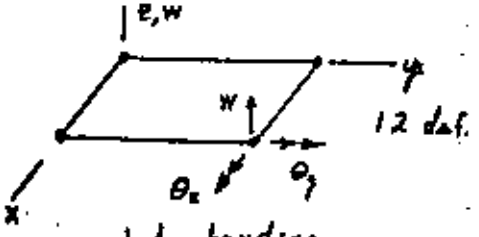

plate bending

shell

SOME ASSEMBLAGES

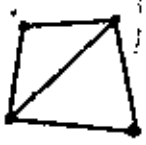

5 tetrahedra combine into a hexahedron

edge beam on a plate

solid propellant in rocket case

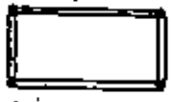

four stringers on shear panel

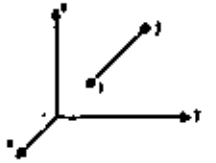

a. TRUSS ELEMENT

b. THREE DIMENSIONAL BEAM ELEMENT

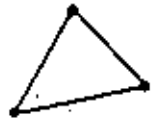

c. PLANE STRESS, PLANE STRAIN AND AXISYMMETRIC ELEMENTS

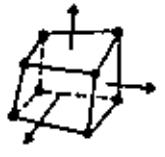

d. THREE DIMENSIONAL SOLID

e. THICK SHELL ELEMENT

f. THIN SHELL AND BOUNDARY ELEMENT

TANGENT

BEND

g. PIPE ELEMENT

FIGURE 7: ELEMENT LIBRARY OF SAP

Design Improvement of a Friction Brake Plate Through Finite Element Analysis

V. H. MUCINO

V. PAVELIC

R. G. TASCHNER

The University of Wisconsin-Milwaukee,
Milwaukee, Wisc.

The finite element method is applied to conduct the stress analysis of the friction brake plate used in the rear axle system of agricultural tractors. External loads on the plate are considered to be applied to the spline and fixed boundary conditions at the friction material area. The original design of the friction plate is analyzed and shown to have an uneven distribution of load on the teeth of the spline, causing high stresses at some critical areas of the plate. Design changes are made on the analysis model, having as a primary interest the reduction of peak stresses to an acceptable level, without severe modifications to the original design. With a minimum of computer manipulations, the finite element model used yielded the best configuration of the brake plate for the given loads.

Contributed by the Design Engineering Division of The American Society of Mechanical Engineers for presentation at the Design Engineering Conference & Show, Chicago, Illinois, May 7-10, 1979. Manuscript received at ASME Headquarters February 22, 1979.

Copies will be available until February 1, 1980.

Design Improvement of a Friction Brake Plate Through Finite Element Analysis

V. H. MUCINO V. PAVELIC R. G. TASCHNER

NOMENCLATURE

A_f = flank area of the teeth
d_{ri} = radial displacement at the tip of the tooth (i)
d_{ti} = tangential displacement at the tip of the tooth (i)
f_i = load distribution factor
F_n = normal force acting on the flank of the teeth
F_r = radial force acting on the flank of the teeth
F_t = tangential component of the normal force (F_n)
m = slope of loading line in Goodman diagram
P_e = equivalent pressure on the flank of the teeth
r = stress ratio of alternating stress (s_{ai}) to mean stress (s_{mi})
S_{ai} = alternating stress at tooth (i)
S_{mi} = mean stress at tooth (i)
$S_{max,\ i}$ = maximum stress at tooth (i)
S_{vmi} = Von Mises criterion of failure
S_1, S_2, S_3 = principal stresses
T_i = torque carried by tooth (i)
T_{in} = input torque in the spline shaft
T_{pl} = torque carried by one friction plate
ϕ = pressure angle of the spline teeth

INTRODUCTION

The system considered in this analysis is a multiple disk brake, which is used in a typical rear axle of an agricultural tractor. The main objective of the analysis is the design improvement of the brake system which depends upon the performance of the friction plates. These friction plates are subject to fluctuating loads that may cause fatigue failure of the system. Therefore, the analysis is carried out having as primary interest the reduction of peak stresses occurring at the critical area of the friction plate.

In pursuing the objective it is desirable to keep the overall modifications to a minimum.

This paper demonstrates the application of the finite element method as an efficient tool to identify critically stressed areas of a typical friction plate, and also as a tool to qualitatively evaluate the design modifications proposed in order to reduce the critical stresses.

Fig. 1 shows the main components of the rear axle assembly which consists of a differential gear train (A), a clutch system (B), a dual brake system (C&C') and the planetary gear train systems (D&D'). The various components in the assembly of each brake system, are shown separately in Fig. 2.

The operation of a multiple disk brake system may be described briefly as follows: the friction plates rotate along with the shaft to which they are attached through the spline, and the steel plates are attached to the housing in such a way that rotation is prevented. Axial displacement is allowed for both the friction plates and steel plates. When hydraulic pressure is applied to the brake cylinder, the brake piston moves axially and presses the friction plates against the steel plates, the acting torque in the shaft is transmitted to the friction plates through the spline, and then transmitted to the steel plates through the friction material on the friction plates, the absorbed braking torque from the steel plates is finally transmitted to the housing which is attached to the frame of the tractor. The heat generated during the brake application is absorbed by coolant fluid which circulates on either side of the friction plate through the holes provided on the plate.

The braking loads imposed on the friction plates, induce high stress concentration at the root of the teeth in the spline, which are sub-

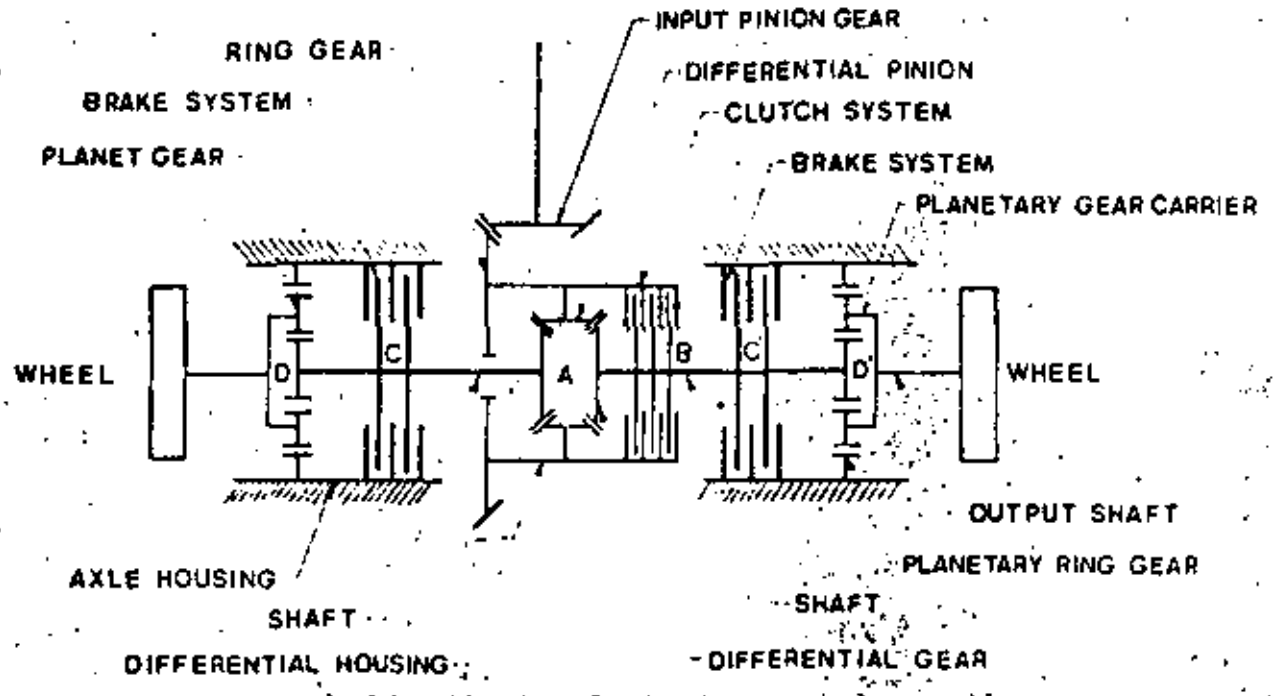

Fig. 1 Schematic view of a tractor rear axle assembly

ject to a stress variation ranging from zero value (idle mode) to some maximum value (brake application).

Fig. 3 shows schematically torques applied to the friction plate, the geometry of the spline, and the location of the coolant circulation holes.

LOADING CONSIDERATIONS

Due to the repetitive nature of the loads, these can be expressed by means of a static (mean) component, and a dynamic (alternating) component, for the purpose of analysis. These loads are distributed among the teeth on the friction plate, in such a way that the ratio of alternating stress to steady stress at any location of the plate is always constant. This is due to the fact that the load varies from zero to some maximum value in each brake application. However, the load that a particular tooth carries is not necessarily equal to the load carried by a different tooth in the spline.

Fig. 4 shows qualitatively the variation of stresses with respect to time, at three arbitrary locations of the friction plate. Also plotted in the same Fig. 4 is the variation of the load with respect to time. It can be appreciated that the maximum stresses at any of the locations shown are reached when the applied load is maximum, this is, the stress peaks are in phase with the load peaks.

Using the notation of Juvinall (1),[1] the stress ratio can be expressed as follows:

$$r = \frac{S_{ai}}{S_{mi}} \qquad (1)$$

where Sai is the alternating stress component Smi is the mean stress component and for the particular case in which the load varies from zero to a maximum value then r = 1; or

$$S_{ai} = S_{mi} \qquad (2)$$

Fig. 5 shows the Goodman diagram and the loading line for the teeth in the spline of the friction plate. The slope of the loading line is such that:

$$S_{max,i} = S_{mi} + S_{ai} \qquad (3)$$

by substituting the equality (2) in equation (3) it results

$$S_{max,i} = 2S_{mi}$$

therefore, the slope of the loading time in the Goodman diagram is

$$m = 2$$

[1] Underlined numbers in parentheses designate References at end of paper.

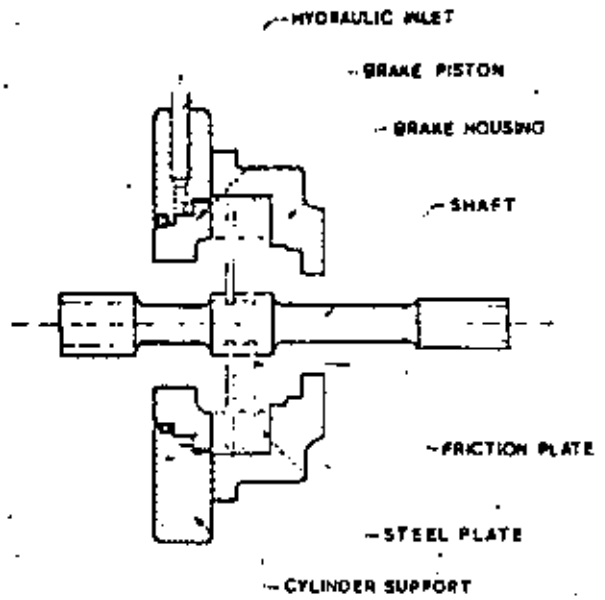

Fig. 2 Brake assembly system

Based on these stress relationships and for the particular case treated in this analysis, the following considerations can be made in order to formulate the finite element model.

1 From fatigue theory as treated by Sors (2), the alternating stress component must be as small as possible in order to improve the fatigue life of the part.
2 Due to the nature of the loads, and by inspection of equations (2) and (3), the reduction of the maximum peak stress at any location of the part will result in a reduction of the dynamic component of stress.
3 Since both the steel plates and friction plates are allowed to displace in the axial

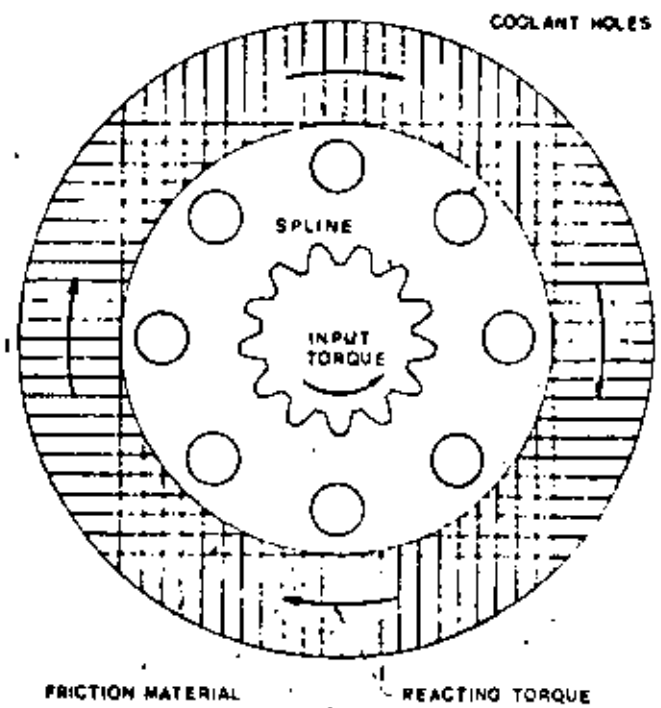

Fig. 3 Torques applied and geometry of the friction plate

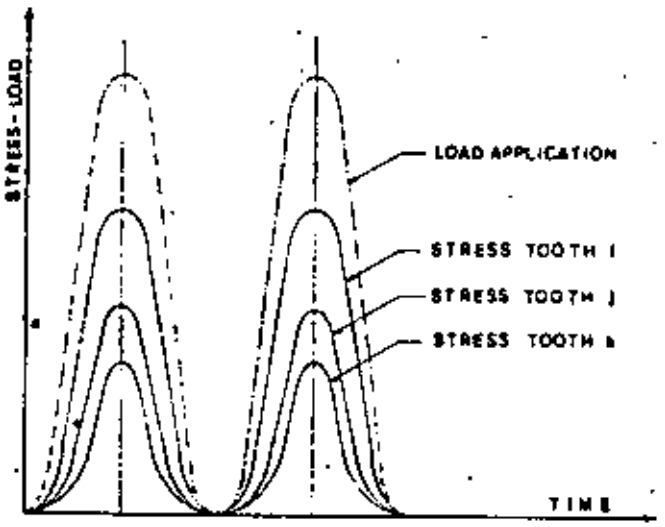

Fig. 4 Variation of load and stresses at three arbitrary locations of the friction plate

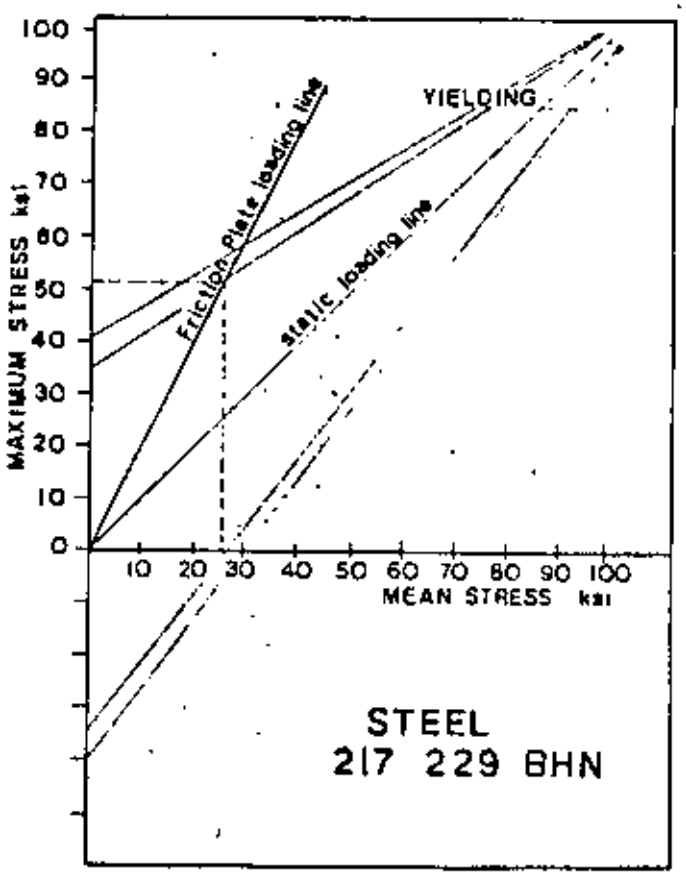

Fig. 5 Goodman diagram and loading line for the friction plate

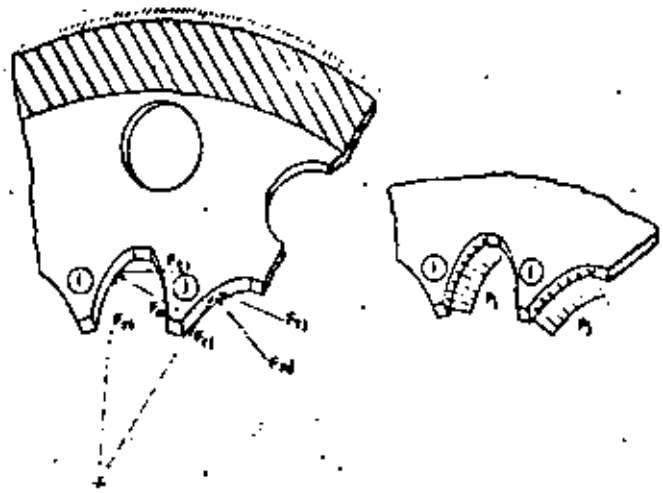

Fig. 6 Application of the load on the friction plate spline teeth

direction the load on the friction plate can be considered to be acting only in the plane of the plate and it has no component in the axial direction.

4 The total load acting on the friction plate can be broken down into tangential and radial forces acting on the teeth of the spline, such that the summation of the resulting tangential forces at the pitch circle, multiplied by the corresponding pitch radius is equivalent to the torque provided by the shaft.

5 The loads applied to the teeth of the plate are reacted by the friction material, which transmits the braking torque to the steel plates.

6 A static analysis alone can be performed on the friction plate, to estimate the stress distribution on the plate.

FORMULATION OF THE PROBLEM

Fig. 6 shows schematically the application of the load on the friction plate, at the location of two adjacent teeth, and the boundary conditions at the friction material area of the plate. In order to avoid local effects due to concentrated point loads, it is convenient to represent the applied forces at the teeth as uniform pressures along the flank of each tooth. The resultant force at the pitch circle must hold for the consideration as discussed earlier in item 4.

The total input torque for each wheel is carried by two plates, such that each plate carries one-half of the input torque.

For the numerical portion of this study

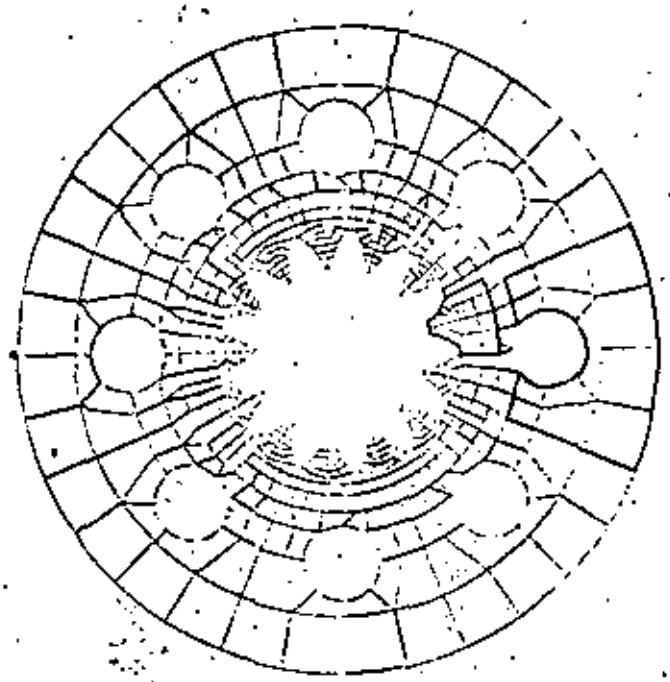

Fig. 7 Computer plot of the original design 8-holes friction plate geometry

and test data available for the particular case, the torque carried by each plate was determined to be as follows:

$$T_{p_1} = \frac{1}{2} T_{in} \qquad (4)$$

Then

$$T_{p_1} = \frac{1}{2}(32400) = 16200 \text{ lb-in} \qquad [1831 \text{ N-m}]^2$$

assuming equal load per tooth, the torque in the plate is distributed equally among the 13 teeth. The torque carried by each tooth is then:

$$T_1 = \frac{1}{13} T_{p_1} \qquad (5)$$

then

$$T_1 = \frac{1}{13}(16200) = 1250 \text{ lb-in} \qquad [141 \text{ N-m}]$$

The equivalent tangential force at each tooth acting at the pitch circle is obtained by dividing the torque by the radius of the pitch circle, this is:

[2] Numbers in brackets indicate the SI equivalence.

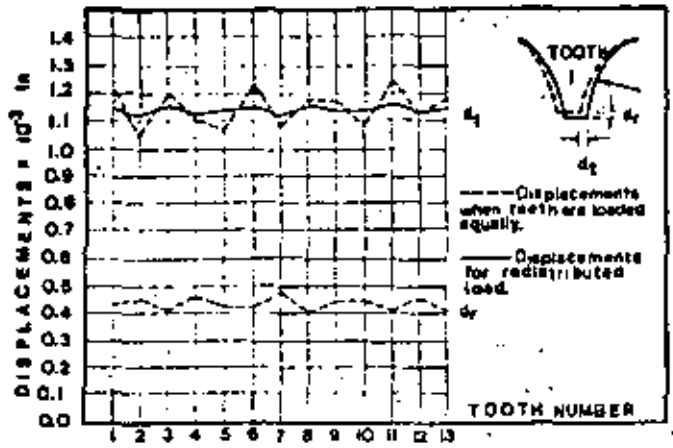

Fig. 8 Displacements at the tip of each tooth for the original 8-holes friction plate model

$$F_{ti} = \frac{T_i}{r_p} \qquad (6)$$

where $r_p = 1.3$ in. Then

$$F_{ti} = \frac{1250}{103} = 960 \text{ lb} \qquad [4276 \text{ N}]$$

The equivalent normal force at the flank of the tooth is obtained as follows:

$$F_{ni} = \frac{1}{\cos\phi} F_{ti} \qquad (7)$$

where ϕ is the pressure angle of the spline geometry. For the present case $\phi = 25$ deg.

The normal force is then:

$$F_{ni} = \frac{1}{\cos 25^\circ} (960) = 1060 \text{ lb} \qquad [4722 \text{ N}]$$

The equivalent pressure at the flank of the teeth is obtained by dividing the normal force by the area of the flank:

$$P_e = \frac{F_{ni}}{A_f} \qquad (8)$$

where A_f is the area of the flank of the tooth for the present case $A_f = 0.04106$ in.^{2} then:

$$P_e = \frac{1060}{.04106} = 25800 \text{ psi} \qquad [178 \text{ M Pa}]$$

The load as uniform pressure on each tooth is estimated to be 25800 psi [178 M Pa] acting on the overall flank of each tooth.

Table 1 Spline Teeth Load Factors Table

Tooth number	Tangential displacement d_{ti}	Inverse $1/d_{ti}$	Percentage %	Nominal percentage %	Percentage difference %	Load factor
1	0.1200	8.3333	7.2684	7.6923	-0.4239	0.9448
2	0.1051	9.4816	8.2753	7.6923	0.5829	1.0750
3	0.1200	8.3333	7.2684	7.6923	-0.4239	0.9448
4	0.1126	8.8809	7.7461	7.6923	0.0537	1.0069
5	0.1088	9.1911	8.0166	7.6923	0.3242	1.0421
6	0.1219	8.2034	7.1511	7.6923	-0.5372	0.9301
7	0.1061	9.3984	8.1974	7.6923	0.5050	1.0655
8	0.1166	8.5765	7.4804	7.6923	-0.2119	0.9724
9	0.1167	8.5689	7.4739	7.6923	-0.2184	0.9716
10	0.1062	9.4250	8.2207	7.6923	0.5283	1.0686
11	0.1220	8.1967	7.1493	7.6923	-0.5450	0.9294
12	0.1091	9.1659	7.9947	7.6923	0.3023	1.0393
13	0.1125	8.8868	7.7530	7.6923	0.0607	1.0079
Total	—	114.6496	100.000	100.000	—	—

THE FINITE ELEMENT MODEL

Due to the type of geometry and loading, plane stress elements were considered adequate for this analysis. Flat plate parabolic elements (8 nodes per element) were chosen to model the geometry of the friction plate.

In order to define the finite element mesh of the structure of the friction plate, node and element generation patterns were used. The procedure is as follows: only one tooth is broken down into finite elements, the location of nodes is defined with respect to a cylindrical coordinate system which origin is at the center of the plate. The element connectivity is also defined for this tooth, then, node generation is performed to define the node locations of the remaining 12 teeth. In the same manner, element generation is performed for the remaining 12 teeth. The generation is done by incrementing the node numbers by 100, at every 27.69 deg twelve times around the center of the plate. A similar approach is used to define the mesh for the outer part of the plate encompassing the coolant circulation holes; in this case one sector is defined and seven sectors are generated around the center of the plate. Finally, quadrilateral and triangular elements are used in order to connect the two sets of sectors together. This is shown in Fig. 7.

The finite element program used, developed by Structural Dynamics Research Corporation (5)

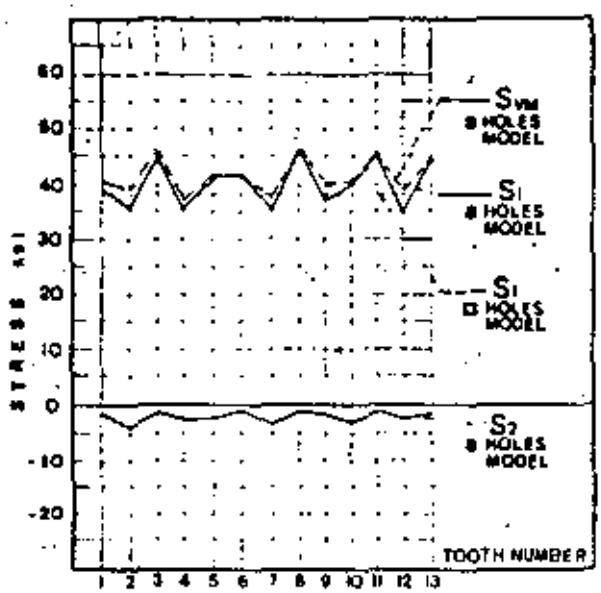

Fig. 9 Stresses at the root of each tooth. The von Mises failure criterion and the principal stresses S_1 and S_2, correspond to the original design. The constant line for S_1 corresponds to the proposed new design

is based on a wave front algorithm solver, therefore, node numbering does not affect the size of the wave front, which is in function of the order in which the elements are defined. (A more detailed description of the wave front algorithm solver can be found in Reference (4) by Nicolas et al.) However, the order in which it is convenient to generate the elements, is not necessarily the most efficient for the wave front size; therefore, a wave front optimizer preprocessor was applied after the mesh generation was accomplished, in order to rearrange the element definition.

The resulting wave front was considerably reduced and the computer costs of this analysis were also reduced.

THE FINITE ELEMENT COMPUTER RUNS

Inspection of the solution yielded by the finite element method application showed that the largest displacement for each tooth occurs at the tip. For the case where the load is considered equally distributed among the teeth, these displacements showed to be different from one tooth to another. Then, the relative differences of displacements are indicative of the particular flexibility of each tooth. Fig. 8 shows graphically the variation of tangential displacements at the tip for all thirteen teeth (dashed line).

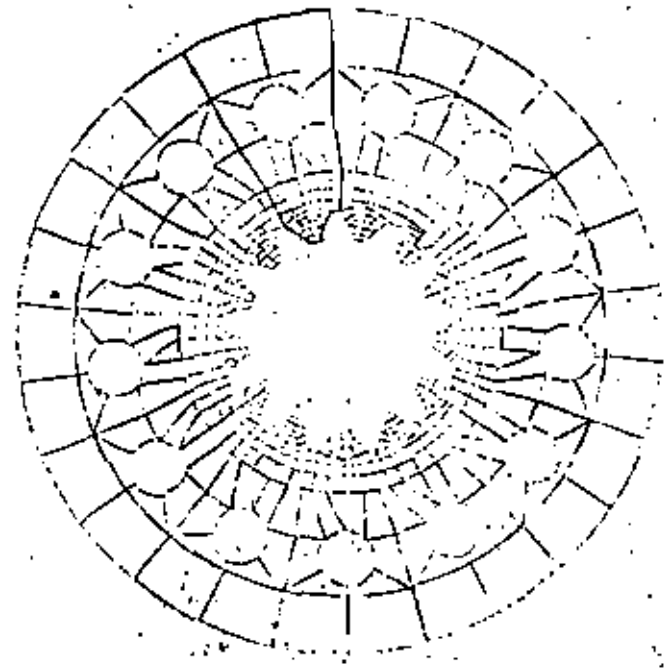

Fig. 10 Computer plot of the proposed 13-holes friction plate

Due to the variation in flexibility for each tooth, the load carried by the most flexible tooth must be less than that for the stiffest tooth. Because of this, a redistribution of the load must be considered, such that the load for a particular tooth is inversely proportional to the tangential displacement at every tooth.

Based on the relative differences of tangential displacements, load factors were developed, in order to redistribute the load on the teeth.

The significance of the load factors is that they indicate the amount of load in percentage carried by each individual tooth.

Table 1 summarizes the calculations made in order to obtain the load factor values for each tooth.

The equivalent pressures applied to the teeth as obtained by equation (8) are then modified as follows:

$$Pe_i = \frac{Fn}{Af}(f_i) \qquad (9)$$

i.e., f_i is the load factor for the ith tooth.

A computer run was performed considering the load factors, and the resulting displacements are shown in Fig. 8 (solid line) for all 13 teeth. The stress solution obtained from this run showed that the maximum stress for each tooth occurs at the base of the root.

Fig. 9 shows the magnitude of the maximum

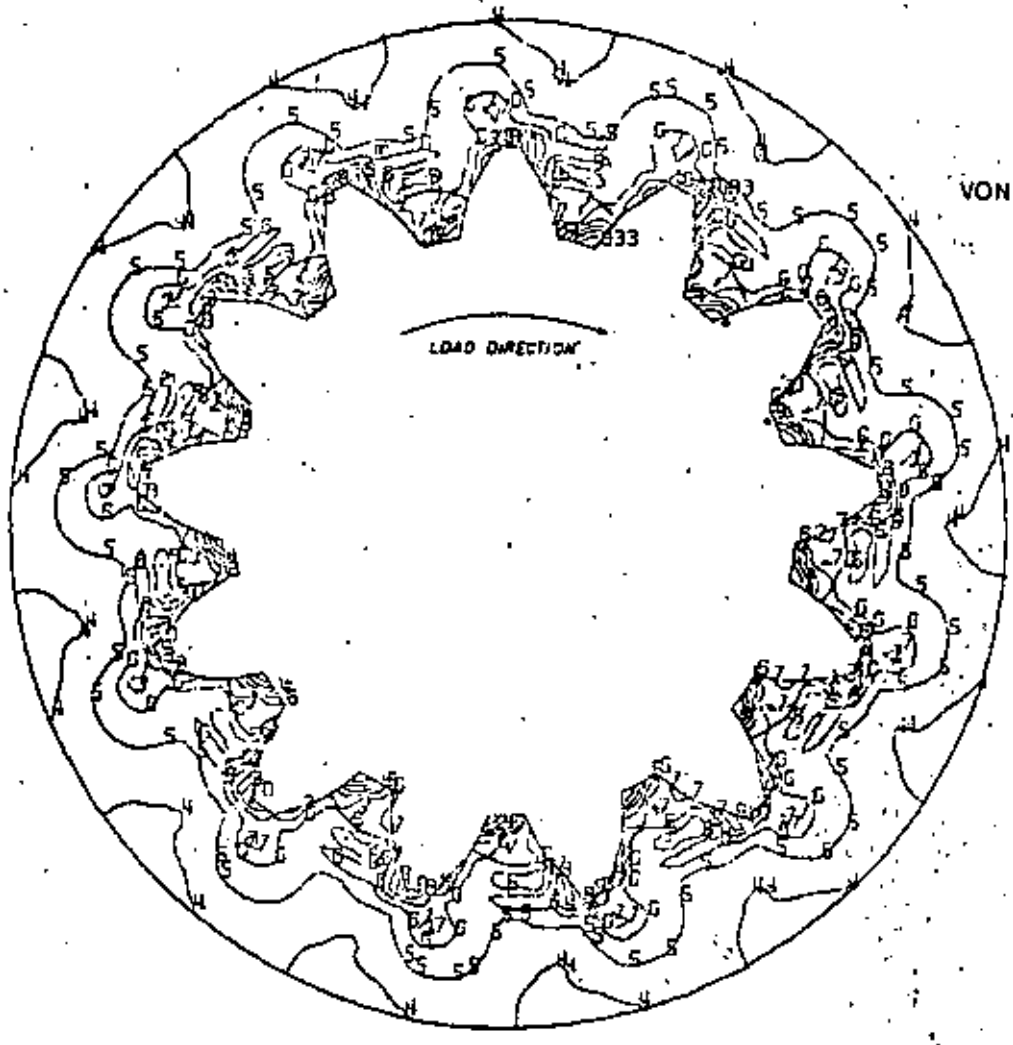

Fig. 11 Stress contour plot for the teeth of the 13-holes friction plate

principal stress (solid line) for all 13 teeth, and also in the same graph, the Von Mises criterion of failure is plotted (dashed line).

The Von Mises criterion of failure as treated by Juvinall (1) is given by the following expression:

$$S_{vm} = \frac{\sqrt{2}}{2} \cdot [(S_2 - S_1)^2 + (S_3 - S_1)^2 + (S_3 - S_2)]^{1/2} \quad (10)$$

where S_1, S_2, S_3 are the principal stresses at the point of consideration.

For the particular case treated in this analysis, $S_3 = 0$ and equation (10) reduces to

$$S_{vm} = \frac{\sqrt{2}}{2} [(S_2 - S_1)^2 + S_1^2 + S_2^2]^{1/2} \quad (11)$$

It can be observed in Fig. 9 that the second principal stress S_2 obtained at the root of the teeth is very small. In the limit, as the mesh is refined S_2 will approach zero.

From the results of the initial computer runs, it was concluded that there exists a significant influence of the relative positions of the coolant circulation holes with respect to each tooth on the spline, some of which will be more susceptible to fail due to fatigue.

A NEW DESIGN MODEL

On the basis of this study, and with the purpose of redistributing the loads and stresses more evenly, a new design having 13 holes equally spaced was suggested. The geometry of the model proposed is shown in Fig. 10.

The main objective of this change as described previously is to obtain a uniform stiffness for all the teeth such that each tooth carries the same load.

One additional computer run was performed considering again equal loading per tooth, and

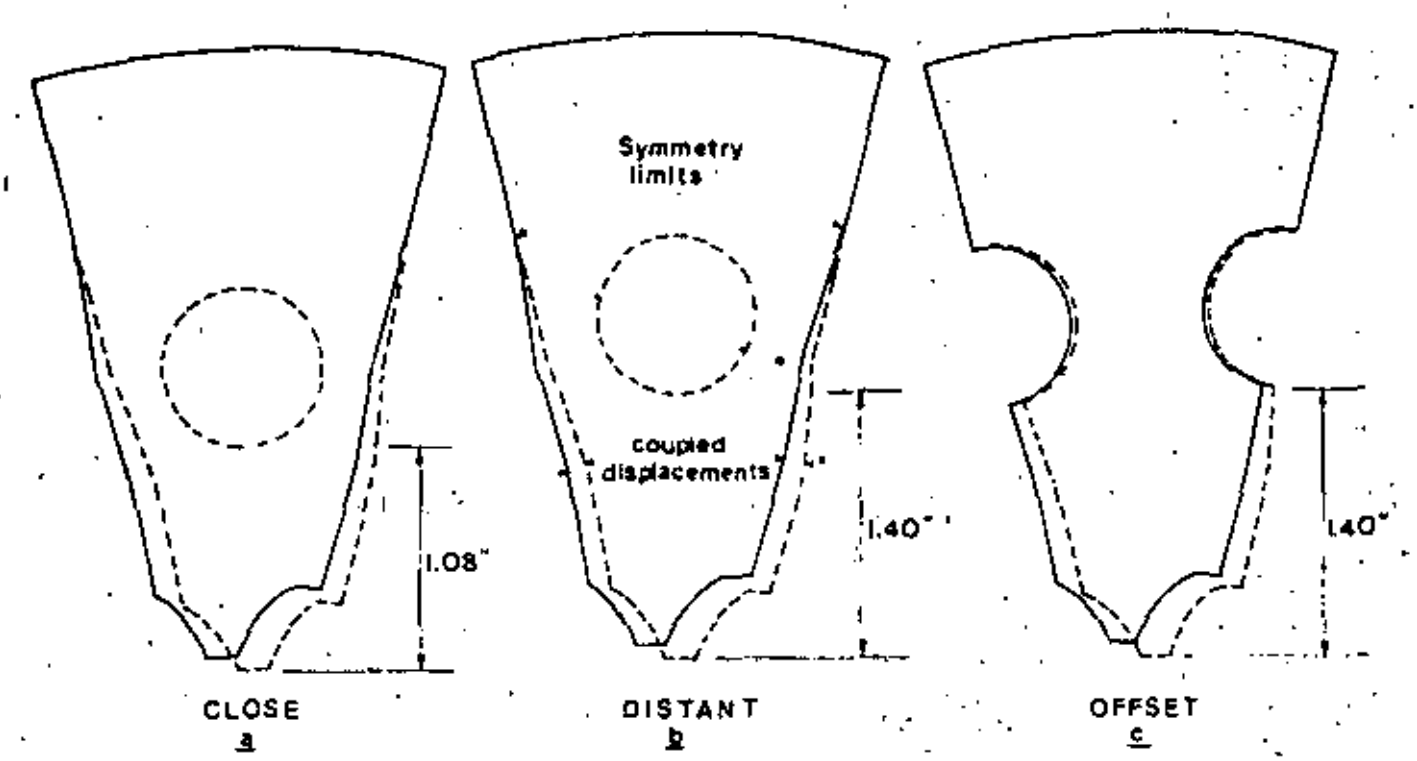

Fig. 12 Additional models of one sector used to determine the most adequate position of the holes with respect to the teeth

the resulting stress distribution (Fig. 11) shows a consistent pattern of stresses which indicates an even distribution of the load on the teeth.

The maximum stress level for the new design plots as the straight line in the graph shown in Fig. 9. As it can be observed, the peak stresses obtained with the original design can be reduced by having the same number of coolant holes than teeth on the plate.

Finally, three additional models were considered in the analysis to determine the most adequate position for the holes with respect to the teeth. These models were made for only one sector encompassing one tooth and one hole. In order to make the one sector model represent to complete structure of the plate, proper boundary conditions were imposed by coupling the displacements of the nodes in the symmetry limits as shown in Fig. 12.

Very good correlation was found between stresses obtained with the complete model and the stresses obtained with the simplified one sector model, (within a 1 percent of difference).

Table 2 summarizes the results obtained from the various computer runs, and provides a reference for the maximum stresses and locations for each case treated.

Table 2 Summary of Results Obtained from the Finite Element Method Computer Runs

RUN No.	MODEL	LOAD DISTRIBUTION	MAXIMUM STRESS LOCATION psi (MPa)	MINIMUM STRESS LOCATION psi (MPa)
1	8 HOLES	Equal load per tooth	S_1 = 46800 (322.7) S_{11} = 1400 (-9.65) S_{up} = 47400 (327.5) Root of tooth No. 2	S_3 = 35600 (251.7) S_{12} = -3900 (-26.99) S_{up} = 35700 (246.9) Root of tooth No. 6
2	8 HOLES	Distributed load by load factor	S_1 = 45500 (313.72) S_{11} = 1600 (11.0) S_{up} = 46300 (319.2) Root of tooth No. 8	S_3 = 35200 (242.70) S_{12} = -3900 (-26.90) S_{up} = 37300 (257.19) Root of tooth No. 11
3	13 HOLES	Equal load per tooth	S_1 = 56500 (389.44) S_{11} = -6000 (-41.37) S_{up} = 39500 (272.36) Root of all 13 teeth	same
4	ONE SECTOR Hole 1.40" from tooth	Uniform Pressure	S_1 = 38000 (262.0) S_{11} = -3000 (-20.68) S_{up} = 40500 (279.26) Root of tooth	
5	ONE SECTOR Hole 1.08" from tooth	Uniform Pressure	S_1 = 39000 (268.90) S_{11} = -3000 (-20.68) S_{up} = 41000 (282.70) Root of tooth	
6	ONE SECTOR Hole Offset from tooth	Uniform Pressure	S_1 = 39000 (268.90) S_{11} = -3000 (-20.68) S_{up} = 41000 (282.70) Root of tooth	

CONCLUSIONS

From the results in this analysis, the following conclusions can be drawn:

1 The distribution of stresses on various teeth in the original design is uneven due to the unique position of each tooth with respect to the coolant circulation holes.
2 A uniform distribution of stresses among the teeth can be obtained by having the same number of holes and teeth.
3 The maximum stresses for the new 13-holes design are 22 percent lower than the stresses obtained with the 8-holes model, for the same loading condition.
4 The most adequated position of the holes with respect to the teeth is above the thick section of each tooth as shown in Fig. 12(b).

The new design produced by this analysis did not require any modification to any of the components of the assembly, and the reduction of the peak stresses resulted in an improvement of the life expectancy of the friction plate.

Laboratory tests have shown an improvement of 100 percent in the fatigue life of the new friction plate, as compared to the original design.

This represents a significant improvement in the performance of the brake system in the rear axles under dynamic loading conditions.

There exists several other parts in the tractor system, which have similar characteristics to the part analyzed herein, and it is visualized that the present analysis method provides the fundamental base for some of the most important aspects to perform a finite element analysis.

ACKNOWLEDGMENT

The authors wish to acknowledge the support provided by the J. I. Case Company of Racine, Wisc., for this study and analysis.

REFERENCES AND BIBLIOGRAPHY

1 Juvinall, R. C., Stress, Strain and Strength, McGraw-Hill, New York, 1967.

2 Sors, L., Fatigue Design of Machine Components, Pergamon Press, New York, 1971.

3 S.D.R.C, "SUPERB," A General Finite Element Program, Cincinnati, Ohio, 1976.

4 Nicolas, V. T., and Citipitioglu, E., "A General Isoparametric Finite Element Program," S.D.R.C.* "SUPERB," Second National Symposium on Computerized Structural Analysis and Design, George Washington University, Washington, D. C., 1976.

5 Citipitioglu, E., Nicolas, V. T., and Tolani, S. K., "Finite Element Method in Stress Analysis Practice," Second International Conference on Vehicle Mechanics, Southfield, Mich., April 18-20, 1977, SAE.

6 Segerlind, L. J., Applied Finite Element Analysis, Wiley, New York, 1976.

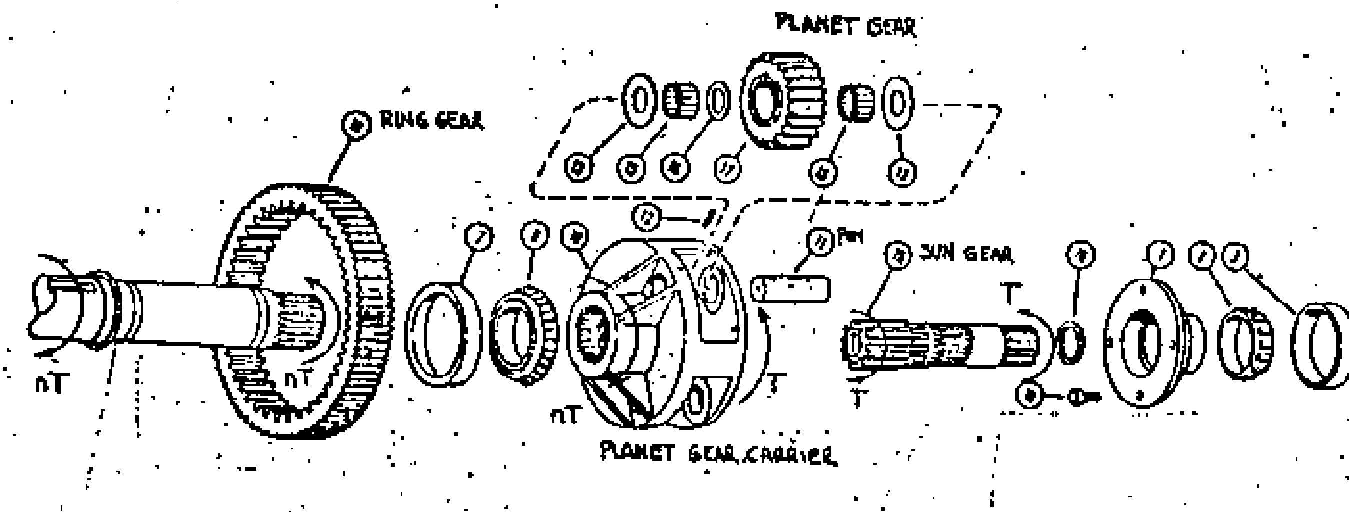

FIG 2

PLANETARY GEAR TRAIN SYSTEM

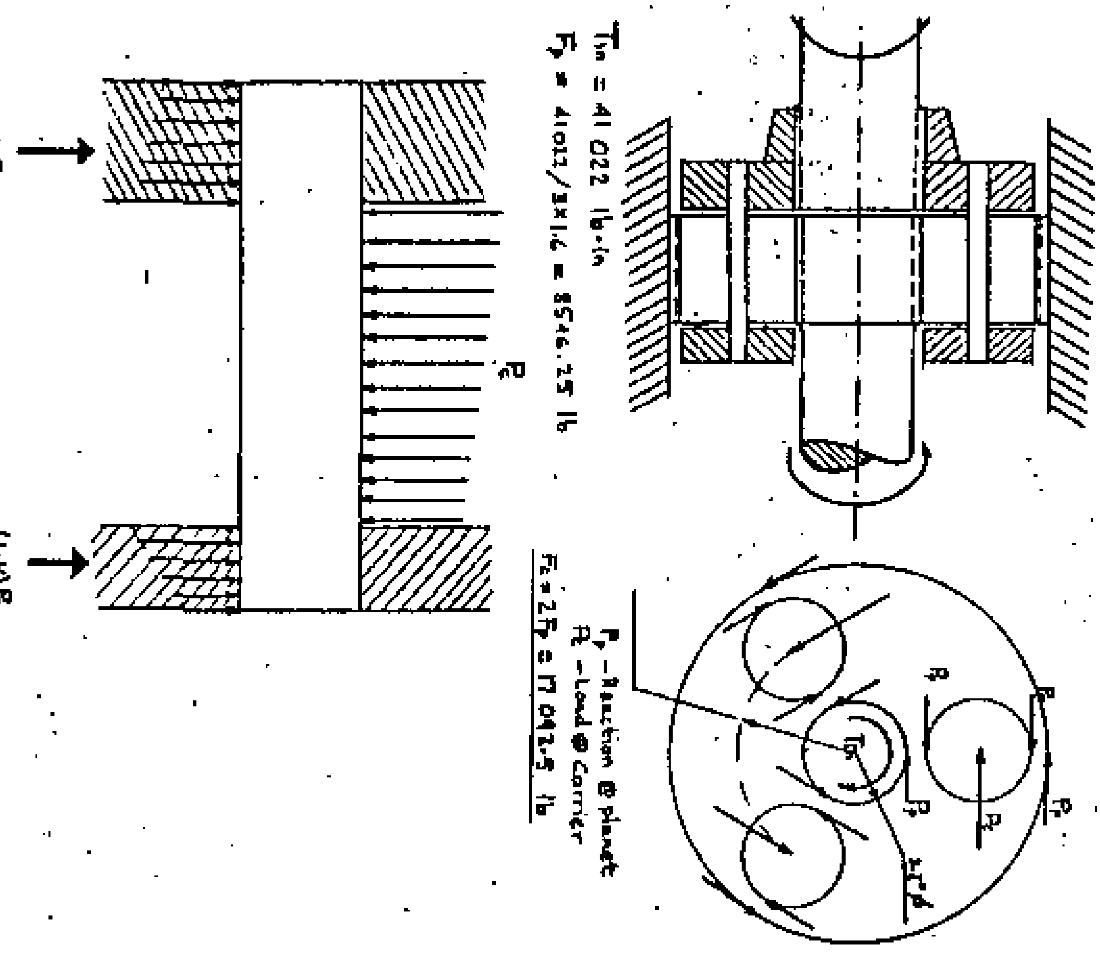

FIG 3

FREE BODY DIAGRAM AND REACTIONS

56

57

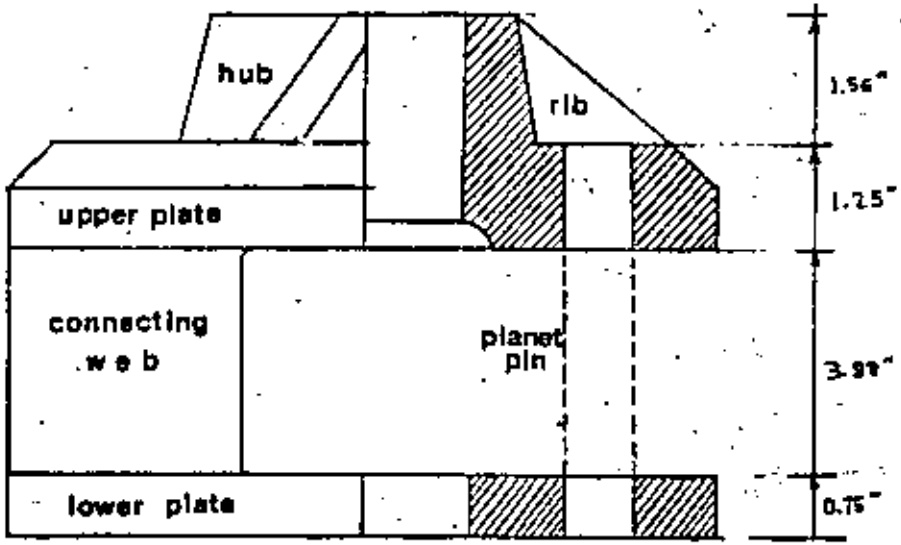

FIG 4

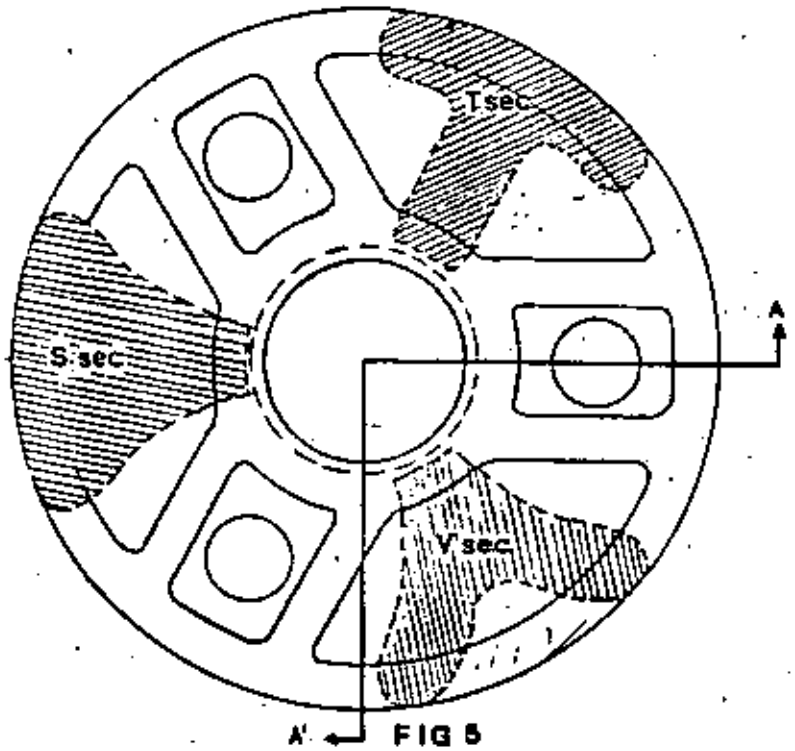

FIG 5

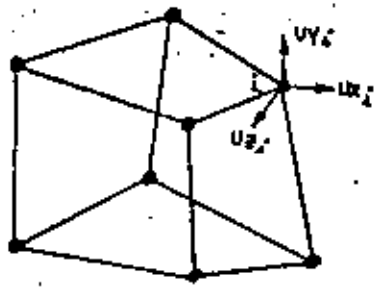

8 NODE BRICK
(LINEAR) ELEMENT

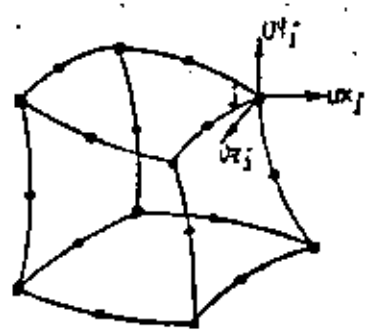

20 NODE BRICK
(PARABOLIC) ELEMENT

FIG 6

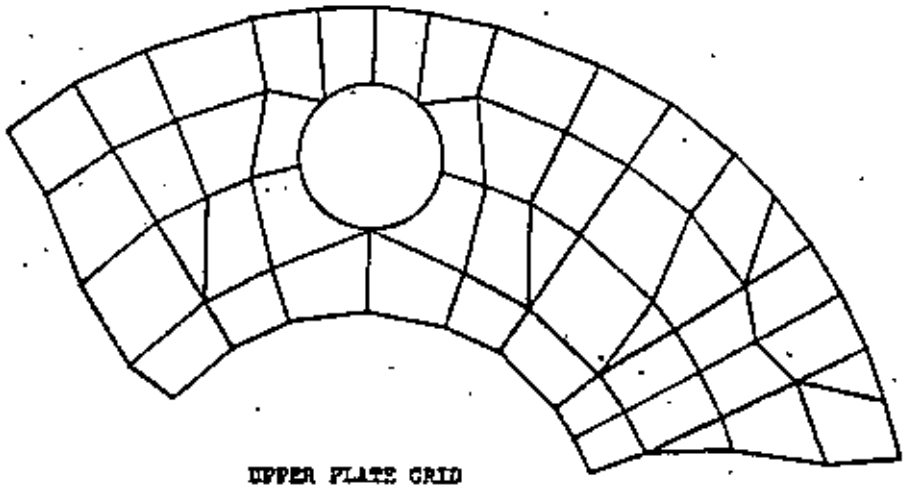

UPPER PLATE GRID

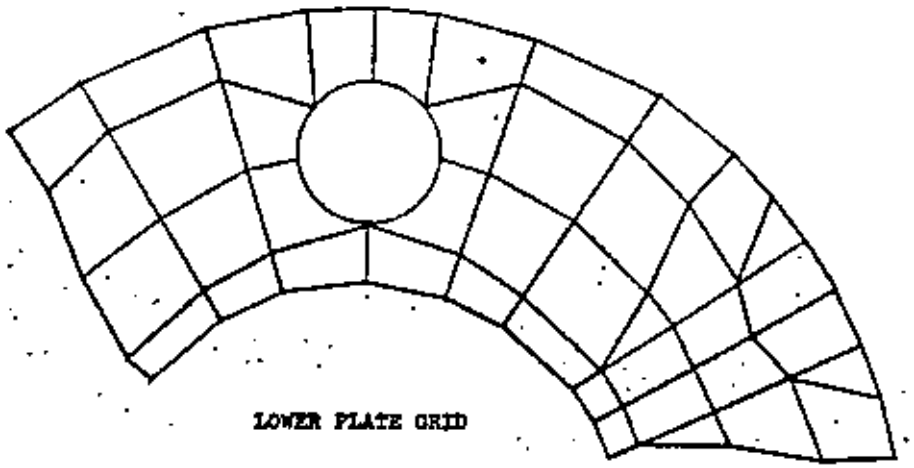

LOWER PLATE GRID

FIG 8 .- GEAR CARRIER FEM MODEL

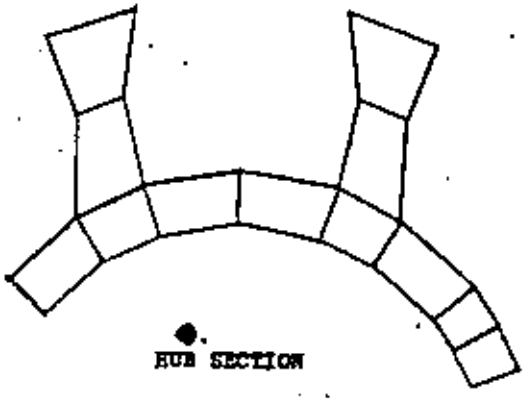

HUB SECTION

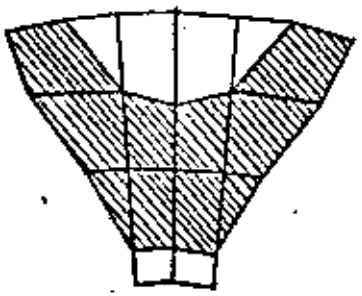

"V"-SECTION
CONNECTING WEB

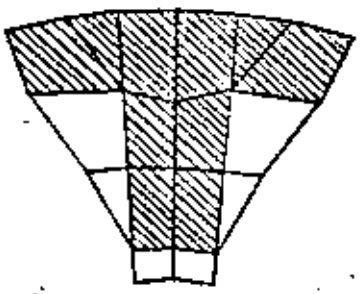

"I"- SECTION
CONNECTING WEB

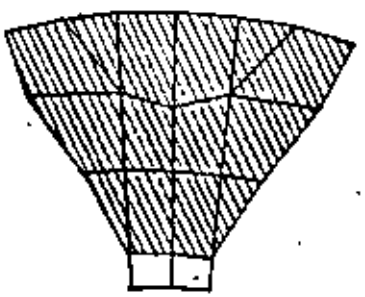

"S"-SOLID SECTION
CONNECTING WEB

FIG. 8

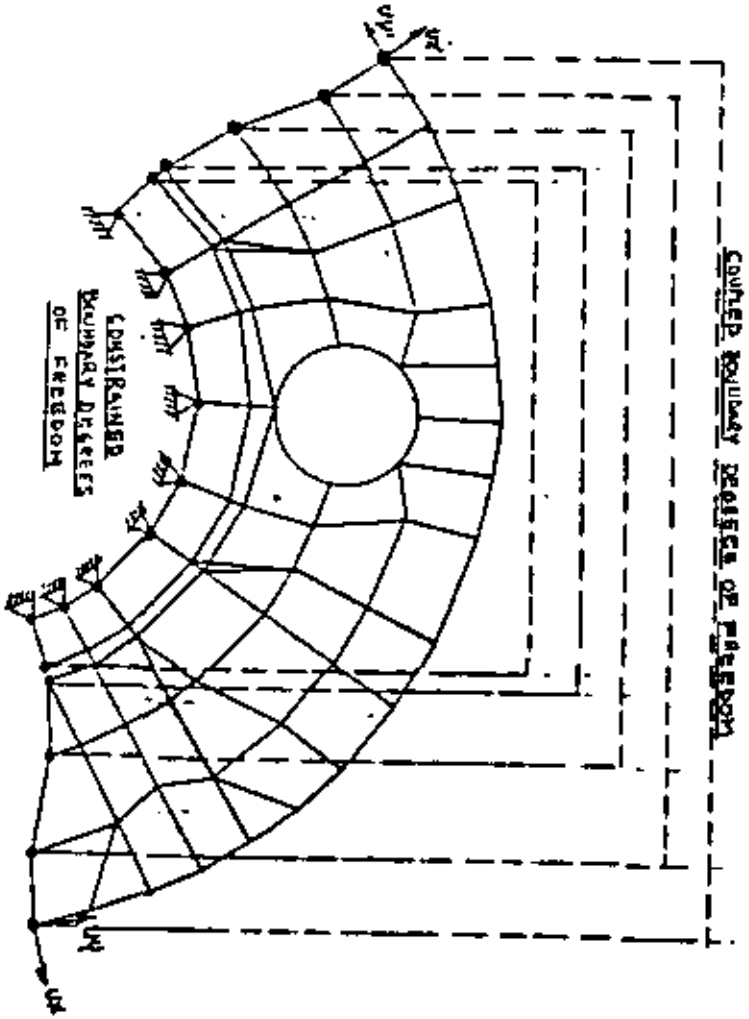

FIG 9

Table 1 - Coupled Node Displacements

Node 1	Node 2	Directions
1	1001	UX, UY, UZ
27	1027	UX, UY, UZ
40	1040	UX, UY, UZ
55	1055	UX, UY, UZ
70	1070	UX, UY, UZ
85	1085	UX, UY, UZ
102	1002	UX, UY, UZ
119	1119	UX, UY, UZ
215	1215	UX, UY, UZ
651	1651	UX, UY, UZ
664	1664	UX, UY, UZ
667	1667	UX, UY, UZ
709	1709	UX, UY, UZ
728	1728	UX, UY, UZ
747	1747	UX, UY, UZ
764	1764	UX, UY, UZ
781	1781	UX, UY, UZ

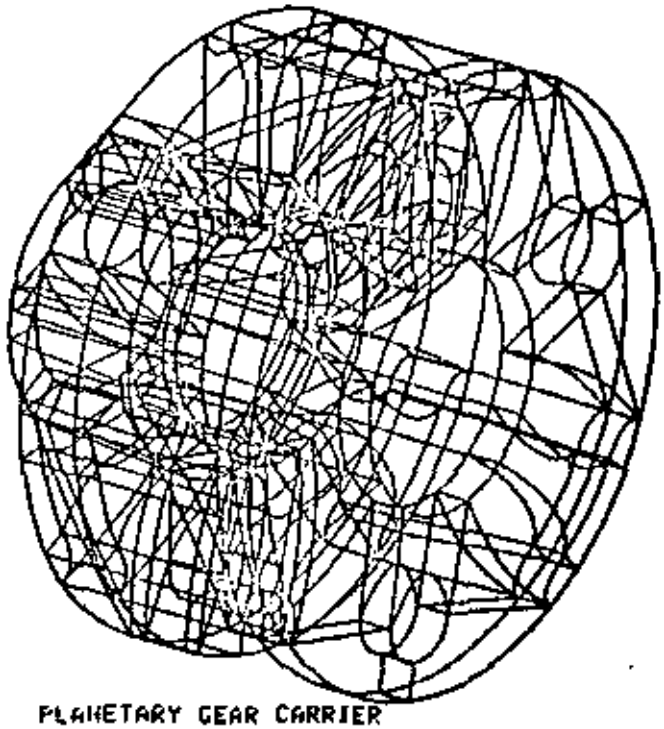

PLANETARY GEAR CARRIER

PLOT NO. 1 FIG 10

Table 2 - Summary of Computer Runs for the Planetary Gear Carrier Project

RUN No.	Model	Structure Size	Element Type	Loading Type	Connecting Web	Computer System*	F.E.M. Codes**
1	1370 Carrier	Complete Structure	20 Nodes Solid	Plates Loaded	"I"	C.D.C.	SUPERB SDRC
2	1370 Carrier	120° Sector	20 Nodes Solid	Plates Loaded	"I"	G.E.	SUPERB SDRC
3	XA-54/55 Carrier	120° Sector	8 Nodes Solid	Plates Loaded	"V"	U.C.S.	ANSYS SASI
4	XA-54/55 Carrier	120° Sector	8 Nodes Solid	Plates Loaded	"I"	U.C.S.	ANSYS SASI
5	XA-54/55 Carrier	120° Sector	8 Nodes Solid	Plates Loaded	"S"	U.C.S.	ANSYS SASI
6	XA-54/55 Carrier	120° Sector	8 Nodes Solid	Pin Loaded	"S"	U.C.S.	ANSYS SASI
7	XA-54/55 Carrier	120° Sector	8 Nodes Solid	Plates Loading	"S"	C.D.C.	ANSYS SASI

* C.D.C. - Control Data Corporation
G.E. - General Electric
U.C.S. - United Computing System

** SDRC - Structural Dynamics Research Corporation; SASI - Swanson Analysis System Inc.

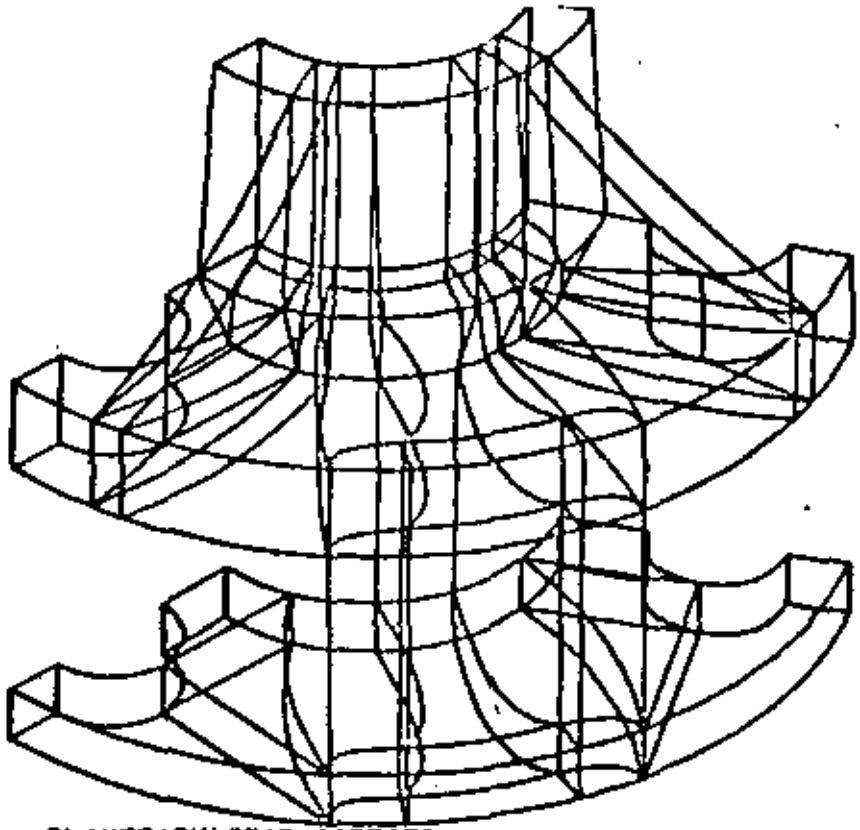

PLANETARY GEAR CARRIER

PLOT NO. 1

FIG 11

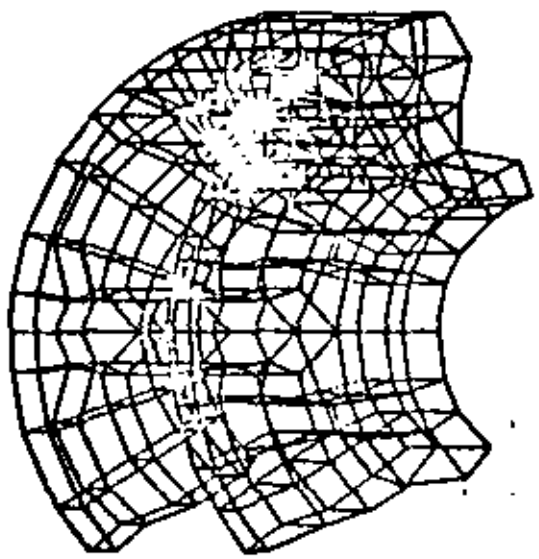

FIG 12

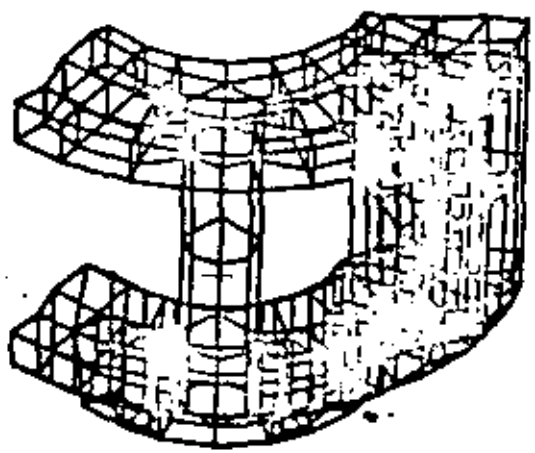

Fig 13

	V section	Tsection	S section	Ssec/pin
$U_{61}^{\cdot}$	0.005305	0.004900	0.004031	0.00372
U_{63}	0.005324	0.004914	0.004049	0.00375
U_{275}	0.005630	0.005221	0.004260	0.004175
U_{277}	0.006351	0.005945	0.004967	0.004149
U_{417}	0.001577	0.001614	0.001645	0.002155
U_{419}	0.002169	0.002208	0.002235	0.002148
U_{717}	0.001788	0.001817	0.001798	0.001773
U_{719}	0.002117	0.002145	0.002127	0.001766
$\alpha_1^{\cdot\cdot}$	0.001044	0.000929	0.000679	0.000520
α_2	0.001077	0.000963	0.000704	0.000515

TABLE 3

$U_{(I)}^{\cdot}$ - Tangential displacement node I

$\alpha_{(J)}^{\cdot\cdot}$ - Slope of pin side J

FIG 14

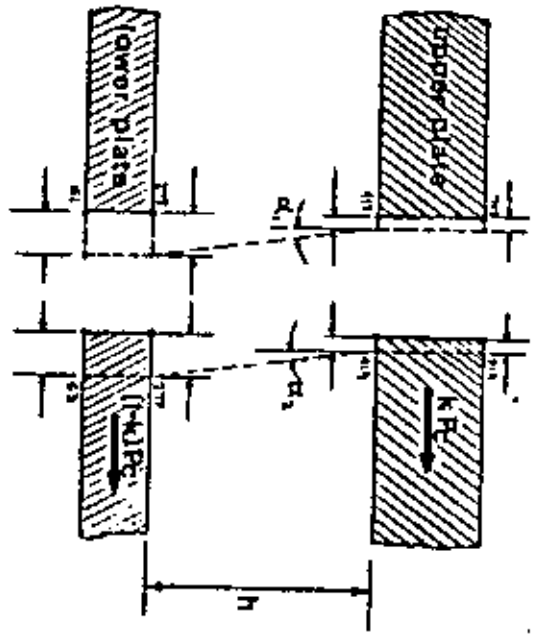

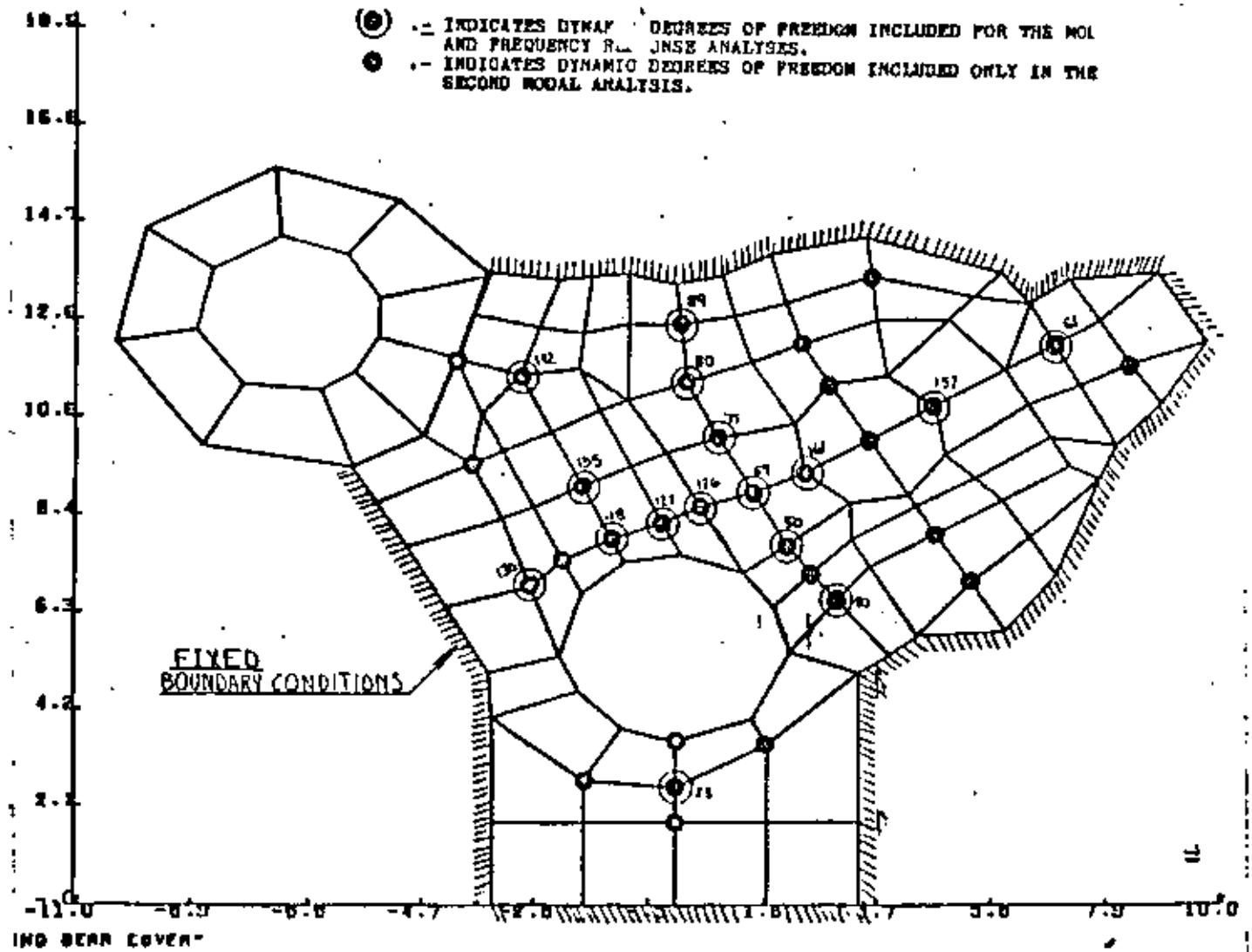

IND BEAR COVER"

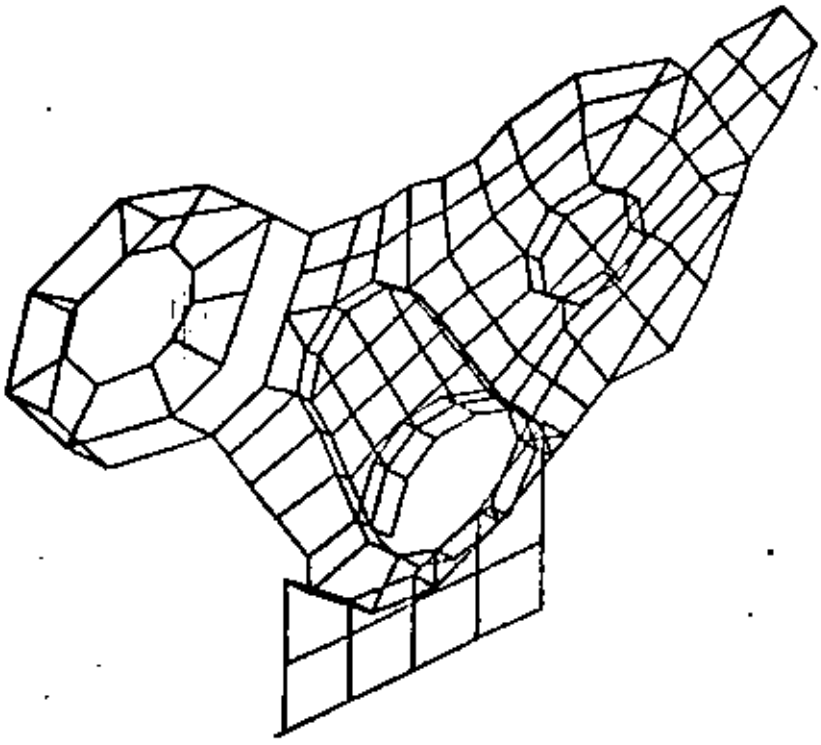

"TIMING GEAR COVER"

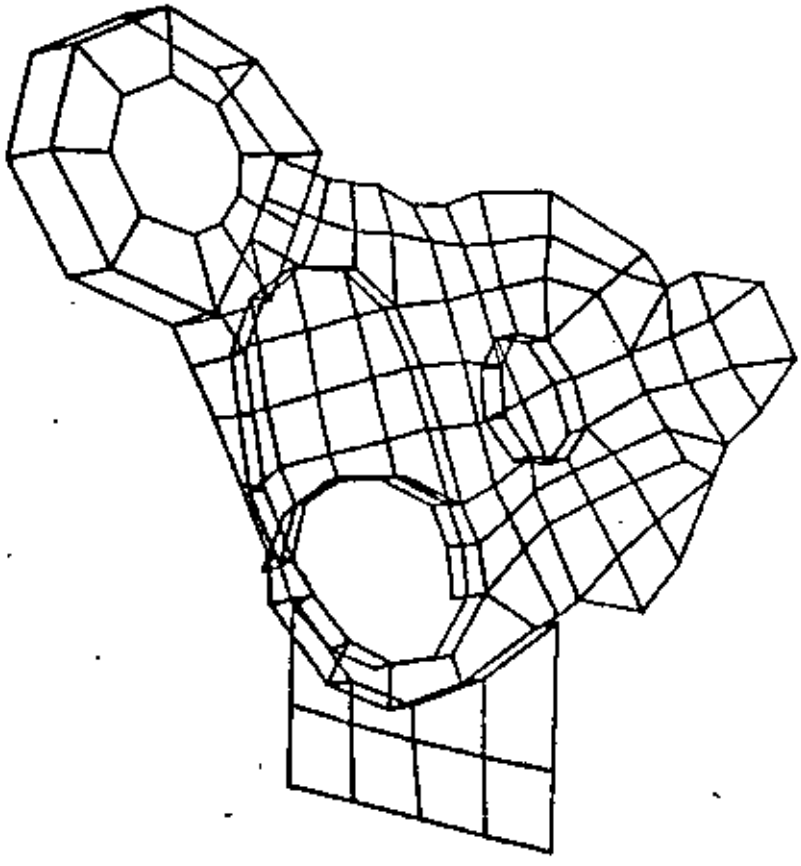

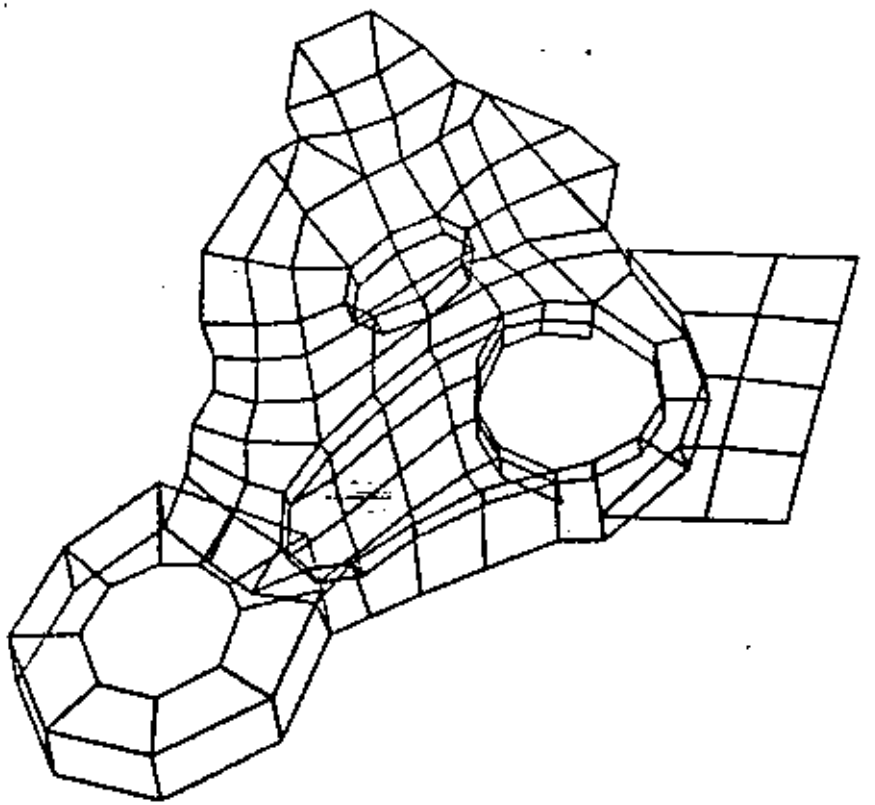

NATURAL FREQUENCIES TABLE

RESULTS		
15 d.o.f.	33 d.o.f.	experimental
571.7	667.0	1123.0
1231.7	1196.6	1215.0
1823.4	1762.0	1259.0.
2000.3	1969.7	1366.0
2530.0	2166.3	1393.0
2635.0	2499.8	1427.0
3490.1	3015.2	1496.0
4441.1	3093.3	1571.0
5147.2	4277.1	1778.0
5776.2	4336.3	1967.0
6693.1	5087.7	2006.0
7990.8	5534.2	
11271.0	5717.6	
12178.0	6223.8	
15557.0	6254.1	
	6821.6	
	7792.0	
	8474.8	
	9053.9	
	9711.9	
	10642.0	
	11493.0	
	11915.0	
	12170.0	
	14205.0	
	15591.0	
	15913.0	
	16701.0	
	24056.0	
	74901.0	
	76946.0	
	79464.0	
	83710.0	

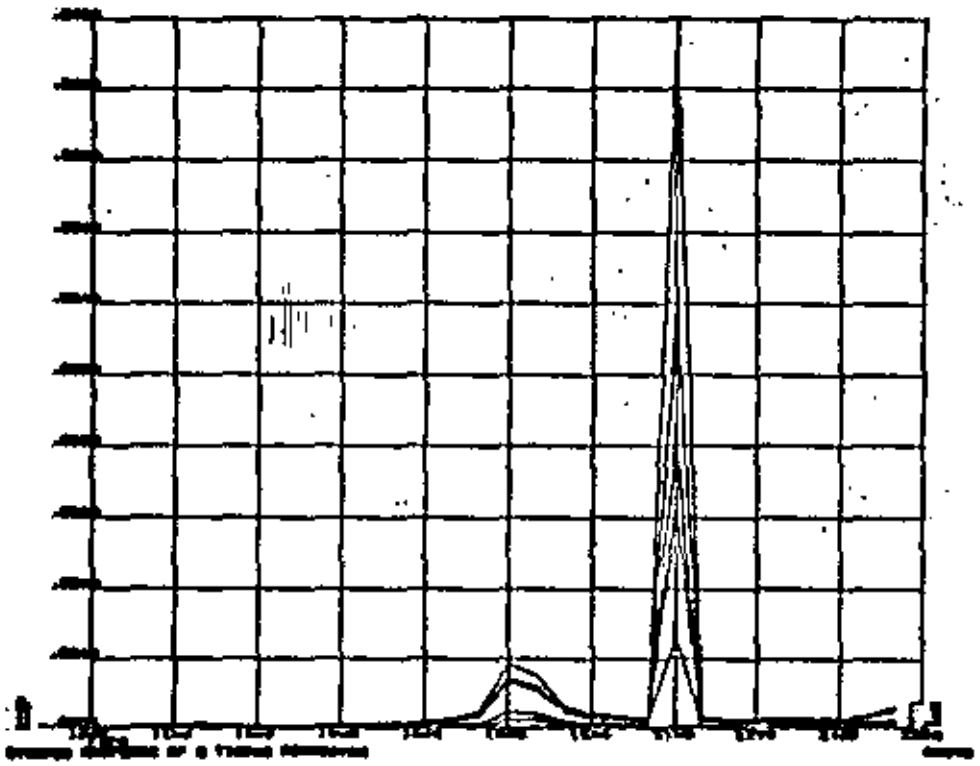

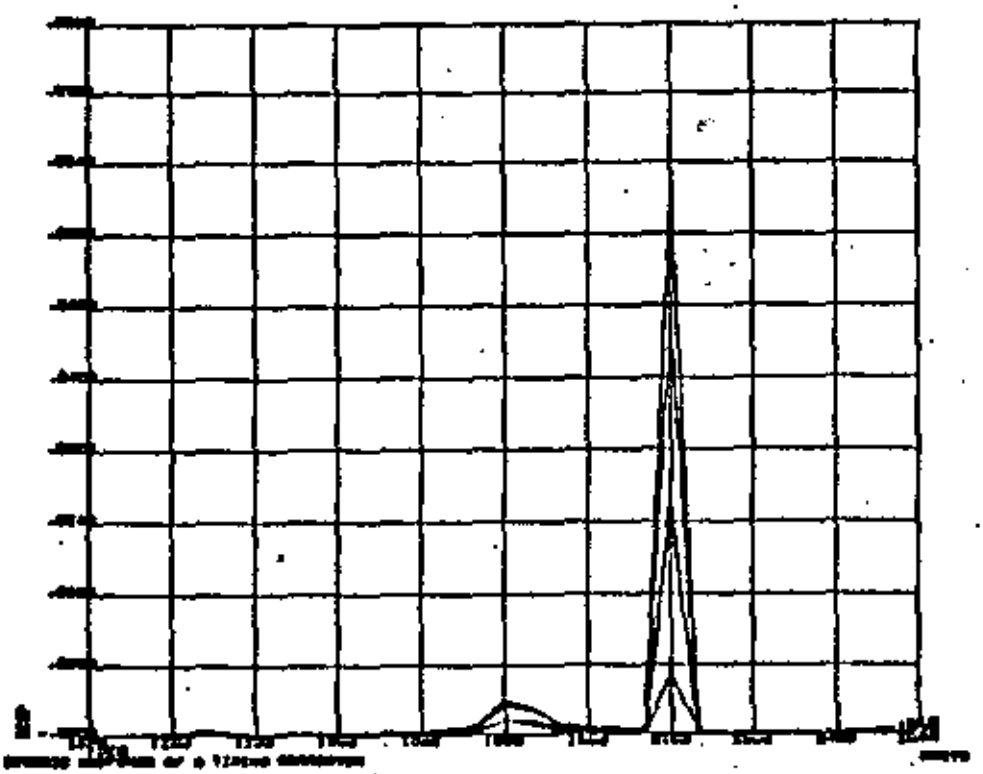

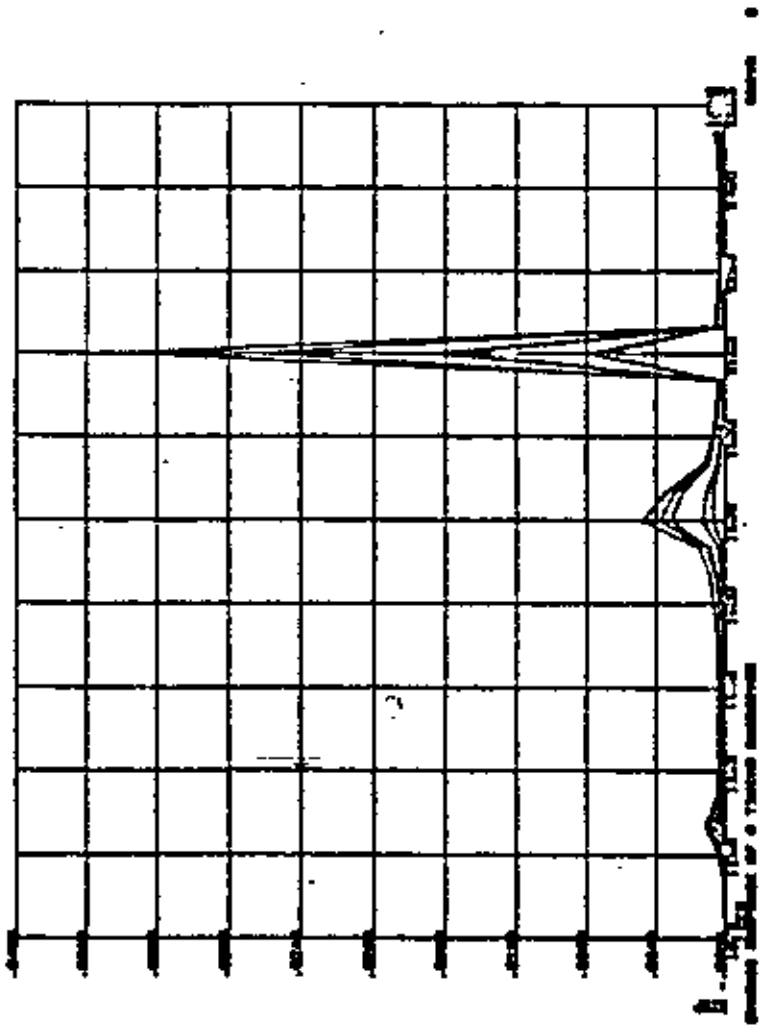

REFERENCES

1. O.C. Zienkiewicz, "The Finite Element Method in Engineering Science", McGraw-Hill, London, 1971.

2. L.J. Segerlind, "Applied Finite Element Analysis", John Wiley & Sons, Inc., New York, 1976.

3. R.D. Cook, "Concepts and Applications of Finite Element Analysis", John Wiley & Sons, Inc., New York, 1974.

4. C.S. Desi & J.F. Abel, "Introduction to the Finite Element Method", Van Nostrand Co., New York, 1972.

5. DeSalvo, C.J. & Swanson, J.A., "ANSYS User's Manual", Swanson Analysis Systems, Inc., 1978.

6. Wilson, Bathe & Peterson, "SAP IV" Structural Analysis Program, University of California - Berkeley, 1974.

7. C.E. McCormick, ed., "The MASTRAN User's Manual", National Aeronautics and Space Administration, Special Publication 222(01), Washington, D.C., May, 1974.

8. SDRC "SUPERB" Finite Element Program, Structural Dynamics Research Corporation, Cincinnati, Ohio, 1978.

EL METODO DEL ELEMENTO FINITO EN LA INGENIERIA MECANICA

ECUACIONES DE EQUILIBRIO

DR. PORFIRIO BALLESTEROS BAROCIO

ABRIL, 1982

METODO DE ANALISIS POR ELEMENTOS FINITOS.

INTRODUCCION.

El ingeniero en la busca de los valores numéricos adecuados para describir su proceso de diseño, se encontraba generalmente con formulaciones matemáticas difíciles. Por ejemplo, considerando el simple caso de teoría de flexión de placas, bajo las hipótesis de pequeñas deformaciones y que las secciones planas permanecen planas después de la deformación, la ecuación diferencial que gobierna el análisis para un material elástico lineal homogeneo e isotrópico es

$$\frac{\partial^4 W}{\partial x^4} + 2\frac{\partial^4 W}{\partial x^2 \partial y^2} + \frac{\partial^4 W}{\partial y^4} = \frac{q}{D} \qquad (1)$$

donde W es la deflexión en el punto (x, y), q es la intensidad de la carga en el punto (x, y), y $D = \frac{E h^3}{12(1-\nu^2)}$ es la rigidez flexionante de la placa la cual depende del modulo de elasticidad E, el espesor de la placa h y la relación de Poisson ν. En la Fig. 1 se presenta un elemento diferencial de la placa y las acciones y reacciones sobre él. Combinando la flexión simple en dos direcciones se obtiene para los momentos y cortantes por unidad de longitud de placa lo siguiente:

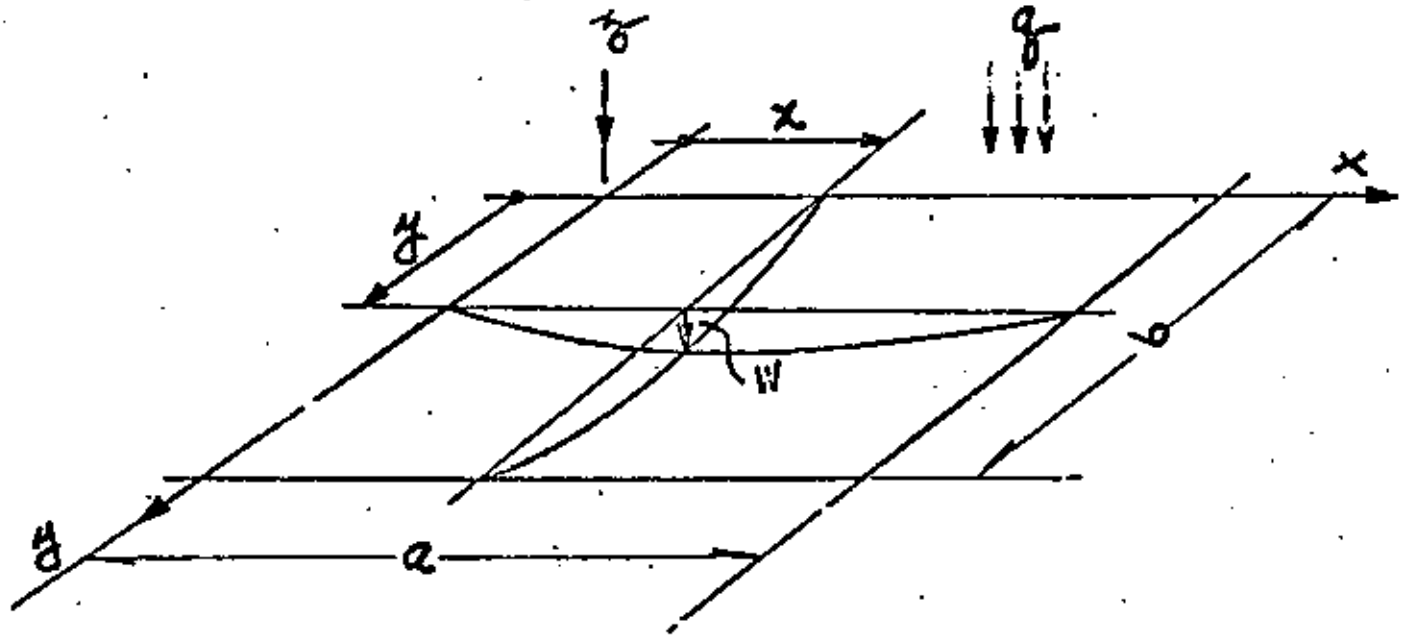

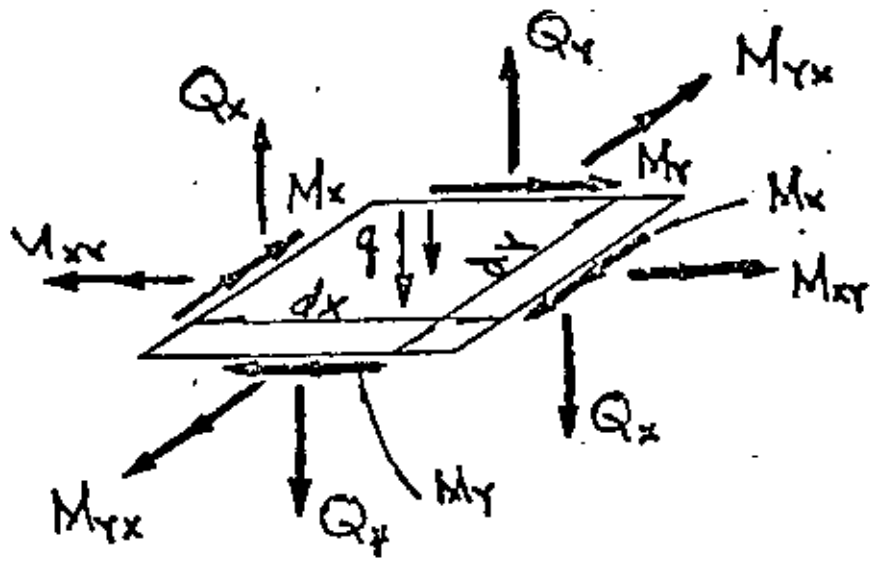

Fig. 1 Superficie media de una placa, y un elemento diferencial dx, dy.

$$M_x = -D\left(\frac{\partial^2 W}{\partial x^2} + \nu \frac{\partial^2 W}{\partial y^2}\right)$$

$$M_y = -D\left(\frac{\partial^2 W}{\partial y^2} + \nu \frac{\partial^2 W}{\partial x^2}\right)$$

$$M_{xy} = D(1-\nu)\frac{\partial^2 W}{\partial x \partial y} \qquad (2)$$

$$Q_x = -D\frac{\partial}{\partial x}\nabla^2 W$$

$$Q_y = -D\frac{\partial}{\partial y}\nabla^2 W$$

donde $$\nabla^2 W = \frac{\partial^2 W}{\partial x^2} + \frac{\partial^2 W}{\partial y^2}$$

Para el caso particular de la placa libremente apoyada, y rectangular, cuyas condiciones en la frontera (Fig. 2) son:

$$W(0,y) = 0$$

$$W_{xx}(0,y) + \nu W_{yy}(0,y) = 0 \qquad (3)$$

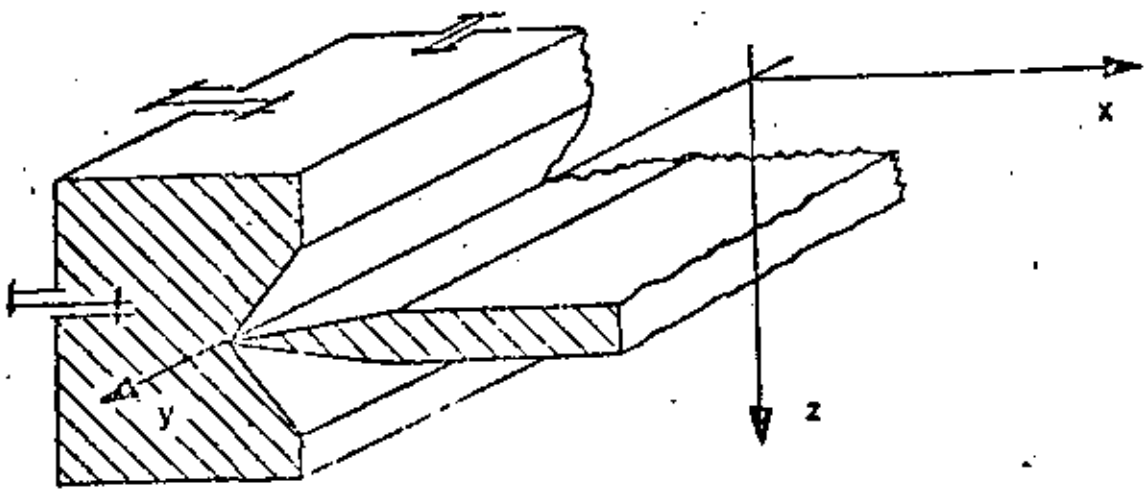

Navier en 1820 presentó a la Academia Francesa de Ciencias, la solución representando la carga q (x, y), por medio de una serie trigonométrica doble

$$q(x,y) = \sum_{m=1}^{\infty}\sum_{n=1}^{\infty} a_{mn} \operatorname{sen}\frac{m\pi}{a}x \operatorname{sen}\frac{n\pi}{b}y \qquad (4)$$

substituye (4) en (1) y considerando las propiedades de ortogonalidad de las series trigonométricas obtiene la solución de la ecuación diferencial bi-armónica (1) como

$$W = \frac{1}{\pi^4 D}\sum_{m=1}^{\infty}\sum_{n=1}^{\infty}\frac{a_{mn}}{\left(\frac{m^2}{a^2}+\frac{n^2}{b^2}\right)^2} \operatorname{sen}\frac{m\pi}{a}x \operatorname{sen}\frac{n\pi}{b}y \qquad (5)$$

en donde el coeficiente Amn viene expresado por

$$a_{mn} = \frac{4}{ab}\int_0^a\int_0^b q(x,y) \operatorname{sen}\frac{m\pi}{a}x \operatorname{sen}\frac{n\pi}{b}y \, dx\, dy \qquad (6)$$

El procedimiento de Navier consiste en lo siguiente: Conocida la función de carga q (x,y), se substituye en (6) y se obtiene el coeficiente Amn el cual - nuevamente se substituye en (5) y se obtiene la deflexión W (x, y), y por medio las ecuaciones (2) se obtienen los momentos y cortantes {M} y {Q.}

Es importante observar que las limitaciones de Navier se refieren a una placa - rectangular libremente apoyada y con una función de carga q (x,y) impar con - respecto a x, y con respecto a Y, es decir, $f(x) = -f(-x)$ y

Si la función fuese par, la representación de - q (x,y) sería mediante una serie de cosenos, y si q (x, y) fuese una función cual

quiera, se representaría mediante una serie trigonométrica doble completa de senos y cosenos, y se tendrían problemas en satisfacer las condiciones en la frontera. Generalmente la convergencia de la serie (5) es lenta, y en algunos casos es necesario considerar más de 500 términos para asegurar la solución correcta.

Posteriormente en 1900 M. Levy cambia de posición los ejes coordenados (Fig. 3) e utiliza una serie trigonométrica simple

$$w = \sum_{m=1}^{\infty} f_m(y) \operatorname{sen} \frac{m\pi}{a} x \qquad (7)$$

El procedimiento de Levy consiste en substituir (7) en (1) obteniendo una ecuación diferencial lineal de cuarto orden en fm(y) con coeficientes constantes no homogenea con la cual ya es posible satisfacer diferentes condiciones en la frontera $y = \pm \frac{b}{2}$. pero continua limitado a una placa rectangular libremente apoyada en las fronteras x = o y x = a.

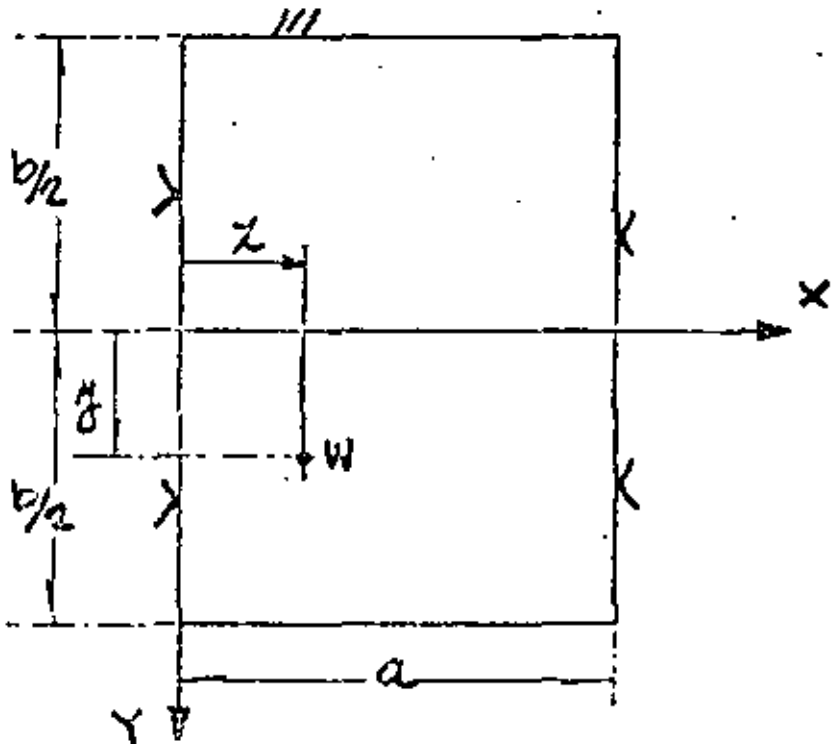

Las limitaciones de análisis tan restringidas, como los ejemplos anteriores aparecían en innumerables problemas de ingeniería, lo cual originó el principio de los métodos numéricos, el cual presenta dos etapas de desarrollo. Antes de la época de las computadoras, donde representa un importante papel el Prof. Southwell del Colegio Imperial de Inglaterra, desarrollando y aplicando los métodos numéricos de relajación y diferencias finitas, superando las limitaciones restringidas de los métodos analíticos de solución.

Durante la era de las computadoras digitales, el método de análisis por elementos finitos ha obtenido gran popularidad, puesto que en este procedimiento como resultado de la discretización del medio por analizar, se obtienen sistemas grandes de ecuaciones algebraicas lineales simultáneas, lo cual actualmente su solución no representa ningún problema. Por ejemplo, en el caso de análisis elástico lineal de placas, podemos tener cualquier condición de apoyo, de geometría y de cargas, prácticamente se eliminan la mayoría de las restricciones de las soluciones analíticas mencionadas, el problema más importante es verifiar adecuadamente su convergencia.

El primer trabajo referente al método se debe a Hrenikoff Ref. 1 publicado en 1941, y el segundo a McHenry publicado en 1943 en ambos trabajos (Fig. 4) se verifican soluciones de problemas de elasticidad bidemensional en estado plano de esfuerzos, discretizando el medio y buscando la analogía con la solución estructural.

Posteriormente en 1949 Newmark, en su libro de Métodos Numéricos Ref. 3 , presenta los métodos de Hrenikoff y McHenry. Sin embargo, el

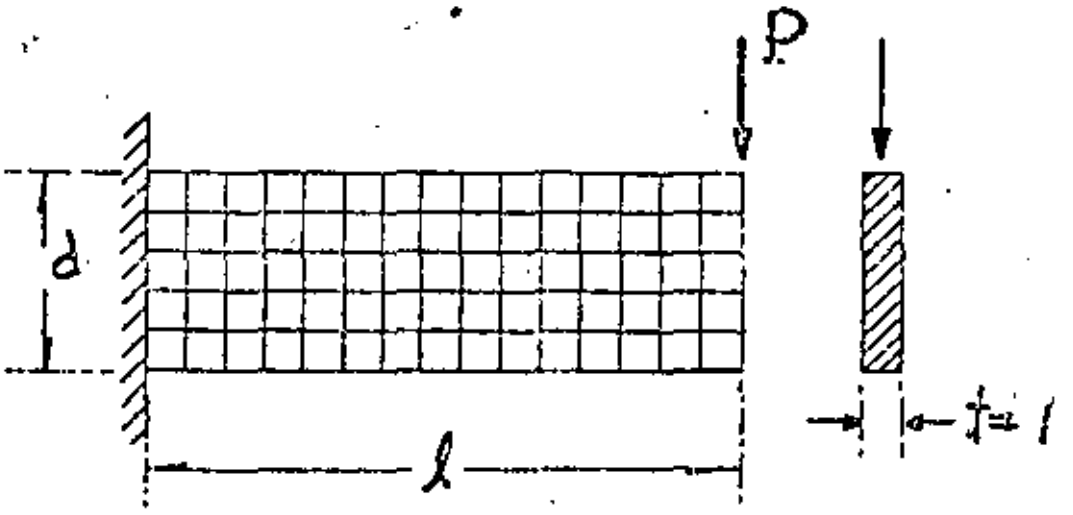

Fig. 4 Primera solución presentada por Hrenikoff en 1941.

crédito de aplicarlo a medios continuos es de Turner, Clough, Martin y Topp Ref. 5 , y no es, sino hasta 1960 con Clough, Ref. 6 nace por primera vez el nombre mágico de "Elemento Finito" , derivando más correctamente las propiedades básicas del elemento triangular y el rectangular, y el hecho de que en el mismo tiempo la computadora comienza a ser una herramienta muy efecti va, conduce rápidamente a la solución numérica de problemas elástico lineales complejos, en los cuales una solución analítica no era posible.

Se inician la derivación de las propiedades de rigidez de los elementos finitos, el campo de desplazamientos en el medio se expresa en función de los desplaza - mientos nodales del elemento, satisfaciendo continuidad, las fuerzas internas se definen aplicando el principio del trabajo virtual, la identidad de este proceso con el de minimizar la energía potencial total, o sea, el proceso de Rayleigh-Ritz Ref. 7 es obvia. El desarrollo anterior se acentúa en el campo de la Mecá- nica de Sólidos y posteriormente Zienkiewicz Ref. 13 y Wilson Ref. 14 lo aplican en Mecánica de fluídos y en problemas de análisis de conducción de calor.

Se presenta al final una lista de referencias de importancia del método del elemento finito

Al iniciar la determinación de esfuerzos y desplazamientos en cierto problema de diseño, las ecuaciones que gobiernan el problema en cualquier forma deben satisfacer equilibrio y continuidad.

El Método del Elemento Finito es un procedimiento analítico, y cuando se aplica a un medio continuo, éste se modela analíticamente subdividiéndolo en sub-regiones (los elementos finitos) en los que el comportamiento de cada uno es definido por grupos separados de funciones que supuestamente definen esfuerzos y desplazamientos en esa región, las funciones se seleccionan en forma tal que se satisfaga la condición de continuidad a través de todo el medio, por lo tanto, el método del elemento finito en común con las soluciones por series y diferencias finitas representa una aproximación a la solución del problema

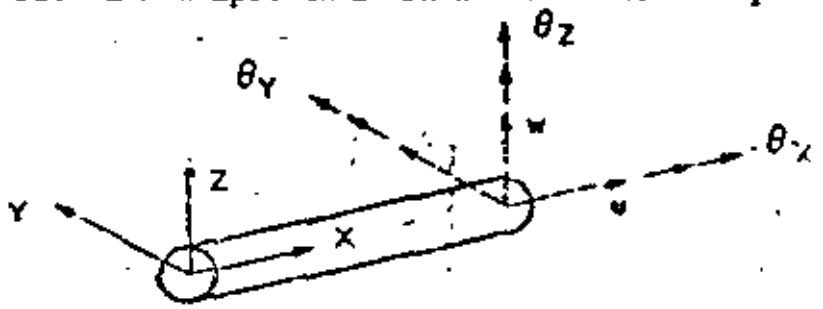

a) Elemento estructural

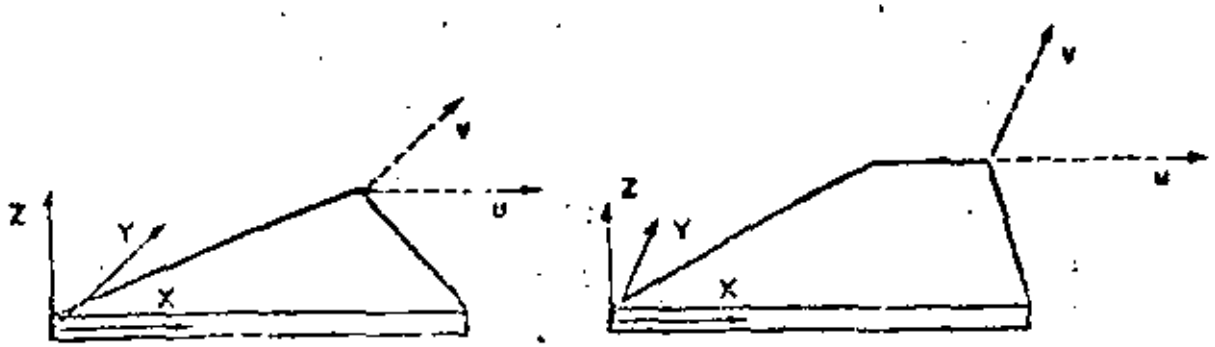

$$\gamma_{XY} = \frac{\partial u}{\partial Y} + \frac{\partial v}{\partial X}$$

b) Esfuerzos planos

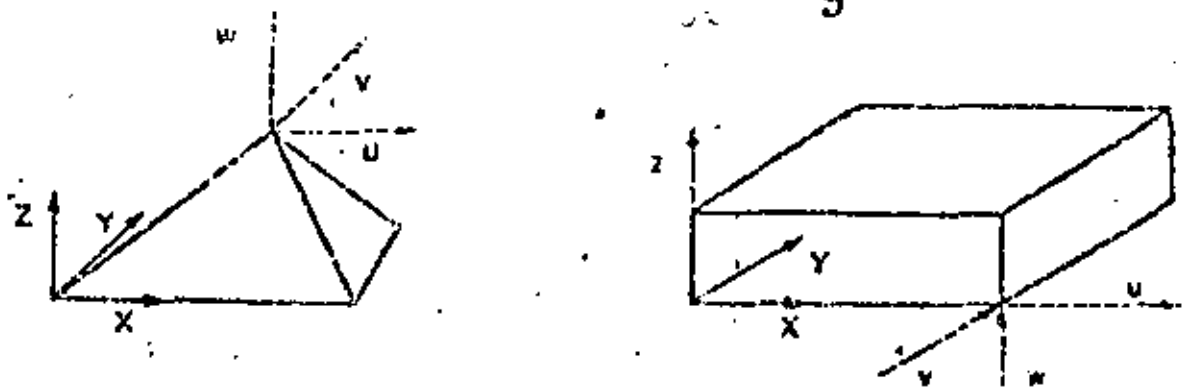

c) Elementos sólidos

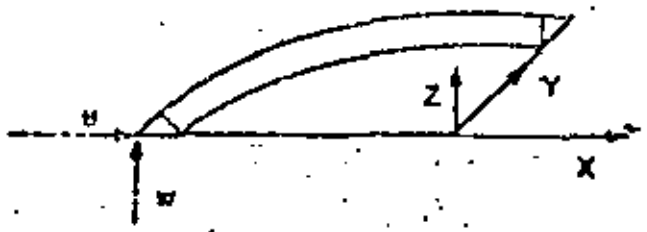

d) Sólidos axisimetricos

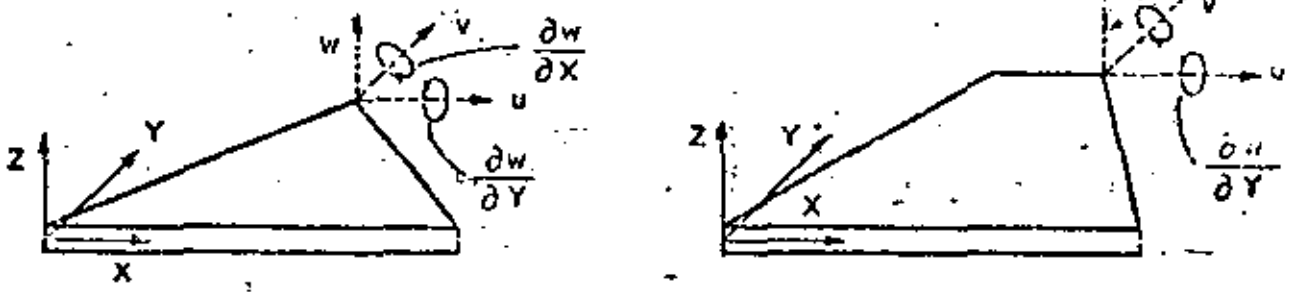

e) Flexión de placas

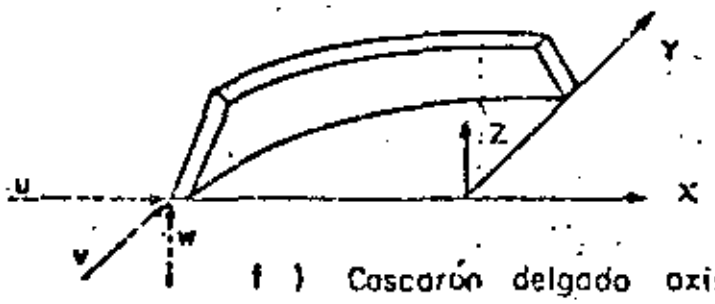

f) Cascarón delgado axisimétrico

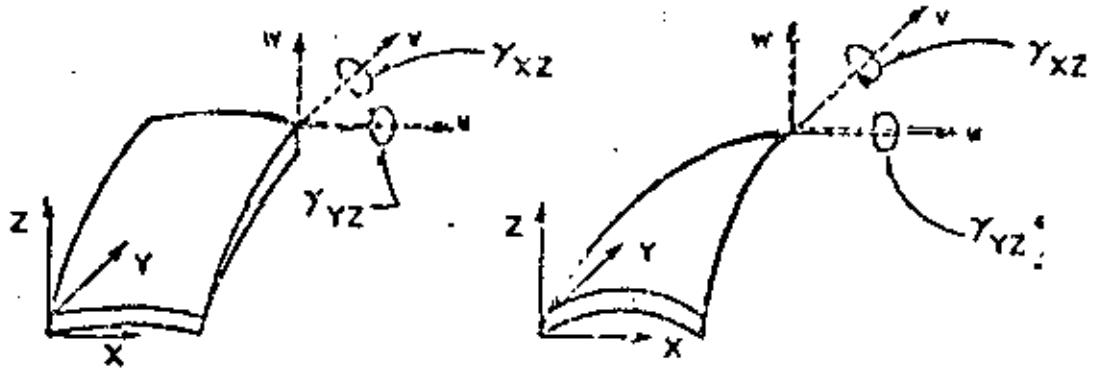

g) Cascarones delgados curvos

Fig 5 Tipos de elementos finitos

TIPOS DE ELEMENTOS.

Elementos que son usados comunmente en la práctica son ilustrados en la Fig. 5.

El elemento estructural simple, Fig. 5 (a), es un miembro de la familia - total de elementos finitos. Cuando se usa con elementos del mismo tipo describe armaduras y estructuras espaciales. Cuando se combina con elementos de tipo diferente, especialmente con elementos de placa generalmente se describen miembros de rigidez.

Los elementos básicos en análisis por elementos finitos son placas delgadas con cargas contenidas en su plano (condición de esfuerzos planos), triangulares y cuadriláteros se ilustran en la Fib 5b. Se denominan básicos porque los primeros desarrollos concernientes con el método se refieren a ellos.

Los elementos sólidos, Fig. 5 (c), son la generalización tridimensional de los elementos de esfuerzos planos. El tetrahedro y el hexaedro son las formas más comunes y son esenciales para modelar analíticamente problemas de mecánica de suelos, rocas y estructuras nucleares. Es conveniente mencionar que la única forma práctica de resolver problemas tridimensionales prácticos, es el método de elementos finitos.

Uno de los campos más importantes de aplicación del método de elementos finitos es en el análisis de "sólidos axisimétricos", Fig. 5 (d). Una gran variedad de problemas de ingeniería caen en esta categoría, incluyendo concreto, tanques, recipientes nucleares, rotores, pistones, flechas de motores, y la cabeza de los roquets. Generalmente son medios de carga y geometría axisimétrica.

En la Fig. 5 (d) se muestra el elemento triangular, también se usan secciones cuadriláteras.

Elemento de placa plana en flexión es empleado no solo en conección con el comportamiento de placas planas, sino también en cascarones y miembros de - pared delgada. Fig. 5 (e).

Estructuras de cascarón delgado axisimétricas, Fig. 5 (f), tienen el mismo rango de significado en la aplicación práctica que los sólidos axisimétricos. Sin- embargo, las relaciones gobernantes se derivan de la teoría de cascarones delga dos.

Cuando una estructura de cascarón delgado que de hecho es curva, es prefe- rible emplear elementos de cascarón curvos delgados para el modelo analítico, tienen la ventaja de describir más aproximadamente la superficie curva del casca rón, y la apropiada representación del acoplamiento de deformación y equilibrio entre cada elemento. Elementos típicos de cascarones de doble curvatura se mues tran en Fig. 5 (g). Gran número de formulaciones para este elemento existen.

ALGUNAS APLICACIONES DE ELEMENTOS FINITOS.

Examinaremos algunas aplicaciones delmétodo de elementos finitos en diseño estructural con el objeto de ilustrar la forma en la cual se usan los elementos - de la Fig. 5, y la escala y complejidad de los problemas.

El desarrollo del método del elemento finito se debe a los investigadores re- lacionados con la industria aeronáutica. La Figura 6 muestra la forma en que -

(11)

se aplicó el análisis por elementos finitos de una porción del avión Boeing 747. La estructura del fuselaje de un avión consiste de laminas de aluminio ligadas a una estructura interna formada por armaduras y atiezadores. La experiencia ha mostrado que los efectos locales de flexión en el cascarón son despreciables, por lo tanto, se supone que consiste de elementos en condición plana de esfuerzos Fig. 5(b). El análisis de elementos finitos del Boeing 747, de la parte achurada, región que conecta el cuerpo o Cascarón Monocoque con las alas, área achurada en Fig. 6, consiste de 7000 incógnitas. Por lo tanto, es común en la práctica dividir la estructura en regiones, o subestructuras, y analizar cada una por elementos finitos con el objeto de producir un superelemento. Los superelementos se ligan entre sí por medio de un procedimiento convencional que determina la fase final del análisis.

El esquema de subestructuración del Boeing 747 es mostrado en la Fig. 6 y los detalles son listados en la Tabla 1.

Sub-Estructura	Descripción	Nodos	Condición Carga	Elemento Viga	Elemento Placa	Grados libertad interacción elementos	Grado de libertad total
1	Ala	262	14	355	363	104	796
2	Centro ala	267	8	414	295	198	880
3	Cascarón Monocoque	291	7	502	223	91	1,026
4	Cascarón M.	213	5	377	185	145	820
5	Cascarón M	292	7	415	241	200	936
6	Caja Tren Aterrizaje	170	10	221	103	126	696
7	Cascarón M	285	6	392	249	233	909
8	Caja Tren Aterrizaje	129	10	201	93	148	503
9	Cascarón M	286	7	497	227	92	1,038
TOTAL		2,195	63	3,374	1,979	555	7,594

Tabla 1 Subestructuración del Boeing 747

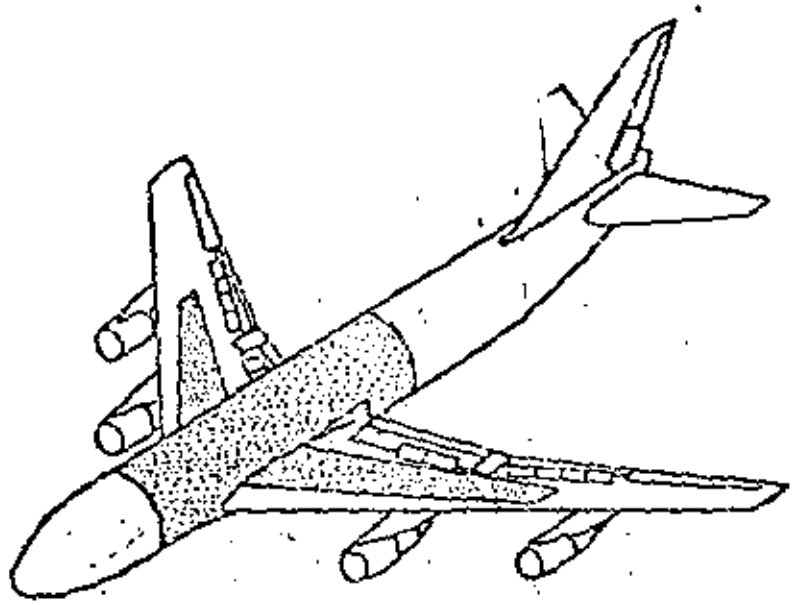

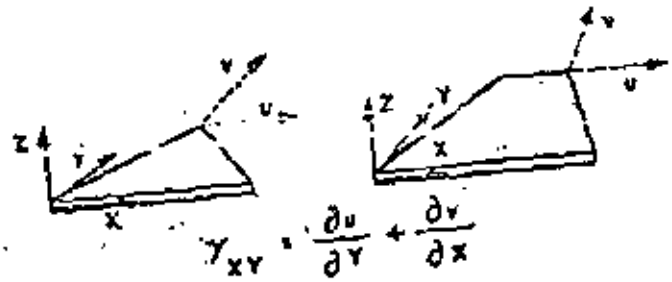

Esfuerzos planos

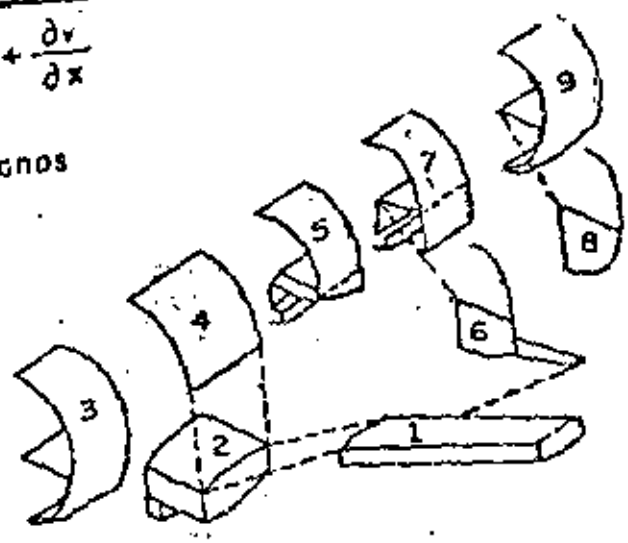

Fig 6 Boeing 747

Como es usual en el diseño de aviones, se hicieron pruebas en el prototipo y los resultados se compararon con la solución por elementos finitos, coincidiendo como se muestra en la Fig. 7

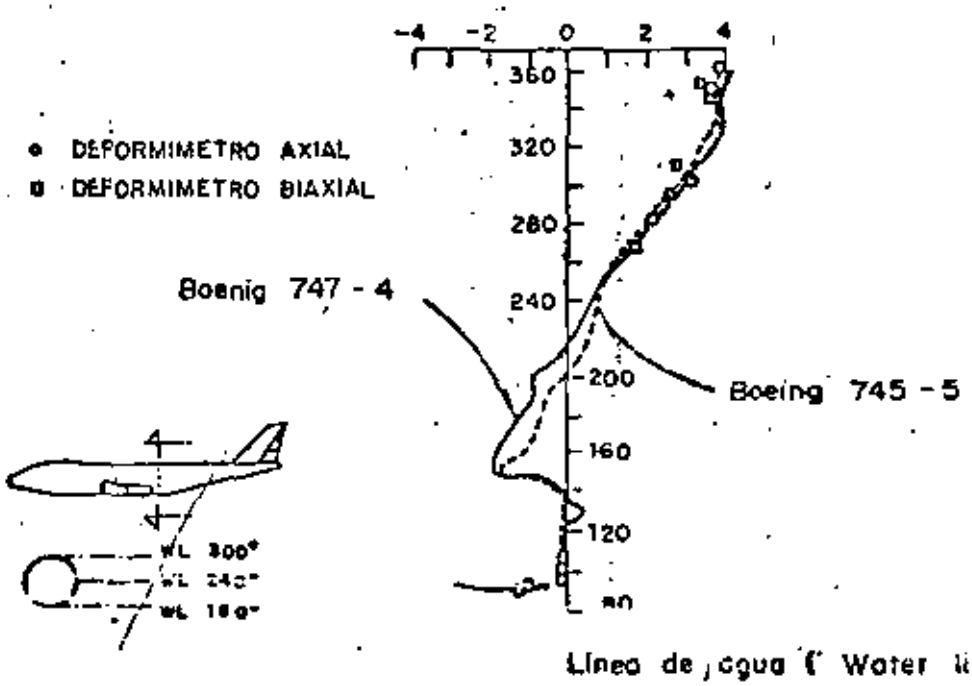

Fig. 7 Comparación entre análisis y experimentación del Boing 747

Es importante agregar que la respuesta dinámica de un avión es muy importante, así como su inestabilidad elástica es una forma importante de falla. Ninguno de estos fenómenos puede tratarse por los métodos simplificados, pero su análisis usando el método de elementos finitos ha probado ser muy aceptable.

Problemas similares se encuentran en Arquitectura Naval. Figura 8 una porción de una estructura de un transbordador. La parte plana es representada por elementos en estado plano de esfuerzos, Fig. 5 (b). Elementos estructurales, Fig. 5 (a), son empleados en la representación de la estructura interna.

El número total de incógnitas para definir las partes importantes de un barco es del orden de 50,000, y de nuevo se subdivide el problema en subestructuras obteniendo menos incógnitas.

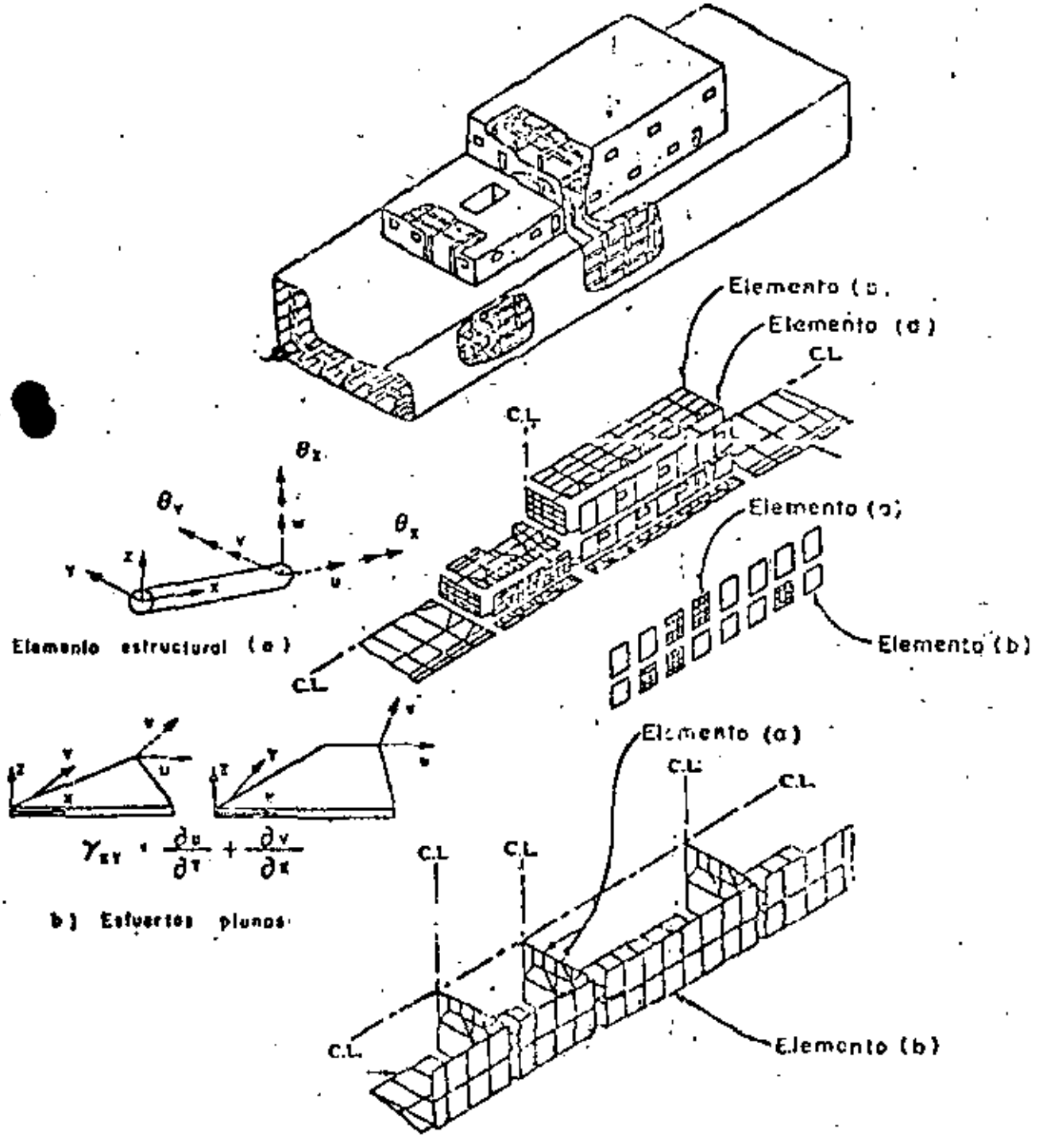

Fig. 8 Análisis por elemento finito de estructura de un transbordador

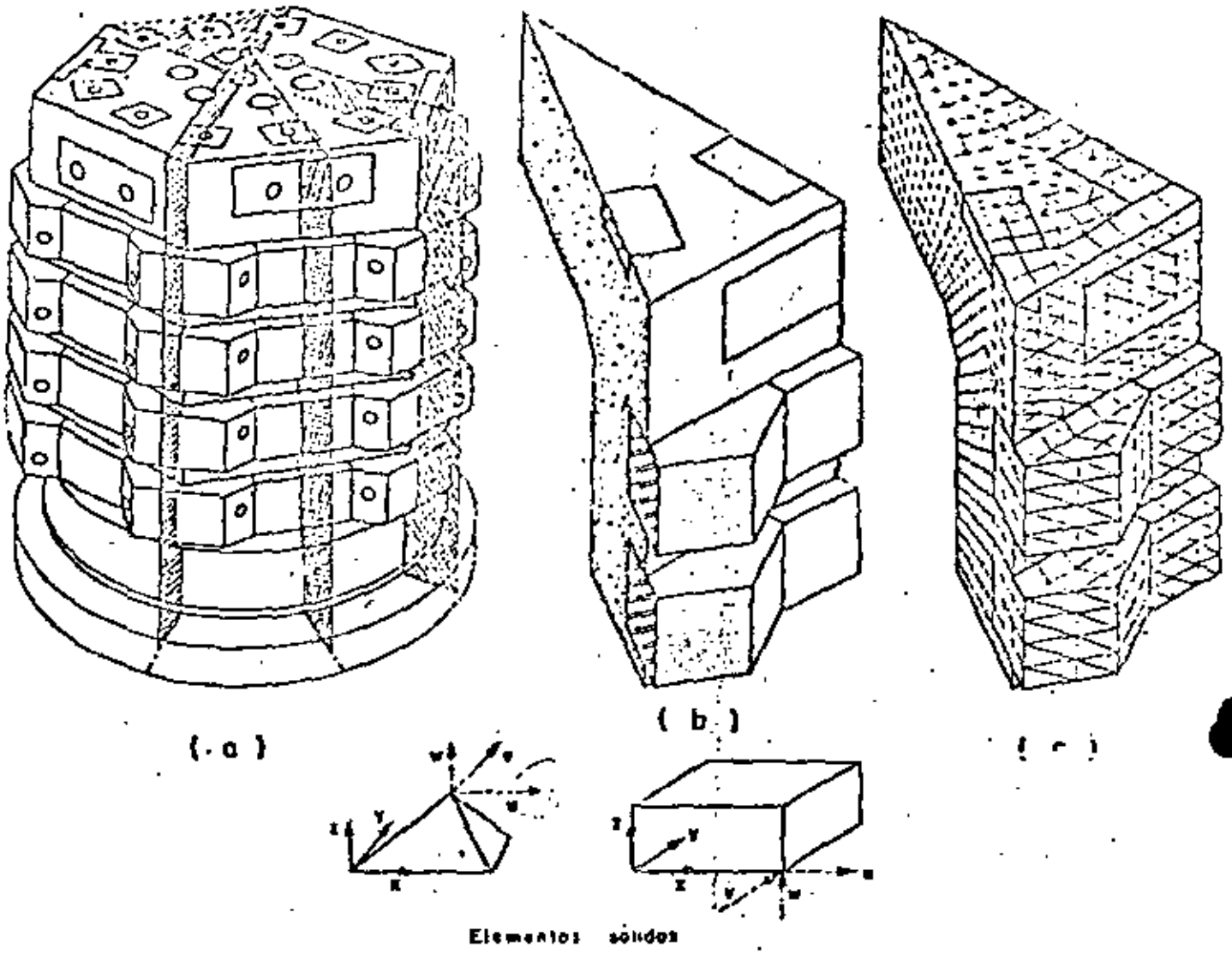

Fig 9 Analisis por elementos finitos de un recipiente reactor de concreto presforzado

Requerimientos de seguridad en el diseño estructural de los reactores nucleares han causado que la industria use ampliamente el análisis por elementos finitos. Figura 9 (a) un recipiente reactor de concreto presforzado. Debido a la simetría es posible analizar solamente un doceavo de la estructura total, Fig. 9 (b). Su volumen se modela analíticamente en un ensamble de elementos tetaedrales y hexaedrales, Fig. 5(c). En problemas de este tipo, el número de incógnitas es del orden de 20,000, y muy común hacer el análisis en condiciones no lineales en material y geometría.

(16)

No todos los problemas de aplicación del método de elementos finitos son de proporciones monumentales. Las figuras 10 y 11 muestran aplicaciones básicas a ciertos problemas de ingeniería civil. Una forma de incrementar la eficiencia de diseño en secciones roladas de acero estructural es cortando el alma en la forma dentada mostrada en la Fig. 10 (a), colocando una sección sobre la otra y soldándolas, Fig. 10 (b). Y se obtiene una viga más aperaltada reduciendo el acero en el alma, y por supuesto que en este problema rutinario de diseño, no es necesario el uso del método de elementos finitos.

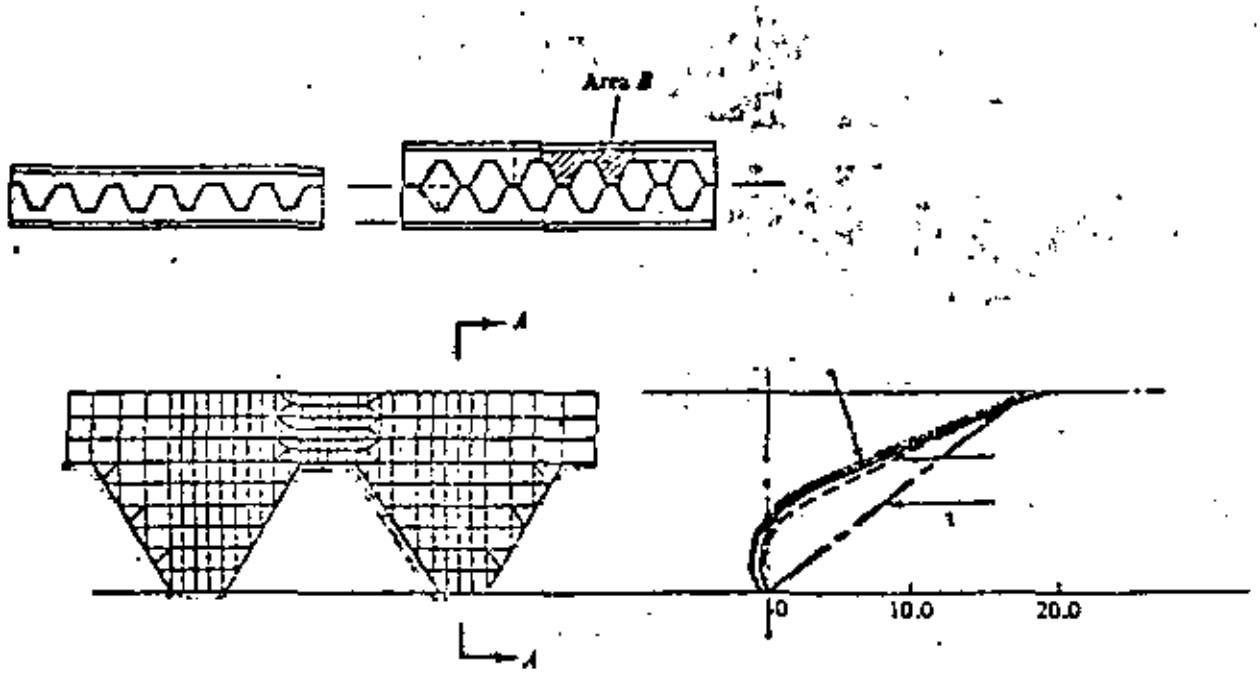

Fig. 10 Análisis de elementos finitos de una viga aperaltada en celosía.

Un problema todavía más común es el de una viga de concreto reforzado, Fig. 11, para el cual se conoce muy poco respecto a la adherencia entre el acero de refuerzo y el concreto, y la formación y crecimiento de las grietas al aumentar la carga. La Figura 11 (a) muestra el modelo analítico de ele-

mentos finitos y la descripción de las trayectorias de grietas y las gráficas de esfuerzos se muestran en la Fig. 11 (b).

Los pocos ejemplos mostrados muestran que el método de elementos finitos puede ser usado ventajosamente en cualquier situación que se requiera la predicción de esfuerzos y deformaciones internas, desplazamientos, vibraciones, inestabilidad elástica, mecánica de fluídos, transferencia de calor. Situaciones que se levantan de diversos campos que tradicionalmente han sido considerados como disciplinas ingenieriles separadas. Ejem., Ingeniería Civil, Mecánica, - Aeroespacial, Arquitectura Naval. El método del elemento finito proporciona una tecnología unificada de análisis en casi todos los campos.

Es nuestro intento en este curso desarrollar los conceptos teóricos básicos y estudiar problemas específicos de carácter práctico. Un compendio de tales problemas llenaría muchos volumenes, por lo tanto es recomendable consultar las memorias de congresos y publicaciones periódicas correspondientes.

PROGRAMAS DE PROPOSITOS GENERALES.

Se ha indicado que las ecuaciones del método de elementos finitos son de una forma tal que su carácter general permite teóricamente escribir un solo programa de computadora que resuelva la mayoría de los problemas que se presentan en la Mecánica de Medio Continuos. Programas de computadora con este objetivo, aún en escala restringida, son llamados programas "de propósitos generales". La ventaja de programas de propósitos generales no es sólo su capacidad,

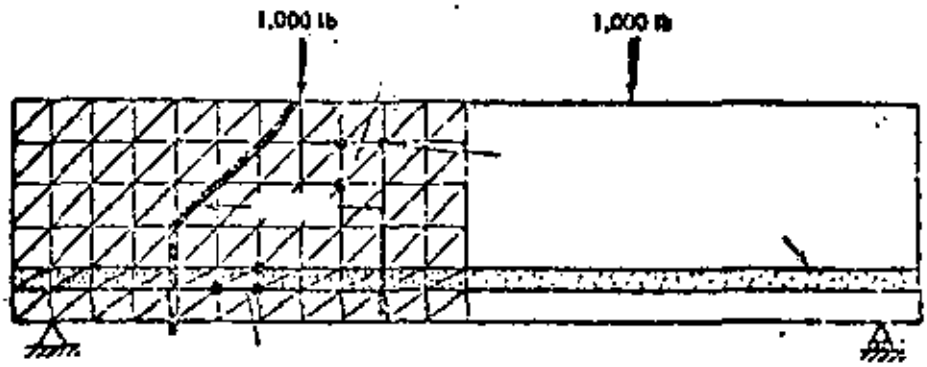

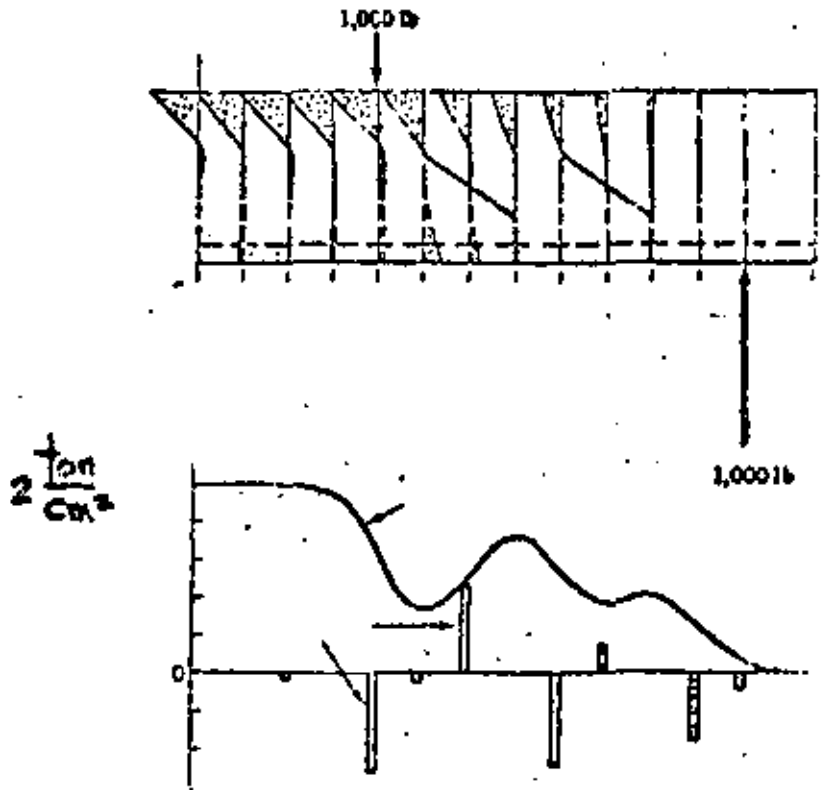

Fig. 11 Análisis por elementos finitos de una viga de concreto reforzado.

sino también en la instrucción de los probables usuarios respecto a la interpretación de la documentación, los datos y procedimientos de entrada y salida de resultados.

El costo de desarrollo de un programa de propósitos generales es usualmente muy alto por lo que la amortización de la inversión es esencial. Ciertos programas de propósitos generales son codificados en un lenguaje computacional que permite operar el programa a muchas organizaciones diferentes localizadas en grandes separaciones geográficas. Otros programas de propósitos especiales de limitada capacidad se usan en organizaciones industriales y gubernamentales con un costo menor en su desarrollo y operación.

Las cuatro componentes mostradas en el diagrama de flujo de la Fig. 12. son comunes en el desarrollo de programas de propósitos generales, fase de datos de entrada, requiere del usuario información del medio o material, descripción geométrica de la representación por elementos finitos y las condiciones de carga y de frontera. Los programas de propósitos generales más sofisticados facilitan el proceso de entrada como propiedades constitutivas del material, almacenados previamente, esquemas de modelar analíticamente el medio, trazar esterográficamente la idealización por elementos finitos en forma tal que los errores pueden detectarse antes de efectuar los cálculos.

La fase de biblioteca de elementos finitos es de interés primordial en el curso. En ella se tienen los procesos de codificación formulativos para los elementos individualmente. La mayoría de los programas de propósitos generales contienen todos los elementos de la Fig. 5, así como ciertas otras alternativas de formulación para un tipo dado de elemento, por ejemplo el trián-

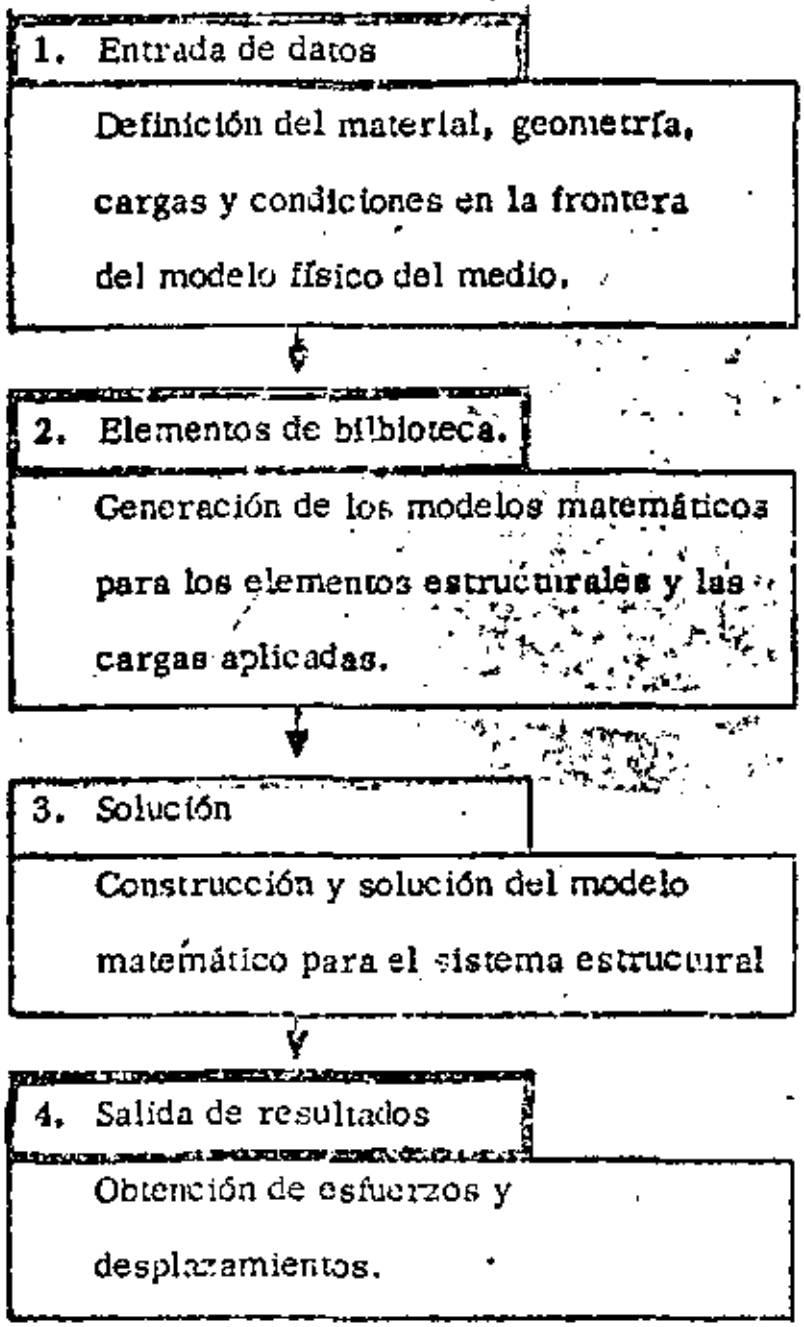

Fig. 12 Diagrama de flujo computacional en Análisis Estructural.

gulo en flexión. Teóricamente el elemento biblioteca es de extremos abiertos y capaz de acomodar cualquier nuevo elemento de cualquier grado de complejidad.

La fase elemento de biblioteca recibe los datos almacenados y establece las relaciones algebráicas del elemento por medio de la aplicación de los procesos formulativos relevantes de codificación. Esta fase del programa de propósitos generales también incluye todas las relaciones algebráicas para interconectar los elementos vecinos y la conección del proceso en sí. Las operaciones posteriores producen un conjunto de ecuaciones algebráicas lineales simultáneas para representar la estructura completa por elementos finitos.

La fase solución del programa de propósitos generales opera sobre las ecuaciones del problema formadas en la fase anterior. En el caso de un problema de análisis estructural solo significa la solución de un conjunto de ecuaciones lineales algebráicas. Soluciones para respuesta dinámica requerirán computaciones más extensas sobre la historia-tiempo de las cargas aplicadas. En algunos casos hay que operar en regiones subdivididas como en el caso del análisis del Boeing 747, o efectuar operaciones especiales en las ecuaciones construídas originalmente. Incluídas en esta fase están las operaciones necesarias de substitución para obtener todos los aspectos deseados de la solución.

La fase salida de resultados presenta el análisis con un registro de la solución sobre la cual se pueden tomar decisiones respecto al dimensionamiento estructural o diseño. El registro comunmente es presentado mediante una lista impresa de esfuerzos y desplazamientos de los respectivos elementos. Así como en la fase de entrada existe una fuerte tendencia a la representación gráfica de datos,

tales como gráficas de trayectorias principales de esfuerzos o modos de pandeo y vibración.

ALGUNOS PROGRAMAS DE PROPOSITOS GENERALES.

ICES-STRUDL II, Integrated Civil Engineering System, (ICES), MIT, Maneja problemas de deformación y esfuerzos planos, cascarones rebajados, sólidos tridimensionales, flexión de placas con y sin deformación axial. Su uso en problemas muy especializados resulta caro. ASKA, Automatic System for Kinematic Analysis. Desarrollado por J. H. Argyris, H. A. Kamel y otros en la Universidad de Stuttgar. Sistema general muy potente el cual incluye una biblioteca de 42 elementos diferentes. Puede ser costoso para un usuario especializado. SAP, A General Structural Analysis Program, elaborado por E. L. Wilson de la Universidad de California. Incluye análisis lineal estático y dinámico de estructuras elásticas, estructuras tridimensionales, sólidos axisimétricos, sólidos tridimensionales, esfuerzos y deformación plana, placas y cascarones.

Zienkiewcz, O.C., programa desarrollando en la Universidad de Wales, - Swansea. Incluye lo de los programas anteriores y problemas de Mecánica de Fluídos y transferencia de calor.

NASTRAN, NAsa STRuctural ANalysis. Desarrollado por U. S. National - Aeronautical and Space Administration para análisis elástico de varias estructuras incluye, análisis de expansión térmica, respuesta dinámica a cargas transitorias - y exitaciones random, cálculo de valores característicos reales y complejos, esta

SAMIS, Structural Analysis and Matrix Interpretative System. Desarrollado por Jet Propulsion Laboratory, y Manned Spacecraft Center. Contiene un elemento unidimensional general y elementos triangulares para deformaciones por flexión y membrana.

ELAS y ELAS 8, Equilibrium Problems of Linear Structures. Desarrollado por el Jet Propulsion Laboratory. Incluye una biblioteca de elementos unidimensionales triangulares, cuadriláteros, tetaedros, hexaedros, cónicos, sólidos axisimétricos de secciones cuadriláteros y triangulares.

MARC, elaborado por P. V. Marcal. Incluye análisis lineal y no lineal de problemas de Mecánica de Medios Continuos.

LISTA DE REFERENCIAS EN ORDEN CRONOLOGICO DEL METODO DE ELEMENTOS FINITOS

(1) Hrenikoff, A., "Solution of problems in elasticity by the framework method, J. Appl. Mech. 8, A 169-175, 1941.

(2) McHenry, D., " A lattice analogy for the solution of plane stress problems," J. Inst. Civ. Eng 21, 59-82, 1943.

(3) Newmark, N. M., "Numerical methods of analysis in bars plates and elastic bodies," "Numerical Methods of Analysis in Engineering," edited by L. E. Grinter, MacMillan (1949).

(4) Turner, M. J., Clough, R. W., Martin, H. C., and Topp, L. J., Stiffness and deflection analysis of complex structures," J. Aero Sci. 23, 805-823, 1956; AMR 10 (1957), Rev. 1776.

(5) Clough, R. W., "The finite element in plane stress analysis," Proc. 2nd. ASCE Conf. on Electronic Computation, Pittsburgh, Pa., Sept. 1960.

(6) Argyris, J. H., "Energy Theorems and structural analysis," Butterworth, London (1960). (Reprinted from Aircraft Eng. 1954-55); AMR 15 (1962), Rev. 2705.

(7) Clough, R. W., "The finite element method in structural mechanics," (Ch. 7 "Stress Analysis", O. C. Zienkiewicz and G. S. Hollister, edited by, J. Wiley & Son (1965); chapter in AMR 20 (1967), Rev. 3942.

(8) Courant, R., "Variational methods for the solution of problems of equilibrium and vibration," Bull. Am. Math. Soc. 49, 1-23, 1943.

(9) Prager, W., and Synge, J. L., "Approximation in elasticity based on the concept of function space," Quart. Appl. Math. 5, 241-69, 1947.

(10) Synge, J. L., "The hypercircle in mathematical physics, Cambridge Univ. Press (1957); AMR 11 (1958), Rev. 733.

(11) Schmelzer, J., "The energy method of networks of arbitrary shape in problems of theory of elasticity," Proc. IUTAM Symp. on Non-homogeneity in Elasticity and Plasticity, W. Olszak, edited by, Pergamon Press (1959).

(12) Zienkiewicz, O. C., and Cheung, Y. K., "Finite elements in the solution of field problems," Engineer. 220, 507-510, Sept. 1965.

(13) Wilson, E. L., and Nickell, R. E., "Application of finite element method to heat conduction analysis," Nuclear Eng. and Design 3, 1-11, 1966.

(95) Arlett, P. L., Bahrani, A. K., and Zienkiewicz, O. C., "Application of finite elements to the solution of Helmholtz's equation (wave guides)," Proc. Inst. El. Eng. 115, 1762-1964, 1968.

(96) Zienkiewicz, O. C., and Newton, R. E., "Coupled vibrations of a structure submerged in a compressible fluid," Int. Symp. on finite element techniques in shipbuilding, Stuttgart, 1969.

(97) Taylor, C., Patil, B. S., and Zienkiewicz, O. C., "Harbour oscillation in a numerical treatment for undampted modes," Proc. Inst. Civ. Eng. 43, 1941-153, 1969.

(98) Archer, J. S., and Rubin, C. P., "Improved linear axisymmetric-shell - fluid model for launch vehicle longitudinal response analysis," Proc. Conf. Mat. Meth. in Struct. Mech., Wright-Patterson AFB, Ohio, 1965.

(99) Zienkiewicz, O. C., Irons, B., and Nath P., "Natural frequencies of complex free or submerged structures by the finite element method," Symp. on Vibration in Civ. Eng., Inst. Civ. Eng., (Butterworth), London, 1965.

(100) Sandhu, R. S., and Wilson, E. L., "Finite element analysis of seepage in elastic media." J. of Engnr. Mech. Div., Proc. ASCE 95, 641-651, 1969.

(101) Rashid, Y. R., "Three-dimensional analysis of elastic solids," Int. J. Solids Struct., " Part I: Analysis procedure," 5, 1311-33, 1969; Part II: " The computational problem," 6, 195-207, 1970.

(102) Irons, B. M., "A frontal solution program for finite element analysis," Int. J. Num. Meth. in Eng. 2, 5-32, 1970.

(103) Johnson, W. M., and Mclay, R. W., "Convergence of the finite element method in the theory of elasticity," J. Appl. Mech. Trans. ASME, 274-278, June 1968.

(104) Przemieniecki, J. S., "Theory of matrix structural analysis," McGraw-Hill, 1968.

(105) Jenkins, W. M., "Matrix and digital computer methods in structural analysis," McGraw-Hill, 1969.

(106) Pope, G. G., " The application of the matrix displacement method in plane elastoplastic stress problems," Proc. Conf. Matrix Meth. in Struct. Mech., Wright-Patterson AFB Ohio, 1965.

(107) Miller, R. E. and S. D. Hansen, "Large Scale Analysis of Current Aircraft," On General Purpose Finite Element Computer Programs, P. V. Marcal (ed), ASME Special Publication, New York, N. Y., 1970.

(108) Smith, C. S. and G. Mitchell, "Practical Considerations in the Application of Finite Element Techniques to Ship Structures," Proc. of Symposium on Finite Element Techniques, U. of Stuttgart, Stuttgart, Germany, June, 1969.

(109) Corum, J. M. and J. E. Smith, "Use of Small Models in Design and Analysis of Prestressed-Concrete Reactor Vessels," Report ORNL-4346, Oak Ridge Nat. Lab., Oak Ridge, Tenn., May, 1970.

(110) Cheng, W. K., M. U. Hosain, and V. V. Nels, "Analysis of Coupled Beams by the Finite Element Method," Proc. of Conf. on Finite Element Method in Civil Eng., McGill U., Montreal, Canada, 1972, pp. 1105-1140.

(111) Gallagher, R. H., "Large Scale Computer Programs for Structural Analysis" in On General Purpose Finite Element Computer Programs, P. V. Marcal (ed.), ASME Special Publication, 1970, pp. 3-34.

(112) Marcal, P. V., "Survey of General Purpose Programs for Finite Element Analysis," in Advances in Computational Methods in Structural Mechanics and Design, J. T. Oden, et al. (ed.), U. of Alabama Press, University, Ala., 1972.

(113) Gallagher, R. H. and O. C. Zienkiewicz, Optimum Structural Design, John Wiley & Sons, Inc., New York, N. Y., 1973.

FINITE ELEMENT METHOD
THEORY AND APPLICATION

1. INTRODUCTION

1.1 HISTORICAL BACKGROUND

The finite element method (FEM) has become a powerful numerical technique for solving complex problems in science and engineering mainly due to the advances made earlier in the numerical methods particularly in matrix methods as well as due to the rapid introduction of high speed computers in the market. However, the introduction of concepts and applications of FEM dates back to the era of mathematicians who tried to calculate the perimeter and area of a circle by idealizing it as a regular polygon. It is also interesting to note that the bound solutions which are often discussed in FEM can be traced back to the solution of the area of a circle. If the circle is modelled with an inscribed polygon, a lower bound solution is obtained whereas an upper bound solution is obtained by replacing the circle by a circumscribed polygon. Even though the basic concepts of FEM existed for over two thousand years, for all practical purposes, one can only say that these concepts were actually used for solving physical problems in 1950s by the aeronautical engineers.

In 1956, Turner et al (Ref 1) presented the stiffness analysis for the complex structures, which is the starting point in the rediscovery of FEM. Nevertheless, Clough (Ref 2) was the one who actually used the term FEM in 1960. Since then, a tremendous amount of research has been done in this field and

quite a large number of papers have been published in almost all the journals related to all fields of engineering as well as some in the fields of mathematics and science. In addition, several conferences have been held all over the world and hundreds of papers have been presented in each. The theory and application of FEM have also been presented in numerous text books (Ref 3-22) In order to help the research workers in tracing the references required for their particular work several bibliographics have either been published or under preparation, among them notably Ref (23) is a good source of information.

1.2 APPLICATIONS OF FEM

The FEM is applicable to a variety of boundary value and initial value problems in engineering as well as applied science. Some of these applications are:

1. Stress Analysis of Structures, Stability of Structures, Dynamic response of structures, Thermal Stress Analysis, Torsion of prismatic members
2. Stress Analysis of Geomechanics problems, Soil-Structure Interaction, Slope Stability problems, Soil Dynamics and Earthquake Engineering, Seepage in soils and rocks, Consolidation settlement
3. Solutions in Fluid Mechanics, Harbour oscillations, Pollution Studies, Sedimentation
4. Analysis of Nuclear Reactor Structures
5. Stress Analysis and Flow Problems in Biomechanics
6. Characteristic Study of Composites in Fibre Technology
7. Wave Propagation in Geophysics
8. Field Problems in Electrical Engineering

Apart from the above mentioned areas, the FEM is also applicable to any other problem as long as the analyst makes certain that the problem is amenable to solution based on the assumptions introduced in the formulation of FEM and appropriate material properties can be provided in a realistic manner.

1.3 METHODS OF ANALYSIS

In general, there are four basic methods of analysis in FEM- displacement method, equilibrium method, mixed method and hybrid method. The field variables or unknown quantities in each of these methods are as follows.

Displacement method - displacements and their derivatives
Equilibrium method - stress components
Mixed method - some displacements and some stress components
Hybrid method - displacements or boundary forces

In the displacement method, smooth displacement distribution is assumed within an element, interelement compatibility of displacement is generally assured and minimum potential energy criterion is used in the formulation.

In the equilibrium method, the interior stress distribution is assumed to be smooth, the equilibrium of boundary tractions is maintained and the minimum complimentary energy is the basis for the formulation.

In the mixed method which is generally used for plate and shell problems, both displacements and stresses are assumed smooth

in the interior, the displacement components and the equivalent stress components are considered to be continuous at the inter-element boundaries and the formulation is based on Reissner's principle.

In the hybrid method, depending on whether the model is displacement type or equilibrium type, the distribution of displacements or stresses within the element is considered to be smooth and along the interelement boundary either assumed compatible displacements or assumed equilibrating boundary tractions are ensured and either modified complementary energy or modified potential energy principle is adopted for the formulation.

Among these four methods, the displacement method is the most widely used approach. However, for plate bending problems either the equilibrium or mixed method is preferred and for some field problems hybrid method is more suitable.

1.4 DESCRIPTION OF FEM

A structure, continuum or a domain is divided into a number of arbitrary shaped parts or regions known as *elements*. These elements are interconnected at joints known as *nodes*. The principal unknown is termed as the *field variable*. This field variable can be displacement, temperature, pore-pressure or stress. The distribution of the field variable within an element is approximated by the use of certain polynomial functions. Variational methods or residual methods are employed

to develop the finite element equations which relate the field variables at the nodes to the corresponding action vector at the nodes of the element. This relationship is provided by the so called property matrix which is based on the material and the geometric properties of the element. Finally these finite element equations are assembled to form a system of algebraic equations for the entire domain. The unknown field variable is obtained by solving this system of algebraic equations.

1.5 BASIC STEPS IN FE ANALYSIS

The basic steps in the finite element analysis of general problems are as follows.

1. The continuum is divided into finite elements of any arbitrary shape.
2. A suitable polynomial is chosen to represent the distribution of the field variable within an element in terms of its nodal values. Thus, the field variables at the nodes become the primary unknowns.
3. Using variational methods or residual methods, the finite element equations are formulated.
4. The individual finite element equations obtained in step 3 are assembled to form a set of algebraic equations for the overall continuum.
5. The solution of the algebraic equations obtained in step 4 yields the values of the field variables at the nodes.
6. From the field variables at the nodes, the secondary variables such as stress, strain for an element can be obtained.

REFERENCES

1. TURNER, M. J., CLOUGH, R. W., MARTIN, H. C., and TOPP, L. J., "Stiffness and deflection analysis of complex structures", J. Aero, Sci., Vol. 23, No. 9, 1956, pp 805-823

2. CLOUGH, R. W., "The finite element method in plane stress analysis", Proc. 2nd ASCE Conf. on Electronic Computation, Pittsburgh, 1960, pp 345-378

3. ZIENKIEWICZ, O. C. and CHEUNG, Y. K., The Finite Element Method in Structural and Continuum Mechanics, McGraw-Hill, London, 1967

4. ZIENKIEWICZ, O. C., The Finite Element Method in Engineering Science, McGraw-Hill, London, 1971

5. SMITH, G. N., An Introduction to Matrix and Finite Element Methods in Civil Engineering, Applied Science, London, 1971

6. DESAI, C. S. and ABEL, J. F., Introduction to the Finite Element Method, Van Nostrand and Reinhold, New York, 1972

7. ODEN, J. T., Finite Elements of Nonlinear Continua, McGraw-Hill, New York, 1972

8. URAL OKTAY, Finite Element Method, Intext Educational Publishers, New York, 1973

9. MARTIN, H. C. and CAREY, G. F., Introduction to Finite Element Analysis, McGraw-Hill, New York, 1973

10. STRANG, G. and FIX, G. J., An Analysis of the Finite Element Method, Prentice Hall, N. J., 1973

11. BREBBIA, C. A. and CONNOR, J. J., Fundamentals of Finite Element Technique, Butterworths, London, 1973

12. NORRIS, D. H. and de VRIES, G., The Finite Element Method-Fundamentals and Applications, Academic Press, New York, 1973

13. COOK, R. D., Concepts and Applications of Finite Element Analysis, John Wiley, New York, 1974

14. WACHPRESS, E. L., A Rational Finite Element Basis, Academic Press, New York, 1975

15. FENNER, R. T., Finite Element Method for Engineers, MacMillan Press, London, 1975

16. GALLAGHER, R. H., Finite Element Analysis-Fundamentals, Prentice-Hall, N. J., 1975

17. HUEBNER, K. H., The Finite Element Method For Engineers; John Wiley, New York, 1975

18 ROCKEY, K. C., et al, The Finite Element Method, Crosby, Lockwood, Staples, London, 1975

19. CONNOR, J. J. and BREBBIA, C. A., Finite Element Techniques for Fluid Flow, Butterworths, London, 1976

20. ODEN, J. J. and REDDY, J. N., An Introduction to Mathematical Theory of Finite Elements, John Wiley, New York, 1976

21. SEGERLIND, L. J., Applied Finite Element Analysis, John Wiley, New York, 1976

22. BATHE, K. J. and WILSON, E. L., Numerical Methods in Finite Element Analysis, Prentice-Hall, N. J., 1976

23. NORRIE, D. H. and de VRIES, G., "A Finite Element Bibliography (3 Parts), Report No. 57, Mechanical Engineering Department The University of Calgary, Canada, 1974

DIVISION DE EDUCACION CONTINUA
FACULTAD DE INGENIERIA U.N.A.M.

EL METODO DEL ELEMENTO FINITO EN LA INGENIERIA MECANICA

APLICACIONES: ANALISIS ESTATICO

DR. JORGE ANGELES ALVAREZ

ABRIL, 1982

El MEF es particularmente útil en el proceso de diseño para localizar puntos en los que pueda presentarse falla por un esfuerzo excesivo. Esto requiere el uso de un programa de elemento finito. El programa, a su vez, requiere que el usario le suministre información respecto a la geometría y a la constitución material del elemento de máquina que va a analizarse, así como respecto a los apoyos y las cargas aplicadas. Estos dos últimos conceptos constituyen lo que se conoce como condiciones de frontera. Una vez realizado el análisis mediante el programa utilizado, los resultados son arrojados en forma numérica mediante un listado, o bien en forma gráfica. El suministro de datos al programa constituye lo que se conoce como preprocesamiento, mientras que el suministro de resultados, posprocesamiento. Tanto para el pre- como para el posprocesamiento se requiere contar con sistemas de cómputo (programas y subprogramas) que constituyen lo que se llama software, además de equipo (graficadores, digitalizadores, tubos de rayos catódicos, interfases), que constituye lo que se llama hardware. En la Fig 6.1 se muestra el equipo básico requerido por el MEF.

El análisis estático de elementos de máquina se presenta mediante un ejemplo de diseño de máquinas. En la Fig 6.2 se muestra el eslabón de una cadena de transmisión que en operación ha fallado en el punto F. El fabricante supone que se trata de un problema de concentración de esfuerzo, por lo que ha pedido un análisis mediante elemento finito. Se conoce el material de que está compuesto el eslabón, por lo que se conoce su módulo de elasticidad, E, y se supondrá que presenta un comportamiento linelamente elástico. Dada la doble simetría del eslabón con respecto a los ejes y-y' y z-z', y de las cargas aplicadas, bastará con analizar un cuarto de él, según se muestra en la Fig 6.2 (c La malla de esta figura consiste de elementos triangulares constantes, esto es, que se supone tienen una distribución uniforme de esfuerzo. Esta malla se genera automáticamente de la siguiente forma :

i) Con ayuda del digitalizador se proporcionan las coordenadas de los puntos P_1, P_2, P_3,... etc. de la Fig 6.3, seleccionados con un espaciamiento adecuado sobre un dibujo constructivo.

ii) El generador automático de mallas (software) produce el contorno de la Fig 6.3 mediante interpolación lineal entre los puntos dados. Este generador requiere una partición de toda la pieza en las partes señaladas en esa figura como 1, 2, 3 y 4, que contienen aproximadamente la misma área.

iii) Mediante una instrucción, el generador automático de mallas produce una malla bien de elementos triangulares, como la de la Fig 6.4, o bien una de elementos cuadriláteros, como la de la Fig 6.5.

iv) Mediante un minimizador de banda, se numeran los nodos en forma tal que se produzca una matriz de rigidez de banda mínima. En la Fig 6.6 se muestran diferentes formas de numeración de elementos en una viga rectangular, que producen diferentes anchos de banda.

v) Mediante un balanceador de mallas se eliminan los elementos de lados muy desiguales. En el ejemplo del eslabón de la cadena de transmisión (Figs 6.4 y 6.5), los elementos están bastante balanceados ; pero en una pieza de geometría más complicada, como una carcaza de bomba, los elementos de la malla generada automáticamente pueden ser muy desbalanceados. En la Fig 6.7 se muestra la malla de una carcaza de bomba con elementos triangulares muy desbalanceados, mientras que en la Fig 6.8 se muestra esa misma malla una vez que ha sido balanceada.

vi) Una vez que se ha minimizado la banda de la matriz de rigidez y que se ha disminuido su condición mediante el balanceo de su malla, se procede al cálculo propiamente dicho de elemento finito. Este produce valores de desplazamiento, de deformación y de esfuerzo en los nodos de la malla. La distribución del esfuerzo normalmente presenta discontinuidades "de salto" en los bordes de cada elemento, como se muestra en la Fig 6.9(a). Mediante un procedimiento de posprocesamiento se puede "suavizar" esa distribución, obteniéndose la de la Fig 6.9(b).

vii) Una vez "suavizada" la distribución de esfuerzo se procede a representarla bien sea en forma bidimensional como se muestra en la Fig 6.10, o bien en forma tridimensional como en las Figs 6.11(a) y (b).

El programa utilizado para obtener los resultados de la Fig 6.11 es el llamado DIAN, desarrollado en el Laboratorio de Máquinas Herramientas del Instituto Tecnológico Henano-Westfálico de Aquisgrán, R.F.A. El cálculo corresponde a la malla de la Fig 6.5, de elementos cuadriláteros isoparamétricos. En ese mismo Laboratorio se ha desarrollado otro programa, el llamado FINEL, que cuenta con elementos de esfuerzo constante, que, sin embargo, produce resultados satisfactorios. Con este programa se obtuvo la distribución del esfuerzo en una placa infinita sujeta a cargas σ_1 y σ_2 en dos direcciones perpendiculares, con una perforación elíptica, como se muestra en la Fig 6.12. Los resultados se muestran en la Fig 6.13.

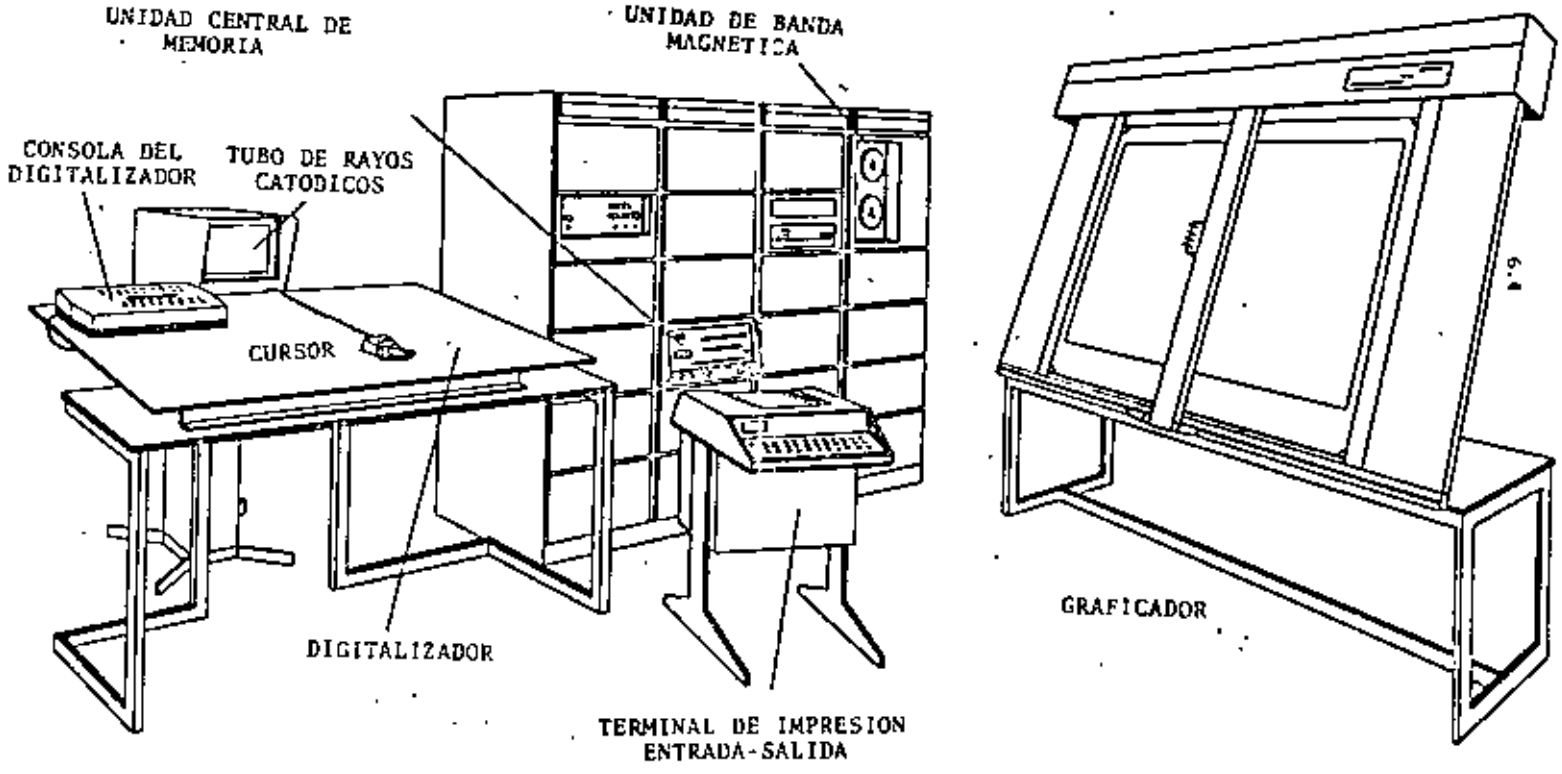

Fig. 6.1 Equipo básico requerido para el MEF (Laboratorio de Máquinas Herramienta de Aquisgrán, RFA)

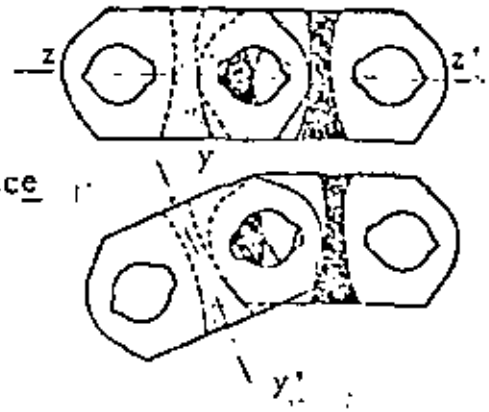

(a)

Eslabones sucesivos de una cadena de transmisión

(c)

Malla de elemento finito de un cuarto del eslabón, en las configuraciones de referencia (r) y final (f).

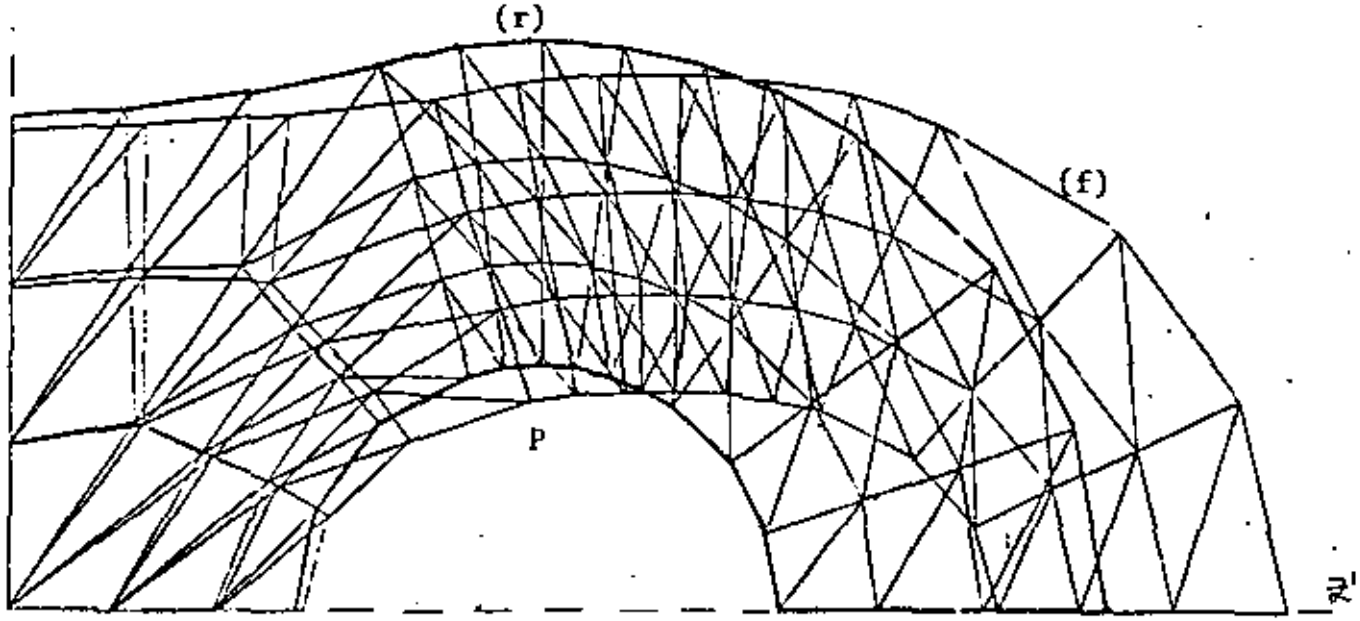

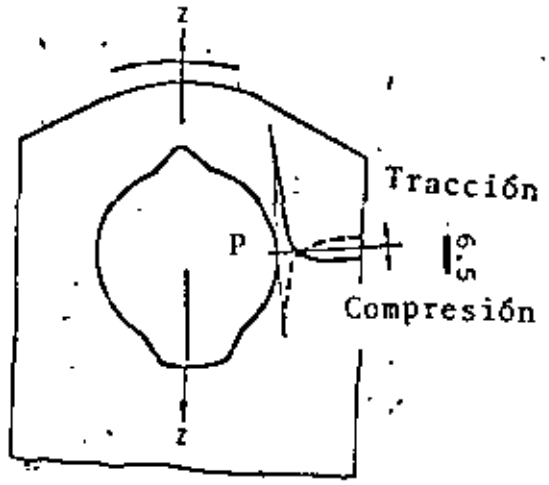

(b)

Distribución del esfuerzo en el borde del eslabón de una cadena de transmisión.

Fig. 6.2 Eslabón de una cadena de transmisión, que presenta concentración de esfuerzos en el punto P, y su modelo de elemento finito.

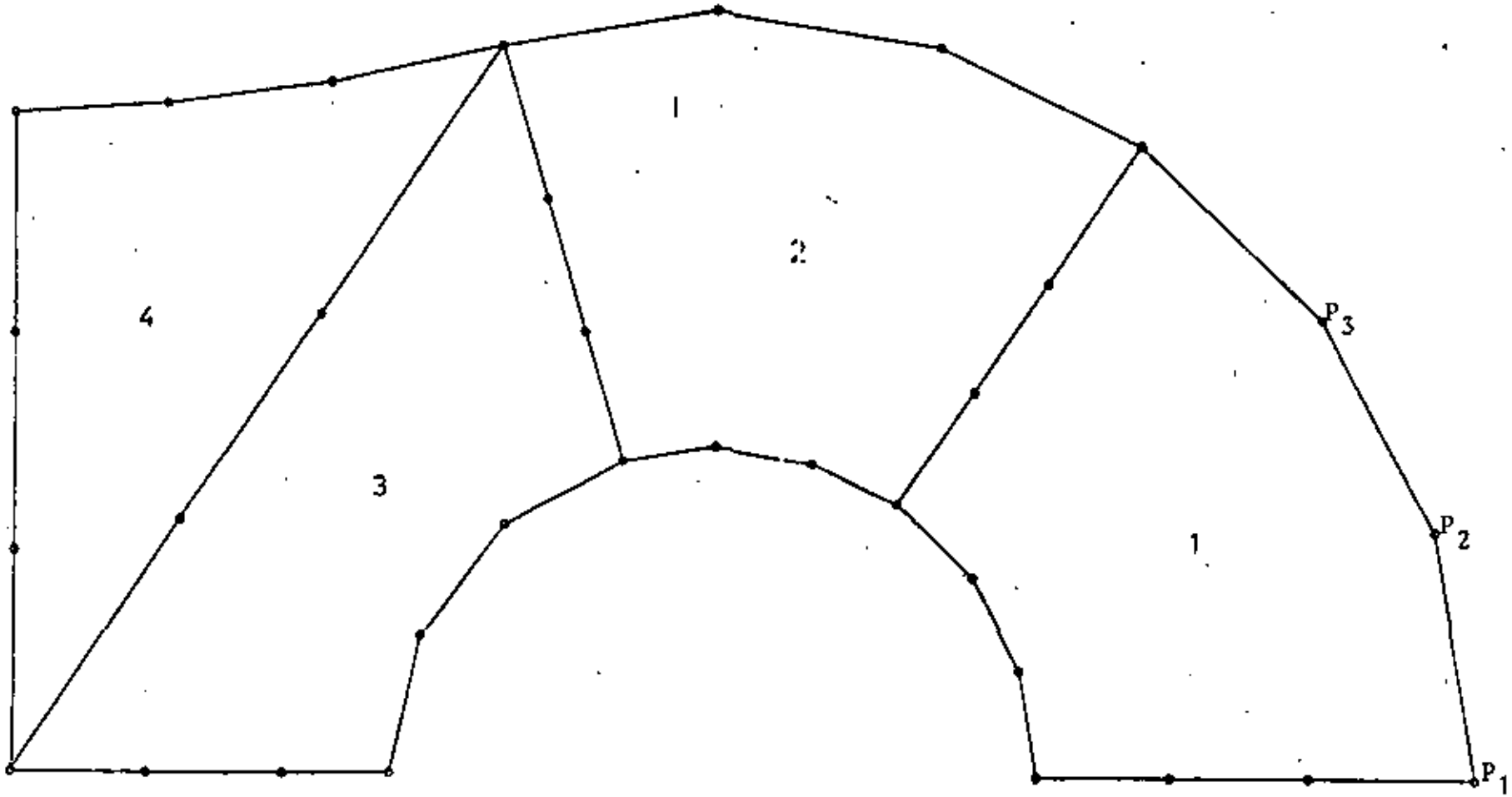

Fig. 6.3 Reproducción automática del contorno de la pieza de máquina y partición para la malla de elemento finito.

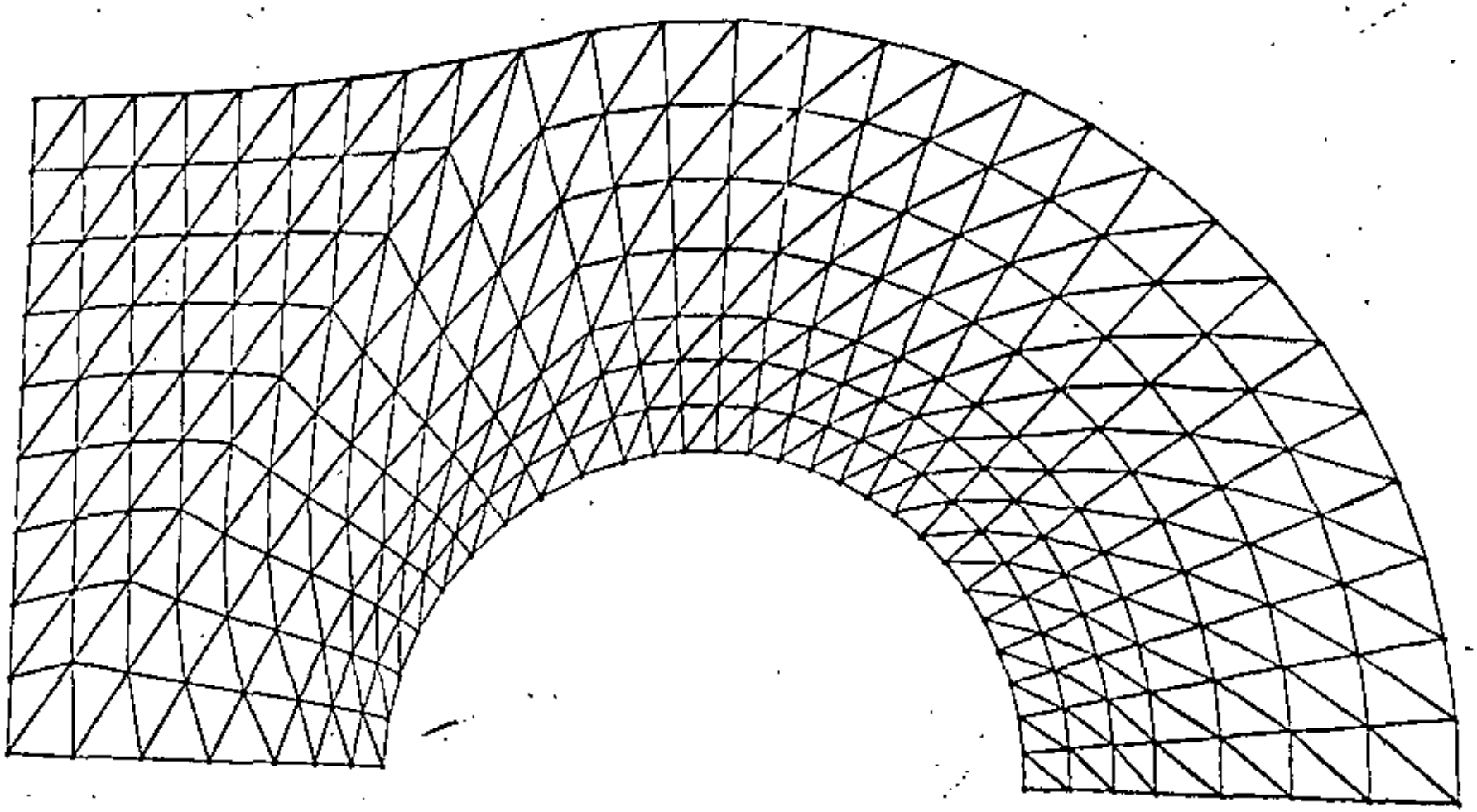

Fig. 6.4 Malla de elementos finitos triangulares, generada automáticamente, con distribución uniforme del esfuerzo en cada elemento.

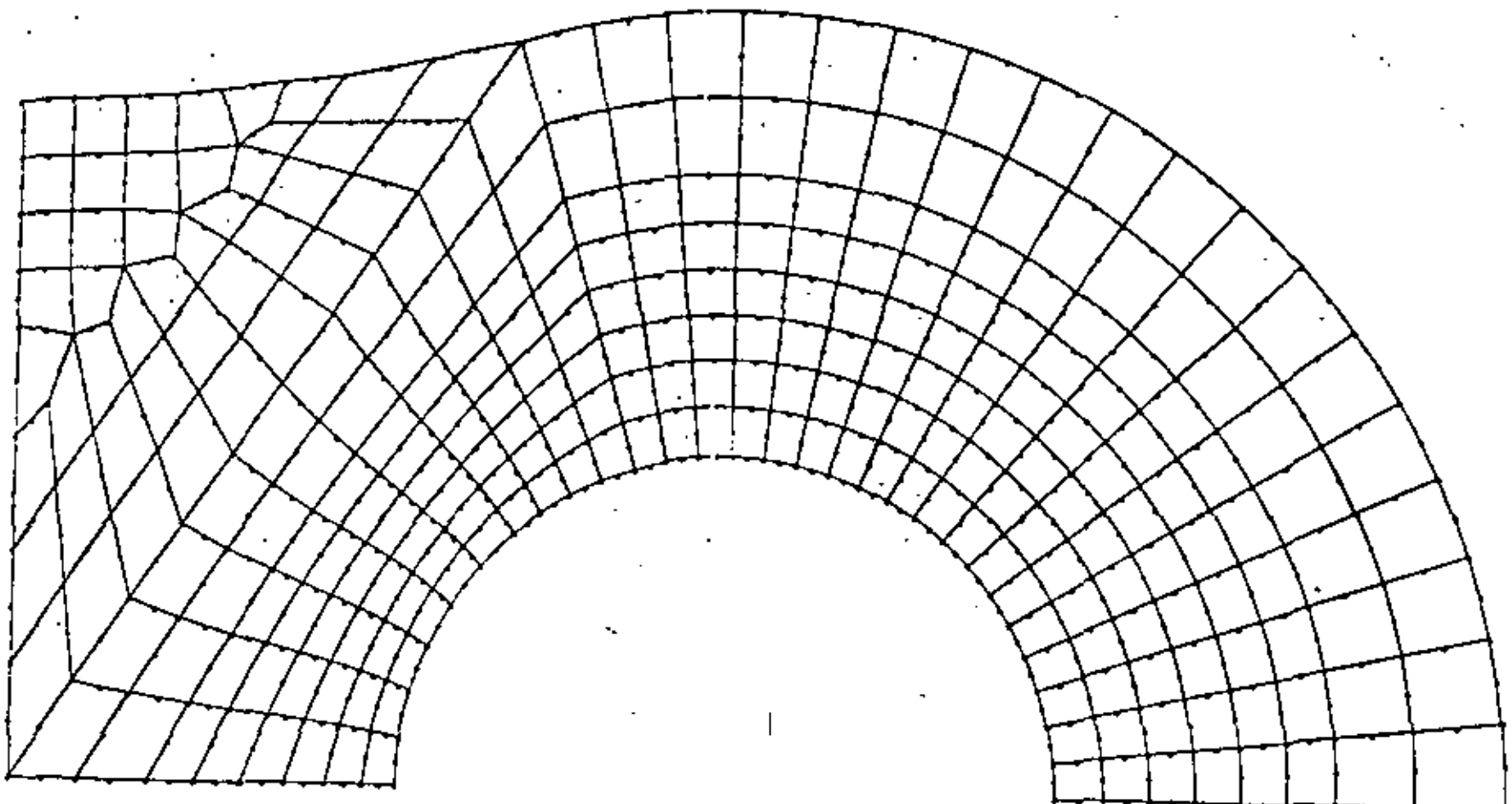

Fig. 6.5 Malla de elementos finitos (isoparamétricos) cuadriláteros, generada automáticamente.

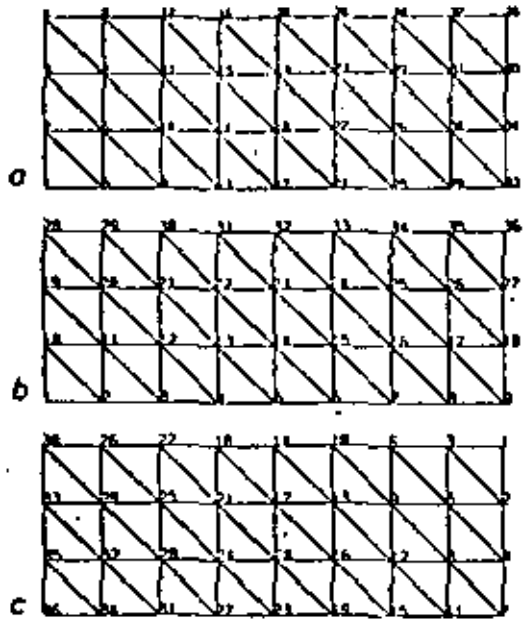

Fig. 6.6 Minimización del ancho de banda de la matriz de rigidez de una viga, con diferente numeración de nodos. Los anchos de banda, d, obtenidos son: a) d=5; b) d=11; c) d=5.

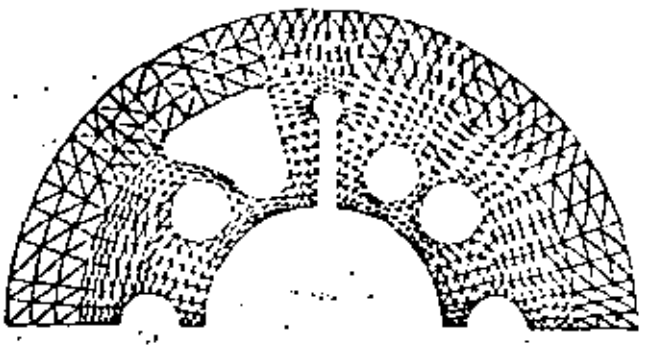

Fig. 6.7 Malla de elementos triangulares, generada automáticamente, de la carcaza de una bomba, que muestra elementos muy desbalanceados.

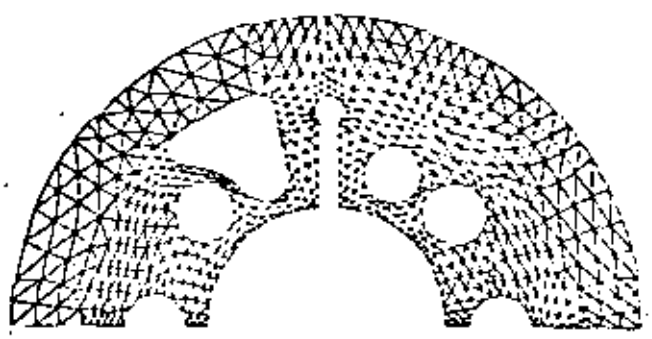

F 6.8 Malla de elementos triangulares de la Fig. 6.7 con elementos balanceados

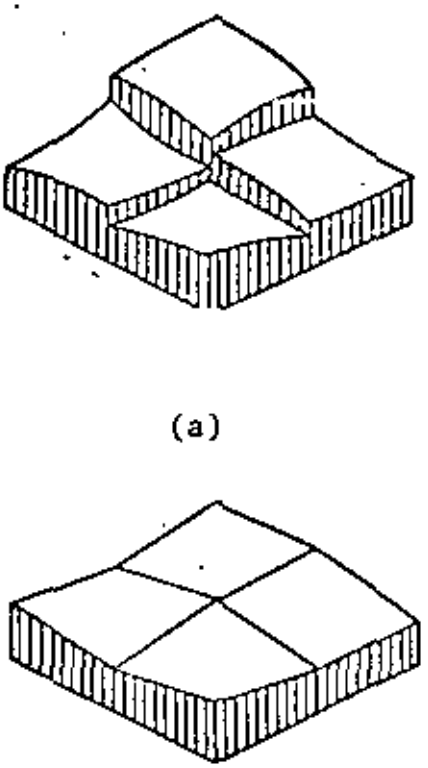

Fig. 6.9 Distribución del esfuerzo en elementos vecinos. (a) discontinua; (b) "suavizada".

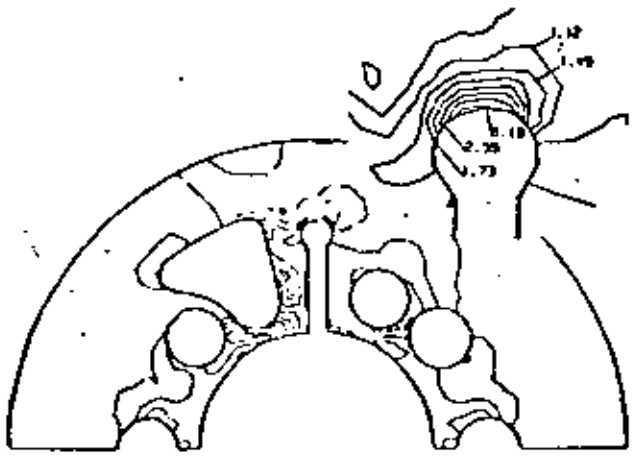

Fig. 6.10 Representación bidimensional de la distribución del esfuerzo en la carcaza de bomba de la Fig. 6.7

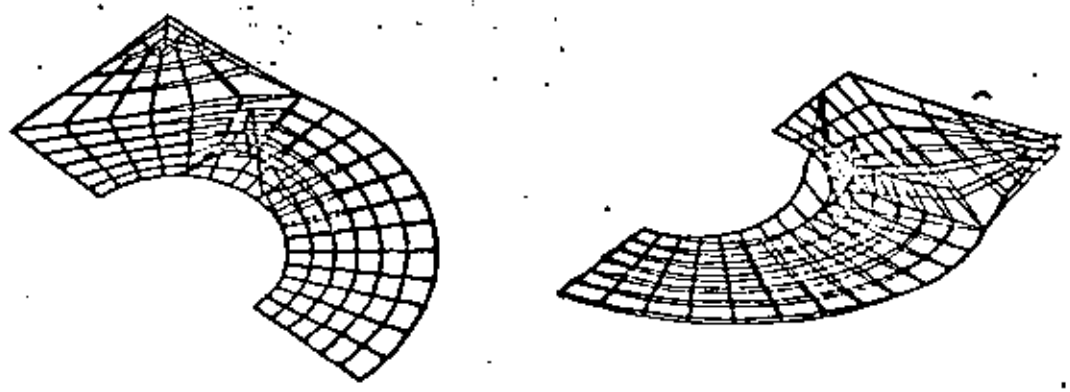

(a) (b)

Fig. 6.11 Representación tridimensional de la distribución del esfuerzo en el eslabón de una cadena de transmisión, de la Fig. 6.2.

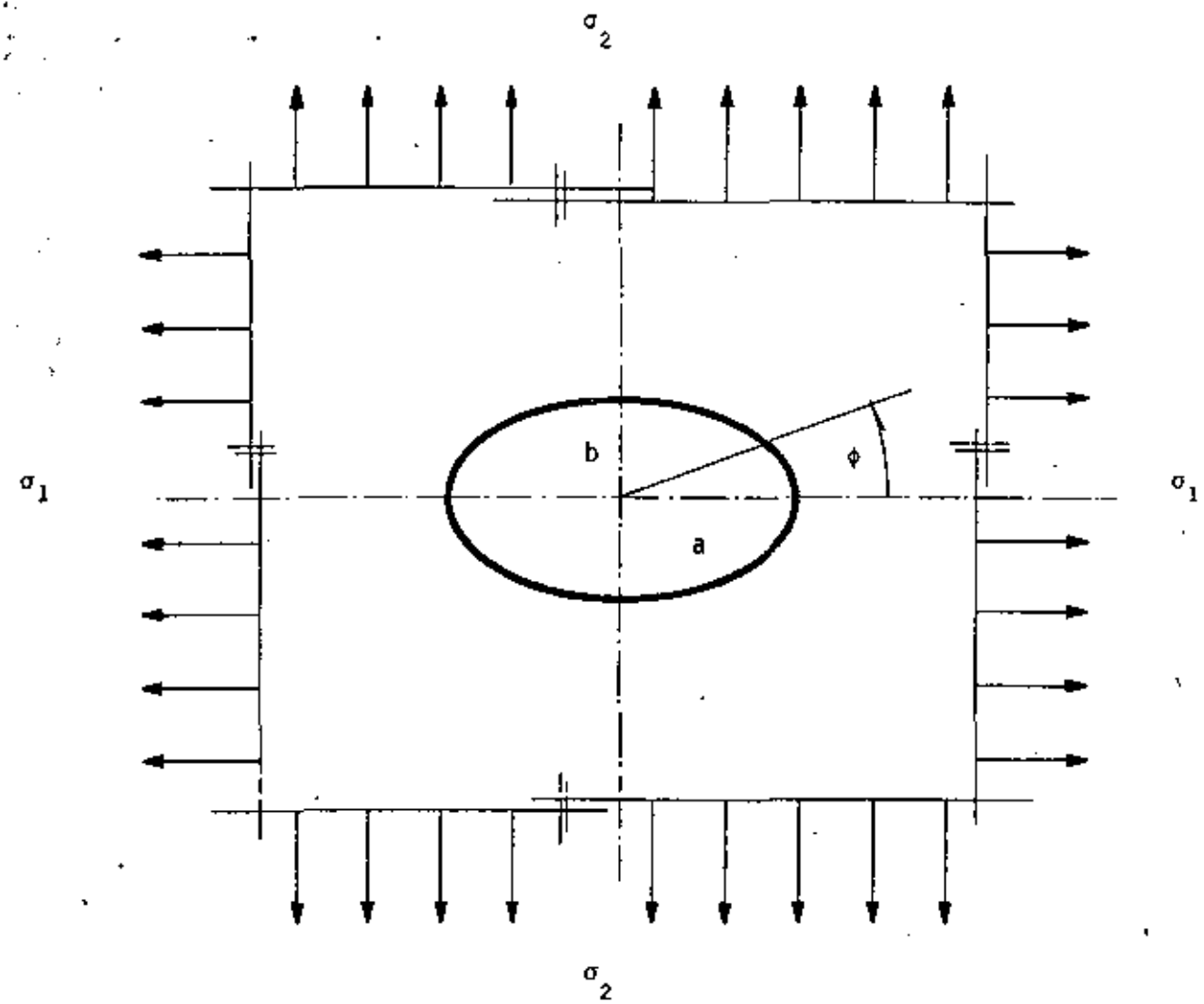

Fig 6.12 Placa cargada en dos direcciones con una perforación

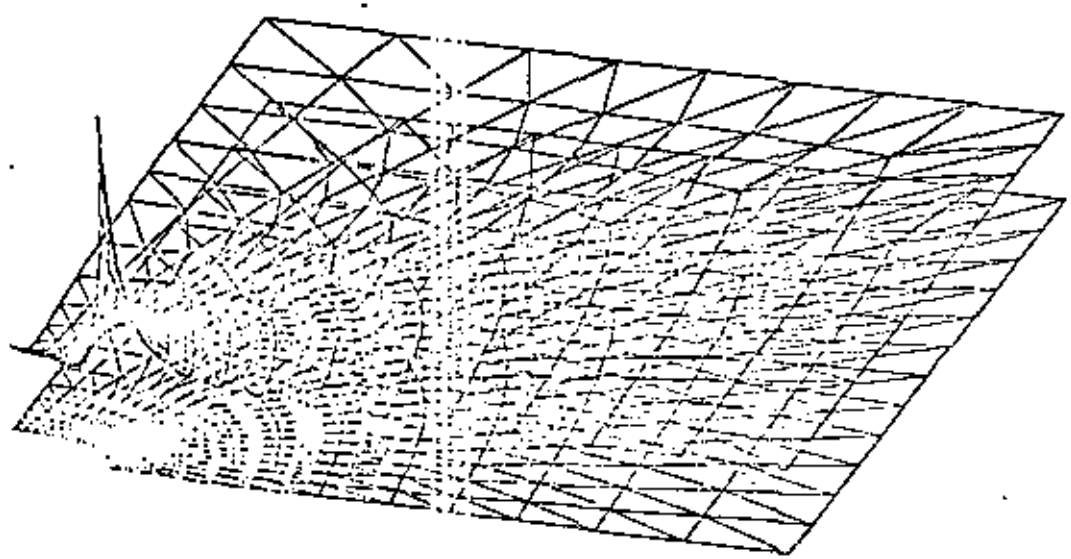

Fig. 6.1 3 Representación tridimensional de la distribución del esfuerzo en la placa de la Fig. 6.12.

DIVISION DE EDUCACION CONTINUA
FACULTAD DE INGENIERIA U.N.A.M.

EL METODO DEL ELEMENTO FINITO EN LA INGENIERIA MECANICA

APLICACIONES DEL METODO DE ELEMENTOS FINITOS A PROBLEMAS DE TERMOFLUIDOS

DR. MIHIR SEN

ABRIL, 1982

CAPITULO I
INTRODUCCIÓN

El desarrollo de la tecnología va a pasos agigantados y el estudio de problemas asociados con ésta, requiere frecuentemente de nuevas técnicas de análisis. A veces estas técnicas provienen de principios ya conocidos, que originalmente tenían poca utilidad por falta de equipos modernos, como por ejemplo la computadora digital.

El estudio de los termofluidos es un caso donde los avances han sido notorios. El movimiento de un fluido real, se describe por medio de un conjunto de ecuaciones diferenciales parciales no lineales. Aún para el problema más sencillo, de un flujo uniforme alrededor de una placa plana inclinada o alrededor de un cilindro, soluciones analíticas tienen que basarse en alguna aproximación y por eso son de uso limitado. Estas aproximaciones pueden ser ángulo de ataque pequeño en el caso de la placa y bajo número de Reynolds en el caso del cilindro.

En situaciones de interés práctico, la presencia de geometrías irregulares sólidas complica aún más la predicción del comportamiento del fluido, es por ello que el análisis teórico debe complementarse, cuando sea posible, con experimentos o métodos numéricos. Este trabajo se enfoca al área de los métodos numéricos; uno de éstos, con gran aceptación actualmente, es el "método de elementos finitos" que será el que se utilice aquí.

No se pretende, ni con mucho, hacer un análisis del método para lo cual existen ya bastantes libros, sino más bien una orientación de su aplicación a las áreas de mecánica de fluidos y transferencia de calor. Para lograr ésto, se resuelven algunos problemas específicos cuya solución analítica es conocida y algunos otros de más alto grado de dificultad.

CAPITULO II
METODO DE ELEMENTOS FINITOS

2.1 METODOS DE RESIDUOS PESADOS

La idea básica del método de residuos pesados (Finlayson, 1972), es obtener una solución aproximada de la siguiente ecuación diferencial

$$A\,\hat{u} + f = 0 \text{ en un dominio} \qquad (2.1)$$

donde A es un operador diferencial, $\hat{u}$ es una variable como puede ser velocidad, temperatura, etc. y f es una función conocida en el dominio. Además está sujeta a las condiciones de frontera

$$H_s(\hat{u}) = b_s \quad \text{en la frontera} \qquad (2.2)$$

Si suponemos una aproximación de la forma

$$\hat{u} \simeq u = \sum_{i=1}^{n} C_i N_i \qquad (2.3)$$

donde las C_i son constantes y las N_i son funciones linealmente independientes que satisfacen las condiciones de frontera, llamadas funciones de base.

Ya que (2.3)es una aproximación de la función $\hat{u}$, si la sustituimos en (2.1) no la va a satisfacer exactamente, sin embargo, la podemos igualar a un cierto residuo ε que será el error que tengamos en la aproximación

$$Au + f = \varepsilon \qquad (2.4)$$

Introduciendo las funciones de peso $w_i (i=1,2,\ldots,n)$ y construyendo el producto interno (ε, w_i) e igualándolo a cero tenemos

$$(\varepsilon, w_i) = 0 \qquad (2.5)$$

lo que es equivalente a decir que la proyección del residuo sobre el espacio de las funciones de peso es cero. Estas ecuaciones se utilizan para encontrar los valores de las C_i. La definición del producto interno que se utliza es la siguiente

$$(u,v) = \int_{\Omega} u\ v d\Omega \qquad (2.6)$$

Hay varias maneras de escoger las funciones de peso w_i entre las que están:

a) Método de Galerkin.- En este método las funciones de peso se hacen igual que las funciones de base, obteniéndose

$$(\varepsilon, N_i) = 0 \qquad (2.7)$$

b) Método de Mínimos Cuadrados. En este método se escogen las funciones de peso igual que el residuo y se minimiza el producto interno con respecto a cada una de las constantes C_i esto es

$$\frac{\partial}{\partial C_i} (\varepsilon, \varepsilon) = 0 \qquad (2.8)$$

c) Método de Momentos. Aquí se escogen las funciones de peso de un conjunto de funciones linealmente independientes como son $1, x, x^2, x^3 \ldots$, para problemas unidimensionales, de tal manera que

$$(\varepsilon, x_i) = 0 \quad i=0,1,2,3,\ldots \qquad (2.9)$$

d) Método de Colocación.- Se escoge un conjunto de N puntos x_i en el dominio Ω como puntos de colocación y la función de peso es

$$w_i = \delta(x-x_i) \qquad (2.10)$$

donde δ es la función de Dirac. Aquí obtenemos

$$(c, \delta(x-x_i)) = c/x_i \qquad (2.11)$$

El error entonces es cero en N puntos de Ω.

Los métodos de Galerkin y Mínimos Cuadrados se adaptan muy bien a las aplicaciones de elementos finitos y los métodos de Momentos y Colocación, no se prestan tan directamente a éstos, ya que son más complicados.

2.2 METODO DE GALERKIN

El método de Galerkin (1915) se adapta muy bien a los problemas que existen en mecánica de fluidos y transferencia de calor, y será el que se utilice a lo largo de este trabajo. Es por ello que se hará un análisis un poco más a fondo de él.

Este método implica la proyección ortogonal del residuo ε sobre un espacio de funciones linealmente independientes lo que se efectúa por medio del producto interno (2.6). Esto es equivalente a decir, que el residuo ε es ortogonal a todo el sistema de funciones $N_i (i=1,2,\ldots,n)$, para lo cual se necesita que ε sea considerado continuo. Ya que sólamente disponemos de n constantes $C_1, C_2, \ldots, C_n$ solo podemos satisfacer n condiciones de ortogonalidad.

Efectuando el proceso anterior para (2.1) tenemos

$$\int_\Omega \varepsilon N_i \, d\Omega = \int_\Omega \left[A\left(\sum_{j=1}^{n} C_j N_j\right) + f \right] N_i \, d\Omega = 0 \qquad (2.12)$$

donde Ω es el dominio del elemento

La ecuación anterior es un sistema de ecuaciones algebraícas, el cual se puede resolver para las constantes C_i. Ya que tanto las C_i como las N_i son arbitrarias, podemos escoger $C_i = u_i$

donde los u_i son valores de la variable en los puntos discretizados del dominio, por lo que la ec. (2,3) se convierte

$$\hat{u} \approx u = \sum_{i=1}^{n} u_i N_i \qquad (2.13)$$

Utilizando esta aproximación en el proceso anterior llegamos a

$$\int_{\Omega} \epsilon N_i d\Omega = \int_{\Omega} \left[A\left(\sum_{j=1}^{n} u_j N_j\right) + f \right] N_i d\Omega = 0 \qquad (2.14)$$

Al resolver este sistema de ecuaciones, se obtiene directamente la solución aproximada, sin necesidad de calcular primero las constantes y luego sustituirlas para obtener el resultado.

Para ejemplificar, tomaremos la ecuación de Poisson

$$\frac{\partial^2 \hat{u}}{\partial x^2} + \frac{\partial^2 \hat{u}}{\partial y^2} + f(x,y) = 0 \qquad (2.15)$$

Si aproximamos la solución por medio de (2.13), el residuo está definido por

$$\frac{\partial^2 u}{\partial x^2} + \frac{\partial^2 u}{\partial y^2} + f(x,y) = \epsilon \qquad (2.16)$$

Efectuando el producto interno entre el residuo y las funciones de base e igualando a cero, nos queda una integral de la forma

$$\int_{\Omega} \varepsilon N_j dxdy = \int_{\Omega} \left(\frac{\partial^2 u}{\partial x^2} + \frac{\partial^2 u}{\partial y^2} + f(x,y)\right) N_j dxdy = 0 \qquad (2.17)$$

Utilizando el teorema de Green, se tiene

$$-\int_{\Omega} \left(\frac{\partial u}{\partial x}\frac{\partial N_i}{\partial x} + \frac{\partial u}{\partial y}\frac{\partial N_j}{\partial y} - f(x,y)N_j\right)dxdy + \int_{\Gamma} \left(\frac{\partial u}{\partial x}N_j dy - \frac{\partial u}{\partial y}N_j dx\right) = 0 \qquad (2.18)$$

donde Γ es la frontera de Ω. Sustituyendo (2.21) en (2.26) y reordenando

$$u_i \int_{\Omega} \left(\frac{\partial N_i}{\partial x}\frac{\partial N_j}{\partial x} + \frac{\partial N_i}{\partial y}\frac{\partial N_j}{\partial y}\right)dxdy = \int_{\Gamma} \left(\frac{\partial u}{\partial x} N_j dx\right) + \int_{\Omega} f(x,y) N_j dxdy \qquad (2.19)$$

Una cualidad muy importante del método de elementos finitos, se puede observar en (2.19). En la forma original de la ecuación de Poisson (2.15) y generalmente cualquier ecuación diferencial, no es evidente como introducir las condiciones de frontera, tanto de Dirichlet, como de Neumann. Sin emabargo en (2.19) podemos aplicar fácilmente las condiciones de frontera de Dirichlet, en la integral de la izquierda, y las condiciones de frontera de Neumann en la primera integral de la derecha. Esta separación de las condiciones de frontera de una y otra clase, es debido a la integración por partes, que se realiza durante el proceso.

Hay que hacer notar, que para todos los problemas de ingeniería, para los cuales existe una funcional, la integral de Galerkin (2.12) da un resultado idéntico al que se obtendría con el método de Raleigh-Ritz (Raleigh, 1877; Ritz, 1909), ade-

más para los problemas en los que no existe una funcional, el método de Galerkin siempre es aplicable.

3. Para la estructura mostrada en la figura 3, determine los diagramas de fuerza normal, cortante y momento flexionante

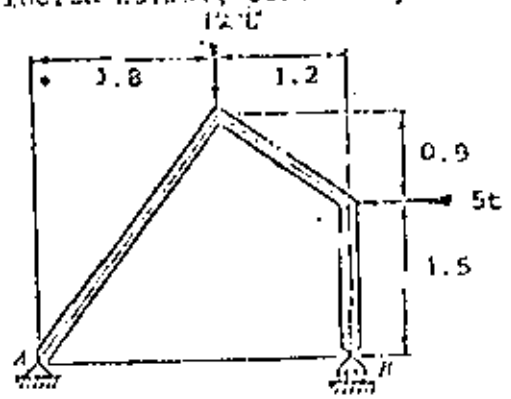

Acotaciones en metros

Fig 3

4. Para la viga mostrada determine el desplazamiento máximo.

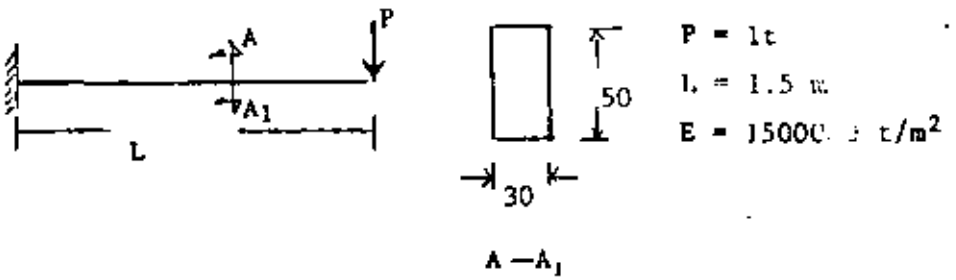

5. Para la viga mostrada en la figura determine el máximo valor de la carga P, al suponer en el punto A, un esfuerzo cortante máximo de 40 kg/cm^2. Despreccie el peso propio de la viga.

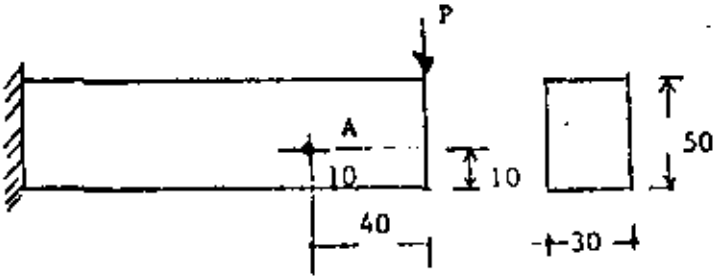

acotaciones en centimetros.

CAPITULO III
CONDUCCION DE CALOR

3.1 GENERAL

Una de las grandes preocupaciones que existen al utilizar un método numérico, es la precisión que se obtendrá al usarlo, ya que hay una diversidad de factores que pueden alterar el resultado.

En el caso del método de elementos finitos, en principio existe un error, al hacer la aproximación de la función, por una sumatoria de funciones evaluados en determinados puntos, ésto es, al hacer la aproximación de la función en un espacio de dimensión infinita a otro de dimensión finita. Varios autores han calculado el error que se obtiene en diferentes problemas, al aplicar el método de elementos finitos, entre ellos están Odon and Reddy(1976), sin embargo utilizan un análisis matemático muy complicado, para obtener únicamente una estimación.

Al error anterior hay que agregarle el que se tiene al utilizar otros métodos numéricos, como son: integración numérica, derivación numérica, solución de sistemas de ecuaciones, métodos iterativos para ecuaciones no lineales, etc., si ésto le agregamos la precisión de la computadora al efectuar las operaciones, resultaría muy difícil efectuar un análisis exacto, del error total obtenido. Por otra parte,al dividir la región en estudio en diferentes elementos, una buena distribución de ellos puede aumentar al precisión del resultado, en cambio, una mala distribución de éstos, puede incluso conducir a resultados localmente muy erróneos además, teóricamente, entre más elementos se utilicen, mayor es la exactitud, pero más constosa es la solución, por lo que es muy difícil precisar cual es el término medio para obtener una solución suficientemente precisa y a la vez la más económica. Se ha llegado incluso a considerar que es arte, el

efectuar la división del dominio en diferentes elementos.

Debido a todo lo anterior, surgió la necesidad de efectuar una comparación, para observar como se comporta el método; es por ello que en este capítulo se resuelven dos problemas de solución analítica conocida por el método de elementos finitos de Galerkin, con lo cual podemos comparar los resultados, además que se aprovechan para dar ciertas normas muy sencillas, pero muy objetivas, en el uso del método.

3.2 PROBLEMA BIDIMENSIONAL EN ESTADO PERMANENTE

El primer problema que se resolverá será el de una placa en dos dimensiones, con transferencia de calor por conducción, en estado permanente, con lo cual se obtendrá la distribución de las temperaturas en toda la superficie. Para ciertas condiciones de frontera, es posible encontrar una solución analítica de este problema y es por ello por lo que se escogió.

3.2.1 Planteamiento de las Ecuaciones y Solución Exacta

La ecuación que define la conducción de calor en dos dimensiones y en estado permanente es (Holman, 1972)

$$\frac{\partial^2 \hat{\theta}}{\partial \hat{x}^2} + \frac{\partial^2 \hat{\theta}}{\partial \hat{y}^2} = 0 \qquad (3.1)$$

que es la ecuación de Laplace bidimensional donde $\hat{\theta}$ es la temperatura y $\hat{x}$ y $\hat{y}$ son las coordenadas cartesianas.

Se definen las siguientes variables adimensionales

$$\tilde{\theta} = \frac{\hat{\theta}}{\theta_0} \; ; \; x = \frac{\hat{x}}{L} \; ; \; y = \frac{\hat{y}}{L} \qquad (3.2)$$

donde θ_0 y L son la temperatura y longitud de referencia respectivamente. Utilizando (3.2) en (3.1) tenemos

$$\frac{\partial^2 \tilde{\theta}}{\partial x} + \frac{\partial^2 \tilde{\theta}}{\partial y} = 0 \qquad (3.3)$$

Si consideramos como ejemplo la placa rectangular mostrada en la Fig. 3.1, tres lados de la placa se mantienen a una tempratura constante θ_1 y el lado superior tiene impuesta una distribución de temperaturas senoidal.

Este problema se puede resolver analíticamente por el método de separación de variables. Utilizando las siguientes condiciones de frontera

$$\begin{aligned} &\tilde{\theta}=\theta_1 \quad \text{en } x=0 \\ &\tilde{\theta}=\theta_1 \quad \text{en } y=0 \\ &\tilde{\theta}=\theta_1 \quad \text{en } x=a \\ &\tilde{\theta}=\theta_m \operatorname{sen}\frac{\pi x}{a}+\theta_1 \text{ en } y=b \end{aligned} \qquad (3.4)$$

y resolviendo la ec. (3.3) usando (3.4) llegamos a

$$\tilde{\theta}=\theta_m \frac{\operatorname{senh}\frac{\pi y}{a}}{\operatorname{senh}\frac{\pi b}{a}} \operatorname{sen}\frac{\pi x}{a} + \theta_1 \qquad (3.5)$$

La ec. (3.5) es la solución analítica del ejemplo propuesto.

3.2.2 Formulación de Elementos Finitos

La temperatura $\tilde{\theta}$ la podemos aproximar en la forma de elementos finitos como

$$\tilde{\theta} \approx \theta = \sum_{i=1}^{n} N_i \theta_i \qquad (3.6)$$

donde n es el número total de nodos en un elemento, N_i son las funciones de interpolación o funciones de base de un elemento

y θ_i son los valores de la tempratura en cada nodo del elemento.

Ya que la función θ es una aproximación de la función $\tilde{\theta}$, al sustituirla en la ec. (3.3) se obtendrá un residuo o error. Entonces tenemos

$$\frac{\partial^2\theta}{\partial x^2} + \frac{\partial^2\theta}{\partial x^2} = \epsilon \qquad (3.7)$$

donde ϵ es el residuo. Considerando la proyección ortogonal del residuo sobre las funciones de base e igualando a cero, que es lo que indica el método de Galerkin se obtiene

$$(\epsilon, N_i) \int_\Omega \left(\frac{\partial^2\theta}{\partial x^2} + \frac{\partial^2\theta}{\partial y^2}\right) N_i \, dxdy = 0 \qquad (3.8)$$

Si a la ec. (3.8) le aplicamos el teorema de Green llegamos a

$$-\int_\Omega \left(\frac{\partial\theta}{\partial x}\frac{\partial N_i}{\partial x} + \frac{\partial\theta}{\partial y}\frac{\partial N_i}{\partial y}\right) dxdy + \int_\Gamma \left(\frac{\partial\theta}{\partial x} N_i \, dy - \frac{\partial\theta}{\partial y} N_i \, dx\right) = 0 \qquad (3.9)$$

Sustituyendo (3.6) en (3.9) y reordenando

$$\theta_j \int_\Omega \left(\frac{\partial N_i}{\partial x}\frac{\partial N_j}{\partial x} + \frac{\partial N_i}{\partial y}\frac{\partial N_j}{\partial y}\right) dxdy = \int_\Gamma \left(\frac{\partial\theta}{\partial x} N_i \, dy - \frac{\partial\theta}{\partial y} N_i \, dx\right) \qquad (3.10)$$

Podemos usar una notación simplificada con lo que escribimos

$$\sum_{j=1}^{n} A_{ij}\theta_j = q_i \quad (i=1,2,\ldots,n) \qquad (3.11)$$

A es llamada matriz de coeficientes de temperaturas y q es el vector de fuentes de calor y son

$$A_{ij} = \int_{\Omega} \left(\frac{\partial N_i}{\partial x}\frac{\partial N_j}{\partial x} + \frac{\partial N_i}{\partial y}\frac{\partial N_j}{\partial y}\right) dxdy \qquad (3.12)$$

$$q_i = \int_{\Gamma} \left(\frac{\partial \theta}{\partial x} N_i dy - \frac{\partial \theta}{\partial y} N_i dx\right) \qquad (3.13)$$

Hay. que hacer notar que debido a la forma de la integral (3.12) la matriz A es simétrica.

Como la formulación que se hizo fué únicamente para un elemento, se deben de juntar las contribuciones de todos los elementos, para obtener el campo de temperaturas en toda la placa. Para lograr ésto, se efectúa un ensamble de todas las ecuaciones, de tal manera, que al final se obtenga un sistema de ecuaciones que contenga todos los nodos de la placa. El sistema global de ecuaciones a resolver será

$$\sum_{j=1}^{m} A^*_{ij}\theta^*_j = q^*_i \quad (i=1,2,\ldots,m \qquad (3.14)$$

donde A^* es la matriz global de coeficientes, θ^* el vector global de temperaturas, q^* el vector globral de flujo de calor y m el número total de nodos.

La forma en que se efectúa el ensamble se explica detalladamente en Cook (1974).

La ec.(3.14) es un sistema algebráico de ecuaciones lineales simétrico y bandeado, que se puede resolver por cualquiera de

los métodos conocidos, como pueden ser Gauss-Jordan, Gauss-Seidel, etc. o algún otro que aproveche las características de la matriz $\bar{A}$ como es el Gauss-Crout modificado para matrices bandeadas, que es el que se utiliza en el programa de computadora presentado.

Es importante observar que la matriz $\bar{A}^*$ es singular; sin embargo, al introducir las condiciones de frontera tanto de Neumann como de Dirichlet en la ec.(3.4), se quita la singularidad, pudiéndose resolver el sistema de ecuaciones resultante.

3.2.3 Ejemplo Numérico

Con el fín de hacer más objetivo cual es el procedimiento que se sigue en elementos finitos, en este inciso se resuelve un problema numérico paso por paso. Este consiste en calcular la temperatura en una placa bidimensional con transferencia de calor por conducción, en estado permanente. Los parámetros que se usan en la solución numérica, son los siguientes

θ_1 = 100 unidades de temperatura
θ_m = 100 unidades de temperatura
a = 12 unidades de longitud
b = 12 unidades de longitud

Unicamente van a existir condiciones de frontera del tipo Dirichlet y son las que se indican en la Fig. 3.1. Por lo tanto, la ecuación de elementos finitos para un elemento es

$$\sum_{j=1}^{n} \theta_j \int_{\Omega} \left(\frac{\partial N_i}{\partial x} \frac{\partial N_j}{\partial x} + \frac{\partial N_i}{\partial y} \frac{\partial N_j}{\partial y} \right) dxdy = 0 \qquad (3.15)$$

o en notación compacta

$$\sum_{j=1}^{n} A_{ij}\ \theta_j = 0 \quad (i=1,2,\ldots,n) \tag{3.16}$$

Para la solución de elementos finitos, se utilizarán elementos triangulares, como muestra la Fig. 3.2, con funciones de interpolación lineal, y son

$$N_i = a_i + b_i x + c_i y \tag{3.17}$$

donde i=1,2,3 debido a que son tres nodos, una función por cada uno y las constantes están dadas por

$$\begin{aligned} a_1 &= (x_2y_3 - x_3y_2)/2\Delta \ ; \ b_1 = (y_2 - y_3)/2\Delta \ ; \ c_1 = (x_3 - x_2)/2\Delta \\ a_2 &= (x_3y_1 - x_1y_3)/2\Delta \ ; \ b_2 = (y_3 - y_1)/2\Delta \ ; \ c_2 = (x_1 - x_3)/2\Delta \\ a_3 &= (x_1y_2 - x_2y_1)/2\Delta \ ; \ b_3 = (y_1 - y_2)/2\Delta \ ; \ c_3 = (x_2 - x_1)/2\Delta \end{aligned} \tag{3.18}$$

aquí Δ es el área del triángulo y se puede obtener por

$$\Delta = \frac{1}{2}\,(x_1y_2 - x_2y_1 + x_3y_1 - x_1y_3 + x_2y_3 - x_3y_2) \tag{3.19}$$

Se observa que la numeración local en el triángulo, está hecha en contra de las manecillas del reloj, para que Δ resulte positiva. La obtención de las funciones de interpolación se encuentra en Segerlind (1976).

Para obtener la matriz A se sustituyen las funciones de interpolación (3.17), en la integral de la ec. (3.10). Por ejemplo para el término A_{11}

$$A_{11} = \int_{\Omega} \left[\frac{\partial}{\partial x}(a_1+b_1x+c_1y)\right]^2 \left[\frac{\partial}{\partial y}(a_1+b_1x+c_1y)\right]^2 dxdy$$

$$= \Delta\ (b_1^2 + c_1^2) \qquad (3.20)$$

Procediendo de la misma manera para los demás coeficientes, llegamos a

$$A = \Delta \begin{bmatrix} b_1^2+c_1^2 & b_1b_2+c_1c_2 & b_1b_3+c_1c_3 \\ b_1b_2+c_1c_2 & b_2^2+c_2^2 & b_2b_3+c_2c_3 \\ b_1b_3+c_1c_3 & b_2b_3+c_2c_3 & b_3^2+c_3^2 \end{bmatrix} \qquad (3.21)$$

donde las constantes son las mismas de la ec. (3.18).

El siguiente paso es evaluar las matrices para cada elemento, para lo cual es necesario numerar, de acuerdo a la malla que se utilice, todos los nodos y los elementos, procurando siempre que la diferencia entre los números asignados globalmente, de los nodos de cada elemento, sea mínima, para que el ancho de banda de la matriz global A^* también sea el mínimo posible. Esto es muy importante, porque en el momento de almacenar la matriz en la memoria en la computadora, se puede hacer en forma bandeada y mientras esta banda sea menor, la memoria que se utilice también es menor, ya que el resto de los coeficients son ceros y no necesitan almacenaje.

Tomando como ejemplo una discretización de pocos elementos, como muestra la fig. 3.3, que es una malla de 7 nodos globales con 7 elementos, se puede observar que con la numeración global de los nodos que se indica, la máxima diferencia entre los nodos de cualquiera de cada uno de los elementos es 3, a este factor se le llama esparcidad y para la malla mostrada es

el mínimo que se puede obtener. El ancho de la banda de la matriz global, se puede obtener sumándole uno a la esparcidad; para nuestro caso el ancho de la banda es 4, ésto es, la matriz tendrá 4 diagonales con valores numéricos no nulos, incluyendo la diagonal principal, ya sea hacia arriba o hacia abajo de ésta última.

Para evaluar las matrices de cada elemento, primero se procede a formar una tabla que relacione las coordenadas, con los nodos globales a las que corresponden, como sigue.

Nodo	1	2	3	4	5	6	7
x	6	0	12	6	0	12	6
y	12	12	12	8	0	0	4

En seguida se forma una tabla que relacione los nodos globales, con los nodos locales de cada elemento.

Elemento / Nodos Locales No	Nodos Globales						
	1	2	3	4	5	6	7
1	2	2	5	5	1	4	4
2	4	5	7	6	4	6	7
3	1	4	4	7	3	3	6

Con las dos tablas anteriores, podemos localizar fácilmente las coordenadas para cada nodo local, las cuales se utilizan para obtener las b's y las c's de la matriz A en la ec. (3.2) y al mismo tiempo el área, así por ejemplo para el elemento 1

$$x_1= \quad ; \quad x_2=6 \quad ; \quad x_3=6$$

$$y_1=12; \quad y_2=8 \quad ; \quad y_3=12$$

aquí los subíndices indican los nodos locales. Con estas coordenadas, podemos evaluar la matriz para el elemento 1 como sigue

$$A^{(1)} = \frac{1}{72}\begin{matrix}\\(2)\\(4)\\(1)\end{matrix}\begin{bmatrix} 24 & 0 & -24 \\ 0 & 54 & -54 \\ -24 & -54 & 78 \end{bmatrix}\begin{matrix}\\(2)\\(4)\\(1)\end{matrix}$$

se observa que como la matriz es simétrica, únicamente se tiene que calcular 6 términos. Los números entre paréntesis a los lados de la matriz, indican los nodos globales a los que pertenecen los renglones y las columnas. Similarmente para los otros elementos, tenemos

$$A^{(2)} = \frac{1}{72}\begin{matrix}\\(2)\\(5)\\(4)\end{matrix}\begin{bmatrix} 45 & -2 & -48 \\ -2 & 26 & -24 \\ -48 & -24 & 72 \end{bmatrix}\begin{matrix}(2)\\(5)\\(4)\end{matrix}$$

$$A^{(3)} = \frac{1}{72}\begin{matrix}\\(5)\\(7)\\(4)\end{matrix}\begin{bmatrix} 24 & -48 & 24 \\ -48 & 150 & -102 \\ 24 & -102 & 78 \end{bmatrix}\begin{matrix}(5)\\(7)\\(4)\end{matrix}$$

$$A^{(4)} = \frac{1}{72}\begin{matrix}\\(5)\\(6)\\(7)\end{matrix}\begin{bmatrix} 39 & 15 & -54 \\ 15 & 39 & -54 \\ -54 & -54 & 108 \end{bmatrix}\begin{matrix}(5)\\(6)\\(7)\end{matrix}$$

$$A^{(5)} = \frac{1}{72}\begin{matrix}\\(1)\\(4)\\(3)\end{matrix}\begin{bmatrix} 78 & -54 & -24 \\ -54 & 54 & 0 \\ -24 & 0 & 24 \end{bmatrix}\begin{matrix}(1)\\(4)\\(3)\end{matrix}$$

$$A^{(6)} = \frac{1}{72}\begin{matrix}\\(4)\\(6)\\(3)\end{matrix}\begin{bmatrix} 72 & -24 & -48 \\ -24 & -2 & -2 \\ -48 & -2 & 45 \end{bmatrix}\begin{matrix}(4)\\(6)\\(3)\end{matrix}$$

$$A^{(7)} = \frac{1}{72}\begin{matrix}\\(4)\\(7)\\(6)\end{matrix}\begin{bmatrix} 78 & -102 & 24 \\ -102 & 150 & -48 \\ 24 & -48 & 24 \end{bmatrix}\begin{matrix}(4)\\(7)\\(6)\end{matrix}$$

En seguida se ensamblan estas matrices en la matriz global, para lo cual se suman los coeficients de cada matriz del elemento, que correspondan al mismo lugar en latriz global, utilizando los números que están entre paréntesis; así por ejemplo, para el coeficiente A^*_{11} de la matriz global, hay contribuciones tanto en la matriz del elemento 1 como en la matriz del elemento 5 y nos queda

$$A^*_{11} = \frac{1}{72}(78+78) = \frac{1}{72}156$$

siguiendo un procedimiento similar para los demás coeficientes, tenemos

$$\frac{1}{72}\begin{bmatrix} 156 & -24 & -24 & -108 & 0 & 0 & 0 & 0 \\ -24 & 69 & 0 & -48 & -48 & -2 & 0 & 0 \\ -24 & 0 & 69 & -48 & -48 & 0 & -2 & 0 \\ -108 & -48 & -48 & 408 & 408 & 0 & 0 & 204 \\ 0 & -2 & 0 & 0 & 0 & 89 & 15 & -102 \\ 0 & 0 & -2 & 0 & 0 & 15 & 89 & -102 \\ 0 & 0 & 0 & -204 & -204 & -102 & -102 & 408 \end{bmatrix} \begin{bmatrix} \theta_1 \\ \theta_2 \\ \theta_3 \\ \theta_4 \\ \theta_5 \\ \theta_6 \\ \theta_7 \end{bmatrix} = \begin{bmatrix} 0 \\ 0 \\ 0 \\ 0 \\ 0 \\ 0 \\ 0 \end{bmatrix} \qquad (3.22)$$

A continuación se introducen las condiciones de frontera. Como se observa en la fig. 3.3, hay 5 nodos en la frontera y 2 en el interior, que son nuestras incógnitas. Los valores de los nodos en la frontera son

$$\theta_1 = 200 \qquad \theta_5 = 100$$
$$\theta_2 = 100 \qquad \theta_6 = 100$$
$$\theta_3 = 100$$

Estos valores se sustituyen en la ec. (3.22), multiplicando las columnas correspondientes y pasándolas del otro lado con signo negativo, ya que los renglones de los nodos conocidos no nos interesan, podemos sustituirlos por un 1 en el coeficiente correspondiente de la diagonal principal y los demás términos del renglón ceros y en el lado derecho el valor del nodo. Haciendo estas operaciones tenemos

$$\begin{bmatrix} 1 & 0 & 0 & 0 & 0 & 0 & 0 \\ 0 & 1 & 0 & 0 & 0 & 0 & 0 \\ 0 & 0 & 1 & 0 & 0 & 0 & 0 \\ 0 & 0 & 0 & 5.66 & 0 & 0 & -2.83 \\ 0 & 0 & 0 & 0 & 1 & 0 & 0 \\ 0 & 0 & 0 & 0 & 0 & 1 & 0 \\ 0 & 0 & 0 & -2.83 & 0 & 0 & 5.66 \end{bmatrix} \begin{bmatrix} \theta_1 \\ \theta_2 \\ \theta_3 \\ \theta_4 \\ \theta_5 \\ \theta_6 \\ \theta_7 \end{bmatrix} = \begin{bmatrix} 200 \\ 100 \\ 100 \\ 433.33 \\ 100 \\ 100 \\ 283.33 \end{bmatrix} \qquad (3.23)$$

En la ec. (3.23) podemos descartar los renglones y columnas 1,2,3,5,6 quedándonos

$$\begin{bmatrix} 5.66 & -2.83 \\ -2.83 & 5.66 \end{bmatrix} \begin{bmatrix} \theta_4 \\ \theta_1 \end{bmatrix} = \begin{bmatrix} 433.33 \\ 283.33 \end{bmatrix} \qquad (3.24)$$

Resolviendo el sistema de ecuaciones anterior, llegamos a

$$\theta_4 = 135.2491$$
$$\theta_7 = 117.6471$$

La solución exacta usando la ec. (3.5) es

$$\theta_4 = 134.6244$$
$$\theta_7 = 110.8182$$

El error en el nodo 4 es de 0.5% y en el nodo 2 es de 6.2%. El hecho de que exista tanta diferencia entre el error de uno y otro nodo, se puede explicar refiriéndose a la Fig 3.3, el nodo 4 pertenece a 6 de los 7 elementos que forman la malla, en cambio el nodo 7 pertenece únicamente a 3 elementos, por lo que tiene menos elementos que contribuyan a su solución. De aquí se concluye inmediatamente, que aumentando el número de elementos, se aumenta la precisión.

El procedimiento anterior se puede implementar en un programa de computadora, ya que para una malla más fina, sería prácticamente imposible efectuarlo a mano y además, se pueden aprovechar las características de simetría y bandeado de la matriz global.

Existen otras formas de efectura el ensamble, que para ciertos problemas son más eficientes, sin embargo, la presentada es la más sencilla y bastante práctica.

3.2.4 Solución de Elementos Finitos Contra Solución Exacta

Para obtener los resultados que se muestran en este inciso, se realizó un programa de computadora, el cual se muestra en el anexo, que sigue casi exactamente los mismos pasos del ejemplo 3.3.3. y que tiene además, una subrutina que calcula el error y otra que calcula lineas de temperatura constante.

El error que se utiliza, es el error raiz medio cuadrático, definido por

$$ERMC = \left(\frac{1}{n}\sum_{i=1}^{n} (\theta_i - \tilde{\theta}_i)^2\right)^{\frac{1}{2}} \qquad (3.25)$$

donde θ_i es la solución de elementos finitos y $\tilde{\theta}$, es la solución exacta y además se toma únicamente por los nodos incógnitos, por lo que n es el número de nodos que no son de frontera.

En la primera prueba que se realiza, se usa una malla como la que se muestra en la Fig.3.4, con 9 nodos, 8 elementos y un solo nodos incógnito y la variación de temperaturas senoidal en la parte de arriba. Los parámetros que se utilizan son los mismos del ejemplo numérico.

Si se desplazan los nodos a, b y c la misma distancia, a lo largo del eje y, manteniendo constante su distancia x, se van a obtener diferentes temperaturas del nodo c, una para cada posición.

Con ésto se intenta ver cual es el comportamiento del método, cuando para una malla con el mismo número de elementos, éstos se hacen más grandes o más pequelos en determinada región, en este caso únicamente se varían en sentido vertical, porque arriba es donde está la mayor variación de temperaturas.

La Fig. 3.5 nos muestra una gráfica posición de la línea $\overline{acb}$ contra temperatura, en la que se representan las curvas de los resultados obtenidos por elementos finitos y la solución exacta. Se observa que a medida que se van haciendo más pequeños los elementos en la parte superior, se va acercando la solución de elementos finitos a la solución exacta, hay un momento en que son iguales y después se aleja otra vez la curva, a pesar de que son todavía más pequeños los elementos.

En la Fig. 3.6 se puede ver más claro este proceso; aquí se grafica posición de la linea $\overline{acb}$ contra el error raiz medio cuadrático, a medida que se van haciendo más pequeños los elementos de la parte superior, el error disminuye, hasta que incluso es cero y después vuelve a aumentar.

De estas dos gráficas podemos concluir, que se deben colocar elementos más pequeños en la zona de mayor variación y más grandes donde no exista tanta variación. El hecho que exista un punto en el que el error vuelvaa aumentar, es debido a que para

las posiciones de la lineas muy altas, los triángulos de la parte superior son muy deformes, ésto es debido a que la base y la altura del triángulo están muy desproporcionados. De aquí se desprende que siempre hay que procurar que los triángulos tiendan a ser equiláteros. Otra razón por la que el error vuelve a aumentar para posiciones muy altas, es que los triángulos de arriba son muy pequeños en comparación de los de abajo, entonces siempre hay que tratar que los triángulos que estén contiguos, tengan una cierta relación de áreas aunque esto último no es tan importante.

El hecho de que llegue un momento en el que el error sea cero, es debido a las peculiaridad de la malla, ya que sólamente existe un solo nodo incógnito. Usualmente es muy difícil obtener una solución exacta por elementos finitos, pero en general se puede obtener una muy buena aproximación, sobre todo para problemas sencillos como éste.

La siguiente prueba consiste en analizar el comportamiento del método, en función del número de elementos y de la posición de éstos, para lo cual primero definiremos tres tipos de mallas.

Mallas tipo S_a, las cuales tienen el mismo número de elementos, en cualquiera de los lados de la placa, como muestra la Fig. 3.7.

Mallas tipo AS_1, las cuales tienen más elementos arriba y abajo, que en los lados de la placa, como muestra la Fig.3.8.

Mallas tipo AS_2, las cuales tienen más elementos a los lados que arriba y abajo de la placa, como muestra la Fig.3.9.

Calculando las temperaturas y el error para todas las mallas anteriores, se obtiene una gráfica como la que muestra la Fig. 3.10, en la que se dibujan las curvas de número de elementos contra error raíz medio cuadrático, para cada tipo de malla. Se observa que para pocos elementos, se obtiene menor error en

las mallas del tipo AS_1, ésto es mallas con más elementos en la zona de variación y mayor error para mallas del tipo AS_2, que son lo contrario de las anteriores. Para más elementos se obtiene un menor error utilizando mallas del tipo S_a. Esto es debido a que los triángulos de estas mallas tienden más a ser equiláteros, que los de las mallas tipo AS_1 y a la vez hay suficientes elementos en la zona de variación, para poder detectar los cambios.

Otra vez podemos concluir, que siempre hay que tratar de poner más elementos en la zona de mayor variación y a la vez procurar que éstos tiendan a ser equiláteros. Las mallas del tipo AS_2 no son recomendables.

Se puede definir otro tipo de mallas, como es la S_b que muestra la Fig. 3.11, en la que el número de elementos en todos los lados de la placa es el mismo. La curva que se obtiene al graficar número de elementos contra error raiz medio cuadrático, es idéntica a la que se obtiene con la malla tipo S_a, sin embargo, con la malla S_b es más fácil aproximar contornos redondeados. Como dato curioso, al utilizar la primera malla de la Fig. 3.11, resulta que la temperatura en toda la placa es constante e igual θ_L ésto es debido a que no hay ningún nodo que detecte que hay una temperatura diferente, por lo que siempre hay que poner suficientes nodos, en las fronteras donde exista variación.

La Fig.3.12 nos muestra una curva, número de elementos contra error raíz medio cuadrático, graficados ambos logarítmicamente para mallas del tipo S_a. Se observa que la curva se asemeja mucho a una recta, por lo que podemos decir que el error disminuye exponencialemnte, a medida que aumente el número de elementos, o en otras palabras, que el método de elementos finitos converge exponencialmente a la solución exacta, a medida que aumenta el número de elementos. Esta conclusión no se puede generalizar para todos los problemas, ya que el caso que estamos tratando es muy sencillo, debido a

que es una ecuación lineal, en la que está definida la temperatura en todas las fronteras y además no existen fuentes de calor. Sin embargo, sí nos damos una muy buena idea de cual es la convergencia del método, sobre todo para problemas similares; ésto es, al principio, a medida que se aumentan los elementos, el método converge rápidamente y al final, aunque se aumente el número de elementos, no se mejora mucho la solución, por lo que hay que tratar de encontrar un justo medio, sobre todo teniendo en cuenta que a más elementos la solución es más costosa. Para lograr esto último se pueden hacer dos o tres mallas con distintos números de elementos, para darse una idea de cual es la diferencia de los resultados entre una y otra, además se puede aprovechar, si es que no se conoce, para detectar cuales son las zonas de mayor variación y colocar en ellas más elementos y más pequeños.

Los resultados anteriores, se resumen en las siguientes normas para el uso del método de elementos finitos:

1.- Dividir la región con una malla gruesa, para observar cuales son las zonas de mayor variación.

2.- Colocar más elementos y más pequeños en las zonas de gran variación.

3.- Dividir la región con una malla más fina y comparar los resultados con los obtenidos con la malla de aproximación, en caso de existir mucha diferencia, utilizar una malla todavía más fina y repetir el procedimiento.

4.- Procurar que los triángulos tiendan a ser equiláteros y evitar aquellos que sean muy deformes. Siempre es posible substituir un triangulo muy deformado por dos triángulos más parecidos a triángulos equiláteros.

5.- Colocar suficientes nodos en las fronteras donde exista variación.

Por último, la Fig. 3.13 muestra líneas de temperatura constante en la superficie de la placa, obtenidas con una malla del tipo S_a, que tiene 49 nodos y 72 elementos y con un error raíz medio cuadrático relativo en la solución de 0.35%.

3.3 PROBLEMA BIDIMENSIONAL EN ESTADO TRANSITORIO

El segundo problema que se resolverá en este capítulo, es el de una placa en dos dimensiones con transferencia de calor por conducción en estado transitorio, para obtener la distribución de temperaturas en toda la superficie, en el transcurso del tiempo. Para el mismo ejemplo del inciso anterior, se puede encontrar una solución analítica a través de series de Fourier, con la que se pueden comparar los resultados obtenidos por elementos finitos.

3.3.1 Planteamiento de las Ecuaciones y Solución Exacta

La ecuación que define la conducción de calor en dos dimensiones y en estado transitorio es, Holman (1972)

$$\frac{\partial^2\hat{\theta}}{\partial\hat{x}^2} + \frac{\partial^2\hat{\theta}}{\partial\hat{x}^2} = \frac{\hat{\rho}c}{K}\frac{\partial\hat{\theta}}{\partial\hat{\tau}} \qquad (3.26)$$

donde $\hat{\theta}$ es la temperatura, $\hat{x}$ y $\hat{y}$ son coordenadas cartesianas, $\hat{\rho}$ es la densidad, C es el calor específico, K es la conductividad térmica del material y $\hat{\tau}$ es el tiempo. Se tomará como constanes las propiedades del material.

Definiendo las siguientes variables adimensionales:

$$\tilde{\theta}=\frac{\hat{\theta}}{\theta_0} \; ; \; x=\frac{\hat{x}}{L} \; ; \; y=\frac{\hat{y}}{L} \; ; \; \tau=\frac{\hat{\tau}}{\hat{\rho}CL^2/K} \qquad (3.27)$$

Aquí θ_0 y L son variables de referencia. Usando (3.27) en (3.26) se tiene

$$\frac{\partial^2 \tilde{\theta}}{\partial x^2} + \frac{\partial^2 \tilde{\theta}}{\partial y^2} = \frac{\partial \tilde{\theta}}{\partial \tau} \qquad (3.28)$$

Considerando un ejemplo similar al de la sección anterior, pero ahora en estado transitorio. Tenemos una placa rectangular, como la mostrada en la Fig. 3.14, donde para tiempo $\tau=0$ toda la placa se encuentra a una temperatura $\tilde{\theta}_o$ y para tiempo $\tau>0$ se cambia la temperatura del lado superior por una distribución de temperaturas senoidal. Para este problema también se puede encontrar una solución analítica como sigue.

Se supone que la solución sea de la forma

$$\tilde{\theta} = G(x,y) + H(x,y,\tau) \qquad (3.29)$$

donde el primer término del lado derecho es la solución en estado permanente y el segudno término es la componente debida al estado transitorio.

La solución en estado permanente se obtiene por medio del método de separación de variables, utilizadno las siguientes condiciones de frontera

$$\begin{aligned} &G=0 \quad \text{en } x=0 \\ &G=0 \quad \text{en } x=a \\ &G=0 \quad \text{en } y=0 \\ &G=\theta_m \operatorname{sen}\frac{\pi x}{a} \text{ en } y=b \end{aligned} \qquad (3.30)$$

La solución del problema permanente está dada en la ec.(3.5), así que

$$G(x,y)=\theta_m \frac{\operatorname{senh}\dfrac{\pi y}{a}}{\operatorname{senh}\dfrac{\pi b}{a}} \operatorname{sen}\frac{\pi x}{a} \qquad (3.31)$$

Por otra parte, la contribución en estado transitorio también se puede obtener por el método de separación de variables, pero ahora se usan las siguientes condiciones de frontera, para tiempo mayor que cero

$$\tau>0\ ;\quad \begin{aligned} H&=0 \quad \text{en } x=0\\ H&=0 \quad \text{en } x=a\\ H&=0 \quad \text{en } y=0\\ H&=0 \quad \text{en } y=b \end{aligned} \tag{3.32}$$

y para tiempo igual a cero las condiciones iniciales son

$$H(x,y,0)=-G(x,y) \quad \text{en} \quad 0\leq x\leq a,\ 0\leq y\leq b \tag{3.33}$$

Sustituyendo $H(x,y,\tau)$ por $\hat{\theta}$ en la ec. (3.28) y resolviéndola usando (3.32) y (3.33) llegamos a una solución de la forma

$$H(x,y,\tau)=\frac{2\theta_m}{\pi}\operatorname{sen}\frac{\pi x}{a}\sum_{n=1}^{\infty}\frac{n(-1)^{n+1}}{b^2/a^2+n^2}\operatorname{sen}\frac{n\pi y}{b}e^{-(\frac{1}{a^2}+\frac{n^2}{b^2})\pi^2\tau} \tag{3.34}$$

La cual es una serie de Fourier senoidal, cuya exactitud depende del número de términos que se tomen en la sumatoria.

Por último, sustityendo (3.31) y (3.34) en (3.29), tenemos

$$\tilde{\theta}=\theta_m\operatorname{sen}\frac{\pi x}{a}\left[\frac{\operatorname{senh}\frac{\pi y}{a}}{\operatorname{senh}\frac{\pi b}{a}}-\frac{2}{\pi}\sum_{n=1}^{\infty}\frac{n(-1)^{n+1}}{b^2/a^2+n^2}\operatorname{sen}\frac{n\pi y}{b}e^{-(\frac{1}{a^2}+\frac{n^2}{b^2})\pi^2\tau}\right] \tag{3.35}$$

que es la solución analítica de la ec. (3.28) para el problema propuesto.

3.3.2 Formulaci[ón] de Elementos Finitos

Debido a q[ue] el problema que estamos considerando se encuentra en est[ado] transitorio, ésto es, depende del tiempo, en la formul[ación] se hace una combinación de dos métodos, el método de el[em]entos finitos en espacio y el método de diferencias finit[as] en tiempo. Para lograrlo, se calcula la distribución de t[em]peraturas en la placa para un tiempo inicial, utilizando [el]ementos finitos, después se incrementa el tiempo por un Δt [y] se vuelve a calcular la distribución de temperaturas por [el]ementos finitos, utilizando los resultados del tiempo an[te]rior, como indica el método de diferencias finitas, así suc[es]ivamente hasta que se llega al estado permanente.

Para la for[mu]lación de elementos finitos se procede de la siguiente man[era]: la temperatura $\tilde{\theta}$ la podemos aproximar de la forma

$$\tilde{\theta}(x,y,\tau)\approx\theta(x,y,\tau)=\sum_{i=1}^{n}\theta_i(\tau)N_i(x,y) \qquad (3.36)$$

donde θ es la fun[ción] aproximada, $\theta_i(\tau)$ son los valores de la temperatura en cad[a] nodo del elemento, N_i son las funciones de interpolación [del] elemento y n es el número total de nodos del elemento.

Debido a qu[e] se hizo una aproximación al sustituir (3.37) en (3.28), se obt[en]drá un residuo como sigue

$$\frac{\partial^2\theta}{\partial x^2}+\frac{\partial^2\theta}{\partial y^2}-\frac{\partial\theta}{\partial\tau}=\varepsilon \qquad (3.37)$$

donde ε es el re[si]duo. Tomando el residuo ortogonal a las funciones de interp[ol]ación

$$(\varepsilon, N_i) = \int_{\Omega} \left(\frac{\partial^2 \theta}{\partial x^2} + \frac{\partial^2 \theta}{\partial y^2} - \frac{\partial \theta}{\partial \tau}\right) N_i \, dxdy = 0 \qquad (3.38)$$

donde Ω es el dominio de un elemento. Aplicando el teorema de Green a la ec. (3.38) llegamos a

$$-\int_{\Omega} \left(\frac{\partial \theta}{\partial x} \frac{\partial N_i}{\partial x} + \frac{\partial \theta}{\partial y} \frac{\partial N_i}{\partial y}\right) dxdy + \int_{\Gamma} \left(\frac{\partial \theta}{\partial x} N_i \, dy - \frac{\partial \theta}{\partial y} N_i \, dx\right) - \int_{\Omega} \frac{\partial \theta}{\partial \tau} N_i \, dxdy = 0 \qquad (3.39)$$

donde Γ es el contorno del elemento. Sustituyendo (3.36) en (3.39) y reordenando

$$\theta_j \int_{\Omega} \left(\frac{\partial N_i}{\partial x} \frac{\partial N_j}{\partial x} + \frac{\partial N_i}{\partial y} \frac{\partial N_j}{\partial y}\right) dxdy + \dot{\theta}_j \int_{\Omega} N_i N_j \, dxdy = \int_{\Gamma} \left(\frac{\partial \theta}{\partial x} N_i \, dy - \frac{\partial \theta}{\partial y} N_i \, dx\right) \qquad (3.40)$$

donde $\dot{\theta}_j \equiv \frac{d\theta_j}{d\tau}$. Usando notación compacta escribimos

$$\sum_{j=1}^{n} (A_{ij} \theta_j + B_{ij} \dot{\theta}_j) = q_i \qquad (3.41)$$

A es la matriz de coeficientes de temperatura estables, B es la matriz de coeficientes de temperatura transitorios y Q es el vector de fuentes de calor y son

$$A_{ij} = \int_{\Omega} \left(\frac{\partial N_i}{\partial x} \frac{\partial N_j}{\partial x} + \frac{\partial N_i}{\partial y} \frac{\partial N_j}{\partial y}\right) dxdy \qquad (3.42)$$

$$B_{ij}=\int_{\Omega} N_i N_j \, dx dy \tag{3.43}$$

$$q_i=\int_{\Gamma} \left(\frac{\partial\theta}{\partial x}N_i\,dy-\frac{\partial\theta}{\partial y}N_i\,dx\right) \tag{3.44}$$

Ahora utilizando el método de diferencias finitas en tiempo, hacemos las siguientes aproximaciones

$$\theta_j = \frac{\theta_j^{k+1}+\theta_j^{k}}{2} \tag{3.45}$$

$$\dot{\theta}_j = \frac{\theta_j^{k+1}-\theta_j^{k}}{\Delta\tau} \tag{3.46}$$

donde K contabiliza los incrementos de tiempo $\Delta\tau$. Sustituyendo (3.45) y (3.47) en (3.41) y agrupando términos tenemos

$$(\Delta\tau A_{ij}+2B_{ij})\theta_j^{k+1}=(-\Delta\tau A_{ij}+2B_{ij})\theta_i^{k}+2\Delta\tau q_i \tag{3.47}$$

lo que se puede escribir como

$$\sum_{j=1}^{n} G_{ij}\theta_j^{k+1}=h_i \quad (i=1,2,\ldots,n) \tag{3.48}$$

donde

$$G_{ij}=\Delta\tau A_{ij}+2B_{ij} \tag{3.49}$$

$$h_i=2\Delta\tau q_i+(-\Delta\tau A_{ij}+2B_{ij})\theta_i^{k} \tag{3.50}$$

Con la ec. (3.48) se pueden encontrar las temperaturas para el siguiente tiempo en función de las temperaturas del tiempo anterior y en nuestro caso, para el tiempo inicial las temperaturas en toda la placa son cero, excepto en la parte superior donde se encuentra la distribución de temperaturas senoidal. Se puede observar que las matrices A y B únicamente se tienen que calcular una vez, ya que éstas dependen solo de la topología del cuerpo y no del tiempo, lo cual facilita mucho los cálculos.

A continuación se procede a efectura el ensamble de las matrices de cada elemento, en la matriz global. También en este caso la matriz global resulta ser simétrica y bandeada, lo cual es debido a la forma de los integrales (3.42) y (3.43).

3.3.3 Solución del Problema por Elementos Finitos Contra Solución Analítica

Los resultados que se muestran a continuación, se obtuvieron de un programa de computadora. En éste, primero se generan las matrices A y B de la ec. (3.47) para cada elemento, con ellas se calcula la matriz G de la ec. (3.48) para el incremento de tiempo y se ensamblan las matrices de todos los elementos, obteniéndose la matriz global G^*. En seguida se genera el vector h para lo cual se utilizan los valores de la temperatura del tiempo anterior. El orden del sistema de ecuaciones (3.48) se reduce a únicamente el número de incognitas sustituyendo las condiciones de frontera del tipo Dirichlet y se resuelve obteniéndose las temperaturas. Este proceso se repite hasta que llega al estado permanente, o sea cuando la diferencia entre las temperaturas del tiempo anterior y el nuevo sea menor que un cierto valor preestablecido. En el posprocesamiento se calcula el error entre la solución analítica y la de elementos finitos para cada instante de tiempo y se interpola linealmente dentro de cada elemento para obtener las coordenadas de las lineas de temperatura constante.

Al igual que la solución en estado permanente, la norma del error, que se utiliza para comparar la solución analítica y la solución de elementos finitos, es el error raíz medio cuadrático definido en la ec. (3.25).

La malla que se utiliza para efectuar los cálculos es del tipo S_a de 25 nodos y 32 elementos, como la que se muestra en la Fig. 3.7, debido a que con esta malla, para el estado permanente, se obtiene un error bastante pequeño al efectuar los cálculos y además no consume mucho tiempo de procesamiento en la computadora.

En la Fig. 3.15 se grafica la variación en el tiempo de la temperatura del nodo central de la malla, obtenida analíticamente y por elementos finitos. Se observa que para tiempos muy pequeños la temperatura obtenida por elementos finitos desciende de la condición inicial y luego vuelve a subir, lo que físicamente no es posible. Después se observa que las dos temperaturas se elevan al mismo tiempo de la condición inicial y se separan hasta que llega un momento en que la diferencia entre una y otra es más o menos constante; esta diferencia es la misma que existe entre la solución de elementos finitos y analítica para estado permanente, lo cual es aceptable, ya que no se puede pedir menor diferencia si se utliza la misma malla. La oscilación no se disminuye al hacer más pequeños los incrementos de tiempo y sí se puede aumentar si éstos son más grandes, por lo que es un defecto del método. Si se utilizan mallas más finas con más elementos en la zona de mayor variación, la oscilación disminuye y la precisión aumenta.

La Fig. 3.16 nos muestra una gráfica de la variación del error raíz medio cuadrático a lo largo del tiempo. En ella se observa que para tiempos muy pequeños el error es grande, debido a las oscilaciones de la tempratura en los nodos, y a medida que transcurre el tiempo, el error se reduce hasta que es igual al que se obtiene en estado permanente. El máximo error es de

5.45%, el cual es bastante pequeño considerando la malla que se utilizó.

Para el ejemplo escogido, la distribución de temperaturas llego al estado permanente en 32 unidades de tiempo aproximádamente y coinciden en este tiempo tanto la solución de elementos finitos como la analítica. La Fig. 3.17 muestra líneas de temperatura constante e igual a 110 unidades en diferentes tiempos, obtenidas a partir de la solución de elementos finitos.

En base a los resultados obtenidos, podemos decir que la combinación del método de elementos finitos y el método de diferencias finitas para resolver problemas parabólicos es efectiva, únicamente teniendo en cuenta que la discretización del dominio debe ser más fina que para un problema elíptico, para disminuir la oscilación que se presenta en los primeros instantes de tiempo.

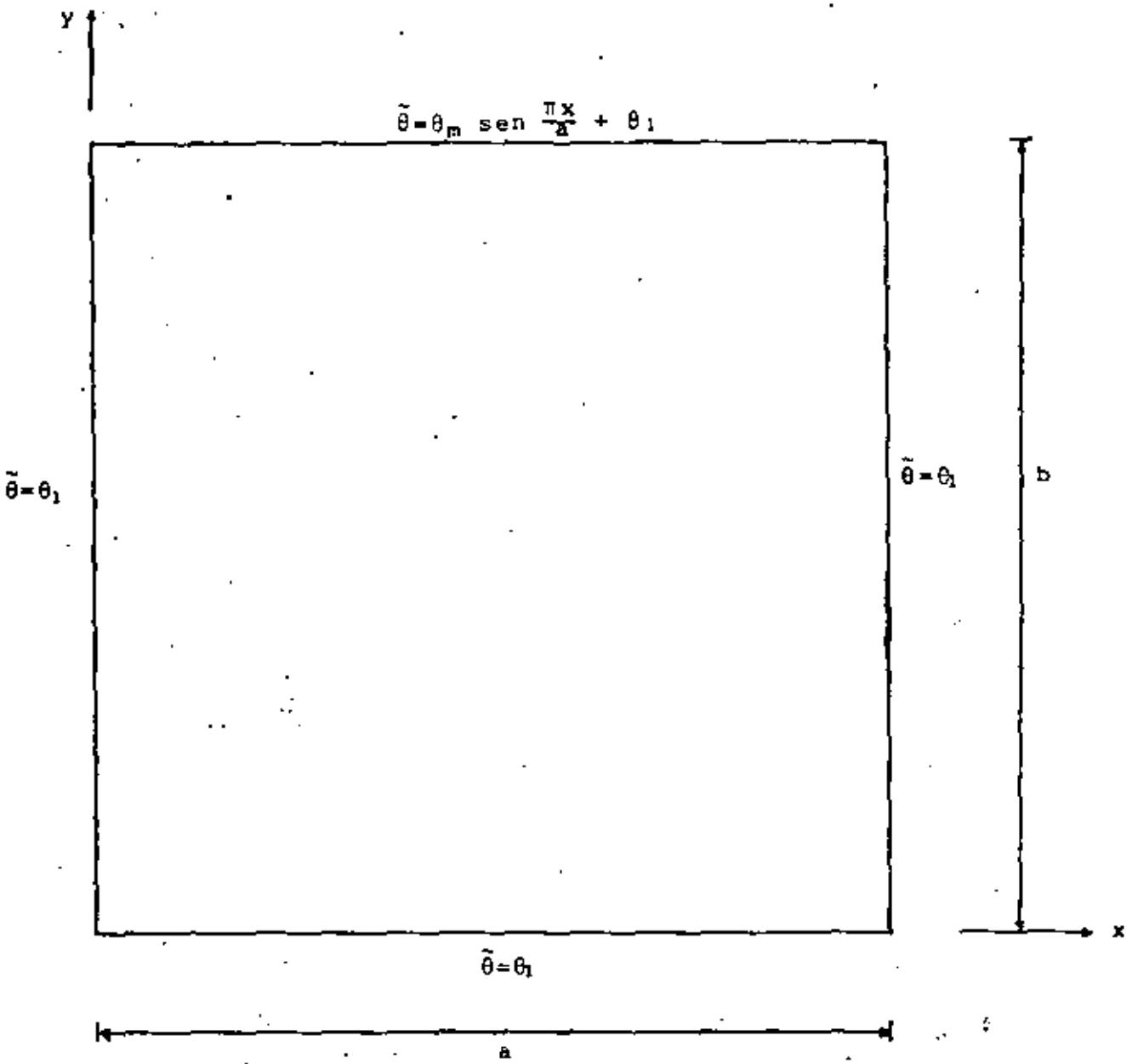

Fig 3.1. Placa rectangular con transferencia de calor por conducción y sus condiciones de frontera

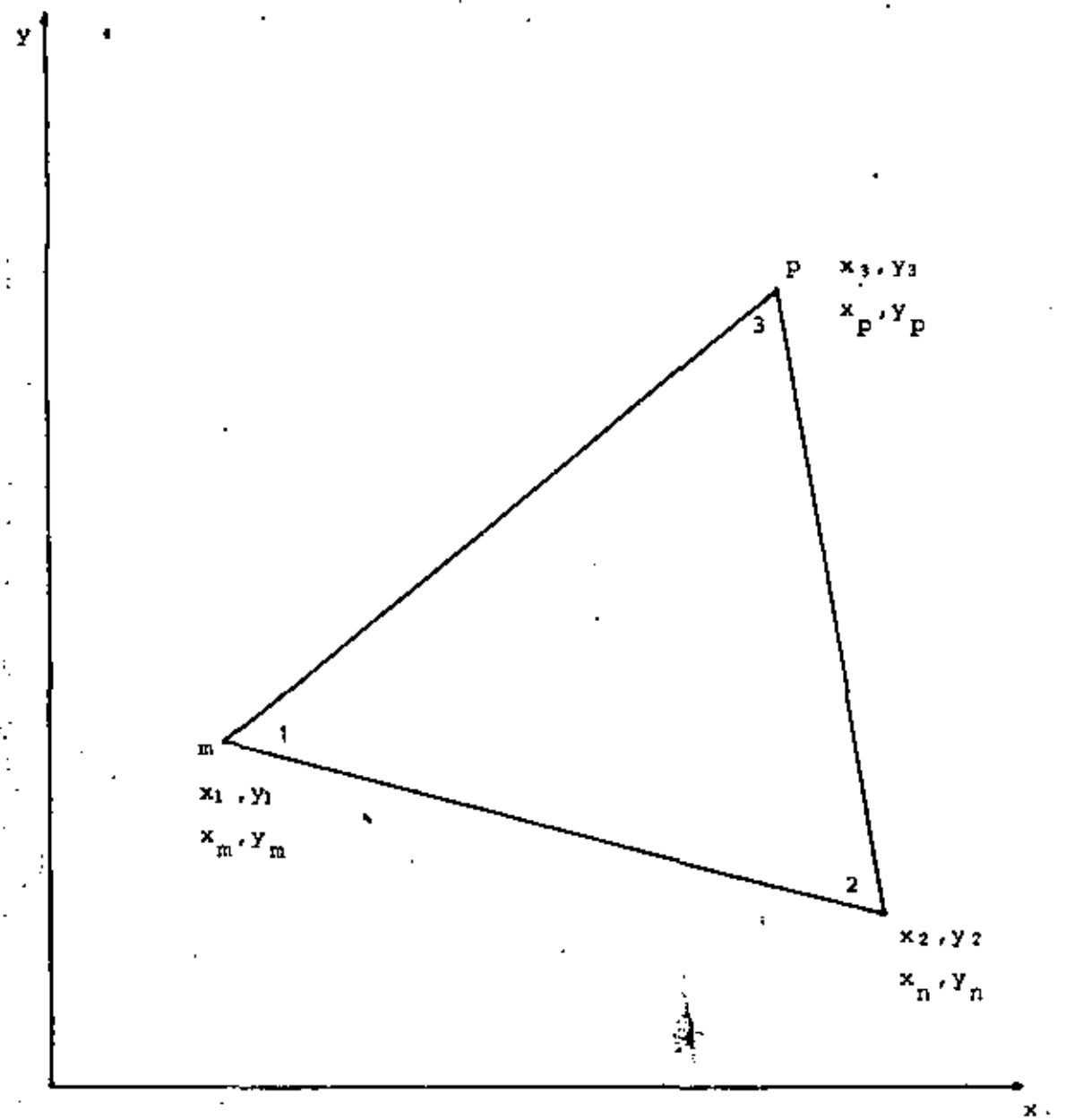

Fig 3.2. Elemento triangular con la numeración local (1,2,3) y la numeración global (n,m,p) y sus respectivas coordenadas cartesianas.

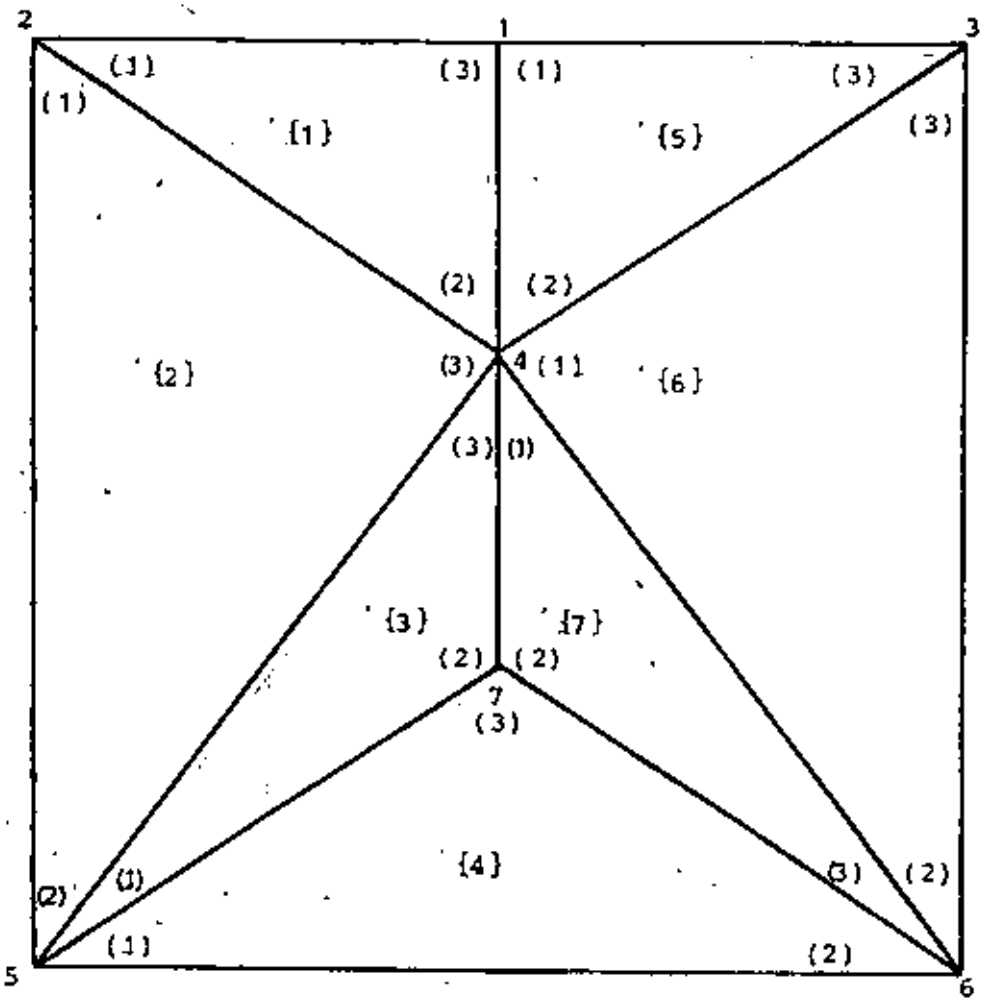

Fig 3.3. Discretización cruda de la placa, mostrando la numeración global, la numeración local y la numeración de los elementos.

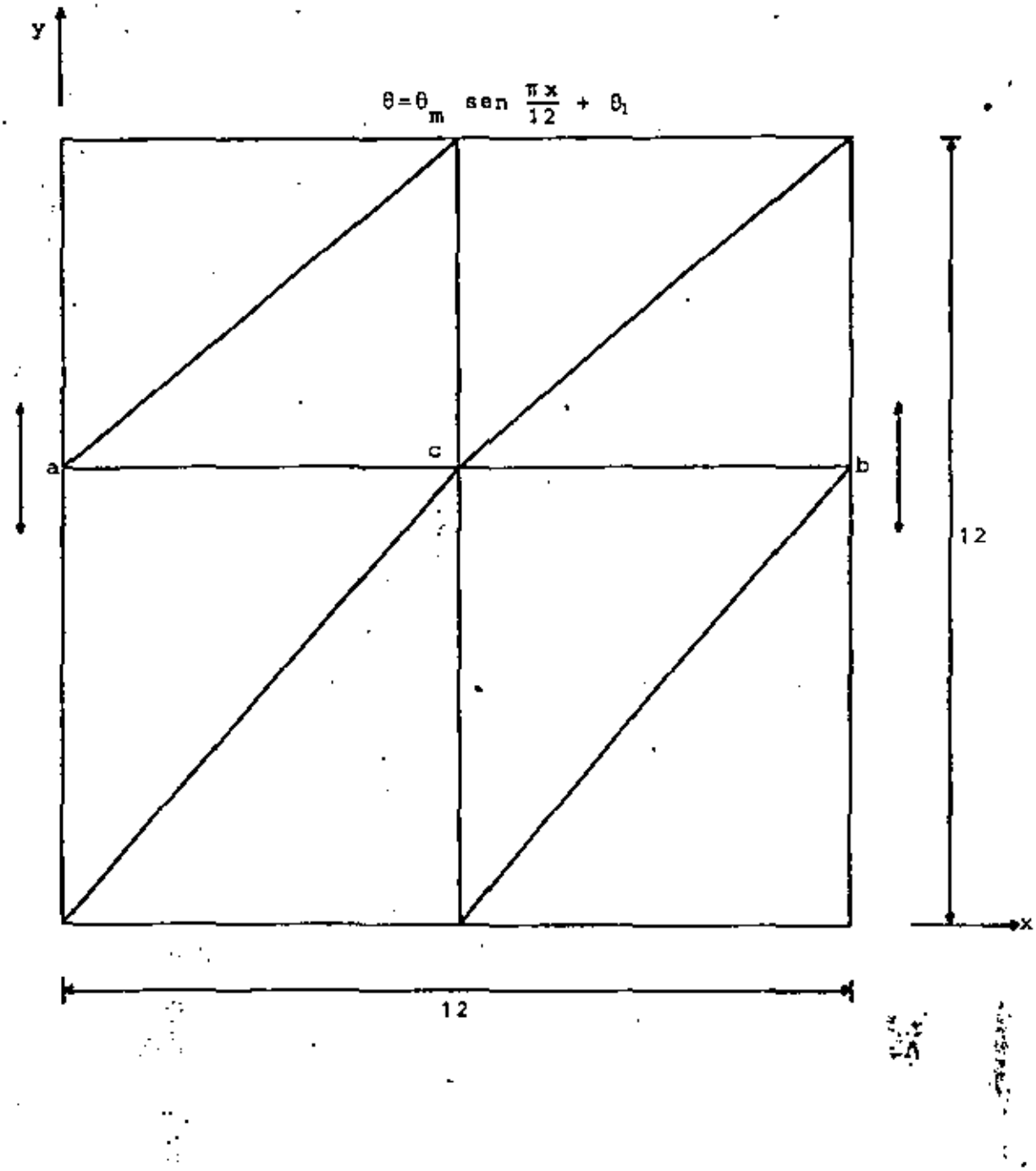

Fig 3.4: Malla con la barra $\overline{acb}$ móvil.

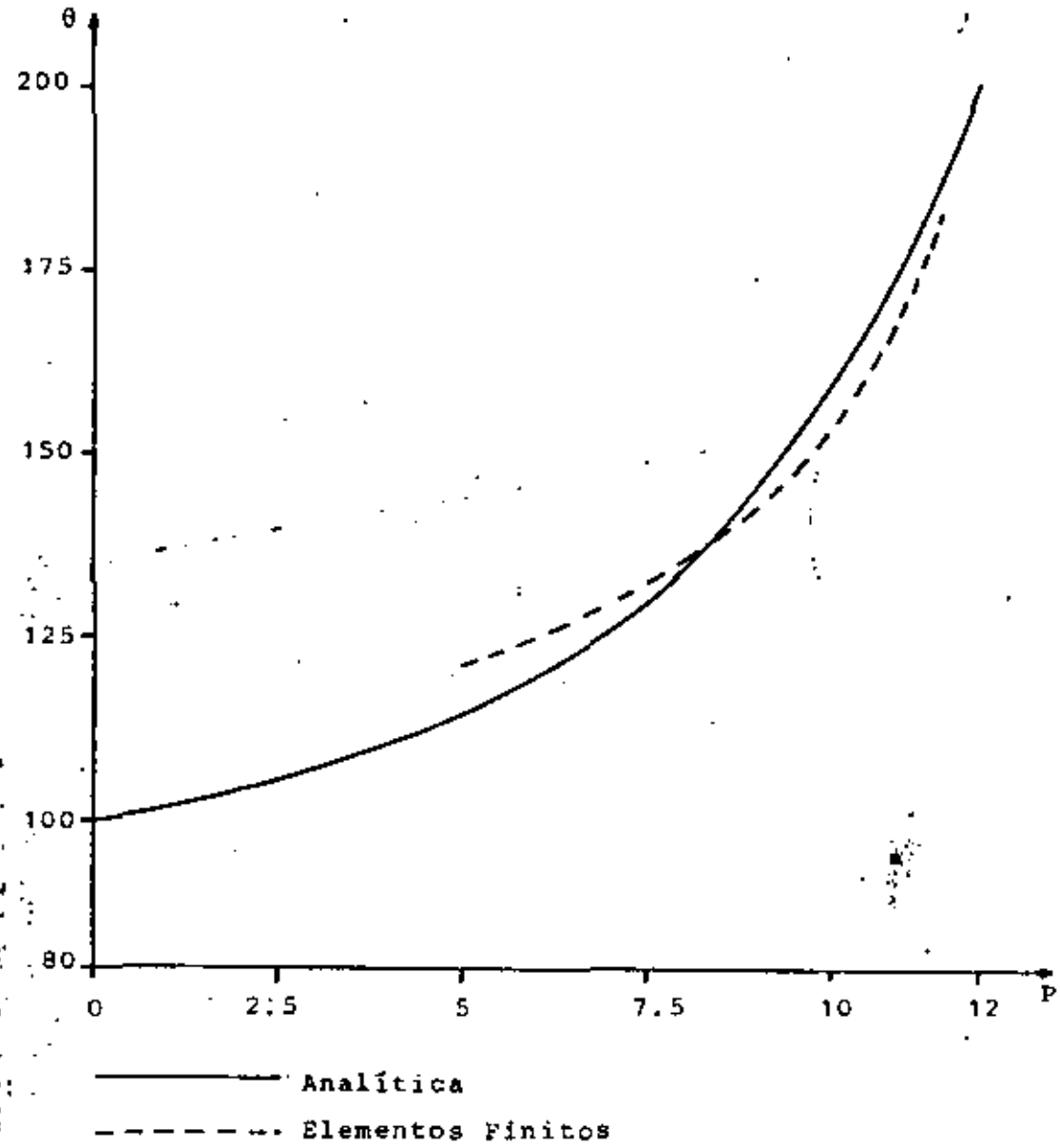

Fig 3.5 Gráfica posición contra temperatura para la solución exacta y de elementos finitos.

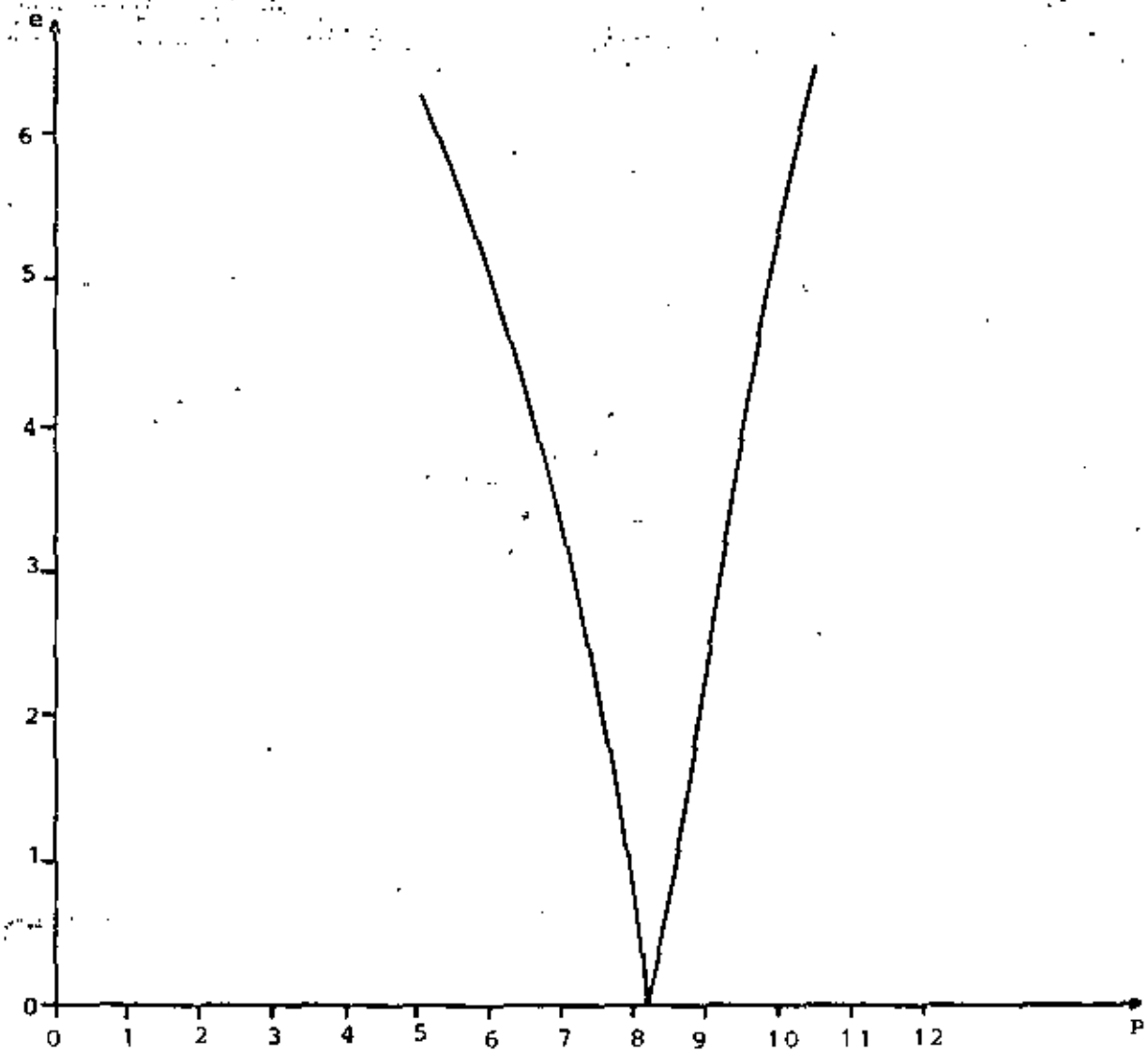

Fig 3.6. Gráfica posición contra error raíz medio cuadrático.

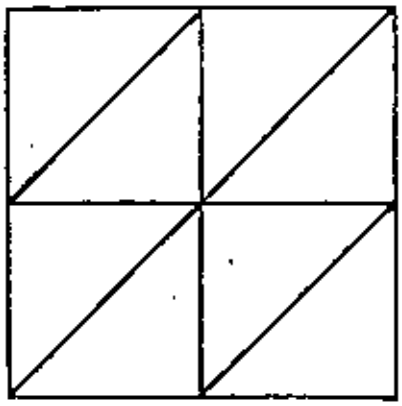

9 Nodos
8 Elementos

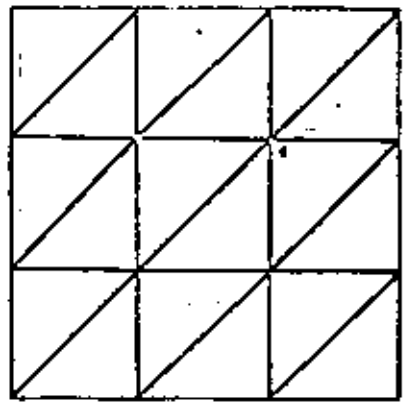

16 Nodos
18 Elementos

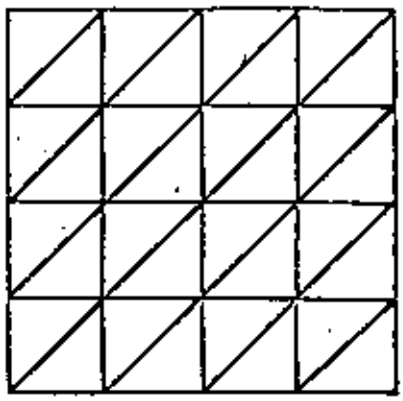

25 Nodos
32 Elementos

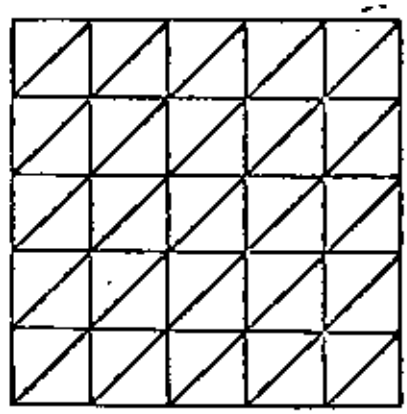

36 Nodos
50 Rlementos

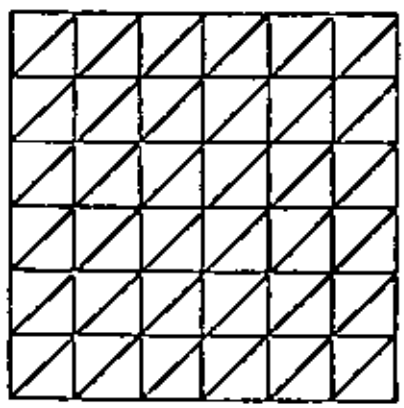

49 Nodos
72 Elementos

Fig 3.7. Mallas tipo S_a.

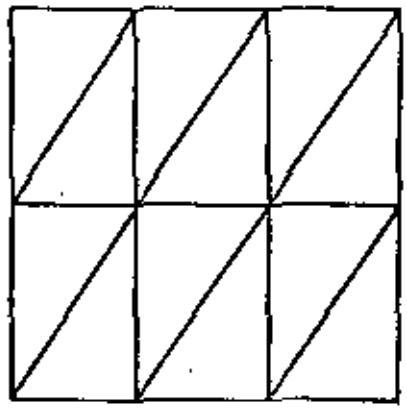

12 Nodos

12 Elementos

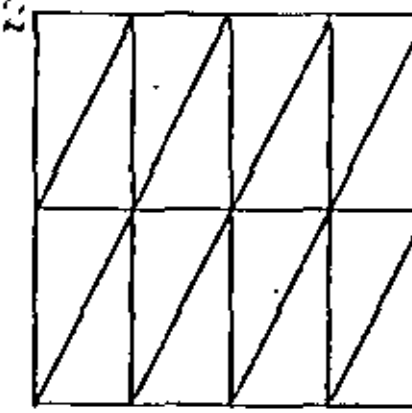

15 Nodos

16 Elementos

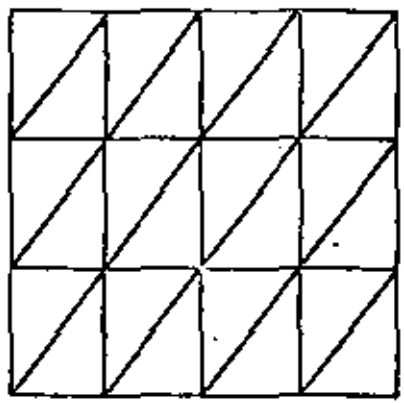

20 Nodos

24 Elementos

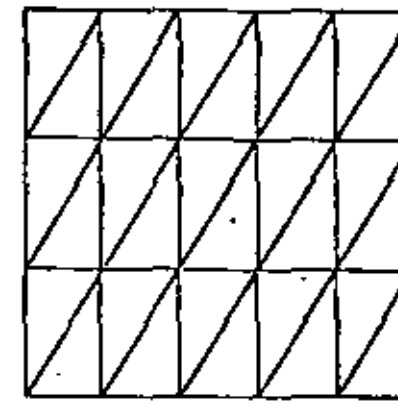

24 Nodos

30 Elementos

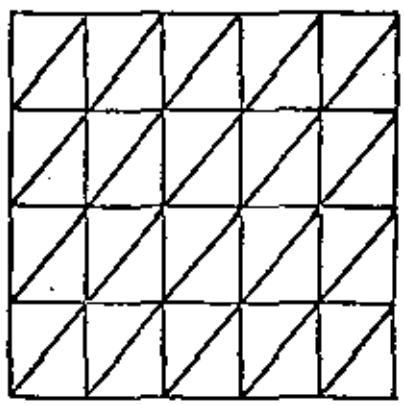

30 Nodos

40 Elementos

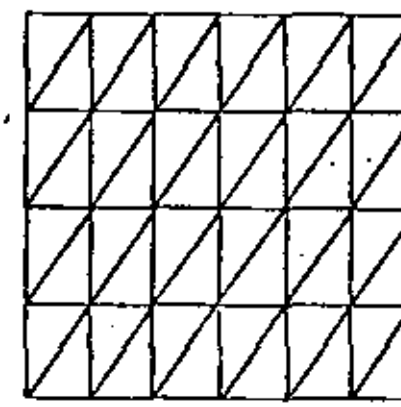

35 Nodos

48 Elementos

Fig 3.8. Mallas tipo AS_1.

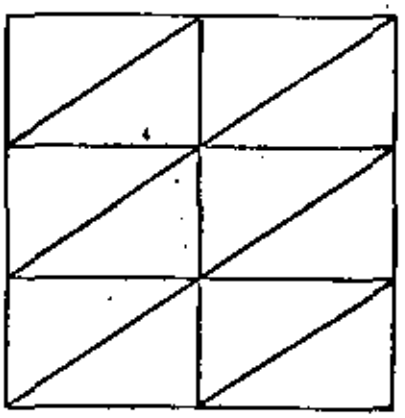

12 Nodos
12 Elementos

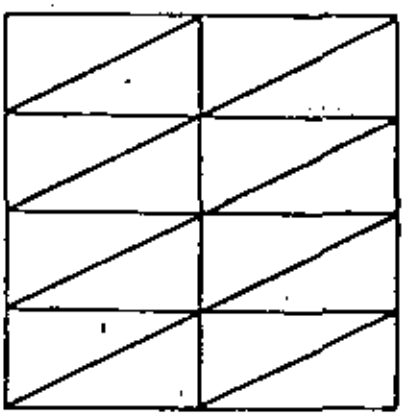

15 Nodos
16 Elementos

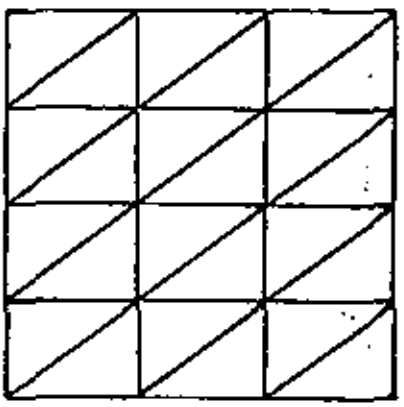

20 Nodos
24 Elementos

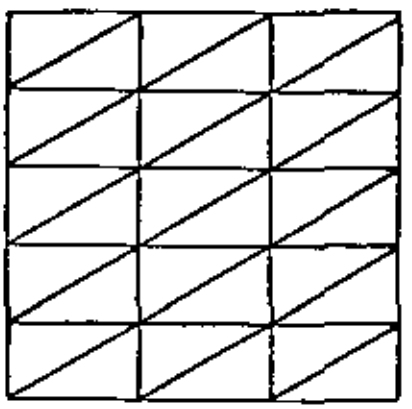

24 Nodos
30 Elementos

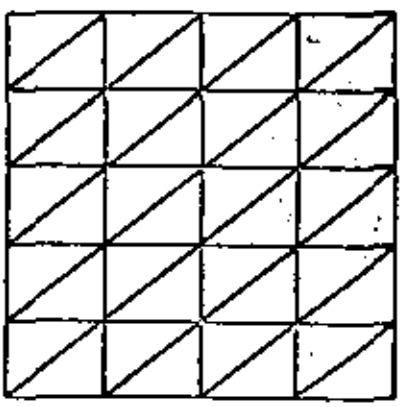

30 Nodos
40 Elementos

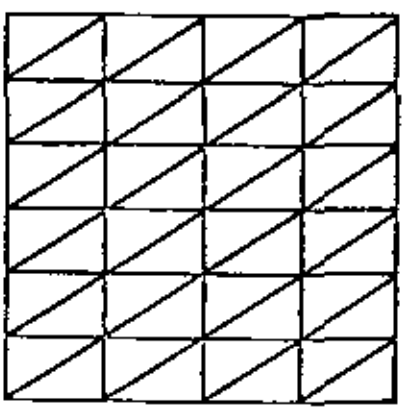

35 Nodos
48 Elementos

Fig 3.9. Mallas tipo AS_2.

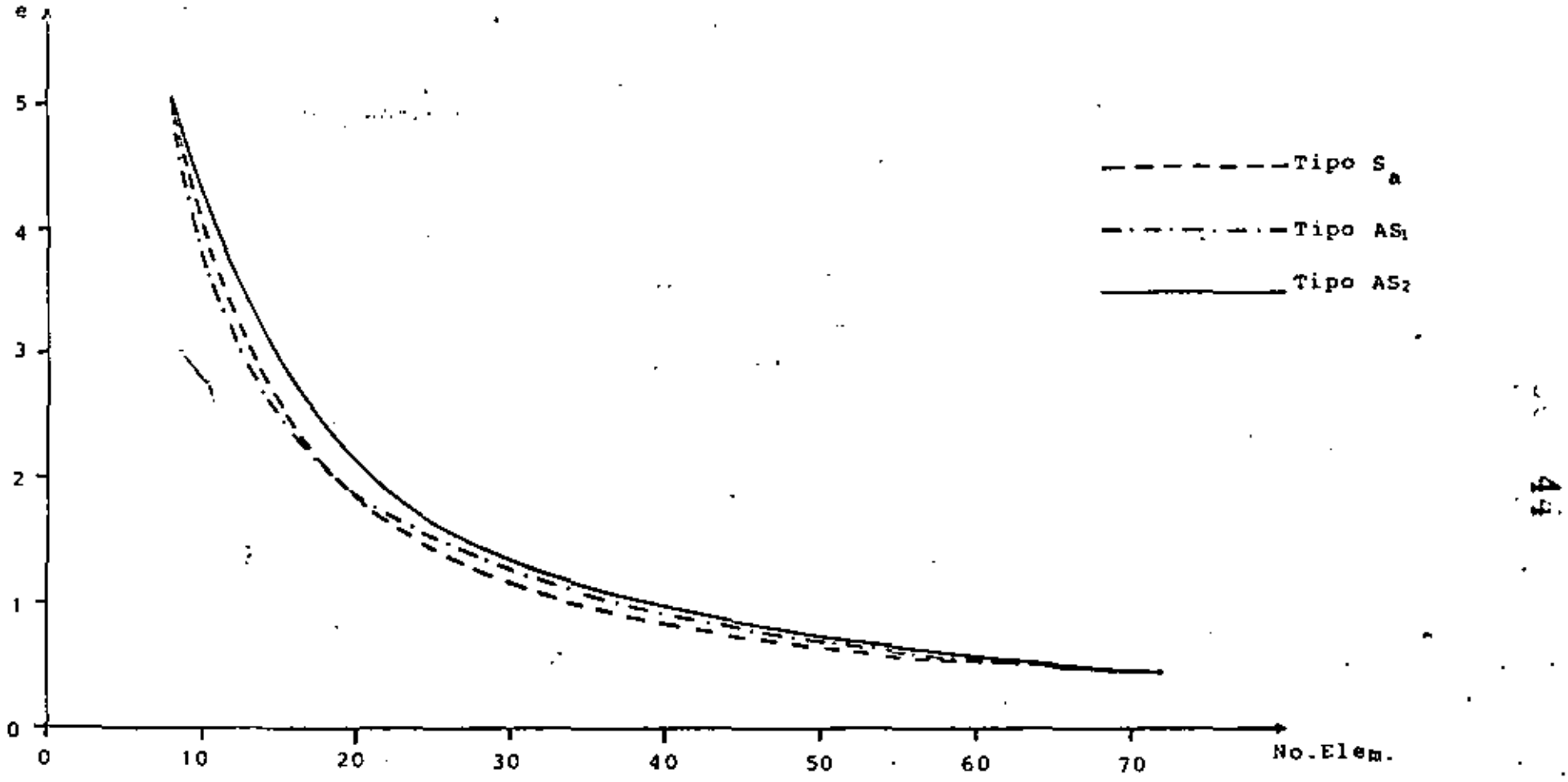

Fig 3.10. Gráfica Número de elementos contra error raíz medio cuadrático para mallas tipo S_a, AS_1 y AS_2

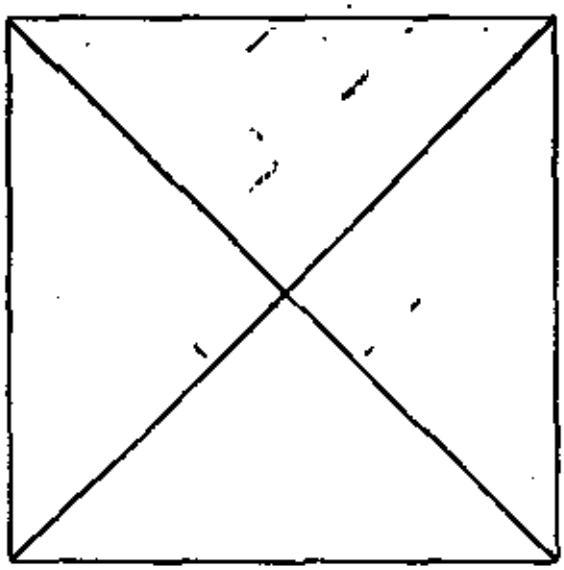

5 Nodos
4 Elementos

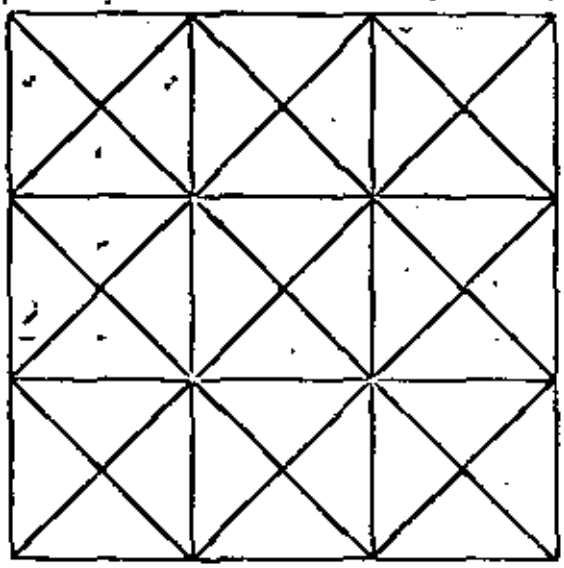

25 Nodos
36 Elementos

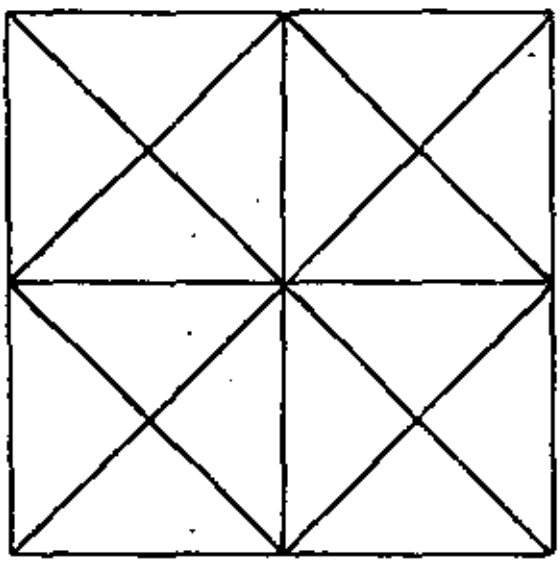

13 Nodos
16 Elementos

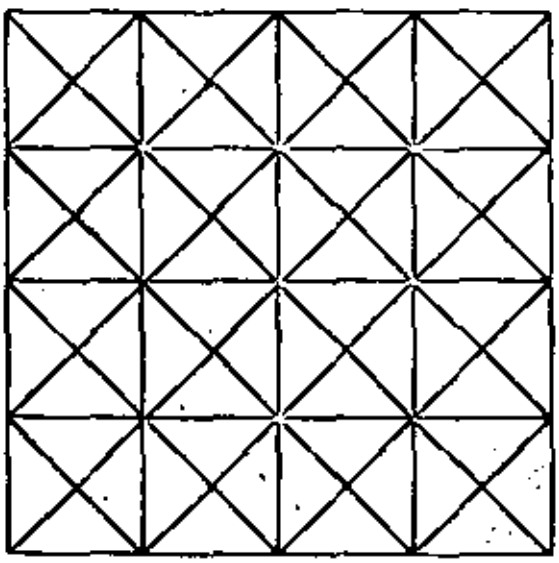

41 Nodos
64 Elementos

Fig 3.11 Mallas tipo S_b

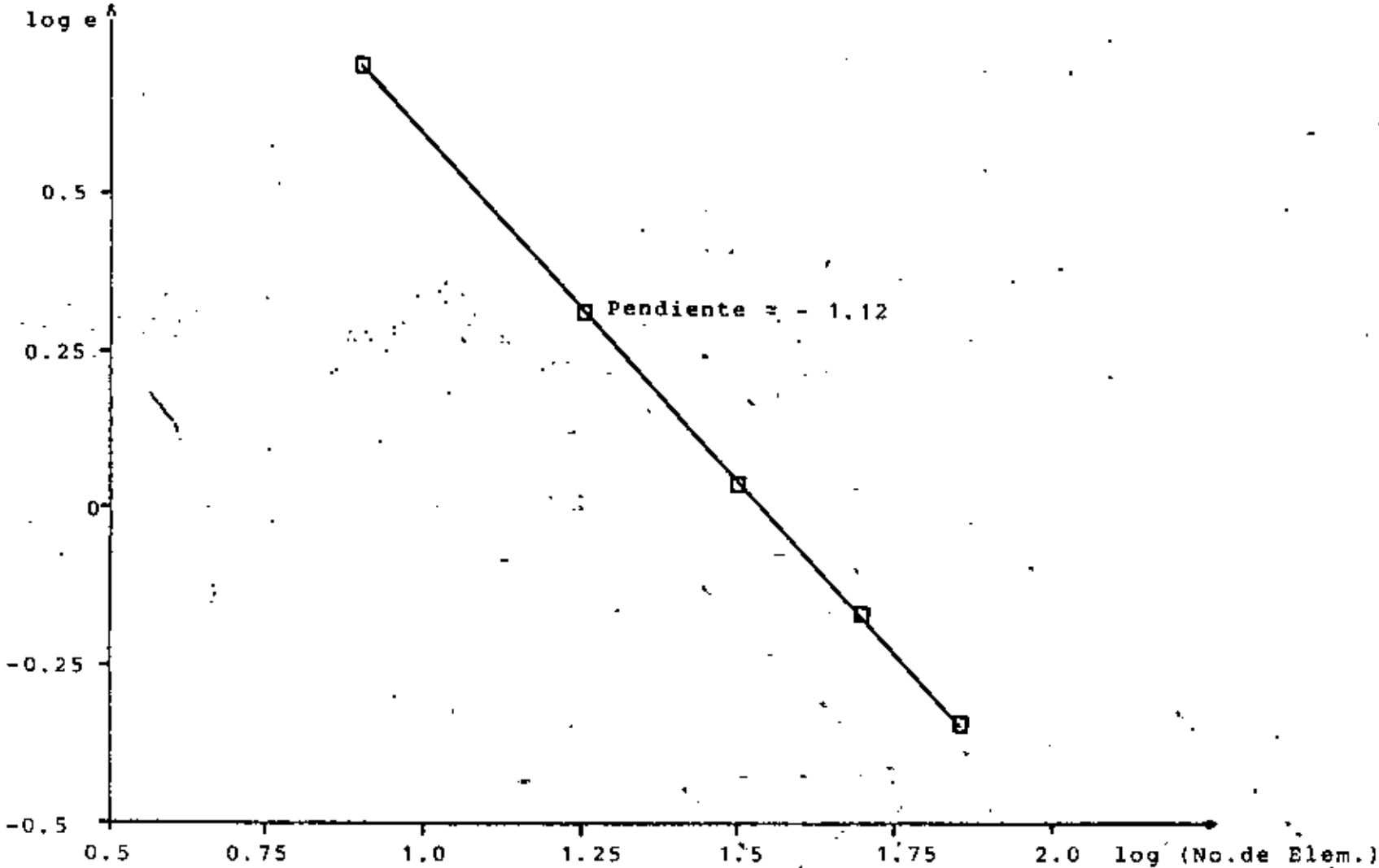

Fig 3.12. Gráfica número de elementos contra error raíz medio cuadrático para mallas de tipo S

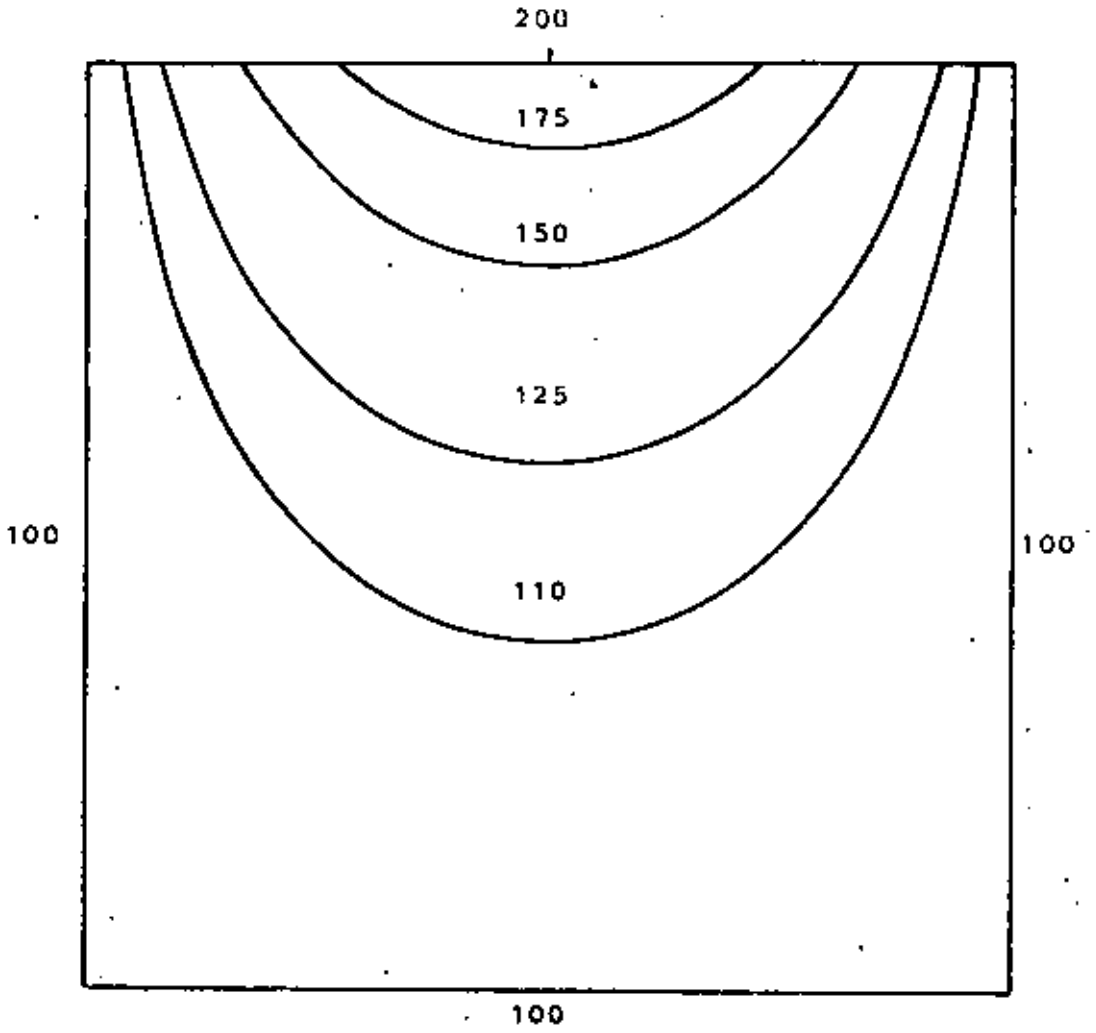

Fig 3.13. Lineas de temperatura constante

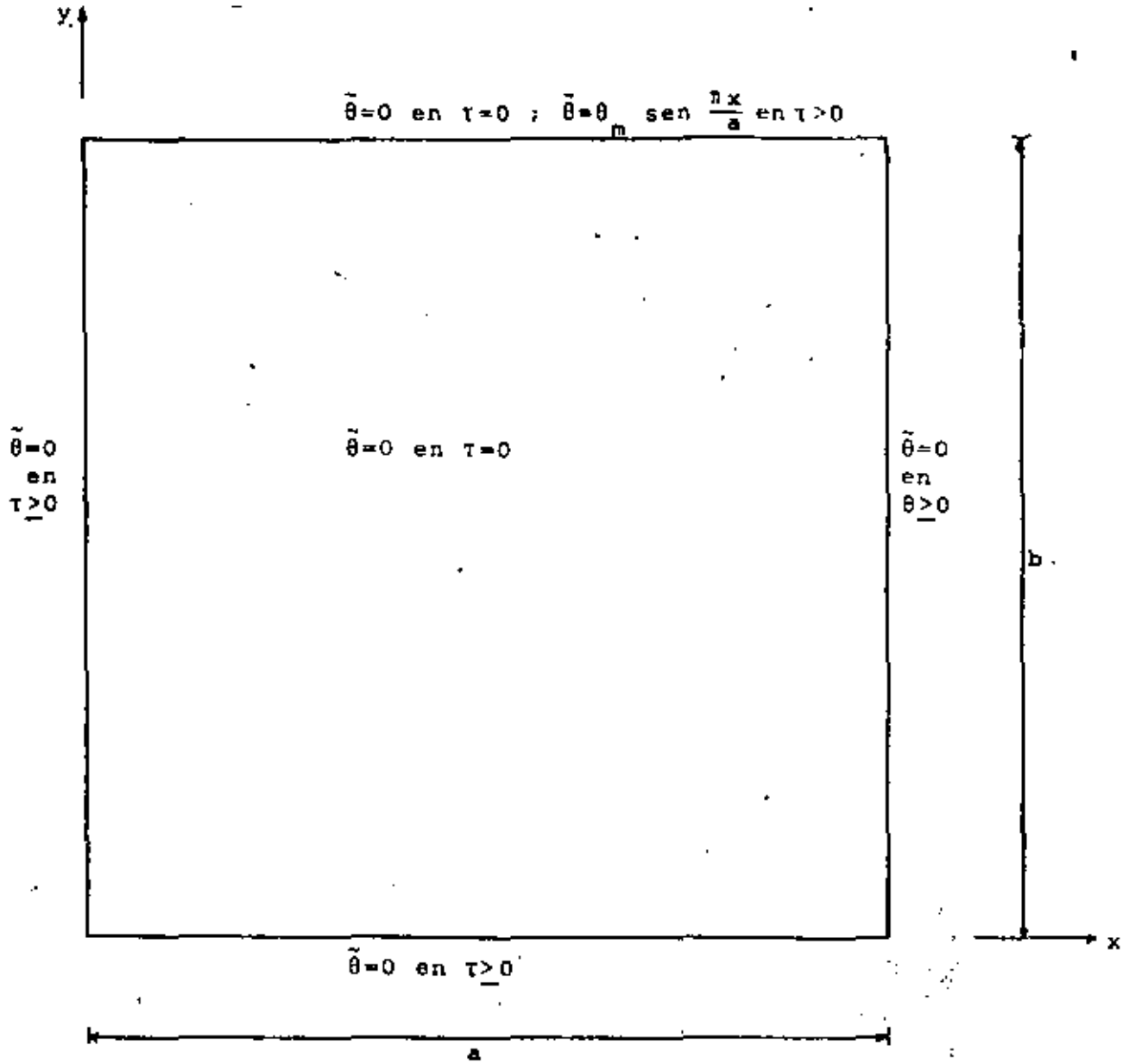

Fig 3.14. Placa con transferencia de calor por conducción con sus condiciones iniciales y de frontera.

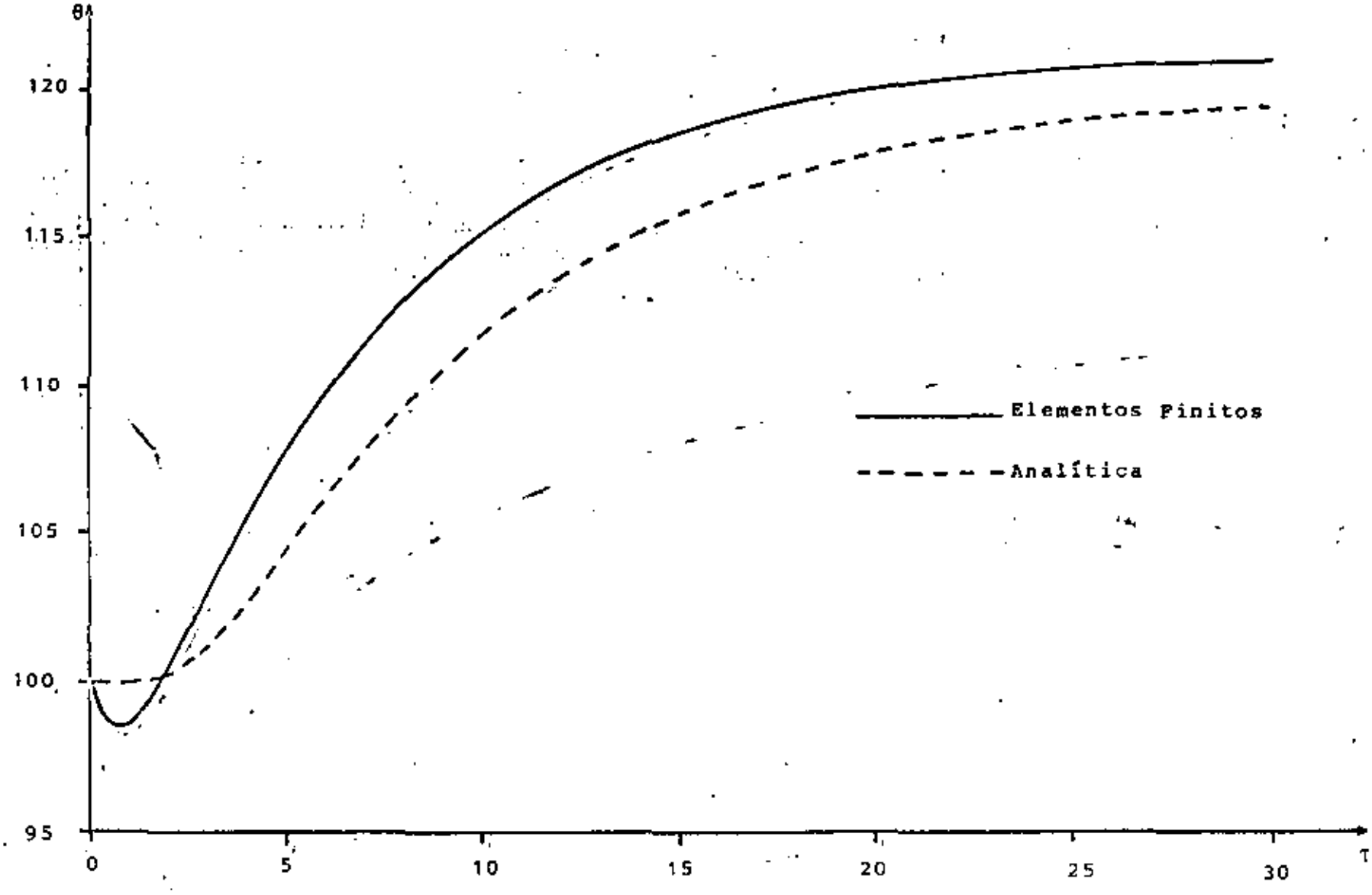

Fig 3.15 Gráfica tiempo contra temperatura para el nodo central de la malla.

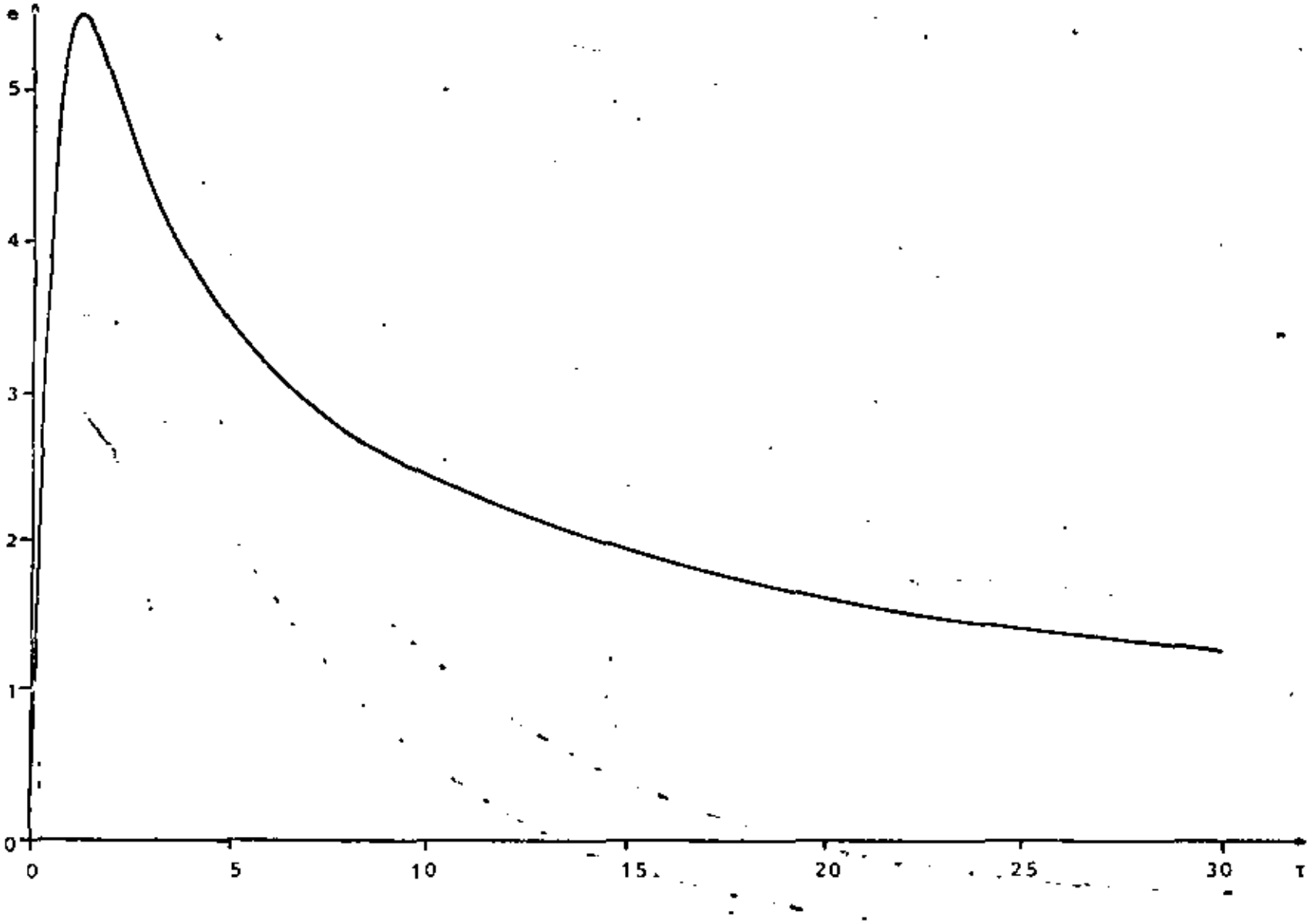

Fig. 3.16. Gráfica tiempo contra error raíz medio cuadrático

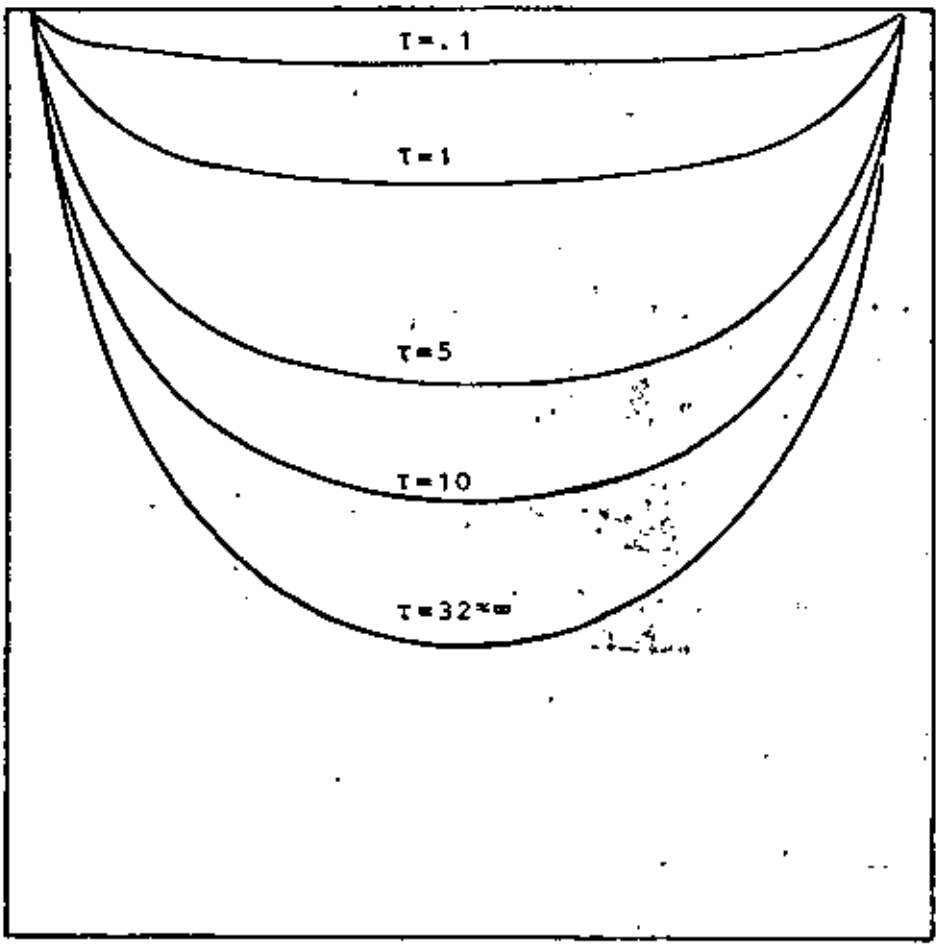

Fig 3.17. Líneas de temperatura constante θ=110 en diferentes tiempos.

CAPITULO IV
FLUJO POTENCIAL INCOMPRESIBLE

4.1 GENERAL

En este capítulo se va a tratar el caso de la solución de un flujo potencial incompresible y no viscoso, o sea un flujo ideal, por medio del método de elementos finitos, en conjunto con el método de Galerkin.

Para ejmplificar, se resolverá el problema de un flujo bidimensional alrededor de un cilindro, el cual se encuentra entre dos placas planas.

Este tipo de flujo puede ser utilizado para obtener una aproximación del comportamiento de un flujo real, con una viscosidad muy pequeña, y con una capa límite muy delgada en la superficie, además de que sea incompresible. Un ejemplo de los flujos que cumplen estas condiciones, son los flujos convergentes o acelerados.

4.2 PLANTEAMIENTO DE LAS ECUACIONES

Ya que lo que nos interesa en un flujo bidimensional, todos los planteamientos que se hagan a continuación serán descritos en dos dimensiones para mayor facilidad.

Un fluido real debe satisfacer las siguientes condiciones:

a) La ecuación de continuidad, que en coordenadas cartesianas es:

$$\frac{\partial \hat{u}}{\partial \hat{x}} + \frac{\partial v}{\partial \hat{y}} = 0 \qquad (4.1)$$

donde $\hat{u}$ y $\hat{v}$ son los componentes de velocidad en las direcciones $\hat{x}$ y $\hat{y}$ respectivamente.

b) La segunda ley de Newton en todos los puntos y en cualquier instar ...

c) El fluido no debe penetrar dentro de cualquier contorno sólido, ni tampoco se deben formar oquedades entre el fluido y el contorno.

d) A las condiciones anteriores le añadimos otra más. El fluido debe ser irrotacional, esto es

$$\frac{\partial \hat{v}}{\partial \hat{x}} - \frac{\partial \hat{u}}{\partial \hat{y}} = 0 \qquad (4.2)$$

El aplicar la segunda ley de Newton a una partícula del fluido, nos conduce a las ecuaciones de Euler y son:

$$\begin{aligned} \frac{\partial \hat{u}}{\partial \hat{t}} + \hat{u}\frac{\partial \hat{u}}{\partial \hat{x}} + \hat{v}\frac{\partial \hat{u}}{\partial \hat{y}} &= -\frac{1}{\rho}\frac{\partial \hat{p}}{\partial \hat{x}} \\ \frac{\partial \hat{v}}{\partial \hat{t}} + \hat{u}\frac{\partial \hat{v}}{\partial \hat{x}} + \hat{v}\frac{\partial \hat{v}}{\partial \hat{y}} &= -\frac{1}{\rho}\frac{\partial \hat{p}}{\partial \hat{y}} \end{aligned} \qquad (4.3)$$

donde $\hat{t}$ es el tiempo, $\hat{\rho}$ es la densidad y $\hat{P}$ es la presión.

Nosotros vamos a considerar un flujo en estado permanente, por lo tanto para este caso el primer término de la ecuación 4.3 desaparece.

Ya que el flujo que estamos considerando es irrotacional, podemos definir un potencial de velocidad a partir de la ec. (4.2) de la siguiente forma

$$\hat{u} = \frac{\partial \hat{\phi}}{\partial \hat{x}} \; ; \; \hat{v} = \frac{\partial \hat{\phi}}{\partial \hat{y}} \qquad (4.4)$$

donde $\hat{\phi}$ es el potencial de velocidad. De esta manera obtenemos una función $\hat{\phi}$ tal, que su derivada con respecto a una dirección cualquiera es la componente de velocidad en esa dirección. Esto

es posible ya que no existe rozamiento, una partícula que esté inicialmente en reposo no puede ponerse a girar, de igual manera una partícula que está girando, no puede alterar su rotacion.

Si substituimos la ec. (4.4) en la ec. de continuidad (4.1) obtenemos

$$\frac{\partial^2 \hat{\phi}}{\partial \hat{x}^2} + \frac{\partial^2 \hat{\phi}}{\partial \hat{y}^2} = 0 \qquad (4.5)$$

que es la llamada ecuación de Laplace en dos dimensiones. Toda función ϕ que satisfaga esta ecuación es un caso posible de flujo irrotacional.

La ec. (4.5) tiene solución analítica para casos muy sencillos, en los que las fronteras no presenten ninguna complicación, sin embargo, para casos en los que las fronteras no son muy regulares, hay que utilizar un método numérico para resolverla.

Para el caso de un flujo bidimensional, también se puede definir una función $\hat{\psi}$, llamada función de corriente, que nos relacione las velocidades en las dos direcciones. A partir de la ec. (4.1) tenemos

$$u = \frac{\partial \hat{\psi}}{\partial \hat{y}} \; ; \; v = - \frac{\partial \hat{\psi}}{\partial \hat{x}} \qquad (4.6)$$

sustituyendo (4.6) en (4.2) se tiene

$$\frac{\partial^2 \hat{\psi}}{\partial \hat{x}^2} + \frac{\partial^2 \hat{\psi}}{\partial \hat{y}^2} = w \qquad (4.7)$$

que es la ecuación de Laplace para la función de corriente y su solución tiene dificultades similares a la del potencial de velocidad.

Se puede demostrar fácilmente, que la línea descrita por la función $\hat{\psi}$=const. es la trayectoria de una partícula del fluido y a esta curva se le llama línea de corriente.

El potencial de velocidad y la función de corriente se realciona de (4.6) y (4.4)

$$\frac{\partial \hat{\phi}}{\partial \hat{x}} = \frac{\partial \hat{\psi}}{\partial \hat{y}} \; ; \; \frac{\partial \hat{\phi}}{\partial \hat{y}} = - \frac{\partial \hat{\psi}}{\partial \hat{x}} \qquad (4.8)$$

Como consecuencia las lineas de corriente y las lineas equipotenciales son perpendiculares entre sí para un flujo ideal.

4.3 FORMULACION DE ELEMENTOS FINITOS

Ya que el mismo tipo de ecuación, ésto es, la ecuación de Laplace, se utiliza para obtener el potencial de velocidad y la función de corriente, la formulación de elementos finitos es idéntica para cualquiera de las dos y la única difencia escriba en las condiciones de frontera que se utilizan. No existe ventaja de una sobre otra formulación si las geometrías son más o menos simples. Por lo tanto únicamente se describirá la formulación de la función de corriente.

Se definen las siguientes variables audimensionales

$$\tilde{\psi} = \frac{\hat{\psi}}{q_\infty D} \; ; \; x = \frac{\hat{x}}{D} \; ; \; y = \frac{\hat{y}}{D}$$

donde q_∞ es la velocidad alejada del cuerpo y D es una distancia característica. Sustituyendo en la ec. (4.8), se tiene

$$\frac{\partial^2 \tilde{\psi}}{\partial x^2} + \frac{\partial^2 \tilde{\psi}}{\partial y^2} = 0 \qquad (4.9)$$

Haciendo la siguiente aproximación para un elemento

$$\tilde{\psi} = \psi = \sum_{i=1}^{n} N_i \psi_i \qquad (4.10)$$

donde ψ es la función aproximada y N_i son las funciones de interpolación o funciones de base de un elemento, n es el número de nodos del elemento y ψ_i es el valor de la función en cada nodo. Sustituyendo (4.10) en (4.9) e igualando a un residuo ε se obtiene

$$\frac{\partial^2\psi}{\partial x^2} + \frac{\partial^2\psi}{\partial y^2} = \varepsilon \qquad (4.11)$$

Considernado una proyección ortogonal del residuo sobre las funciones de peso, que en este caso son iguales a las funciones de base

$$(\varepsilon,\ N_i) = \int_\Omega (\frac{\partial^2\psi}{\partial x^2} + \frac{\partial^2\psi}{\partial y^2}) N_i\, dxdy = 0 \qquad (4.12)$$

donde Ω es el dominio del elemento. Aplicando el teorema de Green en (4.12) llegamos

$$-\int_\Omega (\frac{\partial\psi}{\partial x}\frac{\partial N_i}{\partial x} + \frac{\partial\psi}{\partial y}\frac{\partial N_i}{\partial y})\, dxdy + \int_\Gamma (\frac{\partial\psi}{\partial x}N_i\, dy - \frac{\partial\psi}{\partial y}N_i\, dx) = 0 \qquad (4.13)$$

Sustituyendo (4.10) en (4.13) y reordenando

$$\psi_j \int_\Omega (\frac{\partial N_i}{\partial x}\frac{\partial N_j}{\partial x} + \frac{\partial N_i}{\partial y}\frac{\partial N_j}{\partial y})\, dxdy = \int_\Gamma (\frac{\partial\psi}{\partial x}N_i\, dy - \frac{\partial\psi}{\partial y}N_i\, fx) \qquad (4.14)$$

Usando una notación simplificada escribimos

$$\sum_{j=1}^{n} A_{ij}\psi_j = \phi_i \quad (i=1,2,\ldots,n) \qquad (4.15)$$

Aquí A y ϕ son llamados matriz de coeficientes y vector de flujo respectivamente y son

$$A_{ij}=\int_{\Omega}\left(\frac{\partial N_i}{\partial x}\frac{\partial N_j}{\partial x}+\frac{\partial N_i}{\partial y}\frac{\partial N_i}{\partial y}\right)dxdy \qquad (4.16)$$

$$\delta_i=\int_{\Gamma}\left(\frac{\partial\psi}{\partial x}N_i\,dy-\frac{\partial\psi}{\partial y}N_i\,dx\right) \qquad (4.17)$$

Para obtener el sistema de ecuaciones global, se ensamblan las ec. (4.15) de todos los elementos, obteniéndose

$$\sum_{j=1}^{m} A^*_{ij}\psi^*_j=\delta^*_i \quad (i=1,2,\ldots,m) \qquad (4.18)$$

donde m es el número total de nodos.

4.4 SOLUCION Y RESULTADOS

El problema específico escogido como ejemplo, es el del flujo alrededor de un cilindro de radio D=1 entre placas planas separadas una distancia 4D y suponiendo que el flujo uniforme se encuentra a una distancia 3.5D, medida desde el centro del cilindro, Fig 4.1.

Por simetría se utiliza una cuarta parte del dominio, sección a-b-c-d-e. Por inspección notamos que las fronteras a-b y e-d-c son líneas de corriente y como referencia tomaremos $\tilde{\psi}=0$ en e-d-c. Ya que la velocidad es constante en a-e podemos poner

$$\frac{\partial\tilde{\psi}}{\partial y}=u=1 \qquad (4.19)$$

Integrando

$$\tilde{\psi}=y+\text{const.} \qquad (4.20)$$

lo que significa que la función de corriente varía linealmente con respecto a y, en la frontera a-e. Sustituyendo los valores de $y,\tilde{\psi}$ en la ec. (4.20), para la frontera a-b llegamos a $\tilde{\psi}=2$.

Todas las condiciones de frontera que hemos definido hasta el momento son del tipo Dirichlet. Lo único que resta es definir la condición de frontera para el lado b-c, sabemos que la línea de corriente es perpendicular a ese lado, por lo que definimos $\frac{\partial\tilde{\psi}}{\partial n}=0$, siendo esta del tipo Neumann. Las condiciones de frontera se presentan en la Fig 4.2.

Para resolver este problema, se escogieron elementos triangulares, con funciones de interpolación lineal, por lo que sólamente tienen 3 nodos cada elemento. Los elementos y las funciones son los mismos utilizados en la sección 3.2.3 donde se pueden consultar.

En el programa de computadora que se realizó, primero se generan las matrices de coeficientes $\hat{A}$ de cada elemento, mismas que se ensamblan en la matriz global $\hat{A}^*$. Para el vector $\hat{f}$ en los nodos en la frontera que tienen la condición de Neumann la integral (4.17) debe evaluarse. En nuestro caso resulta ser cero. En los demás nodos con la condición de Dirichlet esta integral tiene valor desconocido pero ya que la función de corriente es conocida allí, no es necesario calcularla. Las condiciones de frontera del tipo Dirichlet se sustituyen en el sistema (4.19), reduciéndose con ello el orden de la matriz global, a únicamente el número de incognitas y se resuelve el sistema resultante obteniéndose los valores de ψ. En el posprocesamiento, se interpola linealmente dentro de cada elemento para obtener las coordenadas de las líneas de corriente, además, por medio de la ec. (4.23), se calculan las velocidades arriba de la cresta del cilindro.

Se utilizan dos discretizaciones del dominio como muestra las figuras 4.3 y 4.4. La primera es una malla gruesa de 10 nodos, usada tanto para probar el programa como para observar las zonas de mayor variación. La segunda es una malla fina de 73 nodos con 111 elementos, que se realizó tomando en cuenta los resultados obtenidos con la malla anterior.

En la Fig. 4.5 se muestran las líneas de corriente y la variación de la velocidad en la cresta del cilindro, se comparan con la solución analítica aproximada, obtenida por el método de imágenes[4] de la siguiente forma (Chung, 1978)

$$\tilde{\psi}=q_\infty \left\{y-\frac{H}{2\pi}\operatorname{senh}^2\left(\frac{\pi b}{H}\right)\operatorname{sen}\left(\frac{2\pi y}{H}\right)\Big/\left[\cosh^2\left(\frac{\pi x}{H}\right)-\cos^2\left(\frac{\pi y}{H}\right)\right]\right\} \qquad (4.24)$$

donde x,y son coordenadas con origen en el centro del cilindro, b es el radio y H es la distancia vertical entre las dos placas.

Se observa que existe bastante diferencia entre los resultados obtenidos con la malla gruesa y la solución analítica, el error raíz medio cuadrático relativo es de 8.5%. Sin embargo,al comparar los resultados de la malla fina con la solución analítica, el error raíz medio cuadrático relativo, en la desviación de las curvas de líneas de corriente, es de 0.9% el cual es bastante pequeno; en la figura se ve claramente que casi coinciden las curvas.

También se observa como la velocidad aumenta en la cresta del cilindro al acercarse a éste y la poca diferencia que existe entre la curva de la malla fina y la solución analítica.

Concluyendo, los resultados demuestran la utilidad del método de elementos finitos de Galerkin en la solución de problemas de flujo potencial incompresible y como,con una buena discretización se pueden obtener resultados bastantes precisos.

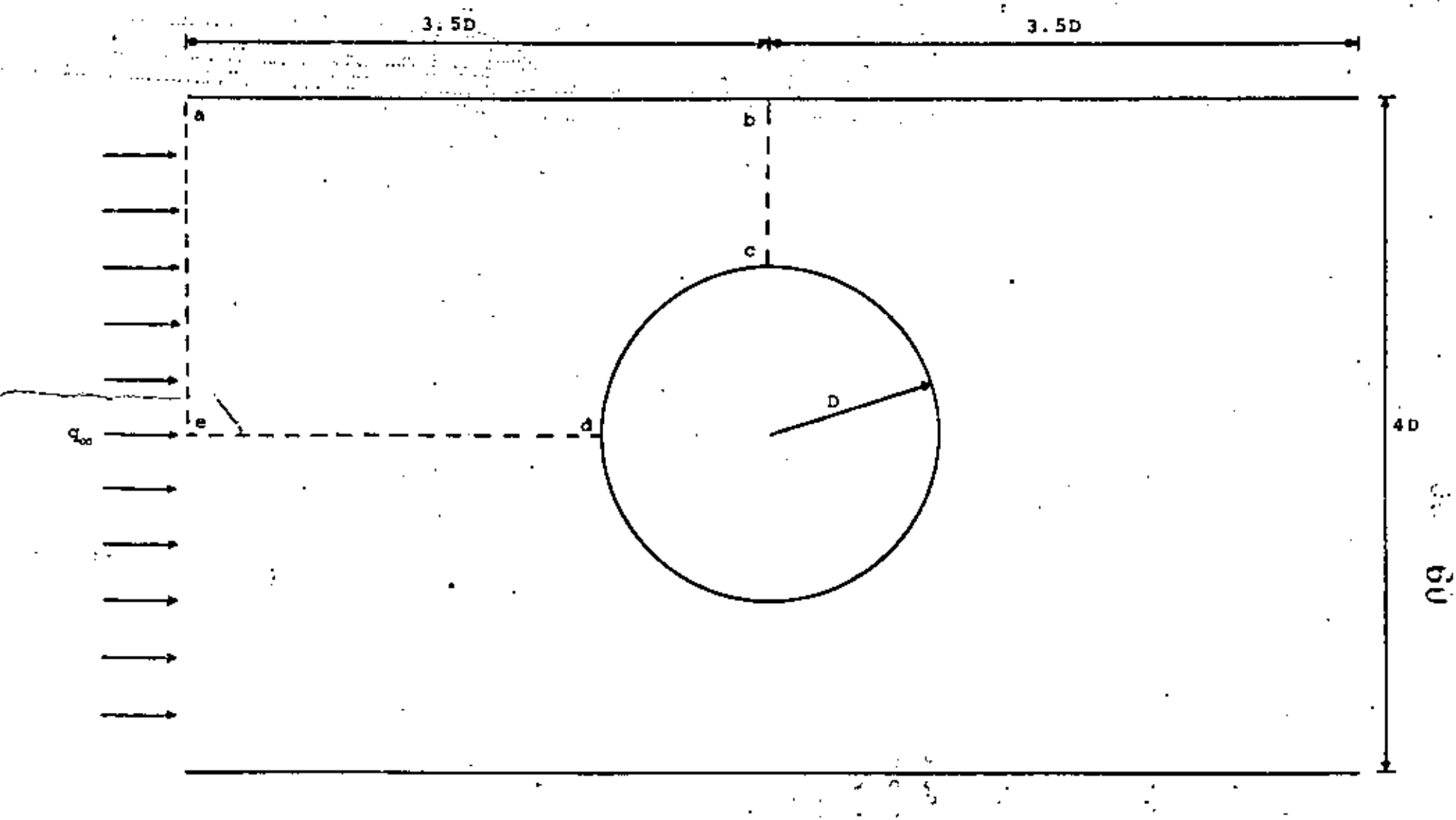

Fig 4.1 Flujo uniforme alrededor de un cilindro entre placas planas.

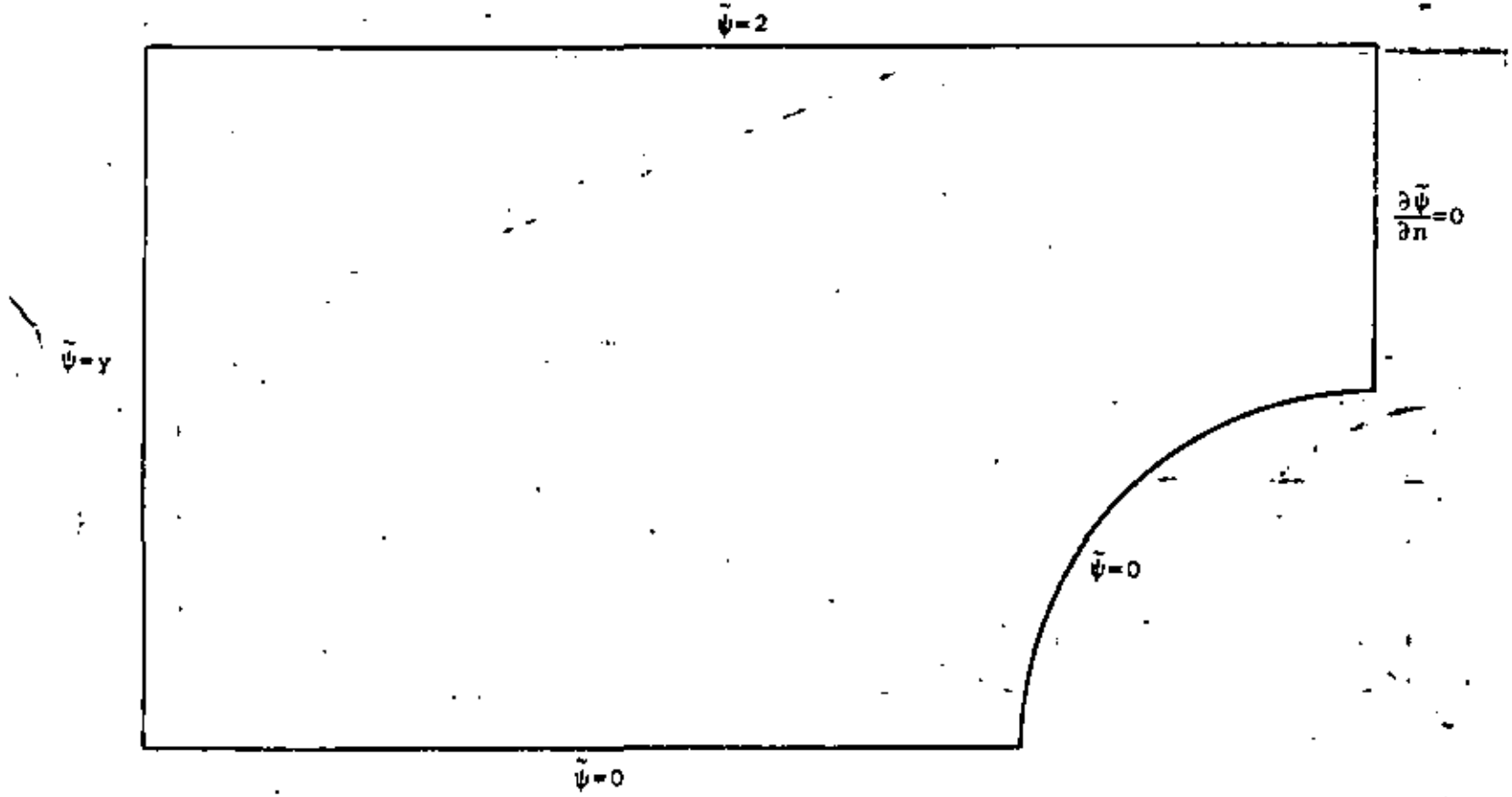

Fig 4.2. Condiciones de frontera.

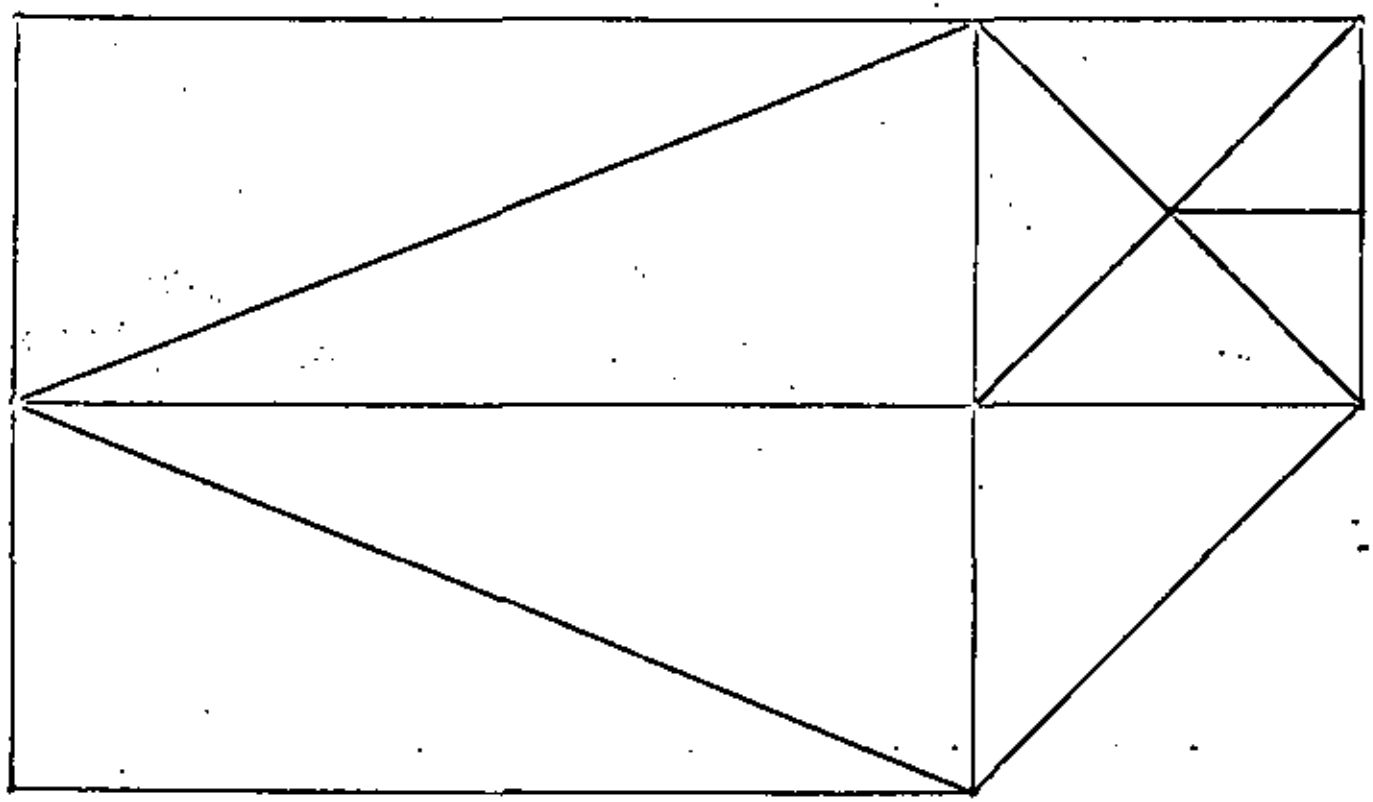

Fig 4.3. Malla gruesa.

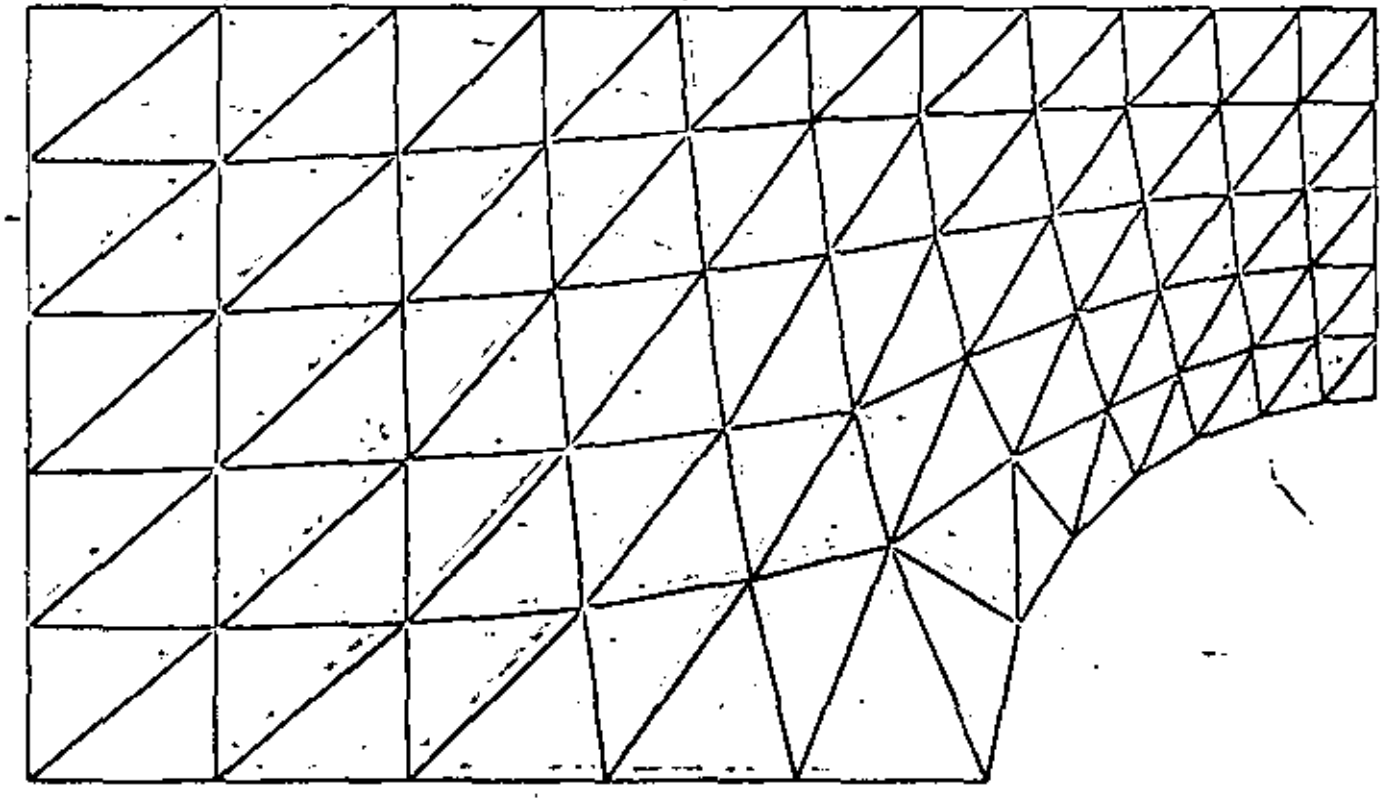

Fig 4.4. Malla Fina.

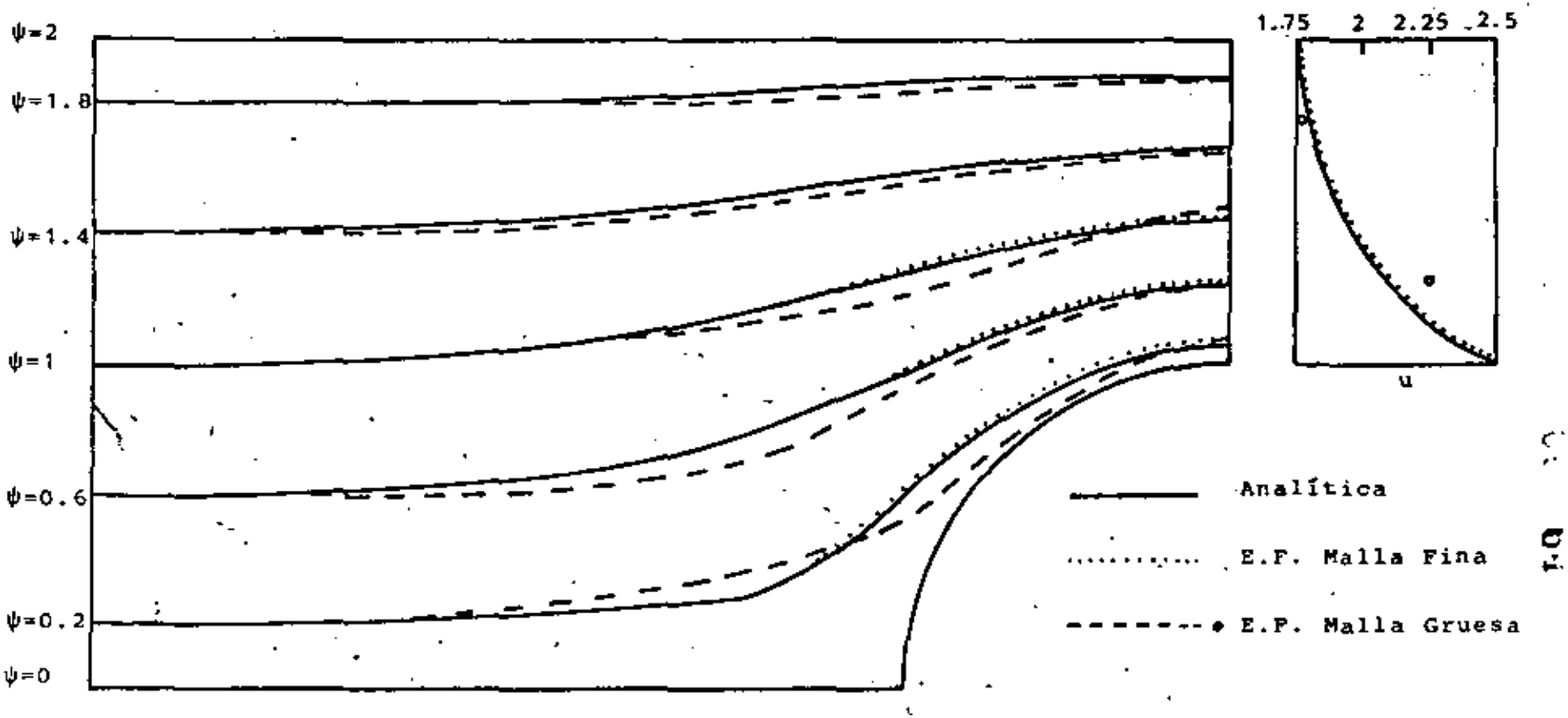

Fig 4.5 Líneas de corriente y variación de la velocidad arriba de la cresta del cilindro.

CAPITULO V
FLUJO POTENCIAL COMPRESIBLE

5.1 GENERAL

Cuando se estudian flujos alrededor de cuerpos sumergidos, normalmente no se pueden resolver las ecuaciones de movimiento en forma analítica, debido a la no linealidad de las mismas, es por ello que en el presente capítulo se estudiará la solución de un flujo potencial compresible subsónico y no viscoso, por medio del método de elementos finitos, usando el método de residuos pesados de tipo Galerkin.

El caso de flujos subsónicos ha sido estudiado principalmente utilizando los principios variacionales (Shen, 1977). Entre los trabajos más importantes se encuentra el de Carey (1975), el cual utiliza un principio variacional, en combinación con una expansión de perturbaciones. Sin embargo, como se muestra en Martín del Campo y Sen (1981), se puede resolver el problema de flujos potenciales más sencillamente, con un método iterativo combinado con el método de elementos finitos. En esta forma se pueden calcular las líneas de corriente y equipotenciales, así como el número de Mach local en cada punto del espacio.

Para ejemplificar, se resolverá el problema de un flujo bidimensional alrededor de un cilindro sin circulación, el cual se encuentra entre dos placas. Este problema puede ser extendido fácilmente a el tratamiento de flujos compresibles alrededor de perfiles aerodinámicos, para lo cual únicamente habría que añadir la circulación.

5.2 PLANTEAMIENTO DE LAS ECUACIONES

Al igual que en el capítulo anterior, ya que lo que se va a tratar es un flujo bidimensional, todos los desarrollos que se hagan a continuación, serán descritos en dos dimensiones.

En primer lugar se plantearán las ecuaciones para un flujo potencial compresible permanente. La ecuación de balance de cantidad de movimiento, para un fluido en estado permanente y no viscoso, está dado por

$$\hat{u}\frac{\partial \hat{u}}{\partial x} + \hat{v}\frac{\partial \hat{u}}{\partial y} = -\frac{1}{\hat{\rho}}\frac{\partial \hat{p}}{\partial x}$$

$$\hat{u}\frac{\partial \hat{v}}{\partial x} + \hat{v}\frac{\partial \hat{v}}{\partial y} = -\frac{1}{\hat{\rho}}\frac{\partial \hat{p}}{\partial y} \qquad (5.1)$$

donde $\hat{u}$ y $\hat{v}$ son las componenetes cartesianas de la velocidad en las direcciones x,y respectivamente, $\hat{\rho}$ es la densidad y $\hat{p}$ la presión. Para un proceso isoentrópico se cumple la siguiente relación

$$\frac{\hat{p}}{\hat{\rho}^{\gamma}} = \text{const} \qquad (5.2)$$

donde γ es la relación de calores específicos, la velocidad del sonido para un gas perfecto está dada por

$$c = \frac{\partial \hat{p}}{\partial \hat{\rho}} = \gamma R\hat{\theta} = \frac{\gamma \hat{p}}{\hat{\rho}} \qquad (5.3)$$

donde R es la constante del gas y $\hat{\theta}$ la temperatura absoluta. Utilizando (5.2) y (5.3) se puede llegar a la siguiente relación

$$\frac{\partial \hat{p}}{\partial x} = \hat{c}^2\frac{\partial \hat{\rho}}{\partial x}$$

$$\frac{\partial \hat{x}}{\partial y} = c^2\frac{\partial \hat{\rho}}{\partial y} \qquad (5.4)$$

que es la ecuación que define la velocidad del sonido, en función de las velocidades y de la relación de calores específicos y $\hat{q}$ es

$$\hat{q} = \hat{u}^2 + \hat{v}^2$$

Multiplicando por $\hat{u}$ la primera ecuación y por $\hat{v}$ la segunda de las ec. (5.5), sumándolas y sustituyendo la ec. (5.6) tenemos

$$\left[1-\left(\frac{\hat{u}}{\hat{c}}\right)^2\right]\frac{\partial \hat{u}}{\partial x} + \left[1-\left(\frac{\hat{v}}{\hat{c}}\right)^2\right]\frac{\partial \hat{v}}{\partial y} - \frac{\hat{u}\hat{v}}{\hat{c}^2}\left(\frac{\partial \hat{u}}{\partial y} + \frac{\partial \hat{v}}{\partial x}\right) = 0 \qquad (5.10)$$

Si a la ec. (5.10) le sumamos y restamos $\frac{\hat{u}\hat{v}}{\hat{c}^2}\frac{\partial \hat{u}}{\partial y}$ y sustituimos la ec. (5.7) llegamos a

$$\left[1-\left(\frac{\hat{u}}{\hat{c}}\right)^2\right]\frac{\partial \hat{u}}{\partial x} + \left[1-\left(\frac{\hat{v}}{\hat{c}}\right)^2\right]\frac{\partial \hat{v}}{\partial y} - \frac{2\hat{u}\hat{v}}{\hat{c}^2}\frac{\partial \hat{u}}{\partial y} = 0 \qquad (5.11)$$

De la ecuación de irrotacionalidad (5.7) se puede definir un potencial de velocidad $\hat{\phi}(x,y)$ que satisface

$$\hat{u} = \frac{\partial \hat{\phi}}{\partial x} \; ; \; \hat{v} = \frac{\partial \hat{\phi}}{\partial y} \qquad (5.12)$$

Sustituyendo (5.12) en (5.11) se obtiene

$$\left[1-\frac{1}{\hat{c}^2}\left(\frac{\partial \hat{\phi}}{\partial x}\right)^2\right]\frac{\partial^2 \hat{\phi}}{\partial x^2} + \left[1-\frac{1}{\hat{c}^2}\left(\frac{\partial \hat{\phi}}{\partial y}\right)^2\right]\frac{\partial^2 \hat{\phi}}{\partial x^2} - \frac{2}{\hat{c}^2}\frac{\partial \hat{\phi}}{\partial x}\frac{\partial \hat{\phi}}{\partial y}\frac{\partial^2 \hat{\phi}}{\partial x \partial y} = 0 \qquad (5.13)$$

Sustituyendo (5.4) en (5.1) tenemos

$$\hat{u}\frac{\partial \hat{u}}{\partial x} + \hat{v}\frac{\partial \hat{u}}{\partial y} + \frac{\hat{c}^2}{\hat{\rho}}\frac{\partial \hat{\rho}}{\partial x} = 0$$

$$\hat{u}\frac{\partial \hat{v}}{\partial x} + \hat{v}\frac{\partial \hat{v}}{\partial y} + \frac{\hat{c}^2}{\hat{\rho}}\frac{\partial \hat{\rho}}{\partial y} = 0 \qquad (5.5)$$

que es la ecuación de balance de cantidad de movimiento en función de la densidad y la velocidad del sonido. La ecuación de conservación de masa para un fluido compresible es

$$\hat{u}\frac{\partial \hat{\rho}}{\partial x} + \hat{v}\frac{\partial \hat{\rho}}{\partial y} + \hat{\rho}\left(\frac{\partial \hat{u}}{\partial x} + \frac{\partial \hat{v}}{\partial y}\right) = 0 \qquad (5.6)$$

Un flujo bidimensional e irrotacional debe cumplir la siguiente condición

$$\frac{\partial \hat{v}}{\partial x} - \frac{\partial \hat{u}}{\partial y} = 0 \qquad (5.7)$$

Finalmente la ecuación de la energía es

$$\hat{h}^2 + \frac{1}{2}\hat{q}^2 = h_\infty + \frac{1}{2}q_\infty^2 \qquad (5.8)$$

donde $\hat{h}$ es la entalpía específica, el subíndice ∞ indica condiciones alejadas del cuerpo sumergido. De las ecuaciones (5.3) y (5.8) se obtiene, para un gas peferfecto

$$\hat{c}^2 = c_\infty^2 + \left(\frac{\gamma-1}{2}\right)(q_\infty^2 - \hat{q}^2) \qquad (5.9)$$

Las ecuaciones (5.9) y (5.13) forman un sistema acoplado en la incognita $\hat{\phi}(x,y)$. Definiendo las siguientes variables adimensionales

$$x = \frac{\hat{x}}{D} \; ; \; y = \frac{\hat{y}}{D} \; ; \; \tilde{\phi} = \frac{\hat{\phi}}{Dq_\infty} ; \qquad (5.14)$$

$$c = \frac{\hat{c}}{c_\infty} \; ; \; q = \frac{\hat{q}}{q_\infty}$$

donde D es una distancia característica, las ecuaciones (5.9) y (5.13) transforman

$$\frac{\partial^2 \tilde{\phi}}{\partial x^2} + \frac{\partial^2 \phi}{\partial y^2} = \frac{M_\infty^2}{c^2}\left[\left(\frac{\partial \tilde{\phi}}{\partial x}\right)^2 \frac{\partial^2 \tilde{\phi}}{\partial x^2} + 2\frac{\partial \tilde{\phi}}{\partial x}\frac{\partial \tilde{\phi}}{\partial y}\frac{\partial^2 \tilde{\phi}}{\partial x \partial y} + \left(\frac{\partial \tilde{\phi}}{\partial y}\right)^2 \frac{\partial^2 \tilde{\phi}}{\partial y}\right] \qquad (5.15)$$

$$c^2 = 1 + \left(\frac{\gamma-1}{2}\right) M_\infty^2 \left[1 - \left(\frac{\partial \tilde{\phi}}{\partial x}\right)^2 - \left(\frac{\partial \tilde{\phi}}{\partial y}\right)^2\right] \qquad (5.16)$$

donde $M_\infty = \frac{q_\infty}{c_\infty}$. M_∞ es el número de Mach alejado del cilindro.

En seguida se procede a obtener la ecuación para la función de corriente. De la ecuación de conservación de masa (5.6) podemos definir una función de corriente $\hat{\psi}(x,y)$ que satisface

$$u = \frac{\rho_\infty}{\hat{\rho}} \frac{\partial \hat{\psi}}{\partial \hat{y}} \; ; \; v = -\frac{\rho_\infty}{\hat{\rho}} \frac{\partial \psi}{\partial x} \qquad (5.17)$$

sustituyendo (5.17) en la condición de irrotacionalidad (5.7) llegamos a

$$\frac{\partial^2 \hat{\psi}}{\partial \hat{x}^2} + \frac{\partial^2 \hat{\psi}}{\partial \hat{y}^2} = \frac{1}{\hat{\rho}}\left(\frac{\partial \hat{\rho}}{\partial \hat{x}}\frac{\partial \hat{\psi}}{\partial \hat{x}} + \frac{\partial \hat{\rho}}{\partial \hat{y}}\frac{\partial \hat{\psi}}{\partial \hat{y}}\right) \qquad (5.18)$$

5.3 FORMULACION DE ELEMENTOS FINITOS

Para el potencial de velocidad $\tilde{\phi}(x,y)$, escribimos la ec. (5.15) como una ecuación de poisson de la siguiente forma

$$\frac{\partial^2\tilde{\phi}}{\partial x^2} + \frac{\partial^2\tilde{\phi}}{\partial y^2} - \tilde{g}(\tilde{\phi}) = 0 \qquad (5.23)$$

donde

$$\tilde{g}(\tilde{\phi}) = \frac{M_\infty^2}{c^2}\left[(\frac{\partial\tilde{\phi}}{\partial x})^2 \frac{\partial^2\tilde{\phi}}{\partial x^2} + 2\,\frac{\partial\tilde{\phi}}{\partial x}\,\frac{\partial\tilde{\phi}}{\partial y}\,\frac{\partial^2\tilde{\phi}}{\partial x\,\partial y} + (\frac{\tilde{\phi}}{\partial y})^2 \frac{\partial^2\tilde{\phi}}{\partial y^2}\right] \qquad (5.24)$$

Haciendo la aproximación para un elemento

$$\tilde{\phi}(x,y) \simeq \phi(x,y) = \sum_{i=1}^{n} N_i \phi_i \qquad (5.25)$$

donde ϕ es la función aproximada y N_i son las funciones de interpolación de un elemento, n el número de nodos del elemento y ϕ_i es el valor de la función en cada nodo. Sustituyendo (5.25) en (5.23) se obtiene un residuo.

$$\frac{\partial^2\phi}{\partial x^2} + \frac{\partial^2\phi}{\partial y^2} - \tilde{g} = \epsilon \qquad (5.25)$$

Se hace el residuo ortogonal a las funciones de interpolación tal que

$$(\epsilon, N_i) = \int_\Omega (\frac{\partial^2\phi}{\partial x^2} + \frac{\partial^2\phi}{\partial y^2} - \tilde{g}) N_i \, dx\,dy = 0 \qquad (5.26)$$

donde Ω es el dominio del elemento. Tomando la siguiente aproximación

Esta ecuación, aparte de no ser lineal, tiene dos incógnitas $\hat{\psi}$ y $\hat{\rho}$. De las ec. (5.5) podemos despejar los términos $\frac{1}{\rho}\frac{\partial \hat{\rho}}{\partial \hat{y}}$ y sustituirlos en (5.18) con lo se obtiene

$$\frac{\partial^2 \hat{\psi}}{\partial \hat{x}^2} + \frac{\partial^2 \hat{\psi}}{\partial \hat{y}^2} = -\frac{1}{c^2}\left(\hat{u}\frac{\partial \hat{u}}{\partial \hat{x}}\frac{\partial \hat{\psi}}{\partial \hat{x}} + \hat{v}\frac{\partial \hat{u}}{\partial \hat{y}}\frac{\partial \hat{\psi}}{\partial \hat{x}} + u\frac{\partial \hat{v}}{\partial \hat{x}}\frac{\partial \hat{\psi}}{\partial \hat{y}} + \hat{v}\frac{\partial \hat{v}}{\partial \hat{y}}\frac{\partial \hat{\psi}}{\partial \hat{y}}\right) \quad (5.19)$$

Otra vez, sería muy difícil resolver esta ecuación, ya que ahora está en función de las velocidades que no conocemos. Sin embargo si sustituimos el potencial de velocidad en lugar de las velocidades, (5.12) en (5.19),

$$\frac{\partial^2 \hat{\psi}}{\partial \hat{x}^2} + \frac{\partial^2 \hat{\psi}}{\partial \hat{y}^2} = -\frac{1}{c^2}\left(\frac{\partial \hat{\phi}}{\partial \hat{x}}\frac{\partial^2 \hat{\phi}}{\partial \hat{x}^2}\frac{\partial \hat{\psi}}{\partial \hat{x}} + \frac{\partial \hat{\phi}}{\partial \hat{y}}\frac{\partial^2 \hat{\phi}}{\partial \hat{x}\partial \hat{y}}\frac{\partial \hat{\psi}}{\partial \hat{x}}\right.$$

$$\left. + \frac{\partial \hat{\phi}}{\partial \hat{x}}\frac{\partial^2 \hat{\phi}}{\partial \hat{x}\partial \hat{y}}\frac{\partial \hat{\psi}}{\partial \hat{y}} + \frac{\partial \hat{\phi}}{\partial \hat{y}}\frac{\partial^2 \hat{\phi}}{\partial \hat{y}^2}\frac{\partial \hat{\psi}}{\partial \hat{y}}\right) \quad (5.20)$$

nos queda una ecuación de la función de corriente en términos del potencial de velocidad, el cual podemos calcular de la ec. (5.15), al igual que la velocidad del sonido de la ec. (5.16), Definiendo las siguientes variables adimensionales

$$x = \frac{\hat{x}}{D}\,;\quad y = \frac{\hat{y}}{D}\,;\quad \tilde{\psi} = \frac{\hat{\psi}}{Dq_\infty}\,;$$

$$\tilde{\phi} = \frac{\hat{\phi}}{Dq_\infty}\,;\quad c = \frac{\hat{c}}{c_\infty}. \quad (5.21)$$

y sustituyéndolas en (5.20), se tiene

$$\frac{\partial^2 \tilde{\psi}}{\partial x^2} + \frac{\partial^2 \tilde{\psi}}{\partial y^2} = -\frac{M_\infty^2}{c^2}\left(\frac{\partial \tilde{\phi}}{\partial x}\frac{\partial^2 \tilde{\phi}}{\partial x^2}\frac{\partial \tilde{\psi}}{\partial x} + \frac{\partial \tilde{\phi}}{\partial y}\frac{\partial^2 \tilde{\phi}}{\partial x \partial y}\frac{\partial \tilde{\psi}}{\partial x}\right.$$

$$\left. + \frac{\partial \tilde{\phi}}{\partial x}\frac{\partial^2 \tilde{\phi}}{\partial x \partial y}\frac{\partial \tilde{\psi}}{\partial y} + \frac{\partial \tilde{\phi}}{\partial y}\frac{\partial^2 \tilde{\phi}}{\partial y^2}\frac{\partial \tilde{\psi}}{\partial y}\right) \quad (5.20)$$

$$\tilde{g} = g = \sum_{j=1}^{n} N_j g_j \tag{5.27}$$

y aplicando el teorema de Green a (5.26) resulta

$$\phi_j \int_\Omega \left(\frac{\partial N_i}{\partial x}\frac{\partial N_j}{\partial x} + \frac{\partial N_i}{\partial y}\frac{\partial N_j}{\partial y}\right) dxdy = \int_\Gamma \left(\frac{\partial \phi}{\partial x} N_i dy - \frac{\partial \phi}{\partial y} N_i dx\right)$$

$$- g_j \int_\Omega N_i N_j dxdy \tag{5.28}$$

Usando notación simplificada escribimos

$$\sum_{j=1}^{m} A^*_{ij}\, \phi_j = f^*_i + t^*_i \quad (i=1,2,\ldots,m) \tag{5.29}$$

A^* es la matriz de coeficientes, f^* es el vector de flujo t^* es el vector que representa los términos no lineales y son

$$A_{ij} = \int_\Omega \left(\frac{\partial N_i}{\partial x}\frac{\partial N_j}{\partial x} + \frac{\partial N_i}{\partial y}\frac{\partial N_j}{\partial y}\right) dxdy \tag{5.30}$$

$$f_i = \int \left(\frac{\partial \phi}{\partial x} N_i dy - \frac{\partial \phi}{\partial y} N_i dx\right) \tag{5.31}$$

$$t_i = -g_j \int_\Omega N_i N_j d\Omega \tag{5.32}$$

El vector g se obtiene sustituyendo (5.25) en (5.24) como

$$g_j=\frac{M_\infty^2}{c^2}\left[(\phi_i\frac{\partial N_i}{\partial x})^2\,\phi_j\frac{\partial^2 N_j}{\partial x^2} + 2(\phi_i\frac{\partial N_i}{\partial x})(\phi_j\frac{\partial N_j}{\partial y_i})(\phi_k\frac{\partial^2 N_k}{\partial x\partial y}) + (\phi_i\frac{\partial N_i}{\partial y})^2\,\phi_j\frac{\partial^2 N_j}{\partial y^2}\right] \qquad (5.33)$$

y la velocidad del sonido

$$c^2=1+(\frac{\gamma-1}{2})M_\infty^2\left[1-(\phi_i\frac{\partial N_i}{\partial x})^2-(\phi_i\frac{\partial N_i}{\partial y})^2\right] \qquad (5.34)$$

A continuación se ensamblan las ecuaciones de todos los elementos obtenidos

$$\sum_{j=1}^{m} A^*_{ij}\phi^*_j=f^*_i+t^*_i \quad (i=1,2,\ldots,m) \qquad (5.35)$$

Ya que el vector t de la ec. (5.35) está en función de los valores del potencial de velocidad en los nodos, esta ecuación se resuelve por medio de iteraciones, para lo cual en la primera iteración se resuelve

$$A^*\phi = f^* \qquad (5.36)$$

Para $M_\infty=0$. Los valores obtenidos de $\phi(x,y)$ se sustituyen en el vector t de (5.35) y se resuelve la ecuación obteniéndose con ella nuevos valores de $\phi(x,y)$, los que se utilizan en la siguiente iteración. Así sucesivamente, hasta que la diferencia del valor anterior y el nuevo sea menor que una cierta magnitud.

Para la formulación de la función de corriente, se sigue un procedimiento similar al utilizado en el potencial de velocidad, llegando a

$$\sum_{j=1}^{n} A_{ij}\psi_j = \delta_i + \delta_i \qquad (i,1,2,\ldots,n) \tag{5.37}$$

y el vector δ se obtiene a partir de

$$\delta_i = \ell_j \int_{\Omega} N_i N_j \, dxdy \tag{5.38}$$

donde ℓ esta dado por

$$\ell_j = \frac{-M_\infty^2}{c^2}\left[(\phi_i \frac{\partial N_i}{\partial x})(\phi_j \frac{\partial^2 N_j}{\partial x^2})(\psi_k \frac{\partial N_k}{\partial x}) + (\phi_i \frac{\partial N_i}{\partial y})(\phi_j \frac{\partial^2 N_j}{\partial x \partial y})(\phi_k \frac{\partial N_k}{\partial x})\right.$$

$$\left. + (\phi_i \frac{\partial N_i}{\partial x})(\phi_j \frac{\partial^2 N_j}{\partial x \partial y})(\psi_k \frac{\partial N_k}{\partial y}) + (\phi_i \frac{\partial N_i}{\partial y})(\phi_j \frac{\partial^2 N_j}{\partial y^2})(\psi_k \frac{\partial N_k}{\partial y})\right] \tag{5.39}$$

donde c^2 se obtiene de la misma forma que en la ec. (5.34). Al igual que para el potencial de velocidad, se efectúa un ensamble de todas las matrices de los elementos (5.37), para obtener la matriz global de coeficientes, lo que se representa

$$A^* \psi = \delta^* + \delta^* \tag{5.40}$$

En este caso el vector δ^* de la ec. (5.40) está en función de los valores del potencial de velocidad y de la función de corriente en los nodos, sin embargo los primeros ya se conocen de la solución de la ec. (5.35), por lo que se pueden sustitutir aquí, quedando la ecuación únicamente en función de $\psi(x,y)$. Nuevamente se utiliza un método de iteraciones,

igual al usado en el potencial de velocidad para encontrar $\psi(x,y)$.

5.4 SOLUCION Y RESULTADOS

El problema específico escogido como ejemplo, es el del flujo uniforme alrededor de un cilindro de radio D, entre placas planas separadas por un distancia 2 H y se supone que el flujo uniforme se encuentra a una distancia 3.5D del centro del cilindro Fig.5.1. Por la simetría del flujo, se puede tomar para el cálculo solamente un cuadrante del dominio total.

Las condiciones de frontera, tanto para el potencial de velocidad como para la función de corriente, se muestran en la Fig. 5.2.

Para la discretización del dominio se utilizan elementos triangulares. Las funciones de interpolación para cada elemento son cuadráticas, para poder sustituirlas en las ec. (5.33) y (5.39), ya que de menor grado se anularían. Es por ello que cada elemento tiene 6 nodos uno por cada función de interpolación, las cuales son

$$\begin{aligned} N_1 &= 2L_1 - L_1 & N_4 &= 4L_1 L_2 \\ N_2 &= 2L_2 - L_2 & N_5 &= 4L_2 L_3 \\ N_3 &= 2L_3 - L_3 & N_6 &= 4L_3 L_1 \end{aligned} \qquad (5.41)$$

donde L_1, L_2, L_3 son las coordenadas de área y su relación con las coordendas cartesianas de

$$L_i = a_i + b_i x + c_i y \qquad (5.42)$$

donde las constantes a_i, b_i, c_i están definidas por la ec. (3.23). Se utilizan coordenadas de área por su facilidad al efectuar operaciones, así por ejemplo las derivadas de las funciones de

interpolación se obtienen por la regla de la cadena como

$$\frac{\partial N_i}{\partial x} = \frac{\partial N_i}{\partial L_1}\frac{\partial L_1}{\partial x} + \frac{\partial N_i}{\partial L_2}\frac{\partial L_2}{\partial x} + \frac{\partial N_i}{\partial L_3}\frac{\partial L_3}{\partial x}$$

$$\frac{\partial N_i}{\partial y} = \frac{\partial N_i}{\partial L_2}\frac{\partial L_2}{\partial y} + \frac{\partial N_i}{\partial L_2}\frac{\partial L_2}{\partial y} + \frac{\partial N_i}{\partial L_3}\frac{\partial L_3}{\partial y} \qquad (5.43)$$

y las integralaes que aparecen en las ecuaciones se resulven a través de

$$\int_\Omega L_1^n\, L_2^m\, L_3^p\, dxdy = 2\Delta\, \frac{n!m!p!}{(n+m+p+2)!} \qquad (3.44)$$

donde Δ es el área del elemento triangular.

Se realizó un programa de computación que calcula las matrices y vectores de elementos finitos y también efectúa las iteraciones. Para el potencial de velocidad, primero se generan las matrices de coeficientes A de cada elemento, mismas que se ensamblan en la matriz global A^*. Se calcula la integrla (5.31) utilizando las condiciones de frontera del tipo Neumann y estas ya ensambladas forman el vector global f^*. El vector t^* se calcula con los valores obtenidos de ϕ en la iteración anterior. Las condiciones de frontera del tipo Dirichlet se sustituyen en el sistema de ecuaciones (5.29), con lo que se reduce la matriz global a únicamente el número de incognitas y se resuelve, obteniéndose nuevos valores de ϕ. La matriz A^* y el vector f^* únicamente se calculan una vez, ya que son los mismos para cada iteración, lo único que cambia es el vector t^*, en el cual se introducen los nuevos valores de ϕ, hasta que haya una convergencia dentro de una magnitud predoterminada. En el pos-

procesamiento se interpola cuadráticamente dentro de cada elemento, para obtener las coordenadas de las líneas equipotenciales.

El programa para la función de corriente sigue un procedimiento similar al anterior. La matriz A de la ec. (5.40) es la misma que la del potencial de velocidad, ya que ésta depende únicamente de la malla y las funciones de interpolación que se utilicen. En el vector ϕ^* se utilizan los valores ϕ obtenidos en el programa anterior.

El dominio primero se discretiza con una malla gruesa, como muestra la Fig. 5.3, la cual tiene 10 elementos y 28 nodos. Esto tiene dos finalidades: La primera probar y corregir el programa de computación y la segunda observar donde se encuentran las zonas de mayor variación, para hacer una mejor discretización.

La Fig. 5.4 muestra una malla más fina con 37 elementos y 92 nodos, la que se realizó tomando en cuenta los resultados obtenidos por la malla anterior.

En la Fig 5.5 se presentan las lineas de corriente para las dos mallas en el caso de flujo incompresble. En las Figurs 5.6, 5.7 y 5.8 se muestran las líneas de corriente y equipotenciales para números de Mach 0.1, 0.2 y 0.3 respectivamente, obtenidos con la malla fina. Estas figuras también indican la variación del número de Mach local, sobre la cresta del cilindro.

Se observa una diferencia entre el caso de flujo incompresible comparado con el flujo compresible y esta diferencia es notable para altos números de Mach. Se nota también que en el caso de flujo compresible, el número de Mach aumenta al acercarce al cilindro. Esto puede presentar problemas para un porfil aerodinámico si el número de Mach local se acercara a la unidad.

Para bajos números de Mach, se necesitan pocas iteraciones para la convergencia, como muestra la siguiente tabla:

M_∞	ERMC	Interaciones para ϕ	Iteraciones para ψ
0.1	0.0001	4	3
0.2	0.0001	9	3
0.3	0.0001	20	3

La función de corriente necesita menos iteraciones para converger, ya que se parte de valores exactos obtenidos del potencial de velocidad.

Para la malla gruesa se logra convergencia hasta para número de Mach 0.5, sin embargo los resultados obtenidos para este número, no son confiables, debido a lo grueso de la discretización, es por ello que no se presentan.

Por último las soluciones numéricas demuestran la utilidad del método de elementos finitos de Galerkin, en combinación con un método iterativo, en la solución de problemas de flujo potencial subsónico.

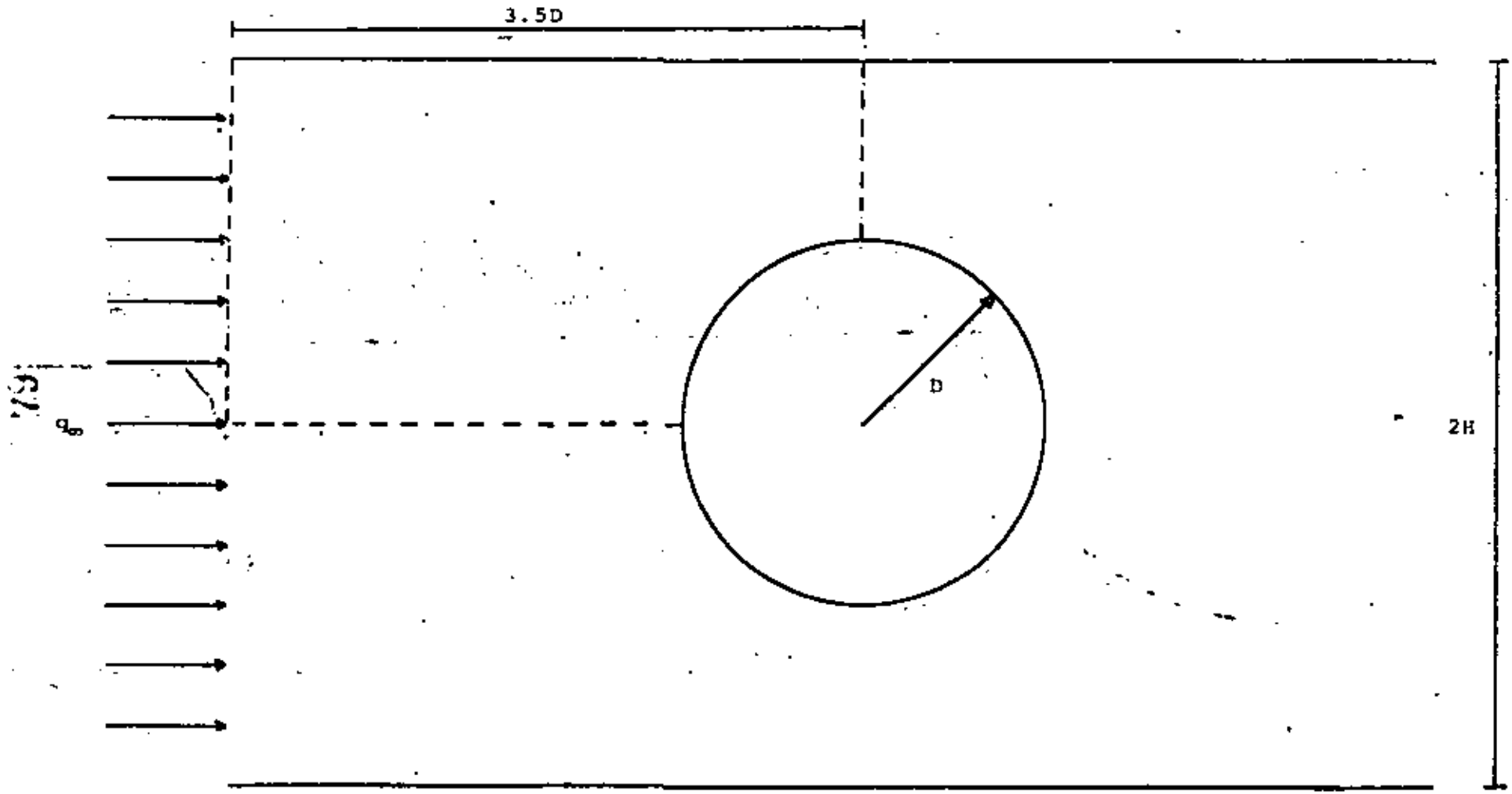

Fig 5.1. Flujo compresible alrededor de un cilindro entre placas planas.

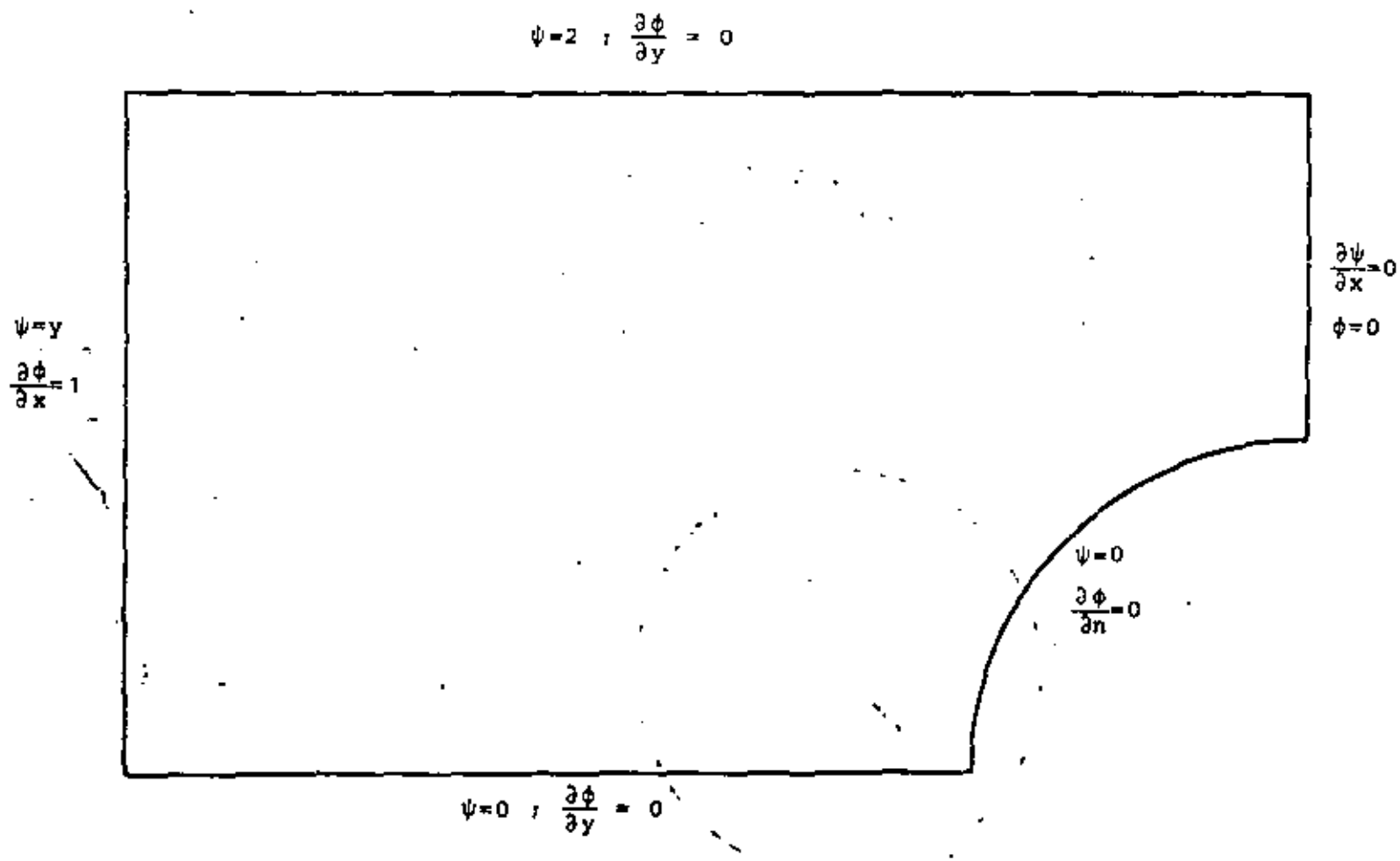

Fig 5.2. Condiciones de frontera.

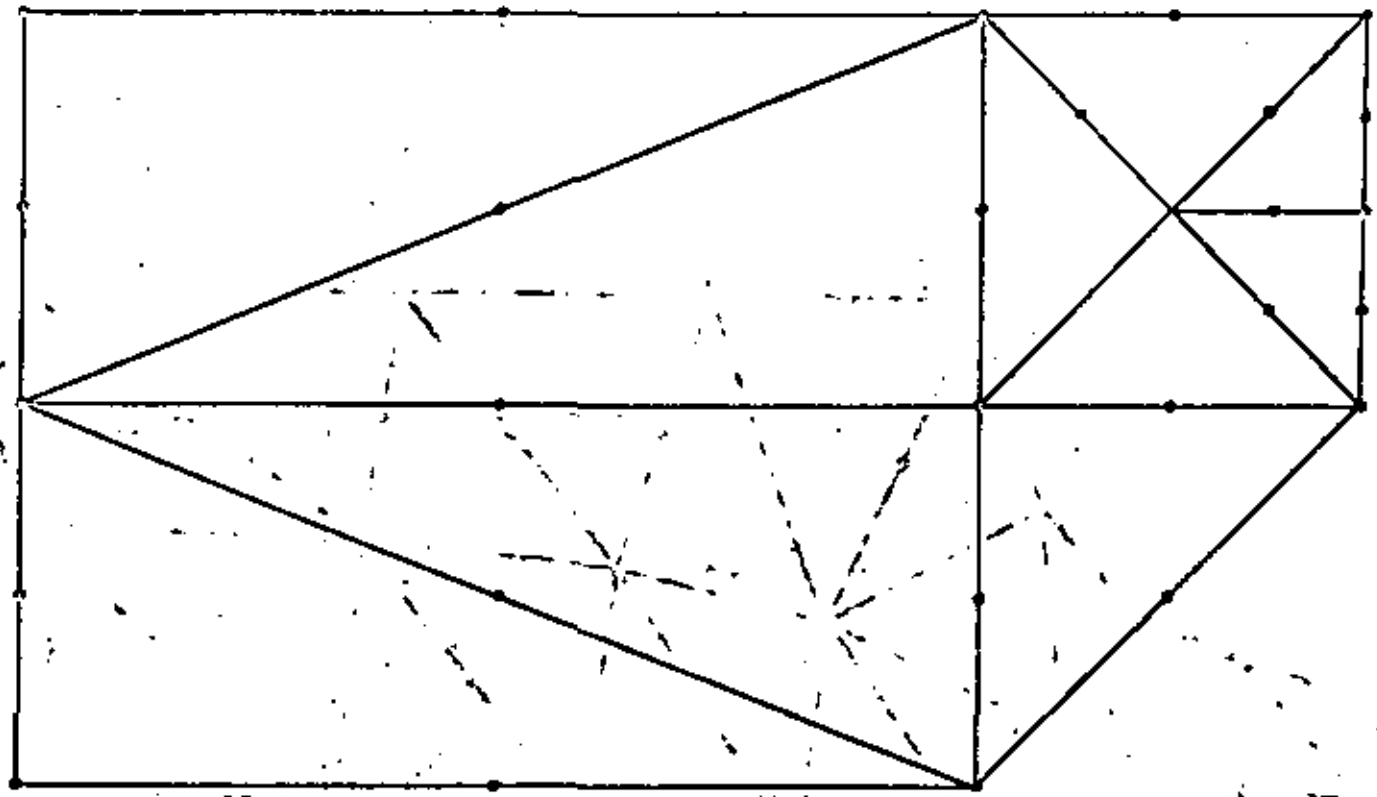

Fig 5.3. Malla gruesa con sus nodos.

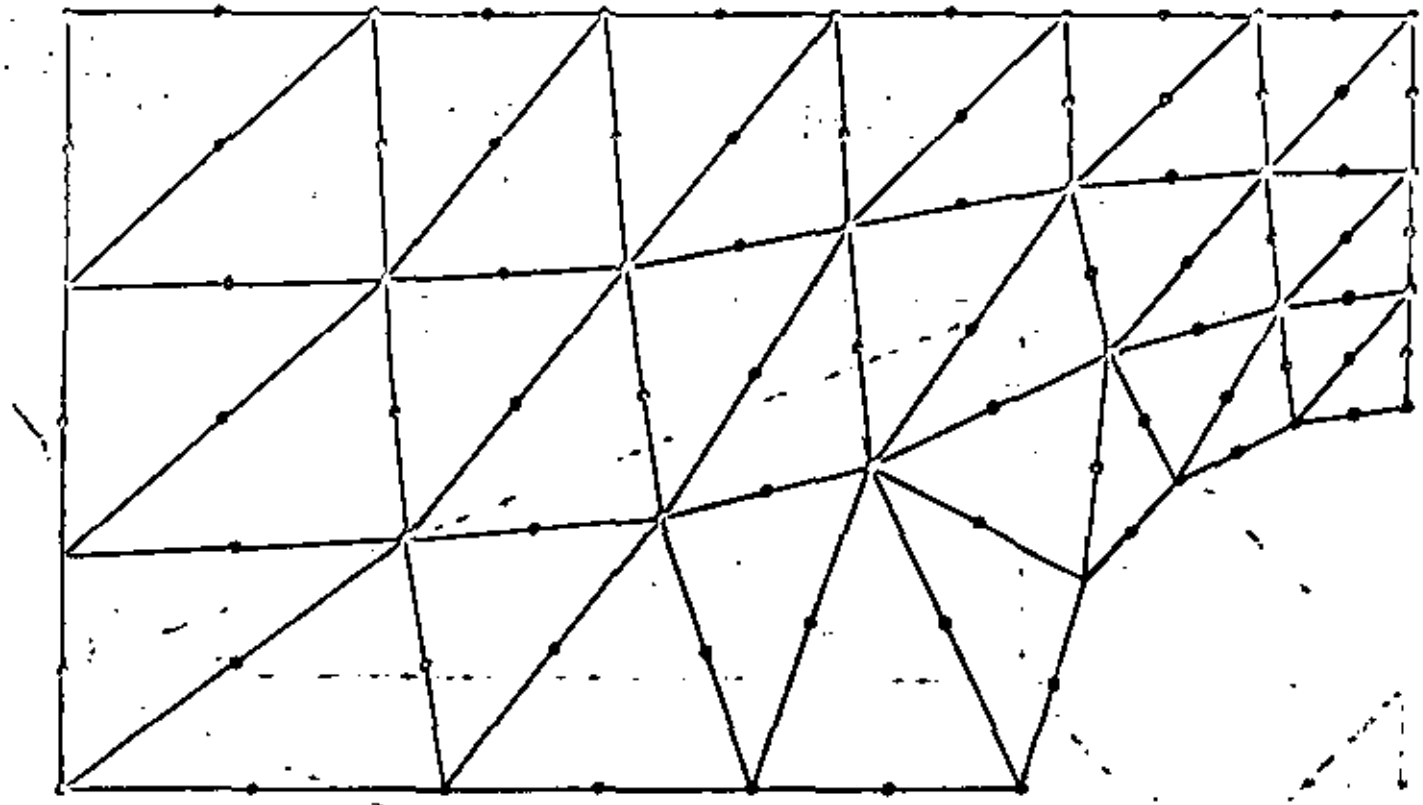

Fig 5.4. Malla fina con sus nodos.

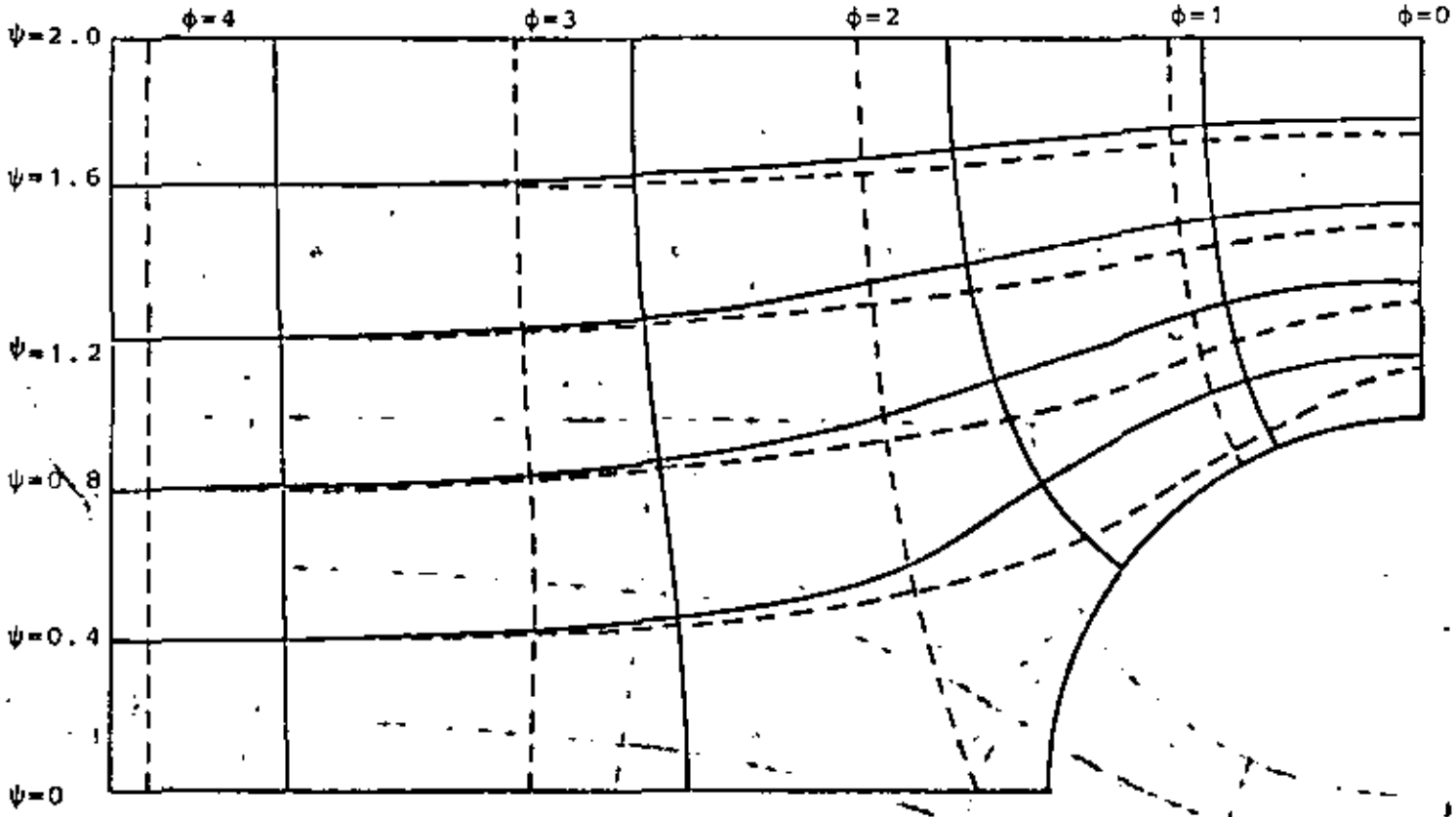

Fig 5.5 Líneas de corriente para las dos mallas, M_∞=0, Línea punteada malla gruesa, Línea continua: Malla fina.

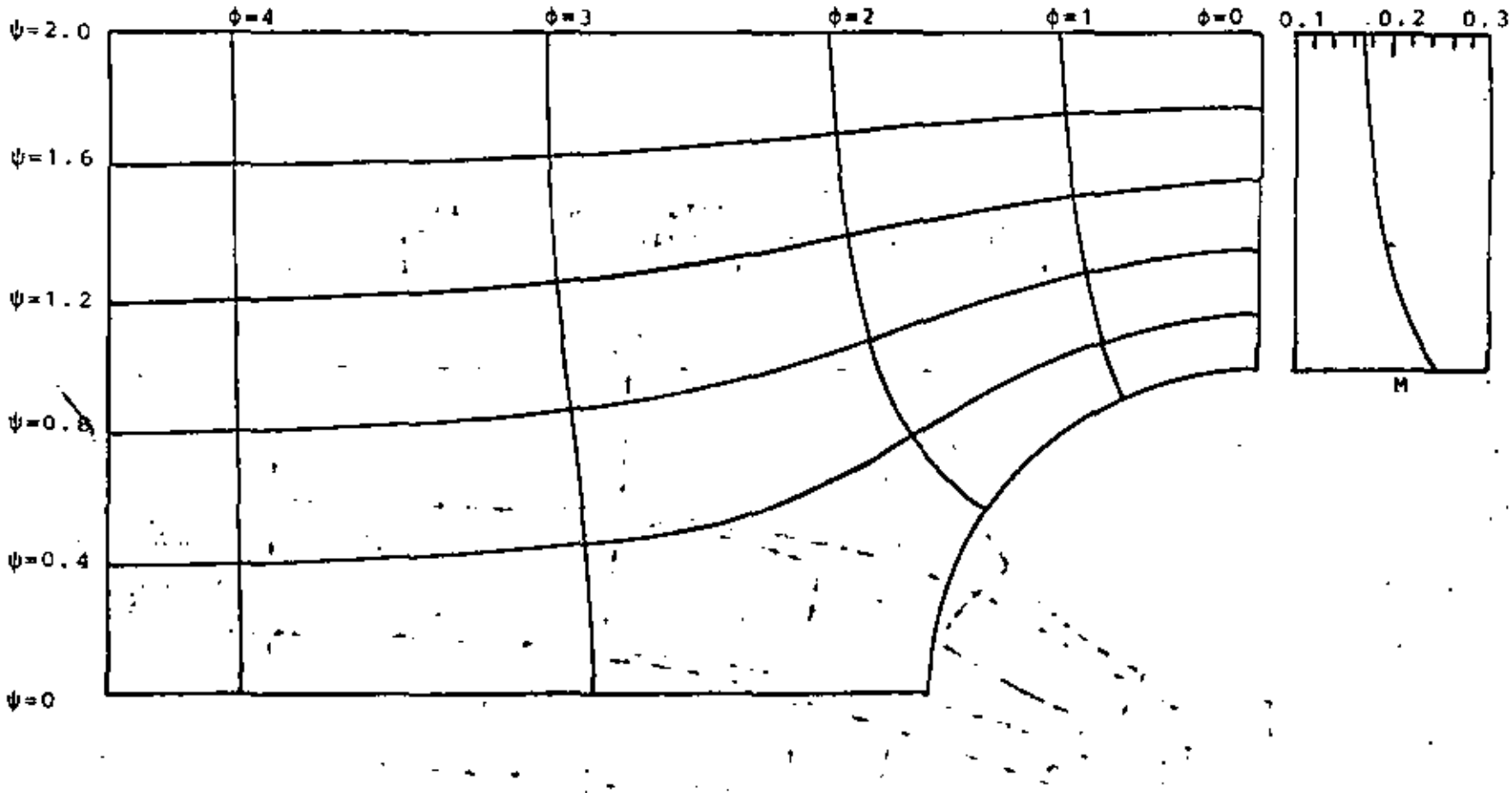

Fig 5.6. Líneas equipotenciales y líneas de corriente para M=0.1 y variación del número de Mach local en la cresta del cilindro.

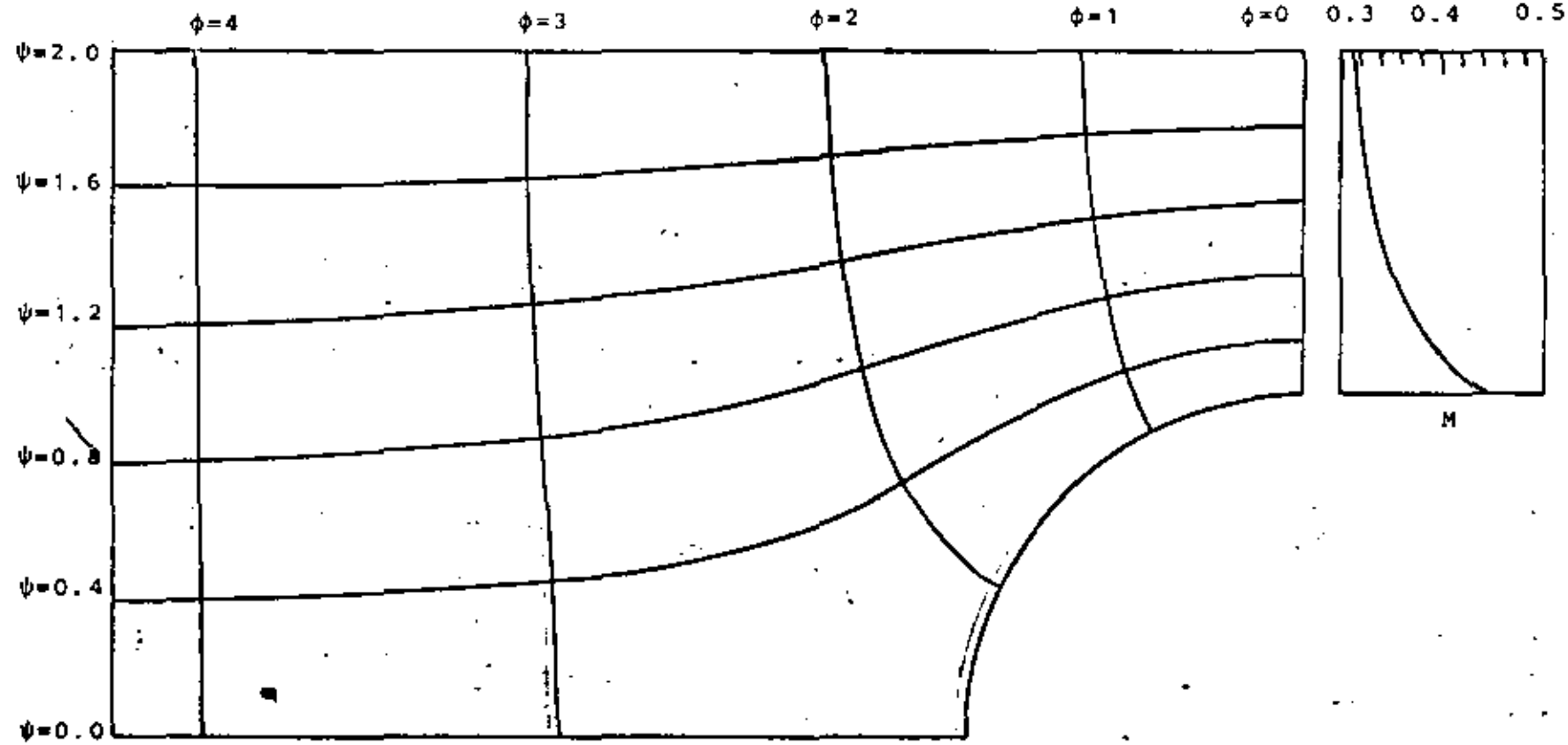

Fig 5.7. Líneas equipotenciales y líneas de corriente para M=0.2 y variación del número de Mach local en la cresta del cilindro.

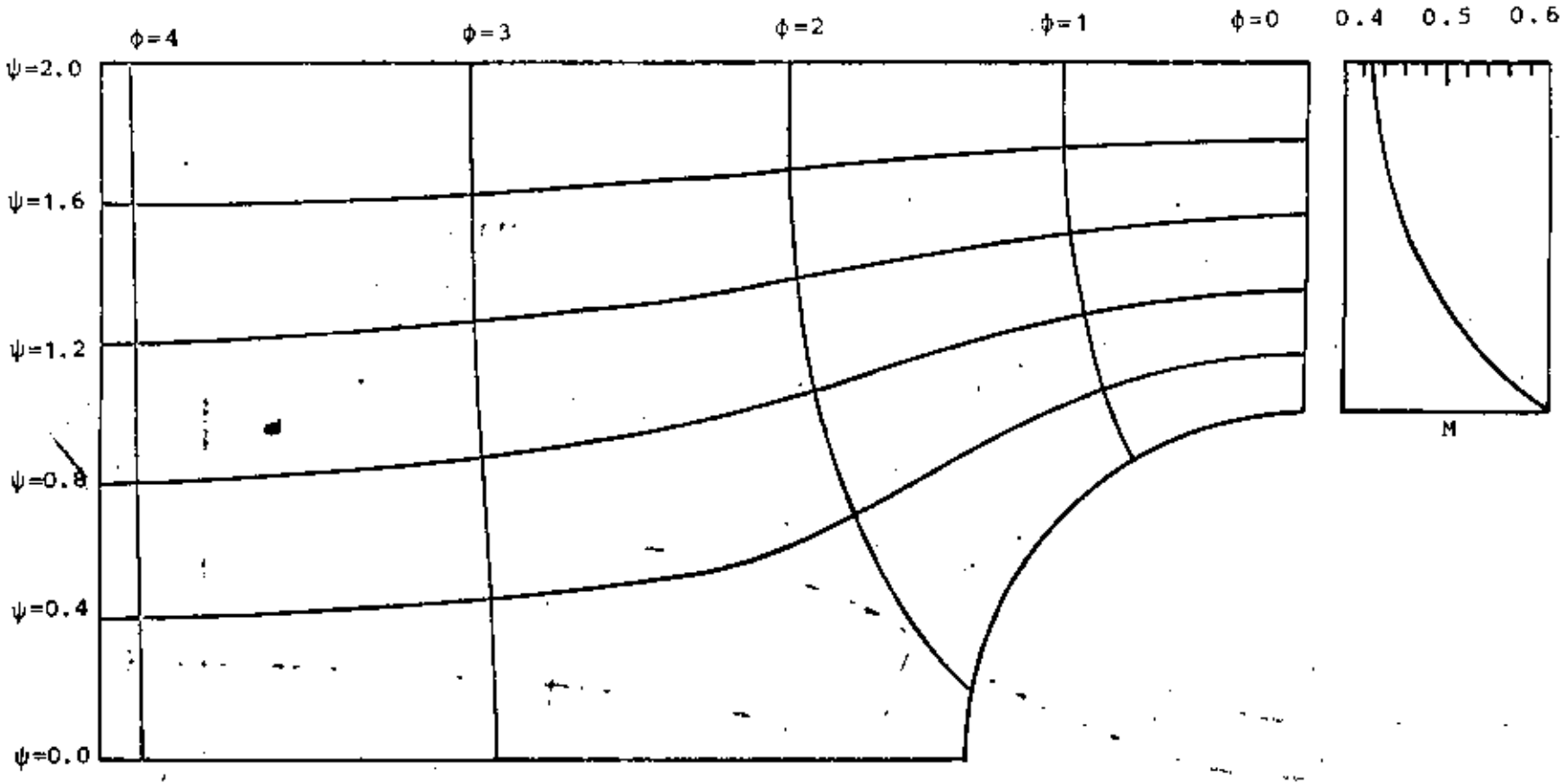

δυ

Fig 5.8. Líneas equipotenciales y líneas de corriente para M=0.3 y variación del número de Mach local en la cresta del cilindro.

DIVISION DE EDUCACION CONTINUA
FACULTAD DE INGENIERIA U.N.A.M.

EL METODO DEL ELEMENTO FINITO EN LA INGENIERIA MECANICA

APLICACIONES: ANALISIS ESTATICO

DR. JORGE ANGELES ALVAREZ

ABRIL 1982

Twist & MAX TORSION. PROBLEM

MS SPLINE DRIVER

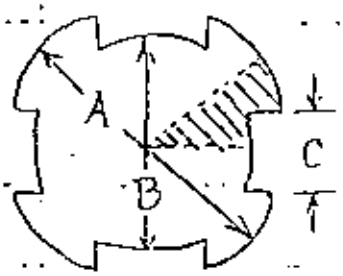

C/B	θ	τ_{max} N/cm²	V	f
.1	.52	9150	1.763	1.43
.3	.70	10900	1.31	1.703
.5	.95	11350	.965	1.773
.6	1.08	11550	.849	1.805

$$T = 2VG\theta R^4 \quad , \quad R = A\ (?)$$

$$\tau_{MAX} = f\,T\,R^3$$

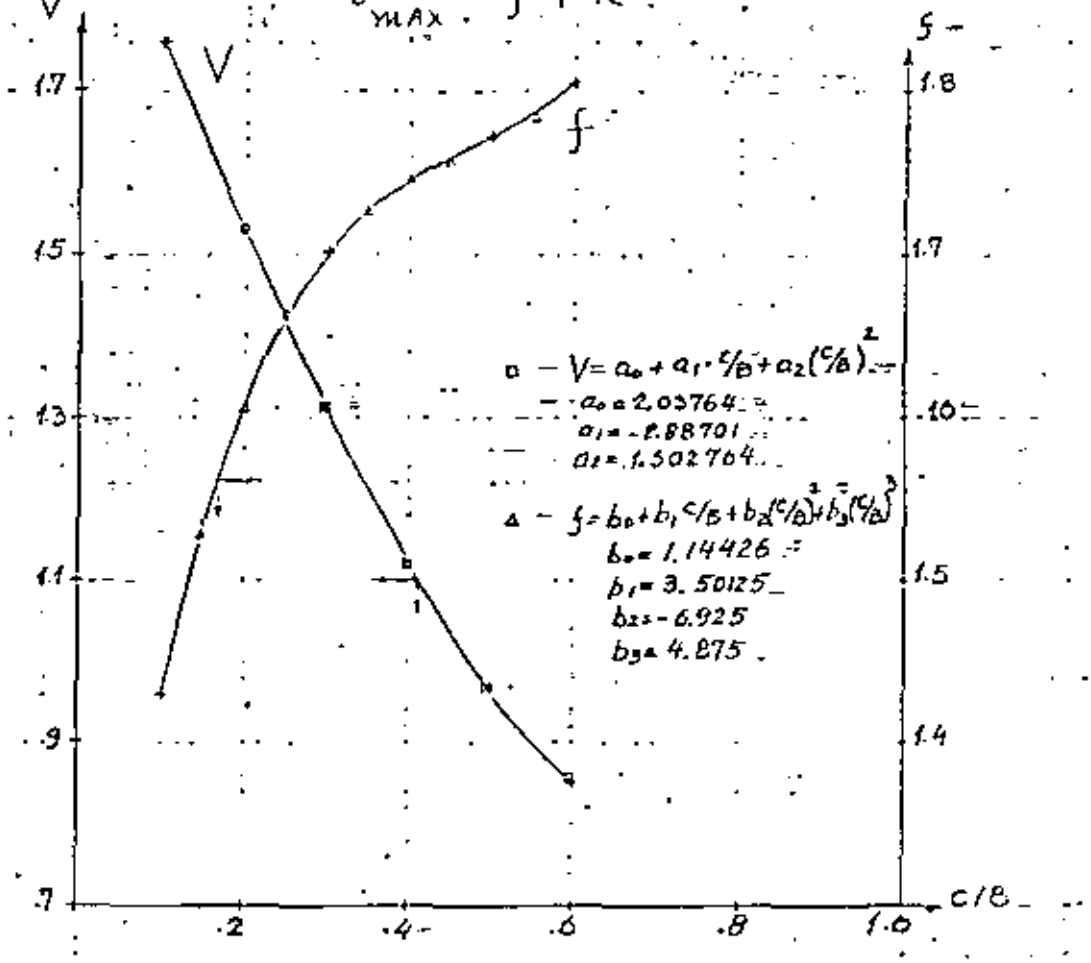

N.J. SALAMON & F.E. CLASS 1981

3.4

C/B = .6

MICRO-ZUM

	EL. 176			EL. 192			EL. 208		
	S CM^2	S/Smax —	τ N/CM^2	S CM^2	S/Smax —	τ N/CM^2	S CM^2	S/Smax —	τ N/CM^2
1	$8.37 \cdot 10^{-5}$	.528	10057	$7.59 \cdot 10^{-5}$	.605	10348.2	$9.55 \cdot 10^{-5}$	9/2	10324
2	$1.583 \cdot 10^{-4}$	1.	9140	$1.254 \cdot 10^{-4}$	1.	9669	$1.06 \cdot 10^{-4}$	1.	9954
3	$1.857 \cdot 10^{-5}$	.117	122543	$3.29 \cdot 10^{-5}$	.262	11063	$4.31 \cdot 10^{-5}$	.463	10539
4	$1.21 \cdot 10^{-4}$	.764	9357.7	$1.01 \cdot 10^{-4}$	.805	9985	$9.08 \cdot 10^{-5}$	.857	101392
5	$5.11 \cdot 10^{-5}$	.323	10714.9	$5.44 \cdot 10^{-5}$	.434	10702	$6.23 \cdot 10^{-5}$	.588	10470

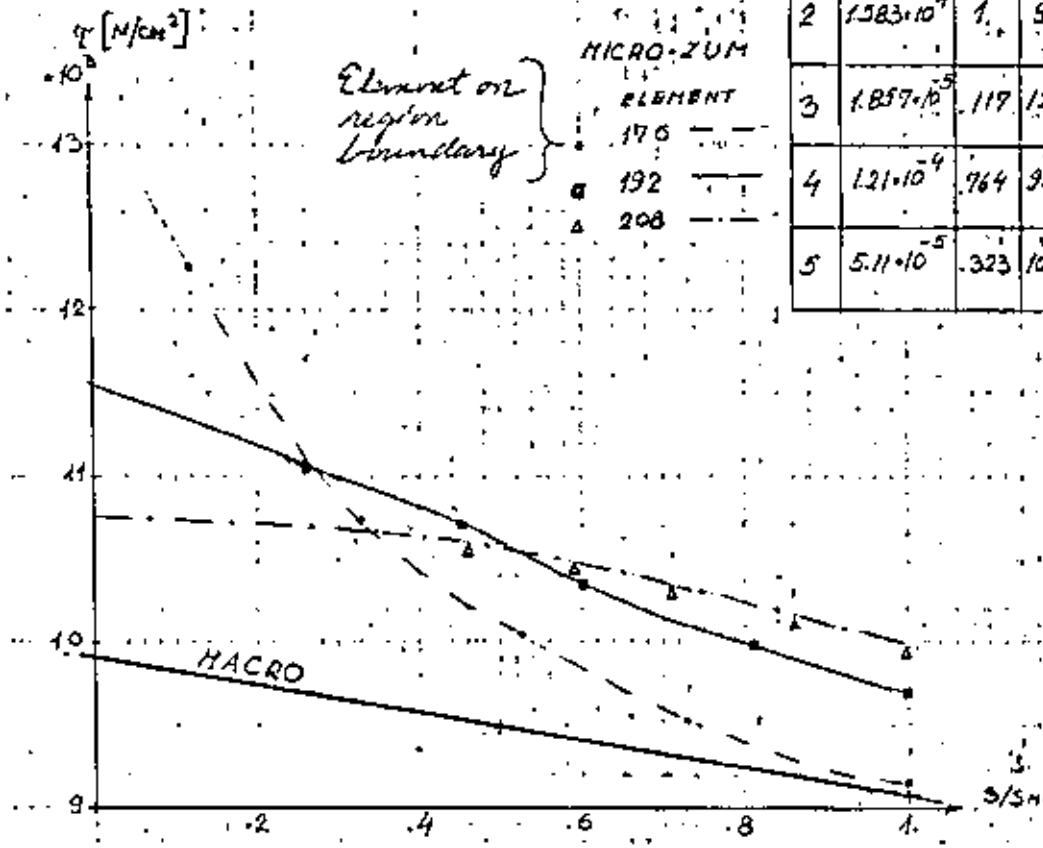

MACRO

	S CM^2	S/Smax —	τ N/CM^2
1	$3953 \cdot 10^{-4}$	1.	9095
2	$1.976 \cdot 10^{-4}$	.5	9477

$\theta = 1.08$ °

N.I. SALAMON

FINITE ELEMENT

CLASS 1981

3.4 MACRO 1

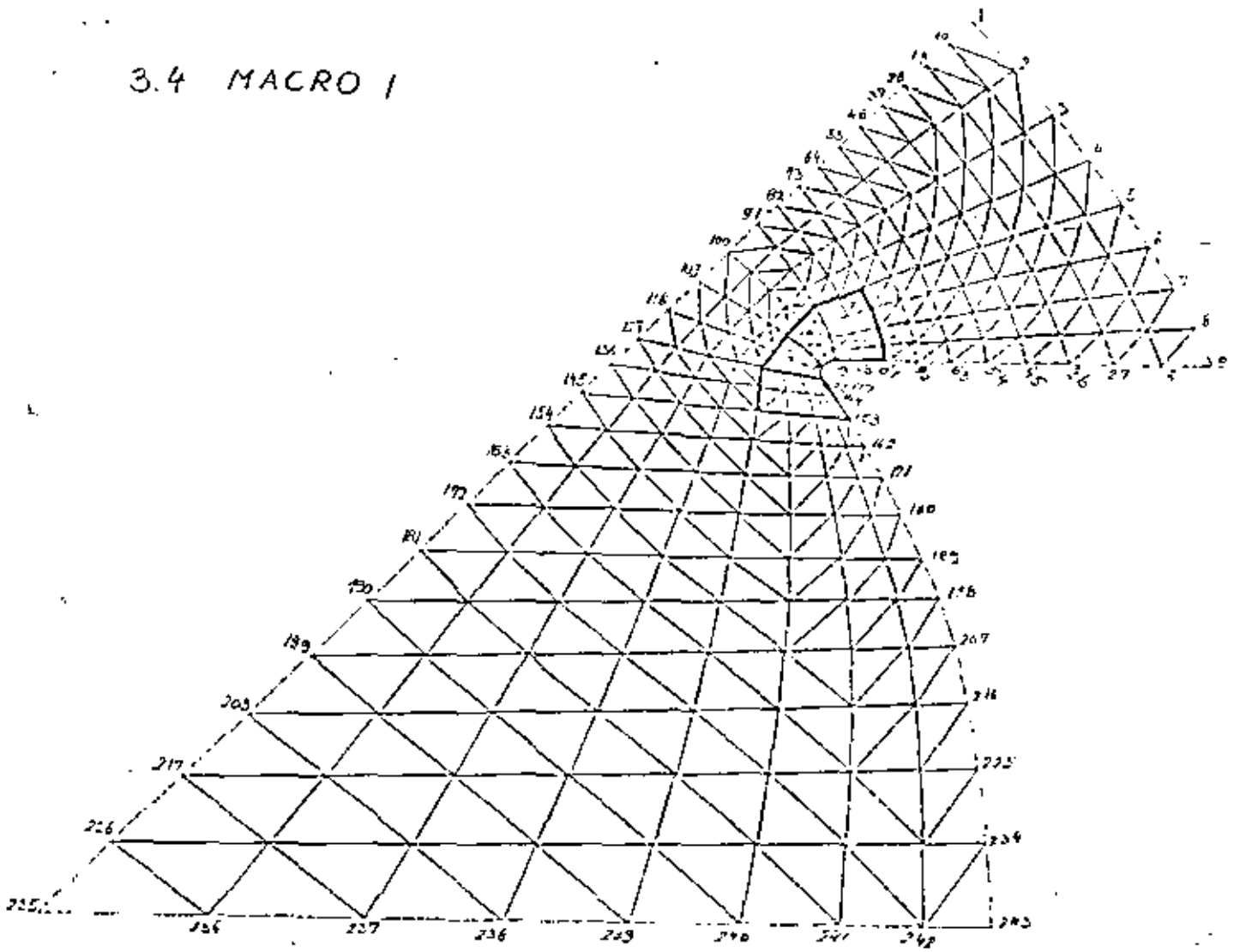

K.J. SALAMON — P.E. CLASS 1981

(4)

3.4 MICRO 1

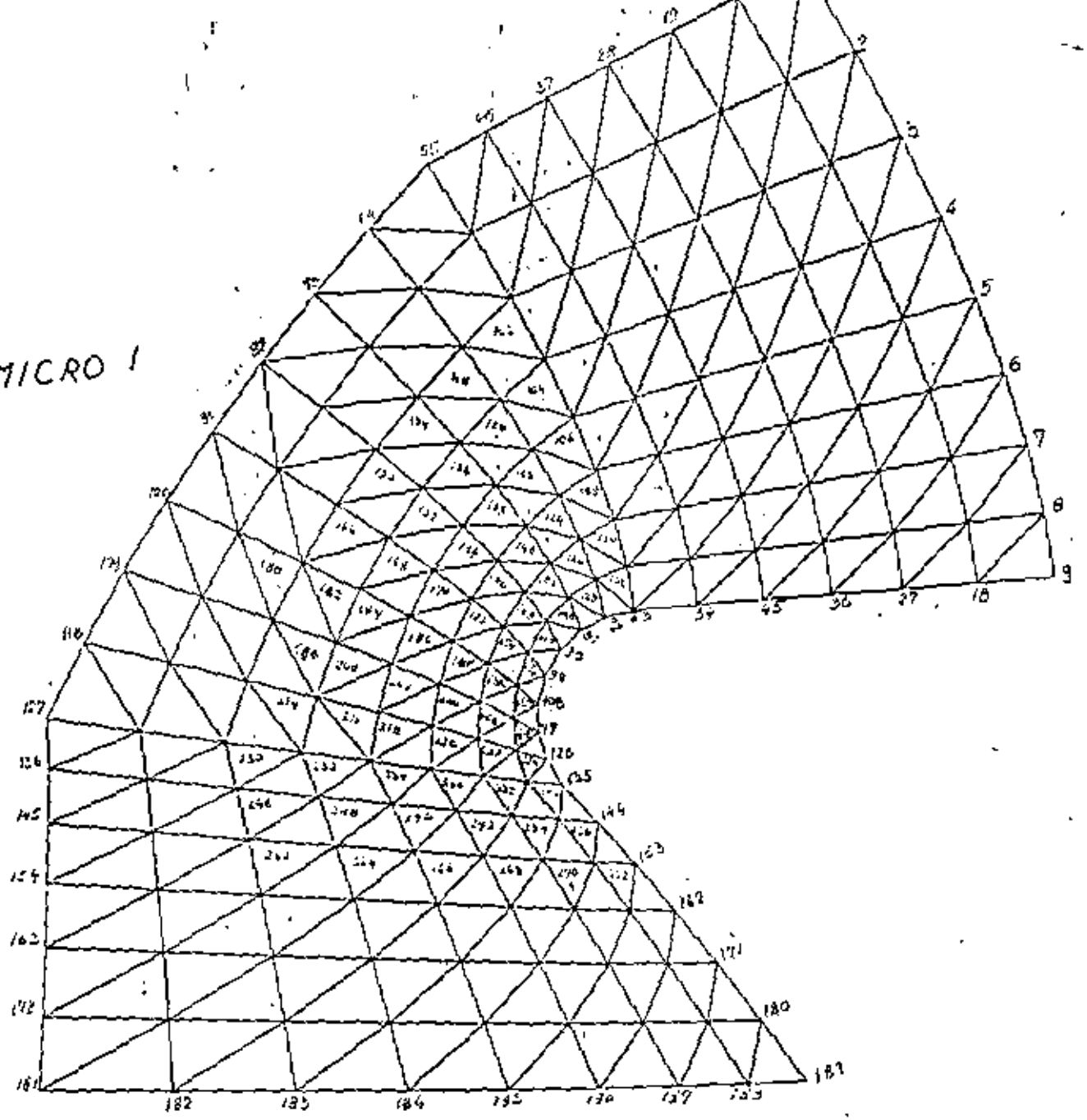

NEE SOLAMON & F.E. CLASS 1971

DIVISION DE EDUCACION CONTINUA
FACULTAD DE INGENIERIA U.N.A.M.

EL METODO DEL ELEMNTO FINITO EN LA INGENIERIA MECANICA

PAQUETES COMPUTACIONALES

DR. PORFIRIO BALLESTEROS

ABRIL 1982

Applications Software

The user (designer, draftsman, engineer or technician) interacts with a CAD system through applications software. The programs "talk" the user's language as opposed to the computer implementation language which is, hopefully, isolated from the user in lower levels of utilities and system software. The usefulness of applications software is related to the human engineering of its interface with the user (command language, user I/O hardware devices, software design, etc.) as much as the technical content and features of the program.

Applications software can be divided into two categories: standalone and turnkey. The standalone software is available from a software vendor and frequently runs on several different manufacturer's computers. The turnkey software is available as part of a packaged hardware/software system from a turnkey vendor. The turnkey vendor typically buys computer equipment from a computer manufacturer and combines this with his own software, hardware packaging, and workstation design. A few turnkey vendors offer modified software from another software vendor. A few also produce their own hardware components, particularly microprocessors for speeding up interactive graphics response.

Standalone applications software has the primary advantage of flexibility. It often can be implemented on computers over a broad size/speed range in organizations having diverse computing machinery. Standalone software dominates engineering analysis, where turnkey systems either don't offer capabilities or are very weak. Turnkey systems, on the other hand, have the primary advantage of being available from one source, avoiding the potential problems of multi-vendor scenarios. They have achieved a dominance in the area of geometric modeling and drafting (particularly 2D).

This section reviews the standalone applications software used in CAD. Turnkey systems are discussed in Section VII. The big news in standalone CAD software is the migration to smaller computers.

CAD Software Vendors/Distributors

1. Professor K. J. Bathe
   Massachusetts Institute of Technology
   Room 3-365
   Cambridge, MA 02139

2. Swanson Analysis Systems, Inc.
   Box 65
   Houston, PA 15342

3. Merlin Technologies, Inc.
   977 Town and Country Village
   San Jose, CA 95128

4. Atkins Research and Development
   Woodcoge Grove, Ashley Road
   Epson, Surrey, U.K.

5. IKOSS GmbH
   Vaihinger Str. 49
   D-7000 Stuttgart 80
   West Germany

6. C.E.G.B.
   Berkeley Nuclear Labs.
   Gloucestershire, England

7. Engineering Information Systems, Inc.
   5120 Campbell Ave.
   Suite 240
   San Jose, CA 95130

8. COSMIC
   112 Barrow Hall
   University of Georgia
   Athens, GA 30602

9. MacNeal-Schwendler Corp.
   7442 North Figueroa Street
   Los Angeles, CA 90041

10. Marc Analysis Research Corp.
    260 Sheridan, Suite 200
    Palo Alto, CA 94036

11. Universal Analytics, Inc.
    7740 W. Manchester Bldg.
    Playa del Ray, CA 90291

12. Engineering Mechanics Res. Corp.
    P.O. Box 696
    Troy, MI 48099

13. PAFEC, Ltd.
    Strelley Hall
    Main Street, Strelley
    Nottingham, NG8 6PE
    England

14. SAP Users Group
    Denney Research Bldg., USC
    University Park
    Los Angeles, CA

15. A. S. Computas
    Veritasveien 1
    P.O. Box 310
    N-1322 Hovik, Norway

16. GTICES Systems Laboratory
    School of Civil Engineering
    Georgia Institute of Tech.
    Atlanta, GA 30332

17. Structural Dynamics Research Corporation
    2000 Eastman Drive
    Milford, OH 45150

18. T-Programm GMBH
    Gustav-Werner-Str. 3
    D-7410 Reutlingen
    West Germany

19. MCAUTO
    Dept. K161/270A
    P.O. Box 515
    St. Louis, MO 63166

20. SIA Ltd.
    23 Lower Belgrave Street
    London, SW 1
    England

21. Jordan, Apostal, Ritter Assoc. Inc.
    Administration Bldg. 7
    Davisville, RI 02854

p.376 (3)

22. Interactive Graphics
Engineering Lab
University of Arizona
College of Engineering
AME Bldg. 16, Room 210A
Tucson, AZ 85721
(602) 626-1650

23. PDA Engineering
1740 Garry Ave., Suite 201
Santa Ana, CA 92705
USA

24. Manufacturing & Consulting
Services
3195A Airport Loop Drive
Costa Mesa, CA 92626

25. Lockheed, Burbank
Building 67, Plant A-1
Department 8034
Burbank, CA 91501

26. Evans and Sutherland
Computer Corp.
580 Arapeen Drive
Salt Lake City, Utah 84108

27. Production Automation
Project
College of Engineering and
Applied Science
University of Rochester
Rochester, NY 14627

28. MAGI
3 Westchester Plaza
Elmsford, NY 10523

29. MATRA-Datavision UK, Ltd.
Systems Engineering
Laboratories
Rafferty House
2-4 Sutton Court Road
Sutton, Surrey SM1 4SY
England

30. MCAUTO
Dept. K507
P.O. Box 516
St. Louis, MO 63166

31. Technische Datenverarbeitung
A-8010, Graz
Luthergasse 4, Austria

32. Washington University
Technology Associates
8049 Litzinger Road
St. Louis, MO 63144

33. SCIA
Attenrodestraat 6
3385 Meensel-Kiezegam
Belgium

34. Advanced Engineering
Consultants AB
Box 3044
S-580 03 Linkoping
Sweden

35. Engineering Computer
Services, Ltd.
Piccadilly, Tamworth, Staffs
B78 2ER, England

36. Computational Mechanics
125 High Street
Southhampton, Hampshire
SO1 0AA, England

37. SOCOTEC
"Les Quadrants"
3 Avenue du Centre
78182 St Quentin en Yvelines
Cedex, France

38. Dr. Edward L. Wilson
1050 Leneve Place
El Cerrito, CA 94530

39. IMSL, Inc.
6th Floor NBC Building
7500 Bellaire Blvd.
Houston, TX 77036

40. A. D. Little, Inc.
20 Acorn Park
Cambridge, MA 02140

41. Quadrex Corporation
1700 Dell Avenue
Campbell, CA 95008

42. Structural Software
Development
1930 Shattuck Avenue
Berkeley, CA 94704

43. MCAUTO
Dept. K246
P.O. Box 515
St. Louis, MO 63166

44. AAA Technology and
Specialities Co., Inc.
P.O. Box 37189
Houston, TX 77036

45. Fitech, Ltd.
Mississippi State Univ.
Drawer KJ
Mississippi State, MS 39762

46. Mr. Ronald T. Bradshaw
85 Central Street
Waltham, MA 02154

47. Gulley Computer Associates
2300 E. 14th
Tulsa, OK 74104

48. Structural Members Users
Group, Ltd.
P.O. Box 3958
Univ. of Virginia Station
Charlottesville, VA 22903

49. Genesys Limited
Lisle Street
Loughborough, LE11OAY
England

50. ECOM Associates
5678 W. Brown Deer
Milwaukee, WI 53223

51. Synercom Technology
P.O. Box 27
Sugerland, TX 77478

52. CONCAP Computing Systems
7700 Edgewater Drive
Suite 700
Oakland, CA 94621

53. Structural Programming, Inc.
83 Boston Post Road
Subury, MA 01776

54. Shabler Associates
1959 Chalice Way
Toledo, OH 43613

55. SysComp Corporation
2042 Broadway
Santa Monica, CA 90404

56. Holguin and Associates, Inc.
5822 Cromo Drive
P.O. Box 12990
El Paso, TX 79912

57. Zeiler-Pennock, Inc.
2727 Bryant Street
Denver, CO 80211

58. Stress Analysis Associates
4529 Angeles Crest Highway
Suite 104
La Canada, CA 91011

59. Computer Mart
560 West 14 Mile Road
Clawson, MI 48017

60. Northern Research and
Engineering Corp.
39 Olympia Avenue
Woburn, MA 01801

Software Referral Catalogs

1. HP 1000 Guide to OEMs and Software Suppliers
   OEM Market Development
   Hewlett-Packard Data Systems Division
   11000 Wolfe Road
   Cupertino, CA 95014

2. Engineering System Software Referral Catalog
   Digital Equipment Corp.
   Engineering Systems Group
   200 Forest Street
   Marlboro, MA 01752

Distribution Agencies for Software

1. ASIAC (Aerospace Structures Information and Analysis Center)
   AFFDL/FBR
   Wright Patterson Air Force Base
   Dayton, OH 45433

2. CEPA (Society for Computer Applications in Engineering, Planning and Architecture, Inc.)
   358 Hungerford Drive
   Rockville, MD 20850

3. COSMIC
   Suite 112, Barrow Hall
   The University of Georgia
   Athens, GA 30602

4. National Information Service-Earthquake Engineering Computer Applications
   519 Davis Hall
   The University of California, Berkeley
   Berkeley, CA 94720

5. National Technical Information Center
   5285 Port Royal Road
   Springfield, VA 22161

6. NESC (National Energy Software Center)
   9700 South Cass Avenue
   Argonne, IL 60439

P173

COMPUTER-AIDED ENGINEERING METHODS

General Electric CAE International Inc.
300 TechneCenter Drive
Milford, Ohio 45150
Tel: 513-576-3800

Who's Who in the GE/SDRC Joint Venture

Structural Dynamics Research Corporation

SDRC, a privately owned corporation, was organized in 1967 as a consulting engineering services company dedicated to serving the mechanical market. It presently specializes in the application of computer-aided engineering techniques to mechanical product design and problem solving.

As a CAE pioneer, the Milford, OH, firm has achieved a world-wide reputation for engineering excellence with its work for clients in these basic industries: automotive, aerospace, machine tools, primary metals, power generation, hydrocarbon processing and agriculture-construction-mining equipment.

SDRC provides on-site electronic testing to solve vibration, stress, fatigue and failure problems in plant equipment and structures, and computer analysis to predict dynamic behavior and prevent problems before they occur. Through its SDRC/CAE International subsidiary, organized in April, 1981, it has offered CAE software encompassing all aspects of the engineering design process from concept through manufacturing.

The firm has 400 employees, including more than 225 engineers. Sales for the fiscal year ending March 31, 1981, were $21.5 million.

General Electric CAE International Inc.

The Milford, OH, based joint venture of GE and SDRC is responsible for marketing of its extensive offering of CAE software and for the development of new products for the mechanical marketplace. It also assumes responsibility for the marketing of N/C factory automation software formerly in the General Electric Information Services Company's product line.

GE-CAE International software also will be offered by the GE-owned Calma Company and other leading computer suppliers, as well as selected computer network vendors.

In addition to marketing its software, GE-CAE International plans a worldwide network of Productivity Centers where customers can experiment with CAD/CAM and CAE, receive technical assistance, and develop custom applications software without an initial investment. Centers are now open in San Diego and Cincinnati. Others are nearing completion in Wiesbaden, Paris, London, Tokyo, and Detroit. Additional locales are in the planning stage.

-more-

p. 3 of 3 (1)

General Electric Information Services Company

GE Information Services, a major supplier of computing services, will distribute GE-CAE International products. The firm has a worldwide distribution and technical force of over 3,000 located in 190 sales offices in 25 countries around the world.

GE Information Services operates the world's largest commercially available teleprocessing network, which includes 500 processing and communications computers.

This communications network provides the vehicle for a paperless flow of design and manufacturing data to and from the large numbers of component suppliers serving end-product manufacturers.

Calma Company

GE's CAD/CAM subsidiary offers mechanical design, drafting and manufacturing software with its turnkey graphics systems.

Calma's line of sophisticated interactive-graphics products will be expanded to include GE-CAE International software. Calma hardware will also be utilized in GECI Productivity Centers.

The Santa Clara, CA, headquartered firm, acquired by GE in April, 1981, has 1,000 employees and offices in 20 U.S. cities and 10 foreign countries. It expects to ship $100 million in equipment in 1981.

GE Industrial Electronics Group

The Industrial Electronics Group is the focal point of GE's massive effort to be a worldwide leader in supplying the automated Factory of the Future. This thrust was announced in April, 1981, when GE completed the acquisitions of Intersil, a major microelectronics supplier, and Calma Company.

In addition to these wholly owned subsidiaries, the Group has two divisions. The Electronic Components division includes the Semiconductor Products, Tube Products, Capacitor Products and Electronic Components Sales department, plus the Instrument Products Section, Power Supply Operation and Liquid Crystal Display Operation.

The Industrial Electronic Systems Division comprises the Industrial Control and Drive Systems departments, and the Programmable Control and Speed Variator Products operations.

An Industrial Electronic Development Laboratory, located at Group headquarters in Charlottesville, VA, will be occupied in the Spring, 1982.

New Manual

Consolidation

One manual explains the usage of static, dynamic and plot options; a flow chart illustrates analysis functions

Index Tabs

Each major data section/function is highlighted with index tab separator sheets

NODES	RESPONSE SPECTRUM
ELEMENTS	TIME HISTORY
LOADS	E2PLOT
STATIC OUTPUT	E2SPEC
DYNAMICS	APPENDICES

Card Layouts

Each data section begins with a card layout strip illustrating the format used for each card type

Output Explanations

Examples of printed output are pictured for each element type with explanations of sign convention and output headings

Output Processors

All output quantities can be diverted to a disk or tape file; processors (FORTRAN programs) which read these external files are given in the Appendices

EASE2

Static and Dynamic Finite Element Analysis System

EASE2 has long been noted for its ability to handle large structural systems at very low costs. Its no-nonsense approach to user documentation is so straightforward that most users code their first problems directly from the manual without any need for time-consuming training sessions or expensive seminars.

New Users Manual

Now the user's manual has been redesigned to allow for even greater ease of input.

Card images are included for every data item input so that the user can visualize each parameter. This is useful to engineers who use the timesharing/free format input options.

All variables are defined with a name and reference to detailed notes explaining the use of the variable and any effect it has on the analysis. This is especially beneficial to first-time users who need to familiarize themselves with nomenclature and definitions.

All New EASE2 Manual

Engineering/Analysis Corporation
1611 South Pacific Coast Highway
Redondo Beach, California 90277

STRUCTURAL SOFTWARE DEVELOPMENT, INC.
ANNOUNCES
SUPPORT SERVICES FOR COMPUTER SOFTWARE DISTRIBUTED BY NISEE/COMPUTER APPLICATIONS

SOFTWARE SUPPORT SERVICES

Structural Software Development Inc. (S.S.D.) has initiated a software support service for several computer programs distributed by the National Information Service for Earthquake Engineering. The purpose of this service is to provide NISEE program users with fast, reliable, and accessible consultation services on the use and interpretation of heavily used NISEE structural analysis programs. An outline of these services is presented below:

- program familiarization for new users
- aid in structural idealization and appropriate modelling
- general problem diagnosis
- input/output understanding and interpretation
- additional, in depth, services upon request

Most problems and questions can be handled via direct phone consultation.

SUPPORTED PROGRAMS

Support service subscriptions are available for the following programs:

TABS — three-dimensional linear elastic analysis of buildings (uncoupled frames/rigid floors)
ETABS — three-dimensional linear elastic analysis of buildings (limited frame coupling/rigid floors)
SAP — general linear elastic structural analysis
ANSR — general non-linear structural analysis
DRAIN-2D — inelastic analysis of plane structures
DRAIN-TABS — three-dimensional inelastic analysis of buildings

STAFF

S.S.D. maintains a full time staff experienced in the development, use and support of these programs. Personnel are available for phone consultation 9 a.m. through 5 p.m. (PST) weekdays.

SUBSCRIPTION RATES

The subscription rate for any single program is $250.00 and includes a maximum of 10 hours consultation over a period of 12 months. Subscriptions for multiple program support or other alternative support arrangements are negotiable. Subscriptions are limited.

Interested parties should contact:

STRUCTURAL SOFTWARE DEVELOPMENT, INC.
1930 Shattuck Avenue
Berkeley, CA 94704
Telephone 415/849-3458

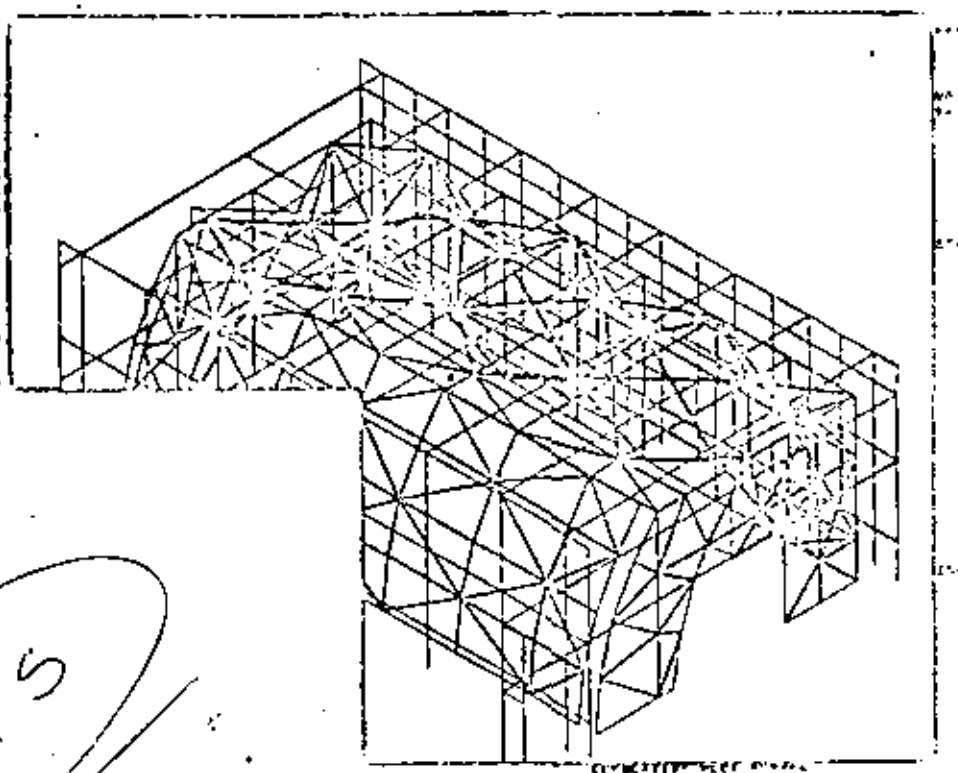

ANSYS

SM Computer Leasing Services

Swanson Analysis Systems, Inc.

JOHNSON ROAD P.O. BOX 65, HOUSTON, PA 15342 USA

(412)746-3304 TWX 510-690-8555

ENGINEERING MECHANICS RESEARCH CORPORATION
P.O. BOX 696 • TROY, MICHIGAN 48099 U.S.A. • PHONE: (313) 968-1606

NON-NISA

NON–LINEAR NUMERICALLY INTEGRATED ELEMENTS FOR STRUCTURAL ANALYSIS

A FINITE ELEMENT STRUCTURAL PROGRAM

NON–NISA is a finite element computer program for non-linear (geometrical and material) structural analysis. The program has two– and three– dimensional isoparametric elements. At present the program has 4 & 8 node isoparametric elements for plane stress, plane strain, and axisymmetric elements for two dimensional analysis. For three dimensional analysis, 16 node isoparametric thick shell and 8 and 20 node isoparametric solids are available.

Large displacement kinematics (geometric nonlinearity) is based on the total Lagrangian formulation. A number of material models such as linear elastic, linear elastic orthotropic, nonlinear elastic-plastic and nonlinear elastic incompressible (Mooney-Rivlin material) are included. . In elastic-plastic model, Von-Mises yield condition is being used with several hardening rules like isotropic, kinematic, combined isotropic-kinematic, and mechanical sublayers. Both static and dynamic analysis are possible. In dynamic analysis, Wilson's Theta and Newmark's time integration methods are available.

In solving the non-linear equilibrum equations, a step-by-step incremental formulation is used. At each step, equilibrum iteration is performed (if desired) using modified Newton–Raphson method until a convergence solution is obtained, and then , the the non-linear stiffness matrix is updated for the solution of the next step. Equations can be solved either by an in-core or an out-of-core solver depending on the problem size and available core size of a given computer system.

ELEMENT TYPE	DISPLACEMENT ORDER / DEGREES OF FREEDOM	LINEAR	PARABOLIC
2D ISOPARAMETRIC • PLANE STRESS • PLANE STRAIN • AXISYMMETRIC	UX UY		
3D ISOPARAMETRIC • THICK SHELL (DESCRIBED BY TOP AND BOTTOM NODES)	UX UY UZ	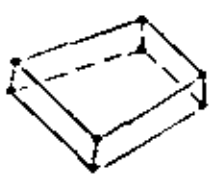	
3D ISOPARAMETRIC • HEXAHEDRON	UX UY UZ		

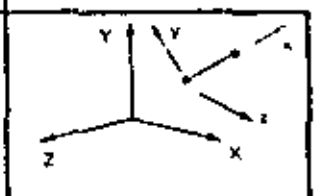

UNITED COMPUTING SYSTEMS, INC.

(15)

p. 1 of 3

BRANCH OFFICES

California

LOS ANGELES
Suite 410
901 Continental Boulevard
El Segundo, California 90245
Phone (213) 640-0891

NEWPORT BEACH
Suite 104
3819 Westerly Place
Newport Beach, California 92660
Phone (714) 752-9551

PALO ALTO
Suite 165
710 Laiteway
Sunnyvale, California 94086
Phone (408) 737-7900

SAN FRANCISCO
525 Hearst Building
3rd & Market Streets
San Francisco, California 94103
Phone (415) 495-6850

Colorado

DENVER
Suite 100
9034 E. Easter Place
Englewood, Colorado 80112
Phone (303) 773-0339

Connecticut

HARTFORD
Suite 712
750 Main Street
Hartford, Connecticut 06103
Phone (203) 522-3534

Florida

FORT LAUDERDALE
Suite 103
1500 N.W. 62nd Street
Fort Lauderdale, Florida 33309
Phone (305) 491-6575

ORLANDO
Suite 111
930 Woodcock Road
Orlando, Florida 32803
Phone (305) 896-3710

TAMPA
Suite 518
1000 Ashley Drive
Tampa, Florida 33602
Phone (813) 223-3921

Georgia

ATLANTA
Suite 106, Building 1
5825 Glenridge Drive N.E.
Atlanta, Georgia 30328
Phone (404) 256-3610

Illinois

CHICAGO
Suite 1016
150 North Wacker Drive
Chicago, Illinois 60606
Phone (312) 782-0865

Kansas

KANSAS CITY
Suite 230
4801 W. 110th Street
Overland Park, Kansas 66211
Phone (913) 341-9330

TELEPHONE SALES
Suite 200A
4801 W. 110th Street
Overland Park, Kansas 66211
Phone (913) 341-9150

Massachusetts

BOSTON
303 Wyman Street
Waltham, Massachusetts 02154
Phone (617) 894-6700

Michigan

DETROIT
Suite 960, Tower 14
21700 Northwestern Highway
Southfield, Michigan 48075
Phone (313) 557-4707

Minnesota

MINNEAPOLIS
Suite 685
300 South County Road
Minneapolis, Minnesota 55426
Phone (612) 545-6999

Missouri

ST. LOUIS
Suite 170
1030 Woodcrest Terrace Dr.
Clayton, Missouri 63141
Phone: (314) 434-6633

New Jersey

NEWARK
900 Route 9
Woodbridge, New Jersey 07095
Phone (201) 634-1290

New York

NEW YORK
Suite 1650
2 Pennsylvania Plaza
New York, New York 10001
Phone (212) 563-8484

North Carolina

RALEIGH
Suite 213
3725 National Drive
Raleigh, North Carolina 27612
Phone: (919) 781-4948

Ohio

CLEVELAND
Suite 460
3690 Orange Place
Beachwood, Ohio 44122
Phone (216) 464-9205

COLUMBUS
Suite 100
6797 North High Street
Worthington, Ohio 43085
Phone (614) 885-8513

Oklahoma

OKLAHOMA CITY
Jamestown Executive Center
3005 N.W. 63rd Street
Oklahoma City, Oklahoma 73116
Phone (405) 843-9784

TULSA
Suite 404
18 East 16th Street
Tulsa, Oklahoma 74119
Phone (918) 582-7291

Pennsylvania

PHILADELPHIA
Suite 2026
2 Penn Center Plaza
Philadelphia, Pennsylvania 19102
Phone: (215) 568-6300

PITTSBURGH
Suite 312
1000 RIDC Plaza
Pittsburgh, Pennsylvania 15238
Phone: (412) 963-8700

Texas

DALLAS
Suite 1301
8150 North Central Expressway
Dallas, Texas 75206
Phone: (214) 696-8030

HOUSTON
Suite 346
4544 Post Oak Place
Houston, Texas 77027
Phone: (713) 622-5351

Virginia

WASHINGTON D.C.
Suite 250
7700 Leesburg Pike
Falls Church, Virginia 22043
Phone: (703) 821-1022

Washington

SEATTLE
15436 N.E. Bellevue - Redmond Road
Redmond, Washington 98052
Phone: (206) 747-6581

Wisconsin

MILWAUKEE
Suite 1175
2300 North Mayfair Road
Wauwatosa, Wisconsin 53226
Phone (414) 475-9392

Canada*

CALGARY
Suite 3070
Bow Valley Square 3
P.O. Box 9235
Calgary, Alberta
Canada T2P 2W5
Phone: (403) 265-4926

EDMONTON
Suite 500
10089 Jasper Avenue
Edmonton, Alberta
Canada T5J 1V1
Phone: (403) 428-8350

MONTREAL
Suite 1050
1253 McGill College Avenue
Montreal, Quebec
Canada H3B 2Y5
Phone: (514) 875-7050

DATACENTERS

NATIONAL DATACENTER
2525 Washington
Kansas City, Missouri 64108
Phone (816) 221-8700

CHICAGO DATACENTER
10 West 31st Street
Chicago, Illinois 60616
Phone (312) 567-8000

DALLAS DATACENTER
14838 Ventura
Dallas, Texas 75234
Phone (214) 620-2375

WALTHAM DATACENTER
335 Bear Hill Road
Waltham, Massachusetts 02154
Phone (617) 890-6820

HEADQUARTERS

P.O. Box 8551
Kansas City, Missouri 64114
Phone: (913) 341-9161

*Registered in Canada as United Computing Systems Canada, Ltd.

(6)

p. 293

APEX/SL ENGINEERING

United Computing Systems' APEX/SL Program Library offers you a complete range of advanced engineering programs suitable for operation in the time-sharing, remote batch and/or remote job entry mode(s). Listed here are the major engineering programs and graphic interface systems available to you on the APEX/SL system. A brief description of each program's function follows.

These two pages indicate and describe some of the many software systems available through UNITED COMPUTING SYS

CHEMICAL/PETRO-CHEMICAL

AIDEX II
CHEMTRAN[T]
CONCEPT
DESIGN/2000[®]
DISTIL[®]
ECONRUN
HEXTRAN[SM]
HTRCST1
HTRIST4
HTRRKH1
HTRRTF2
HYPROP
HFRAC2
PIPEFLO
REFINE[®]
SSIVLE
SYMBOL[®]
TPFLOW
WELLFLO

CIVIL

CNCGRD
COGO
EARTHWK
EARTHWORK PROGRAMS
FLOORR
FLOORT
HEC PROGRAMS
POSTEN
SECS
SUBPLAT PROGRAMS
TRIDRIL[®]
TRIMAT

COMPUTER GRAPHICS

CALCOMP BASIC & FUNCTIONAL SOFTWARE PACKAGES
CPS-1
DISSPLA[®]
DISSPOP
HEWLETT PACKARD PLOT/21 PROGRAMS
PLOTIT
PLOTREQ
SACM
SUPERTAB
TEKTRONIX PROGRAMS
UNIDRAW
UNIGRAF[®]

ELECTRONIC PRODUCTS

Circuit Simulation

HSPICE
METACKT

Device & Process Simulation

SUPREME

Microwaves

AMPSYN[®]
CADSYN[®]
COMPACT[®]
DFELAY[®]
FILSYN[®]

ENERGY

DOE2
ECUBE3
FCHART
MEDSI
POGOS
SOLCOST

MECHANICAL

ENVIRONS PROGRAMS (PROG1/PROG2/PROG3)
FRP
FIRE SPRINKLER DESIGN PROGRAMS
INTERCOMP PROGRAMS[®]
WERCO

PIPING

ADLPIPE
ANSYS[®]
AUTOFLEX[®]
DYNAFLEX[®]
EZFLEX[®]
FLANGE
PIPA
TRIFLEX[®]
TRIFLR[®]
TRIVESL[®]
WAVENET

NUMERICAL CONTROL

APT
CUTSII
UCS/APT

PROJECT MANAGEMENT

EZPERT[®]
TIMETABLE[®]

STRUCTURAL

Nonlinear Analysis

ANSYS®
EDI PROGRAMS
GIFTS IV
KSHEL
MARCS PROGRAMS
MSC/NASTRAN®
UAI/NASTRAN®

Linear Analysis

ANSYS
DESIGNS
EDI PROGRAMS
GIFTS IV
KSHEL
MARCS PROGRAMS
SAP4
SPACE4
SPAR/EAL
STAAD-III
STRAN

Heat Transfer Analysis

ANSYS
MARCS PROGRAMS
MSC/NASTRAN
UAI/NASTRAN

Marine Analysis

ANSYS
EDI PROGRAMS
MARCS PROGRAMS
MSC/NASTRAN
UAI/NASTRAN

Design

DESIGNS
STAAD-III

SYSTEMS PROFESSIONAL

Business Applications	Concrete	General Analysis	Masonry	Steel	Wood
MANAGE	BOXCUL COLFTG1 COMFTG1 CONCOL FLPLT NONPBM PRISBM PRSTRS PRSTRU RETWAL2	COLLDS DETTRS EQKSWL REGFRM RIGFRM SHWINT SIMPBM SPSTRESS	BRGWAL1 EQPIER1	BASPLT COMPBA COMPBU STLBMU STLCOL1 WELDBM	GLULAM TIMBER

ALPHABETICAL LISTING OF APEX/SL ENGINEERING APPLICATIONS

ADLPIPE

Generates static, stress and dynamic piping analyses and reports which meet current ANSI and ASME codes.

AIDEX

Handles heat transfer for tubular heat exchangers as well as sensible heat, condensing or vaporizing change-of-phase on either the shellside or tubeside of any TEMA heat exchanger.

AMPSYN®

Uses direct synthesis techniques to calculate amplified input, output and interstage networks; meets user-specified bandwidth, ripple and gain slope requirements.

ANSYS®

Solves engineering analysis problems using the matrix displacement method based upon infinite element idealization.

Material Nonlinearities

MARC Analysis Research Corporation
World Headquarters
260 Sheridan Avenue
Palo Alto, CA 94306
Telephone: (415) 326-7511
TWX 910 373 2013

MARC contains an extensive library of material behaviors. All types of behavior which make physical sense may be present in a single analysis. All material properties may be temperature dependent, and arbitrary anisotropy (eg. layered orthotropic shells) may be defined as a function of position through user subroutines. Examples of constitutive characterizations available in the program are:

- Isotropic, kinematic or combined hardening of elastic-plastic materials with Mises or Mohr-Coulomb yield surfaces.
- Associated or non associated flow rules.
- Creep analysis — stress induced. Special high-temperature theories (ORNL equations for nuclear components).
- Irradiation induced creep swelling.
- Coulomb friction.
- Concrete cracking.
- Nonlinear elasticity (e.g., Mooney Material).
- Incompressible elements, potential fluid flow.
- Metal working.
- J-integral evaluation and C.O.D. predictions for fracture mechanics.

Figure 8

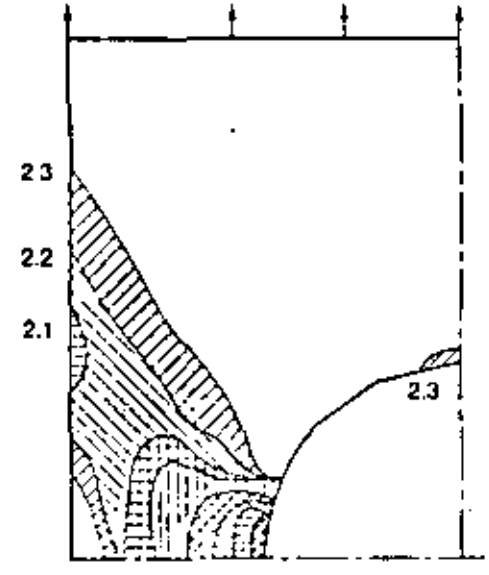

PROGRESSIVE YIELDING OF PERFORATED STRIP
DIA : WIDTH OF STRIP = 1:2

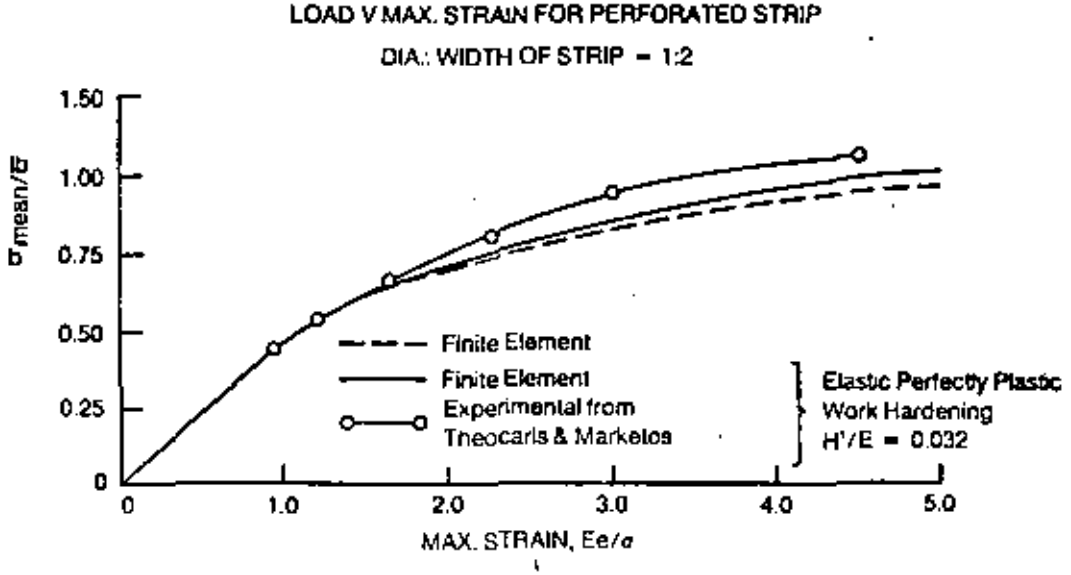

Photoelastic Measurements
Finite Element Analysis

You know that lab or field testing combined with theoretical analysis is the best approach to many design problems. At Engineering Methods, photoelastic measurements are used together with finite element analyses to reduce your design time and costs.

Photoelastic measurements made on actual hardware are used to verify the finite element analysis of your present design. They can be applied under varying temperature and humidity conditions and they show full-field strain patterns for either static or dynamic load cases. Design changes are then prototyped within the computer using the finite element analysis; you reduce the number of hardware prototypes needed.

Engineering Methods helps you pinpoint and correct problem areas in your design – whether it is in the field, in the lab, or on the drawing board.

If you already use photoelastic measurements, use Engineering Methods to help relieve work overload, to check critical analyses, or to provide advanced expertise.

To get the right answer in less time for less money,
Don't Use Conventional Methods,
Use Engineering Methods.

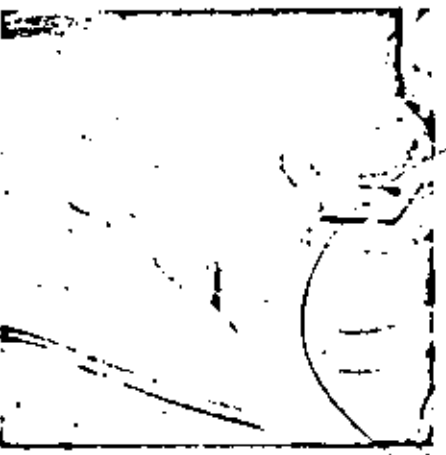

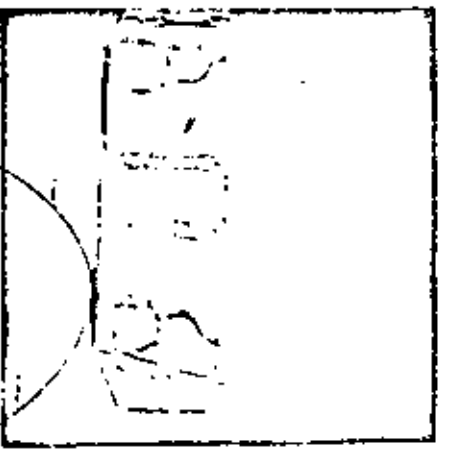

Engineering Methods Inc.

EMI

301 North 5th Street
Lafayette, IN 47901
317/742-0047

Professionals in Stress Analysis

COMPUTER REQUIREMENTS

The BERSAFE stress analysis package is written in FORTRAN 4 for the IBM 370. A few extensions to standard ANSI fortran have been used but in general it is easily converted for other machines.

Versions of the package have been installed over the years on various machines produced by the following manufacturers:

IBM, ICL, DIGITAL, UNIVAC, PRIME,

CDC, BURROUGHS, GEC.

The most recent versions of the programs are available for the larger IBM machines from IBM 4331 to IBM 370, and the Digital VAX 11/780.

If you would like details regarding the installation of the BERSAFE package please contact the:

BERSAFE Advisory Group
CEGB Berkeley Nuclear Laboratories
Berkeley
Gloucestershire GL13 9PB

Tel: Dursley - 810451 Ext. 221

Specially known for applications to fracture mechanics.

Computational
Mechanics
Consultants

3601A Chapman Highway
Knoxville, TN 37920
Phone: (615) 577-5494

COMOC: Q1D-EULER

FINITE ELEMENT COMPUTER PROGRAM FOR SOLUTION OF THE QUASI-ONE-DIMENSIONAL INVISCID NAVIER-STOKES (EULER) EQUATIONS

Also:
- Computer-aided Drafting
- 2-D, 3-D Unsteady Heat Transfer
- Interactive Data Management

FEATURES

- ✓ Linear and Quadratic Basis
- ✓ Implicit, Time-Accurate
- ✓ Phase-Selective Non-Linear Dissipation
- ✓ Mixed Flows with Shocks
- ✓ Accurate and Efficient

DISTRIBUTED BY

COMCO PRODUCTS, INC.

3601-A CHAPMAN HIGHWAY

KNOXVILLE, TENNESSEE 37920

Note: This material forms a portion of an Air Force Wright Aeronautical Laboratories Technical Report summarizing a research project on finite element numerical methods for the multi-dimensional Navier-Stokes equations. This report will be published approximately June, 1982.

DIVISION DE EDUCACION CONTINUA
FACULTAD DE INGENIERIA U.N.A.M.

EL METODO DEL ELEMENTO FINITO EN LA INGENIERIA MECANICA

LIBRERIA DE ELEMENTOS

DR. NICHOLAS J. SALOMON

ABRIL 1982

CAE APPLICATIONS SOFTWARE

Computerized Engineering System

The CAE integrated applications software system likewise must address all functions and applications required in mechanical product development. The software must be distributed and portions of each package must run on intelligent graphic workstations, supermini product computers, large mainframes in a batch mode, and on network foreground and background processors.

The core of the applications software runs in an interactive mode on the new virtual memory "supermini" mid-range mainframes, i.e., DEC VAX 11/780 and/or IBM 4341, as shown in Figure 15. When these machines get loaded, or large computations are required, processing is automatically deferred to large in-house mainframes and/or to network computers. Such processing is performed in a batch mode and returned to the product computer when completed. The system command executive and product data base management system automatically "spawn" particular applications software packages and provide all appropriate data required (available) for the application.

Particular applications on interactive graphics minicomputer workstations are used to offload the product computer with those input/output graphic and computational activities that require the highest level of interactivity with the operator.

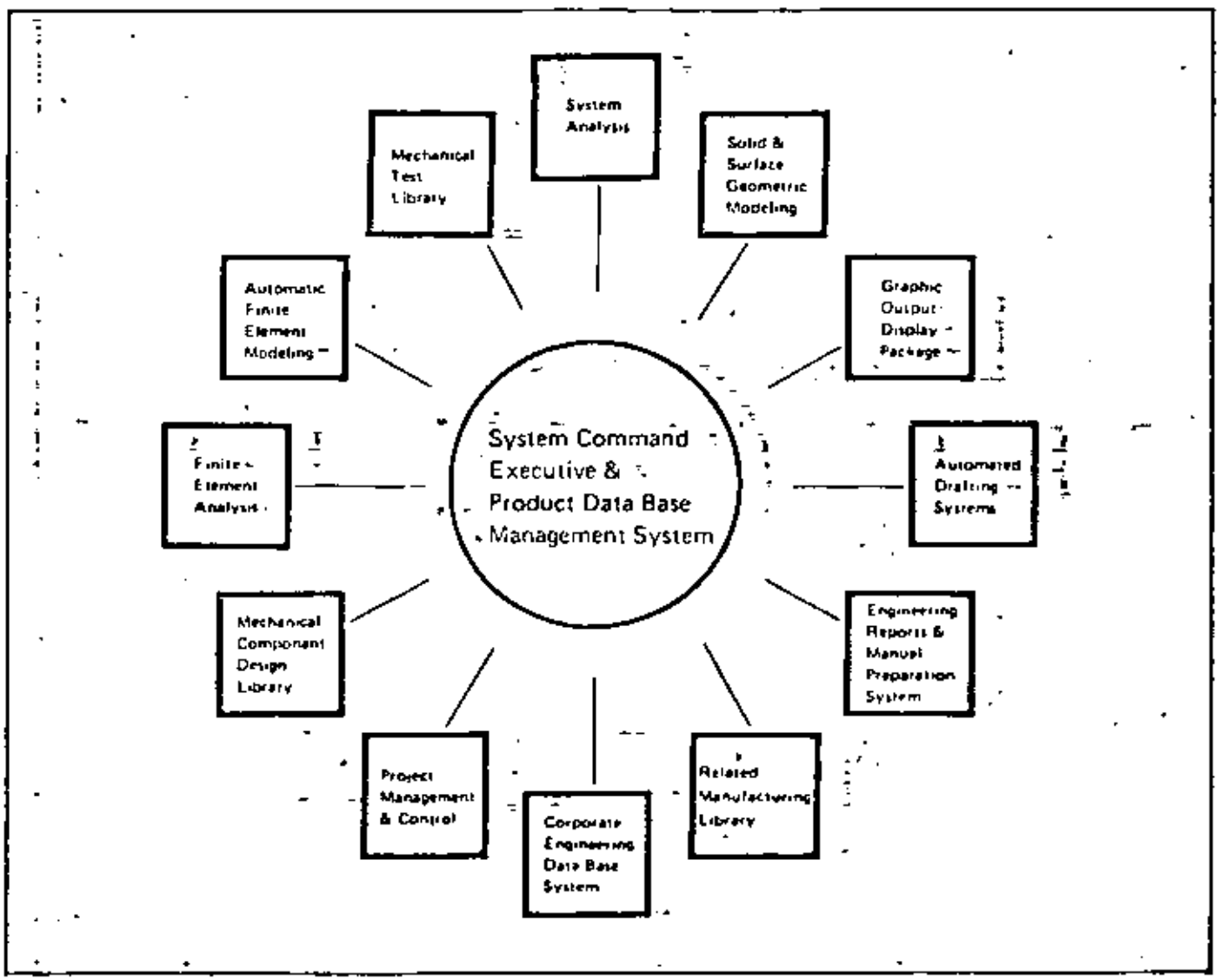

Figure 15. CAE Integrated Applications Software System

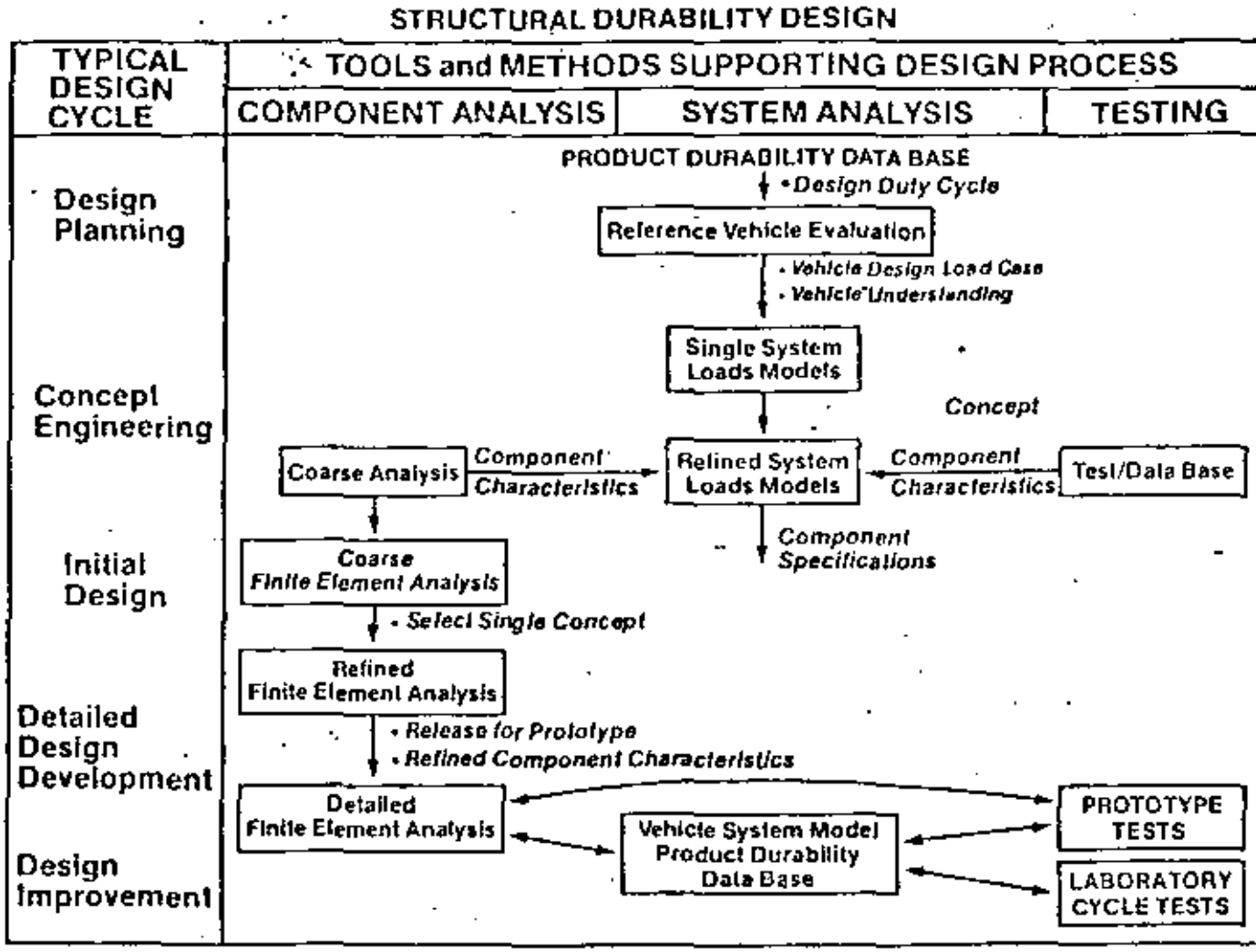

Figure 11. CAE Approach for Structural Durability Design

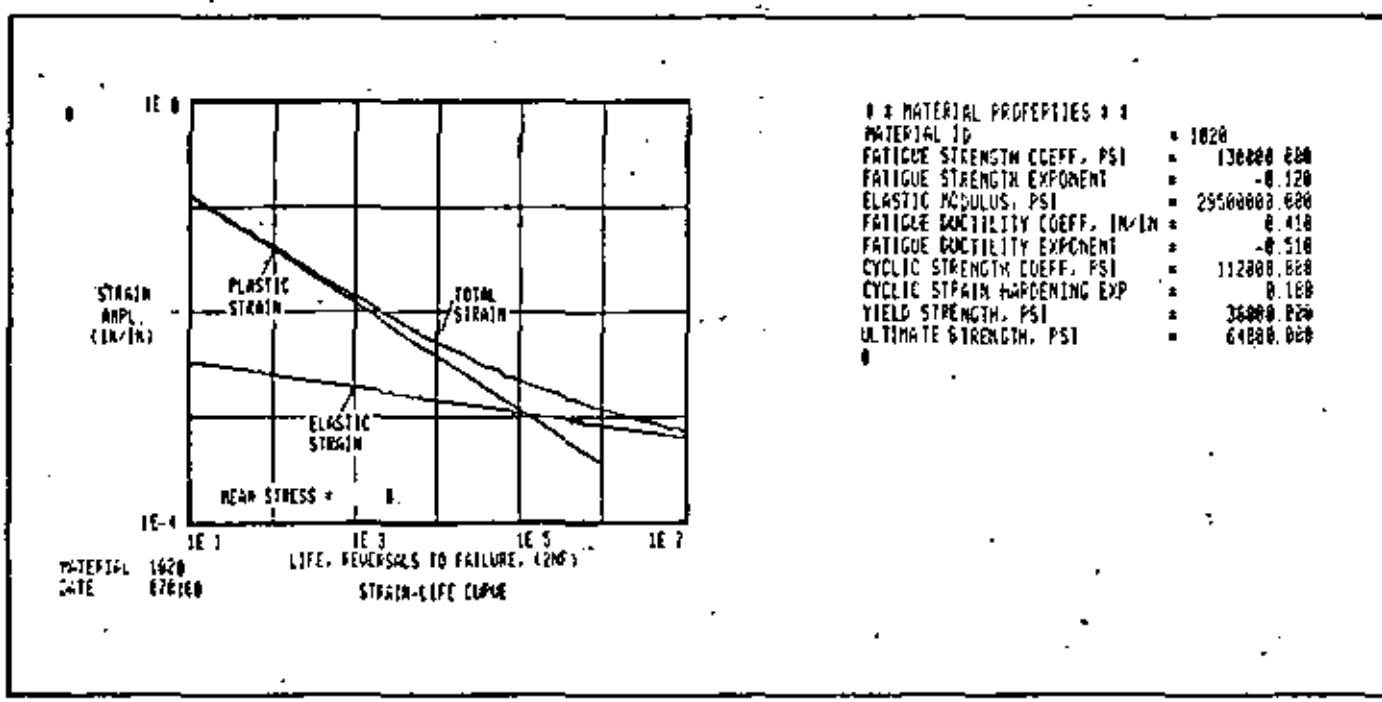

Figure 12. Material Properties from the Corporate (or Division) Engineering Data Base System

ELEMENTS AND SOME POPULAR (?) COMPUTER CODES

PROGRAM	AUTHORS
SUPERB	STRUCTURAL DYNAMICS RESEARCH CORPORATION (SDRC)
EASE2	ENGINEERING ANALYSIS CORPORATION (EAC)
STARDYNE	MECHANICS RESEARCH INC. (MRI)
NASTRAN	MCNEAL-SCHWENDLER CORP. (MSC)
ANSYS	SWANSON ANALYSIS SYSTEMS (SAS)
MARC-CDC	MARC ANALYSIS CORP.

1978

TYPES OF ANALYSIS

ANALYTICAL CAPABILITY		PROGRAM					
		EASE2	STARDYNE	NASTRAN	ANSYS	MARC	SUPERB
LINEAR STATICS	MECHANICAL LOADS	•	•	•	•	•	•
	TEMPERATURE LOADS	•	•	•	•	•	•
	EULER BUCKLING			•		•	
	INERTIA RELIEF			•			
DYNAMICS	MODE/FREQUENCY	•	•	•	•	•	
	FREQUENCY RESPONSE		•	•	•		
	TRANSIENT RESPONSE	•	•	•	•	•	
	SHOCK SPECTRA	•	•		•		
	RANDOM RESPONSE		•	•			
	NONLINEAR TRANSIENT			•	◦	•	
NONLINEAR STATICS	NONLINEAR BUCKLING					◦	
	LARGE DISPLACEMENT				◦	•	
	PLASTICITY			•	•	•	
	CREEP				•	◦	
	VISCOELASTICITY			•		•	
	LARGE STRAINS					◦	
HEAT TRANSFER	STEADY STATE			•	•	•	•
	TRANSIENT			•	•	•	
SUBSTRUCTURES (SUPER-ELEMENTS)	STATIC		•	•	•		
	DYNAMIC		•	◦	•		
	CYCLIC SYMMETRY			•			
MISCELLANEOUS	FRACTURE MECHANICS				◦	•	
	FLUIDS			•	•	◦	
	ELECTRIC CIRCUITS				◦		
	OPTIMIZATION			◦			
	ACOUSTIC CAVITIES			•			
	FATIGUE DAMAGE				◦		

STRUCTURAL ANALYSIS ELEMENT/MATRIX LIBRARY

ELEMENT			PROGRAM					
			EASE2	STARDYNE	NASTRAN	ANSYS	MARC	SUPERB
LINE ELEMENTS	ROD				•	•	•	
	BEAM		•	•	•	•	•	•
	TAPERED BEAM					•	•	
	OFFSET BEAM		•	•	•	BEAM OFFSET		•
	PINNED END BEAM		•	•	•			•
	CURVED BEAM							
FLAT MEMBRANES AND PLATES	3 NODE TRIANGLE	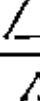	•	•	•	•	M	
	6 NODE TRIANGLE	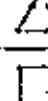			M		M	C
	SHEAR PANEL				•			
	4 NODE QUAD	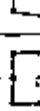	•	•	•		M	•
	8 NODE QUAD					S	M	S
CURVED SHELLS	3 NODE TRIANGLE							
	6 NODE TRIANGLE							C
	4 NODE QUAD						•	•
	8 NODE QUAD							S
	REDUCED THICK SHELL				J			

NOTES:

- M Membrane and/or plane strain only (no plate bending)
- S Includes sub parametric forms with fewer nodes
- C Also includes cubic isoparametric element with two midside nodes

STRUCTURAL ANALYSIS.
ELEMENT/MATRIX LIBRARY (continued)

ELEMENT				PROGRAM					
				EASE2	STARDYNE	NASTRAN	ANSYS	MARC	SUPERB
AXI-SYMMETRIC ELEMENTS	SHELLS	CONICAL				•	•	D	
		CURVED				•		•	
	TRIANGULAR RINGS	3 NODE				•	•	•	D
		6 NODE				•		D	C
	QUAD RINGS	4 NODE				•	•	•	•
		8 NODE					S	•	S,
SOLID ELEMENTS	TETRA-HEDRON	4 NODE			•	•	•	D	
	WEDGES	6 NODE		•	•	•	•	D	D
		15 NODE						•	D
	HEXA-HEDRONS	8 NODE		•	•	•	•	•	•
		20 NODE				S		•	S,
PIPE ELEMENTS		STRAIGHT		•	•	•	•	•	
		ELBOW		•	•		•	•	
		TEE			•				

NOTES:

- S Includes subparametric forms with fewer nodes
- C Also includes cubic isoparametric element with two midside nodes
- D Degenerate case

STRUCTURAL ANALYSIS
ELEMENT/MATRIX LIBRARY (continued)

ELEMENT				PROGRAM					
				EASE2	STARDYNE	NASTRAN	ANSYS	MARC	SUPERB
GENERAL STIFFNESS ELEMENTS		SPRING	K	1	•		•	•	•
		SCALAR SPRING				•			
		6 x 6 or 12 x 12 MATRIX			•	•	•		•
		GENERAL MATRIX				•			
MASSES	ELEMENT	LUMPED (DIAGONAL)		2	2	2	2		
		CONSISTENT				2	2	2	
	NON-STRUCTURAL	SCALAR (DOF)				•		•	
		NODAL		•	•	•	•		
		DISTRIBUTED				•			
		GUYAN REDUCTION			•	•	•		
		GENERAL MATRIX				•	•		
DAMPING		SCALAR				•			
		DASHPOT				•	•		
		DISCRETE VISCOUS [C] = α[K] + β[M]		•	•	•	•	•	
		STRUCTURAL (1 + ig)[K]				•			
		MODAL VISCOUS		•	•	•		•	
		GENERAL MATRIX	F			•	•		
OTHER ELEMENTS		GAP					•	•	
		FRICTION					•	•	
		RIGID		3	•	•			
		REBAR SOLID						•	
		ELASTIC FOUNDATION						•	
		CRACK TIP					•	•	
		LAMINATED SHELL					•	•	
		PLOT ONLY			•	•			

NOTES:
1. See restraints
2. Generated from density
3. See constraints

HEAT TRANSFER–CONDUCTING ELEMENTS

ELEMENT			PROGRAM					
			EASE2	STARDYNE	NASTRAN	ANSYS	MARC	
LINEAR					•	•	•	
PLANAR	3 NODE TRIANGLE				•	•	•	P
	4 NODE QUAD				•	•	•	
	8 NODE QUAD					S	•	S
	TRANSVERSE CONDUCTING SHELL					•		
AXISYMMETRIC	TRIANGULAR RING				•	•	•	P
	4 NODE QUAD RING				•	•	•	
	8 NODE QUAD RING					S	•	
SOLID	TETRAHEDRON				•	•		
	WEDGE				•	•	D	
	8 NODE BRICK				•	•	•	
	15 NODE WEDGE						D	
	20 NODE BRICK						•	
GENERAL MATRIX INPUT					•			

NOTES:

- S Contains subparametric forms with fewer number of nodes
- P Also contains parabolic isoparametric element with one midside node
- C Also contains cubic isoparametric element with two midside nodes
- D Degenerate case

COORDINATE SYSTEMS AND MATERIAL PROPERTIES

		FEATURE	PROGRAM				
			EASEZ	STARDYNE	NASTRAN	ANSYS	MARC
COORDINATE SYSTEMS	BASIC (GLOBAL)	CARTESIAN	•	•	•	•	•
		CYLINDRICAL	•	•	•	•	
		SPHERICAL		•	•	•	
		GENERAL					1
	SKEWED (LOCAL)	CARTESIAN	•	•	•	•	•
		CYLINDRICAL	•	•	•	•	
		SPHERICAL			•	•	
		GENERAL					1
		MIXED	•	•	•	•	•
MATERIAL PROPERTIES		ISOTROPIC	•	•	•	•	•
		2-D ORTHOTROPIC		•	•	•	1
		3-D ORTHOTROPIC				•	1
		TEMPERATURE DEPENDENT	•		•	•	•
		STRESS DEPENDENT			•	•	•
		TIME DEPENDENT				•	•
		NONLINEAR ELASTIC					•
	WORK HARDENING	ISOTROPIC				•	•
		KINEMATIC				•	•
		COMBINED					•
		DRNL 10 CYCLE					•
		GENERAL					1

NOTES:

1 = Performed by user subroutine

BOUNDARY CONDITIONS

FEATURE				PROGRAM					
				EASE2	STARDYNE	NASTRAN	ANSYS	MARC	
LOADING	STATIC	CONCENTRATED		•	•	•	•	•	
		DISTRIBUTED (BEAM)		•	•	•	•	•	
		PRESSURE	PLATES/SHELLS	•	•	•	•	•	
			AXISYMMETRIC ELEMENTS			•	•	•	
			SOLIDS	•	•	•	•	•	
		TEMPERATURE		•	•	•	•	•	
		ACCELERATION		•	•	•	•	•	
		ROTATIONAL VELOCITY		•	•	•	•	1	
		COMBINATION		•	•	•	•		
		AXI-SYMMETRIC	AXISYMMETRIC SHELLS			•	•		
			AXISYMMETRIC RINGS				•		
	DYNAMIC	TIME DEPENDENT		•	•	•	•	•	
		FREQUENCY DEPENDENT			•	•			
		PSD RANDOM			•	•			
		SHOCK SPECTRUM		•	•		•		
DISPLACEMENT CONSTRAINTS		SINGLE POINT*		•	•	•	•	•	
		MULTI POINT*		2		•	•	•	
		SPECIFIED NONZERO DISPLACEMENT		•	•	•	•	•	
HEAT TRANSFER		HEAT SOURCE/SINK				•	•	•	
		CONVENTION				•	•	•	
		RADIATION				•	•	•	
		SPECIFIED TEMPERATURE				•	•	•	

TES: *Single point constraint ≡ enforced zero translation(s) and/or rotation(s) in coordinate(s) associated with a node point
Multi-point constraint ≡ enforced linear constraint relationships between translation(s) and/or rotation(s) which may b
associated with different node points

1 Applies to some elements
2 Specialized forms of rigid and interface coupling
3 Displacement components set equal on different nodes
4 Stand alone program

PRE- AND POST-PROCESSING

		FEATURE	EASE2	STARDYNE	NASTRAN	ANSYS	MARC	SUPERB
PLOTTING	INPUT	UNDEFORMED GEOMETRY	+	•	•	•	•	•
		NODE LABELS	+	+	•	•	•	•
		ELEMENT LABELS	+		•	•	•	•
		PROPERTY-LABELS			•	•		•
		2-D SECTIONS				•	•	
		BOUNDARY CONDITION LABELS	+		•			
		HIDDEN LINES REMOVED					+	
	OUTPUT	DEFORMED GEOMETRY	+	•	•	•	•	•
		CONTOURS 2D STRUCTURE		+	•	•	•	•
		CONTOURS SOLID STRUCTURE				•	•	•
		TIME HISTORY	4	•	•	•	+	
		FREQUENCY RESPONSE		•	•,4			
		POWER SPECTRAL DENSITY		•	•,4			
		ARBITRARY-X VS. Y				•	+	
DATA GENERATION		NODES	1	1,2	1,2,3	1,2	2,3	1,2
		ELEMENTS	1	1	1,2,3	1,2	2,3	1,2
		RESTRAINTS	1	1	1,2	1	2,3	1
		LOADS	1	1	2	1	2,3	1
OUTPUT SORTING		BY LOAD CASES		•	•	•	•	•
		BY ELEMENT	•		•			
		MAX/MIN SUMMARY	•	•	•			•
		SELECTED NODES AND/OR ELEMENTS		•	•	•	•	
BANDWIDTH MINIMIZATION			•	•	•	W	•,W	+,1

NOTES:
1 Generates data in 1 "dimension"
2 Generates data in 2 "dimensions"
3 Generates data in 3 "dimensions"
4 Printer plots
+ Stand alone program
W Wavefront solution

NISA ELEMENT LIBRARY

ELEMENT TYPE	DISPLACEMENT ORDER / DEGREES OF FREEDOM	LINEAR	PARABOLIC	CUBIC	LINEAR PARABOLIC	LINEAR PARABOLIC	LINEAR CUBIC	PARABOLIC CUBIC	LINEAR PARABOLIC CUBIC
2D ISOPARAMETRIC PLANE STRESS* PLANE STRAIN* AXISYMMETRIC*	UX UY								
3D ISOPARAMETRIC GENERAL SHELL (DESCRIBED BY MIDDLE SURFACE NODES)	UX UY UZ RX RY RZ								
3D ISOPARAMETRIC THICK SHELL* (DESCRIBED BY TOP AND BOTTOM NODES)	UX UY UZ								
3D ISOPARAMETRIC HEXAHEDRON	UX UY UZ								
3D ISOPARAMETRIC SUPER SHELL*	AT CORNER NODES: UX UY UZ AT MIDSIDE NODES: UX UY UZ RX RY								

* STRAIGHT BEAM	3D	2D	SYM. ASYM.	
* STRAIGHT BEAM WITH OFFSETS	3D	2D	SYM, ASYM	
* SPAR	3D	2D	1D	
* AXIAL SPRING	3D	2D	1D	
* TORSIONAL SPRING	3D	2D	1D	

MASS ELEMENTS

- 1D MASS (Mx = M)
- 2D MASS (Mx = M, My = M)
- 3D MASS (Mx = M, My = M, Mz = M)
- 2D GENERAL MASS (Mx, My, It)
- 3D GENERAL MASS (Mx, My, Mz, Ix, Iy, Iz)

OTHER ELEMENTS

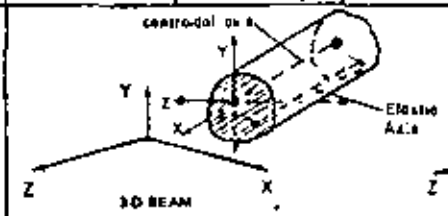

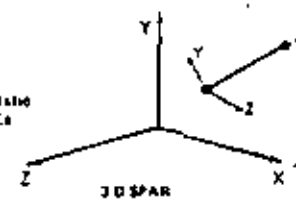

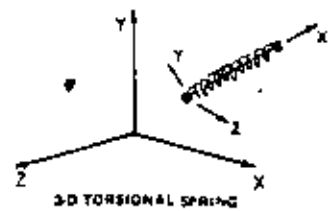

NEW ELEMENTS

6-NODE

16-NODE

9-NODE

12-NODE

AXISYMMETRIC ELEMENT WITH UNSYMMETRIC LOADING 8-NODE

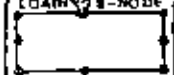

SANDWICH SHELLS
TYPICAL CONSTRUCTION METAL-FOAM-METAL COMPOSITE-HONEY COMB-COMPOSITE MAY BE MULTI-TIERED

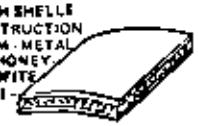

LAMINATED COMPOSITE SHELLS
SYMMETRICAL OR UNSYMMETRICAL LAYUP

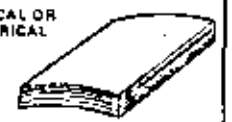

* THESE ELEMENTS ARE ALSO AVAILABLE FOR STEADY STATE AND TRANSIENT HEAT TRANSFER, SEEPAGE, TORSION AND OTHER FIELD PROBLEMS

3.4 PROBLEM FORMULATION

The explanation of any complex activity must be subdivided into phases or steps in order to be intelligible. In the case of a computer program for structural analysis it is convenient to divide the total effort into a Problem Formulation Phase and a Problem Solution Phase. The termination of the Problem Formulation Phase is arbitrarily chosen to occur at the point where the properties of the structure have been reduced to matrix form. (In the case of basic static analysis this occurs between blocks 4 and 5 in the flow diagram of Figure 1, Section 3.2.)

3.4.1 Structural Modeling

The beginning of the Problem Formulation Phase occurs in the mind of the analyst. He contemplates nature (or his navel, or whatever), decides what he needs to know, and constructs a mathematical problem whose solution, he hopes, will provide relevant answers to his questions. He will, naturally, require computational tools to solve his mathematical problem and, fortunately or unfortunately, the available tools have a strong influence on the analyst's choice of a mathematical problem. It would, after all, do no good to formulate a problem that could not be solved.

The range of choice in mathematical problem formulation provided by NASTRAN is, however rich in detail, limited to one basic approach, namely the use of finite element structural models. This means that the substitute mathematical problem refers to an idealized model with a finite number of degrees of freedom, a particular selection of topological objects (grid points and elements), and a limited range of structural behavior. The relevance of the behavior of the idealized structural model to the analyst's questions clearly depends on the particular choice of components for the model. This procedure, referred to as "structural modeling," is the most important step in the problem formulation phase, since the results of an analysis can be no better than the initial assumptions.

The User's Manual contains a chapter on structural modeling. Section 14 of the Theoretical Manual describes some advanced modeling techniques that utilize special features of NASTRAN. For the present, a small example will serve to indicate the general nature of the modeling process and some of the features of NASTRAN that relate to it.

Figure 1a shows a typical aircraft structure, a ring frame with a partial bulkhead acting as a floor support. Although poor results are obtained when such structures are analyzed without

From: The NASTRAN Theoretical Manual (Level 15), Richard H. MacNeal, Edit., April 1972, NASA, Wash., D.C., USA.

considering the shell to which the frame is attached, the analyst may have a special reason for doing so. The resulting idealized model of the frame can, in any case, serve as part of the model for the complete shell.

The idealized model selected by the analyst, Figure 1b, contains

13 grid points

4 Bar elements (B)

2 Rod elements (R)

2 Triangular Plate Elements (T)

3 Quadrilateral Plate Elements (Q)

Each grid point has six degrees of freedom (three translations and three rotations). The analyst has, however, elected to analyze the response of the frame to a pair of vertical loads so that it is unnecessary to consider out-of-plane motions of the frame. The out-of-plane motions are eliminated by applying single point constraints to three of the degrees of freedom (two rotations and one translation) at each gridpoint (This can be implemented with a single data card).

One of the necessary tasks in preparing input data is to specify the location of grid points. In NASTRAN grid point locations can be specified by rectangular, cylindrical or spherical coordinate systems (see Figure 2) and there may be an unlimited number of coordinate systems of each type in a given problem. All that is required is that they be related, directly or indirectly, to each other and to a "basic" coordinate system, which is rectangular. In the example of Figure 1, the analyst found it convenient to locate grid points on the ring frame (points 1 to 4) with a cylindrical coordinate system and to locate points on the floor bulkhead (points 5 to 13) with a rectangular coordinate system.

(see Fig. 2)

A separate task is the selection of coordinate systems to express the components of motion at grid points. In the example of Figure 1, the coordinate systems for motion have been selected to be identical to the coordinate systems for grid point location, although this is not required.

It will be noted in Figure 1b that the grid points for the ring frame are located on the outer edge of the frame rather than along its centerline. This will not result in poor accuracy if the provision for offsetting the neutral axis of Bar elements is exercised. Reinforcing Rod elements (R1 and R2), which have axial stiffness only, are placed between grid points 11, 12, and 13 to

simulate the stiffener along the centerline.

The Plate elements (T's and Q's) are selected to contain membrane (plane stress) properties only, since out of plane bending is precluded by the nature of the loading. No restraint on in-plane rotation (θ_z) is provided by the plate elements so that the θ_z component of motion must be eliminated by more single point constraints at gridpoints 6 to 13. A special problem occurs at grid point 5 because of the requirement to maintain compatibility of inplane rotation between the adjacent bar element (B_4) and the adjacent triangular plate (T_1). The problem is solved by means of a multipoint constraint between inplane rotation (θ_z) at grid point 5 and the vertical motions (u_y) at grid points 5 and 6. The equation of constraint is

$$\theta_{z5} = \frac{u_{y5} - u_{y6}}{x_5 - x_6} \qquad (1)$$

Additional single point constraints are required along the centerline of symmetry to constrain motions in the x direction (including the θ direction at gridpoint 1). A special type of single point constraint, known as a reaction, is used to constrain vertical motion at grid point 13. Constraints of this type are automatically removed when a static analysis is followed by a dynamic analysis. In addition, a special check calculation is provided (see Section 3.5.5) to determine whether the input impedance at reaction points is correct.

It will be noted that the grid points in Figure 1 have been numbered consecutively starting at the top. More than a sense of orderliness is involved since the sequencing of grid point numbers affects the bandwidth of the stiffness matrix and the resulting computer solution time (see Section 2.2). Grid point sequencing strategy is discussed in the User's Manual. The main idea is that the arithmetic differences between the sequence numbers of grid points that are physically adjacent should be minimized.

In order to facilitate grid point sequencing for the preservation of bandwidth, the user is permitted to specify grid point numbers in two different ways. The external identification numbers can be assigned to grid points in any manner the user desires. Element connection and load information prepared by the user refers to the external identification numbers. The internal sequence numbers are generated by the user in a paired list that relates external and internal numbers. Since the internal sequence numbers appear nowhere else in the input data, they may easily be changed, if desired, to reflect an improved banding strategy. Preparation of the paired list is

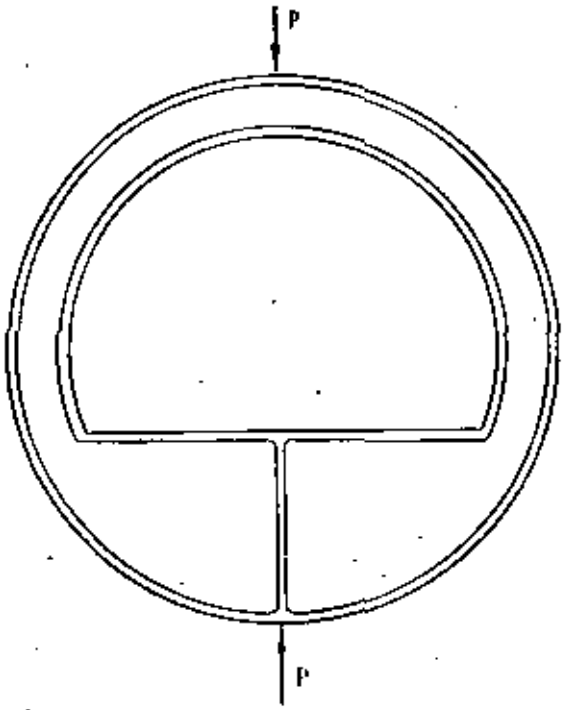

a. Ring frame with floor bulkhead.

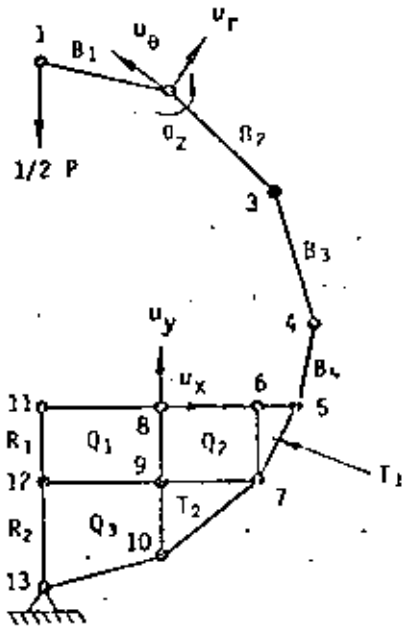

b. Idealized structural model.

Figure 1. Example of structural modeling.

Figure 2

COMMON COORDINATE SYSTEMS

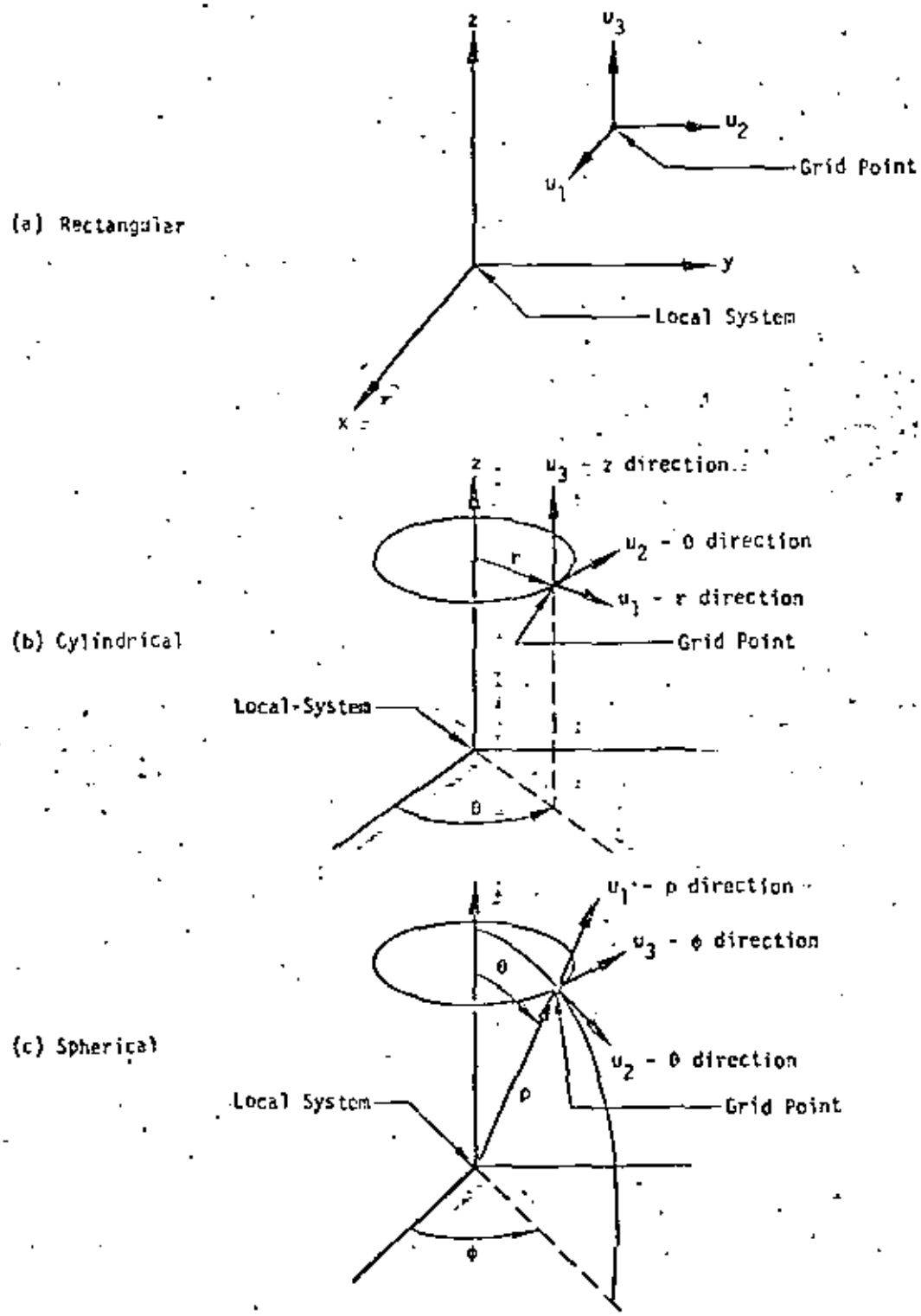

VII CONGRESSO BRASILEIRO DE ENGENHARIA BIOMÉDICA

PLATE DESIGN CONSIDERATIONS FOR THE STUDY OF HUMAN POSTURAL SWAY

C. F. HARRIS, Ph.D., N. J. SAIAMON, Ph.D., and R. C. WEBER, Ph.D.

THE MEDICAL COLLEGE OF WISCONSIN
MILWAUKEE, WISCONSIN, USA

ABSTRACT

The high cost of commercially available force plates instrumented to quantify postural sway can be prohibitive. Custom plate design and construction within the institutional environment therefore is not uncommon. Some plate designs however, may yield erroneous measurements. Several models of flat, square-shaped plates which are corner supported are discussed. The kern of the plate surface is described which relates plate loading to support reactions. Loads placed inside this area result in support compression, while those placed outside cause at least one support to experience tension. A set of equations are derived through the use of curve fitting procedures to describe the kern boundary as a function of support stiffness. The findings indicate that the type of force transducer used for corner support (unidirectional or bidirectional), the type of connection between the plate and transducers, plate weight and dimensions, subject weight, and transducer preloads are all critical to accurate measurements. An aid is suggested for the static calibration of plates which utilize bidirectional transducers.

RESUMO

O custo das plataformas de medida de força comerciais com instrumentacao para medir instabilidade de postura pode ser proibitivo. Torna-se então comum o projeto e a construcao de plataformas especiais pelas instituicoes interessadas. Alguns destes projetos, entretanto, produzem medidas erroneas. Varios modelos de plataformas quadradas planas com suporte nos cantos sao discutidos. A superficie da plataforma (kern) que relaciona carga aplicada e reacao nos suportes e descrita. Cargas dentro desta superficie resultam em compressao dos suportes, enquanto que cargas fora desta area resultam em tensao em ao menos um dos suportes. Equacoes sao obtidas usando curvas de aproximacao para descrever os limites desta superficie em funcao da rigidez dos suportes. Os resultados indicam que o tipo de transdutor de força usado nos suportes de canto (unidirecional ou bidirecional), o tipo de conexao entre plataforma e suporte, o peso e dimensoes da plataforma, o peso da pessoa sendo testada, e a carga inicial dos transdutores sao todos parametros criticos para medicao correta. Sugestoes para calibracao estatica da plataforma com transdutores bidimensionais sao apresentadas.

INTRODUCTION

The quantitative study of human postural sway is classically performed by placing a subject on an instrumented platform. Data from such tests describes the position history of the body center of pressure during the test epoch. This information is then used to define ranges of normal sway, and to diagnose various pathological conditions.

The purpose of this paper is to present the results of a detailed study of the support reactions of a plate which is square in shape and corner supported. In the loading of these plates, there exists a locus of load points which produce zero force in at least one support. All load points interior to this locus produce compression in all supports and this region is called the kern of the section, i.e., Singer [5]. If loads are located exterior to the kern causing tension to occur in any support, then only bidirectional force transducers which are pinned at the plate corners will transduce correct information. The concern therefore is with those designs in which the force transducers are pinned to the plate and are only compression sensitive. The results of this work establish the kern boundaries for plate designs incorporating various support stiffnesses. The plate dimensions and material properties were selected to conform with a design common to both research and clinical applications. It was found that the kern is not only sensitive to support stiffness and plate flexibility, but also to plate and subject weight, plate dimensions, and transducer preloading.

METHODS

Three methods are employed in this investigation. The first concerns the analysis of a rigid plate pinned to non-rigid corner supports, Fig. 1. In this case, the four unknown support reactions may be determined in closed form. Force and moment equilibrium considerations provide three equations, while displacement compatibility requirements provide the fourth. Inertial shear terms in the plane of the plate in the X and Y directions are included in the moment equilibrium equations, and can be estimated through the use of an inverted pendulum model, Gurfinkel (3). For a typical sway frequency of 1Hz and sway amplitude of 5.08 cm, these terms produce a maximum angular vertical reaction force of only .093% of the static component of the applied downward load, W. This negligible vertical component may be safely excluded in the solution of the equilibrium equations for the support reactions, A, B, C, and D.

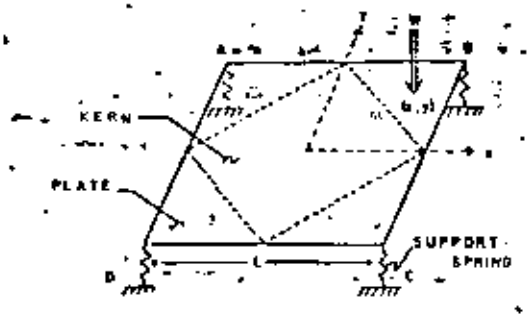

Fig.1: Corner supported, square plate.

The kern boundary of the plate is defined by the equations which result from consecutively setting each support reaction to zero. The regions inside or outside of the kern are associated with support reactions greater or less than zero respectively. For instance, at support D, one finds these regions determined by

$$Y \geq -X + L/2 \text{ for } D \geq 0 \quad (1)$$

where X, Y denote the position of W, L is a plate length dimension, and D is the support reaction taken as positive if the spring is in compression. Equation (1) defines the kern over a single plate quadrant which because of symmetry allows complete kern mapping.

Inclusion of plate weight, P, in the closed form analysis requires an additional term in the kern solution. Once again looking at support D, the expanded equation is

$$Y \geq -X + L/2 + PL/2W \text{ for } D \geq 0 \quad (2)$$

This demonstrates the combined effects of plate weight, subject weight, and plate side length upon the kern boundary location. Similar results are obtained when the supports are compressively preloaded. In order to generalize the solution, plate weight and preload values are therefore set equal to zero.

Finite element analysis (FEA) techniques are employed in the second method to investigate plates having nonzero relative support-to-plate stiffnesses, Bathe et al (1).

The plate/thin shell quadrilateral element is chosen to model the flat plate under plane stress conditions and the truss element is chosen for the springs. The plate dimensions are taken to be 76.2 cm long and 1.27 cm thick; aluminum having an elastic modulus of 6.89×10^{10} N/m^2 and Poisson's ratio of 0.33 is chosen for the plate material. The truss elements are pinned (ball and socket joint) to the plate corners and rigidly attached to the support surface. Each corner of the plate is constrained from lateral motion, while bending and vertical deflection are permitted here and throughout the plate. The lateral motion restraint at the corners serves to restrain the plate from rigid body motion. Local lateral motion at these contact points is also restrained, however, the magnitude of such motions is sufficiently small to proceed despite this limitation.

The loading consists of the plate weight (196.16 N) modelled through the use of a uniform surface pressure distribution exerted on the upper plate face, and a single concentrated nodal load (890 N) to represent W. The plate is descretized into 72 elements (90 nodes) in order to maintain solution economy and yet retain adequate resolution of kern boundary points. The plate model takes advantage of plate symmetry and consists of quadrilateral elements densely packed into a single quarter of the plate and sparsely located throughout the remainder, Fig. 2.

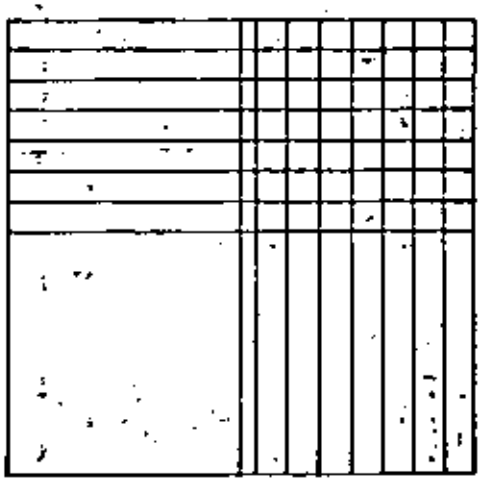

Fig.2: 72 element grid over plate surface.

The kern map is obtained by placing W at selected nodes and noting all support conditions. If a support attains a value of

plate weight only, this load location is noted as a kern boundary point. This method of mapping eliminates the effects of plate weight and allows a more generalized solution. As the analysis demonstrates that support reaction varies linearly with load point in the X and Y directions in the plane of the plate, linear interpolation is used to precisely locate the kern boundary point.

The final method employed in the study consisted of an experimental analysis of two square balance platforms of differing dimensions. The kern of these plates was mapped by placing a cylindrical lead weight (18 N) with center drilled hole at various locations and noting when one or more of the support transducers indicated a plate only load. The position of the lead weight in such a case was noted as lying on the kern boundary.

RESULTS

The kern for a massless rigid plate on elastic supports is found to be diamond shaped as shown by the dashed boundary of Fig. 1. This kern also represents a limiting shape as the relative support-to-plate stiffness is zero. The FEA modelling results are presented in Fig. 3. A family of kern shapes for support stiffnesses ranging from the theoretical minimum of 0 N/m to the theoretical maximum of ∞ are shown over one quadrant of the symetrical massless plate. It is clear that the kern boundary shifts outward from the center as support stiffnesses increase. The diamond shaped kern corresponds to a support stiffness approaching 0 N/m for a nonrigid plate. At the other extreme, the plate-shaped kern corresponds to an infinite support stiffness. It follows that the two extremes can be viewed as independent of plate stiffness and dependent upon support stiffnesses ranging from 0 N/m to ∞. Intermediate to the extremes, however, there occur an infinite set of possible kern shapes which are functions of both support and plate stiffness.

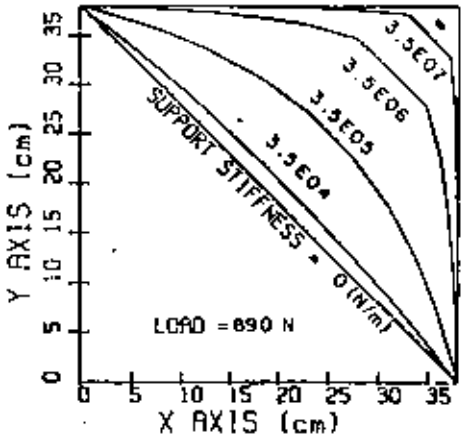

Fig.3: Kern boundary shapes over one plate quadrant.

Even though the kern is affected by the stiffness of the plate, the elastic slopes of the plate are negligible and the maximum corner-to-corner plate tilt for these cases studied is 0.0236 rad for a support stiffness of 3.5×10^4 N/m. With this in mind, it is safe to assume that the linear elastic theory sufficiently describes the behavior.

The effect of varying the plate dimensional parameters, L and t, the elastic modulus, E, and Poisson's ratio, ν, is also of concern in the analysis. A useful parameter in the description of plate stiffness (4), is

$$\kappa = \pi t^3/(L^2 - \nu^2 L^2) \approx \pi t^3/L^2 \quad (3)$$

Results from several models confirmed the usefulness of eqn. 3. These plates had different dimensions and material properties, yet same stiffness parameter, κ, and produced the same set of kern boundaries. Thus, the results of this study apply to the family of plates having a κ value of 2.73×10^5 N/m, regardless of E, t, L and ν values.

Results from a laboratory test of two square plates of unequal dimension resting upon supports of stiffnesses greater than 1.5×10^5 N/m are depicted in Fig. 4. The shape and location of the kern boundary in these tests closely approximates that expected based upon the FEA results.

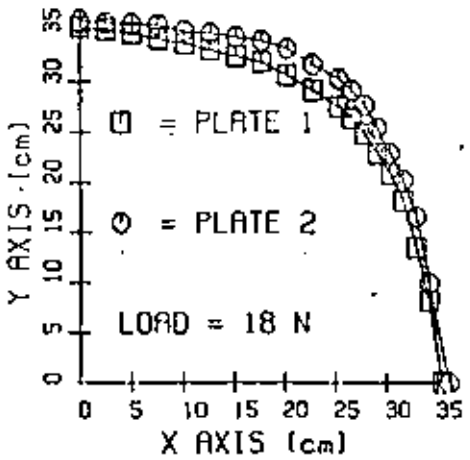

Fig.4: Kern boundary points found through physical testing of 2 dissimilar plates.

DISCUSSION

It is clearly demonstrated that for a massless corner supported plate having a stiffness parameter of 2.73×10^5 N/m, the kern boundary loci are a function of support stiffness. For the case of a rigid plate on elastic supports, the kern boundary may be described in closed form and is shown to occupy 50% of the total plate area. At the other extreme, any plate resting upon rigid supports possesses a kern boundary defined

by the plate edges and occupies 100% of the plate area. The crucial factors in this analysis are plate stiffness and support stiffness, with the kern boundary existing as a function of support stiffness alone for any given plate stiffness. If the support stiffness is held constant, the kern boundary is shown to depend upon a plate stiffness parameter κ as given by eqn. 3.

Further inspection of the relationship between support stiffness and kern boundary location for a given family of plates (i.e. κ = constant) yields the equation

$$X^n + Y^n = R^n \qquad (4)$$

where X, Y define the kern location, $R = L/2$ and n is a function of support stiffness. Clearly if $n = 1$, eqn. 4 defines a straight line which represents the diamond shape in the first quadrant; if $n = 2$, the kern shape is a circle. Not so obvious is that as $n \to \infty$, eqn. 4 approaches the function $Y = R = L/2$, $0 \le X \le L/2$, which describes the top edge of the plate. Hence n varies as the stiffness of the supports to produce a family of curves.

To be of practical use, a relationship between n and spring stiffness K is necessary. Attempts to find a linear correlation revealed a log-log transformation as the optimal choice. The first and second order equations are

1st order: $\log n = 0.33119 \log K - 1.53089$ with $F = 1.639 \times 10^{-2}$ (5a)

2nd order: $\log n = 6.6790 \times 10^{-2} (\log K)^2 - 0.4762 \log K + 0.81764$ with $F = 4.8731 \times 10^{-4}$ (5b)

where F is the least squares error (2) defined by

$$F = \min \left\{ \sum_{i=1}^{N} (Y_i - f(X_i))^2 \right\}$$

and where $Y_i = \log n_i$ given by 4, $f(X_i) = \log n_i$ given by 5, i is a particular point in the (n,K) system and N is the total number of points. The 1st and 2nd order fitted results are illustrated in Fig. 5.

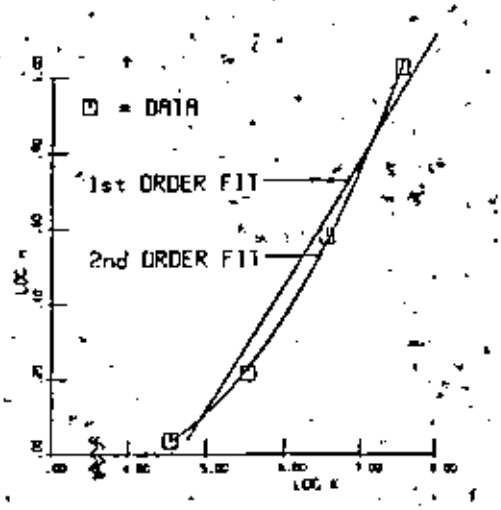

Fig.5: Curve fit results relating K to n.

SUMMARY

It has been shown that certain plate designs, dependant upon (1) type of transducers used for support (unidirectional or bidirectional) and (2) type of support-to-plate attachment (pinned or unpinned) may produce erroneous results if the load falls outside of the kern boundary. Inclusion of plate weight in the analysis causes the kern to shift an additional amount according to the relation, $PL/2W$. Compressive transducer preloads shift the kern towards the plate edges.

A curve fitting procedure employing the relation given in eqn. 4 is shown to be effective in mapping the kern boundary shape under all conditions of plate and support stiffness. Through further curve fitting, the dependent variable n in eqn. 4 is shown to be a function of the support stiffness K as expressed through eqns. 5 for a given plate stiffness parameter κ.

A means to aid in static plate calibration has also been indicated. Thus, for the family of plates described, employing pinned corner supports, one can readily check plate balance and transducer calibration by placing an object along the kern boundary and noting whether or not the diagonally opposed support indicates a load due to plate weight only.

The analysis presented in this paper should prove useful to those concerned with the quantification of human postural sway. Furthermore, this will be useful to anyone who employs corner supported plates as a measurement device. Yet, these results cannot be limited to users alone, but should prove important to platform designers as well.

ACKNOWLEDGMENTS

We gratefully acknowledge the financial support given through the Shriners Hospital for Crippled Children, Chicago, Illinois. We would also like to thank Dr. S. Silber of Clinical Technology Corp., Kansas City, Mo., and Dr. A. Nancea, Jr., Professor of Biomedical Engineering, Marquette University, Milwaukee, WI, for their continued and valuable suggestions and discussions throughout the course of investigation.

REFERENCES

1. Bathe, K., Wilson, E.L., Peterson, F.E., SAP IV, A Structural Analysis Program for Static and Dynamic Response of Linear Systems, A report to the National Science Foundation, Report No. EERC 73-11, June, 1973, revised April 1974.

2. Bendat, J.S., and Piersol, A.G., Random Data: Analysis and Measurement Procedures, 1st ed., Wiley-Interscience, New York, 1971, pp. 130,289.

3. Gurfinkel, E.V., "Mechanical Analysis of the Stabilographic Method," Bulletin of Experimental Biology and Medicine, Vol. 77, 1974, pp. 585-587.
4. Langhaar, H., Energy Methods in Applied Mechanics, 1st ed., John Wiley and Sons, New York, 1962, p. 162.
5. Singer, F.L., Strength of Materials, 2nd ed., Harper and Row, New York, 1962, pp. 320-324.

Also see: G.F. Harris, M.J. Salamon, R.C. Weber, "Effects of Subject Position on Balance Platform Measurements", J. Biomechanical Engineering, Vol. 103, 213-216, 1981.

Determine the stress concentration factor for the circular fillet in the axially loaded member shown in Fig. 12.4. The width of the member changes from 8 to 4 cm while the thickness remains constant at 0.50 cm. The normal stress at a point far to the right of the fillet has a uniformly distributed value of 44000 N/cm^2. The member is made from steel that has an elastic modulus of 2×10^7 N/cm^2 and a Poisson's ratio of 0.25.

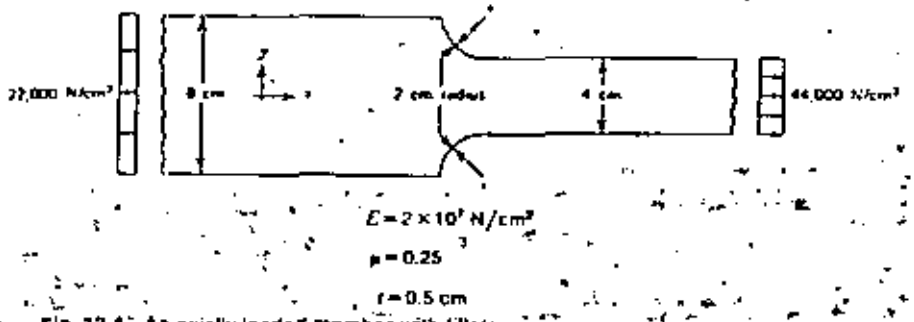

Fig. 12.4 An axially loaded member with fillets.

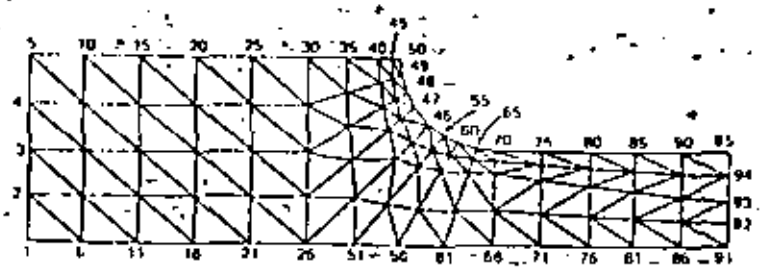

Fig. 12.6 Final subdivision of elements and boundary node numbers.

The calculated horizontal displacements for the nodes along the right edge are uniform at 0.0247 cm. These values indicate that we have reached a region of uniform strain, and thus stress, and that the length of the model is acceptable.

The stress components obtained in the solution are constant over the region of the element. The nodal values can be obtained by applying the consistent element resultant theory discussed in Chapter 6. The nodal values of the largest principal stress in a region around the fillet are presented in Fig. 12.7. The largest value occurs at node 65 and is 64567 N/cm^2. The stress concentration value relative to the 44000 N/cm^2 stress is 1.47. This value is reasonably close to the value of 1.42 given by Singer (1962, Table 13-1). This example will be considered again in Chapter 16.

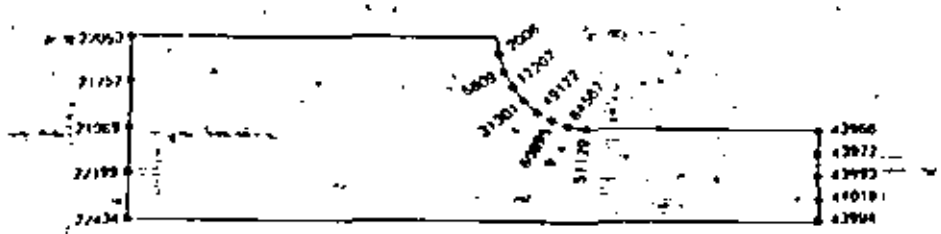

Fig. 12.7 Nodal values of σ_1 in the region of the fillet and at the ends.

(Ref: Segerlind, L.J., Applied Finite Element Analysis, John Wiley & Sons, Inc, N.Y. 76.)

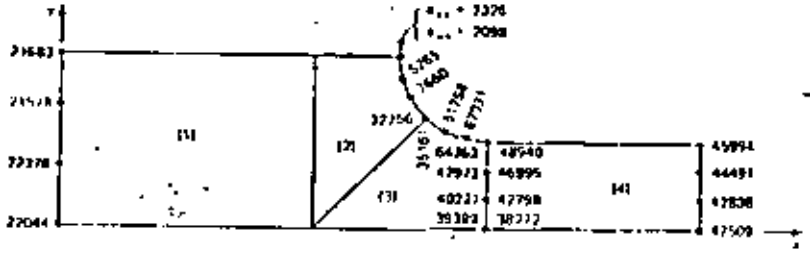

Fig. 16.7 Some values of σ_1 for the four element quadrilateral model.

The principal stress values, σ_1, at the ends and in the region of the fillet for the four-element model are shown in Fig. 16.7. The nodal values of σ_1 at the left and right ends, average out to 21,918 and 43,952 N/cm^2, respectively, which are close to the correct values of 22,000 and 44,000 N/cm^2. The values of σ in the region of the fillet, however, are suspect. First, the values of σ_{xx} and σ_{yy} at the square corner are not zero as they should be but instead are in the range of 2000 N/cm^2. The nodal value at the upper common corner of elements three and four differ by about 15,000 N/cm^2. This is an indication that the element grid is not fine enough. The stress values along the curved boundary of the fillet change significantly from one end to the other and more than two equations are needed to model these values. The maximum value of σ_1 is around 67,000 N/cm^2, which is equivalent to a stress concentration of 1.52, which differs from the accepted value of 1.42 by 7 percent.

An improvement in the stress values would be expected to accompany a finer grid of elements. The determination of the node locations and the punching of the data for a finer grid starts to become time consuming and the higher-order elements are no longer the quickest way to solve the problem. The solution given in Chapter 12 is probably the most painless to obtain and is the favored option. The use of a large number of small simple elements also makes possible the approximation of the displacements along the fillet boundary with a good degree of accuracy. The primary disadvantage in using the simplex elements is the need to solve another system of equations in order to obtain nodal values for the stress component.

Element Convergence Comparison for Plate with Hole

30° Series

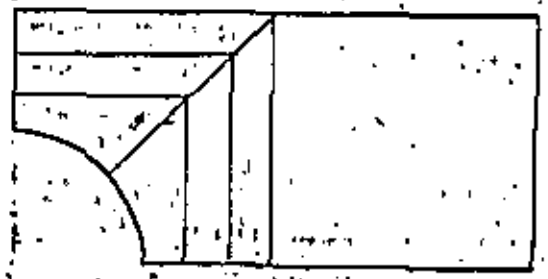

45° Series

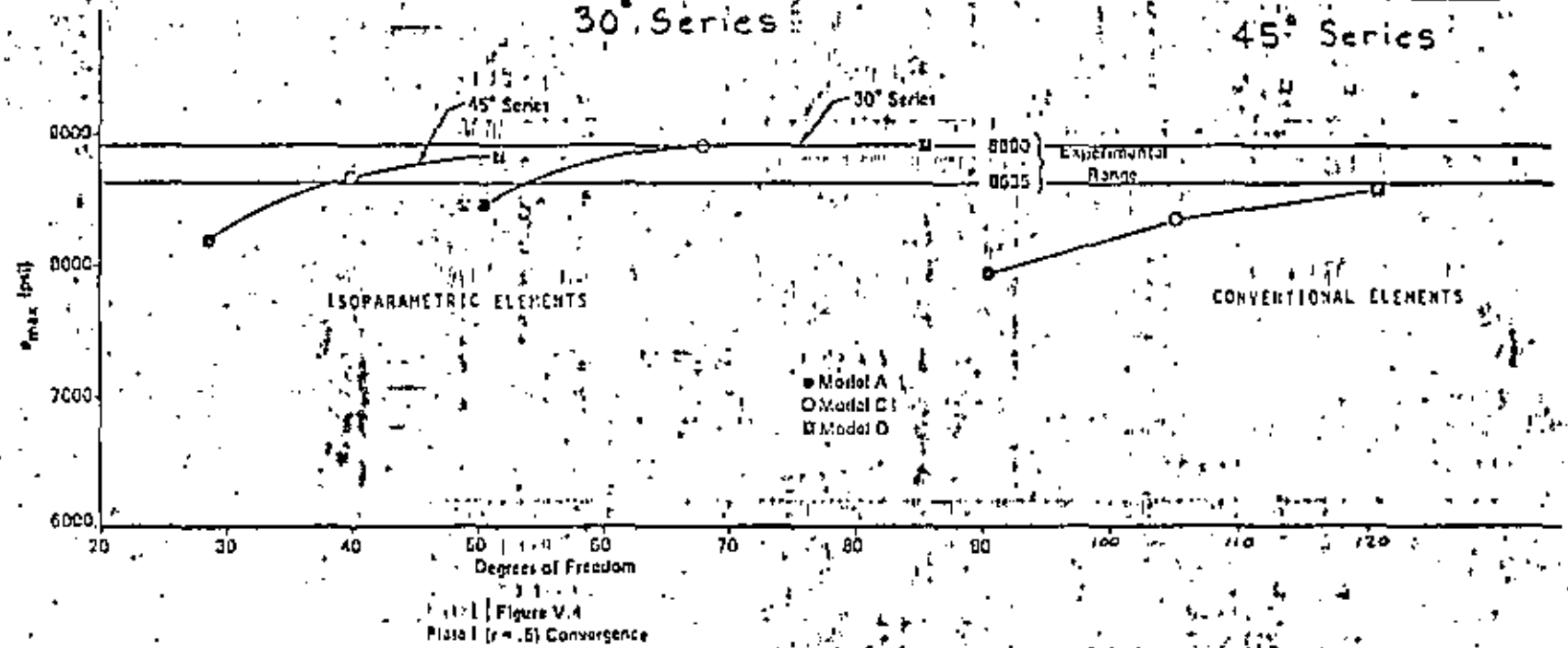

Figure V.4
Plate I (r = .5) Convergence

Compliments of SDRC

(26)

From: J.R. Lemon, S.K. Tolani, G.L. Klosterman, "Integration and Implementation of CAE and Related Micmufacturing ..." presented at GI-Jahrestagung 1980, Saarbrücken, W. Germany, 1 Oct. 1980.

EXAMPLE 1 – ROBOTIC DESIGN

In creating designs for the next generation of high-performance industrial robots, computer-aided engineering techniques prove cost-effective at each stage of the development process and from evaluating alternative machine geometries, to analyzing stress distribution in structural components and predicting system time-response characteristics.

For certain of these problems, computer-aided engineering proves indispensible; that is to say, one is not able to develop design solutions on a practical time schedule without a well-considered application of these tools.

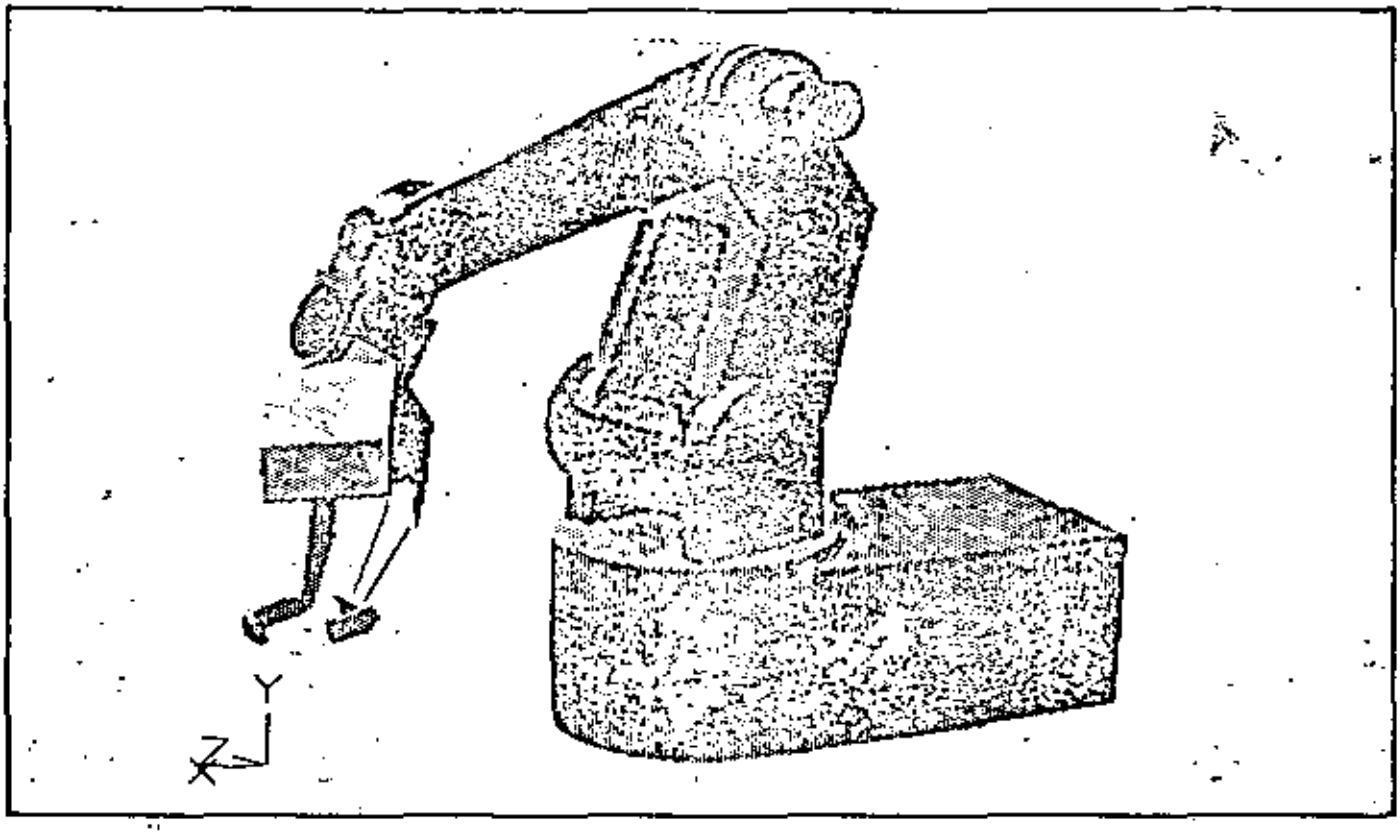

Figure 5. Computer Output Display of a High-performance Robotic Manipulator

In this example a set of functional specifications was outlined for an advanced industrial robot which demonstrated performance capabilities superior to contemporary devices. For example, a one-meter device having a maximum payload of 20 kg was required to accelerate a typical 3 kg payload at over 3 g's in an arm-sweep motion commencing in any linkage orientation within the working envelope of the linkage. Additionally, the manipulator was to have the capability to achieve terminal velocities at the tool point exceeding 3 meters per second with a static position error of 0.20 mm. A design was to be developed which could act as a prototype for a line of commercial products having a range of sizes and payloads. Preliminary design specifications for the servomechanism called for a versatile, anthropomorphic configuration, Figure 5, providing as many degrees of freedom as proved useful for applications like discrete-parts assembly, but having a modular construction which permitted the elimination of joints and actuators not required for any particular application. The system was to utilize electric servomotors. The design was to permit the incorporation of advanced-technology subsystems, such as passive or instrumented compliant wrists, integral-stress-strain feedback for overload protection, and so on.

Based on these and other functional specifications, a hypothetical development program was undertaken in which computer-aided engineering methods were utilized to solve key structural and servomechanism design problems which determine robot performance.

The general CAE applications strategy outlined in the text, Figure 4, commences with accumulating certain engineering data necessary for preliminary simulation and design efforts. Since this project involved the development of a device which was in many respects the first of its kind . . . that is, it was not a redesign but incorporated many new mechanical elements . . . the engineering data base which would normally be available as input to conceptual design was not extensive. In order to establish standards, commercially-available manipulators of similar configuration were used for reference testing. Key performance values for the systems and certain components were derived using modal analysis testing to collect, analyze and display data from excitation tests, and using interactive systems analysis software to generate system models. Gear reducer performance, for example, which was anticipated to be critical to system response and positioning, was thus characterized prior to design.

At this stage, characterizations of the operational requirements for typical manipulation processes, such as "worst-case" and "representative" payload, trajectory, and time standards were also defined. These characterizations were subsequently used in computer simulations to evaluate and compare proposed system concepts.

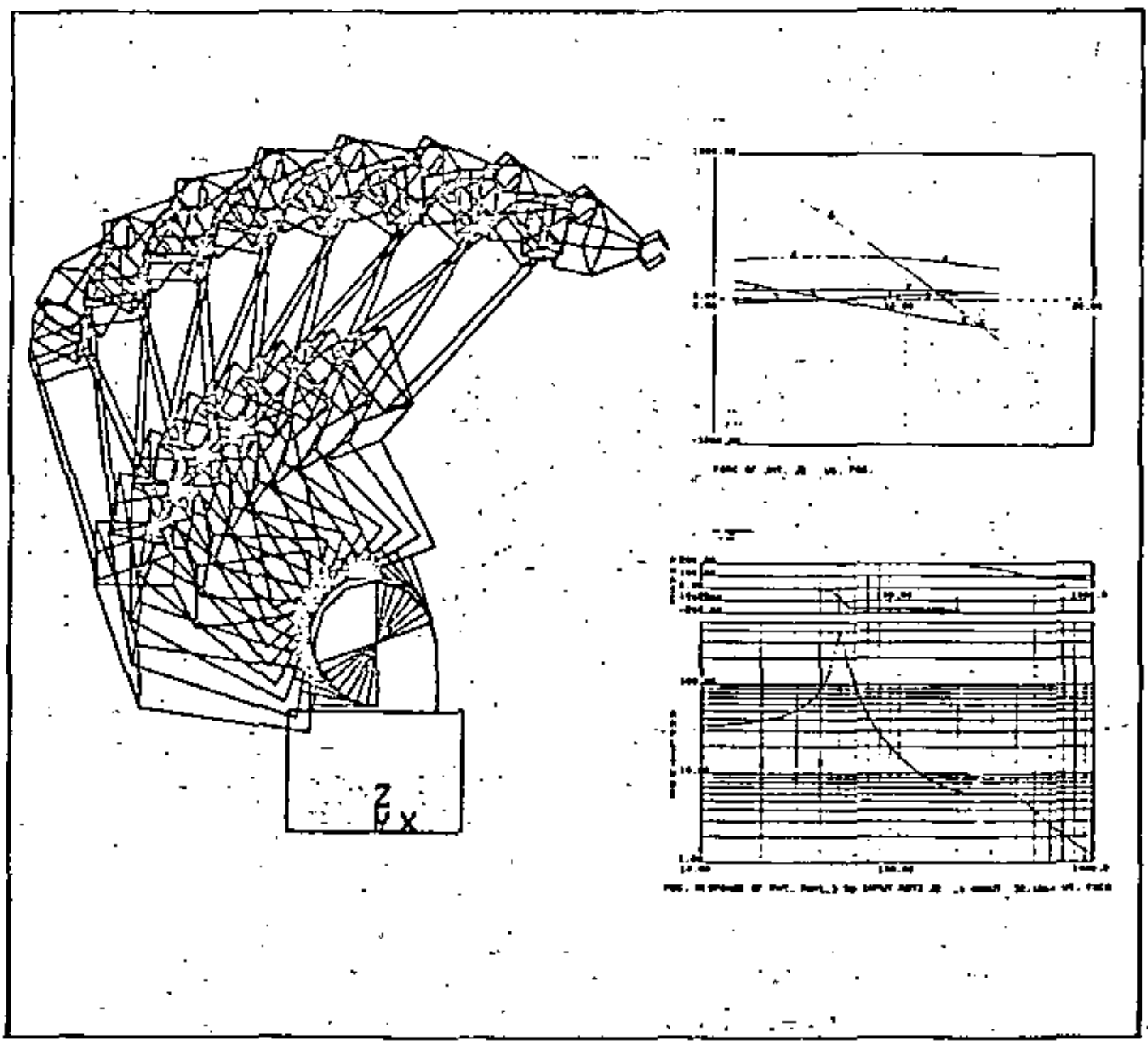

Figure 6. Graphic Output from Integrated Mechanism Program

The conceptual design phase began with the definition of alternative system concepts, each describing a mechanism geometry, drive scheme, packaging concept, control scheme, etc. These machine concepts were developed in parallel and were analyzed on an interactive basis to the degree of detail necessary for decisions to be made, weighing the relative merits of the alternatives as to which concept was generally most optimal. Some pencil and paper work was involved in this effort, but at an early stage solid volumetric models were created and a design data base began to form. The main analytical tool employed during conceptual design was an integrated mechanisms program. This program, run on a supermini through an interactive graphics terminal, was used both to evaluate linkage kinematics, including such characteristics as link/joint disposition and volumetric interferences, and also to examine linkage kinetics.

Figure 6 shows an example of the integrated mechanism program output. For example, the actuator torque requirements and induced loads were determined given certain prescribed linkage topologies and payload accelleration.

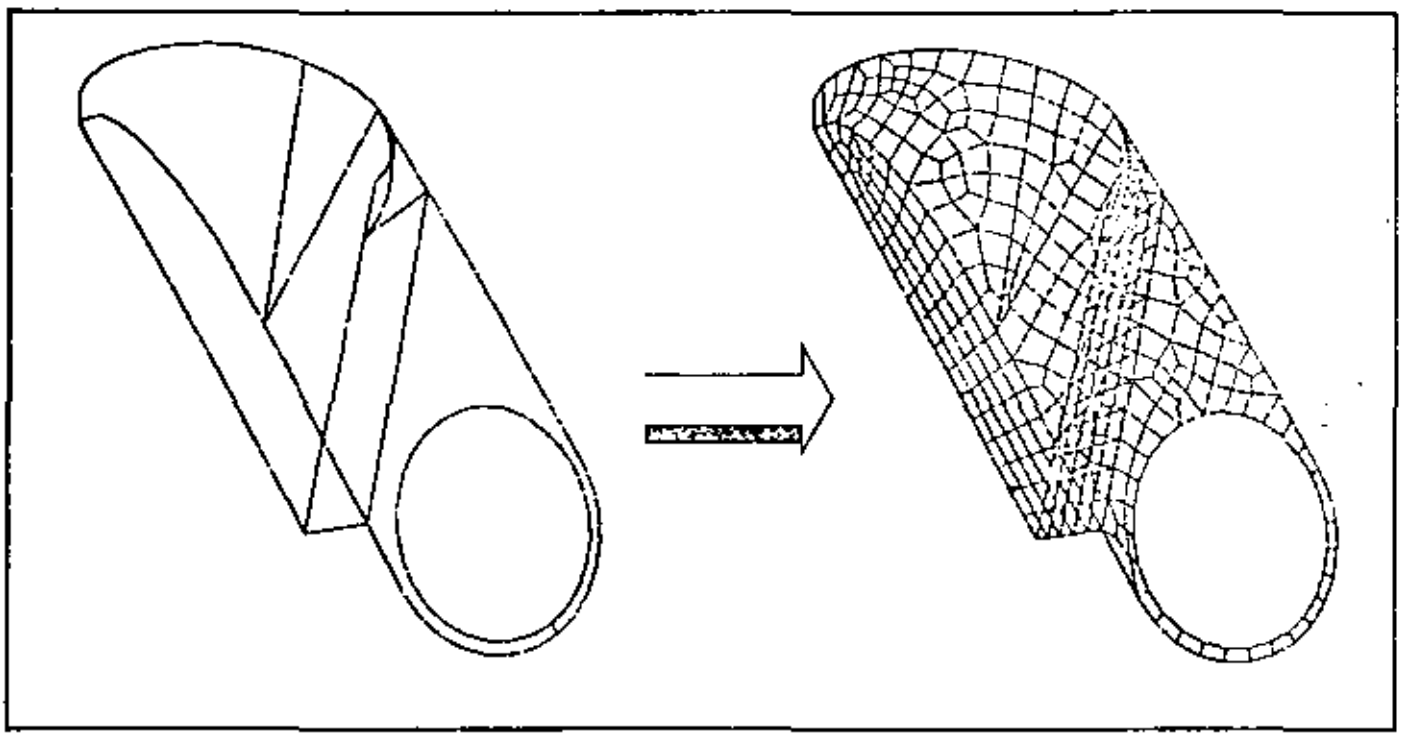

Figure 7. Boundary Edge Description of Robot Component—Left
Automatically Generated Finite Element Model—Right

Following the selection of system concepts which held potential for meeting overall product specifications, the system models were exercised to develop detailed component design specifications and design loads, i.e., component space, connection degrees of freedom and characteristics, component weight objectives, relative center of gravity and principal axes locations and directions, desired strength, stiffness, fatigue-life, joint damping, etc. Engineering then focused on two related aspects of structure/servomechanism interaction: component structural design and analysis, and control system design and analysis. Individual component designs were geometrically modeled in the computer and analyzed using finite element methods with automatic mesh generation software, Figure 7. A solid model, hidden-surface display of a linkage member with all associated structural properties derived automatically from geometry, in exactly the form necessary to compare against component design specifications are shown in Figure 8.

Strength, stiffness, weight, fatigue life and damping are critical structural characteristics of individual components and influence speed, accuracy and stability of the overall manipulator significantly. In this context, it can be seen that geometric modeling of components with automatic analysis capabilities, to assure component behavior at the earliest design stages, is an extremely useful and productive tool in these applications.

```
 MASS OF OBJECT =       100.265
CENTER OF GRAVITY =
      6.310          15.384          39.987
MOMENTS OF INERTIA ABOUT C.G.:

IXX =  0.40933E+06
IYY =  0.23555E+06
IZZ =  0.46588E+06
IXY = -0.41560E+05
IYZ =  0.94016E+05
IXZ =  0.24170E+05

MOMENTS OF INERTIA ABOUT THE ORIGIN:

IXX =  0.59313E+06
IYY =  0.39986E+06
IZZ =  0.49734E+06
IXY = -0.31877E+05
IYZ =  0.15537E+06
IXZ =  0.49478E+05

PRINCIPAL AXES:
     -0.213          -0.920          0.330
     -0.972           0.235          0.029
      0.103           0.315          0.944
PRINCIPAL MOMENTS OF INERTIA
I11 =  0.19221E+06
I22 =  0.41868E+06
I33 =  0.58385E+06
 DO YOU WANT TO DISPLAY THE C.G. ?
```

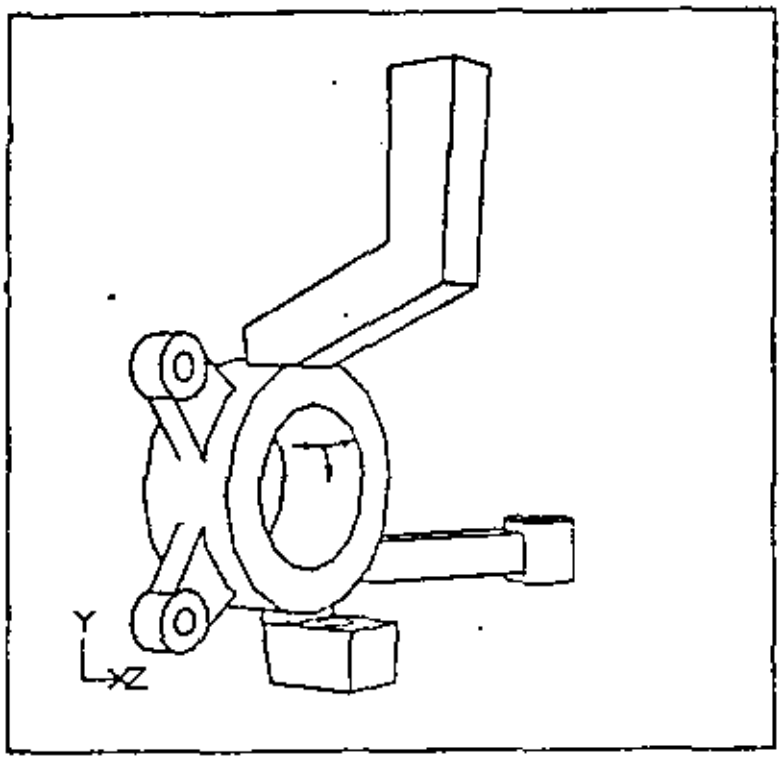

Figure 8. Three-dimensional Solid Model of Linkage Member with all Required Structural Characteristics Derived Automatically

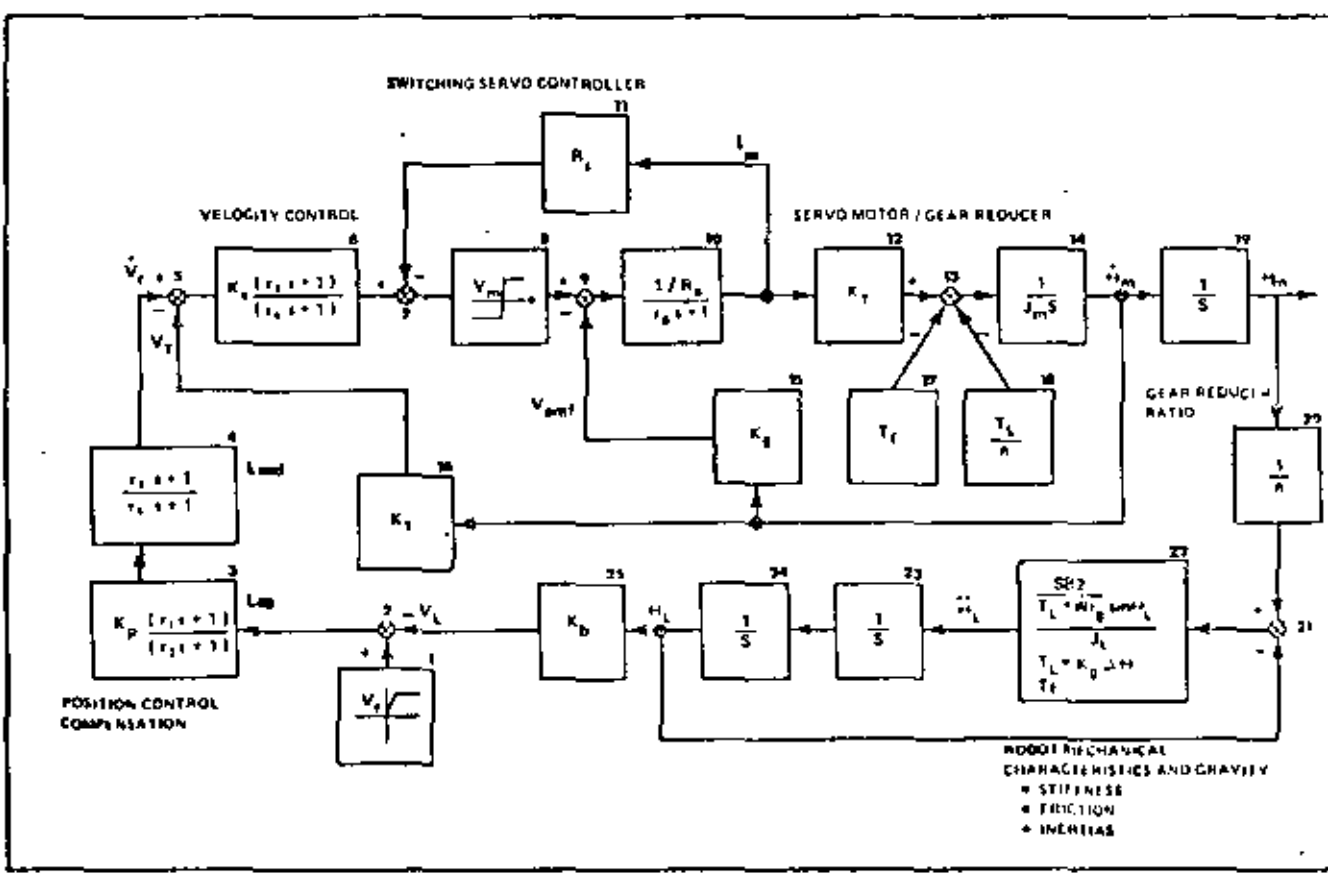

Figure 9. Control System Model for Single Joint

Servocontrol systems were designed and system performance evaluated using a block-oriented system simulation digital computer program. In this approach, a very comprehensive and accurate model was created of the control system for each joint, Figure 9. The model included values for all key parameters of the servocontrol, actuator and system kinetics – such as time-constraints, gains, friction torques, reflected inertias, gravity, and so on. The model was exercized with various control values and modified as necessary to establish the proper design for each joint control to assure an overall system demonstrating the levels of performance described in the functional specifications. System response stability, path-following capabilities and settling times were all investigated repeatedly as individual component designs and joint controls became detailed.

Computer-aided drafting systems were utilized for the first time in the detailed design phase to accomplish both mechanical and electrical system layouts. The design data base was futher expanded as part drawings and associated manufacturing data, i.e., process planning, N/C tapes, tool designs, etc., were created for prototypes of the final proposed manipulator.

Partitioning Schemes

▷ References

(1) NASTRAN Theoretical Manual, MacNeal-Schwendler Corp., 1974.

(2) ANSYS®, Engineering Analysis System Theoretical Manual, Swanson Analysis Systems, Inc., 1977.

(3) Cook, R.D., Concepts ... F.E. Analysis, 1974.

▷ Element condensation

Consider the QUAD-5 element shown.

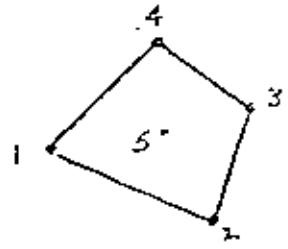

$$\left[\begin{array}{cccc|c} k_{11} & k_{12} & \cdots & k_{14} & k_{15} \\ k_{12} & k_{22} & \cdots & k_{24} & k_{25} \\ \vdots & & \cdots & k_{34} & k_{35} \\ k_{14} & k_{24} & \cdots & k_{44} & k_{45} \\ \hline k_{15} & k_{25} & k_{35} & k_{45} & k_{55} \end{array}\right] \left[\begin{array}{c} \bar{\Phi}_1 \\ \bar{\Phi}_2 \\ \bar{\Phi}_3 \\ \bar{\Phi}_4 \\ \hline \bar{\Phi}_5 \end{array}\right] = \left[\begin{array}{c} r_1 \\ r_2 \\ r_3 \\ r_4 \\ \hline r_5 \end{array}\right] \qquad \text{(PS1.1)}$$

The element stiffness matrix may be partioned:

$$\left[\begin{array}{c|c} \bar{k} & k_5 \\ \hline k_5^T & k_{55} \end{array}\right] \left[\begin{array}{c} \bar{\Phi} \\ \hline \bar{\Phi}_5 \end{array}\right] = \left[\begin{array}{c} \bar{r} \\ \hline r_5 \end{array}\right] \qquad \text{(PS1.2)}$$

Simple reduction $\Rightarrow$

$$[k_5]^T \{\bar{\Phi}\} + [k_{55}] \{\bar{\Phi}_5\} = \{r_5\} \qquad \text{(PS1.3)}$$

or that

$$\{\bar{\Phi}_s\} = [k_{ss}]^{-1}\left(\{r_s\} - [k_s]^T\{\bar{\Phi}\}\right). \qquad (PS2.1)$$

The first row in (PS1.2) $\Rightarrow$

$$[\bar{k}]\{\underline{\bar{\Phi}}\} + [k_s][k_{ss}]^{-1}\left(\{r_s\} - [k_s]^T\{\underline{\bar{\Phi}}\}\right) = \{\bar{r}\}$$

or

$$\left([\bar{k}] - [k_s][k_{ss}]^{-1}[k_s]^T\right)\{\bar{\Phi}\} = \{\bar{r}\} - [k_s][k_{ss}]^{-1}\{r_s\}. \qquad (PS2.2)$$

Recognizing scalars $\Rightarrow$

$$\underbrace{\left([\bar{k}] - [k_s][k_s]^T/k_{ss}\right)}_{[k]}\{\bar{\Phi}\} = \underbrace{\{\bar{r}\} - [k_s]r_s/k_{ss}}_{\{r\}}.$$

or

$$[k]\{\bar{\Phi}\} = \{r\}. \qquad (PS2.3)$$

Thus we have a higher order element in terms of the same number of D.O.F.

D Superelements (ANSYS, ref. (2))

A. Statics

Beginning with the basic form of the static equations of equilibrium (equation (1.1.1)):

$$[K]\{u\} = \{F\} \tag{1.9.1}$$

The equations may be partitioned into two groups, the master (retained) degrees of freedom, here denoted by the subscript "m", and the slave (removed) degrees of freedom, here denoted by the subscript "s".

$$\left[\begin{array}{c|c} K_{mm} & K_{ms} \\ \hline K_{sm} & K_{ss} \end{array}\right] \left\{\begin{array}{c} U_m \\ \hline U_s \end{array}\right\} = \left\{\begin{array}{c} F_m \\ \hline F_s \end{array}\right\} \tag{1.9.2}$$

or, expanding:

$$[K_{mm}]\{u_m\} + [K_{ms}]\{u_s\} = \{F_m\} \tag{1.9.3}$$

$$[K_{sm}]\{u_m\} + [K_{ss}]\{u_s\} = \{F_s\} \tag{1.9.4}$$

The master degrees of freedom are input as the dynamic degrees of freedom on the K cards. They should include all boundary nodes. If accelerations are used (or if the problem is dynamic) master (dynamic) degrees of freedom throughout the rest of the structure should be used in order to characterize the distributed mass. The selection of master (dynamic) degrees of freedom is discussed in more detail in the ANSYS User's Manual (Reference 7).

Solving equation (1.9.4) for (u_s).

$$(u_s) = [K_{ss}]^{-1}(F_s) - [K_{ss}]^{-1}[K_{sm}](u_m) \tag{1.9.5}$$

Substituting (u_s) into equation (1.9.3):

$$\left([K_{mm}] - [K_{ms}][K_{ss}]^{-1}[K_{sm}]\right)(u_m) = \left((F_m) - [K_{ms}][K_{ss}]^{-1}(F_s)\right) \tag{1.9.6}$$

or, $$[\hat{K}](\hat{u}) = (\hat{F}) \tag{1.9.7}$$

where: $$[\hat{K}] = [K_{mm}] - [K_{ms}][K_{ss}]^{-1}[K_{sm}] \tag{1.9.8}$$

$$(\hat{F}) = (F_m) - [K_{ms}][K_{ss}]^{-1}(F_s) \tag{1.9.9}$$

$$(\hat{u}) = (u_m)$$

$[\hat{K}]$ and $(\hat{F})$ are the substructure stiffness matrix and load vector, respectively.

B. Dynamics

The general form of the equations of motion for dynamics is (equation (1.2.1)):

$$[M](\ddot{u}) + [C](\dot{u}) + [K](u) = (F) \tag{1.9.17}$$

For substructuring, an equation of the form:

$$[\hat{M}](\ddot{\hat{u}}) + [\hat{C}](\dot{\hat{u}}) + [K](\hat{u}) = (F) \tag{1.9.18}$$

is needed. $[K]$ and (F) are computed identically as they are for the static case (equation (1.9.8) and (1.9.9)). The computation of the reduced mass matrix is done by:

$$[\hat{M}] = [M_{mm}] - [K_{ms}][K_{ss}]^{-1}[M_{sm}] - [M_{ms}][K_{ss}]^{-1}[K_{sm}]$$

$$+ [K_{ms}][K_{ss}]^{-1}[M_{ss}][K_{ss}]^{-1}[K_{sm}] \tag{1.9.19}$$

This simplification was suggested by Guyan (Reference 11), because direct partitioning and condensation are not practical, since the condensed matrices would be functions of the time derivatives of displacement and very awkward to implement. The damping matrix is handled similarly:

$$[\bar{C}] = [C_{mm}] - [K_{ms}][K_{ss}]^{-1}[C_{sm}] - [C_{ms}][K_{ss}]^{-1}[K_{sm}] \qquad (1.9.20)$$

$$+ [K_{ms}][K_{ss}]^{-1}[C_{ss}][K_{ss}]^{-1}[K_{sm}]$$

C. Thermal (Steady State and Transient)

The governing equation for a transient thermal analysis is:

$$[\bar{C}]\{\dot{T}\} + [\bar{K}]\{T\} = \{Q\} \qquad (1.9.21)$$

where: $[\bar{C}]$ = specific heat matrix

$[\bar{K}]$ = thermal conductivity matrix

$\{T\}$ = vector of nodal temperatures

$\{Q\}$ = vector of nodal heat flows.

By analogy with the dynamic equation of motion, equation (1.9.17), it is readily obtained that the governing equation for the thermal substructure is:

$$[\hat{\bar{C}}]\{\dot{\hat{T}}\} + [\hat{\bar{K}}]\{\hat{T}\} = \{\hat{Q}\} \qquad (1.9.22)$$

where: $[\hat{\bar{K}}] = [\bar{K}_{mm}] - [\bar{K}_{ms}][\bar{K}_{ss}]^{-1}[\bar{K}_{sm}]$

$$[\hat{\bar{C}}] = [\bar{C}_{mm}] - [\bar{K}_{ms}][\bar{K}_{ss}]^{-1}[\bar{C}_{sm}] - [\bar{C}_{ms}][\bar{K}_{ss}]^{-1}[\bar{K}_{sm}]$$

$$+ [\bar{K}_{ms}][\bar{K}_{ss}]^{-1}[\bar{C}_{ss}][\bar{K}_{ss}]^{-1}[\bar{K}_{sm}]$$

$$\{\hat{Q}\} = \{Q_m\} - [\bar{K}_{ms}][\bar{K}_{ss}]^{-1}\{Q_s\}$$

$$\{\hat{T}\} = \{T_m\}$$

and the back substitution equation is:

$$\{T_s\} = [\bar{K}_{ss}]^{-1}\{Q_s\} - [\bar{K}_{ss}]^{-1}[\bar{K}_{sm}]\{T_m\} \qquad (1.9.23)$$

T — P.S-6

Reduction of Stiffness and Mass Matrices

ROBERT J. GUYAN*
North American Aviation, Inc., Downey, Calif.

JUST as it is often necessary to reduce the size of the stiffness matrix in statical structural analysis, the simultaneous reduction of the nondiagonal mass matrix for natural mode analysis may also be required. The basis for one such reduction technique may follow the procedure used in Ref. 1 for the stiffness matrix, namely, the elimination of coordinates at which no forces are applied.

Arrange the structural equations $\{F\} = [K]\{x\}$ so that after partitioning in the form

$$\begin{Bmatrix} F_1 \\ F_2 \end{Bmatrix} = \begin{bmatrix} A & B \\ B' & C \end{bmatrix} \begin{Bmatrix} x_1 \\ x_2 \end{Bmatrix}$$

the forces F_2 are to be zero. The two resulting equations yield

$$F_1 = (A - BC^{-1}B')x_1$$

from which the reduced stiffness matrix is seen to be

$$K_1 = A - BC^{-1}B'$$

The foregoing amounts to a coordinate transformation $x = Tx_1$ or

$$\begin{Bmatrix} x_1 \\ x_2 \end{Bmatrix} = \begin{bmatrix} I \\ -C^{-1}B' \end{bmatrix} \{x_1\}$$

If the structure energies are written $T = \frac{1}{2}\dot{x}'M\dot{x}$ and $V = \frac{1}{2}x'Kx$ and the foregoing transformation is employed, the result is

$$T = \tfrac{1}{2}\dot{x}_1'T'MT\dot{x}_1$$

$$V = \tfrac{1}{2}x_1'T'KTx_1$$

The reduced stiffness matrix is seen to be $K_1 = T'KT$ and the reduced mass matrix $M_1 = T'MT$. Then with

$$[M] = \begin{bmatrix} \bar{A} & B \\ B' & C \end{bmatrix}$$

the reduced mass matrix becomes

$$M_1 = \bar{A} - \bar{B}C^{-1}B' - (C^{-1}B')'(\bar{B}' - \bar{C}C^{-1}B')$$

In the case of the reduced stiffness matrix, none of the structural complexity is lost since all elements of the original stiffness matrix contribute. However, in the reduced mass matrix, combinations of stiffness and mass elements appear. The result is that the eigenvalue-eigenvector problem is closely but not exactly preserved. Some comparative results are reported in Ref. 2 for beam vibrations.

References

[1] Turner, M. J., Clough, R. W., Martin, H. C., and Topp, L. J., "Stiffness and deflection analysis of complex structures," J. Aeronaut. Sci. 23, 805–824 (1956).

[2] Archer, J. S., "Consistent mass matrix for distributed mass systems," Proc. Am. Soc. Civil Engrs. 89, 161–178 (August 1963).

Received September 8, 1964.

* Research Specialist, Space and Information Systems Division. Member AIAA.

Ref. Cook, § 12.4-.

(3)

GUIDELINES FOR FINITE ELEMENT IDEALIZATION

Papers presented at
THE NATIONAL STRUCTURAL ENGINEERING MEETING OF
THE AMERICAN SOCIETY OF CIVIL ENGINEERS
NEW ORLEANS, LOUISIANA
APRIL 14-18, 1975

Sponsored by
THE TASK COMMITTEE ON AUTOMATED
ANALYSIS AND DESIGN,
THE COMMITTEE ON ELECTRONIC COMPUTATION
STRUCTURAL DIVISION OF THE ASCE

Compiled by
ALAN M. EBNER, M. ASCE
UNITED ENGINEERS & CONSTRUCTORS, INC.
PHILADELPHIA, PENNSYLVANIA

THE AMERICAN SOCIETY OF CIVIL ENGINEERS

United Engineering Center 345 East 47th Street New York, N.Y. 10017

GENERAL COMMENTS

Of these responses, the overwhelming opinion was in favor of the project, (18 for and 2 against), if one considers those who contributed additional guidelines as being in favor of the project. Some of the more thought provoking comments were:

1. "Finite element idealization requires a substantial amount of judgment based on the problem at hand and the immediate capability to attack that problem. I feel that that judgment cannot be condensed into a list of 'rules of thumb'. For almost every item on the ad-hoc list enclosed in your letter I could think of exceptions which I felt were important. These exceptions and possible misdirectives alone, however, are not sufficient to condemn the list.

   "A more fundamental and far reaching effect of the list would be its apparent acceptance and sanction by ASCE. It would become a pseudo standard by which finite element idealizations are judged. I am confident that I can defend finite element analyses that I perform against arguments based on logic and engineering judgment. I cannot, nor is it reasonable to, defend them against a checklist. For this reason, I do not believe that publication of this list is in the best interest of finite element analysts or those who judge their work."

2. "General guidelines for finite element procedures may be of academic interest but for practical situations are of ambiguous value. There are too many exceptions and such guidelines foster the belief that given a few rules 'we're all set to go.' I would think a more practical benefit to a methodology for 'learning the rules' which would start with an apprentice period of linear elastic static, simple structure and move through linear dynamics, to nonlinear statics, to nonlinear dynamics, to 3D, to complicated structures, etc. At each stage these homilies might be introduced to sprinkle a few bits of wisdom on the discussion.

   "Finally, who would be significantly effected by such guidelines should seriously question whether 'he's working over his head' and whether he should seek out professional guidance."

3. "I guess we all use 'rules of thumb', but I tend to do so with as open a mind as possible. I am very hesitant about generalizing, on paper, without tying the statement to a backup study or specific problem."

4. "This is an interesting exercise, trying to collect experience in this 'art form'."

5. "Your problem is going to be to make a coherent whole of these stray suggestions."

In the following, the sample list of guidelines is repeated, succeeded by the comments generated in the responses to each of them. This is then followed by the additional list of guidelines contributed by the respondees.

In the words of one respondee, " as you understand, these are guidelines and in special cases they may not apply."

AD HOC GUIDELINES

for

FINITE ELEMENT IDEALIZATION

1. Finite element gridworks should be uniform where this is practical. However, nonuniformity is often necessary to achieve refinement of the gridwork in regions of rapid changes in loading and/or behavior.

2. Strains imposed by thermal load terms should not impose a higher degree of variation in strain than can be accomodated in the strains implied by the assumed displacement functions because this may lead to unusable stress predictions.

3. Quadrilateral finite elements should be used except where triangular shapes are necessary to effect grid refinement or accommodate irregularity in geometry and/or loading.

4. Analyses to obtain displacement (or force) behavior do not require as refined a gridwork as is required to obtain strain (or stress) behavior.

5. Analyses including nonlinearity in geometry or material usually require a more refined idealization than linear analyses.

6. Vibration analyses using lumped mass models usually yield slightly lower frequency values than are obtained from consistent mass models.

7. Prediction of modes of vibration usually requires a more refined idealization than does the prediction of frequencies of vibration.

8. Where possible, gridpoints should be numbered from regions of large displacement toward regions of small displacement (e.g., from tip toward root for a cantilever beam).

9. Condensation of the stiffness matrix in substructing calculations or in preparation for vibration calculations may expand the bandwidth such that the total calculation is increased.

10. Monotonic convergence characteristics are seldom guaranteed with respect to behavior at a point; an exception may be the displacement under a single concentrated load.

11. When flat elements are used in the polygonal approximation of curved shell surfaces, rotation about the normal to the curved surface should usually be retained as a degree of freedom. However, the retention of such degrees of freedom may yield an ill-conditioned stiffness matrix. If these degrees of freedom are suppressed, it is important to check that the resulting reactions are acceptably small.

12. Eigenvalue buckling loads can be calculated even in cases where they are not meaningful. The displacement implied by the buckling load should be examined regarding the possible influence of pre-buckling displacements. Often, buckling calculations referenced to a deformed position are required.

13. The use of constraint equations as a means of imposing special connections and boundary conditions may increase the bandwidth substantially.

14. The use of constant strain triangle finite elements should be avoided wherever possible.

15. Where convenient it is advisable to use a thermal finite element to calculate temperatures which results in a degree of temperature variation equal to that of the strain variation provided in the stress finite element of the follow-on stress analysis.

16. Polygonal approximation of curved surfaces yields usable predictions of displacement with much less grid refinement than is required to obtain usable stress predictions.

17. The recommended first checks on predicted behavior are equilibrium checks using loads, reactions and forces.

18. Aspect ratio limits vary from element to element; however, a general guideline is to keep element aspect ratios below 10 for deformation analysis and below 5 for stress analysis.

19. Curvature of sides of isoparametric elements should be employed only to represent curved boundary geometry or curvature of stress isorelities (where this can be reasonably inferred from the geometry and loading).

20. Nonuniform distribution of intermediate nodes on the sides of higher order elements should be avoided wherever possible.

(10)

CHAPTER III BASIC ELEMENTS

Part I

THE CONSTANT STRAIN TRIANGLE AND ASSOCIATED QUADRILATERAL

By
M. R. Case and J. B. Mason*

APPENDIX–NOTATION

AR	=	BEAM ASPECT RATIO (ℓ/d)
AR_e	=	ELEMENT ASPECT RATIO (ℓ_e/d_e)
d	=	BEAM DEPTH
d_e	=	ELEMENT DEPTH (n/ND)
E	=	YOUNGS MODULUS
ℓ	=	BEAM LENGTH
ℓ_e	=	ELEMENT LENGTH (ℓ/NL)
ND	=	NUMBER OF ELEMENTS THROUGH BEAM DEPTH
NL	=	NUMBER OF ELEMENTS ALONG BEAM LENGTH
t	=	BEAM THICKNESS
T	=	BEAM TEMPERATURE
u,v	=	BEAM DEFLECTIONS
u_c, v_c	=	COMPARISON SOLUTION DEFLECTIONS
α	=	COEFFICIENT OF THERMAL EXPANSION
ν	=	POISSON RATIO
σ_x, τ_{xy}	=	BEAM STRESSES
$\sigma_{x_c}, \tau_{xy_c}$	=	COMPARISON SOLUTION STRESSES

FIG. III.3.1

BEAM GEOMETRY AND PROPERTIES

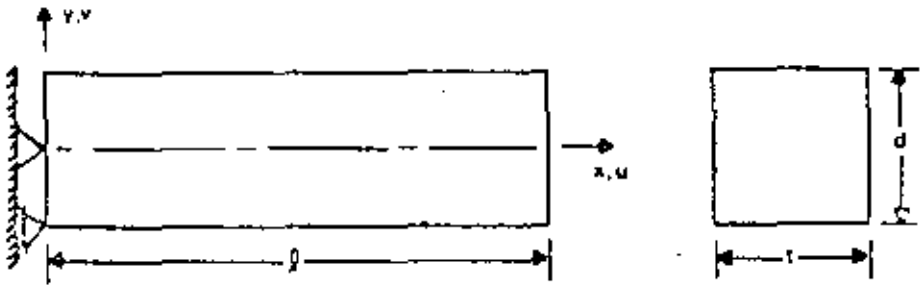

$$\ell = \begin{cases} 15 \text{ INCH SLENDER BEAM} \\ 2 \text{ INCH DEEP BEAM} \end{cases}$$

$d = 1$ INCH

$t = 1$ INCH

$E = 28 \times 10^6$ LB/IN^2

$\nu = 0.3$

$\alpha = 9.4 \times 10^{-6}$ IN/IN/$^\circ$F

$u = v = 0$ AT $x = y = 0$ AND $u = 0$ AT $x = 0$, $y = -d/2$

TABLE III. 1 (a)

FINE MESH SOLUTIONS USED AS BASIS FOR ERROR CALCULATIONS

BEAM	LOADING	v_C (INCHES)		σ_{x_C} (psi)		τ_{xy_C} (psi)	
		THEOR.	FINE MESH	THEOR.	FINE MESH	THEOR.	FINE MESH
DEEP	END MOMENT	-1.4285×10^{-7}	-1.4756×10^{-7}	1.0	.9997	0	10^{-7}
	END SHEAR	-1.1161×10^{-7}	-1.1138×10^{-7}	0.5	.4994	.1250	.1247
	UNIFORM LOAD	–	-8.7494×10^{-8}	–	–	–	–
	TEMPERATURE	–	-1.7086×10^{-3}	–	–	–	–
SLENDER	END MOMENT	-8.0357×10^{-6}	-8.0083×10^{-6}	1.0	.9972	0	10^{-5}
	END SHEAR	-5.3735×10^{-6}	-5.3538×10^{-6}	0.5	.4985	.010687	.010529
	UNIFORM LOAD	–	-4.0187×10^{-6}	–	–	–	–
	TEMPERATURE	–	-1.0341×10^{-1}	–	–	–	–

1) v_C IS DEFLECTION AT $x = \ell, y = 0$

2) σ_{x_C} IS STRESS AT $x = \ell/2, y = d/2$

3) τ_{xy_C} IS STRESS AT $x = \ell/2, y = 0$

FIG III 12
BEAM LOADS

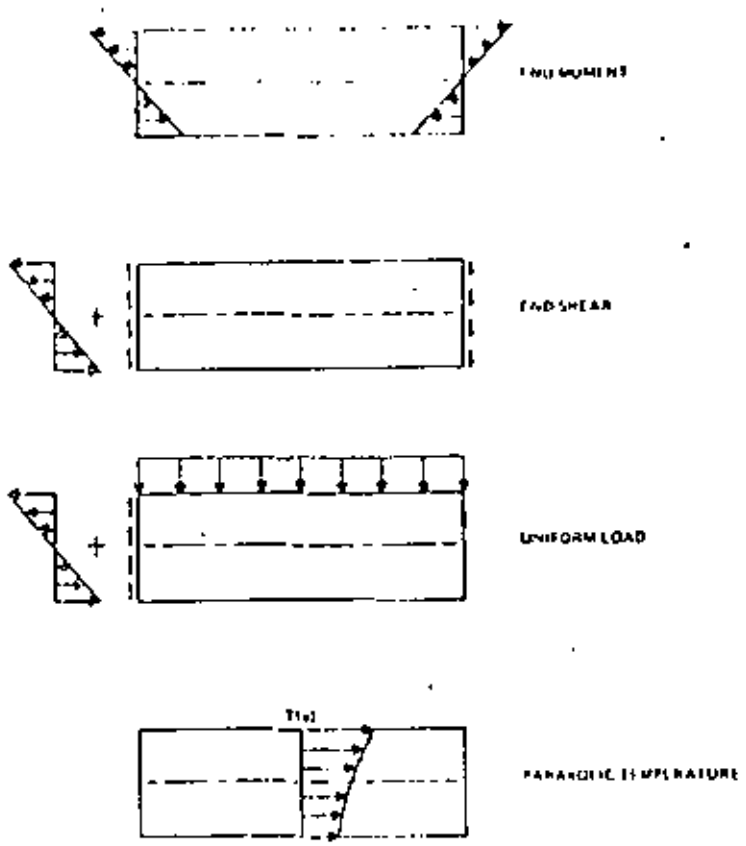

FIG III 13
FINITE ELEMENT MODEL MESH PATTERNS

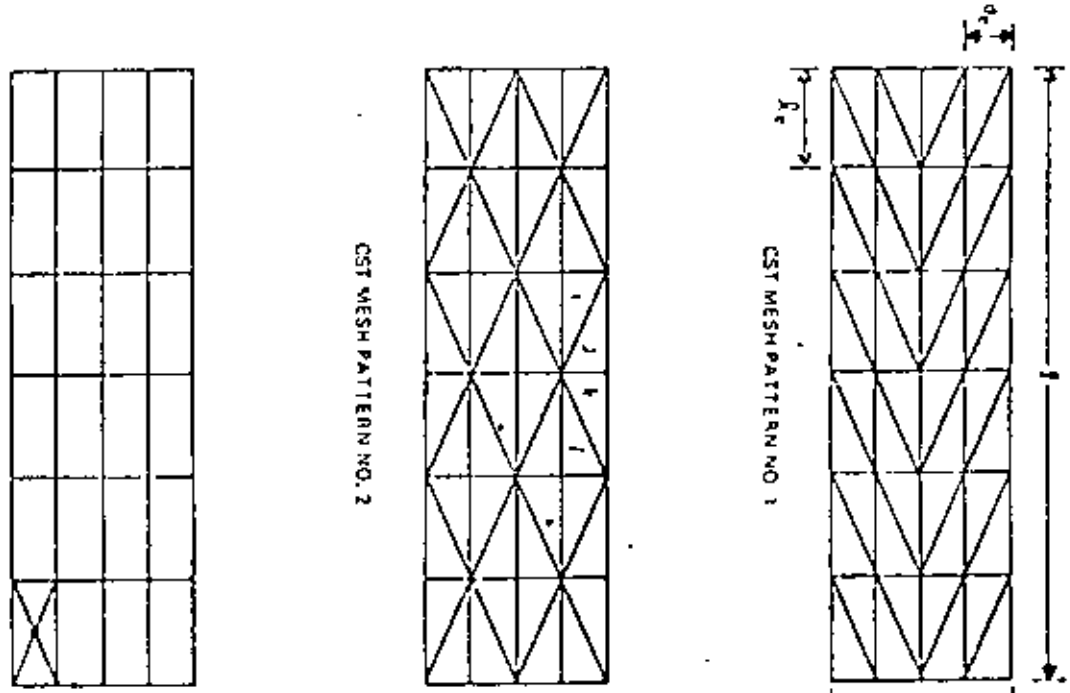

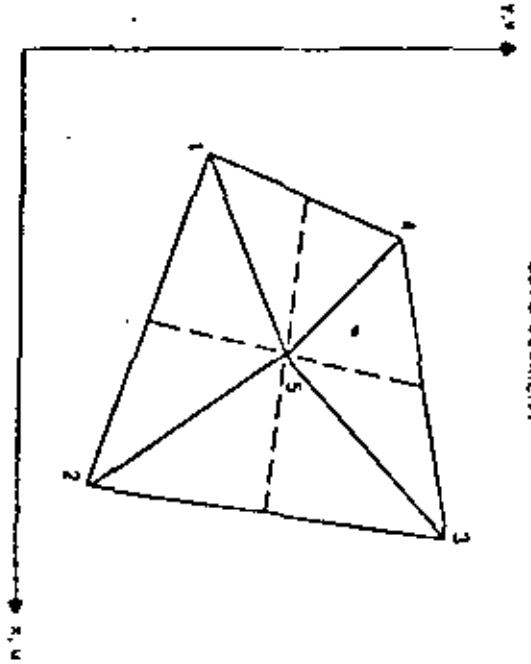

FIG. III .1.5
CSTQ ELEMENT

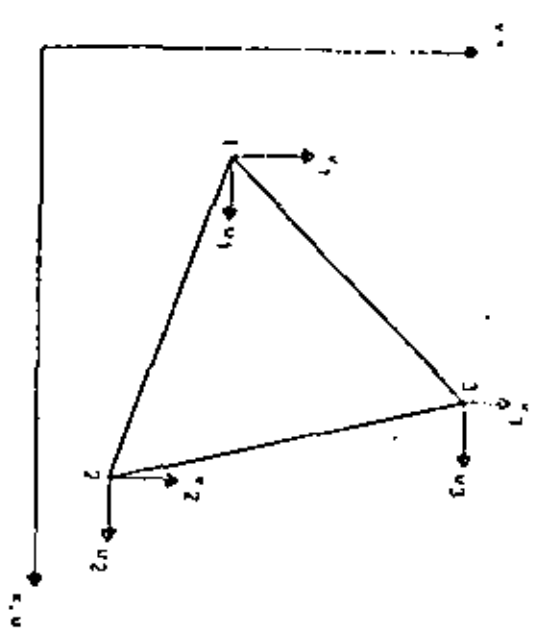

FIG. III .1.6

TIP DEFLECTION ERROR
SLENDER BEAM–END MOMENT, END SHEAR, UNIFORM LOAD
(MESH SIZE STUDY)

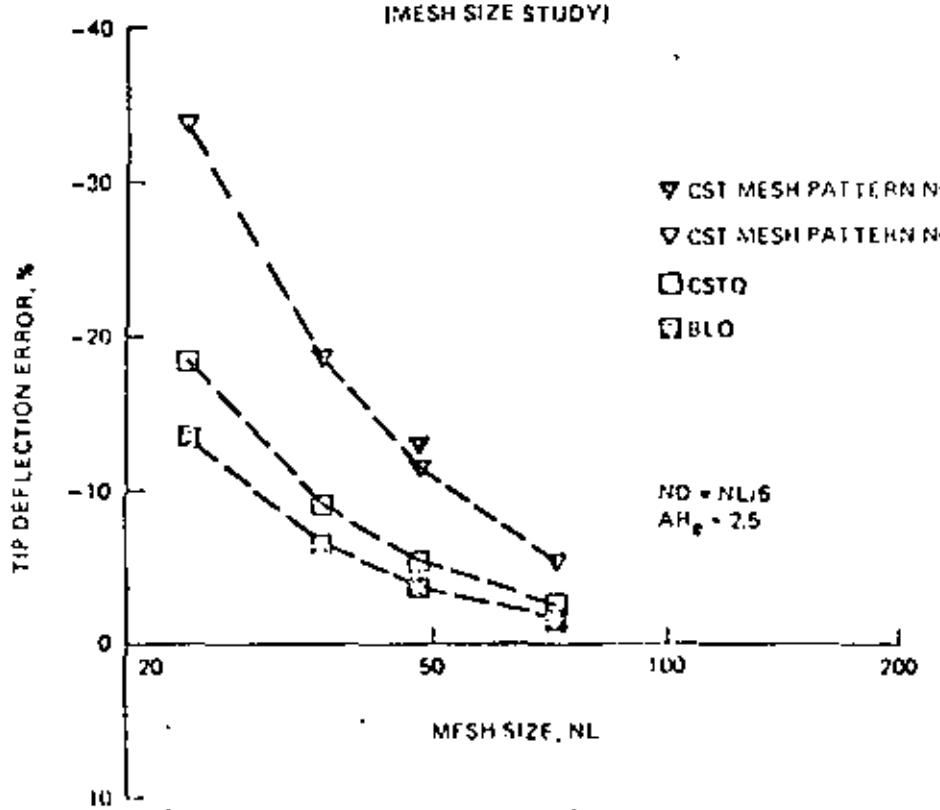

FIG. III.1.7

TIP DEFLECTION ERROR
SLENDER BEAM–PARABOLIC TEMPERATURE
(MESH SIZE STUDY)

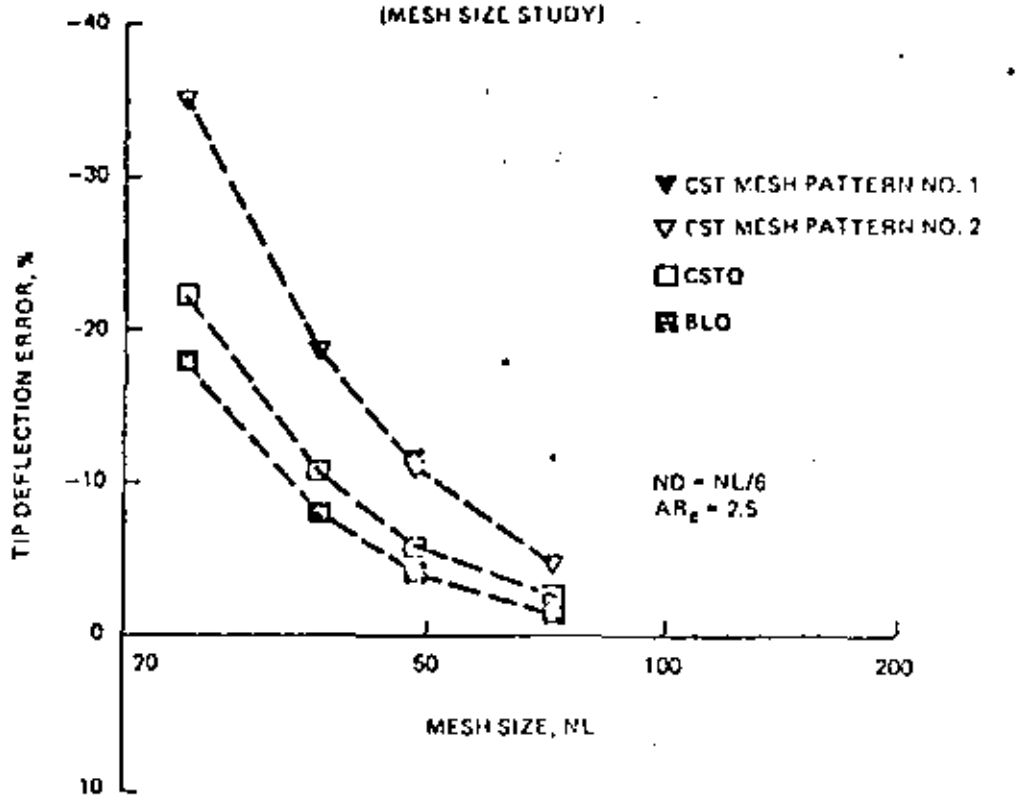

FIG. III.1.8

DIRECT STRESS ERROR
SLENDER BEAM–END MOMENT AND END SHEAR LOADING
(MESH SIZE STUDY)

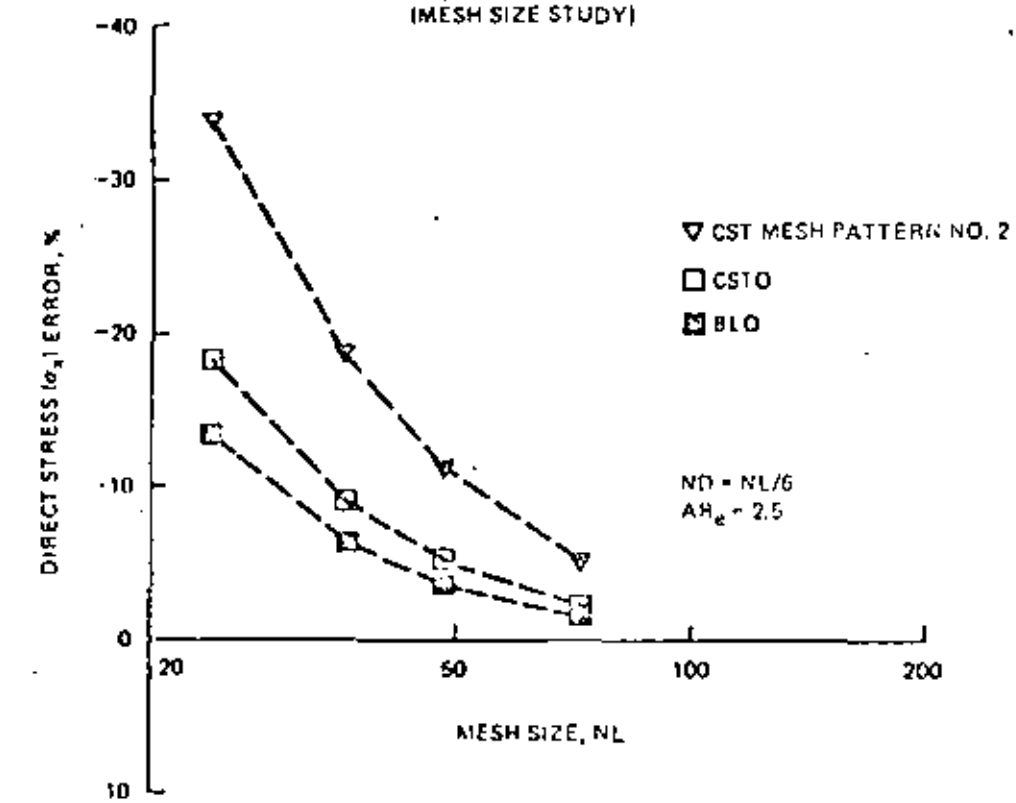

FIG. III.1.9

SHEAR STRESS ERROR
SLENDER BEAM—END MOMENT AND END SHEAR LOADING
(MESH SIZE STUDY)

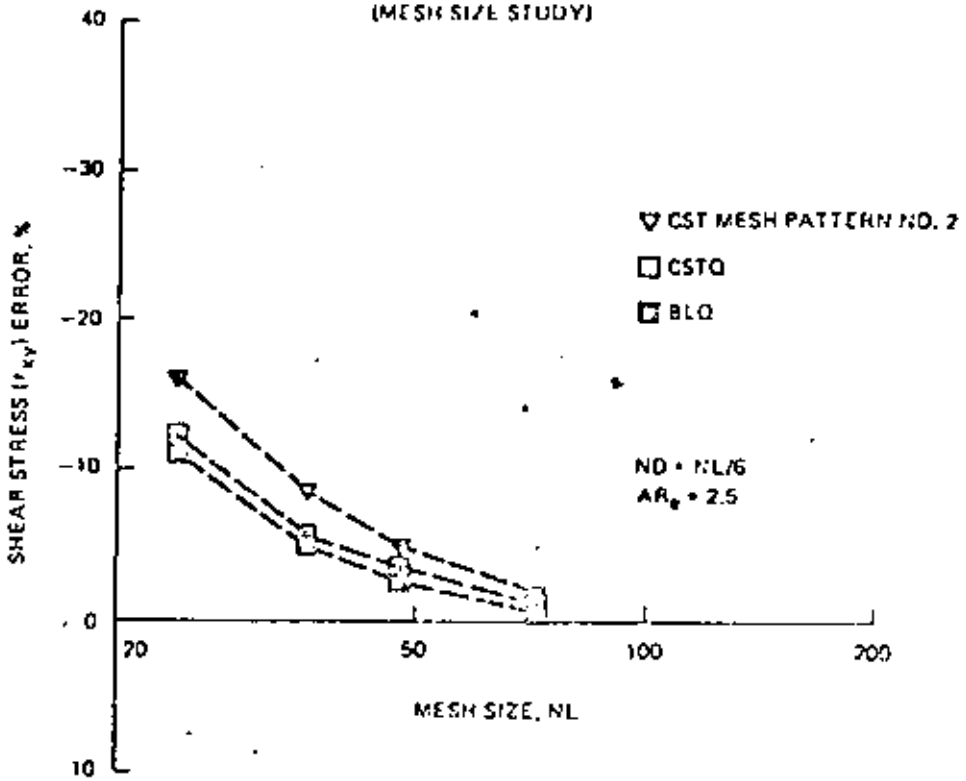

FIG. III.1.10

TIP DEFLECTION ERROR
SLENDER BEAM—END MOMENT, END SHEAR, UNIFORM LOAD
(ASPECT RATIO STUDY)

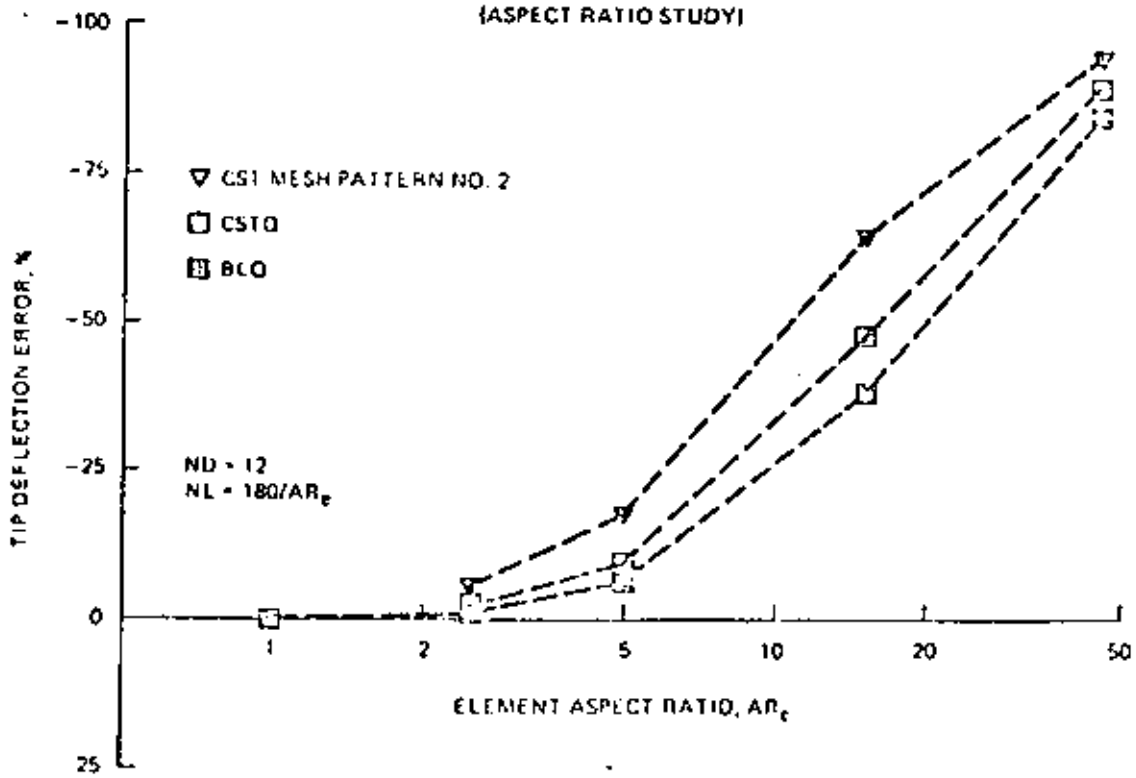

FIG III 3.11
MID-SPAN STRESS DISTRIBUTIONS
SLENDER BEAM-END SHEAR LOADING
NL = 24, ND = 4

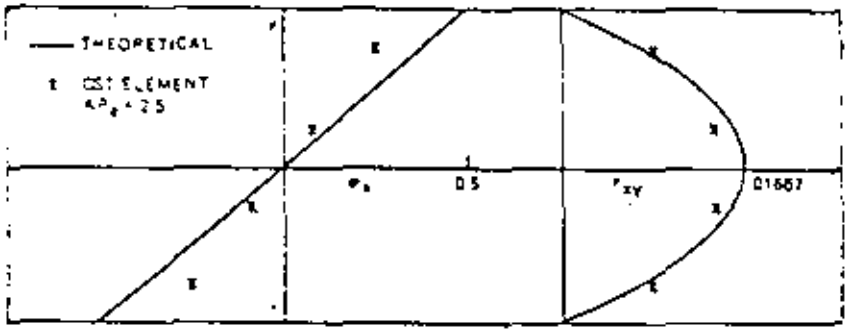

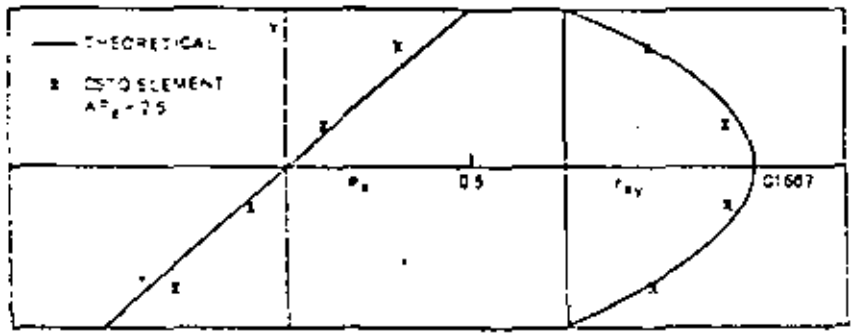

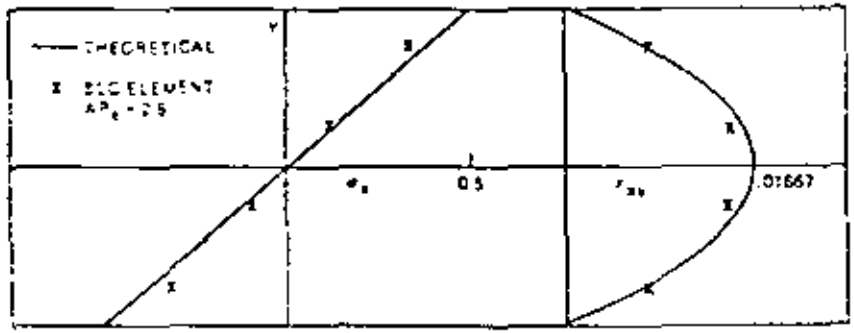

FIG III 3.12
MID-SPAN STRESS DISTRIBUTIONS
SLENDER BEAM-END SHEAR LOADING
ND = 12

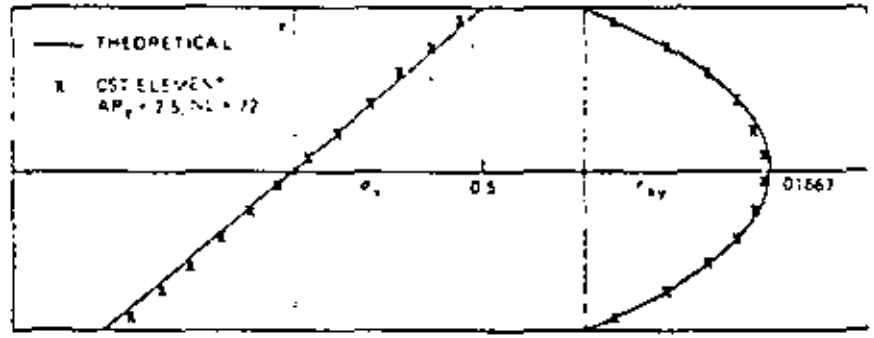

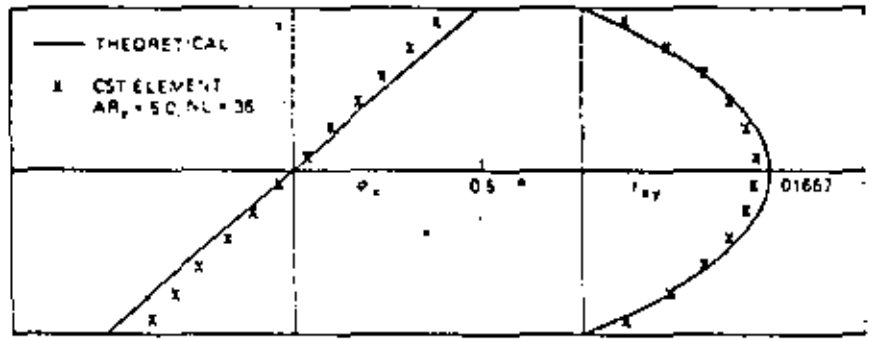

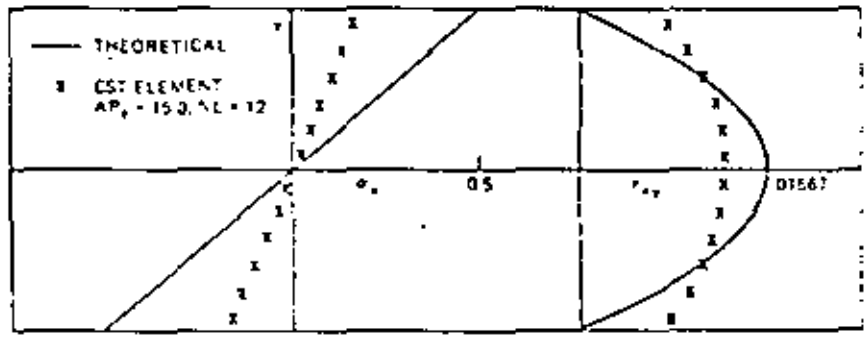

FIG. III.1.13
MID-SPAN STRESS DISTRIBUTIONS
SLENDER BEAM - END MOMENT AND END SHEAR LOADING
NL = 160, ND = 12

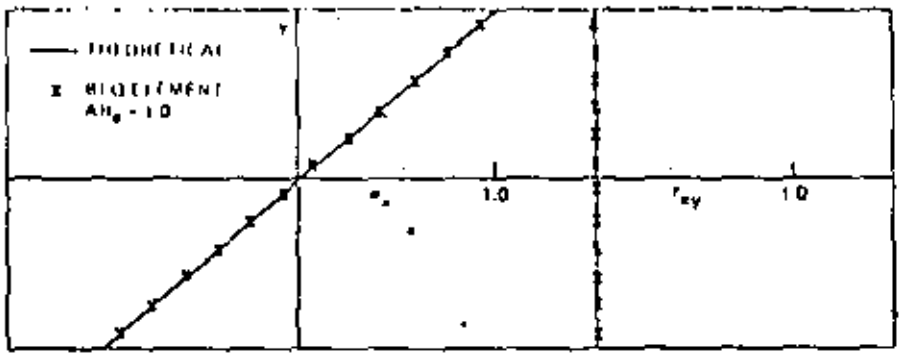

END MOMENT LOADING

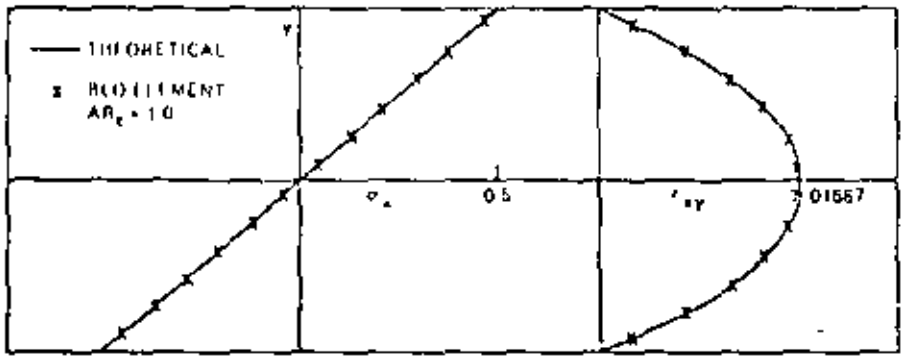

END SHEAR LOADING

FIG. III .1.14

TIP DEFLECTION ERROR
DEEP BEAM—END MOMENT LOADING
(MESH SIZE STUDY)

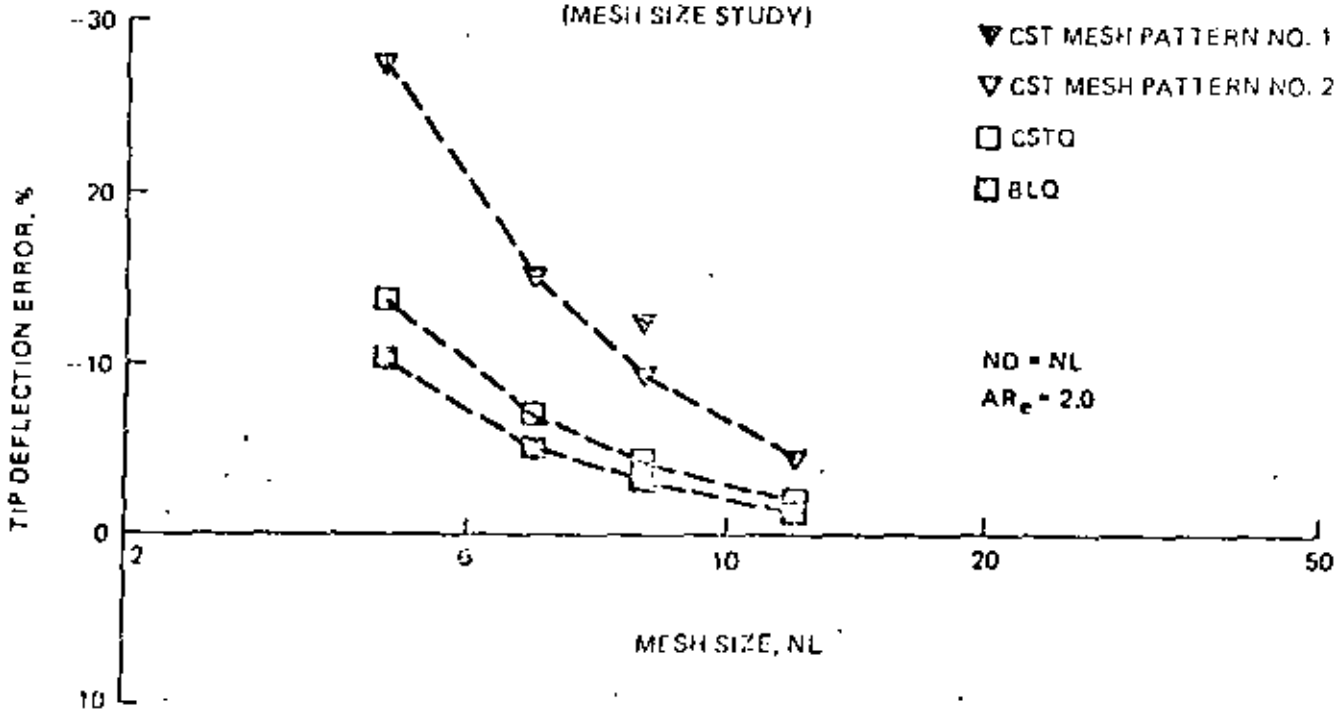

FIG. III .1.15

DIRECT STRESS ERROR
DEEP BEAM–END MOMENT AND END SHEAR LOADING
(MESH SIZE STUDY)

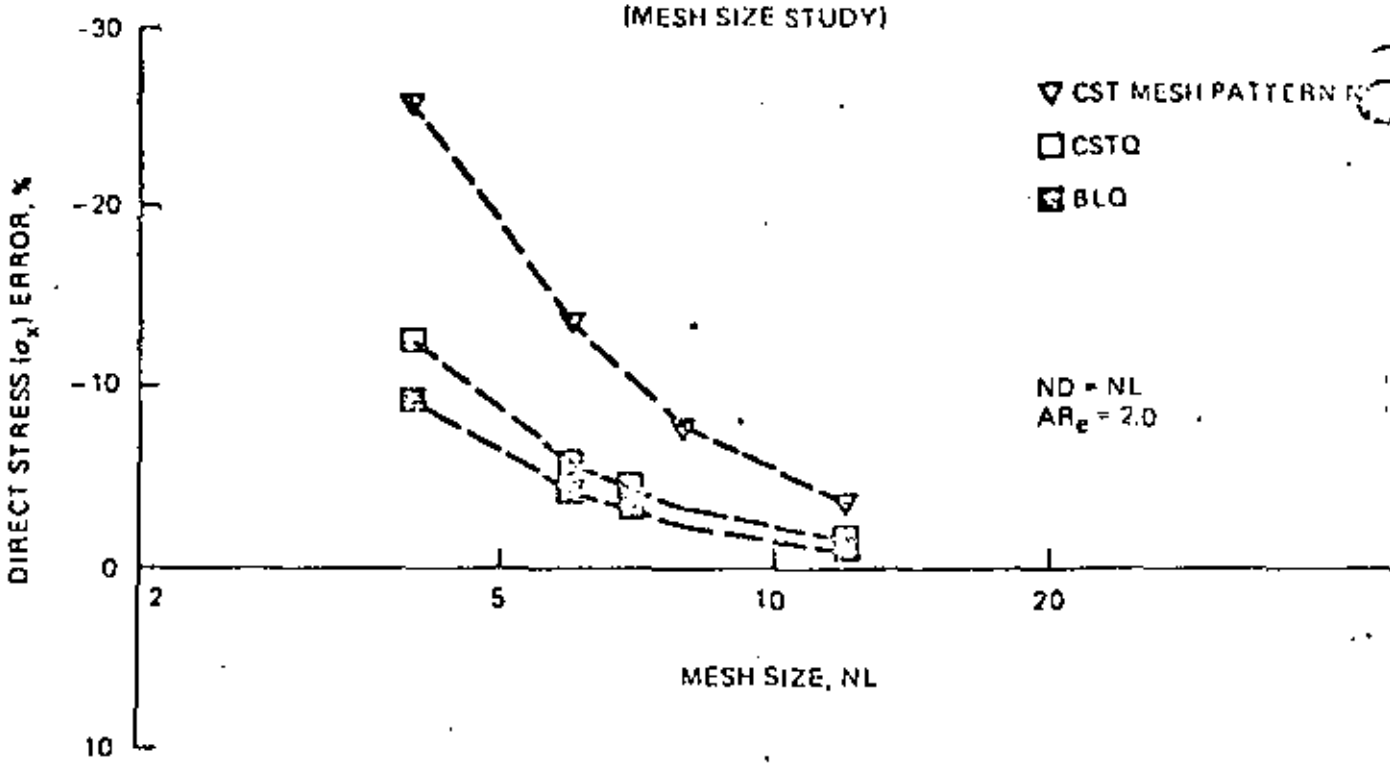

FIG. III .1.16

SHEAR STRESS ERROR
DEEP BEAM–END MOMENT AND END SHEAR LOADING
(MESH SIZE STUDY)

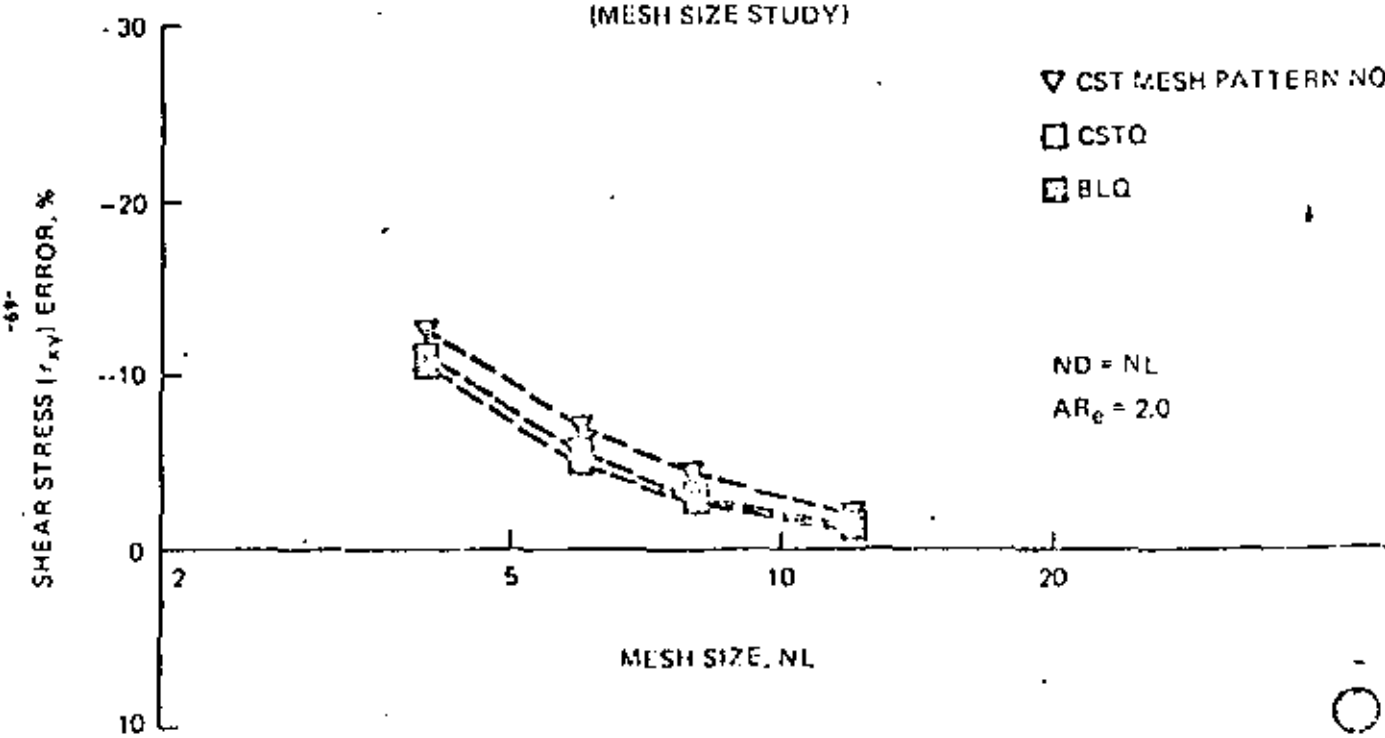

FIG. III.1.17

TIP DEFLECTION ERROR
DEEP BEAM–END MOMENT LOADING
(ASPECT RATIO STUDY)

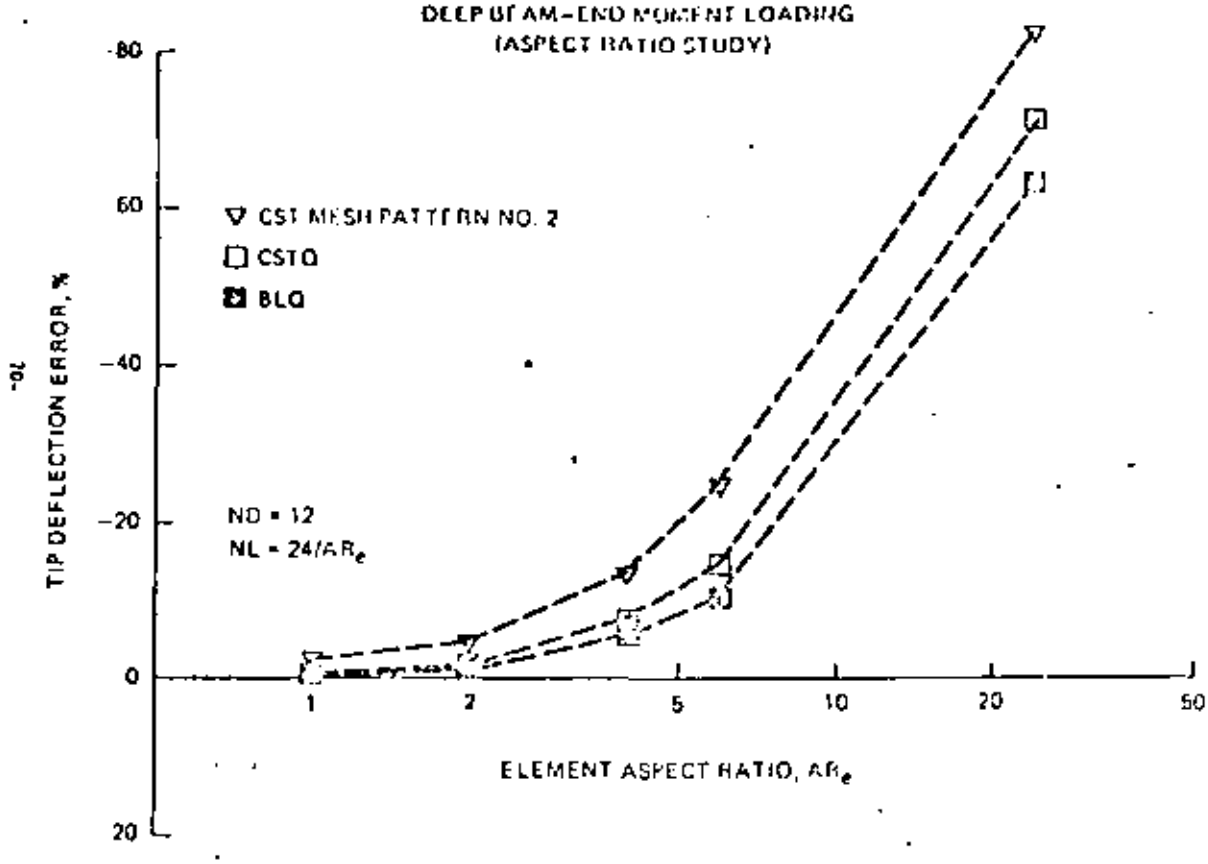

FIG. III.1.18

SHEAR STRESS ERROR
DEEP BEAM–END SHEAR LOADING
(ASPECT RATIO STUDY)

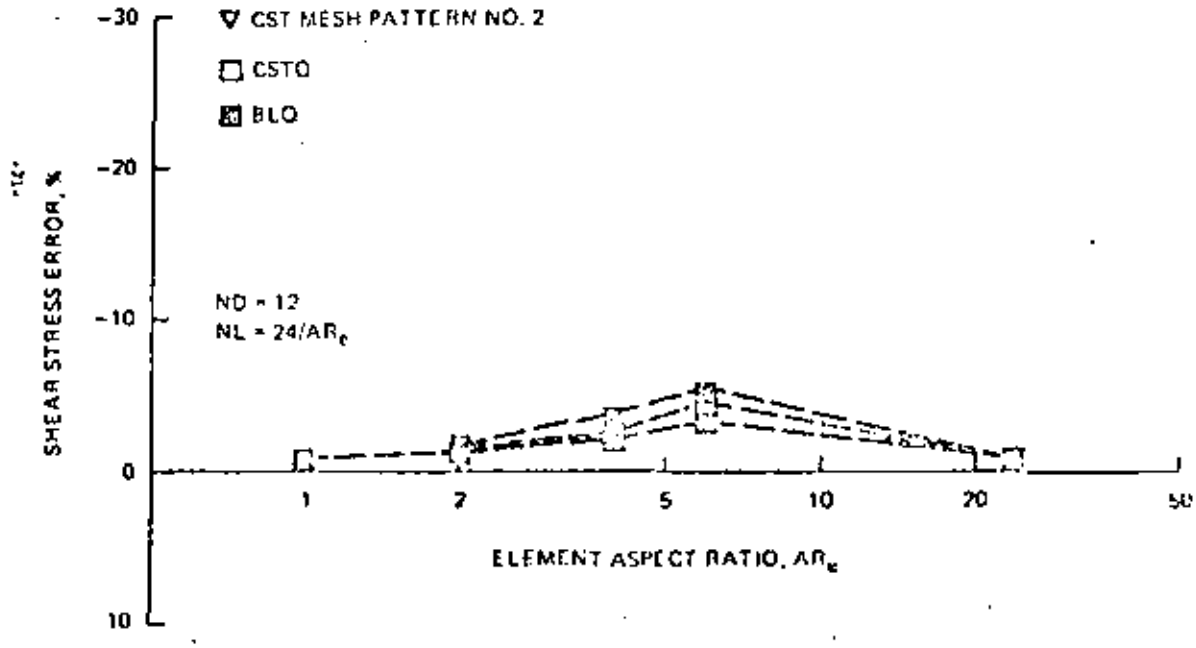

FIG. III 3.19

MID-SPAN STRESS DISTRIBUTIONS
DEEP BEAM - END SHEAR LOADING
NL = ND = 4

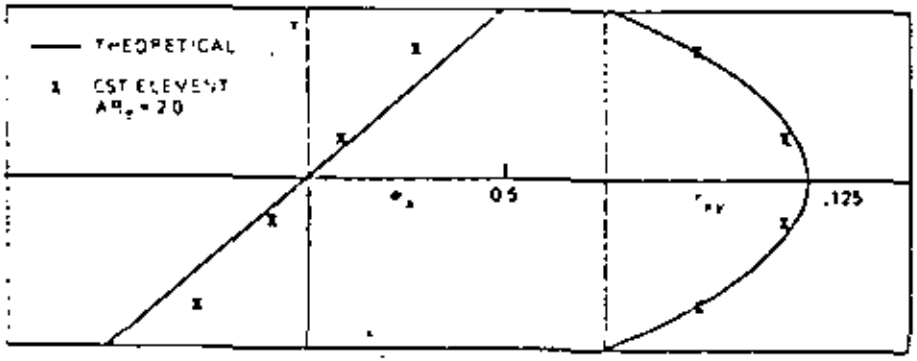

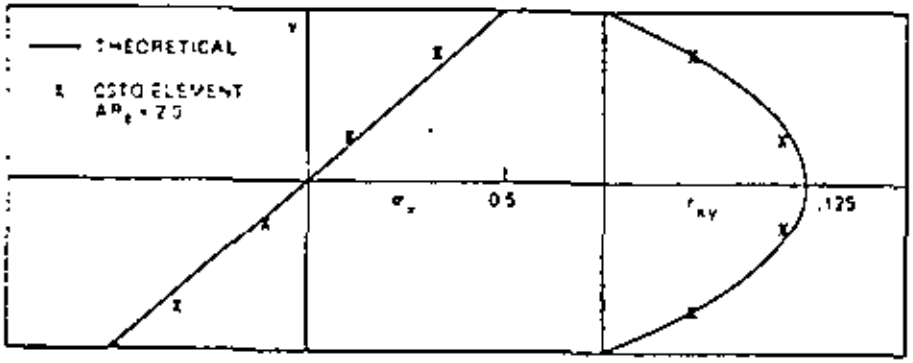

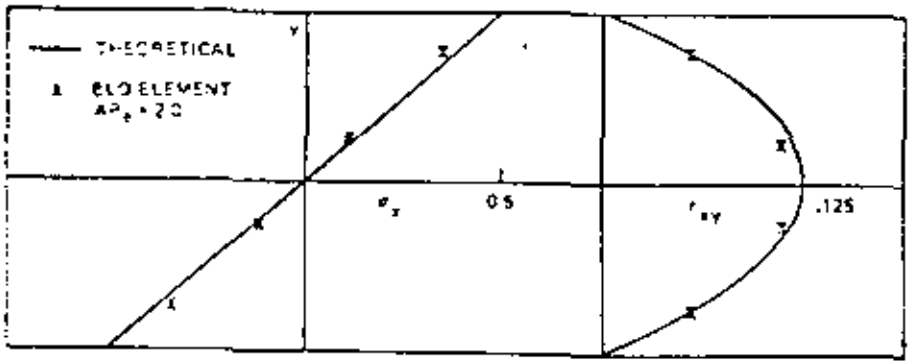

FIG. III 3.20

MID-SPAN STRESS DISTRIBUTIONS
DEEP BEAM - END SHEAR LOADING
ND = 12

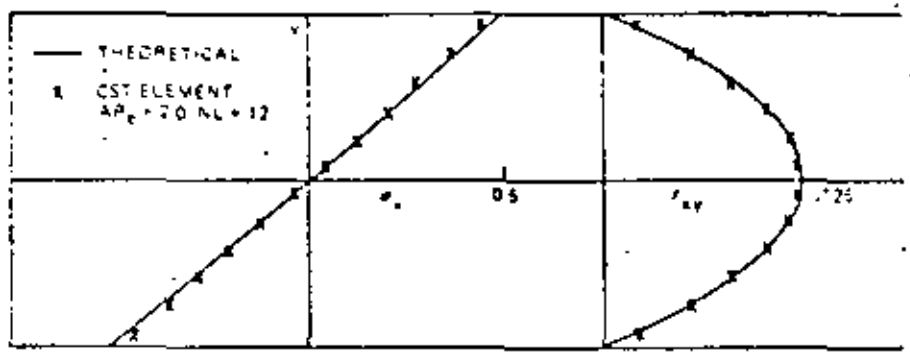

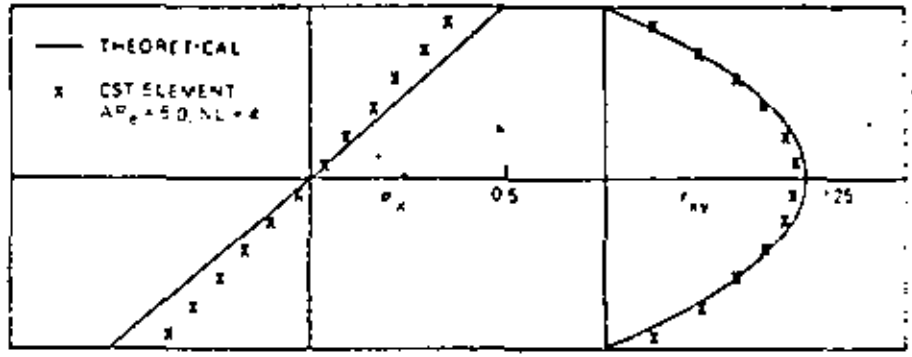

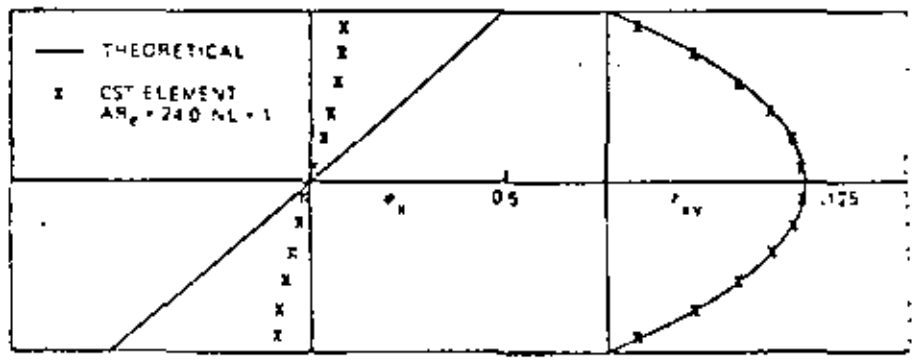

FIG. III.1.21

MID-SPAN STRESS DISTRIBUTIONS
DEEP BEAM–END MOMENT AND END SHEAR LOADING
NL = 43, ND = 24

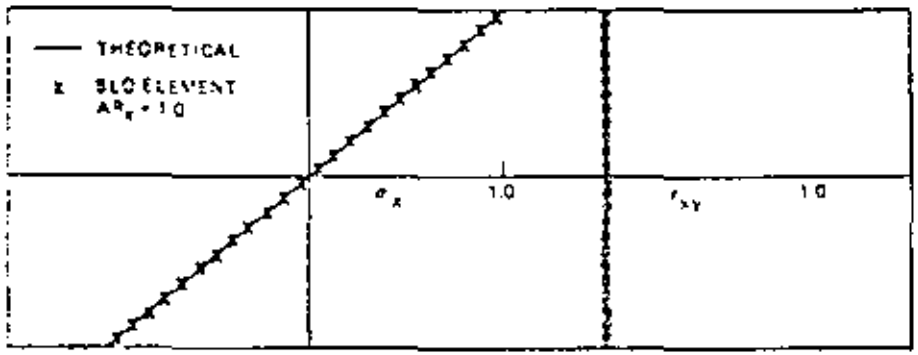

END MOMENT LOADING

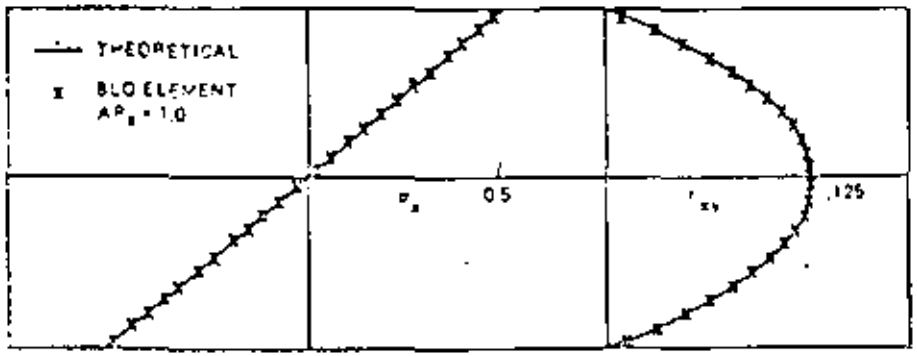

END SHEAR LOADING

FIG III 1.22

MID-SPAN STRESS DISTRIBUTIONS
DEEP BEAM–UNIFROM LOAD AND PARABOLIC TEMPERATURE
NL = 46, ND = 24

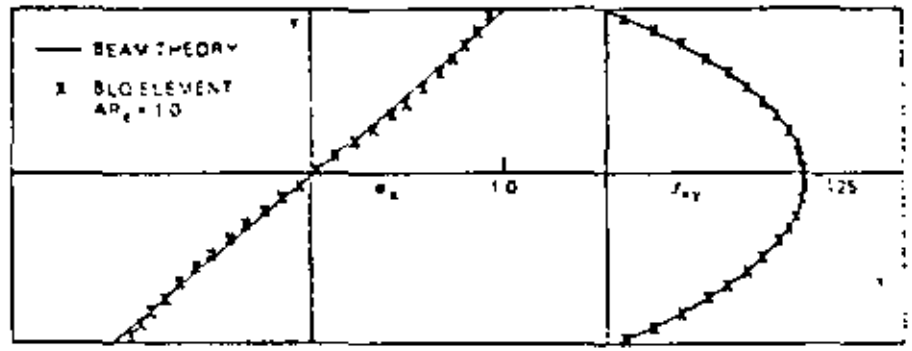

UNIFORM LOAD

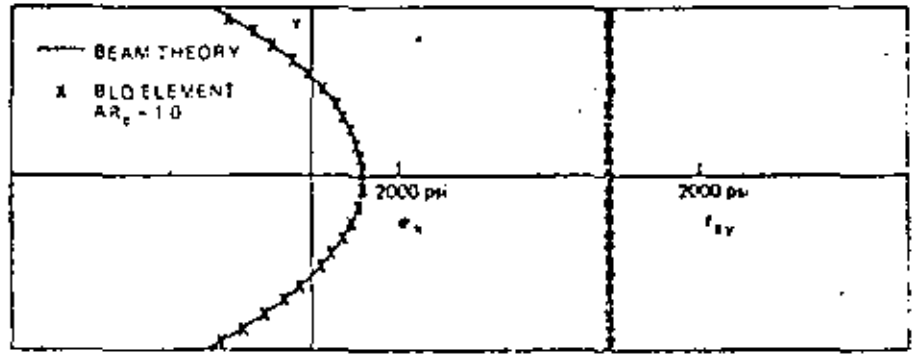

PARABOLIC TEMPERATURE

FIG. III.1.23

MID-SPAN BENDING STRESS DISTRIBUTIONS
DEEP BEAM-END MOMENT LOADING
NL = 4, ND = 4

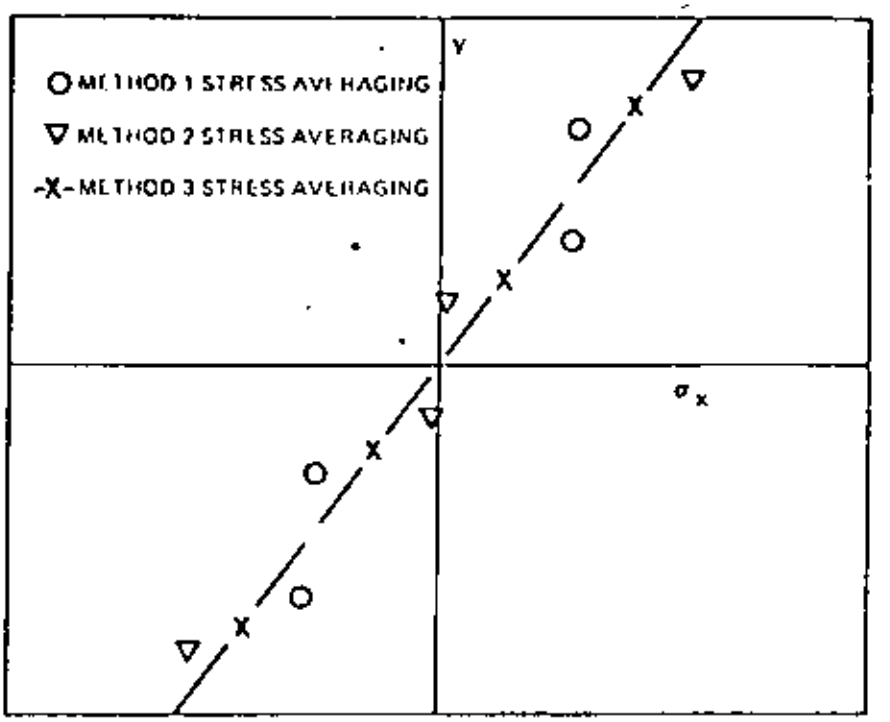

FIG. III. 1.24
TIP DEFLECTION ERROR
DEEP BEAM-END MOMENT LOADING
(TIMING STUDY)

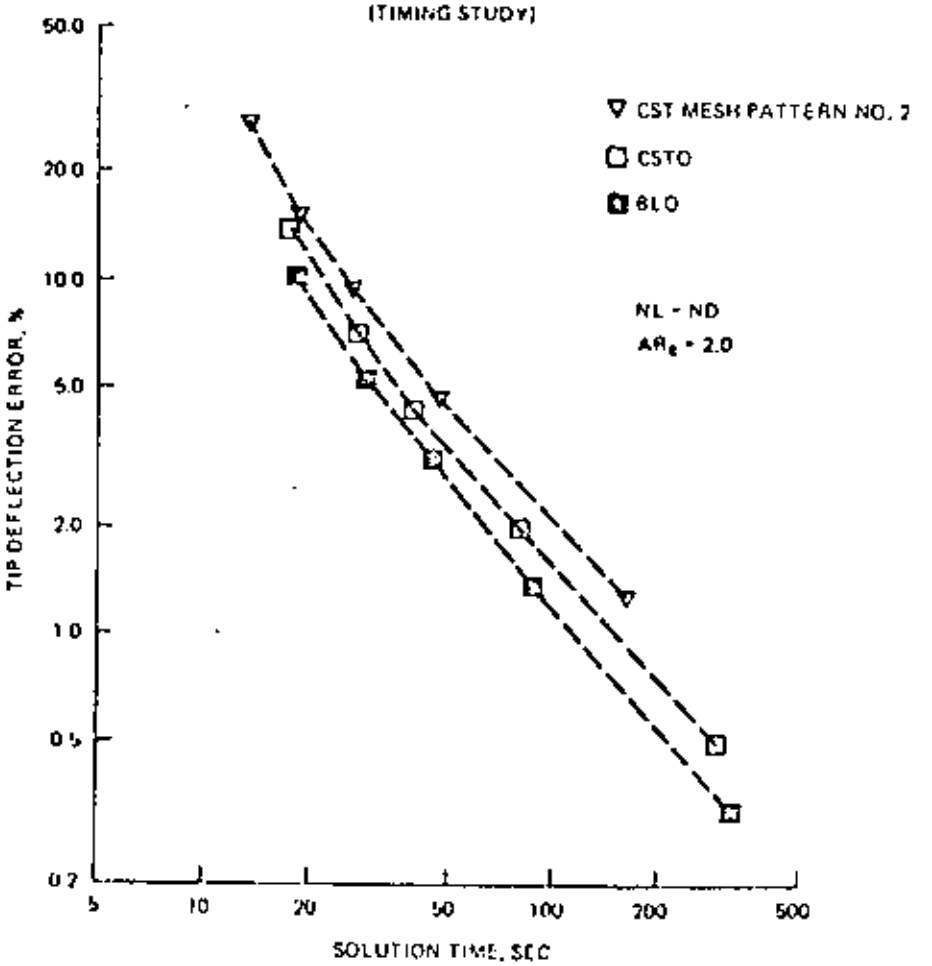

(C-3)

Part 2 - The Quadratic Quadrilateral

by Albert P. Burg, A.M. Asce[1] and
Vinod L. Kinodia [2]

4.2.1 Introduction

The quadratic quadrilateral finite element is the second higher-order element to be considered in this study. Because of its greater degree of sophistication, the element is more versatile than and generally superior to the lower order elements. It is the purpose of this portion of the chapter to present the analysis description, results and conclusions in conjunction with the overall purpose of establishing finite element idealization guidelines for the practicing engineer.

4.2.2 Element Description

The quadratic quadrilateral (QQ) is a second-order, isoparametric two-dimensional finite element (element number 26 of the MARC-CDC Non-Linear Finite Element Analysis Program). The element is defined in space by the locations of four corner and four mid-side nodes (Fig. 1) and belongs to what Zienkiewicz calls the Serendipity family (7). The addition of a mid-side node along each edge enables the user to approximate a curved boundary along each edge with a parabolic interpolation function. A much greater degree of accuracy is available with the QQ than with the bilinear quadrilateral. Exact stress and strain results are possible when the strain variation through an element is linear; exact displacement results are possible when the displacement function is quadratic. Nine integration points, whose positions are determined by Gaussian interpolation, provide locations within each element for stress and strain output.

---

(1) Engineer, United Engineers and Constructors, Inc., Philadelphia, PA

(2) Grad. Student, Dept. of Civil Engr., Cornell Univ., Ithaca, NY; formerly, Engineer, United Engineers and Constructors, Inc., Philadelphia, PA

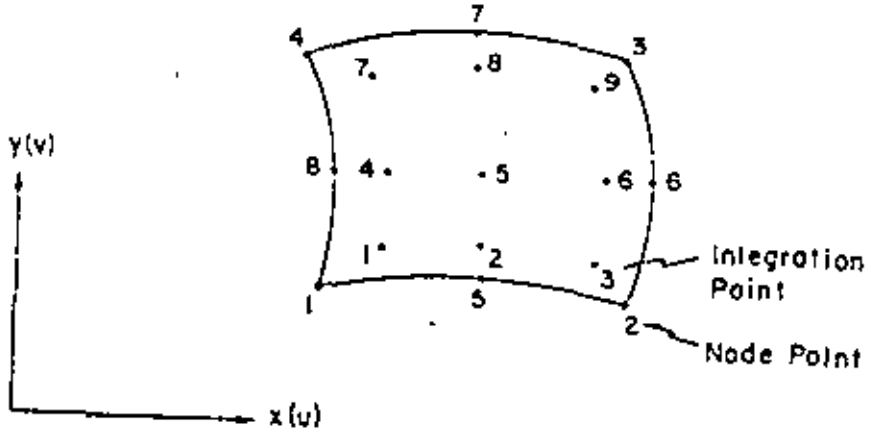

FIG. 1 — QUADRATIC QUADRILATERAL ELEMENT IN THE GLOBAL XY—PLANE

4.2.3 Model Description

Two structures of unit thickness are analyzed - a relatively slender beam of length to depth ratio 15 to 1 and a short deep beam of length to depth ratio 2 to 1. Each structure is modeled with five different mesh variations in order that the effects of a constant and a variable element aspect ratio can be compared. Figures 2 and 3 show the deep and slender mesh configurations, respectively. Table 1 lists the individual characteristics of each model.

The following material properties are used in the analysis:

modulus of elasticity = 29×10^6 psi

Poisson's ratio = 0.3

Linear coefficient of thermal expansion = 9.4×10^{-6} in/in/°F

Mass density is not considered because body loads are not included in the general loading conditions.

4.2.4 Boundary Conditions

Two distinct sets of boundary conditions are employed - one for the first three load cases (end moment, end shear, uniformly distributed) and one for the nonuniform temperature loading case. The boundary conditions in the first set are only those required to eliminate rigid body motion; i.e., the left end mid-side node is restrained vertically and horizontally and the left end bottom node is restrained horizontally only. In order to simulate the correct boundary conditions for a cantilevered beam, the proper equivalent loads, namely a parabolic shear distribution and a linear normal distribution, are applied to the left end.

Temperature loading case boundary or constraint conditions are applied to both the left and right ends. On the left end, the mid-side node is restrained vertically and horizontally while the remainder of the nodes are restrained horizontally only. The effect is to eliminate axial displacements at all of the fixed end nodes. The free (right) end of the beam is constrained to a linear displacement in order that temperature stresses do not vanish near the end.

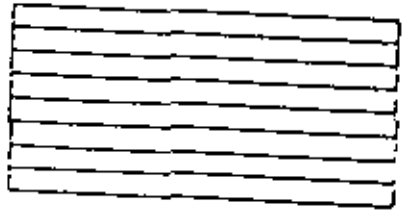

D3L1 - 8 X 1

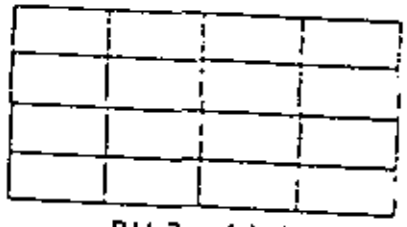

D1L2 - 4 X 4

D3L2 - 8 X 4

D2L3 - 6 X 6

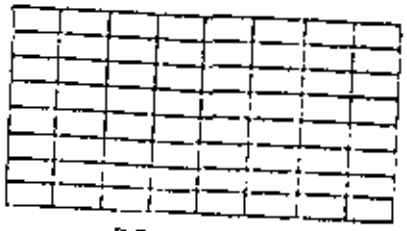

D3L4 - 8 X 8

FIG. [redacted] – DEEP BEAM CONFIGURATIONS

D3L1 - 8 X 4

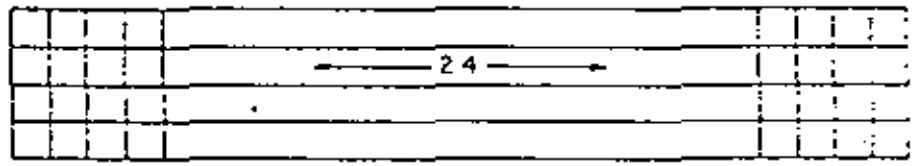

D1L3 - 4 X 24

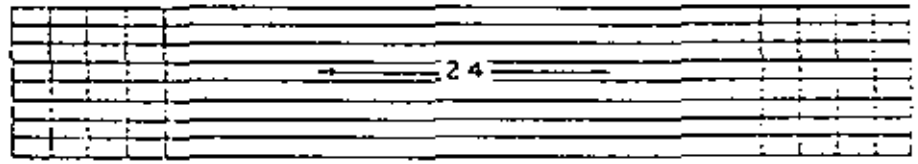

D3L3 - 8 X 24

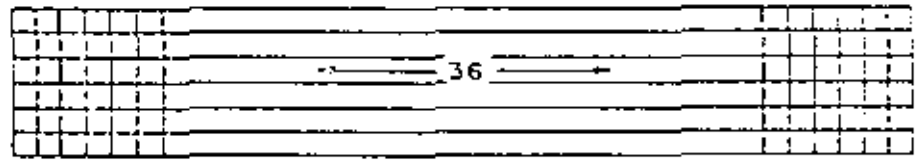

D2L4 - 6 X 36

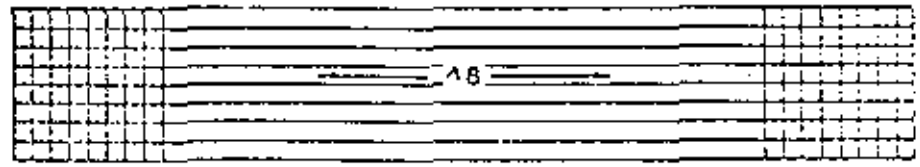

D3L5 - 6 X 48

FIG. 3 – SLENDER BEAM CONFIGURATIO[redacted]

TABLE 1 - BEAM CHARACTERISTICS

Mesh	Nodes	DOF	Elements	El. Along Length	El. Thru Depth	El. Aspect Ratio *
D3L1 DP	43	86	8	1	8	16:1
D1L2 DP	65	130	16	4	4	2:1
D3L2 DP	121	242	32	4	8	4:1
D2L3 DP	133	266	36	6	6	2:1
D3L4 DP	225	450	64	8	8	2:1
D3L1 SL	121	242	32	4	8	30:1
D1L3 SL	345	690	96	24	4	2.5:1
D3L3 SL	641	1282	192	24	8	5:1
D2L4 SL	733	1466	216	36	6	2.5:1
D3L5 SL	1265	2530	384	48	8	2.5:1

4.2.3 Loading Conditions

Four load cases (Fig. 4) have been considered for each of the ten models used - end moment, end shear, a uniformly distributed load, and a nonuniform temperature distribution. In each of the first three cases, the correct self-equilibrating loads are applied at the left (fixed) end of the beam in order to simulate cantilevered boundary conditions. In addition, the respective distributed loads (uniform, linear, and quadratic) must be applied as work equivalent nodal forces. When this is done, the same nodal deflections of the structure are produced as if the distributed loads are applied directly. The following relationship exists between the nodal work equivalent loads and distributed load intensities:

$$\begin{Bmatrix} P_1 \\ P_2 \\ P_3 \end{Bmatrix} = \frac{d}{30} \begin{bmatrix} 4 & -1 & 2 \\ -1 & 4 & 2 \\ 2 & 2 & 16 \end{bmatrix} \begin{Bmatrix} P_1' \\ P_2' \\ P_3' \end{Bmatrix}$$

where P_1, P_2, P_3 = nodal work equivalent loads

P_1', P_2', P_3' = distributed load intensities at the nodes

d = depth of beam

The quadratic displacement expansion, represented by the above equation, is presented in Fig. 3.

The loading configurations for all load cases are shown in Fig. 4. A maximum value of unit normal stress is assumed for each of the first three cases with the corresponding shear and uniform loads calculated accordingly. In the temperature case, the following nonuniform parabolic temperature distribution is applied (8):

$$T(y) = 1050 + 100y + 30y^2$$

The extreme and mid-point values of the temperature gradient are shown in Figure 4. The distribution is applied uniformly along the length of the beam and parabolically at each integration point through the depth.

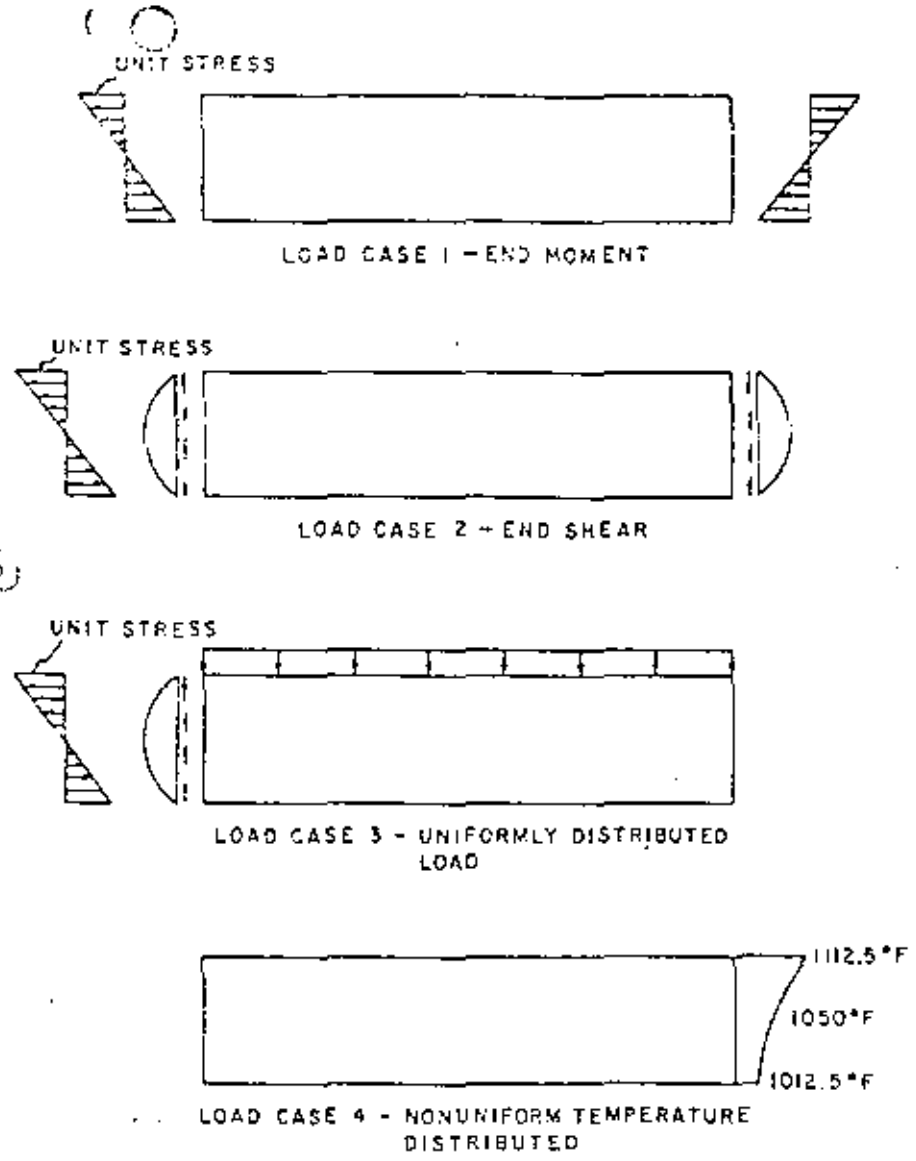

FIG. 4 – LOAD CASES

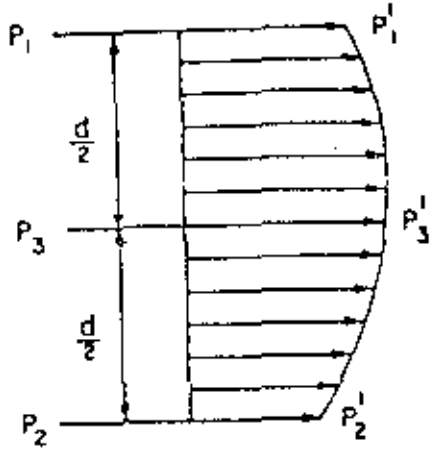

P_1, P_2, P_3 = Nodal Work Equivalent Loads

P_1', P_2', P_3' = Distributed Load Intensities at the Nodes

FIG. 5 – WORK EQUIVALENT LOADS ALONG THE EDGE OF A PLANAR ELEMENT

4.7.5 Results:

In each of the four load cases considered, mid-length, normal and shear stress distributions and mid-depth, free end deflections are presented. The mid-length stresses have been calculated by averaging the stresses at the two adjacent integration points and then by extrapolating the resulting stress distribution to the extreme fibers. Generally, displacement results possess greater accuracy than stress results.

4.7.6a End Moment Case

The classical elasticity solution to a beam loaded in pure bending can be found by using a stress function in the form of a third degree polynomial (3). The following stress distributions result:

$$\sigma_x = My/I$$

$$\sigma_y = 0$$

$$\tau_{xy} = 0$$

The mid-depth, free end deflection (v) becomes $v = ML^2/2EI$. The QQ element is capable of giving exact results for this particular loading since the stress is linear in the y-direction; therefore, it can be predicted that the percent error from the classical solution will be zero. For all ten of the deep and slender beam cases, deviation from the actual values of normal stress and tip deflection is zero (Table 2) as predicted. Figure 6 shows the stress distribution at mid-length for all deep and slender beams. Figures 7 and 8 show the percentage deviation from theoretical vertical free end deflection for the deep and slender beams, respectively.

4.7.6b End Shear Case

The classical elasticity solution (4) to a beam loaded in end shear gives the following values for direct and shear stresses:

$$\sigma_x = \frac{-P(L-X)y}{I}$$

$$\sigma_y = 0$$

$$\tau_{xy} = \frac{P}{2I}(c^2 - y^2)$$

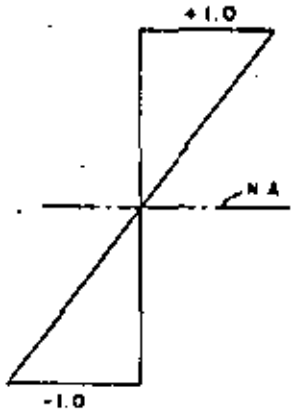

FIG. 6 — MID-LENGTH NORMAL STRESS DISTRIBUTION DUE TO END MOMENT LOADING OF ALL DEEP AND SLENDER BEAMS

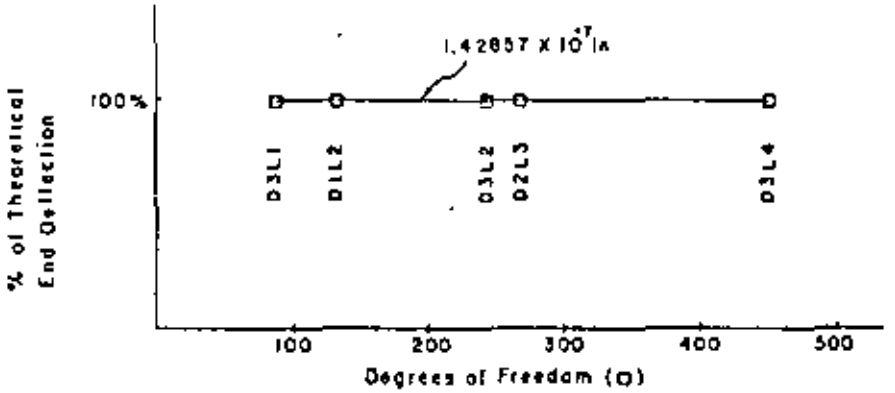

FIG. 7 — FREE END DEFLECTION DUE TO END MOMENT LOADING OF ALL DEEP BEAMS

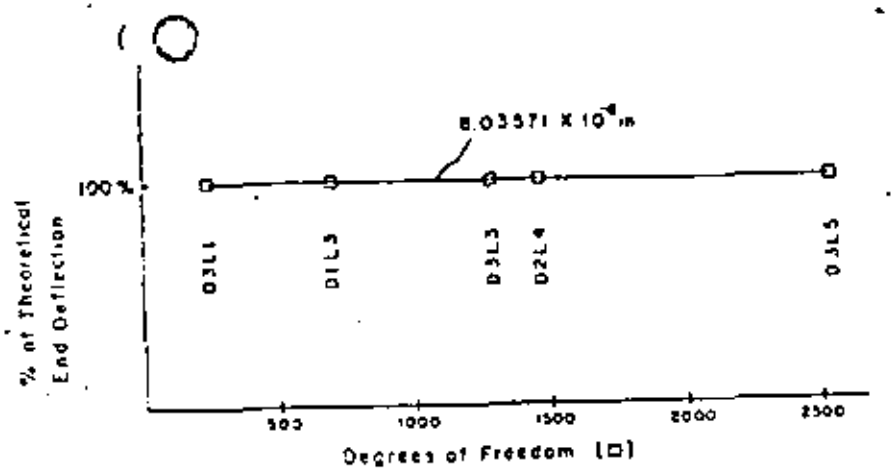

FIG. 8 — FREE END DEFLECTION DUE TO END MOMENT LOADING OF ALL SLENDER BEAMS

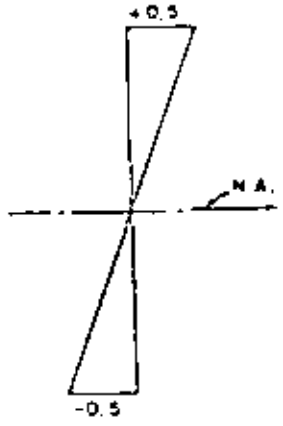

FIG. 9 — MID-LENGTH NORMAL STRESS DISTRIBUTION DUE TO END SHEAR LOADING OF ALL DEEP AND SLENDER BEAMS

-140-

upon the proper application of the boundary conditions, the following horizontal (u) and vertical (v) deflections are found at mid-depth of the free end:

$$u = 0$$

$$v = \frac{Pl^3}{3EI}$$

Because the normal stress σ_x is a linear function through the beam depth, the QQ element should give an exact stress distribution for all deep and slender beams. Shear stress and vertical end deflection vary quadratically through the depth and cubically along the length, respectively. Exact shear stress and deflection solutions with the QQ element are not possible, although very good approximations are possible.

Slender beam results are presented in Figures 9, 10, and 11. Figure 9 shows that the normal stress distribution for all of the deep and slender beams is exact, as would be expected. Figure 10 presents the mid-length shear stress distributions. Except for the D3L1 slender beam with element aspect ratio 30 to 1, the mid-depth shear stress values vary by less than 6% from the theoretical value (Table 2). The free end mid-depth vertical deflection values of the slender beams (Fig. 11) vary by less than 1% from the theoretical value (Table 2).

As in the cases with slender beams, the normal stress distribution for deep beams is exact (Fig. 9). The mid-length deep beam shear stress distributions are presented in Figure 12. With the exception of the D3L1 deep beam with element aspect ratio 16 to 1, the mid-depth stress values vary by no greater than 4% from theoretical values (Table 3). The free end mid-depth vertical deflection values of the deep beams (Fig. 13), except for the D3L1 deep beam case, vary by no greater than 2% from theoretical values.

Note that in the case of deep beams with small span to depth ratios, the deflection due to shear must by considered in addition to the bending deflection. Reference 5 gives the following vertical deflection term due

-141-

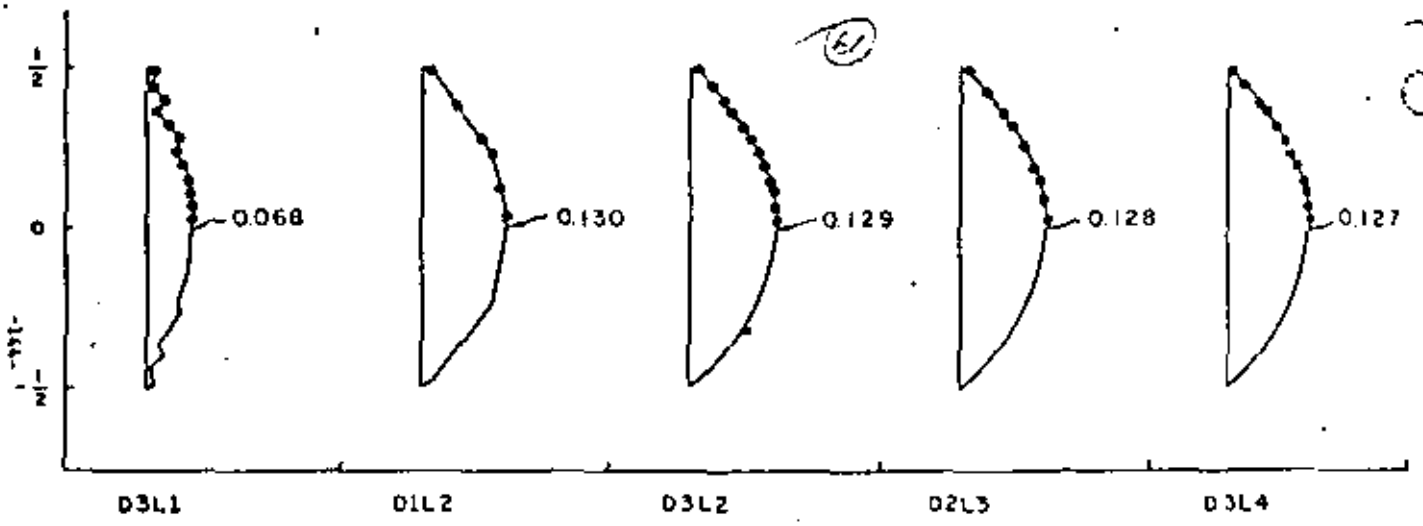

FIG. 12 – MID-LENGTH SHEAR STRESS DISTRIBUTION DUE TO END SHEAR LOADING (ALSO DISTRIBUTED LOADING) OF ALL DEEP BEAMS

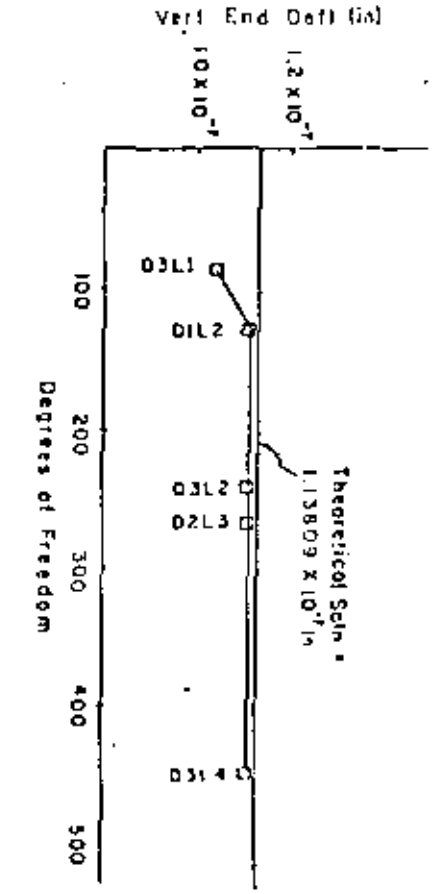

FIG. 13 – FREE END MID-DEPTH DEFLECTION DUE TO END SHEAR LOADING OF DEEP BEAMS

TABLE 2 - STRESS AND DEFLECTION COMPARISONS WITH THEORETICAL SOLUTIONS

Load Case	Beam	σ_x	Th. Soln.	% Error	τ_{xy}	Th. Soln.	% Error	Vert. Defl.	Th. Soln.	% Error
1 End Moment	D3L1 DP	1.0	1.0	0.0	——	——	——	1.428572E-07	1.428572E-07	0.0
	D1L2 DP	1.0	1.0	0.0	——	——	——	1.428572E-07	1.428572E-07	0.0
	D3L2 DP	1.0	1.0	0.0	——	——	——	1.428572E-07	1.428572E-07	0.0
	D2L3 DP	1.0	1.0	0.0	——	——	——	1.428572E-07	1.428572E-07	0.0
	D3L4 DP	1.0	1.0	0.0	——	——	——	1.428572E-07	1.428572E-07	0.0
	D3L1 SL	1.0	1.0	0.0	——	——	——	8.035714E-06	8.035714E-06	0.0
	D1L3 SL	1.0	1.0	0.0	——	——	——	8.035714E-06	8.035714E-06	0.0
	D3L3 SL	1.0	1.0	0.0	——	——	——	8.035714E-06	8.035714E-06	0.0
	D2L4 SL	1.0	1.0	0.0	——	——	——	8.035714E-06	8.035714E-06	0.0
	D3L5 SL	1.0	1.0	0.0	——	——	——	8.035714E-06	8.035714E-06	0.0
2 End Shear	D3L1 DP	0.5	0.5	0.0	.068	.125	45.6	1.040668E-07	1.138095E-07	8.6
	D1L2 DP	0.5	0.5	0.0	.130	.125	4.0	1.111440E-07	1.138095E-07	2.0
	D3L2 DP	0.5	0.5	0.0	.129	.125	3.2	1.113514E-07	1.138095E-07	2.0
	D2L3 DP	0.5	0.5	0.0	.128	.125	2.4	1.115589E-07	1.138095E-07	2.0
	D3L4 DP	0.5	0.5	0.0	.127	.125	1.6	1.117664E-07	1.138095E-07	1.9
	D3L1 SL	0.5	0.5	0.0	.0324	.0167	94.4	5.325078E-06	5.357143E-06	0.6
	D1L3 SL	0.5	0.5	0.0	.0176	.0167	5.6	5.373348E-06	5.357143E-06	0.3
	D3L3 SL	0.5	0.5	0.0	.0175	.0167	5.0	5.373348E-06	5.357143E-06	0.3
	D2L4 SL	0.5	0.5	0.0	.0171	.0167	2.6	5.373348E-06	5.357143E-06	0.3
	D3L5 SL	0.5	0.5	0.0	.0169	.0167	1.4	5.375618E-06	5.357143E-06	0.3

NOTES
1. σ_x measured at extreme fiber of mid-length cross section.
2. τ_{xy} measured at mid-depth of mid-length cross section.
3. Vert. defl. measured at mid-depth of free end.

TABLE 2 - STRESS AND DEFLECTION COMPARISONS WITH THEORETICAL SOLUTIONS (CONTINUED)

Load Case	Beam	σ_x	Th. Soln.	% Error	τ_{xy}	Th. Soln.	% Error	Vert. Defl.	Th. Soln.	% Error
3 Uniformly Distributed	D3L1 DP	.318	.25	27.2	.068	.125	45.6	7.946397E-02	8.035650E-02	1.1
	D1L2 DP	.234	.25	6.4	.130	.125	4.0	8.246238E-08	8.035650E-08	2.6
	D3L2 DP	.233	.25	6.8	.129	.125	3.2	8.339502E-08	8.035650E-08	3.3
	D2L3 DP	.235	.25	6.0	.128	.125	2.4	8.253767E-08	8.035650E-08	2.5
	D3L4 DP	.235	.25	6.0	.127	.125	1.6	8.261730E-08	8.035650E-08	2.5
	D3L1 SL	.258	.25	3.2	.0324	.0167	94.4	3.899058E-05	4.020790E-05	1.5
	D1L3 SL	.250	.25	0.0	.0176	.0167	5.6	4.033643E-05	4.020790E-05	0.1
	D3L3 SL	.250	.25	0.0	.0175	.0167	5.0	4.023331E-05	4.020790E-05	0.1
	D2L4 SL	.250	.25	0.0	.0172	.0167	3.2	4.033528E-05	4.020790E-05	0.1
	D3L5 SL	.250	.25	0.0	.0169	.0167	1.4	4.033618E-05	4.020790E-05	0.1
4 Parabolic Temperature Distribution	D3L1 DP	——	——	——	——	——	——	1.875918E-03	1.88E-03	0.2
	D1L2 DP	——	——	——	——	——	——	1.847335E-03	1.88E-03	1.7
	D3L2 DP	——	——	——	——	——	——	1.848031E-03	1.88E-03	1.7
	D2L4 DP	——	——	——	——	——	——	1.848385E-03	1.88E-03	1.7
	D3L4 DP	——	——	——	——	——	——	1.848668E-03	1.88E-03	1.7
	D3L1 SL	——	——	——	——	——	——	.10578	.10575	0.1
	D1L3 SL	——	——	——	——	——	——	.10572	.10575	0.0
	D3L3 SL	——	——	——	——	——	——	.10572	.10575	0.0
	D2L4 SL	——	——	——	——	——	——	.10572	.10575	0.0
	D3L5 SL	——	——	——	——	——	——	.10572	.10575	0.0

NOTES:
1. σ_x measured at extreme fiber of mid-length cross section.
2. τ_{xy} measured at mid-depth of mid-length cross section.
3. Vert. defl. measured at mid-depth of free end.

to shear:

$$\delta_{ys} = 1.2\,\frac{PL}{AG}$$

The above value for the vertical deflection is sufficient for beams with span to depth ratio 3 to 1 or greater. The deep beams analyzed, however, have a span to depth ratio of 2 to 1. This is a possible explanation for the fact that the deep beam percent error for the theoretical value is a consistent 2%.

The effects of varying element aspect ratios depends on which stress or deflection result is considered. For normal stress distribution, variable element aspect ratios had no effect since exact answers were possible. For shear stress distribution, convergence to theoretical value was quite apparent as aspect ratios became smaller. The vertical end deflection was not greatly effected by varying the aspect ratio. When the element aspect ratio remained constant and only the grid refinement was varied, accurate results were available in all cases.

4.2.4c Uniformly Distributed Load Case

The stress distribution for a slender cantilever beam under a uniformly distributed load is as follows:

$$\sigma_x = -\frac{My}{2I}\,(L - x)^2$$

$$\sigma_y = 0$$

$$\tau_{xy} = -\frac{w}{2I}\,(L - x)\,(c^2 - y^2)$$

When proper boundary conditions are applied, the following mid-depth, free end deflections are found:

$$u = 0$$

$$v = \frac{wL^4}{8EI}$$

The QT element should give exact results for direct stress since the direct stress varies linearly through the beam depth. Exact results for shear stress and vertical end deflection are not available since the shear stress varies parabolically through the depth and the displacement varies to the fourth degree.

Slender beam results under distributed loading are presented in Figures 14, 10, and 15. Figure 14 shows that the mid-length normal stresses are exact except for the D3L1 beam. The mid-length shear stress values are the same as those for end shear loading and are presented in Figure 10. With the exception again of the D3L1 beam (element aspect ratio 30 to 1), mid-depth shear stress values vary less than 6% from theoretical values (Table 2). Free end, mid-depth vertical deflections of the slender beams (Fig. 15) vary by 1.5% or less from the theoretical value (Table 2).

The deep beam results (Figs. 16,12, 17) listed in Table 2 are in greater error from theoretical values than are the slender beam results. Mid-length normal stress values (Fig. 16) consistently vary by about 6.5% from theoretical except the D3L1 beam stress varies by 27.2%. Shear stress values are identical to those of the end shear case (Fig. 12). The mid-depth free end vertical deflections vary by a consistent 8.5% from theoretical (Fig. 17). As in the case of end shear, the deflection for deep beams loaded uniformly across the length must include a shear term as given in Reference 5:

$$\delta_{ys} = 1.2\,\frac{wL}{2AG}$$

Since this equation is only sufficient for beams with span to depth ratio 3 to 1 or greater and since a linear stress distribution is not valid for short deep beams (5), a possible source of error exists which could explain the large discrepancy in deflection results.

The effects of varying or holding constant the element aspect ratios are similar to those of the end shear case. Stress results for both the D3L1 deep and slender beams are in considerable error from theoretical. Element aspect ratios for the two beams are 15 to 1 and 30 to 1, respectively. The displacement results are not as adversely effected by severe aspect ratios.

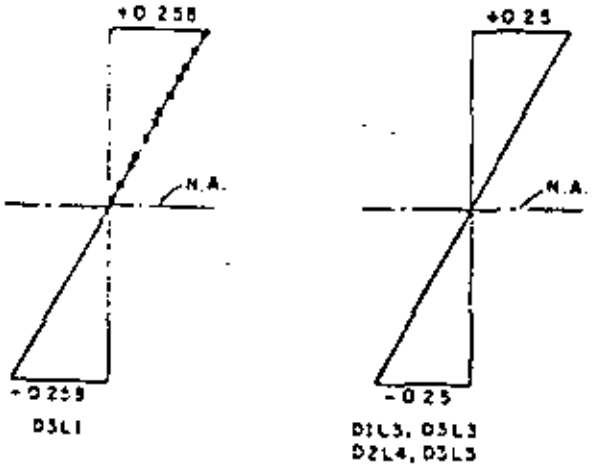

FIG. 14 – MID–LENGTH NORMAL STRESS DISTRIBUTION DUE TO DISTRIBUTED LOADING OF ALL SLENDER BEAMS

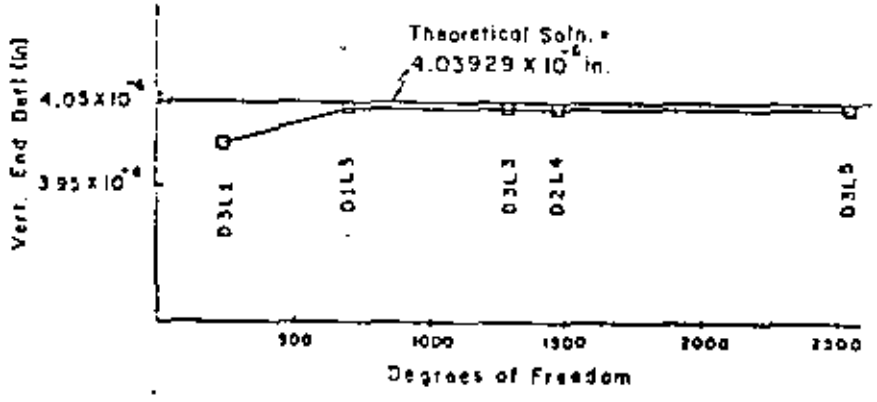

FIG. 15 – FREE END MID–DEPTH DEFLECTION DUE TO DISTRIBUTED LOADING OF SLENDER BEAMS

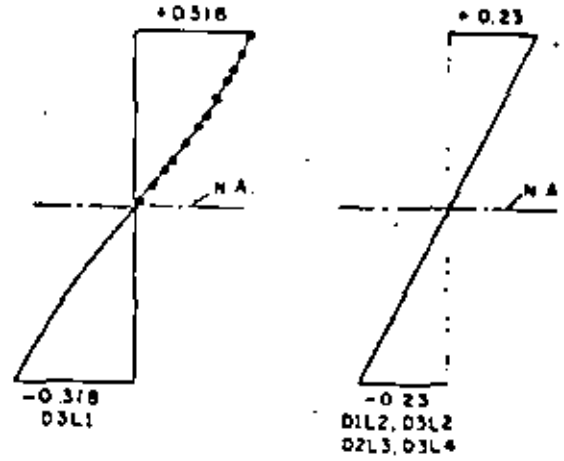

FIG. 16 – MID–LENGTH NORMAL STRESS DISTRIBUTION DUE TO DISTRIBUTED LOADING OF ALL DEEP BEAMS

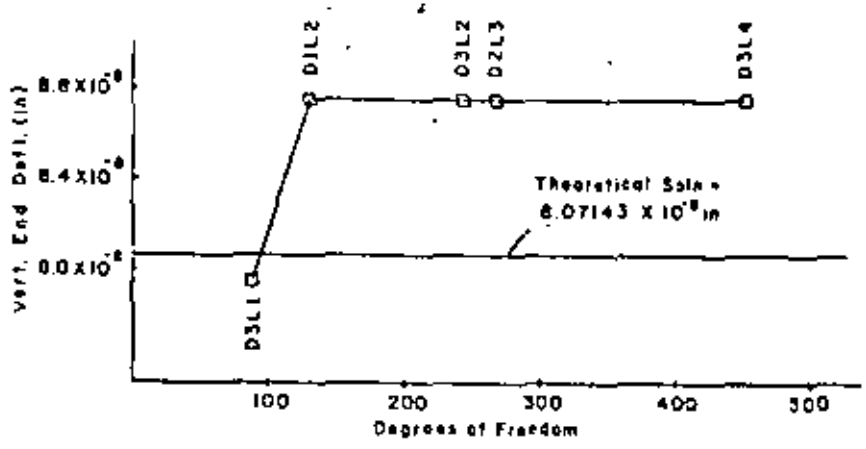

FIG. 17 – FREE END MID–DEPTH DEFLECTION DUE TO DISTRIBUTED LOADING OF ALL DEEP BEAMS

4.2.6c Temperature Case

The theoretical solution to a beam subjected to the nonuniform parabolic temperature distribution previously described gives the following values for normal and shear stresses:

$$\sigma_x = 50\ \alpha\ E\ (\tfrac{1}{3}c^2 - y^2)$$

$$\sigma_y = \tau_{xy} = 0$$

When the proper boundary conditions for a cantilever beam are applied, the horizontal (u) and vertical (v) deflections are found as follows:

$$u = \alpha\, x(1050 + 100y + \tfrac{50}{3}c^2)$$

$$v = \alpha\ (1050 + 50y^2 + \tfrac{50}{3}y^3 - 50x^2)$$

Exact solutions for the normal stress and vertical end deflection are not possible because of the respective quadratic and cubic variations in y. The Q4 element, in spite of the fact that exact solutions are available for linear functions only, provides quite accurate results for the normal stress and vertical end deflections.

The mid-length normal stress distributions of the slender and deep beams are shown in Figures 18 and 19, respectively. With the exception of the D3L1 deep beam, computer stress results do not vary significantly from theoretical results. Note in Figure 19 for the D3L1 case that the linear stress interpolation through the depth of an element is clearly represented by the eight straight-line segments which compose the stress diagram. The free end mid-depth vertical deflections of the slender and deep beams are shown in Figures 20 and 21, respectively. Slender beam deflections are virtually exact for every case except the coarsest mesh; deep beam deflections vary by not greater than 2% from theoretical results.

4.2.7 Overall Results

1. Computer results for the free end vertical deflection of deep beams for end shear, distributed, and temperature loadings are at a constant variance from the theoretical results for each case - 2% for end shear, 5.3% for distributed, and 1.7% for temperature. A possible explanation

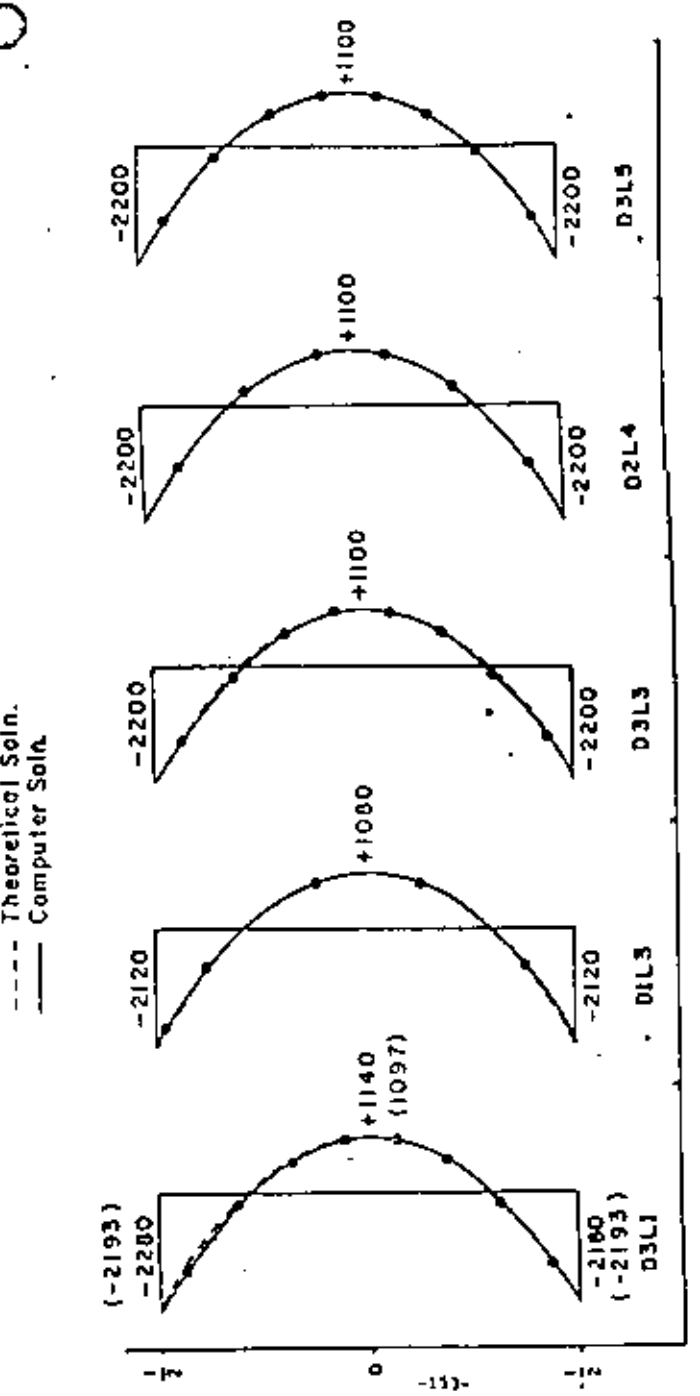

NOTE: Theoretical Stress Values in Parentheses

FIG. 18 – MID-LENGTH NORMAL STRESS DISTRIBUTION DUE TO TEMPERATURE LOADING OF ALL SLENDER BEAMS

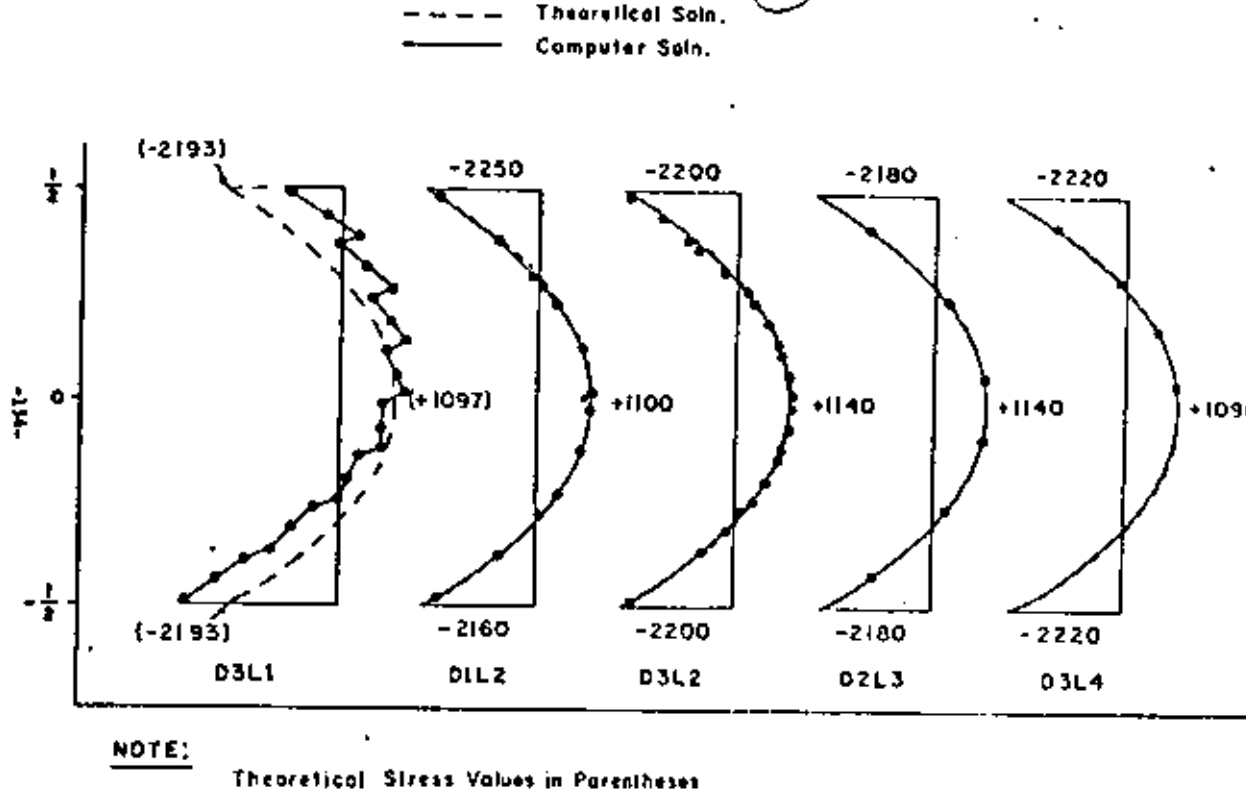

FIG. 19 – MID–LENGTH NORMAL STRESS DISTRIBUTION DUE TO TEMPERATURE LOADING OF ALL DEEP BEAMS

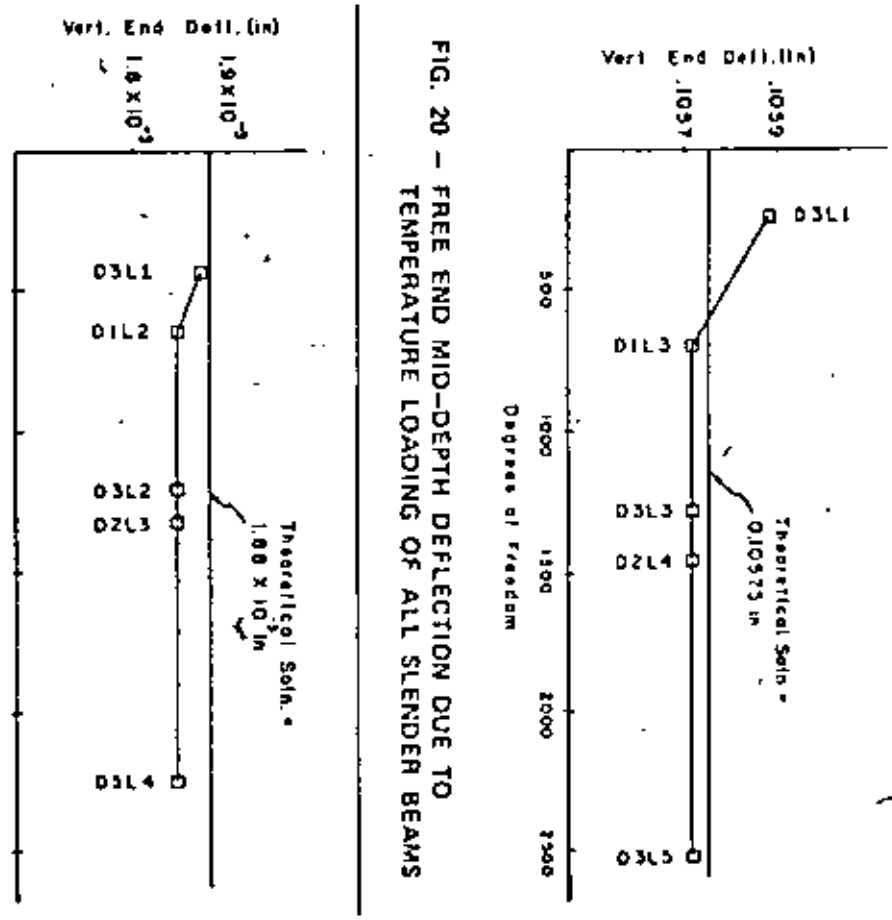

FIG. 20 – FREE END MID–DEPTH DEFLECTION DUE TO TEMPERATURE LOADING OF ALL SLENDER BEAMS

FIG. 21 – FREE END MID–DEPTH DEFLECTION DUE TO TEMPERATURE LOADING OF ALL DEEP BEAMS

for this behavior is that since the theoretical results cannot be calculated exactly, the computer results could be closer to the "correct" value than the theoretical results.

2. For each load case and for each set of deep and slender beams with constant element aspect ratios, there is little variation in computer results among those beams; i.e., beams with constant aspect ratios have very consistent results. A study in which the grid pattern becomes successively coarser would show, however, that accuracy is sacrificed with loss in refinement, regardless of aspect ratio. Dramatic differences can be seen when the aspect ratio varies from large to small. Percentage error from theoretical is much larger for the DILI deep beam with aspect ratio 16 to 1 and for the DILI slender beam at 30 to 1 than for beams at 4 or 2 to 1.

3. The assumption that the QQ element is capable of providing better displacement than stress results is shown to be correct by inspection of Table 2. Whereas stress results for beams with large element aspect ratios vary considerable from theoretical, the corresponding displacement results - keeping in mind the explanation of paragraph 1 above - are more consistent with the theoretical.

4.2.8 Conclusions

Upon inspection of the stress and deflection results and the comparisons with theoretical values, it is seen that the quadratic quadrilateral element is capable of producing quite accurate results with relatively few elements in a mesh. Because of the linear strain capabilities of the element, the exact solution is obtained for the pure bending case. Parabolic distributions of shear stress are within a few percentage of points of the theoretical values for most of the beams analyzed.

As the element aspect ratios become larger, accuracy is sacrificed. The

most severe aspect ratios for both the deep and slender beams (16 to 1 and 30 to 1, respectively) give results with much greater deviations from the theoretical value than beams with smaller element aspect ratios. The beam with the next higher element aspect ratio (8 to 1) has results no greater than 3% from theoretical for all stresses and deflections. Therefore, an element aspect ratio of up to 5 to 1 can be used with confidence in the accuracy of the results; element aspect ratios as high as, perhaps, 8 or 10 to 1 produce proportionately less accurate, but acceptable, results.

Accuracy of the results is a function of grid refinement. Generally, results will improve in accuracy as the number of elements increases. However, rapid convergence, as demonstrated with the 16-element mesh (DIL2 deep beam), is achieved with the QQ element. Since the objective of any finite element model is to most efficiently produce the desired accuracy at the minimum cost, care should be exercised that the problem is not modelled with an excess of nodes and elements. The advantages of the QQ element in achieving accurate results with small numbers of nodes and elements should be fully exercised by the user.

5.3 General Conclusions

As with any finite element model, the accuracy of the results is a direct function of the quality of the model. This is measured by how well the model can represent the actual stress and displacement distributions from the real structure. Good modelling, then, is partially a function of the engineer's understanding beforehand of how the stresses will be distributed. This implies that he or she should, to some extent, know the answers before the problem is run. The linear strain elements reduce the negative consequences of a poor choice of mesh relative to both the problem geometry and the particular loading conditions. This is particularly true in areas of high stress gradients, since stress distributions and boundary geometries which are quadratic functions may be modelled exactly.

In general, since the accuracy of the linear strain models is so much better than corresponding constant strain models, fewer elements need be used to obtain comparable, or even better, accuracy. The problems are consequently easier to set up, modelling time is reduced, the opportunity to make errors and their consequences are reduced. In addition, for a given level of accuracy, the costs may be expected to be less than for a constant strain model.

The user should take care not to use the linear strain elements indiscriminately. In cases where a constant strain model is sufficient, the linear strain models are significantly more expensive for the same mesh size. For example, in the models shown in this discussion, an axial load would yield nearly a constant strain situation. This could be modelled very accurately and with a significant cost savings by a coarse mesh of constant strain elements. On the other hand, the results show the need for a linear strain element for the distributed load case. This reinforces the need for consideration of the load distribution, as well as the geometry, in deciding the mesh size and type of element to be used in a particular problem solution.

REFERENCES

1. Fraeijs de Veubeke, B., "Displacement and Equilibrium Models in the Finite Element Method", Chapter 9 of Stress Analysis, edited by Zienkiewicz and Holliester, Wiley, 1965.
2. Felippa, C.A., "Refined Finite Element Analysis of Linear and Non-Linear Two-Dimensional Structures", Report 66-22, Department of Civil Engineering, University of California, Berkeley, Oct., 1966.
3. Connor, J.J., and Will, G., "Computer-Aided Teaching of the Finite Element Displacement Method", Report 869-23, Department of Civil Engineering, M.I.T., Cambridge, Mass., Feb., 1969.
4. Timoshenko, S., and Goodier, J.N., Theory of Elasticity, Second Edition, McGraw-Hill Book Company, Inc., New York, 1951.
5. Roark, R.J., Formulas for Stress and Strain, Fourth Edition, McGraw-Hill Book Company, Inc., New York, 1965.
6. Ergatoudis, I., Irons, B.M., and Zienkiewicz, O.C., "Curved, Isoparametric, 'Quadrilateral' Elements for Finite Element Analysis," Int. Journal of Solids and Structures, vol. 4, pp. 31-42, 1968.
7. Zienkiewicz, O.C., The Finite Element Method in Engineering Science, McGraw-Hill Book Company, Inc., New York, 1971.
8. Bruhn, E. F., Analysis and Design of Flight Vehicle Structures, Tri-State Offset Co., 1965.
9. Volterra, Enrico and Gaines, J.H., Advanced Strength of Materials, Prentice-Hall, Inc., Englewood Cliffs, N.J., 1971.

DIVISION DE EDUCACION CONTINUA
FACULTAD DE INGENIERIA U.N.A.M.

EL METODO DEL ELEMENTO FINITO EN LA INGENIERIA MECANICA

APLICACIONES: ANALISIS DINAMICO

DR. NICHOLAS JOHN SALAMON

ABRIL, 1982

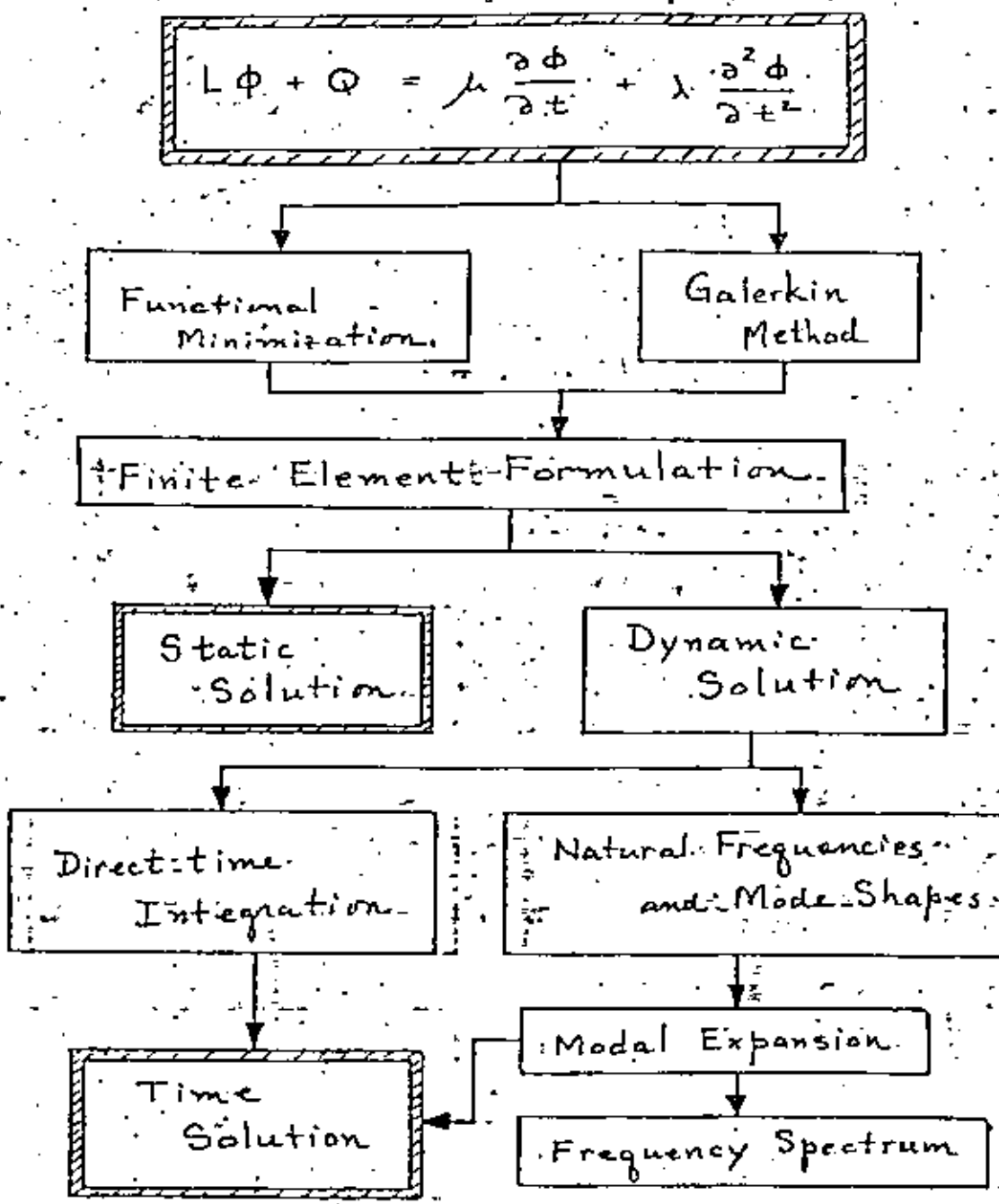

Flow Chart of Finite Element Solution Procedures

(e)

N.J. SALAMON

REFERENCES FOR NUMERICAL ANALYSIS

1. Przemieniecki, J., Theory of Matrix Structural Analysis, McGraw-Hill, 1968. (TA 642 .P77)

2. Zienkiewicz, O.C., The F.E. Method in Eng'g. Sci., McGraw-Hill, 1971. (TA 646 .Z54)

3. Desai, C., & Abel, Intro. to the F.E. Method, Van Nostrand, 1972. (TA 640 .2 .D48)

4. Oden, J.T., Finite Elements of Nonlinear Continua, McGraw-Hill, 1972.

5. Cook, R.D., Concepts and Applications of Finite Element Analysis, John Wiley, 1974.

6. Gallagher, Oden, et. al., Finite Elements in Fluids, Vol. 1,2, John Wiley, 1975.

7. Bathe, K.J. and Wilson, E.L., Numerical Methods in F.E. Analysis, Prentice-Hall, 1976. (TA 347 .F5 .B37)

8. Segerlind, L.J., Applied F.E. Analysis, John Wiley, 1976.

9. Connor, J.J. and Brebbia, C.A., Finite Element Techniques for Fluid Flow, Transatlantic, 1977.

10. Gudehus, G., Finite Elements in Geomechanics, John Wiley, 1977.

11. Norrie, D.H. and deVries, G., An Introduction to Finite Element Analysis, Academic Press, 1978.

12. Segerlind, Larry J., Applied Finite Element Analysis, John Wiley, New York, 1976.

13. Bathe, Klaus-Jurgen, Finite Element Procedures in Engineering Analysis, Prentice-Hall, Englewood Cliffs, N.J., 1982.

14. Becker, Eric B., Carey, G.F., Oden, J.T., Finite Elements, An Introduction, Vol I, Prentice-Hall, 1981.

KEY PERIODICALS

1. Int. J. for Numerical Methods in Eng'g. (TA 335 .I57)
2. Computers and Structures (TA 641 .C65)
3. Computers and Fluids (TA 357 .C59)
4. Earthquake Eng'g and Structural Dynamics (TA 654 .6 .E37)
5. Computer Methods in Applied Mechanics and Engineering
6. Int. J. for Numerical and Analytical Methods in Geomechanics.
7. Computer Programs in Science and Technology (QA 76 .C6X)
8. Computer Program Abstracts (NASA) (QA 76 .C5716)
9. Association of Computing Machinery (ACM) Special Interest Group - Numerical Mathematics (SIGNUM) Newsletter.
10. Int. J. of Heat and Mass Transfer (QC 320 .I55)
11. Numerical Heat Transfer

ELEMENTARY REFERENCES

1. Ural, Oktay., Finite Element Method - Basic Concepts and Applications, Intext, 1973.
2. Nath, B., Fundamentals of Finite Elements for Engineers, Athlone Press, 1974.
3. Desai, Chandrakant S., Elementary Finite Element Method, Prentice-Hall, Englewood Cliffs, N.J., 1979.

MISCELLANEOUS REFERENCES

1. Segui, W.T., Computer Programs for the Solution of Systems of Linear Algebraic Equations, NASA CR-2173, 1973.
2. Gregory, R.T. and Karney, D.L., A collection of Matrices for Testing Computational Algorithms, John Wiley, 1969. (QA 263 .G68)

▷ Formulation by Galerkin's Method (c 1915)* GM-1

⊙ The governing PDE in V is

$$L\varphi + Q = \frac{\partial}{\partial x}\left(D_{xx}\frac{\partial \varphi}{\partial x}\right) + \frac{\partial}{\partial y}\left(D_{yy}\frac{\partial \varphi}{\partial y}\right) + \frac{\partial}{\partial z}\left(D_{zz}\frac{\partial \varphi}{\partial z}\right) + Q = 0 \quad \text{(GM1.1)}$$

subject to the B.C. (BV-1b). For a simple derivation, consider on the interval (a,b)

$$\begin{aligned} Lu + f &= 0 \quad , \quad u \text{ exact} \\ Lv + f &= \epsilon \quad , \quad v \text{ approx. } \neq \epsilon = \text{error fctn.} \end{aligned} \quad \text{(GM1.2)}$$

subject to B.C. : $u = v = 0$ @ a, b.

$$\int_a^b \left[v\,Lu + v f = 0 \right] dx$$

$$\rightarrow \quad + \int_a^b u\,\underbrace{Lv}_{\epsilon - f}\,dx + \underbrace{u'v\Big|_a^b}_{0} - \underbrace{uv'\Big|_a^b}_{0} + \int_a^b v f\,dx = 0 \quad \text{(GM1.3)}$$

$$\int_a^b u\epsilon\,dx - \int_a^b u f\,dx$$

{ Not obvious: Since L is Order 2, ⇒ integrate by parts twice, i.e., $\int v\,d^2u \rightarrow -\int u'v' \rightarrow -\int v'\,du \rightarrow \int u\,d^2v$

$$\therefore \quad \int_a^b u\epsilon\,dx = \int_a^b (u - v) f\,dx \underset{v \to u}{\overset{\lim}{=}} 0 \quad \text{(GM1.4)}$$

Thus the exact solution is orthogonal to the error. Since $\epsilon = Lv + f$ and letting $u = \sum_i W_i U_i$ ⟶

$$\sum_i \int_a^b W_i U_i (Lv + f)\,dx = 0$$

---

* (i) Segerlind, L.J.
(ii) Sokolnikoff, I.S. Math. Th. Elasticity, McGraw-Hill, 1946

GM-2

$$\sum_i U_i \int_e^b W_i (Lv + f)\, dx = 0$$

or

$$\int_e^b W_i (Lv + f)\, dx = 0 \quad , \quad i = 1, 2, \ldots \qquad (GM2.1)$$

defines the general method of weighted residuals.

⇒ Collocation, least squares, Galerkin methods.

⊙ : Let $W_i \longrightarrow N_i$, the interpolation fctns, then

$$\int_V [N]^T (L\phi + Q)\, dV = 0 \qquad (GM2.2a)$$

Galerkin's Method

where

$$\phi = [N]\{\Phi\} \qquad (GM2.2b)$$

RESTRICTION: Since $\int_V = \sum_e \int_{V_e}$ in F.E., smooth transitions between elements are required of the field quantities. However finite jumps "increasingly acceptable" as discretization → ∞ (small elements) or if gradients are small.

Extremely large (→ ∞) jumps between elements ⇒ error in the sum $\sum_e \int_{V_e}$, i.e.,

$$\int_V - \sum_e \int_{V_e} = \text{error}$$

∴ Derivatives in L can only be one greater than continuous order of N_i.

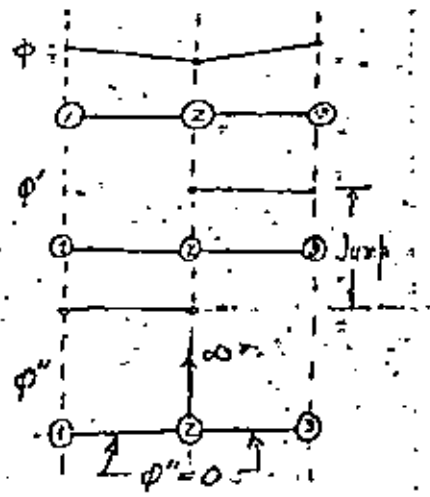

GM-3

This ⇒ acceptance of at most inter-element jumps.
For the present cases (figure), $\varphi'' \sim N'' \to \infty$
⇒ N is of order zero, N' has a jump. ∴
⇒ L must be ≤ order one. In fact most N_i are not continuous in N' between elements. Similar arguments apply to functional minimization, except note that the highest derivatives in (BV-2a) are 1st order.
Note: This requirement comes in at Eq. (GM 1.3) where we may be willing to accept a jump in L_V, ∴

⊙ Formulation of $L\varphi + Q$; (GM-1.1):

$$\int_{V_e} [N]^T \left[\frac{\partial}{\partial x}\underbrace{\left(D_{xx}\frac{\partial \varphi}{\partial x}\right)}_{\psi} + \frac{\partial}{\partial y}(\ ) + \dots + Q \right] dV = 0 \qquad (GM3.1)$$

Note: Reduce order of derivatives:

$$\int_{V_e} [N]^T \frac{\partial}{\partial x}\psi \, dV \overset{\text{PARTS}}{=} -\int_{V_e} \left[\frac{\partial}{\partial x}N^T\right]\psi \, dV + \underbrace{\int_{V_e} \frac{\partial}{\partial x}(N^T\psi)\, dV}$$

Gauss ⇒ $\dots + \int_{S_e} [N]^T \psi \, c\theta_x \, dS$

$$-\left\{ \int_{V_e}\left[\frac{\partial}{\partial x}N^T\right] D_{xx}\frac{\partial \varphi}{\partial x}\, dV + \int_{V_e}\left[\frac{\partial}{\partial y}N^T\right] D_{yy}\frac{\partial \varphi}{\partial y}\, dV + \int_{V_e}\left[\frac{\partial}{\partial z}N^T\right] D_{zz}\frac{\partial \varphi}{\partial z}\, dV \right\}$$

$$+ \int_{S_e} [N]^T \underbrace{\left\{ D_{xx}\frac{\partial \varphi}{\partial x}c\theta_x + D_{yy}\frac{\partial \varphi}{\partial y}c\theta_y + D_{zz}\frac{\partial \varphi}{\partial z}c\theta_z \right\}} dS$$

$$+ \int_{V_e} [N]^T Q \, dV = 0$$

$-q - h(\varphi - \varphi_\infty)$ from (BV-1b)

GM-4

Using (GM2-2b) and factoring $\{\bar{\Phi}\}$ $\Rightarrow$

$$0 = \left[\int_{V_e} \underbrace{\left\{\left[\frac{\partial}{\partial x}N\right]^T D_{xx}\left[\frac{\partial}{\partial x}N\right] + \cdots + \left[\frac{\partial}{\partial z}N\right]^T D_{zz}\left[\frac{\partial}{\partial z}N\right]\right\}}_{[B]^T[D][B]} dV\right]\{\bar{\Phi}\}$$

$$+ \int_{S_1^{(e)}} [N]^T q \, dS + \underbrace{\int_{S_4^{(e)}} [N]^T h\left([N]\{\bar{\Phi}\} - \phi_\infty\right) dS}$$

$$- \int_{V_e} [N]^T Q \, dV \qquad \int_{S_4^{(e)}} \left\{h[N]^T[N]\{\bar{\Phi}\} - h[N]^T\phi_\infty\right\} dS$$

$$\Rightarrow \underbrace{\left\{\int_{V_e} [B]^T[D][B]\,dV + \int_{S_4^{(e)}} h[N]^T[N]\,dS\right\}}_{[k]_e}\{\bar{\Phi}\}$$

$$\{f\}_e \begin{cases} -\int_{V_e} Q[N]^T dV + \int_{S_1^{(e)}} q[N]^T dS \\ \int_{S_4^{(e)}} h\phi_\infty [N]^T dS \end{cases} = 0 \qquad \text{(GM4-1)}$$

$$\Rightarrow [K]\{\bar{\Phi}\} = \{F\} \quad \text{as in E.O.'s (BY-4)}$$

⊙ Why Galerkin?

- The principle advantage is that a functional need not be derived and one can work directly from the PDE.

GM-5

▷ Formulation for transient fields

Ref. (i) Zienkiewicz, Ch. 16.
(ii) Segerlind, Ch. 11.

○ The PDE is

$$\frac{\partial}{\partial x}\left(D_{xx}\frac{\partial \varphi}{\partial x}\right)+\frac{\partial}{\partial y}\left(D_{yy}\frac{\partial \varphi}{\partial y}\right)+\frac{\partial}{\partial z}\left(D_{zz}\frac{\partial \varphi}{\partial z}\right)+Q=\mu\frac{\partial \varphi}{\partial t}+\rho\frac{\partial^2 \varphi}{\partial t^2} \quad (GM5.1)$$

with B.C. as in (BV-1a, b), initial conditions (I.C.) given and D_{ii}, Q, μ, ρ fctns. of time (t) at most. Treating time as a parameter

$\Rightarrow$

$$Q \longrightarrow \left(Q-\mu\frac{\partial \varphi}{\partial t}-\rho\frac{\partial^2 \varphi}{\partial t^2}\right). \quad (GM5.2)$$

So that the "Q-integral" in (BV-4b) becomes

$$\mathcal{J}=-\int_{V_e}[N]^T Q\,dV \longrightarrow -\int_{V_e}[N]^T\left(Q-\mu\frac{\partial \varphi}{\partial t}-\rho\frac{\partial^2 \varphi}{\partial t^2}\right)dV.$$

$$=-\int_{V_e}[N]^T Q\,dV+\int_{V_e}[N]^T\mu\frac{\partial \varphi}{\partial t}\,dV+\int_{V_e}[N]^T\rho\frac{\partial^2 \varphi}{\partial t^2}\,dV$$

Since $\varphi = [N(x,y,z)]\{\Phi(t)\}$

Then $$\frac{\partial \varphi}{\partial t}=[N]\frac{\partial\{\Phi\}}{\partial t} \quad \text{and} \quad \frac{\partial^2 \varphi}{\partial t^2}=[N]\frac{\partial^2\{\Phi\}}{\partial t^2} \quad (GM5.3)$$

$\Rightarrow$

$[c]_e$ ← Capacitance Matrix

$$\mathcal{J}=-\int_{V_e}[N]^T Q\,dV+\overbrace{\int_{V_e}[N]^T\mu[N]\,dV}\frac{\partial}{\partial t}\{\Phi\}$$

$[m]_e$ ← Mass Matrix

$$+\overbrace{\int_{V_e}[N]^T\rho[N]\,dV}\frac{\partial^2}{\partial t^2}\{\Phi\}. \quad (GM5.4)$$

Eq.s (BV-4) ≠ (GM5.4) ⇒

$$[k]_e \{\bar{\Phi}\} + [c]_e \frac{\partial}{\partial t}\{\bar{\Phi}\} + [m]_e \frac{\partial^2}{\partial t^2}\{\bar{\Phi}\} + \{f\}_e = 0$$

which upon assembly becomes (GM6.1)

$$[K]\{\bar{\Phi}\} + [C]\frac{\partial}{\partial t}\{\bar{\Phi}\} + [M]\frac{\partial^2}{\partial t^2}\{\bar{\Phi}\} = \{F\} \quad (GM6.2)$$

where $[C]$ ≡ Global capacitance matrix

$[M]$ ≡ Global mass matrix

Note: These matrices are not "lumped", say at nodes or Gauss points, but are <u>distributed</u> via the interpolation fctns in (GM5.4). For this reason, they are sometimes termed "consistent".

⊙ Example: 1-D linear element w/ k, ρ constant

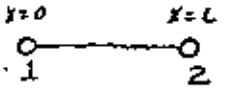

⇒

(1) $[N] = [(1-\frac{x}{L}) \quad \frac{x}{L}]$

(2) $[c]_e \overset{(GM5.4)}{=} k \int_{V_e} \begin{bmatrix} 1-x/L \\ x/L \end{bmatrix} [1-\frac{x}{L} \quad \frac{x}{L}] \underbrace{A\,dx}_{dV}$

$$= k \int_0^L \begin{pmatrix} (1-\frac{x}{L})^2 & \frac{x}{L}(1-\frac{x}{L}) \\ \frac{x}{L}(1-x/L) & (\frac{x}{L})^2 \end{pmatrix} A\,dx \quad (k, A \text{ constant})$$

$$= \frac{kAL}{2}\begin{bmatrix} 2/3 & 1/3 \\ 1/3 & 2/3 \end{bmatrix}$$

(3) Similarly

$$[m]_e = \frac{\rho AL}{2}\begin{bmatrix} 2/3 & 1/3 \\ 1/3 & 2/3 \end{bmatrix}$$

Note: for "lumped" mass:

$$[m]_e^{lumped} = \frac{\rho AL}{2}\begin{bmatrix} 1 & 0 \\ 0 & 1 \end{bmatrix}$$

⊙ Direct time integration ~ finite difference GM-7

Ref. (i) Bathe & Wilson, Ch. 8 & 9.
(ii) Segerlind, Ch. 11

Technique is a "marching" method as solutions in previous time are used to step out into or advance in time ⇒ solutions in future time.

Thus

$$\varphi_{t+\Delta t} = \varphi_{t-\Delta t} + \frac{\partial \varphi}{\partial t}(2\Delta t) + O(\Delta t)^3$$

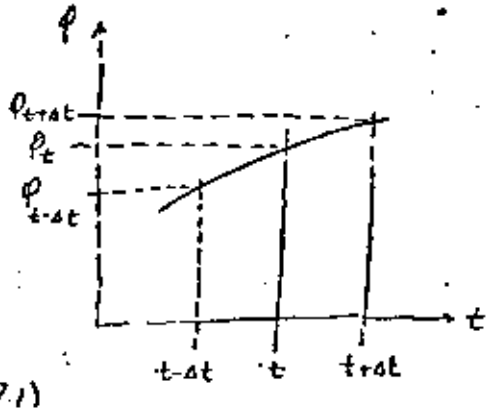

⇒

$$\left.\frac{\partial \varphi}{\partial t}\right|_t = \frac{1}{2\Delta t}\left[\varphi_{t+\Delta t} - \varphi_{t-\Delta t}\right] + \underline{O(\Delta t)^2}$$

discretization error (GM 7.1)

By a more elaborate procedure *

$$\left.\frac{\partial^2 \varphi}{\partial t^2}\right|_t = \frac{1}{(\Delta t)^2}\left[\varphi_{t+\Delta t} + \varphi_{t-\Delta t} - 2\varphi_t\right] + O(\Delta t)^2 \qquad (GM 7.2)$$

For finite element application

$$\frac{\partial}{\partial t}\{\Phi\}\Big|_t = \frac{1}{2\Delta t}\left[\{\Phi\}_{t+\Delta t} - \{\Phi\}_{t-\Delta t}\right] + O(\Delta t)^2$$

$$\frac{\partial^2}{\partial t^2}\{\Phi\}\Big|_t = \frac{1}{(\Delta t)^2}\left[\{\Phi\}_{t+\Delta t} + \{\Phi\}_{t-\Delta t} - 2\{\Phi\}_t\right] + O(\Delta t)^2 \qquad (GM 7.3)$$

where the $O(\Delta t)^2$ is dropped in practice.

---

* See: Forsythe & Wasow, Finite-diff. Meth. for PDE, Wiley, 1960.

GM-8

Substitution of (GM 7.3) in (GM6.2) $\Rightarrow$

Note: $t+\Delta t \to 3$, $t \to 2$, $t-\Delta t \to 1$

$$[K]\{\ddot{\Phi}\}_2 + [C]\cdot\frac{1}{2\Delta t}\left\{\{\Phi\}_3 - \{\Phi\}_1\right\}$$

$$+ [M]\cdot\frac{1}{\Delta t^2}\left\{\{\Phi\}_3 + \{\Phi\}_1 - 2\{\Phi\}_2\right\} = \{F\}_2$$

$\therefore$

$$\left\{\frac{1}{(\Delta t)^2}[M] + \frac{1}{2\Delta t}[C]\right\}\{\Phi\}_{t+\Delta t} = \{F\}_t - \left\{[K] - \frac{2}{(\Delta t)^2}[M]\right\}\{\Phi\}_t$$

$$- \left\{\frac{1}{(\Delta t)^2}[M] - \frac{1}{2\Delta t}[C]\right\}\{\Phi\}_{t-\Delta t} \qquad (GM8.1)$$

Thus future values follow directly from past values. However @ $t=0$, a starting procedure is needed as $\{\Phi\}_{0-\Delta t}$ appears. From (GM7.3)

$$\{\Phi\}_{-\Delta t} \overset{t=0}{=} (\Delta t)^2\frac{\partial^2}{\partial t^2}\{\Phi\}\Big|_0 - \{\Phi\}_{\Delta t} + 2\{\Phi\}_0$$

$$-2\Delta t\frac{\partial}{\partial t}\{\Phi\}\Big|_0 - \{\Phi\}_{-\Delta t}$$

$\therefore$

$$\{\Phi\}_{-\Delta t} = \frac{1}{2}\left\{\Delta t^2\{\ddot{\Phi}\}_0 - 2\Delta t\{\dot{\Phi}\}_0 + 2\{\Phi\}_0\right\} \qquad (GM8.2)$$

where $\{\Phi\}_0$ & $\{\dot{\Phi}\}_0$ are usually known and $\{\ddot{\Phi}\}_0$ may be computed from (GM6.2) if unknown.

In essence then, (GM8.1) is of the form (GM8.3)

$$[MCP]_{NOW}\{\Phi\}_{NEW} = \{F\}_{NOW} - [KM]_{NOW}\{\Phi\}_{NOW} - [MC]_{NOW}\{\Phi\}_{OLD}.$$

⊙ Flow chart for finite-difference on time GM-9
(Ref.: Bathe, p. 311).

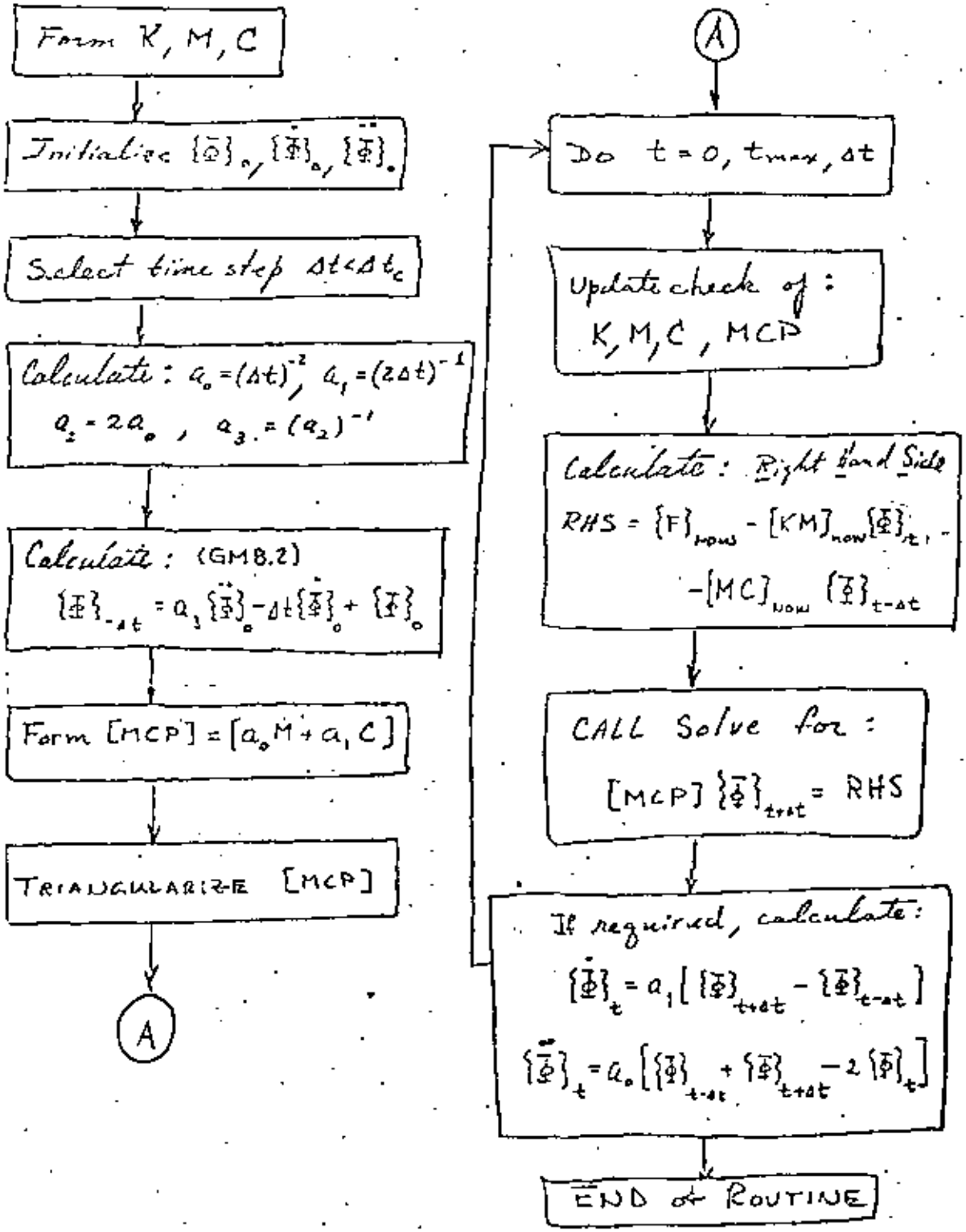

GM-10

○ Comments on integration over time.

• The explicit procedure developed is only conditionally stable; that is $\Delta t \leq \Delta t_{critical}$ for bounded error. Since $\Delta t_{critical}$ is mass dependent, this should only effect acceleration problems. (The stability of a system is not to be confused with accuracy. Stability infers clear deviation from physical reason marked by wild oscillations or exponential growth in error [blow-up]. Whereas accuracy may not be very good even when a procedure is stable, it may often be improved upon. Accuracy may also be difficult to detect.)

• The critical time step may be estimated as

$$\Delta t_{critical} \sim \left(\frac{\text{Natural Period}}{\pi}\right)_m \sim [\pi \cdot \text{Natural Frequency}]_m^{-1}$$

where subscript m refers to that element in the system which yields the smallest $\Delta t_{critical}$.

• Stable integration procedures may be developed by employing implicit schemes (versus explicit above). These frequently involve iterating a residual error to zero, e.g., the Newton-Raphson method.

• References

(i) Texts: Bathe & Wilson, Segerlind, Zienkiewicz.

(ii) W.L. Wood, IJNME, 11, 1519-1528, 1977.
12, 1717-1726, 1978.

EARTHQUAKE ENGINEERING AND STRUCTURAL DYNAMICS, VOL. 5, 413–418 (1977)

SHORT COMMUNICATION

A NEW LOOK AT THE NEWMARK, HOUBOLT AND OTHER TIME STEPPING FORMULAS. A WEIGHTED RESIDUAL APPROACH

O. C. ZIENKIEWICZ*

Department of Civil Engineering, University College of Swansea, University of Wales, Swansea, U.K.

SUMMARY

The Newmark time stepping algorithm which was introduced in 1959, using constants γ and β which average the integration process, can be rederived as the most general finite element-weighted residual algorithm involving three consecutive sets of displacements. This derivation is much simpler than that involved originally in the Newmark presentation, and indicates a very wide range of possibilities of approximation. The application of the process to four point (cubic) algorithms leads to another family of formulas of which the Houbolt algorithm is a particular case.

The use of the generalized expressions in the context of first-order equations is indicated and shows how some new, as well as some of the old, formulas can be developed.

INTRODUCTION

The classical problem of deriving a recurrence formula for the differential equation

$$\mathbf{M}\ddot{\mathbf{x}}+\mathbf{C}\dot{\mathbf{x}}+\mathbf{K}\mathbf{x}+\mathbf{f}=\mathbf{0} \tag{1}$$

has been subject to much investigation. In 1959, Newmark developed his well-known algorithm[1] by considering the change of velocity and displacement between two time stations n (at t) and $n+1$ (at $t+\Delta t$).

Noting that the Taylor expansion of velocity is

$$\dot{\mathbf{x}}_{n+1}=\dot{\mathbf{x}}_n+\ddot{\mathbf{x}}_n\Delta t+\dddot{\mathbf{x}}\Delta t^2/2+\dots \tag{2}$$

we can write for sufficiently smooth functions

$$\dot{\mathbf{x}}_{n+1}=\dot{\mathbf{x}}_n+\hat{\ddot{\mathbf{x}}}\Delta t \tag{3}$$

where $\hat{\ddot{\mathbf{x}}}$ represents some value of $\ddot{\mathbf{x}}$ intermediate to $\ddot{\mathbf{x}}_n$ and $\ddot{\mathbf{x}}_{n+1}$. Thus, we can write

$$\dot{\mathbf{x}}_{n+1}=\dot{\mathbf{x}}_n+(1-\gamma)\ddot{\mathbf{x}}_n\Delta t+\gamma\ddot{\mathbf{x}}_{n+1}\Delta t \tag{4}$$

where γ is a constant ($0\leqslant\gamma\leqslant 1$).

Similarly, expanding the displacements and truncating the series we can write

$$\mathbf{x}_{n+1}=\mathbf{x}_n+\dot{\mathbf{x}}_n\Delta t+(1-2\beta)\ddot{\mathbf{x}}_n\Delta t^2/2+2\beta\ddot{\mathbf{x}}_{n+1}\Delta t^2/2 \tag{5}$$

where β is again arbitrary ($0\leqslant 2\beta\leqslant 1$).

Writing equation (1) for $n+1$ we have

$$\mathbf{M}\ddot{\mathbf{x}}_{n+1}+\mathbf{C}\dot{\mathbf{x}}_{n+1}+\mathbf{K}\mathbf{x}_{n+1}+\mathbf{f}_{n+1}=\mathbf{0} \tag{6}$$

and assuming $\mathbf{x}_n$, $\dot{\mathbf{x}}_n$ and $\ddot{\mathbf{x}}_n$ are known the three equations (4)–(6) allow $\mathbf{x}_{n+1}$, $\dot{\mathbf{x}}_{n+1}$ and $\ddot{\mathbf{x}}_{n+1}$ to be determined.

If the integration process is applied to the time step $n-1$, n we have two additional relations of the form of (4) and (5). In addition, if the governing equation (1) is written at times n and $n-1$, we have a total of seven equations from which the six velocities and accelerations can be eliminated, leaving a general recurrence relation between three successive values of displacement ($\mathbf{x}_{n-1}$, $\mathbf{x}_n$ and $\mathbf{x}_{n+1}$). This general expression has

* Professor.

Received 21 July 1976

GM·11

▷ Time problem without acceleration or mass

Nullify mass in (GM 8.1) ⇒

$$\frac{1}{2\Delta t} C \Phi_{t+\Delta t} = F_t - K \Phi_t + \frac{1}{2\Delta t} C \Phi_{t-\Delta t} . \qquad (GM\,11.1)$$

Equations (GM 7.3) ⇒

i/ $\left.\frac{\partial^2 \Phi}{\partial t^2}\right|_t = 0 = \Phi_{t+\Delta t} + \Phi_{t-\Delta t} - 2\Phi_t$ @ any t.

or

$$\Phi_0 = \frac{1}{2}\left[\Phi_{t+\Delta t} + \Phi_{t-\Delta t}\right], \qquad (GM\,11.2)$$

ii/ $$\left.\frac{\partial \Phi}{\partial t}\right|_t = \frac{1}{2\Delta t}\left[\Phi_{t+\Delta t} - \Phi_{t-\Delta t}\right] . \qquad (GM\,11.3)$$

Without mass, Eq. (GM 11.1) is a discrete model of a first order differential equation in time. Therefore we need only <u>one</u> initial condition which is merely the value of the field quantity at time zero Φ_0. In addition (GM 11.2) provides the starting value

$$\Phi_{-\Delta t} = 2\Phi_0 - \Phi_{\Delta t} . \qquad (GM\,11.4)$$

Thus (GM 11.1) serves all iterations over $t > 0$, but requires modification for the initial

GM-12

start, that is at $t = 0$, (GM 11.4 in 11.1) $\Rightarrow$

$$\frac{1}{2\Delta t} C \ddot{x}_{\Delta t} = F_0 - K x_0 - \frac{1}{2\Delta t}(2x_0 - x_{\Delta t})$$

$\Rightarrow$

$$\frac{1}{\Delta t} C \dot{x}_{\Delta t} = F_0 + \left(\frac{1}{\Delta t} C - K\right) x_0 . \qquad \text{(GM 12.1)}$$

Let $H = \Delta t$ and the algorithm is:

$$\frac{1}{H} C \dot{x}_1 = F_0 + \left[\frac{1}{H} C - K\right] x_0 \quad @ \text{ time } 0,$$

$$\frac{1}{2H} C \ddot{x}_{i+1} = F_i - K x_i + \frac{1}{2H} C x_{i-1} \quad @ \text{ time } i, \qquad \text{(GM 12.2)}$$

where $i = 1, 2, 3, \ldots$

This is fine, but note Eq. (GM 11.2). We see that when acceleration is zero, the intermediate time step t may be eliminated from the algorithm and we may reformulate it using what we might term a 'double time step'. (See assignment problem 11.1.) Thus (GM 11.1) becomes

$$\frac{1}{2\Delta t} C \ddot{x}_{t+\Delta t} = F_t - K * \frac{1}{2}\left(x_{t+\Delta t} + x_{t-\Delta t}\right) + \frac{1}{2\Delta t} C x_{t-\Delta t} . \qquad \text{(GM 12.3)}$$

Combining like terms ⟹

$$\frac{1}{2}\left[K + \frac{1}{\Delta t}C\right]\Phi_{t+\Delta t} = F_t + \frac{1}{2}\left[\frac{1}{\Delta t}C - K\right]\Phi_{t-\Delta t}. \qquad (GM\,13.1)$$

From the figure we see that elimination of the intermediate point t permits $\Delta t \rightarrow \Delta t^*/2$ so that

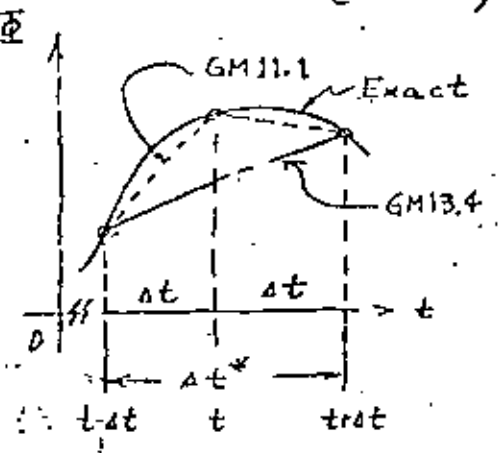

$$\left[K + \frac{2}{\Delta t^*}C\right]\Phi_{t+\Delta t^*/2}$$

$$= 2F_t + \left[\frac{2}{\Delta t^*}C - K\right]\Phi_{t-\Delta t^*/2}. \qquad (GM\,13.2)$$

But it is clear that t is at the midpoint of the Δt^* interval. Thus at t_i,

$$F_t = \frac{1}{2}\left[F_{t+\Delta t} + F_{t-\Delta t}\right] \equiv F_t^{AV} \qquad (GM\,13.3)$$

and we have

$$\left[K + \frac{2}{\Delta t^*}C\right]\Phi^{AV}_{t+\Delta t^*/2} = 2F_t^{AV} + \left[\frac{2}{\Delta t^*}C - K\right]\Phi^{AV}_{t-\Delta t^*/2}$$

where the 'AV' refers to the relation (GM13.3). (GM 13.4)

Note that t never equals zero because we insist that zero time start at left-most end of the interval Δt^*. Thus at time zero $t = \Delta t$ and

if we set index i to correspond to the left most end of any interval, then

$$i \equiv t - \Delta t^*/2 \quad \text{and} \quad i+1 \equiv t + \Delta t^*/2$$

so that (GM 13.4) becomes (GM14.1)

$$\left[K + \frac{2}{\Delta t^*} C\right] \Phi_{i+1} = 2F^{AV} + \left[\frac{2}{\Delta t^*} C - K\right] \Phi_i$$

where (GM14.2)

$$F^{AV} = \frac{1}{2}\left[F_{i+1} + F_i\right] \quad (GM14.3)$$

Eq'ns (GM14.2 and 3) serve as the operational algorithm and no special initial starting procedure is required as it was in (GM12.2).

⊙ Comments on integration of 1st order rate problems

- The explicit procedure given by (GM14.2) may not converge for large time steps. For example, in the case of a heat transfer

problem, the time step must satisfy

$$\Delta t^* \leq \frac{(\Delta x)^2}{\alpha}\left[2 + \bar{h}\frac{(\Delta x)}{k}\right]^{-1}, \quad \alpha = k/\rho c. \quad \text{(GM15.1)}$$

Otherwise physically impossible solutions will result. For further details, see:

1. Smith, G.D. "Numerical Solution of Partial Differential Equations", Oxford, London, 1965.

2. Adams, J. Alan and Rogers, David F., Computer-aided Heat Transfer Analysis, McGraw-Hill Book Co., 1973.

- The problem of a critical time step may be circumvented by employing a fully or partially implicit integration scheme, e.g., the Crank-Nicolson method. See:

3. Dahlquist, Germund, Björck, Åke. and Anderson, Ned (trans.), "Numerical Methods", Prentice-Hall, Inc., 1974.

Time Integration Schemes in Heat Conduction.
Salamon/Chen 1980

Results Analysis and Discussion ..

There are 2 cases studied in this report. numerical solutions by Euler method, Crank-Nicolson method and pure implicit method and Graphs are presented in the following pages. The two cases are,

1. the example problem in prob. 104. Segerlind, the governing differential equation and boundary condition and Initial condition are given in Pg. 7 of this report.
2. the example problem in Sec 9.4 Meyer, the governing equation and conditions are given in Pg. 10.

a) : P value changing from 0.1 to 10, the results for pure implict and crank nicolson methods are always stable, however the solution of .. Euler method turns out to be unstable as $P > 0.16$ ($P = 0.16$ stable, $P = 0.17$, unstable for both two cases), the oscillatory limits for the finite element method are more severe than for the finite-difference method. An oscillation in the calculated values usually occurs in the numerical values even though the method itself is stable.

b) Since $\Delta t = \frac{\rho (\Delta x)^2}{K/\rho c}$, the only variables that are adjustable are the element size, Δx, and the time step, the reduction of element size and ρ will reduce the time step that the solution will approach to the exact solution and the time of computation is increasing. Convergence is achieved through increasing discretization, but leads to increasing computer cost.

There is a steady state solution in Pg. 14.6, Segerlind and as time increases the solution of each time step is approaching to a constant value that means the steady state is reached. In the following a comparision with the available datas in segerlind is made. T_1 T_2 T_3 T_4 T_5 T_6 ($\rho=1$)

5 elements	150,	88.84,	61.74,	49.82,	44.76,	43.0
* exact solution in segerlind	150,	89.9,	62.8,	50.6,	45.2,	43.3
Crank-Nicolson 5 elements	150,	88.836,	61.745,	49.824,	44.757,	43.008
Crank-Nicolson 20 elements	150,	89.871,	62.682,	50.475,	45.186,	43.321
pure implicit 5 elements	150,	88.831,	61.744,	49.823,	44.756,	43.007
pure implicit 20 elements	150,	89.863,	62.668,	50.456,	45.166,	43.304

exact

From the above datas, reducing the element size, the numerical solution will approach to exact solution and

the solution of Crank-Nicolson is a little better than the pure implicit. Fig 4 is the solution of prob. 104 scanned and solved by crank-Nicolson method with elements = 20 and 5 at p=1

c) When the boundary of this thin rod is insulated no convective heat loss from the boundary, then case 1, problem in pg 24 becomes case 2, the difference is only let h=0, substitute the boundary conditions in pg. 10, Solutions of case 2 are presented in Fig 5 by crank-Nicolson method and Fig. 6 by pure implicit method with p=1

time = 0.25

	T_1	T_2	T_3	T_4	T_5
Crank-Nicolson elements = 4	0.0	.2772	.5394	.6871	.7471
Crank-Nicolson elements = 20	0.0	.2653	.4886	.6363	.6876
Pure implicit elements = 4	0.0	.2866	.5179	.6624	.7108
pure implicit elements = 20	0.0	.2652	.4882	.6354	.6866

In here for elements = 20, the solutions ≒ exact sol

time = 0.50

	T_1	T_2	T_3	T_4	T_5
Crank-Nicol, E=4	0.0	.1522	.2841	.3681	.4012
Crank-Nicol, E=20	0.0	.14231	.2629	.3436	.3719
pure-impli., E=4	0.0	.15477	.2857	.3750	.4035
Pure-impli., E=20	0.0	.1424	.2632	.3438	.3722

time = 0.75	T_1	T_2	T_3	T_4	T_5
Crank-Nicol. E=4	0.0	.0817	.1514	.1972	.2102
Crank-Nicol. E=20	0.0	.0768	.1419	.1853	.2006
pure impli. E=4	0.0	.0865	.1600	.2088	.2260
pure impli. E=20	0.0	.0780	.1440	.1882	.2037

as elements = 4, It is clear the solution of Crank-Nicholson is better than the pure implicit. From the above datas and Fig 5, 6, reducing the element size, both of pure implicit and Crank-Nicolson solutions will approach to exact solution. Observation of the output solution of the three numerical methods will show oscillations occur at smaller value of ρ. for $\rho = 0.1$.

Euler method for $\rho = 0.1$

```
TIME STEP=      .100
T=   .00025000     .00000    1.00136     .99999    1.00000    1.00000
T=   .00050000     .00000     .99421    1.00002    1.00000    1.00000
T=   .00075000     .00000    1.00568     .99994    1.00000    1.00000
T=   .00100000     .00000    1.00221    1.00011    1.00000    1.00000
T=   .00125000     .00000     .99925     .99994    1.00000    1.00000
T=   .00150000     .00000     .99767     .99996    1.00000    1.00000
T=   .00175000     .00000     .99746    1.00001    1.00000    1.00000
T=   .00200000     .00000     .99814    1.00002    1.00000    1.00000
T=   .00225000     .00000     .99927    1.00002    1.00000    1.00000
```

Since the oscillation is very small, it is not noticable from Fig. 4, 5, 6. in the above figures ρ is equal to 1.

4) The Euler method is workable only for $\rho \leq .16$, otherwise solution will blow up. Since ρ smaller, Δt is smaller too, it will increase the cost of computation for a tiny time step, so avoid this method.

VI) Figures

P = 1, Crank Nicolson

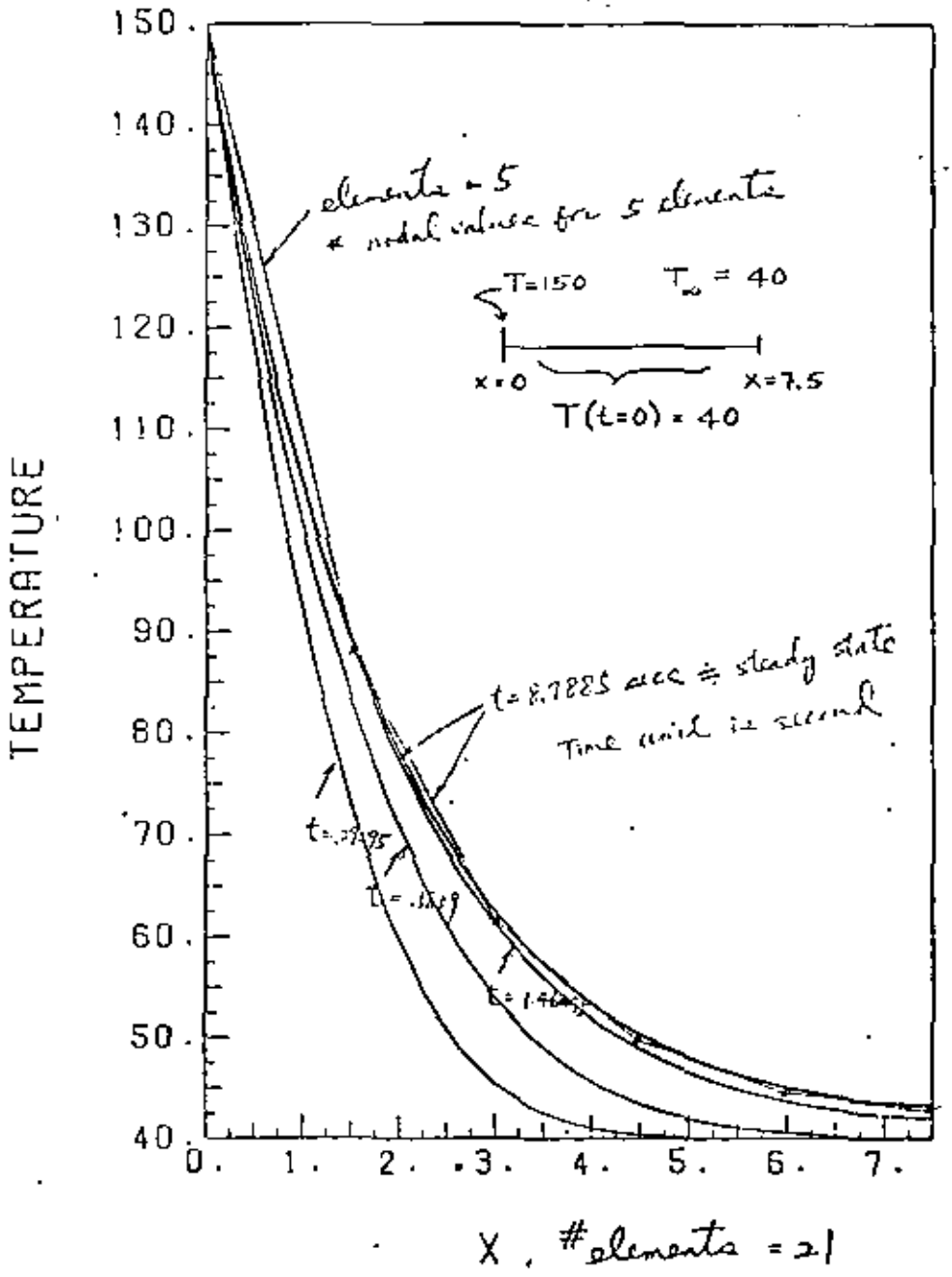

Fig 4. Crank Nicolson finite element solution for Prob. 104 Seely Smith.

P = 1 Crank Nicolson

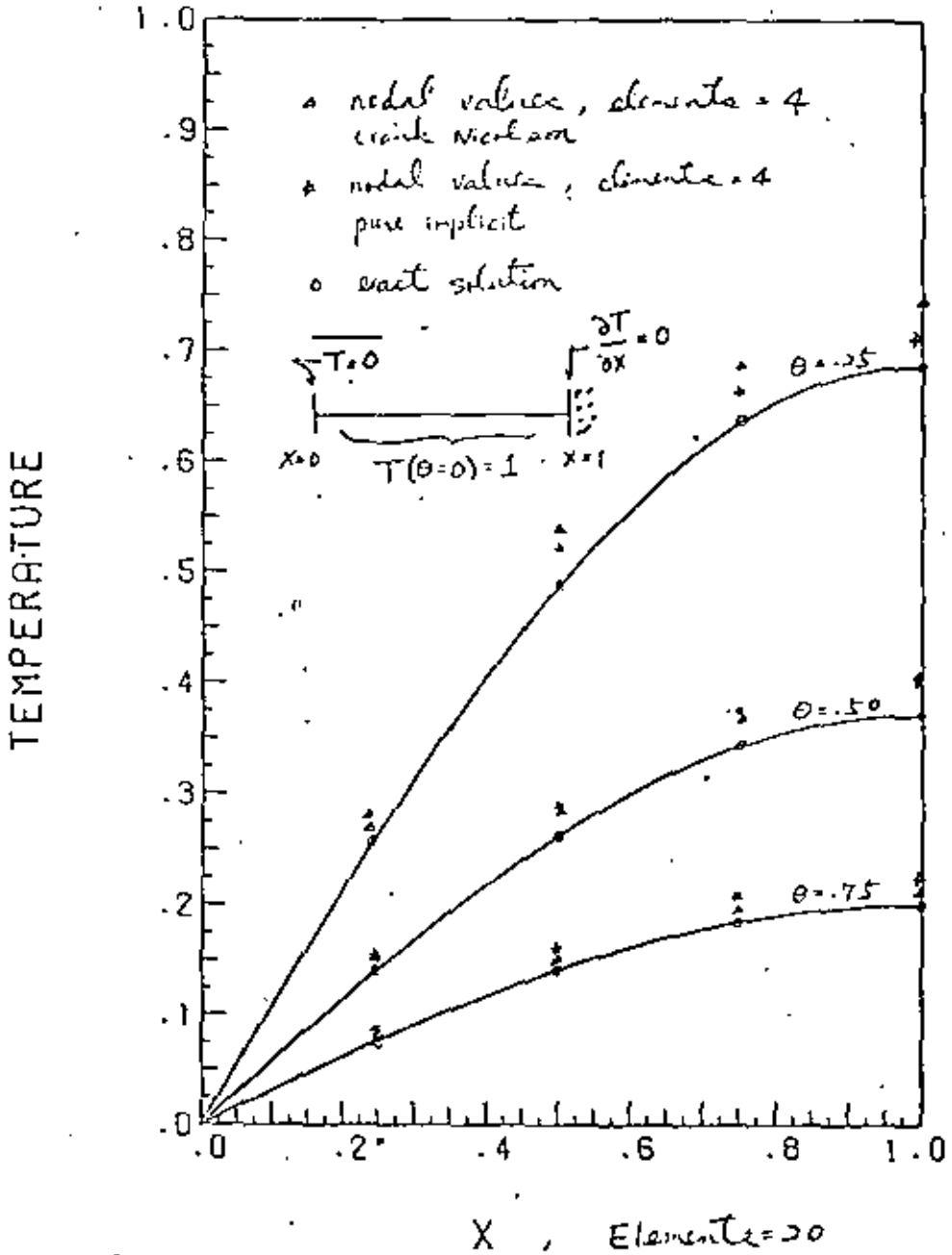

Fig 5. Crank Nicolson element solution for Prob. Sec. 9.4 Meyer.

Elasto-Dynamics

Ref: (i) Cook
(ii) Zienkiewicz
(iii) Bathe & Wilson

▷ Energy formulation

⊙ Kinetic energy, v = velocity.

$$T = \frac{1}{2} m v^2 \Rightarrow T_e = \int_{V_e} \{\dot{f}\}^T \frac{\rho}{2} \{\dot{f}\}\, dV \qquad \text{(ED-1a)}$$

where

$$\{f\} \overset{\text{EF-1a}}{=} [N]\{D\} \; ; \; \{d\} \text{ expanded} \qquad \text{(ED-1b)}$$

and

$$\{\dot{f}\} = \frac{\partial}{\partial t}\{f\} = [N]\frac{\partial}{\partial t}\{D\} = [N]\{\dot{D}\} \qquad \text{(ED-1c)}$$

$\therefore$

$$T_e = \int_{V_e} \{\dot{D}\}^T [N]^T \frac{\rho}{2} [N] \{\dot{D}\}\, dV$$

$$= \frac{1}{2}\{\dot{D}\}^T \underbrace{\int_{V_e} [N]^T \rho\, [N]\, dV}_{[m]_e \text{ see (GM5.4)}} \{\dot{D}\} \qquad \text{(ED-1d)}$$

$$= \frac{1}{2}\{\dot{D}\}^T [m]_e \{\dot{D}\}$$

Upon assembly

$$T = \sum_{e=1}^{M} T_e = \frac{1}{2}\{\dot{D}\}^T \overbrace{\left(\sum_{e=1}^{M} [m]_e\right)}^{[M]} \{\dot{D}\} \qquad \text{(ED-1e)}$$

$\Rightarrow$

$$T = \frac{1}{2}\{\dot{D}\}^T [M] \{\dot{D}\} \qquad \text{(ED-1f)}$$

⊙ Dissipation forces (damping)

. Think of lost energy which only occurs during energy transfer (say from kinetic to potential, i.e., 1) heat loss 2) viscous flow resistance). Let this energy, F, be velocity dependant, but a fctn. of a hypothetical constant, μ, which is velocity *in*dependant. Then

$$F_e = -\frac{1}{2}\{\dot{D}\}^T \underbrace{\int_{V_e} [N]^T \mu [N]\, dV}_{[C]_e \text{ as (GM5.4)}} \{D\} \qquad \text{(ED-2a)}$$

$F \sim -\frac{1}{2}\mu v^2$ viscous damping

or

$$F_e = -\frac{1}{2}\{\dot{D}\}^T [C]_e \{D\} \qquad \text{(ED-2b)}$$

$\Rightarrow$

$$F = \sum_{e=1}^{M} F_e = -\frac{1}{2}\{\dot{D}\}^T [C] \{D\}$$

Note: Damping is difficult, if not impossible to quantify. See Bathe & Wilson, § 8.3.3.

ED-3

⊙ Potential Energy (π)

Substitution of (EF-4) into (EF-3b) $\Rightarrow$

$$\pi = \{D\}^T \left[\tfrac{1}{2} [K] \{D\} - \{R\} \right] \qquad \text{(ED-3a)}$$

⊙ The Lagrangian (L)

$$L = T - \pi \; ; \text{ net system energy} \qquad \text{(ED-3b)}$$

Note

$$L = \begin{matrix} \text{Net} \\ \text{Energy} \end{matrix} \Rightarrow \begin{cases} = 0 \rightarrow T = \pi \text{ (conservative)} \\ \neq 0 \Rightarrow \text{Dissipation} \end{cases}$$

$$L = \tfrac{1}{2} \{\dot{D}\}^T [M] \{\dot{D}\} - \{D\}^T \left[\tfrac{1}{2} [K] \{D\} - \{R\} \right]$$

The Lagrangian principle states (ED-3c)

$$\frac{\partial}{\partial t} \left\{ \frac{\partial L}{\partial \dot{D}} \right\} - \left\{ \frac{\partial L}{\partial D} \right\} = \left\{ \frac{\partial F}{\partial \dot{D}} \right\} \qquad \text{(ED-3d)}$$

$\Rightarrow$

$$\frac{\partial}{\partial t} \left\{ [M] \{\dot{D}\} \right\} + [K] \{D\} - \{R\} = -[C] \{\dot{D}\}$$

$\therefore$

$$\underbrace{[M] \{\ddot{D}\}}_{\text{Inertial}} + \underbrace{[C] \{\dot{D}\}}_{\text{Damping}} + \underbrace{[K] \{D\}}_{\text{Stiffness}} = \overbrace{\{R\}}^{\text{Loading}} \qquad \text{(ED-3e)}$$

Forces:

(see (GM6.2))

▷ Response to periodic input ED-4

Take the periodic input to be (force):

$$\{R\} = \{A\}\cos\omega t + \{B\}\sin\omega t \qquad \text{(ED-4a)}$$

where $\{A\}$ or/and $\{B\}$ may be null* and the output, displacement, to be

$$\{D\} = \{a\}\cos\omega t + \{b\}\sin\omega t \qquad \text{(ED-4b)}$$

$\Rightarrow$

$$\{\dot{D}\} = -\omega\{a\}\sin\omega t + \omega\{b\}\cos\omega t,$$

$$\{\ddot{D}\} = -\omega^2\{a\}\cos\omega t - \omega^2\{b\}\sin\omega t.$$

Substitution into (ED-3e) $\Rightarrow$

$$\left[\left[-\omega^2[M]\{a\} + \omega[C]\{b\} + [K]\{a\}\right]\cos\omega t + \left[-\omega^2[M]\{b\} - \omega[C]\{a\} + [K]\{b\}\right]\sin\omega t\right] \qquad \text{(ED-4c)}$$

$$= \{A\}\cos\omega t + \{B\}\sin\omega t$$

or equating the harmonic terms, $\Rightarrow$

$$\begin{aligned} ([K]-\omega^2[M])\{a\} + \omega[C]\{b\} &= \{A\} \\ -\omega[C]\{a\} + ([K]-\omega^2[M])\{b\} &= \{B\} \end{aligned} \qquad \text{(ED-4d)}$$

---

* If both $\{A\}$ & $\{B\}$ are null, $\Rightarrow$ transient sol'n.

$\Rightarrow$ ED-5

$$\begin{bmatrix} [K]-\omega^2[M] & +\omega[C] \\ -\omega[C] & [K]-\omega^2[M] \end{bmatrix} \begin{Bmatrix} \{a\} \\ \{b\} \end{Bmatrix} = \begin{Bmatrix} A \\ B \end{Bmatrix} \quad \text{(ED-5a)}$$

Note: The above system is not positive-definite. (Zienk.)

▷ Free Vibrations, $[C] = [0]$

From (ED-5a):

$$\{[K]-\omega^2[M]\}\{D_0\} = \{0\} \quad \text{(ED-5b)}$$

which is a "linear" eigenvalue problem ($K, M \neq f(\omega)$)

where $\{D_0\}$ replaces $\{a\}$ or $\{b\}$ in (ED-4b), i.e.,

$$\{D\} = \{D_0\}\sin\omega t \text{ or } \{D_0\}\cos\omega t \quad \text{(ED-5c)}$$

For a nontrivial sol'n,

$$\left| [K]_{n\times n} - \omega^2 [M]_{n\times n} \right| = 0, \quad n = \text{Global D.O.F} \quad \text{(ED-5d)}$$

The sol'n $\Rightarrow$ n (*) real roots ω_i^2, $i = 1, n$.

which constitute the natural frequency spectrum.

Each $\omega_i \Rightarrow$ one $\{D_0\} \equiv \{D_0^1\ D_0^2\ D_0^3 \cdots D_0^n\}$

which is the mode shape corresponding to that particular ω_i.

(*) If $[M]$ contains null '0' rows (if $[M]$ of lumped form), then $n = n - \#$ of 0 rows.

▷ Solution – The standard form ED-6

To permit use of standard eigen-solution packages*, we desire the standard form

$$[H]\{X\} = \lambda\{X\} \qquad \text{(ED-6a)}$$

where $[H]$ is a symmetric, positive definite matrix. To obtain this form, multiply (ED-5b) by $[K]^{-1}$ or $[M]^{-1}$ and factor either $[K]$ or $[M]$ into Cholesky lower triangular form. Procedure follows:

⊙ Factor $[K]$ using Cholesky

Eq. (ED-5b) $\Rightarrow$

$$[\underbrace{K^{-1}K}_{[I]} - \frac{1}{\lambda}K^{-1}M]\{D_o\} = \{0\}$$

$\Rightarrow$

$$\underbrace{[K]^{-1}[M]}_{\text{Not symmetric in general}}\{D_o\} = \lambda\{D_o\} \qquad \text{(ED-6b)}$$

∴ Use Cholesky lower triangularization $\Rightarrow$

$$[K] = [L][L]^T \Rightarrow [K]^{-1} = [L]^{T^{-1}}[L]^{-1} \qquad \text{(ED-6i)}$$

---

* Basically iterative routines commonly referred to as (Givens, Householder, QR, Jacobi or combinations) factorization.

ED-7

where

$[L] \Rightarrow$ 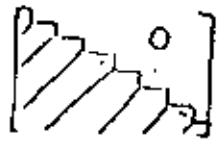

then

$$[L]^T * \left[[L]^{T^{-1}} [L]^{-1} [M] \{D_o\} = \lambda \{D_o\} \right]$$

$\Rightarrow$

$$[L]^{-1} [M] \{D_o\} = \lambda [L]^T \{D_o\}$$

Now let

$$\{X\} = [L]^T \{D_o\} \Leftrightarrow \{D_o\} = [L]^{T^{-1}} \{X\} \qquad \text{(ED-7c)}$$

Substitution $\Rightarrow$

$$\underline{[L]^{-1} [M] [L]^{-1}}^T \{X\} = \lambda \{X\}$$

$[H]$ ~ note symmetry since $[M]$ is sym.

$\therefore$

$$[H] = [L]^{-1} [M] [L]^{-1^T}, \quad \lambda = \frac{1}{\omega^2} \qquad \text{(ED-7b)}$$

Preferred form for lower natural frequencies since λ large $\Rightarrow$ more accuracy.
Results from eigen solution yield natural modes $\{D_o\}$ via eq. (ED-7c).

ED-8

⊙ Factor [M] using Cholesky

Eq. (ED-5b) ⟹

$$[\underbrace{M^{-1}K}_{} - \omega^2 \overbrace{\underbrace{M^{-1}M}_{[I]}}^{\lambda}][D_o] = \{0\} \qquad \text{(ED-8a)}$$

$[L]^{-1^T}[L]^{-1}$ where by Cholesky: $M = [L][L]^T$

⇒

$$[L]^T\left[[L]^{-1^T}[L]^{-1}[K]\{D_o\} = \lambda\{D_o\}\right] \qquad \text{(ED-8b)}$$

Let

$$\{X\} = [L]^T\{D_o\} \Leftrightarrow \{D_o\} = [L]^{T^{-1}}\{X\} \qquad \text{(ED-8c)}$$

Substitution ⟹

$$\underbrace{[L]^T[L]^{-1^T}}_{[I]}\underbrace{[L]^{-1}[K][L]^{-1^T}}_{[H]}\{X\} = \lambda\{X\}$$

and we have the standard form

$$[H]\{X\} = \lambda\{X\} \qquad \text{(ED-8d)}$$

where

$$[H] = [L]^{-1}[K][L]^{-1^T}, \quad \lambda = \omega^2$$

This form is preferred for higher mat. freq.

Mode shapes are recovered from (ED-8c).

ED-9

⊙ Conversion of lumped mass form

1) Let $[M]^{1/2} = \text{Diag}\left[\sqrt{M_{11}}\ \sqrt{M_{22}}\ \sqrt{M_{33}} \ldots \sqrt{M_{nn}}\right]$

$$\Rightarrow \quad [M]^{-1/2} = \text{Diag}\left[\frac{1}{\sqrt{M_{11}}}\ \frac{1}{\sqrt{M_{22}}}\ \frac{1}{\sqrt{M_{33}}} \cdots \frac{1}{\sqrt{M_{nn}}}\right] \tag{ED-9a}$$

where

$$[M] = [M]^{1/2}[M]^{1/2} \tag{ED-9b}$$

2) $[M]^{-1/2} * \text{Eq.}(\text{ED-5b}) \Rightarrow$

$$[M]^{-1/2}[K]\{D_0\} - \lambda [M]^{-1/2}\underbrace{[M]}_{[M]^{1/2}[M]^{1/2}}\{D_0\} = \{0\}$$

$$\underbrace{[M]^{-1/2}[M]^{1/2}}_{[I]}$$

$$\Rightarrow \quad [M]^{-1/2}[K]\{D_0\} = \lambda\,[M]^{1/2}\{D_0\} \tag{ED-9c}$$

3) Let $\{X\} = [M]^{1/2}\{D_0\} \Leftrightarrow \{D_0\} = [M]^{-1/2}\{X\}$ (ED-9d)

4) $$\underbrace{[M]^{-1/2}[K]\,[M]^{-1/2}}_{[H]}\{X\} = \lambda\{X\}$$

and we have the standard form

$$[H]\{X\} = \lambda\{X\},\ [H] = [M]^{-1/2}[K][M]^{-1/2},\ \lambda = \omega^2 \tag{ED-9e}$$

Mode shapes follow from (ED-9d).
This form fails if any element $M_{ii} = 0$.

Example: Direct solution {Bathe, Ex. 10.6} ED-10

Let $[K] = \begin{bmatrix} 3 & -3 \\ -3 & 3 \end{bmatrix}$, $[M] = \begin{bmatrix} 2 & 1 \\ 1 & 2 \end{bmatrix}$, $\lambda = \omega^2$

Then (ED-5d) $\Rightarrow$

1) $\det \left| K - \lambda [M] \right| = \det \left| \begin{bmatrix} 3 & -3 \\ -3 & 3 \end{bmatrix} - \lambda \begin{bmatrix} 2 & 1 \\ 1 & 2 \end{bmatrix} \right|$

$= \det \begin{vmatrix} 3-2\lambda & -3-\lambda \\ -3-\lambda & 3-2\lambda \end{vmatrix}$. $\overbrace{(3-2\lambda)^2}^{9-12\lambda+4\lambda^2} - \overbrace{(3+\lambda)^2}^{-9-6\lambda-\lambda^2}$

$= 3\lambda^2 - 18\lambda$

Define the characteristic polynomial

$p(\lambda) = \det \left| [K] - \lambda [M] \right| \overset{\text{simple}}{=} 3\lambda^2 - 18\lambda$ (ED-10a)

$\Rightarrow$ $p(\lambda) = 0 = 3\lambda(\lambda - 6) \Rightarrow$ Roots $\begin{cases} \lambda_1 = 0 \\ \lambda_2 = 6 \end{cases}$

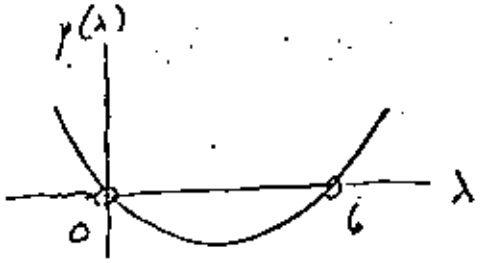

2) (i) for $\lambda_1 = 0$,

$$\begin{bmatrix} 3 & -3 \\ -3 & 3 \end{bmatrix} \begin{Bmatrix} D_0^{(1)} \\ D_0^{(1)} \end{Bmatrix} = \begin{Bmatrix} 0 \\ 0 \end{Bmatrix}$$

(ED-10b)

$\Rightarrow$ $3 D_0^{(1)} - 3 D_0^{(1)} = 0$ $\Rightarrow$ let $D_0^{(1)} = 1$

$-3 D_0^{(1)} + 3 D_0^{(1)} = 0$ then $D_0^{(1)} = 1$

Define the mass orthonormality condition for the i,j modes associated with ω_i and ω_j. ED-11

$$\{D_o\}_i^T [M] \{D_o\}_j = \delta_{ij} = \begin{cases} 1, & i=j \\ \epsilon \to 0, & i \neq j \end{cases} \quad \text{(ED-11a)}$$

$\Rightarrow$ mass normalize each vector:

$$\therefore \{D_o\}_1 = \frac{\begin{Bmatrix} 1 \\ 1 \end{Bmatrix}}{\left[\begin{Bmatrix} 1 & 1 \end{Bmatrix}\underbrace{\begin{bmatrix} 2 & 1 \\ 1 & 2 \end{bmatrix}\begin{Bmatrix} 1 \\ 1 \end{Bmatrix}}_{\begin{bmatrix} 3 \\ 3 \end{bmatrix}}\right]^{1/2}} = \frac{\begin{Bmatrix} 1 \\ 1 \end{Bmatrix}}{\sqrt{3+3}} = \begin{Bmatrix} 1/\sqrt{6} \\ 1/\sqrt{6} \end{Bmatrix}$$

Here we are merely scaling all components (of each vector) to $\Rightarrow$ consistency for comparisons.

(ii) $\lambda_2 = 6$, $\begin{bmatrix} -9 & -9 \\ -9 & -9 \end{bmatrix}\begin{Bmatrix} D_o^{(1)} \\ D_o^{(2)} \end{Bmatrix} = \begin{Bmatrix} 0 \\ 0 \end{Bmatrix}$ from $[K-\lambda M]\begin{Bmatrix} D_o^{(1)} \\ D_o^{(2)} \end{Bmatrix}_2 = \begin{Bmatrix} 0 \\ 0 \end{Bmatrix}$ (ED-11b)

$\Rightarrow -9 D_o^{(1)} - 9 D_o^{(2)} = 0 \quad \to \quad D_o^{(2)} = -D_o^{(1)} \stackrel{\text{say}}{=} -1$

$$\therefore \{D_o\}_2 = \frac{\begin{Bmatrix} 1 \\ -1 \end{Bmatrix}}{\left[\begin{Bmatrix} 1 & -1 \end{Bmatrix}\underbrace{\begin{bmatrix} 2 & 1 \\ 1 & 2 \end{bmatrix}\begin{Bmatrix} 1 \\ -1 \end{Bmatrix}}_{\begin{Bmatrix} 1 \\ -1 \end{Bmatrix}}\right]^{1/2}} = \frac{\begin{Bmatrix} 1 \\ -1 \end{Bmatrix}}{\sqrt{1+1}} = \begin{Bmatrix} 1/\sqrt{2} \\ -1/\sqrt{2} \end{Bmatrix}$$

(iii) Then the 1) $\lambda_1 = 0$. 2) $\lambda_2 = 6$

two modes: ① —— ② ① —— ②

$1/\sqrt{6}$ $1/\sqrt{6}$ $1/\sqrt{2}$ $1/\sqrt{2}$

Rigid Body Oscillation

ED-12

△ Eigenvalue shifting

- Application to free or partially free structures (i.e., aircraft, vehicles, etc) and iteration. solution
- Problem: Lack of complete B.C. ⇒ singular $[K]$.
- Solution: Use the following artifice to alter $[K]$. Add & subtract $\alpha[M]$ in (ED-5b) where α = const. ≥ 0 open to choice. Thus (ED-5b) becomes

$$\left\{ \underbrace{[K]+\alpha[M]}_{[K_s]} \underbrace{-\omega^2[M]-\alpha[M]}_{-(\omega^2+\alpha)[M]=-\omega_s^2[M]} \right\} \{D_o\} = \{0\}$$

⇒

$$\left\{ [K_s] - \omega_s^2 [M] \right\} \{D_o\} = \{0\} \quad \text{(ED-12a)}$$

and solve for ω_s in the usual manner. Then recover ω from

$$\omega^2 = \omega_s^2 - \alpha \quad \text{(ED-12b)}$$

For alternate approaches, see ref. in Cook. Also Bathe § 10.2.3.

▷ Solution – Iteration. ED-13

⊙ Shifting eigenvalues ω_i, $\lambda_s = \omega_s^2 = \omega^2 + \alpha$

i) Let λ be the eigenvalues for $[K]\{D_o\} = \lambda [M]\{D_o\}$ and λ_s be the shifted eigenvalues for $[K_s]\{D_s\} = \lambda_s [M]\{D_s\}$, then $\{D_s\} = \{D_o\}$ (ED-134) (ED-136)
where $[K_s] = [K] + \text{constant} \cdot [M]$
$\therefore \quad \lambda = \lambda_s \pm \text{constant}$. In other words, shifting the eigenvalues does not effect the eigenvectors.

2) The eigenvalues are roots of the characteristic polynomial $p(\lambda) = \det |[K] - \lambda [M]|$. (ED-136)

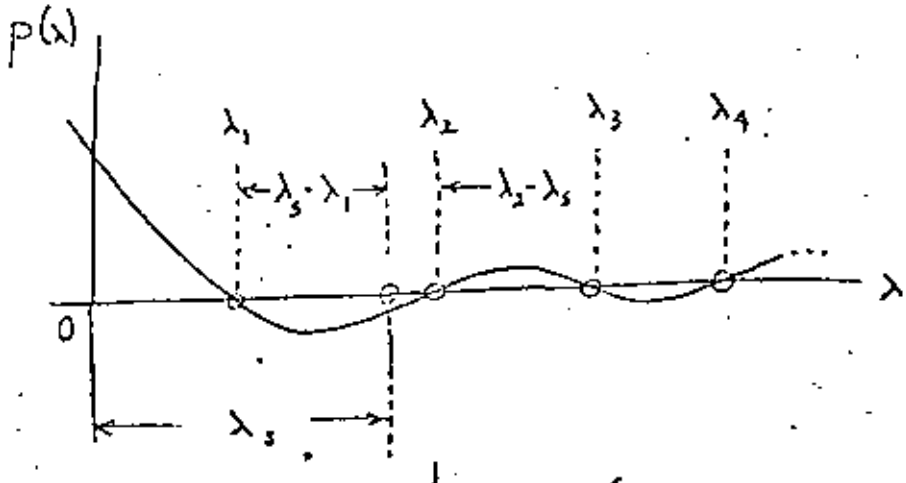

The shifted eigenvalue λ_s will always converge to the nearest eigenvalue λ, i.e., here $\lambda_s \to \lambda_2$ and $\{D_s\} \to \{D_o^{(2)}\}$, the 2nd mode shape.

3) The Rayleigh quotient

$\{D_o\}^T *$ (ED-56) $\Rightarrow$ $(\lambda = \omega^2)$

$$\{D_o\}^T [K] \{D_o\} - \lambda \{D_o\}^T [M] \{D_o\} = \{0\}$$

$\Rightarrow$

$$\lambda = \frac{\{D_o\}^T [K] \{D_o\}}{\{D_o\}^T [M] \{D_o\}} \qquad \text{(ED-14a)}$$

Thus we can determine the eigenvalues from estimates of the vectors $\{D_o\}$.

Note: From (ED-11a), the determinator will be normalized to 1.
∴ If $D_o = D_o + \epsilon$, the error in λ is of the order ϵ^2.

Example: Eigenvalue shifting, let $\alpha = +2$.

For the previous example (ED-10):

1) $$[K_s] = [K] + \alpha [M] = \begin{bmatrix} 3 & -3 \\ -3 & 3 \end{bmatrix} + 2 \begin{bmatrix} 2 & 1 \\ 1 & 2 \end{bmatrix} = \begin{bmatrix} 7 & -1 \\ -1 & 7 \end{bmatrix}$$

Eq. (ED-13a) $\Rightarrow$

$$\left\{ \begin{bmatrix} 7 & -1 \\ -1 & 7 \end{bmatrix} - \lambda_s \begin{bmatrix} 2 & 1 \\ 1 & 2 \end{bmatrix} \right\} \begin{Bmatrix} D_s^{(1)} \\ D_s^{(1)} \end{Bmatrix} = \begin{Bmatrix} 0 \\ 0 \end{Bmatrix} \qquad \text{(ED-14b)}$$

2) $$p(\lambda_s) = \det \begin{vmatrix} (7-2\lambda_s) & (-1-\lambda_s) \\ (-1-\lambda_s) & (7-2\lambda_s) \end{vmatrix} = \begin{matrix} 49 - 28\lambda_s + 4\lambda_s^2 \\ -1 - 2\lambda_s - \lambda_s^2 \end{matrix}$$

$$= 3\lambda_s^2 - 30\lambda_s + 48 \Rightarrow \lambda_s^{(1)} = 2, \quad \lambda_s^{(2)} = 8.$$

Eq. (ED-13b) $\overset{126}{\Rightarrow}$ $\lambda = \lambda_s - \alpha$

$\therefore$ $\lambda_1 = 0$, $\lambda_2 = 6$ as before.

3) From step 1) & 2) the eigenvectors are

i) $\lambda_s = 0$

$$\begin{bmatrix} 3 & -3 \\ -3 & 3 \end{bmatrix} \begin{Bmatrix} D_2^{(1)} \\ D_2^{(2)} \end{Bmatrix} = \begin{Bmatrix} 0 \\ 0 \end{Bmatrix}$$ same as (ED-10b).

NOTE: The shifted eigenequation (ED-14b) reduces to (ED-10b).

ii) $\lambda_s = 8$ The same thing happens for ii).

$$\begin{bmatrix} -9 & -9 \\ -9 & -9 \end{bmatrix} \begin{Bmatrix} D_0^{(1)} \\ D_0^{(2)} \end{Bmatrix} = \begin{Bmatrix} 0 \\ 0 \end{Bmatrix}$$ same as (ED-11b).

Thus the shift in eigenvalues allows recovery of desired eigenvalues and does not alter the mode shapes.

⊙ Reverse Matrix iteration for the 1st eigenvalue

In eq'ns. (ED-13a), do not shift λ.

But then $\Rightarrow$ $[K]\{A\} = \rho[M]\{A\}$

(ED-15a)

or $[K]\{A\} = [M]\{B\}$

and simply absorb ρ (unknown) in $\{B\}$.

ED-16

We desire $\{1\} \rightarrow \{D_1\}$ and if this is achieved, λ follows from Rayleigh's Quotient. With shift = 0, we anticipate the 1ST eigenvalue. Let $\{y\}$ be iterated upon. $\{x\}$ be the resulting eigenvector.

Algorithm: Assume $\{X\}_1$, ϵ.

START → (1) $\{y\}_1 = [M]\{x_1\}$

→ (2) Do (8) $k = 1$, IQUIT

Note [K] must be (+) definite!

(3) $\{X\}_{k+1} = [K]^{-1}\{y\}_k$

(4) $\{y\}_{k+1} = [M]\{x\}_{k+1}$

Rayleigh's Quotient

(5) $\rho_k = \dfrac{\{x\}_{k+1}^T \{y\}_k}{\{x\}_{k+1}^T \{y\}_{k+1}}$

Test convergence

(6) If $k > 1$, $CK = \dfrac{|\rho_{k+1} - \rho_k|}{\rho_{k+1}}$

(7) If $CK < \epsilon$, $K =$ IQUIT

Normalize $\{y\}$ (8) $\{y\}_{k+1} = \{y\}_{k+1} / \left[\{x\}_{k+1}^T \{y\}_{k+1}\right]^{1/2}$

Normalize $\{x\}$ (9) $\{x\}_{k+1} = \{x\}_{k+1} / \left[\{x\}_{k+1}^T \{y\}_{k+1}\right]^{1/2}$

Calculate λ (Note: $\{x\}^T[M]\{x\} = 1$ from (9).) (10) $\rho_k = \{x\}_{k+1}^T [K] \{x\}_{k+1}$

ED-17

Example: Iteration {Batlie Ex. 10.1}

1/ $[K] = \begin{bmatrix} 5 & -2 \\ -2 & 2 \end{bmatrix}$; $[M] = \begin{bmatrix} 5/4 & 0 \\ 0 & 1/5 \end{bmatrix} \cdot \begin{bmatrix} 1.25 & 0 \\ 0 & .2 \end{bmatrix}$

2/ Exact values

ⓐ $\{D_n\}_1 = \begin{Bmatrix} -\frac{4}{5} \\ 1 \end{Bmatrix} = \begin{Bmatrix} .800 \\ 1.000 \end{Bmatrix}$ for $\lambda_1 = 2$ } Exact Values Batlie Ex. 10.1

ⓑ $\{D_n\}_2 = \begin{Bmatrix} 2/5 \\ -2 \end{Bmatrix} = \begin{Bmatrix} .400 \\ -2.000 \end{Bmatrix}$ for $\lambda_2 = 12$ }

3/ $[K]^{-1} = \frac{1}{6 \cdot 10 - 4} \begin{bmatrix} 2 & 2 \\ 2 & 5 \end{bmatrix} = \begin{bmatrix} .333 & .333 \\ .333 & .833 \end{bmatrix}$

4/ Let ⓐ $x_1 = \begin{Bmatrix} 1 \\ 1 \end{Bmatrix} \Rightarrow \{y_1\} = [M]\{x_1\} = \begin{Bmatrix} 1.25 \\ .2 \end{Bmatrix}$

Item #1

ⓑ $\{x_2\} = [K]^{-1}\{y_1\} = \begin{Bmatrix} .499 \\ .583 \end{Bmatrix} \Rightarrow \{y\}_2 = [M]\{x_2\}$

$= \begin{Bmatrix} .624 \\ .117 \end{Bmatrix}$

ⓒ $\rho_1 = \frac{\{x_1\}^T\{y_1\}}{\{x_1\}^T\{y_2\}} = \frac{.720}{.360} = 2.00$

ⓓ $\{y_2\} = \frac{\{y_2\}}{\left[\{x_2\}^T\{y_2\}\right]^{1/2}} = \frac{1}{.360}\begin{Bmatrix} .624 \\ .117 \end{Bmatrix} = \begin{Bmatrix} 1.678 \\ 0.325 \end{Bmatrix}$

$\{x_3\} / \left[\{x_3\}^T \overline{[M]\{x_3\}}\right]^{1/2}$

ⓔ $\|\{x_3\}\|' = \frac{1}{.6}\{x_2\} = \begin{Bmatrix} .805 \\ .972 \end{Bmatrix}$

II-1 ex. #2 ↓ ED-18

(a) $\{X_3\} = [K]^{-1}\{Y_2\} \rightarrow \begin{Bmatrix} .668 \\ .830 \end{Bmatrix}$

(b) $\{Y_3\} = [M]\{X_3\} = \begin{Bmatrix} .835 \\ .166 \end{Bmatrix}$

(c) $\rho_2 = \dfrac{\{X_3\}^T\{Y_2\}}{\{X_3\}^T\{Y_3\}} = \dfrac{1.39}{.696} = 1.999$

(d) $\epsilon = \dfrac{|\lambda_2 - \lambda_1|}{\lambda_2} = \dfrac{|1.999 - 2.000|}{1.999} = .001 \rightarrow$ ok.

(e) $\|\{X_3\}\| = \dfrac{\{X_3\}}{\left[\{X_3\}^T \underbrace{[M]\{X_3\}}_{\{Y_3\}}\right]^{1/2}} = \dfrac{1}{.834}\{X_3\} = \begin{Bmatrix} .801 \\ .995 \end{Bmatrix} \equiv \{X_3\}$

5/ Determine λ_1 using Rayleigh Quotient.

$$\therefore \lambda \approx \rho_3 = \frac{\{X_3\}^T[K]\{X_3\}}{\{X_3\}^T[M]\{X_3\}} = \frac{\begin{Bmatrix} .801 \\ .995 \end{Bmatrix}^T \underbrace{\begin{bmatrix} 5 & -2 \\ -2 & 2 \end{bmatrix}\begin{Bmatrix} .801 \\ .995 \end{Bmatrix}}_{\begin{Bmatrix} 2.015 \\ .319 \end{Bmatrix}}}{\begin{Bmatrix} .801 \\ .995 \end{Bmatrix}^T \underbrace{\begin{bmatrix} 1.25 & 0 \\ 0 & .2 \end{bmatrix}\begin{Bmatrix} .801 \\ .995 \end{Bmatrix}}_{\begin{Bmatrix} 1.001 \\ .199 \end{Bmatrix}}}$$

$= 2.000075$

1.000 of course from (4e)

Note: if $\{D_2\} \rightarrow \{X\} + \underbrace{\epsilon}_{O(10^{-3})}$

$\{\lambda\} \rightarrow \{\rho\} + \underbrace{\epsilon^2}_{O(10^{-5})}$

IJNME, 14, #3, 459-463. (1979)

A PHYSICAL INTERPRETATION OF THE ARTIFICE USED IN FREQUENCY ANALYSIS OF UNSUPPORTED STRUCTURES

A. PRAMILA†

Department of General Sciences, Helsinki University of Technology, Finland

SUMMARY

A physical interpretation of the method—adding αM to the stiffness matrix—used in frequency analysis of unsupported structures is suggested. The proper choice of α is discussed and a relation between angular natural frequencies of structures with and without elastic support is given.

INTRODUCTION

The free vibration of an elastic structure when analysed by the finite element method (or other discrete methods) leads to the problem of determining the eigenvectors $\bar{a}$ and eigenvalues ω^2 of the system

$$\mathbf{K}\bar{a} = \omega^2\mathbf{M}\bar{a} \tag{1}$$

where K and M are the stiffness and mass matrices, respectively. For unsupported structures K is singular and does not possess an inverse, which is needed to obtain the special eigenvalue problem, for which standard solution algorithms exist. (See e.g. Reference 1, pages 349-350.)

The procedure usually used to enable solution is based on the artifice first suggested by Cox.[2] Equation (1) is simply modified to

$$(\mathbf{K} + \alpha\mathbf{M})\bar{a} = (\omega^2 + \alpha)\mathbf{M}\bar{a} \tag{2}$$

in which α is an arbitrary constant of the same order as the typical ω^2 sought. Matrix $\mathbf{K} + \alpha\mathbf{M}$ is not singular and thus the standard process can be used to find the eigenvalues $(\omega^2 + \alpha)$.

INTERPRETATION

Consider an elastic support of the type

$$\mathbf{f} = -k\mathbf{u} \tag{3}$$

added to the unsupported structure. Here f is the force per domain unit (volume unit in 3-dimensional problems, area unit in plate bending etc.), u is the displacement and if mass per domain unit, m, is function of position the 'spring constant' k is assumed to vary in such a way that the ratio k/m remains constant, say α.

† Research Assistant.

0029-5981/79/0314-0459$01.00

Received 17 April 1978
Revised 18 July 1978

(45)

On frequency shifting by elementary modifications of inertia and stiffness

B. Fraeijs de Veubeke

The problem of shifting eigenvalues presents both a practical interest to avoid resonance and theoretical interest as a computational tool in numerical analysis. In this last context, the general translation of the eigenvalue spectrum is widely used in iteration techniques. Shifting by elementary modifications of the inertia and stiffness matrices opens wider possibilities, especially in the presence of closely spaced eigenvalues or degeneracy. Orthogonal deflation turns out to be one of its particular applications.

1. ELEMENTARY MODIFICATIONS OF INERTIA AND STIFFNESS MATRICES

Consider the eigenvalue problem in n degrees of freedom

$$Kx = \omega^2 Mx \tag{1}$$

where x is the column of modal amplitudes, K and M square symmetric matrices of stiffness and inertia respectively.

By elementary inertia we understand any inertia attached to a given linear form in the generalized coordinates q_i

$$\sum_i^n h_i q_i = h'q$$

where h' denotes the transpose of the column matrix h of the coefficients of the form and q the column matrix of the generalized coordinates. Hence the kinetic energy attached to an elementary inertia μ is of the form

$$\tfrac{1}{2}\mu(h'\dot{q})^2 = \tfrac{1}{2}\dot{q}'(\mu hh')\dot{q}$$

and the addition of this to the already existing kinetic energy

$$\tfrac{1}{2}\dot{q}'M\dot{q}$$

is equivalent to the modification of the inertia matrix M into

$$M + \mu hh'$$

from: Contributions to the Theory of Aircraft Structures: presented to A. van der Neut by Friends, Colleagues and former Students, Delft University Press, 1972.

Similarly an additional potential energy

$$\tfrac{1}{2}\kappa(h'q)^2 = \tfrac{1}{2}q'(\kappa hh')q$$

of stiffness coefficient κ, modifies the stiffness matrix into

$$K + \kappa hh'.$$

The changes in design parameters, that produce such elementary modifications of inertia and stiffness, are easily traced on lumped mass models. They are quite difficult to assess on continuous structures, where the reduction to a finite number of degrees of freedom depends on the type of discretization employed. The integral equation method with point collocation is here to be favored, precisely because of its ability to produce a rational lumped mass approximation to the continuum [1].

2. SPECIAL CASES OF ALTERATIONS IN MODE SHAPES AND FREQUENCIES

The modified eigenvalue problem

$$(K + \kappa hh')y = \omega^2(M + \mu hh')y \tag{2}$$

presents some remarkably simple properties for special choices of the elementary modifications.

a. *Invariance of a modal shape and its associated eigenvalue*

If $x_{(m)}$ is a modal shape of problem (1) associated to the eigenvalue ω_m^2, it remains modal shape of problem (2) without eigenvalue alterations if the coefficients of the linear form are such that $h'x_{(m)} = 0$.

Trivial examples of this property are the addition of a lumped mass or of a spring anchorage, or both, at the level of a node of a flexural vibration mode.

b. *Deflation*

In particular if $h = Mx_{(r)}$, the orthogonality properties of mode shapes

$$x'_{(r)}Mx_{(m)} = 0 \qquad \text{for } r \neq m \tag{3}$$

make all eigensolutions of problem (1) eigensolutions of problem (2) except for one. The exception is $x_{(r)}$ itself that remains a modal shape but whose eigenvalue is shifted to

$$\bar{\omega}_r^2 = \frac{\omega_r^2 + \kappa x'_{(r)}x_{(r)}}{1 + \mu x'_{(r)}Mx_{(r)}}, \tag{4}$$

This property of shifting a single eigenvalue in the spectrum implies the knowledge of the associated modal shape. In iteration techniques it is used

to force convergence towards a modal shape other than the one $x_{(r)}$ that was just obtained. To this effect the inverse eigenvalue $\lambda_r = 1/\omega_r^2$ is usually shifted to zero by taking

$$\kappa = 0 \qquad \mu = -\frac{1}{x'_{(r)}Mx_{(r)}} \tag{5}$$

Thus the matrix K remains unchanged but M becomes

$$M - \frac{Mx_{(r)}x'_{(r)}M}{x'_{(r)}Mx_{(r)}} = MP_r = P_r'M \tag{6}$$

where $$P_r = I - \frac{x_{(r)}(Mx_{(r)})'}{x'_{(r)}Mx_{(r)}}$$

is an orthogonal projection matrix [2], that clearly does not depend on the undetermined scale of $x_{(r)}$ but only on its 'direction'. The direction of $x_{(r)}$ is that of the projection itself since

$$P_r x_{(r)} = 0;$$

moreover the operator projects in a subspace orthogonal to $x_{(r)}$ since for any vector a

$$x'_{(r)}MP_r a = 0 \qquad \text{i.e.} \qquad x'_{(r)}MP_r = 0.$$

This method of removing $x_{(r)}$ from an iterative convergence process is known as 'orthogonal deflation'.

c. *Elimination of zero frequency modes*

The original matrix K is frequently singular because the system possesses rigid body modes or mechanisms; we refer to both of them as kinematical modes. Let $u_{(i)}$ denote an orthogonalized set of such degrees of freedom, whence

$$Ku_{(i)} = 0 \qquad u'_{(i)}Mu_{(j)} = 0 \qquad i \neq j \tag{7}$$

and they can be considered as modal shapes associated to the zero eigenvalue. In this case the direct iteration procedure of Duncan and Collar [4]

$$K^{-1}Mx = \lambda x \tag{8}$$

fails because the static influence coefficients matrix K^{-1} does not exist. The difficulty can be overcome by a generalization of the notion of influence coefficients [1]. If, instead, we try the idea of eigenvalue shifting through (5), the procedure leads to an indeterminacy of the shifted eigenvalue (4) because in this case $\omega_i^2 = 0$. It is thus necessary to use a non zero κ value. In fact, if we modify the stiffness matrix as follows

$$R = K + \sum_i \frac{Mu_{(i)}(Mu_{(i)})'}{u'_{(i)}Mu_{(i)}} = K' \tag{9}$$

we have, by virtue of (7)

$$K u_{(j)} = M u_{(j)} \tag{10}$$

and for the modal shapes of non zero frequency, that are orthogonal to all the kinematical modes

$$u'_{(0)} M x_{(s)} = 0 \qquad K x_{(s)} = K x_{(s)} = \omega_s^2 M x_{(s)} \tag{11}$$

Because the $u_{(j)}$ and $x_{(s)}$ consitute a complete orthogonal base for the x vectors, and $Mu_{(j)}$ and $Mx_{(s)}$ are linearly independent, results (10) and (11) show that the new stiffness matrix is non singular and can thus be inverted. The modified iteration scheme

$$R^{-1} M x = \lambda x$$

has the same modal solutions as problem (1), the kinematical modes $u_{(j)}$ being associated to the inverse eigenvalue $\lambda = 1$ in view of (10) and the other modal shapes $x_{(s)}$ keeping their original inverse eigenvalues $\lambda_s = 1/\omega_s^2$ in view of (11). However, the kinematical modes, which are usually known by simple inspection or by solving directly (7), should still be shifted to $\lambda = 0$ in order to force convergence to the other modes. This can be achieved by a modification of M similar to (5)

$$\bar{M} = M - \sum_j \frac{M u_{(j)} [M u_{(j)}]'}{u'_{(j)} M u_{(j)}} \tag{12}$$

whereby $\bar{M} u_{(j)} = 0 \qquad \bar{M} x_{(s)} = M x_{(s)}$ (13)

Thus the low frequency spectrum of inverse eigenvalues associated to the $x_{(s)}$ can be determined from the modified iteration scheme

$$R^{-1} \bar{M} x = \lambda x \tag{14}$$

with successive orthogonal deflations.

An alternative is the modified iteration scheme

$$A R^{-1} M x = \lambda x \tag{15}$$

where A is an orthogonal projector [1]

$$A = I - \sum_j \frac{u_{(j)} u'_{(j)} M}{u'_{(j)} M u_{(j)}} \tag{16}$$

with the properties

$$A u_{(j)} = 0 \qquad A x_{(s)} = x_{(s)} \tag{17}$$

R^{-1} can then be recognized as a matrix of extended influence coefficients [1].

d. *Invariance under any elementary modification*

If we call

$$\theta = (\kappa/\mu)^{\frac{1}{2}} \tag{18}$$

the 'alteration (circular) frequency', any modal shape of problem (1) remains modal shape of problem (2) with the same eigenvalue ω^2, provided $\theta^2 = \omega^2$; this result is independent of the particular linear form involved in the elementary modification of the matrices. The proof is by direct verification.

3. ALTERATIONS OF MODES AND EIGENVALUES IN THE GENERAL CASE

The general solution of the modified problem (2) can be found by expansion of the eigenvectors y in the basis of the eigenvectors of problem (1).

We do not have to distinguish here the kinematical modes, if any, and use the general notation $x_{(r)}$ $(r = 1, 2, \ldots, n)$ for the eigenvectors of problem (1).

Setting $y = \sum_r \alpha_r x_{(r)}$, (19)

substituting into (2) and using (11) we find

$$\sum_r (\omega_r^2 - \omega^2) \alpha_r M x_{(r)} + \mu(\theta^2 - \omega^2)\Big(\sum_r \alpha_r \beta_r\Big) h = 0 \tag{20}$$

where $\beta_r = h' x_{(r)}$ (21)

If this is premultiplied by $x'_{(m)}$ and due account is taken of the orthogonality relations (3), there comes

$$\gamma(\omega_m^2 - \omega^2)\alpha_m + \mu(\theta^2 - \omega^2)\Big(\sum_r \alpha_r \beta_r\Big)\beta_m = 0 \quad (m = 1, 2, \ldots, n) \tag{22}$$

This set of linear and homogeneous equations in the unknown coefficients α_m poses an eigenvalue problem for ω^2 equivalent to (2); it contains the additional assumption that the eigenvectors of problem (1) are normed as follows

$$x'_{(m)} M x_{(m)} = \gamma > 0. \tag{23}$$

Equations (22) are linked to a rather remarkable form of frequency equation; written in the equivalent form

$$\frac{\alpha_m}{\mu(\theta^2 - \omega^2)} + \frac{\beta_m}{\gamma(\omega_m^2 - \omega^2)}\Big(\sum \alpha_r \beta_r\Big) = 0 \tag{24}$$

multiplied by their respective coefficient β_m and added, they yield after cancellation of the common factor $(\sum \alpha_r \beta_r)$

$$\phi(\omega^2) = \frac{1}{\mu(\theta^2 - \omega^2)} + \sum_r \frac{\beta_r^2}{\gamma(\omega_r^2 - \omega^2)} = 0. \tag{25}$$

For $\mu > 0$, $\kappa > 0$ and consequently θ real, ϕ is a monotonic increasing

function of its argument ω^2. It jumps from plus to minus infinity each time it overtakes an eigenvalue ω_i^2 of problem (1) (provided $\beta_{ii} \neq 0$) and also when it overtakes the value θ^2. Its zeros are the new eigenvalues. Consequently each original frequency is normally shifted towards the alteration frequency but keeps its rank in the frequency spectrum.

The exceptional cases, like the vanishing of a β_{ii} or the coalescence of the alteration frequency with some original frequency, were dealt with in section 2. If the modifications brought to M and K are small enough to be treated as perturbations, explicit forms can be given to the shifts in eigenvalues

$$\omega_i^2 = \frac{\gamma\omega_i^2 + \alpha\omega_i^4}{\gamma + \mu\beta_i^2} \tag{26}$$

and to the new modal shapes

$$y_{(i)} = x_{(i)} + \sum_{r \neq i} a_{ir} x_{(r)} \tag{27}$$

$$a_{ir} = -\frac{\mu(\theta^2 - \omega_i^2)\beta_i\beta_r}{\gamma(\omega_r^2 - \omega_i^2)} \tag{28}$$

4. DEGENERACY

For simplicity take first a case of simple degeneracy: two linearly independent mode shapes $x_{(i-1)}$ and $x_{(i-2)}$ belong to the same eigenvalue ω_i^2 in problem 1. There always exists some non trivial linear combination

$$a_{ir} = \varepsilon_1 x_{(i-1)} + \varepsilon_2 x_{(i-2)}$$

of the mode shapes, such that for an arbitrarily given h

$$h' a_{ir} = 0.$$

Indeed the linear homogeneous equation in ε_1 and ε_2

$$(h' x_{(i-1)})\varepsilon_1 + (h' x_{(i-2)})\varepsilon_2 = 0$$

has always at least one non trivial solution. But then, as shown in section 2.a, a_{ir} which is a modal shape of eigenvalue ω_i^2 of problem (1) remains an eigensolution of problem (2). The generalization is obvious, if problem (1) has an index of degeneracy p for some ω_i^2, $q < p$ elementary modifications of the matrices M and K with arbitrary coefficients, will leave at least $p - q$ eigensolutions invariant.

5. CLOSELY SPACED EIGENVALUES

For exact degeneracy the iteration procedure involves theoretically no difficulties. Convergence must occur to some modal shape of the linear

manifold belonging to the degenerate eigenvalue. Subsequent deflation will force convergence to an orthogonal mode shape of the same manifold and the procedure may in principle be repeated until this manifold has been completely spanned. In practice however, round-off errors will tend to replace degeneracy by close spacing of eigenvalues. It is also true that the problem of determining modes and frequencies of modern complex aerospace structures almost invariably leads to the existence of quasi-degeneracy. It may be suspected that in this case the use to which this frequency analysis is directed does not necessarily warrant a very accurate discrimination between closely spaced modal shapes. Nevertheless the problem is an irritating one because of the apparent slowness of convergence and lack of accuracy criteria.

We will restrict our analysis to the case of two closely spaced modal shapes a_1 and a_2 satisfying

$$Ma_1 = \lambda_1 Ka_1 \qquad Ma_2 = \lambda_2 Ka_2 \tag{29}$$

with small difference between the inverse eigenvalues λ_1 and λ_2.

After a sufficient number of iterations, assuming all modal shapes of higher λ to have been deflated, we can obtain an iterate x that is, with sufficient accuracy, a linear combination

$$x = a_1 a_1 + a_2 a_2 \tag{30}$$

of the unknown modal shapes. Without loss of generality it will also be assumed that we have the norms

$$a_1' M a_1 = 1 \qquad a_2' M a_2 = 1 \qquad x' M x = 1. \tag{31}$$

The next iterates will be

$$y = K^{-1} M x = a_1 \lambda_1 a_1 + a_2 \lambda_2 a_2 \tag{32}$$

$$z = K^{-1} M y = a_1 \lambda_1^2 a_1 + a_2 \lambda_2^2 a_2. \tag{33}$$

If the convergence process becomes very slow, we are certain that both a_1 and a_2 are different from zero. Then, setting up the Rayleigh quotient

$$\lambda = \frac{(z + \varepsilon y)' M (z + \varepsilon y)}{(z + \varepsilon y)' K (z + \varepsilon y)} = \frac{(z + \varepsilon y)' M (z + \varepsilon y)}{(z + \varepsilon y)' M (y + \varepsilon x)} \tag{34}$$

it is clear that its extremal values are respectively λ_1 and λ_2.

Indeed the extremizing condition turns out to be a second degree algebraic equation for ε, whose roots will furnish respectively a_1 and a_2 and the associated eigenvalues. Unfortunately, because (32) and (33) have not very different shapes from (30), this approach is known to be unstable by ill-conditioning. This is not too surprising as we would have practically determined two modal shapes through a single iteration sequence.

Let us turn to the possibilities offered by frequency shifting and modify

the mass matrix into

$$\hat{M} = M - \frac{Mxx'M}{x'Mx} \tag{35}$$

whereby our x becomes a modal shape associated to $\lambda = 0$. Since the mode shapes of lower inverse eigenvalues than λ_1 and λ_2 remain eigensolutions of the modified problem, a new iteration cycle will hopefully provide an iterate y, quite different from x, that is a new linear combination of the exact modes

$$y = \beta_1 a_1 + \beta_2 a_2. \tag{36}$$

To this effect we must show that the inverse eigenvalue associated to y remains higher than those of the next modes. In view of the results obtained in the analysis of degeneracy, it may indeed be suspected that in

$$\hat{M}y = \lambda K y \tag{37}$$

the value of λ will lie between λ_1 and λ_2. To prove this we observe that (31) is equivalent to

$$\alpha_1^2 + \alpha_2^2 = 1.$$

If furthermore we norm y

$$y'My = 1 \text{ is equivalent to } \beta_1^2 + \beta_2^2 = 1$$

and $x'My = \alpha_1\beta_1 + \alpha_2\beta_2$.

Consequently we can write

$$\alpha_1 = \cos\phi \quad \alpha_2 = \sin\phi \qquad \beta_1 = \cos\theta \quad \beta_2 = \sin\theta$$
$$x'My = \cos(\phi - \theta).$$

From (35) we find then

$$\hat{M}y = \sin\phi\sin(\phi-\theta)Ma_1 + \cos\phi\sin(\theta-\phi)Ma_2$$

and, in view of (29)

$$\hat{M}y = \sin(\phi-\theta)(\sin\phi\lambda_1 Ka_1 - \cos\phi\lambda_2 Ka_2).$$

Equation (37) is then split into

$$\lambda_1 \sin\phi\sin(\phi-\theta) = \lambda\cos\theta. \tag{38}$$
$$\lambda_2 \cos\phi\sin(\phi-\theta) = -\lambda\sin\theta. \tag{39}$$

Elimination of θ between those equations yields two solutions for λ. One is $\lambda = 0$, requiring $\theta = \phi$, and confirming the shifting of x to zero λ, the other is

$$\lambda = \lambda_1\sin^2\phi + \lambda_2\cos^2\phi \tag{40}$$

which lies, as was hoped, between λ_1 and λ_2.

Furthermore, eliminating λ between (38) and (39), the result

$$\lambda_1\sin\theta\sin\phi + \lambda_2\cos\theta\cos\phi = 0 \tag{41}$$

shows that

$$x'My = \cos(\phi-\theta) = \frac{\lambda_1-\lambda_2}{\lambda_1+\lambda_2}\cos(\phi+\theta) = \varepsilon \tag{42}$$

is small, being a measure of the relative gap between the eigenvalues; hence y is almost orthogonal to x. We find then that

$$\hat{M}y = My - \varepsilon Mx = \lambda Ky$$

from which the useful results

$$x'Ky = 0 \tag{43}$$
$$1 - \varepsilon^2 = \lambda y'Ky \tag{44}$$

We are now able to determine the modes a_1 and a_2 and their eigenvalues from the linear combinations $x + \gamma y$ that extremize the quotient

$$\frac{(x+\gamma y)'M(x+\gamma y)}{(x+\gamma y)'K(x+\gamma y)} = \frac{1+2\varepsilon\gamma+\gamma^2}{\frac{1}{\eta}+\gamma^2\frac{1-\varepsilon^2}{\lambda}} \tag{45}$$

where $$\eta = \frac{x'Mx}{x'Kx} = \frac{1}{x'Kx}. \tag{46}$$

The extremizing condition is found to be

$$\gamma^2 - \frac{\mu-1}{\varepsilon}\gamma - \mu = 0 \qquad \text{where} \qquad \mu = \frac{\lambda}{\eta(1-\varepsilon^2)} \tag{47}$$

The accuracy with which the roots of this equation can be determined still depends on the accuracy of the ratio of the two small numbers $\mu - 1$ and ε. This accuracy is however obtainable because of the near orthogonality of the mode shapes x and y. The same basic idea can obviously be applied to the case where several eigenvalues are nearly coincident.

REFERENCES

1. Fraeijs de Veubeke, B., Iteration in semi-definite eigenvalue problems, *Jl. of the Aer. Sci.*, 22, no. 10, 710–718, 1955.
2. Fraeijs de Veubeke, B., Matrices de projection et techniques d'iteration, Annales de la Société Scientifique de Bruxelles, 70–1, 1956.
3. Householder, A.S., *The theory of matrices in numerical analysis*, Blaisdell Pub. Cy., 1964.
4. Wilkinson, T.H., *The algebraic eigenvalue problem*, Oxford University Press, 1965.

▷ Eigenvalue expansion via normal modes

⊙ Background

In standard analysis, "nice" functions may be represented by a series expansion in orthogonal eigenfunctions (say Fourier). Thus

$$f(x) = \sum_{i=1}^{n} A_n \sin \frac{n\pi x}{L} \qquad \text{(ED-19a)}$$

$$= \underset{1\times n}{\{A\}^T} \underset{n\times 1}{\left\{\sin \frac{n\pi x}{L}\right\}}$$

In vibrations the eigenfunctions (normal modes) serve as such an orthogonal set of expansion vectors.

⊙ Normal mode expansion {ref: Bathe §8.3, Zienk. §17.6}

From (ED-56), the normalized mode shapes $\{D_i\}$, $i=1, n$ modes (one "i" for each ω_i) are obtained. These represent the natural or free (forceless) response characteristics of the system. Now the response to transient loading can be written as

ED-20

$$\{D\} = \left[\{D_o\}_1 \ \{D_o\}_2 \ \ldots \ \{D_o\}_m\right]\{z\} \equiv [\Delta_o]\{z\} \quad \text{(ED-20a)} \ \circledast$$

where

$$\{z\}_{m\times 1} = \{z(t)\}, \text{ unknown} \quad \text{(ED-20b)}$$

proportions + the response in each mode.

Substituting (ED-20a) into (ED-3e) ⇒

$$[\Delta_o]^T\left\{[M][\Delta_o]\{\ddot{z}\} + [C][\Delta_o]\{\dot{z}\} + [K][\Delta_o]\{z\} = \{R\}\right\}$$

Upon multiplying by $\{\Delta_o\}$, we have (ED-20c)

i/ $[\Delta_o]^T[M][\Delta_o]$ ⇒ terms like $\{D_o\}_i^T[M]\{D_o\}_j = \begin{cases} 1, & i=j \\ 0, & i\neq j \end{cases}$ (ED-11a)

so that

$$[\Delta_o]^T[M][\Delta_o] = [I], \text{ off-diag terms vanish} \quad \text{(ED-20d)}$$

ii/ $[\Delta_o]^T[C][\Delta_o]$ ⇒ terms like $\{D_o\}_i^T[C]\{D_o\}_j$

From (GM 5.4), (ED-1d), (ED-2a), we see that $[c]$ differs from $[m]$ only by a constant.

$\circledast$ $\{D_o\}_i = \begin{Bmatrix} D_o^1 \\ D_o^2 \\ \vdots \\ D_o^n \end{Bmatrix}_i$, n D.o.F. ⇒ $[\Delta_o] = \left[\begin{Bmatrix} D_o^1 \\ D_o^2 \\ \vdots \\ D_o^n \end{Bmatrix}_1 \begin{Bmatrix} D_o^1 \\ D_o^2 \\ \vdots \\ D_o^n \end{Bmatrix}_2 \cdots \begin{Bmatrix} D_o^1 \\ D_o^2 \\ \vdots \\ D_o^n \end{Bmatrix}_m\right]_{n\times m}$; each mode is different

Thus if $i \neq j$, $\{D_o\}_i^T [C] \{D_o\}_j = 0$ (ED-21c)

However $\{D_o\}$ is not normalised w.r.t. $[C]$, ∴

if $i = j$, $\{D_o\}_i^T [C] \{D_o\}_i =$ constant

which in keeping with classical vibration theory may be set to $2\omega_i \bar{c}_i$ where

$$\bar{c}_i = \frac{1}{2\omega_i} \{D_o\}_i^T [C] \{D_o\}_i \quad \text{(ED-21b)}$$

In conclusion

$$[\Delta_o]^T [C] [\Delta_o] = 2\omega_i \bar{c}_i [I] \quad \text{(ED-21c)}$$

iii/ $[\Delta_o]^T [K] [\Delta_o] \Rightarrow$ terms like $\{D_o\}_i^T [K] \{D_o\}_j$

look: $\{D_o\}_i^T * \left[[K] \{D_o\}_j \overset{\text{(ED-5b)}}{=} \omega_j^2 [M] \{D_o\}_j \right]$

$\Rightarrow$

$$\{D_o\}_i^T [K] \{D_o\}_j = \omega_j^2 \{D_o\}_i^T [M] \{D_o\}_j \overset{\text{(ED-11c)}}{=} \omega_j^2 \delta_{ij}$$

∴

$$[\Delta_o]^T [K] [\Delta_o] = \omega_i^2 [I] \quad \text{(ED-21d)}$$

Substituting i/— iii/ in (ED-20c) ⇒ ED-22

$$\{\ddot{z}\} + 2\omega_i \bar{c}_i \{\dot{z}\} + \omega_i^2 \{z\} = [\Delta_0]^T \{R\} \qquad \text{(ED-22a)}$$

where as before, $\{R\} = \{R(t)\}$. This equation expanded ⇒ a set of ordinary differential equations in time,

$$\begin{aligned}
&\ddot{z}_1 + 2\omega_1 \bar{c}_1 \dot{z}_1 + \omega_1^2 z_1 = \{D_0\}_1^T \{R\} \\
&\ddot{z}_2 + 2\omega_2 \bar{c}_2 \dot{z}_2 + \omega_2^2 z_2 = \{D_0\}_2^T \{R\} \\
&\qquad\vdots \qquad\qquad\qquad\qquad \vdots \qquad \text{(ED-22b)} \\
&\ddot{z}_m + 2\omega_m \bar{c}_m \dot{z}_m + \omega_m^2 z_m = \{D_0\}_m^T \{R\}
\end{aligned}$$

which can be easily solved for z_i.

Finally, $\{D_i\}$ is recovered via (ED-20a).

⊙ ∴ Solution

The equations (ED-22b) can be solved by elementary means (say variation of parameters) to yield the solution in the Duhamel form:

$$z_i(t) = \frac{1}{\omega_i \sqrt{1-\bar{c}_i^2}} \int_0^t \{D_0\}_i^T \{R(\tau)\} e^{-\bar{c}_i \omega_i (t-\tau)} \sin\left[\omega_i \sqrt{1-\bar{c}_i^2}\,(t-\tau)\right] d\tau + z_{\text{homogeneous}} \qquad \text{(ED-22c)}$$

For a system starting from rest, $z_{i_{homo}} = 0$

⊙ Applications

i/ Impact : $\{R\} = \{R_0\}\delta(t)$

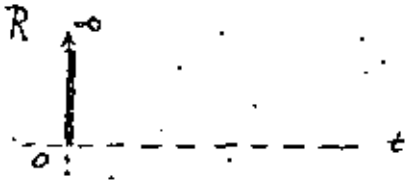

$\Rightarrow$

$$z_i(t) = \frac{1}{\omega_i\sqrt{1-\bar{c}_i^2}}\{D_0\}^T\{R_0\}e^{-\bar{c}_i\omega_i t}\sin\left[\omega_i\sqrt{1-\bar{c}_i^2}\,t\right]$$

(ED-23a)

ii/ Step load :

$$\{R\} = \{R_0\}H(t)$$

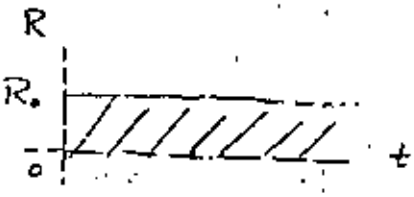

$\Rightarrow$

$$z_i(t) = \frac{1}{\omega_i^2}\{D_0\}^T\{R_0\}\left[1 - \frac{e^{-\bar{c}_i\omega_i t}}{\sqrt{1-\bar{c}_i^2}}\cos\left(\sqrt{1-\bar{c}_i^2}\,\omega_i t - \psi\right)\right]$$

where : $\psi = \tan^{-1}\bar{c}_i/\sqrt{1-\bar{c}_i^2}$

(ED-23b)

iii/ Base excitation ~ Ground motion

To visualize this, consider a 1-D model (frictionless)

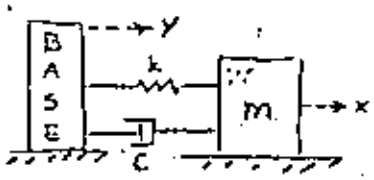

$$\Sigma F = -c\underbrace{(\dot{x}-\dot{y})}_{\dot{\delta}} - k\underbrace{(x-y)}_{\delta} = m\ddot{x}$$

$\Rightarrow$

$$m\ddot{\delta} + c\dot{\delta} + k\delta = -m\ddot{y}$$

$\delta = x - y$, $\dot{\delta} = \dot{x} - \dot{y}$

$\ddot{\delta} = \ddot{x} - \ddot{y}$

(ED-23c)

when the load vector is the acceleration of base (assumed known) acting upon the mass m. It is simple to consider only the relative motion δ between base & structure while viewing $m\ddot{y}$ as an opposing force via d'Alembert's principle. This makes the multi-D.O.F. F.E. problem much easier to formulate for then we can superpose inertial forces equal & opposite to $\ddot{U}$ at all nodes while viewing the base as fixed.

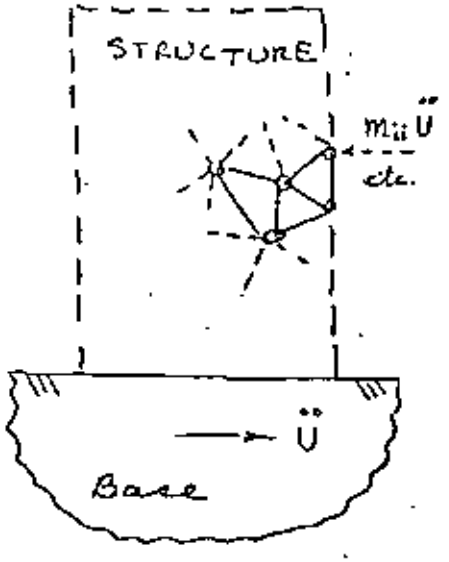

Note that (for a multi-DOF problem, otherwise) the damping and stiffness forces become cumbersome functions of base motion, i.e.

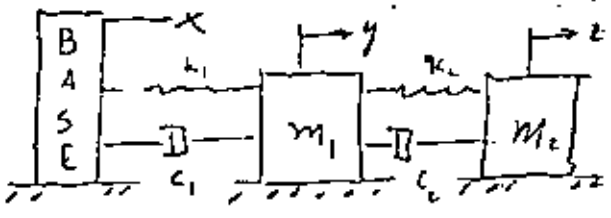

$k_2(z-y)$

$= k_2(z-[\delta+x])$

where $\delta = y - x$

However both m_1 & m_2 sense the accelaration $\ddot{x}^*$ at any moment in time. Therefore from (ED-3c) : (δ = relative motion)

$$[M]\{\ddot{\delta}\} + [C]\{\dot{\delta}\} + [K]\{\delta\} = -[M]\{\Lambda\}\ddot{U} \qquad \text{(ED-25a)}$$

where

$$\{\Lambda\} = \begin{Bmatrix} \vdots \\ \circ \\ \vdots \\ \circ \\ \vdots \end{Bmatrix} \text{ for example, } \ddot{U} \equiv \text{scalar} \qquad \text{(ED-25b)}$$

Now (ED-22a) $\Rightarrow$

$$\{\ddot{z}\} + 2\omega_i \bar{c}_i \{\dot{z}\} + \omega_i^2 \{z\} = -[\Delta_o]^T[M][A^*]\ddot{U} \qquad \text{(ED-25c)}$$

where

$$[A^*] = \left[\begin{Bmatrix} \vdots \\ \circ \\ \vdots \end{Bmatrix} \begin{Bmatrix} \vdots \\ \circ \\ \vdots \end{Bmatrix} \cdots \right]_{n \times m}; \quad \{\delta\} = [\Delta_o]\{z\} \qquad \text{(ED-25d)}$$

Essentially the problem is solved, however I can write once does the following:

i/ Let $\{z\} = [\Delta_o]^T[M][A^*]\{\bar{z}\}$, $\{\dot{z}\} = \ldots \{\dot{\bar{z}}\}$, etc.

ii/ Then i/ $\Rightarrow$ (ED-25e)

$$[\Delta_o]^T[M][A^*] * \left[\{\ddot{\bar{z}}\} + 2\omega_i \bar{c}_i \{\dot{\bar{z}}\} + \omega_i^2 \{\bar{z}\} = -\ddot{U} \right]$$

iii/ Solving $\Rightarrow$ (say starting from rest) (ED-25f)

$$\bar{z}_i = \frac{-1}{\omega_i \sqrt{1-\bar{c}_i^2}} \int_0^t \ddot{U} e^{-\bar{c}_i \omega_i (t-\tau)} \sin\left[\omega_i \sqrt{1-\bar{c}_i^2}\,(t-\tau)\right] d\tau \qquad \text{(ED-25g)}$$

11.3.

(61)

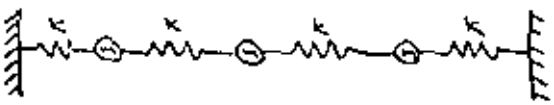

$K = 1$
$m = 1$

$$[K] = \begin{bmatrix} 2 & -1 & 0 \\ -1 & 2 & -1 \\ 0 & -1 & 2 \end{bmatrix}$$

$$[M] = \begin{bmatrix} 1 & 0 & 0 \\ 0 & 1 & 0 \\ 0 & 0 & 1 \end{bmatrix}$$

As this is free vibration: $[C] = [0]$

We wish to solve:

$$\{[K] - \omega^2[M]\}\{D\} = \{0\}$$

We need only find ω = natural frequencies
We know that:

$$\det |[K] - \omega^2[M]| = 0 \quad \text{for a nontrivial solution}$$

Solving

$$\det \begin{vmatrix} 2-\omega^2 & -1 & 0 \\ -1 & 2-\omega^2 & -1 \\ 0 & -1 & 2-\omega^2 \end{vmatrix} = 0$$

$$(2-\omega^2)^3 - 2(2-\omega^2) = 0$$

if $\lambda = \omega^2$

$$(2-\lambda)^3 - 2(2-\lambda)$$
$$= 8 - 12\lambda + 6\lambda^2 - \lambda^3 - 4 + 2\lambda$$
$$= 4 - 10\lambda + 6\lambda^2 - \lambda^3$$

by inspection $\omega = \sqrt{2}$ is one root

$$(2-\omega^2)^2 - 2 = 0$$
$$4 - 4\omega^2 + \omega^4 - 2 = 0$$
$$\omega^4 - 4\omega^2 + 2 = 0$$

3. (cont'd) (62)

by quadratic equation:

$$\omega^4 - 4\omega^2 + 2 = 0 \quad \Longrightarrow \quad \omega^2 = \frac{4 \pm \sqrt{16 - 4(2)}}{2} = 2 \pm \sqrt{2}$$

Thus the natural frequencies are:

$$\omega_1 = \sqrt{2} = 1.414$$
$$\omega_2 = \sqrt{2 - \sqrt{2}} = .765$$
$$\omega_3 = \sqrt{2 + \sqrt{2}} = 1.848$$

To find the mode shapes $\{D\}$, we substitute the frequencies back into the original equation.

FOR $\omega = \sqrt{2}$

$$\begin{bmatrix} 0 & -1 & 0 \\ -1 & 0 & -1 \\ 0 & -1 & 0 \end{bmatrix} \begin{bmatrix} D_1 \\ D_2 \\ D_3 \end{bmatrix} = \begin{bmatrix} 0 \\ 0 \\ 0 \end{bmatrix}$$

The leftmost matrix is singular. We thus pick one value.
if $D_1 = 1$ then $D_2 = 0$ and $D_3 = -1$

$$\{D_0\}_1 = \frac{\begin{bmatrix} 1 \\ 0 \\ -1 \end{bmatrix}}{\left(\begin{bmatrix} 1 & 0 & -1 \end{bmatrix} \begin{bmatrix} 1 & 0 & 0 \\ 0 & 1 & 0 \\ 0 & 0 & 1 \end{bmatrix} \begin{bmatrix} 1 \\ 0 \\ -1 \end{bmatrix} \right)^{1/2}} = \begin{bmatrix} 1/\sqrt{2} \\ 0 \\ -1/\sqrt{2} \end{bmatrix}$$ VIBRATION

This final step simply scales the vectors with respect to the mass.

3. (contd)

For $\omega = \sqrt{2-\sqrt{2}}$

$$\begin{bmatrix} \sqrt{2} & -1 & 0 \\ -1 & \sqrt{2} & -1 \\ 0 & -1 & \sqrt{2} \end{bmatrix} \cdot \begin{bmatrix} D_1 \\ D_2 \\ D_3 \end{bmatrix} = \begin{bmatrix} 0 \\ 0 \\ 0 \end{bmatrix}$$

if $D_1 = 1$ then $D_2 = \sqrt{2}$ and $D_3 = 1$

$$\{D_0\}_2 = \begin{bmatrix} 1/2 \\ \sqrt{3}/2 \\ 1/2 \end{bmatrix}$$

For $\omega = \sqrt{2+\sqrt{2}}$

$$\begin{bmatrix} -\sqrt{2} & -1 & 0 \\ -1 & -\sqrt{2} & -1 \\ 0 & -1 & -\sqrt{2} \end{bmatrix} \begin{bmatrix} D_1 \\ D_2 \\ D_3 \end{bmatrix} = \begin{bmatrix} 0 \\ 0 \\ 0 \end{bmatrix}$$

if $D_1 = 1$ then $D_2 = -\sqrt{2}$ and $D_3 = 1$

$$\{D_0\}_3 = \begin{bmatrix} 1/2 \\ -\sqrt{3}/2 \\ 1/2 \end{bmatrix}$$

Elements may have uniformly distributed structural and nonstructural mass. Structural mass is calculated from material and geometric properties. The mass is assumed to be concentrated in the middle surface or along the neutral axis in the case of rods and bars, so that rotary inertia effects, including the torsional inertia of beams, are absent. Such effects can, of course, be assigned by the user to grid points. The masses of metric structural elements are transferred to the adjacent grid points by either of two methods, referred to as the Lumped Mass and Coupled Mass methods, at the option of the user.

In the Lumped Mass method the mass of an element is simply divided and assigned to surrounding grid points. Thus, for uniform rods and bars, one-half of the mass is placed at each end; for uniform triangles, one-third of the mass is placed at each corner; quadrilaterals are treated as two pairs of overlapping triangles (see Sections 5.3 and 5.8). It will be noted that second mass moments are not preserved with the Lumped Mass method. The virtues of the method derive from its simplicity. Off-diagonal terms in the mass matrix are restricted to those involving a single geometric grid point. Programming effort and computer running time are less, often by an insignificant amount, than for more sophisticated methods of mass assignment. The mass matrix is independent of the elastic properties of elements and the user has a better feel for the character of the matrix. The accuracy of the results, which is the key question, will be examined later.

In Coupled Mass methods, the mass matrix due to a single structural element includes off-diagonal coefficients that couple adjacent grid points. The best known of the Coupled Mass methods is the Consistent Mass Matrix of Archer[1].

The general procedure for generating a consistent mass matrix is as follows. Consider, for simplicity, a one-dimensional structural element whose degrees of freedom are represented by translations and rotations at the two ends of the element. Corresponding to each degree of freedom, u_i, there is a displacement function, $w_i(x)$, within the element obtained by giving unit value to u_i and zero value to all other degrees of freedom. The functions, w_i, satisfy the differential equations of the element. The element M_{ij} of the mass matrix [M] is obtained from the formula

$$f_j = -M_{ij}\ddot{u}_i = -\left(\int_0^{\ell} m(x) w_i(x) w_j(x) dx\right)\ddot{u}_i \quad . \qquad (1)$$

[1] Archer, John S., "Consistent Mass Matrix for Distributed Mass Systems". Journal of the Structural Division, ASCE, Vol. 89, No. ST4, p.161, August 1963.

From: The NASTRAN Theoretical Manual (Level 15), Richard H. MacNeal, Edt., April 1972, NASA, Wash., D.C., USA

TREATMENT OF INERTIA PROPERTIES

Equation 1 is obtained from the principle of virtual work. In essence u_i is regarded as a generalized coordinate for which $w_i(x)$ is the "mode shape". The inertia force acting at x due to u_i is $-m(x)w_i(x)\ddot{u}_i$. Multiplication of the inertia force by w_j gives the generalized force acting on coordinate u_j.

The idea of "consistency" enters because the functions w_i are also used to calculate the stiffness matrix $[K_{ij}]$ from strain energy considerations. It can be shown that the vibration frequencies so obtained are upper bounds. The reason is that the selection of a finite number of specific functions, w_i, is equivalent to the imposition of rigid constraints on the structure.

As an elementary example consider a uniform extensional rod with distributed mass, as shown below

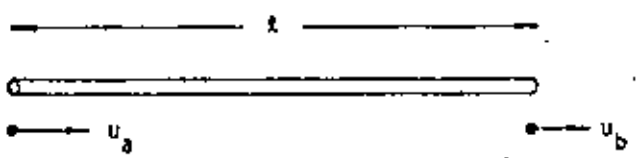

The degrees of freedom are u_a and u_b and the displacement functions are $w_a = 1 - x/\ell$ and $w_b = x/\ell$. The resulting consistent mass matrix is

$$[M^C] = \frac{m\ell}{6}\begin{bmatrix} 2 & 1 \\ 1 & 2 \end{bmatrix} \qquad (2)$$

whereas the lumped mass matrix is

$$[M^\ell] = \frac{m\ell}{2}\begin{bmatrix} 1 & 0 \\ 0 & 1 \end{bmatrix} \qquad (3)$$

The stiffness matrix is

$$[K] = \frac{EA}{\ell}\begin{bmatrix} 1 & -1 \\ -1 & 1 \end{bmatrix} \qquad (4)$$

Some information on the question of accuracy can be gained by calculating the error in natural frequency due to finite element assumptions for simple structures. Analysis of a uniform

rod with any combination of free and fixed ends[2] shows that the error in frequency that results from using Equations 3 and 4 (the lumped mass method) is

$$\left(\frac{\omega_{approx}}{\omega_{exact}}\right)_L = 1 - \frac{1}{6}\left(\frac{\pi}{N}\right)^2 + 0\left(\frac{\pi}{N}\right)^4 \qquad (5)$$

where N is the number of cells per wavelength. The corresponding result for Equations 2 and 4 (the consistent mass method) is

$$\left(\frac{\omega_{approx}}{\omega_{exact}}\right)_C = 1 + \frac{1}{6}\left(\frac{\pi}{N}\right)^2 + 0\left(\frac{\pi}{N}\right)^4 \qquad (6)$$

Note that the consistent mass and lumped mass methods give errors that, for large N, are the same in magnitude but opposite in sign. A much smaller error is achieved if the mass matrices for the two methods, Equations 2 and 3, are averaged.

$$[M^a] = \frac{m\ell}{12}\begin{bmatrix} 5 & 1 \\ 1 & 5 \end{bmatrix} \qquad (7)$$

The error in this case is given by

$$\left(\frac{\omega_{approx}}{\omega_{exact}}\right)_a = 1 + \frac{1}{30}\left(\frac{\pi}{N}\right)^4 + 0\left(\frac{\pi}{N}\right)^6 \qquad (8)$$

The mode shapes are exact for all three methods.

Equation 7 has been adopted in NASTRAN as the coupled mass matrix for the extension of rods and bars. It will also be applied to the torsion of beams, if and when distributed torsional inertia is added as a property of beam elements.

Archer's paper[1] includes a derivation of the consistent mass matrix for the lateral bending of a uniform beam without transverse shear flexibility shown below.

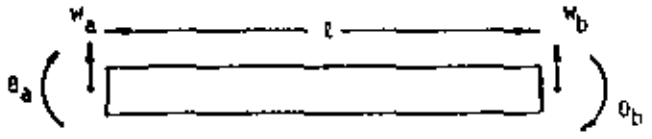

[2] MacNeal, R. H., ELECTRIC CIRCUIT ANALOGIES FOR ELASTIC STRUCTURES. John Wiley & Sons, 1962.

TREATMENT OF INERTIA PROPERTIES

The consistent mass matrix referred to the coordinate set $\{u\} = \{w_a, \theta_a, w_b, \theta_b\}^T$ is

$$[M^C] = \frac{m\ell}{420}\begin{bmatrix} 156 & -22\ell & 54 & 13\ell \\ -22\ell & 4\ell^2 & -13\ell & -3\ell^2 \\ 54 & -13\ell & 156 & 22\ell \\ 13\ell & -3\ell^2 & 22\ell & 4\ell^2 \end{bmatrix} \qquad (9)$$

The paper also includes the results of numerical error analysis for free-free and simply supported beams. For simply supported beams the errors in the lumped mass and consistent mass formulations are approximately equal and opposite, and they are surprisingly small. An equation for the frequency error associated with the lumped mass formulation [2] is

$$\left(\frac{\omega_{approx}}{\omega_{exact}}\right)_{\ell} = 1 - \frac{1}{90}\left(\frac{\pi}{N}\right)^4 + O\left(\frac{\pi}{N}\right)^6 \qquad (10)$$

For free-free beams the error in the consistent mass formulation appears to be of the same order as that given by Equation 10, but the error in the lumped mass formulation is one or two orders of magnitude larger. Similar results may be expected for cantilever beams.

(68)
EARTHQUAKE ENGINEERING AND STRUCTURAL DYNAMICS, VOL. 4, 245-249 (1976)

A NOTE ON MASS LUMPING AND RELATED PROCESSES IN THE FINITE ELEMENT METHOD

E. HINTON, T. ROCK AND O. C. ZIENKIEWICZ
Department of Civil Engineering, The University of Wales, Swansea, Wales

SUMMARY

The general problem of mass lumping and related processes in the finite element method are discussed.

A mass lumping scheme is presented for parabolic isoparametric elements. Examples are presented to show the good accuracy which can be obtained in linear and non-linear dynamic problems using the scheme.

In many problems of structural dynamics, transient heat conduction, etc., the finite element approximation leads to equations of the type (dots referring to time differentiation)

$$\mathbf{P}(\mathbf{a}) + \mathbf{C}\dot{\mathbf{a}} + \mathbf{M}\ddot{\mathbf{a}} = \mathbf{F} \tag{1}$$

after the introduction of basic functions N_i describing the continuous variable as

$$\phi = \sum N_i a_i \tag{2}$$

In this note we restrict our attention to problems of structural dynamics although much of what is discussed has wider application for problems defined by equation (1).

For structural dynamics problems, nodal displacements a_i are represented by the displacement vector a. In the equilibrium relationship expressed in equation (1), the terms on the left side represent the inertia force, damping force and elastic (or non-linear) force vectors, respectively, and the right side is the dynamically applied load vector. In equation (1), the term P(a) generally involves $\hat{m}$th order derivatives of N_i while the damping matrix C and the mass matrix M contain derivatives of order $\bar{m}$ ($\bar{m}$ frequently being zero, i.e. involving no differentiation). A common structure of the matrix M (or C) is of the form

$$M_{ij} = \int_\Omega N_i^T \rho N_j \, d\Omega \tag{3}$$

Ω being the integration domain.

In the solution of such equations it would be extremely useful from the computational viewpoint if the matrices M and C could be made diagonal. In the early days the engineer has (apologetically) lumped his masses or forces by physical reasoning alone and appeared glad when a proper discretization procedure introduced him to consistent mass/force approximations of the form given by equation (3).[1-3] In recent years there has been a partial return to mass lumping as investigators found that the use of consistent masses did not always lead to improved accuracy and *always* involved additional computational work. Clough,[4] Washizu[5] and others[6] have demonstrated this point with the use of simple elements for which lumping procedures are physically obvious. Clough[4] postulated that such lumping is simply the outcome of using substitute basis functions $\bar{N}$ to approximate the terms of equation (3) by

$$M_{ij} = \int_\Omega \bar{N}_i^T \rho \bar{N}_j \, d\Omega \tag{4}$$

in which $\bar{N}$ are piecewise constant, non-overlapping functions covering the whole element. Is this approximation always tenable with respect to convergence? What is a *good form* of such an approximation in the

Received 12 December 1974
Revised 10 March 1975

3–D BODE DIAGRAM

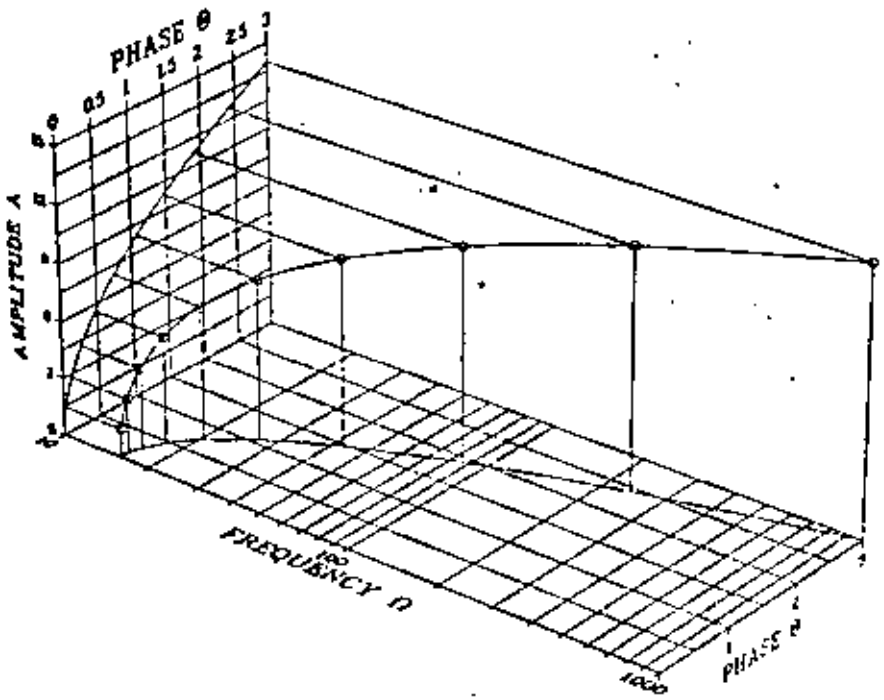

from DISSPLA package; Integrated Software Systems Corp., San Diego, CA

SPACE SHUTTLE REENTRY

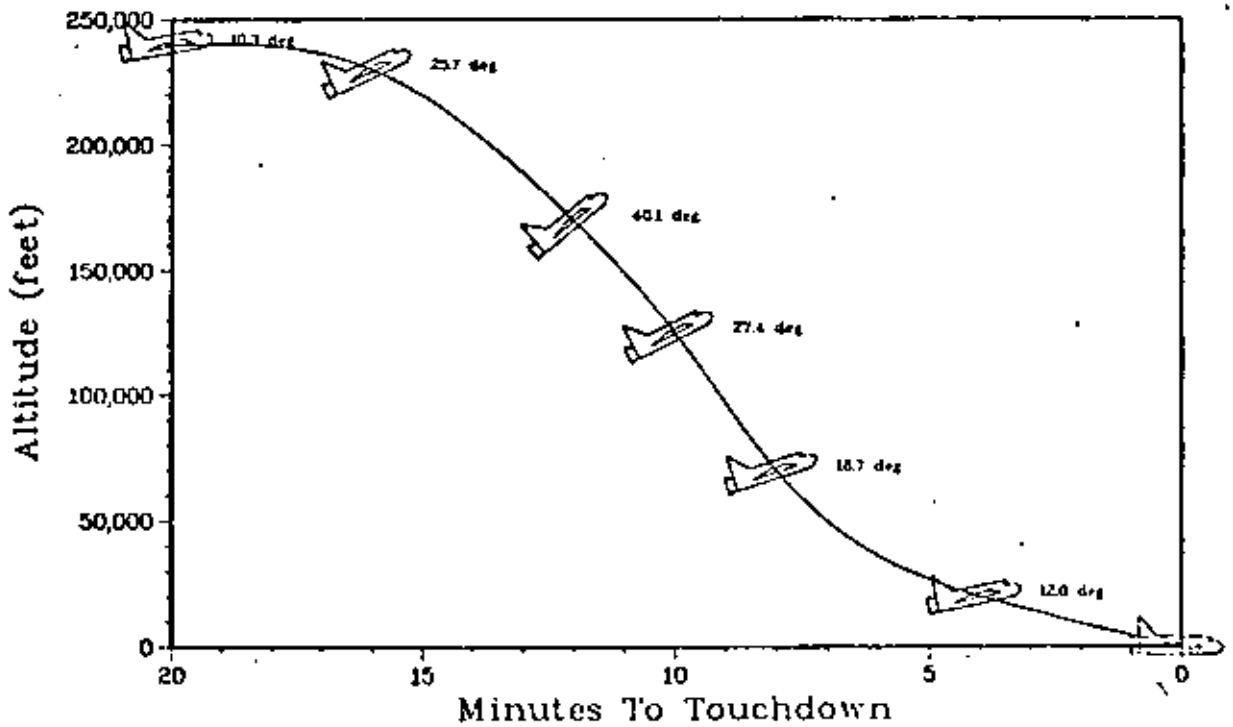

Instrument Tower

1. Configuration 2
2. Configuration 3 includes dotted members.

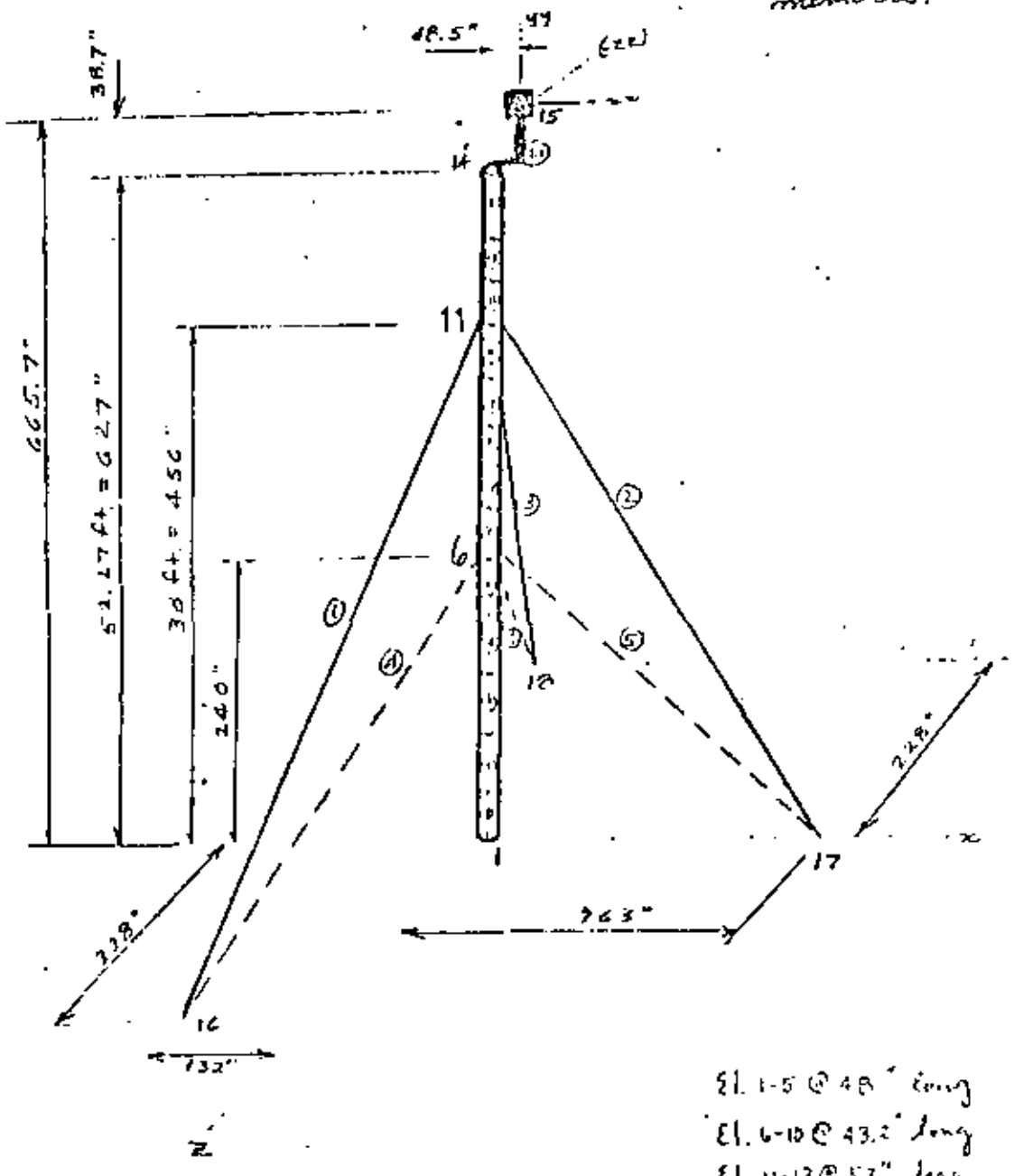

El. 1-5 @ 48" long
El. 6-10 @ 43.2" long
El. 11-13 @ 57" long
El. 14 rigid

(21)

Member Properties	Area (in²)	I (in⁴)	J (in⁴)	ρ (lb/in³)	E (×10⁶ psi)
Beam El. 1-12 (Shaft)	11.40	72.5	145	.283	29.5
14	.84	72.5	1450	.283	29.5
Truss El. (½" cable)	.124	0	0	.283	29.0

(1.00)

Lumped Mass (units, lb)

$wt = 1500^{\#}$, $M = 4.659 \frac{lb\text{-}sec^2}{in}$

$MI_{xx} = 561 \frac{lb\text{-}sec^2}{in} \cdot in^2$

$MI_{zz} = 2811 \frac{lb\text{-}sec^2}{in} \cdot in^2$

$MI_{yy} = 0$

Support conditions

Horizontal rotational releases at 1

Truss element ball joint at both ends

Loads (0 mass at 15)

1) gravity

2) F_y @ 15 = 1800#

3) F_x @ 15 = 1277#

4) M_y @ 14 = 4800 in-lb

5) wx on beam el. 1-12 = 58 #/ft

(1-5)	4.0	116.0	928#
(6-10)	3.6	104.4#	754.7
(11-12)	4.75	137.5#	1303.6

6) 1+2+3+4

7) 1+2+3-5

INPUT DATA : pp. 3 & 4.

```
@ELT.DIL  CAPDS.,ZZ
ELTDTT RLIB70 03/19-16:30:18-(-0)
000001      000
000002      000
000003      000          1         2         3         4         5         6         7
000004      000  1234*6789012345678901234567890123456789012345678901234567890123456789012345678901234567890
000005      000
000006      000
000007      000  INSTRUMENT TOWER--STATIC ANALYSIS--BEAM AND TRUSS ELEMENTS
000008      000    18    2    7
000009      000     1    1    1    1         1
000010      000     2                                        43.
000011      000     6                                       240.                   1
000012      000    11                                       450.                   1
000013      000    16                                       627.                   1
000014      000    15                                 18.5  666.
000015      000    16   -1   -1   -1   -1   -1   -1     -132.          228.
000016      000    17                                   264.
000017      000    18    1    1    1    1    1    1     -132.         -228.
000018      000     1    3    1
000019      000     1  20.E06    1.E-06  7.19E-04      .129     : .793
000020      000
000021      000        -1.
000022      000
000023      000
000024      000     1   16   11    1
000025      000     2   17   11    1
000026      000     3   18   11    1
000027      000     2   19    2    3    2
000028      000     1  29.5E06         .3  7.73E-04      .283
000029      000     2  29.5E06         .3
000030      000     1      8.4                    195.     72.5      72.5  8 IN SCH 40
000031      000     2      84.                   1450.    725.      725.  RIGID LINK
000032      000
000033      000        -1.
000034      000
000035      000     1                -110.                          -928.
000036      000                      -116.                           928.
000037      000     2                -104.9                        -751.7
000038      000                      -104.4                         751.7
000039      000     3                -137.8                       -1300.6
000040      000                      -137.8                        1300.6
000041      000     1    1    2   17    1    1         1
000042      000     5    5    6   17    1    1         1
000043      000     6    6    7   17    1    1         2
000044      000    10   10   11   17    1    1         2
000045      000    11   11   12   17    1    1         3
000046      000    13   13   14   17    1    1         3
000047      000    14   14   15   17    2    2
000048      000    15    2              -1800.
000049      000    15    3        1277.
000050      000    15    4                                    4200.
000051      000    15    5        1277.      -1300.           4200.
000052      000    15    7        1277.      -1800.
000053      000
000054      000        3.
000055      000
```

simulated by high stiffness. (2)

p. 3 of 9

(73)

```
000056      000
000057      000
000058      000                     1.
000059      000          1.
000060      000          1.         1.
000061      000
000062      000

END ELT.
@PCH,S  CARDS
FURPUR 27RZ* RL72-8 01/14/78 16:30:29
@SYM  PUNCH$,,CP1
@FIN


  RUNID: I5237     ACCT: 98100              USER: 196323514
  TIME:     TOTAL: 00:00:02.790    CPSUPS:  0.00229976
            CPU:   00:00:00.299    I/O:  00:00:00.800
            CC/ER: 00:00:01.687    WAIT: 00:00:00.000
  TOAS USED:  $     0.71   TOAS REMAINING: $   399.92
  THE ABOVE DOLLAR CHARGES FOR THIS RUN ARE APPROXIMATE.
  THE ACTUAL COST WILL BE REFLECTED ON YOUR MONTHLY INVOICE.
  IMAGES READ:   69        PAGES:  3          IMAGES PUNCHED:   63
  START:    16:30:15 MAR 14,1978    FIN:  16:30:46 MAR 14,1978
```

1234567890123456789012345678901234567890123456789012345678901234567890123456789012345678901234567890

INPUT DATA

```
@ELT,C CARDS,,27
ELTDT7 RUN 05/31-15:23:21-1.01
000001      000          1         2         3         4         5         6         7
000002      000 1234567890123456789012345678901234567890123456789012345678901234567890
000003      000 INCTRUMENT TOWER--DYNAMIC ANALYSIS--8 BAR AND TRUSS ELEMENTS
000004      000    18    2        10    1
000005      000     1    1    1    1         1
000006      000     2                                        4 K.
000007      000     6                                       20 K.              1
000008      000     7                                       28.2
000009      000    11                                       45 K.              1
000010      000    12                                       51 K.
000011      000    14                                       57 K.              1
000012      000    15                                 13.5  66 K.
000013      000    16   -1   -1   -1   -1   -1   -1   -132.          22.8
000014      000    17                                  26 K.
000015      000    18    1    1    1    1    1    1   -132.         -22.8
000016      000     1    6    1
000017      000     1   20.E06    1.E-06   7.78E-04     .174      2.83
000018      000
000019      000
000020      000
000021      000
000022      000     1   15   11    1
000023      000     2   17   11    1
000024      000     3   19   11    1
000025      000     4   16    6    1
000026      000     5   17    6    1
000027      000     6   18    6    1
000028      000     2   14    2         2
000029      000     1   29.E06         .3   7.33E-04     .287
000030      000     2   29.E06         .3   7.33E-05
000031      000     1     8.4                          195.      72.5      72.5 8 IN SCH 40
000032      000     2    33.6                          580.      290.      290.  RIGID LINK
000033      000
000034      000
000035      000
000036      000     1    1    2   17    1    1
000037      000     5    5    6   17    1    1
000038      000     6    6    7   17    1    1
000039      000    10   10   11   17    1    1
000040      000    11   11   12   17    1    1
000041      000    13   13   14   17    1    1
000042      000    14   14   15   17    2    2
000043      000    15          4.679     4.679     4.679      561.      2811.        0.
000044      000
000045      000
000046      000
000047      000

END ELT.
@FIN
```

RUN ID: 26762 ACCT: 491CO USER: JEFF SELLIN

TIME: TOTAL: 00:00:00.936 CPU: 0000:55.272

P.S. 4-5-85

Simulated by high stiffness. If stiffness is too high → program will not execute.

Master/Slave option does not transfer Point masses & inertias thru link.

(20) 17/18

GENERAL INFORMATION

NUMBER OF NODAL POINTS = 17
NUMBER OF ELEMENT TYPES = 2
NUMBER OF LOAD CASES = 0
NUMBER OF PERTURBATIONS = 10
ANALYSIS CODE (NDMA) = 1
EQ.0: STATIC
EQ.1: MODAL EXTRACTION
EQ.2: FORCED RESPONSE
EQ.3: RESPONSE SPECTRUM
SOLUTION MODE (NSOLN) = 0
EQ.0: EXECUTION
EQ.1: DATA CHECK

output given on this and following pages.

NODAL POINT INPUT DATA

NODE NUMBER	BOUNDARY CONDITION CODES X	Y	Z	XX	YY	ZZ	NODAL POINT COORDINATES X	Y	Z	T
1	1	1	1	0	1	0	.000	-0.00	.00 0	0 .000
2	0	0	0	0	0	0	.000	48.00	.00 0	0 .000
5	0	0	0	0	0	0	.000	240.00	.00 0	1 .000
7	0	0	0	0	0	0	.000	288.00	.00 0	0 .000
11	0	0	0	0	0	0	.000	456.00	.00 0	1 .000
12	0	0	0	0	0	0	.000	504.00	.00 0	0 .000
14	0	0	0	0	0	0	.000	672.00	.00 0	1 .000
15	0	0	0	0	0	0	192.000	672.00	.00 0	0 .000
16	-1	-1	-1	-1	-1	-1	-192.000	.00	288.00 0	0 .000
17	0	0	0	0	0	0	48.000	.00	.00 0	0 .000
19	1	1	1	1	1	1	-192.000	.00	-288.00 0	0 .000

GENERATED NODAL DATA

NODE NUMBER	BOUNDARY CONDITION CODES X	Y	Z	YX	YY	ZZ	NODAL POINT COORDINATES X	Y	Z	I
1	1	1	1	0	1	0	.000	.000	.000	.000
2	0	0	0	0	0	0	.000	48.000	.000	.000
3	0	0	0	0	0	0	.000	96.000	.000	.000
4	0	0	0	0	0	0	.000	144.000	.000	.000
5	0	0	0	0	0	0	.000	192.000	.000	.000
6	0	0	0	0	0	0	.000	240.000	.000	.000
7	0	0	0	0	0	0	.000	288.000	.000	.000
8	0	0	0	0	0	0	.000	336.000	.000	.000
9	0	0	0	0	0	0	.000	384.000	.000	.000
10	0	0	0	0	0	0	.000	432.000	.000	.000
11	0	0	0	0	0	0	.000	480.000	.000	.000
12	0	0	0	0	0	0	.000	528.000	.000	.000
13	0	0	0	0	0	0	.000	576.000	.000	.000
14	0	0	0	0	0	0	.000	624.000	.000	.000
15	0	0	0	0	0	0	13.000	666.000	.000	.000
16	-1	-1	-1	-1	-1	-1	-172.000	.000	228.000	.000
17	-1	-1	-1	-1	-1	-1	20.000	.000	.000	.000
18	1	1	1	1	1	1	-172.000	.000	-228.000	.000

(76)

(77)

EQUATION NUMBERS

N	X	Y	Z	XX	YY	ZZ
1	0	0	0	1	0	2
2	3	4	5	6	7	8
3	9	10	11	12	13	14
4	15	16	17	18	19	20
5	21	22	23	24	25	26
6	27	28	29	30	31	32
7	33	34	35	36	37	38
8	39	40	41	42	43	44
9	45	46	47	48	49	50
10	51	52	53	54	55	56
11	57	58	59	60	61	62
12	63	64	65	66	67	68
13	69	70	71	72	73	74
14	75	76	77	78	79	80
15	81	82	83	84	85	86
16	0	0	0	0	0	0
17	0	0	0	0	0	0
18	0	0	0	0	0	0

(77)

3 of 18

NUMBER OF TRUSS MEMBERS= 6
NUMBER OF DIFF. MEMBERS= 1

4 of 18

TYPE	E	SIGMA	DEN	AREA	WT
1	.2000000+08	.1000000+05	.7340000-01	.1240000+00	.2830000+00

78

ELEMENT LOAD MULTIPLIERS

	A	B	C	D
X-DIR	.000000	.000000	.000000	.000000
Y-DIR	.000000	.000000	.000000	.000000
Z-DIR	.000000	.000000	.000000	.000000
TEMP	.000000	.000000	.000000	.000000

N	I	J	TYPE	ZERO	BEND
1	10	11	1	.00	3
2	17	11	1	.00	3
3	10	11	1	.00	3
4	16	6	1	.00	3
5	17	6	1	.00	3
6	18	6	1	.00	3

5 of 18

(79)

.....THREE DIMENSIONAL BEAM ELEMENTS

(80)

6 of 18

NUMBER OF NODES = 14
NUMBER OF GEOMETRIC PROPERTY SETS = 2
NUMBER OF FIXED END FORCE SETS = 0
NUMBER OF MATERIALS = 2

MATERIAL	YOUNG'S MODULUS	POISSON'S RATIO	MASS DENSITY		
1	29500000.	.30000	.00073	.28300	
2	29500000.	.30000	.00007	.00070	(81)

7 of 18

BEAM GEOMETRIC PROPERTIES

8 of 18

ELEMENT TYPE	AREA X	AREA Y	AREA Z	INERTIA X	INERTIA Y	J INERTIA Z
1	8.400	.000	.000	145.000	72.500	72.500
2	33.600	.000	.000	580.000	290.000	290.000

(82)

ELEMENT LOAD MULTIPLIERS

	A	B	C	D
X-DIR	.000000	.000000	.000000	.000000
Y-DIR	.000000	.000000	.000000	.000000
Z-DIR	.000000	.000000	.000000	.000000

BEAM NO	I	J	K	RATIO OF N NO	NO	FIXED LOADS A	B	C	D	END CODES I	J
1	1	2	17	1	1	0	0	0	0	0	0
2	2	3	17	1	1	0	0	0	0	0	0
3	3	4	17	1	1	0	0	0	0	0	0
4	4	5	17	1	1	0	0	0	0	0	0
5	5	6	17	1	1	0	0	0	0	0	0
6	6	7	17	1	1	0	0	0	0	0	0
7	7	8	17	1	1	0	0	0	0	0	0
8	8	9	17	1	1	0	0	0	0	0	0
9	9	10	17	1	1	0	0	0	0	0	0
10	10	11	17	1	1	0	0	0	0	0	0
11	11	12	17	1	1	0	0	0	0	0	0
12	12	13	17	1	1	0	0	0	0	0	0
13	13	14	17	1	1	0	0	0	0	0	0
14	14	15	17	2	2	0	0	0	0	0	0

9 of 18

(84)

EQUATION PARAMETERS

TOTAL NUMBER OF EQUATIONS	=	85
BANDWIDTH	=	17
NUMBER OF EQUATIONS IN A BLOCK	=	85
NUMBER OF BLOCKS	=	1

10 of 18

85

***** NODAL FORCES/MOMENTS

11 of 18

JOINT NUMBER	LOAD CASE	X-AXIS FORCE	Y-AXIS FORCE	Z-AXIS FORCE	X-AXIS MOMENT	Y-AXIS MOMENT	Z-AXIS MOMENT
15	0	.40790+01	.40790+01	.40790+01	.56100+03	.28110+04	.00000

STRUCTURE LOAD CASE	ELEMENT A	B	LOAD MULTIPLIERS C	D
1	.000	.000	.000	.000

E I G E N V A L U E A N A L Y S I S

12 9 18

DETERMINANT SEARCH SOLUTION IS CARRIED OUT

CONTROL INFORMATION

FLAG FOR PRINTING = 0
EQ.0 FOR NO PRINT
EQ.1 FOR PRINT

FLAG FOR STURM SEQUENCE CHECK = 0
EQ.0 FOR CHECK
EQ.1 FOR NO CHECK

MAXIMUM NUMBER OF ITERATIONS = 10

CONVERGENCE TOLERANCE = .1000-04

CUT-OFF FREQUENCY (CPS) = .1000+09

NUMBER OF STARTING ITERATION VECTORS TO BE READ FROM TAPE10 = 0

SOLUTION IS SOUGHT FOR FOLLOWING EIGENPROBLEM

NUMBER OF EQUATIONS = 86

HALF BANDWIDTH OF STIFFNESS MATRIX = 12

NUMBER OF EQUATION BLOCKS = 1

NUMBER OF EQUATIONS PER BLOCK = 86

NUMBER OF EIGENVALUES REQUIRED = 10

WE SOLVED FOR 10 FOLLOWING EIGENVALUES

.1000+01 .3774+02 .1086+03 .2047+04 .2322+04 .1137+05

.2578+05 .3937+05 .1098+06 .1555+06

PRINT OF FREQUENCIES

MODE NUMBER	CIRCULAR FREQUENCY (RAD/SEC)	FREQUENCY (CYCLES/SEC)	PERIOD (SEC)	TOLERANCE
1	.6885+01	.9685+00	.1033+01	.1000-11
2	.8143+01	.9778+00	.1023+01	.1000-11
3	.2394+02	.9765+01	.2058+00	.1000-11
4	.4095+02	.7473+01	.1338+00	.1000-11
5	.4819+02	.7670+01	.1304+00	.1000-11
6	.7153+02	.1133+02	.8784-01	.1000-11
7	.7251+02	.1154+02	.8666-01	.1000-11
8	.1116+03	.1767+02	.5659-01	.1000-11
9	.1183+03	.1883+02	.5312-01	.1000-11
10	.1664+03	.2965+02	.3373-01	.1000-11

PRINT OF EIGENVECTORS

28

14.5 18

N O D E D I S P L A C E M E N T S / R O T A T I O N S

NODE NUMBER	EIGEN-VECTOR	X-TRANSLATION	Y-TRANSLATION	Z-TRANSLATION	X-ROTATION	Y-ROTATION	Z-ROTATION
13	1	.00000	.00000	.00000	.01000	.00000	.00000
	2	.00000	.00000	.00000	.00000	.00000	.00000
	3	.00000	.00000	.00000	.00000	.00000	.00000
	4	.00000	.00000	.00000	.00000	.00000	.00000
	5	.00000	.00000	.00000	.00000	.00000	.00000
	6	.00000	.00000	.00000	.00000	.00000	.00000
	7	.00000	.00000	.00000	.00000	.00000	.00000
	8	.00000	.00000	.00000	.00000	.00000	.00000
	9	.00000	.00000	.00000	.00000	.00000	.00000
	10	.00000	.00000	.00000	.00000	.00000	.00000
17	1	.00000	.00000	.00000	.00000	.00000	.00000
	2	.00000	.00000	.00000	.00000	.00000	.00000
	3	.00000	.00000	.00000	.00000	.00000	.00000
	4	.00000	.00000	.00000	.00000	.00000	.00000
	5	.00000	.00000	.00000	.00000	.00000	.00000
	6	.00000	.00000	.00000	.00000	.00000	.00000
	7	.00000	.00000	.00000	.00000	.00000	.00000
	8	.00000	.00000	.00000	.00000	.00000	.00000
	9	.00000	.00000	.00000	.00000	.00000	.00000
	10	.00000	.00000	.00000	.00000	.00000	.00000
18	1	.00000	.00000	.00000	.00000	.00000	.00000
	2	.00000	.00000	.00000	.00000	.00000	.00000
	3	.00000	.00000	.00000	.00000	.00000	.00000
	4	.00000	.00000	.00000	.00000	.00000	.00000
	5	.00000	.00000	.00000	.00000	.00000	.00000
	6	.00000	.00000	.00000	.00000	.00000	.00000
	7	.00000	.00000	.00000	.00000	.00000	.00000
	8	.00000	.00000	.00000	.00000	.00000	.00000
	9	.00000	.00000	.00000	.00000	.00000	.00000
	10	.00000	.00000	.00000	.00000	.00000	.00000
15	1	.16[illegible]+00	-.11[illegible]-07	.54[illegible]+03	.19[illegible]-02	-.57[illegible]-03	-.61[illegible]-09
	2	-.[illegible]+00	.35[illegible]-01	.2[illegible]-07	.11[illegible]-09	-.24[illegible]-10	.19[illegible]-02
	3	-.16[illegible]-11	.21[illegible]-11	-.34[illegible]-01	.17[illegible]-03	.28[illegible]-01	.11[illegible]-12
	4	-.96[illegible]-01	.11[illegible]+00	.[illegible]+00	.23[illegible]-10	.11[illegible]-10	.66[illegible]-02
	5	.17[illegible]-10	-.73[illegible]-10	.5[illegible]-01	.14[illegible]-02	.29[illegible]-02	-.41[illegible]-11
	6	.52[illegible]-01	-.8[illegible]-01	.62[illegible]-01	.27[illegible]-10	.23[illegible]-10	-.86[illegible]-03
	7	-.47[illegible]-09	.29[illegible]-09	.[illegible]-01	.27[illegible]-02	.14[illegible]-02	.10[illegible]-12
	8	-.27[illegible]-02	.1[illegible]+00	.17[illegible]-11	.71[illegible]-12	.41[illegible]-11	.31[illegible]-03
	9	.[illegible]-01	-.21[illegible]-10	.42[illegible]-01	.17[illegible]-01	.26[illegible]-02	-.15[illegible]-11
	10	.17[illegible]-01	.2[illegible]+00	.51[illegible]-12	.25[illegible]-12	.16[illegible]-12	.71[illegible]-03
16	1	.11[illegible]-01	-.5[illegible]-11	.3[illegible]-01	.18[illegible]-02	-.57[illegible]-03	-.61[illegible]-09
	2	-.[illegible]+00	.1[illegible]-01	.2[illegible]-07	.11[illegible]-09	-.94[illegible]-10	.14[illegible]-02
	3	.94[illegible]-11	.57[illegible]-11	.[illegible]-01	.10[illegible]-03	.10[illegible]-11	.11[illegible]-12
	4	.11[illegible]+00	.2[illegible]-01	-.9[illegible]-01	.[illegible]-10	.11[illegible]-10	.[illegible]-02
	5	-.[illegible]-01	-.21[illegible]-10	-.[illegible]	.[illegible]-02	.23[illegible]-02	-.[illegible]-11
	6	-.[illegible]-01	-.5[illegible]-02	-.15[illegible]	.24[illegible]-10	.21[illegible]-10	-.[illegible]-02
	7	.47[illegible]-09	.13[illegible]-10	-.11[illegible]-05	.[illegible]-02	.13[illegible]-02	.14[illegible]-12

	8	.3264E+00	.3008E-01	-.5204E-11	.2489E-12	.3397E-13	.8617E-09
	9	.5706E-09	.1459E-10	-.3166E+00	.9601E-07	.1310E-07	-.2078E-11
	10	.2981E+00	.1157E+00	-.8572E-11	.2136E-12	.5547E-14	.6030E-07
13	1	.3271E-07	-.8866E-11	.2565E+00	.1751E-07	-.5191E-08	-.5986E-09
	2	-.2503E+00	.1528E-04	.1533E-07	.1155E-09	-.3129E-10	.1709E-07
	3	.2159E-11	.6177E-13	.2285E+00	.1003E-07	.1658E-08	.3401E-13
	4	.4284E+00	.2563E-07	-.1791E-05	-.1925E-10	-.1005E-10	.4500E-07
	5	-.3264E-09	-.1535E-11	-.4796E-06	.4049E-07	.2551E-08	-.2975E-11
	6	-.3742E+00	-.4926E-07	-.5423E+00	.8157E-10	.1939E-10	-.2004E-07
	7	.1007E-08	-.1536E-10	-.6466E+00	.2567E-02	.1719E-02	.6580E-11
	8	.5811E+00	.2739E-01	-.1744E-10	.6017E-13	-.3093E-13	.7851E-07
	9	-.4875E-09	.1963E-10	-.6745E+00	.2394E-02	.1191E-07	-.3461E-11
	10	.2357E+00	.1457E+00	-.1756E-10	-.7607E-13	.5043E-14	-.6722E-02
17	1	.4254E-07	-.4436E-11	.1813E+00	.1402E-07	-.4672E-08	-.4820E-09
	2	-.1650E+00	.1380E-04	.9733E-04	.3965E-10	-.2025E-10	.1514E-07
	3	.1726E-10	.4660E-13	.1703E+00	.1906E-07	.1579E-01	.4561E-13
	4	.3856E+00	.2419E-07	-.2529E-04	.1092E-10	.3505E-11	.2756E-07
	5	-.4875E-09	-.1735E-11	-.6470E+00	.2734E-02	.2290E-07	-.1932E-11
	6	-.4702E+00	-.4943E-07	-.6459E-06	-.3702E-11	.1756E-10	-.7900E-08
	7	.1179E-08	.1438E-10	-.3654E+00	-.2673E-03	.1097E-07	-.2531E-11
	8	.4241E+00	.2468E-01	-.1487E-10	-.1465E-12	.2773E-13	-.6236E-07
	9	.2047E-09	.1213E-10	-.4736E+00	-.5657E-02	.1072E-07	-.3338E-11
	10	-.2755E+00	.9542E-01	-.1642E-11	-.2555E-12	.4517E-14	-.4054E-02
11	1	.2955E-07	-.3624E-11	.3862E-01	.1034E-07	-.4153E-08	-.3525E-09
	2	-.3779E-01	.2232E-04	.5527E-04	.5159E-10	-.2511E-10	.1107E-07
	3	.1492E-10	.4123E-13	.1167E+00	.3823E-08	.1319E-01	.1144E-13
	4	.7432E+00	.2146E-07	-.2942E-03	.3375E-11	.8076E-11	.5931E-07
	5	-.4951E-09	-.1530E-11	-.7474E+00	.9344E-03	.2041E-02	-.2545E-11
	6	-.2571E+00	-.3923E-07	-.9123E-06	-.4431E-10	.1591E-10	.3171E-07
	7	.3056E-09	.1277E-10	-.3675E+00	-.2766E-02	.3768E-01	-.1913E-11
	8	-.3969E-01	.2195E-01	-.2662E-11	-.2966E-12	.2470E-13	-.5928E-07
	9	.5615E-10	.1086E-10	-.1027E+00	-.5837E-02	.9631E-03	-.1758E-11
	10	-.6086E+00	.8567E-01	-.1172E-10	-.1524E-12	.4834E-14	-.1312E-07
10	1	.1756E-07	-.3550E-11	.4837E-01	.2632E-01	-.4759E-03	-.2479E-09
	2	-.4917E-01	.1425E-04	-.2176E-03	.4015E-10	-.2232E-10	.7707E-08
	3	.1441E-10	.3731E-14	.3506E-01	.7016E-03	.1136E-01	-.1244E-13
	4	.7430E+00	.1933E-07	-.3812E-03	-.1346E-11	.3274E-11	-.6970E-08
	5	-.4790E-09	-.1437E-11	-.7624E+00	-.5470E-03	.1843E-02	.6159E-12
	6	-.4571E-01	-.3611E-07	-.2557E-03	-.6737E-10	.1440E-10	.4604E-08
	7	.2892E-09	.1156E-10	-.1568E+00	-.4141E-02	.3549E-03	-.1379E-10
	8	-.4052E+00	.2530E-01	.3747E-11	-.2525E-12	.2236E-13	-.7378E-07
	9	.1116E-10	.9376E-11	-.3141E+00	-.9777E-02	.9623E-03	-.2355E-11
	10	-.4525E+00	.7735E-01	-.1543E-10	-.1490E-12	.4926E-14	.6568E-07
9	1	.6870E-08	-.3175E-11	.2726E-01	.6008E-03	-.3366E-03	-.1825E-09
	2	-.2154E-01	.9374E-05	-.1246E-03	.3024E-10	-.2035E-10	.5105E-08
	3	.1232E-10	.3340E-14	.6564E-01	.4703E-03	.1067E-01	-.3758E-13
	4	.7014E+00	.1744E-07	-.2820E-03	-.6944E-11	.5513E-11	-.1911E-07
	5	-.4728E-09	-.1430E-11	-.7160E+00	-.1764E-02	.1854E-02	.1900E-11
	6	-.1004E+00	-.3269E-07	-.2504E-01	-.7432E-10	.1250E-10	.4712E-08
	7	-.8501E-09	.1035E-10	-.4928E-01	-.4066E-02	.7878E-03	-.1524E-10
	8	-.4739E+00	.1716E-01	-.1623E-10	-.1245E-12	.2002E-13	-.5196E-07
	9	.2144E-10	.8599E-11	.6763E+00	-.9154E-03	.7725E-03	.6725E-12

	10	-.90751-01	.70101-01	.70113-11	.72405-12	.72703-14	.10788-01
8	1	-.13772-08	-.78011-11	.41815-02	.29707-03	-.29726-03	-.96319-10
	2	-.41933-02	.87350-05	.25284-09	-.17363-10	-.17976-10	.30252-03
	3	.11754-10	.73408-13	.73631-01	.45175-03	-.93830-02	-.56954-17
	4	.58759+00	.15304-07	-.24182-03	-.11150-10	.57521-11	-.29513-02
	5	-.57775-09	-.11378-11	-.61434+02	-.76833-02	.14013-07	.71550-11
	6	.33442+00	-.23516-02	.41832-03	-.32464-10	.21793-10	.40189-07
	7	-.15041-08	.31407-11	.25036+00	-.49017-07	.59053-01	-.14716-10
	8	-.58243+00	.15706-01	.18447-10	.25065-17	.17586-13	.21420-02
	9	.57219-10	.72715-11	.71166+00	-.15663-03	.68725-03	.60567-12
	10	.30048+00	.60137-01	-.39794-11	.25467-12	.28081-14	.90419-02
7	1	-.17768-03	-.24265-11	-.52046-02	.15197-07	-.25702-03	-.49177-10
	2	.56451-02	.70214-05	-.37066-09	.91591-11	-.15996-10	.15486-03
	3	.37196-11	.25556-13	.18726-01	.34270-03	.81411-02	-.51974-13
	4	.34452+00	.13467-07	-.12771-03	-.13451-10	.49033-11	-.33706-02
	5	-.27100-09	-.98509-12	-.42851+00	-.15410-02	.12772-02	-.23753-11
	6	.50275+00	-.24778-07	.75513-03	-.74725-10	.99860-11	.40634-07
	7	-.19037-03	.73371-11	.41407+00	-.45047-07	.50708-01	-.12033-10
	8	-.48772+00	.13209-01	-.14194-10	.16414-12	.15345-13	.66429-07
	9	.31461-10	.66502-11	-.54754+00	.63119-07	-.59196-01	.62220-13
	10	.62069+00	.54072-01	-.12746-10	.12869-12	.75058-14	.24151-07
6	1	-.71866-03	-.20697-11	-.97942-02	.65617-04	-.21858-03	-.21136-10
	2	.10769-01	.64494-05	-.59216-09	.59816-11	-.13717-10	.66397-04
	3	.59744-11	-.71079-13	.79674-02	-.23194-03	.58993-02	-.51364-13
	4	.30934+00	-.11229-02	-.13341-03	-.11191-10	.42295-11	-.27169-02
	5	-.13699-02	-.34429-12	-.34944+00	-.28438-02	.10745-02	.20820-11
	6	.85731+00	-.20396-07	.10636-07	-.87219-10	.33771-11	.36019-02
	7	-.21760-03	.67121-11	.65711+00	-.41734-07	.51383-01	-.11457-10
	8	-.17772+00	.11595-01	.57666-11	.75709-12	.13005-13	.97619-02
	9	.54347-10	.56177-11	.20687+00	.91457-02	.50186-03	-.77609-12
	10	.56134+00	.45921-01	-.14041-10	-.68405-13	.21236-14	-.51401-02
5	1	-.17456-03	-.16416-11	-.11514-01	.32797-05	-.17886-03	-.26109-11
	2	.21749-01	.51555-05	-.69729-09	.50864-12	-.10573-10	.32004-05
	3	.18029-11	.17307-13	-.44643-02	.11377-07	.45194-02	-.35380-13
	4	.19772+00	.89988-01	-.18409-03	-.75404-11	.37836-11	-.16523-02
	5	-.10655-10	-.66757-12	-.29654+00	-.19159-02	.85559-01	.13257-11
	6	.41347+00	-.16731-07	.13381-07	-.40449-10	.67017-11	.21057-02
	7	-.47720-03	.53709-11	.87053-05	-.24200-07	.41090-03	-.66458-11
	8	.25505+00	.92860-02	-.41696-11	.21729-12	.10406-13	.78179-02
	9	.65034-11	.66642-11	-.25544+00	.81021-07	-.40133-03	-.12172-11
	10	.37135+00	.36847-01	-.84056-11	-.23164-12	.15939-14	-.99790-02
4	1	-.51023-09	-.12112-11	-.10731-01	-.77400-04	-.17115-01	.11362-10
	2	.11000-01	-.38028-05	-.81284-09	-.42024-11	-.79299-11	-.37256-04
	3	.24722-11	.12057-13	-.77805-02	.27166-04	.41396-02	-.24527-13
	4	.12643+00	.67393-01	-.50763-03	-.99710-11	.21377-11	-.12776-02
	5	-.50717-10	-.50076-12	-.14804+00	-.13274-02	.64509-01	.79604-12
	6	.40235+00	-.12506-07	.14044-07	.15470-10	-.50263-11	-.11686-02
	7	-.77781-03	.48246-11	-.40116+00	.92971-07	.36916-01	.35804-11
	8	.51040+00	-.59726-07	-.14717-10	-.10784-12	.78029-14	.14517-02
	9	-.55131-10	.35699-11	-.54644+00	.91601-02	-.35079-03	-.10743-11
	10	-.40677+00	.27699-01	.56187-11	-.23051-12	.17241-14	-.45029-02

17.9.18

3	1	-.25675-05	-.82076-17	-.42147-02	-.66402-08	-.37431-04	.27257-10
	2	.13782-07	.25780-05	-.49702-09	-.41409-11	-.52367-11	-.69364-04
	3	.14163-11	.85655-14	-.33573-04	-.79256-04	.27507-02	-.17357-11
	4	.77710-01	.44873-03	-.35770-09	-.42582-11	.15918-11	-.92757-07
	5	-.15852-10	-.33254-17	-.90334-01	-.10769-02	.87179-03	.40540-17
	6	.50781+00	-.84006-07	.11794-07	.79109-10	.73509-11	-.47777-02
	7	-.22726-09	.26600-11	.71993+00	.49504-07	.20545-03	.15022-10
	8	.50471+00	.44466-07	-.15756-10	-.45994-13	.52013-14	-.20878-02
	9	-.43905-10	.24511-11	-.66766+00	-.17753-02	.20086-04	-.72356-13
	10	-.50477+00	.13417+01	.13000-10	-.58174-13	.4943-15	-.18237-02
2	1	-.18737-09	-.41629-12	-.44165-02	-.37712-04	-.41715-04	.25479-10
	2	.45530-07	.12090-05	-.28717-01	-.53087-11	-.20433-11	-.83469-04
	3	.55213-12	.45290-14	-.43660-02	-.81502-04	.13799-02	-.14545-13
	4	.37737-05	-.24683-03	-.17610-09	-.15087-11	.34782-12	-.74249-04
	5	-.50770-11	-.14075-13	-.47214-01	-.97349-03	.21490-03	.16173-12
	6	.19891+00	-.82009-05	.66877-04	.12775-09	.10754+11	-.75501-02
	7	-.13512-08	.13452-11	.41050+00	.73063-02	.10773-03	.24079-11
	8	.77590+00	.24256-07	-.26163-10	-.17744-12	.37009-14	-.66651-07
	9	-.60712-10	.11729-11	-.39194+00	-.66947-07	.10033-03	.05703-12
	10	-.42340+00	.92575-07	.10407-10	.15521-12	-.42472+15	.85151-07
1	1	.00000	.00000	.00000	-.94193-04	.00000	.30563-10
	2	.00000	.00000	.00000	-.56358-11	.00000	-.95053-04
	3	.00000	.00000	.00000	-.85053-04	.00000	-.12219-11
	4	.00000	.00000	.00000	-.34263-11	.00000	-.63475-07
	5	.00000	.00000	.00000	-.80563-03	.00000	.27196-11
	6	.00000	.00000	.00000	.14931-03	.00000	-.85251-07
	7	.00000	.00000	.00000	-.39056-07	.00000	.27373-10
	8	.00000	.00000	.00000	-.72306-12	.00000	-.24454-07
	9	.00000	.00000	.00000	-.22254-07	.00000	.19173-11
	10	.00000	.00000	.00000	.25075-12	.00000	-.24743-07

(16)

SOLUTION TIME LOG

SECONDS - 12.97
POINTS - 1.55

OVERALL TIME LOG

MODAL POINT INPUT	= .58
ELEMENT STIFFNESS FORMATION	= 2.67
MODAL LOAD INPUT	= .15
TOTAL STIFFNESS FORMATION	= 1.07
STATIC ANALYSIS	= .00
EIGENVALUE EXTRACTION	= 14.53
FORCED RESPONSE ANALYSIS	= .00
RESPONSE SPECTRUM ANALYSIS	= .00
TOTAL SOLUTION TIME	= 19.03

$FIN

RUNID: 26327 ACCT: 78152 USER: LW 323518
LOAD 022269 ORZ TAPE -1 78127
TIMES: TOTAL CPU: 12.60 s COST: $7.49
CPU: 00:00:14.04 I/O: 00:00:16.11
SRVCE: 00:00:22.43 WAIT: 00:00:00.71
RUN USED: $ 0.00 RUN REMAINING: $ 250.19
THE ABOVE DOLLAR CHARGES FOR THIS RUN ARE ADDITIONAL
THE ACTUAL COST WILL BE REFLECTED ON YOUR MONTHLY INVOICE.
TAPES READ: 02 PRINTS: 19
START: 10:59:00 MAY 24,1978 FINI: 11:05:33 MAY 24,1978

(12)

DIVISION DE EDUCACION CONTINUA
FACULTAD DE INGENIERIA U.N.A.M.

EL METODO DEL ELEMENTO FINITO EN LA INGENIERIA MECANICA

APLICACIONES AVANZADAS

DR. NICHOLAS JOHN SALAMON

ABRIL, 1982

from: M.J. Salamon, F.F. Mahmoud, "An Elastoplastic Laminated Finite Element", Developments in Mechanics, Vol. 11, Proc. of the 17th Midwestern Mechanics Conference, U. of Michigan, Ann Arbor, 6-8 May 1981, co-Chair: A.S. Wineman, S.K. Clark.

REFERENCES

1 Jones, Robert M., Mechanics of Composite Materials, McGraw-Hill, New York, 1975.

2 Hill, R., The Mathematical Theory of Plasticity, Oxford University Press, London, 1950.

3 Marcal, P. V. and King, I. P., "Elastic-Plastic Analysis of Two-Dimensional Stress Systems by the Finite Element Method," International Journal of the Mechanical Sciences, Vol. 9, 1967, pp. 143-155.

4 Zienkiewicz, O. C., The Finite Element Method in Engineering Science, McGraw-Hill, New York, 1971.

5 Theocaris, P. S. and Marketos, E., "Elastic-Plastic Analysis of Perforated Thin Strips of a Strain-Hardening Material," Journal of the Mechanics and Physics of Solids, Vol. 12, 1964.

6 Bhateja, Sudershan K. and Alfrey, Turner Jr., "Mechanical Interactions in Laminated Sheets - I," Journal Composite Materials, Vol. 14, January 1980, pp. 42-53.

For a three-dimensional code, see:

"Finite Element Analysis of Elastic-plastic Fibrous Composite Structures", Computers and Structures, vol. 13, pp. 321-330, 1981, by Y. A. Bahei-El-Din, G. J. Dvorak and S. Utku.

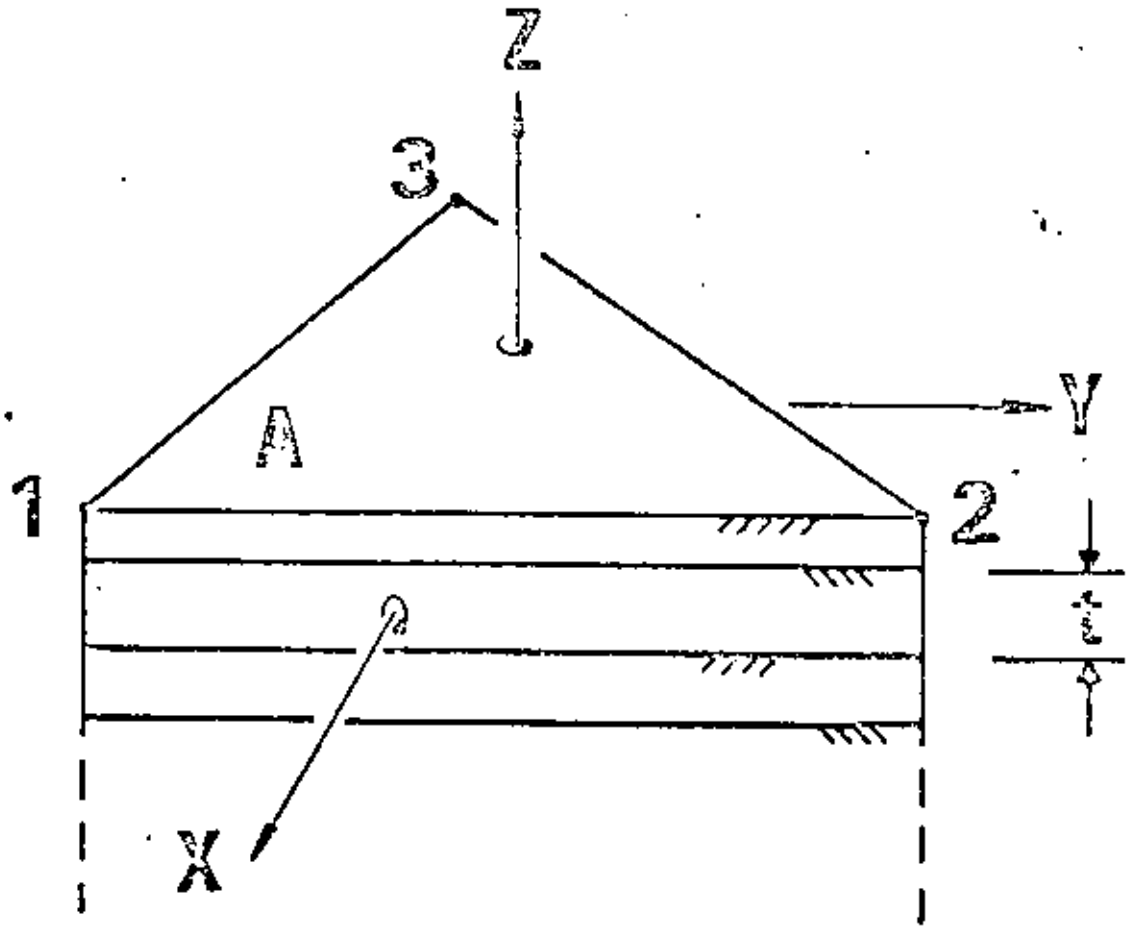

SALAMON - MAHMOUD, 1981

p. 2 of 9

INCREMENTAL STRESS / STRAIN

$$\{\Delta\varepsilon_x^p, \Delta\varepsilon_y^p, \Delta\varepsilon_{xy}^p\}^T = [C]_p \{\Delta\sigma_x, \Delta\sigma_y, \Delta\sigma_{xy}\}^T$$

WHERE PRANDTL-REUSS $\Rightarrow$

$$[C]_p = \frac{1}{H'\sigma_e^2}\begin{bmatrix} (\sigma_x - \frac{\sigma_y}{2})^2 & (\sigma_x - \frac{\sigma_y}{2})(\sigma_y - \frac{\sigma_x}{2}) & 3\sigma_{xy}(\sigma_x - \frac{\sigma_y}{2}) \\ & (\sigma_y - \frac{\sigma_x}{2})^2 & 3\sigma_{xy}(\sigma_y - \frac{\sigma_x}{2}) \\ (SYM) & & 3\sigma_{xy}^2 \end{bmatrix}$$

WITH

$$\sigma_e = \left[\sigma_x^2 + \sigma_y^2 - \sigma_x\sigma_y + 3\sigma_{xy}^2\right]^{1/2}$$

H' = Slope σ_e vs $\varepsilon_e^{(p)}$ in a tension test.

THE FINITE ELEMENT

$$\left\{\Delta\varepsilon_x, \Delta\varepsilon_y, \Delta\varepsilon_{xy}\right\}^T = [B]\{\Delta d\}$$

$$[k] = \int_V [B]^T [D][B]\, dV$$

$$= A[B]^T \left\{\sum_{\text{LAYERS}} t\,[D]\right\}[B]$$

WHERE

$$[D] = \left\{[C]_{el} + [C]_p\right\}^{-1}$$

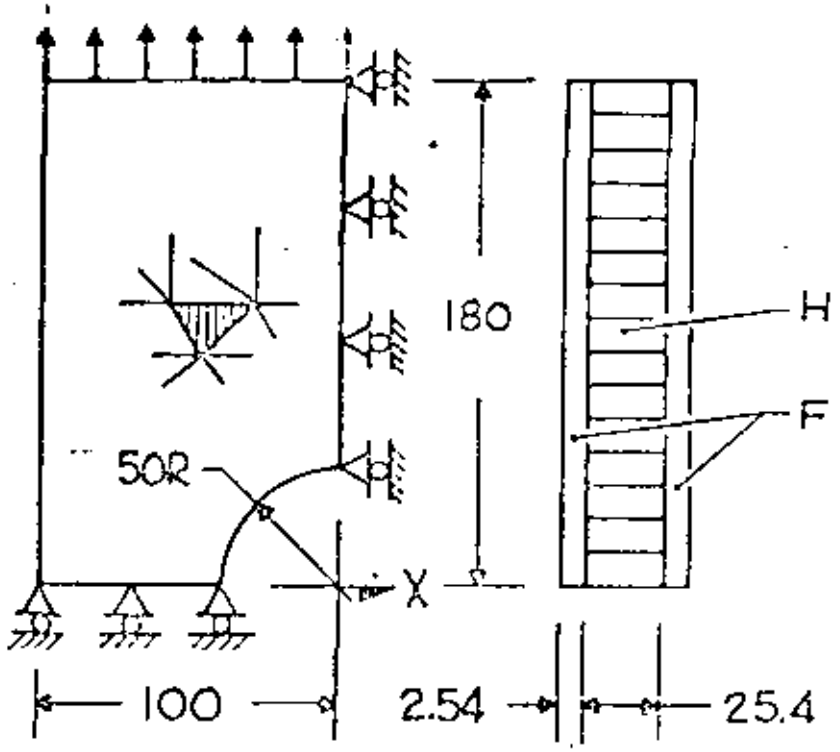

a. PERFORATED STRIP

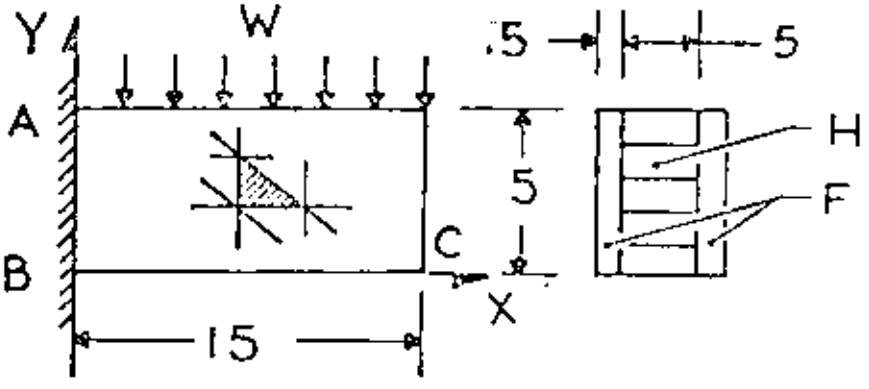

b. CANTILEVER BEAM

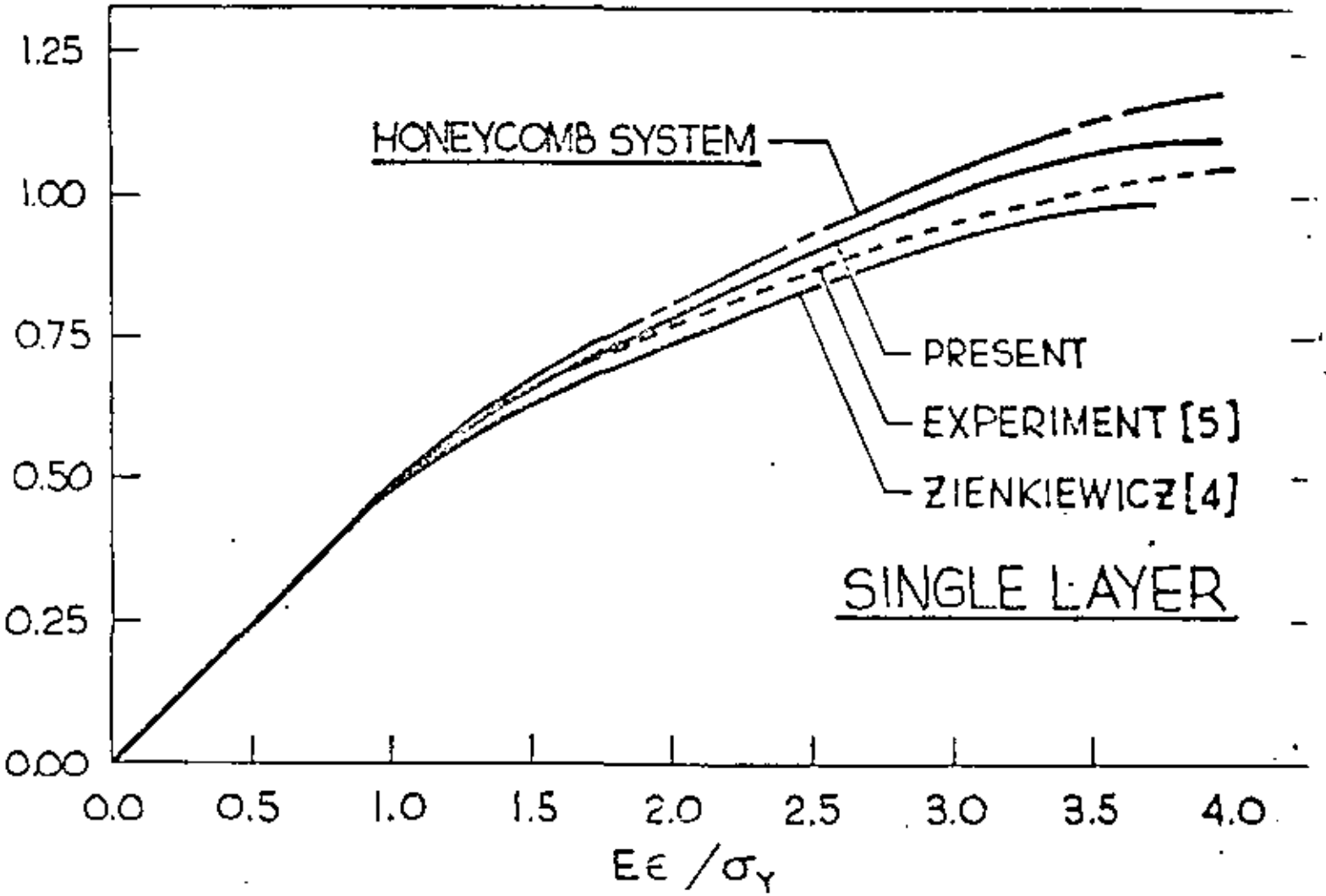
HONEYCOMB SYSTEM
PRESENT
EXPERIMENT [5]
ZIENKIEWICZ [4]
SINGLE LAYER
1.25
1.00
0.75
0.50
0.25
0.00
0.0
0.5
1.0
1.5
2.0
2.5
3.0
3.5
4.0
Eε /σY

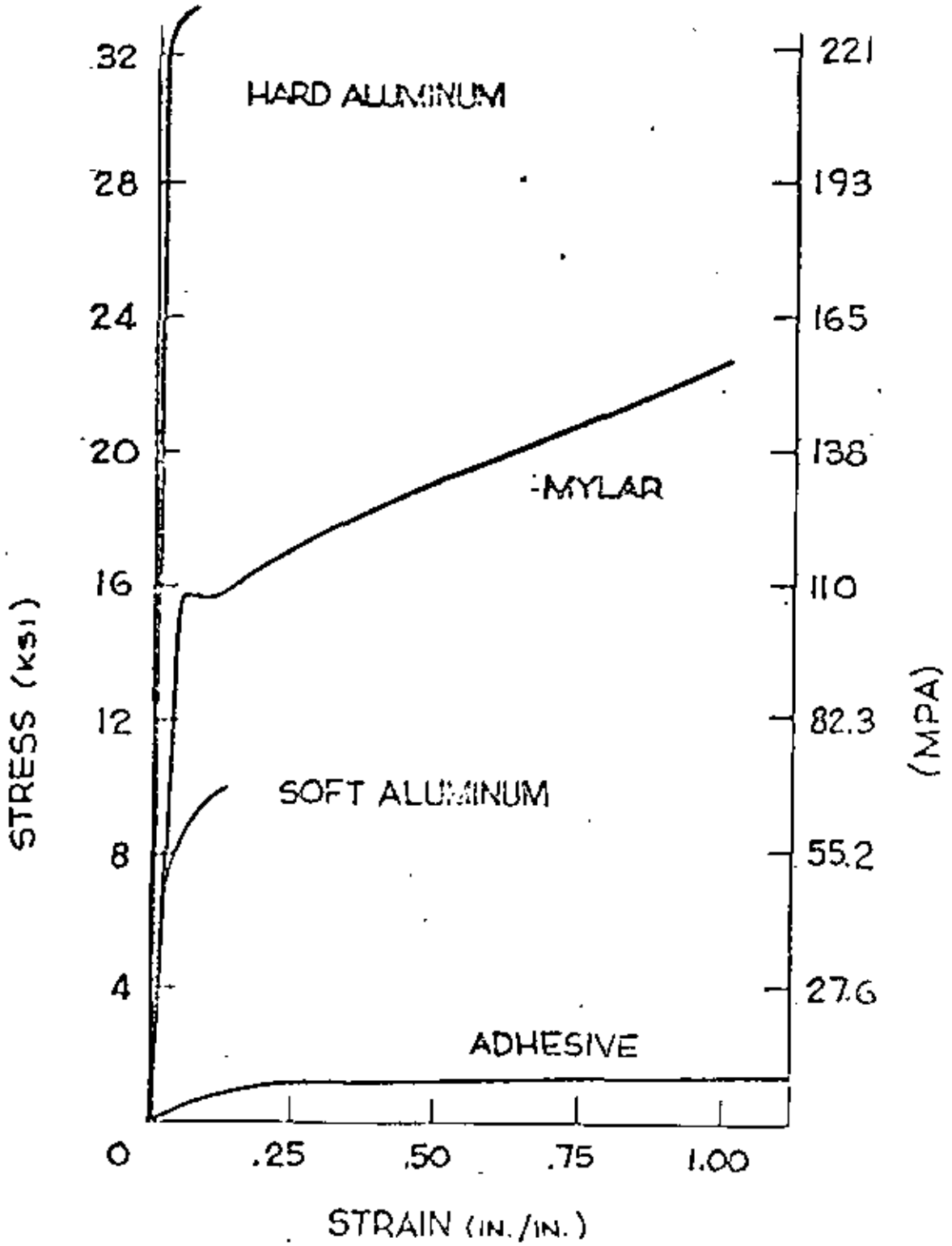
32
28
24
20
16
12
8
4
0
221
193
165
138
110
82.3
55.2
27.6
(MPA)
STRESS (KSI)
HARD ALUMINUM
MYLAR
SOFT ALUMINUM
ADHESIVE
.25
.50
.75
1.00
STRAIN (IN./IN.)

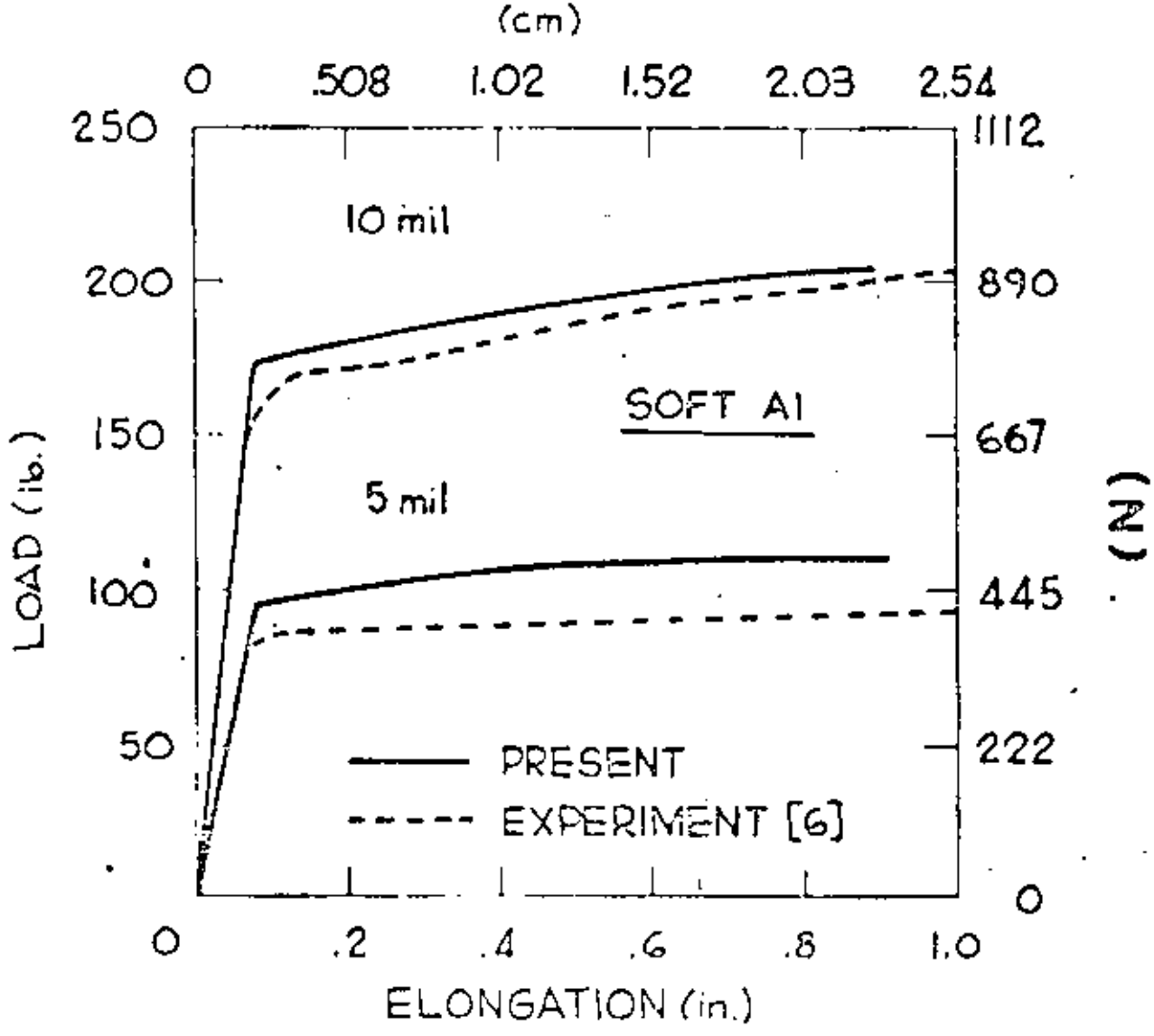
(cm)
0
.508
1.02
1.52
2.03
2.54
250
200
150
100
50
1112
890
667
445
222
0
10 mil
5 mil
SOFT Al
PRESENT
EXPERIMENT [6]
LOAD (lb.)
(N)
0
.2
.4
.6
.8
1.0
ELONGATION (in.)

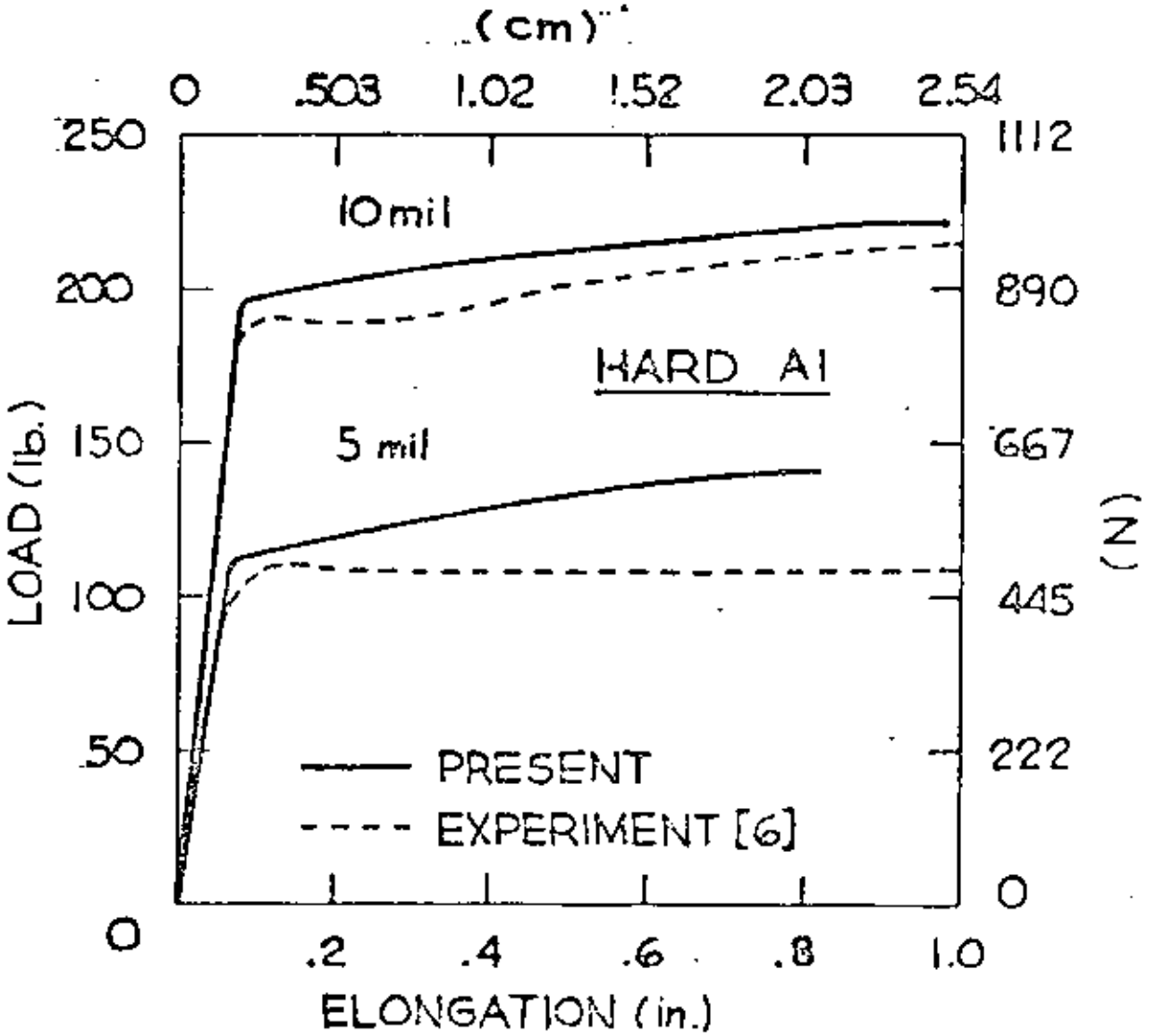
(cm)
0
.503
1.02
1.52
2.03
2.54
250
200
150
100
50
0
1112
890
667
445
222
0
10 mil
5 mil
HARD Al
PRESENT
EXPERIMENT [6]
LOAD (lb.)
(N)
.2
.4
.6
.8
1.0
ELONGATION (in.)

A MODIFIED CONJUGATE GRADIENT METHOD FOR FRICTIONLESS CONTACT PROBLEMS

W. R. Marks
Rexnord Inc., Nordberg Machinery Group
Milwaukee, Wisconsin

N. J. Salamon
College of Engineering and Applied Science
University of Wisconsin Milwaukee
Milwaukee, Wisconsin

ABSTRACT

The solution of elastic bodies in contact through the application of a conjugate gradient technique integrated with a finite element computer code is discussed. This approach is general, easily applied and reasonably efficient. Furthermore the solution method is compatible with existing finite element computer programs and easily incorporated in them. The necessary algorithm for use of the technique is described in detail. Numerical examples for two-dimensional frictionless contact problems are presented. It is found that the extent of the contact region and the displacements and stresses throughout the contacting bodies can be economically computed with precision.

NOMENCLATURE

c	= contact halflength
CG	= abbreviation for conjugate gradient
$\underline{D}$	= vector of nodal displacements
F	= force dimension
$\underline{G}$	= vector of initial separations between interface node pairs prior to load application
[K]	= global stiffness matrix
L	= length dimension
N	= number of global degrees of freedom
NSREL	= number of steps to release, a convergence control parameter
$\underline{R}$	= vector of external nodal loads
s	= step size
$\underline{v}_c$	= conjugate gradient vector
$\underline{v}_s$	= negative of the simple gradient vector
Π	= potential energy of finite element system
σ	= stress

Superscripts denote iteration number, except for T which denotes the transpose of a vector. For iteration k, the quantities s^k, $\underline{v}_c^k$ and $\underline{v}_s^k$ are associated with the step to, not from, $\underline{D}^k$.

INTRODUCTION

The behavior of elastic bodies in contact is critical to the performance of a wide variety of machine elements including roller bearings, gears, and bolted joints. In engineering practice, the analysis of contact problems is usually accomplished through the use of a finite element computer program that incorporates an iterative process to satisfy the contact constraints. However, existing computer codes have certain disadvantages. One such code [1] requires the introduction of special interface elements which often have no physical basis. Another popular method [2,3,4] employs quadratic programming techniques which require considerable effort beyond that normally associated with routine finite element analysis. Much less common in practice is the formulation of the problem as an integral equation which can be solved numerically [5] or, for simple configurations, in closed form. A method best suited for general use by practicing engineers is certainly not agreed upon.

This paper presents an alternative method of solution which is general, easily applied, compatible with existing finite element programs and reasonably efficient. The formulation is based upon modification of a standard conjugate gradient technique [6,7,8] which performs an iterative minimization of potential energy whereby contact constraints are satisfied continuously during the solution process.

The text contains a review of the conjugate gradient (CG) technique for unconstrained linear elastic problems followed by a mathematical definition of the contact constraints and the specific modifications necessary to incorporate the constraints into the CG technique. Numerical examples for two-dimensional frictionless contact problems are presented and conclusions drawn. It is found that the extent of the contact region and the displacements and stresses throughout the contacting bodies can be economically computed with precision.

CONJUGATE GRADIENT METHOD FOR UNCONSTRAINED PROBLEMS

The equilibrium equations for linear elastic analysis by the direct stiffness method can be written in the usual matrix form as

$$[K]\underline{D} = \underline{R} \tag{1}$$

where [K] is the global stiffness matrix, $\underline{D}$ is the global displacement vector and $\underline{R}$ is the vector of external nodal loads. A necessary and sufficient condition for the existence of a unique solution to (1) is a proper specification of kinematic boundary conditions to prevent rigid body modes of displacement. Various texts, e.g. [9], show that these equations are a direct consequence of the principle of minimum potential energy which states that of all feasible displacement configurations, that which minimizes the system's potential energy Π is the equilibrium configuration. For linear elastic structures under external loads $\underline{R}$, the potential energy Π is

$$\Pi = \frac{1}{2}\underline{D}^T[K]\underline{D} - \underline{D}^T\underline{R} \tag{2}$$

The CG method is a convergent iterative scheme to minimize Π without directly solving (1). The algorithm consists of the following operations:

1. Calculate the negative simple gradient vector

$$\underline{V}_s^k = -[K]\underline{D}^{k-1} + \underline{R} \qquad (3)$$

for the k^{th} iteration. The initial $\underline{D}^0$ is usually taken as null.

2. Calculate the conjugate gradient vector

$$\underline{V}_c^k = \underline{V}_s^k + \alpha^k \underline{V}_c^{k-1} \qquad (4)$$

where

$$\alpha^k = \begin{cases} 0, & k = 1, \\ ||\underline{V}_s^k||^2 / ||\underline{V}_s^{k-1}||^2, & k > 1, \end{cases}$$

$$||\underline{V}_s^k||^2 = \sum_{i=1}^{N} (V_{si}^k)^2,$$

where N is the number of global degrees of freedom.

3. Calculate the optimal step size

$$s^k = \frac{\underline{V}_c^T \underline{R} - \underline{D}^T[K]\underline{V}_c}{\underline{V}_c^T[K]\underline{V}_c} \qquad (5)$$

where $\underline{V}_c = \underline{V}_c^k$ and $\underline{D} = \underline{D}^{k-1}$.

4. Determine the end-of-iteration displacement configuration

$$\underline{D}^k = \underline{D}^{k-1} + s^k \underline{V}_c^k . \qquad (6)$$

5. Apply a convergence criterion, such as a sufficiently small percentage decrease in Π, equation (2), to test for termination. Should convergence be unsatisfactory, go to step 1 and continue.

While the above process is straightforward, the operations in steps 1 and 5 should not be accomplished by the direct matrix multiplications indicated in (3) and (2) to determine $\underline{V}_s$ and Π, respectively. Instead, the product $[K]\underline{D}$ required in (2) and (3) is computed more efficiently by accumulating it through consecutive summations than by computing it through direct matrix multiplication. Specifically, the product $[K]\underline{V}_c$ obtained and used in (5) is reused in conjunction with (6) to compute $[K]\underline{D}$ as follows:

$$\Delta\underline{D}^k = \underline{D}^k - \underline{D}^{k-1} = s^k \underline{V}_c^k , \qquad (7)$$

then

$$[K]\Delta\underline{D}^k = s^k [K]\underline{V}_c^k$$

so that for $k \geq 1$,

$$[K]\underline{D}^k = [K]\underline{D}^0 + \sum_{m=1}^{k} s^m [K]\underline{V}_c^m . \qquad (8)$$

Thus even the product $[K]\underline{D}^0$ need not be computed if $\underline{D}^0$ is null.

In the computerized implementation of the CG algorithm, most of the central processor time is spent on the one multiplication per iteration involving $[K]$. Conventional band format storage can be used to advantage in conjunction with a compatible multiplication subroutine for computing the $[K]\underline{V}_c$ product.

While some investigators claim advantages in using the CG technique on unconstrained linear problems, the writers' experience [10] indicates that it is inefficient as compared to Gauss elimination for this application.

CONTACT CONSTRAINTS

The preceding analysis places no constraints on the active degrees of freedom so that the solution state determining the equilibrium configuration is that which produces a stationary value in the potential energy Π. In contrast, the condition of frictionless contact does impose constraints upon the active degrees of freedom in that two adjacent surfaces may not interpenetrate. No constraints apply to tangential displacements due to the assumed absence of friction.

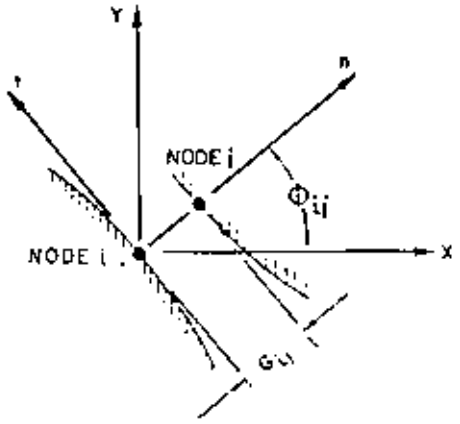

Fig. 1 Interface conventions and coordinate systems: global X, Y and local n, t

In the present analysis, the discretized finite-element model within the linear theory of elasticity requires the establishment of contact node pairs in close proximity directly across all interfaces of potential contact. The variables and coordinate systems used for two-dimensional contact surfaces are illustrated in Fig. 1 where G_{ij} is the initial separation between nodes i and j in the unloaded state. The contact constraint at each node pair requires that

$$D_{in} - D_{jn} \leq G_{ij} \qquad (9)$$

where n denotes a direction approximately normal to the two surfaces. Should contact occur at any node pairs in the loaded state, then internal force reactions exist only at these discrete locations.

Nodal Consolidation at Contacting Surfaces

Consider the nodes i,j of a contact node pair which are presently joined and which are to remain in contact during an iteration. It is apparent from equations (1) and (3) that the negative simple gradient components associated with each node i,j may be viewed as unbalanced nodal forces for an arbitrary displacement configuration. The resultant unbalanced force in the approximate normal direction n for the consolidated node pair is the sum of the component forces as calculated by equation (3) for nodes i and j separately. The equal and opposite contributions from the internal contact forces of course cancel. Consequently in the normal direction, the negative simple gradient resultant $V_{s\,ij\,n}$ is the sum of the negative simple gradient components, specifically

$$V_{sijn} = V_{sin} + V_{sjn} \quad (10)$$

By applying (10) the finite element problem has in effect been changed from a problem with two degrees of freedom in the normal direction at the contact node pair to a problem with one degree of freedom in the normal direction for the joined nodes. Note that in forming the conjugate gradient vector by (4), the summation for $||\underline{V}_s^k||^2$ must only include the single consolidated gradient component V_{sijn}, not V_{sin} and V_{sjn}.

This process is similar to the gradient projection method. It can be shown that for the constraints under consideration, the gradient projection method as applied to the simple negative gradient components yields the following result at contacting node pairs:

$$V'_{sin} = V'_{sjn} = (V_{sin} + V_{sjn})/2$$

where the prime denotes the projected value. If the gradient components are again viewed as unbalanced forces, the two equal, but distinct components V'_{sin} and V'_{sjn} may be summed and equation (10) is recovered.

Special attention is required for contact involving nodes with deleted degrees of freedom. Should contact be maintained at a node pair for which normal direction displacement of either node is prevented by boundary condition specifications, then $V_{sijn} = V_{cijn} = 0$. Any other value would result in displacement of both nodes as required by equation (6).

Making and Breaking Contact

The optimal step size s as given by (5) may cause the displacement vector $\underline{D}$ to leave the set of feasible solutions which means interpenetration of the contacting surfaces will result. In order to prevent this, the CG algorithm for contact problems must minimize Π in the direction of $\underline{V}_c$ by selecting as the step size the smaller of 1) the optimal step size as calculated by equation (5) in which constraints are ignored, or 2) the minimum positive step size to activate any constraint not presently active. Equating the change in displacement at each node pair to the present interface separation, the step size required to close node pair i,j is

$$s_{ij}^k = \frac{G_{ij} - D_{in}^{k-1} + D_{jn}^{k-1}}{V_{cin}^k - V_{cjn}^k} \quad (11)$$

Should the above condition determine the step size, a new node pair will come into contact. Thus for the new configuration, the algorithm must be restarted from equation (3) with $k = 1$ and $\alpha^k = 0$ in equation (4).

During an iteration, it is assumed that all contact node pairs currently joined may possibly release. Should release occur at previously joined nodes, the current model is changed as a previously dependent degree of freedom becomes independent. Again, the new contact status dictates restarting the algorithm as the energy minimization continues on the modified structure. In the subsequent iteration with $k = 1$ in (4), the step direction $\underline{V}_c$ would be the negative simple gradient $\underline{V}_s$. According to (7), joined nodes tend to separate during a step if $V_{sin} < V_{sjn}$. This condition could be considered for a release criterion. However experience has shown that convergence is accelerated if release of contacting nodes is retarded until a specified small number of consecutive iterations NSREL are performed for which $V_{sin} < V_{sjn}$. This device insures a strong tendency to separate and avoids very small nonoptimal steps in an oscillating contact-release-contact cycle.

MODIFIED CONJUGATE GRADIENT ALGORITHM

Once the global stiffness matrix and vector of nodal loads are calculated, the equilibrium configuration for the contact problem may be found as follows:

1. Assume a starting vector of nodal displacements.
2. Calculate $\underline{V}_s$ by equation (3).
3. For all nonrotational degrees of freedom associated with contact node pairs, transform the components of $\underline{D}$ and $\underline{V}_s$ from the global coordinate system to a normal-tangential system.
4. Test for possible separation at all contacting node pairs. Is $V_{sin} < V_{sjn}$ for NSREL iterations?
5. For node pairs remaining in contact, consolidate the negative simple gradient components by equation (10) unless either node is fixed in the normal direction by boundary conditions, in which case V_{sijn} is zero.
6. Apply equation (4) to find the conjugate gradient vector for the remaining independent degrees of freedom. Set iteration number k to 1 if during the last iteration new contact was established or if separation occurs between previously contacting nodes on this iteration.
7. Calculate the minimum positive step size to create contact at any node pair presently open. See equation (11).
8. Transform $\underline{V}_c$ and $\underline{D}$ components of contact node pairs back to the global coordinate system.
9. Calculate the unconstrained optimal step size. See equation (5).
10. Select the smaller of the step sizes calculated in operations 7 and 9.
11. Perform the step to the new displacement vector according to equation (6).
12. Apply equation (8) to find the updated $[K]\underline{D}$ product. The required $[K]\underline{V}_c$ product was calculated to find the optimal step size in operation 9.
13. Using the $[K]\underline{D}$ product found in operation 12, calculate $\underline{V}_s$ for the new displacement vector by equation (3). The updated $\underline{V}_s$ is for use in the next iteration.
14. Calculate Π by equation (2) and test for convergence and termination. An effective criterion is a sufficiently small decimal percentage change in Π on an optimal step for which $V_{sin} > V_{sjn}$ at all presently joined node pairs following an iteration that involved no change in contact status.
15. Go to operation 3 and continue.

NUMERICAL EXAMPLES

The modified conjugate gradient algorithm is incorporated in the Fortran program CONTACT which is listed in [10]. The program has been tested by solving several problems having known exact solutions. Besides the examples included here, the program has also been applied to two-dimensional structural trusses supported by misaligned foundations. The physical parameters and computed results for the examples below are correct for any consistent set of units. Since the choice of units is not relevant to the matter at hand, specific units are not indicated in the figures. However the units of pounds and

inches make these problems physically realistic.

Example 1. Beam On An Elastic Foundation

The beam on an elastic Winkler-type foundation is loaded by a concentrated force as shown in Fig. 2. Because of symmetry, only half of the problem is modeled. The foundation modulus is 5000 (F/L^3). The elastic modulus of the beam is 30×10^6 (F/L^2) and its linear dimensions (L) are: total length, 30, height, 1.0, and width, 3. The finite element model includes fifteen beam spans of length 1.0 (L) each and corresponding discrete springs of stiffness 15,000 (F/L), except at the plane of symmetry where the support spring stiffness is 7500 (F/L). While the initial gap G_{ij} between the beam and the foundation is arbitrary, a value of zero was chosen.

The computed results are compared with the exact solution [11] in Table 1. The numerical results are well corroborated by the exact mathematical solution.

Example 2. Two Cylinders In Contact

Two cylinders of equal radii are pressed together by line-forces directed along a line of centers. Taking advantage of symmetry, this Hertzian problem can be viewed as one cylinder pressed onto a rigid half-space. Furthermore, the entire cylinder need not be modeled. The configuration is illustrated in Fig. 3 with the modeled portion of the cylinder shown shaded. The modulus of elasticity and Poisson's ratio of the cylinder are 1.0×10^6 (F/L^2) and 0.25, respectively.

The numerical results agree nicely with the analytical solution. The calculated half length of contact was .2193 (L), yielding a 0.37% error in comparison with the exact Hertzian solution [12]. The stresses along the plane of loading are shown in Fig.

Aside from the stepped appearance of the numerical solution resulting from the use of simple plane strain triangles, the correlation with the exact solution

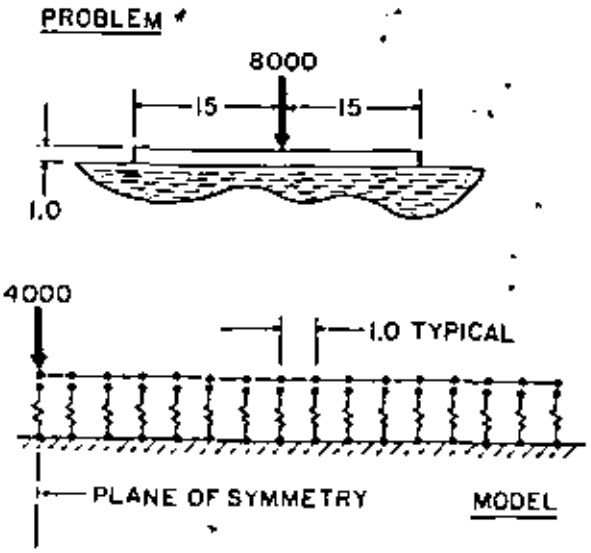

Fig. 2 Beam on elastic foundation problem and finite element model

	Exact	Numerical	% Error
Half length of contact	10.505	10.493*	0.11
Stress at load point	29170	29070	0.34
Displacement at load point	0.04348	0.04348	0.00

*Interpolated

Table 1 Results for the beam on an elastic foundation problem

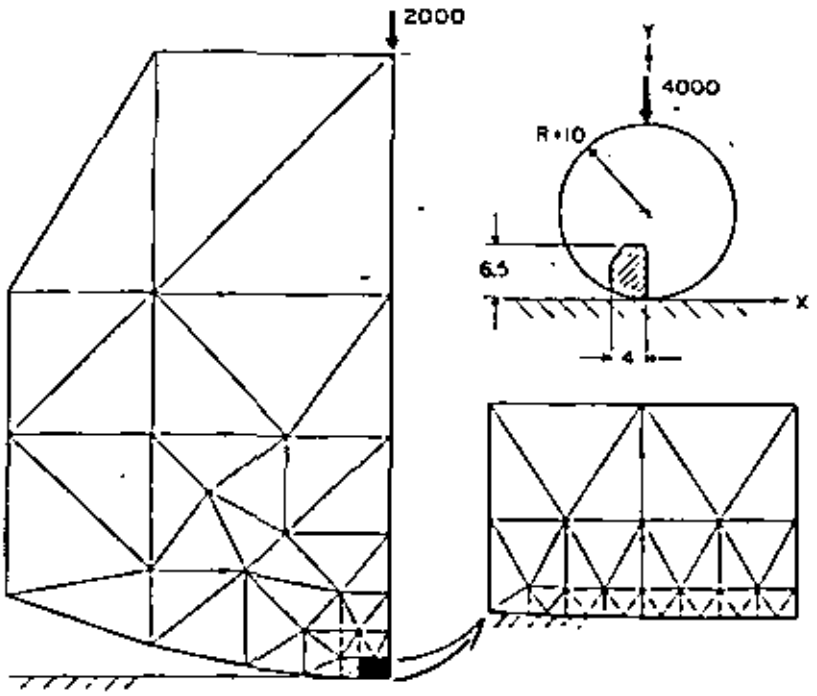

Fig. 3 Cylinder-plane contact problem and finite element model

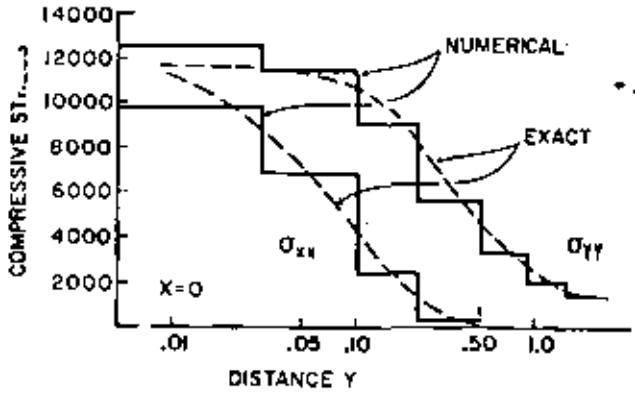

Fig. 4 Stress distribution along line of loading for cylinder-plane problem

is good. In Fig. 5 the normalized pressure distribution between the cylinders is plotted together with the exact solution. A close comparison is apparent.

Example 3. Rigid Punch On An Elastic Half-plane

A rigid punch is pressed without rotation into an elastic half-plane as shown in Fig. 6. The curved contour of the punch face is described by the equation $Y = 0.05\ X^4$ which makes this problem non-Hertzian. Rather than loading the punch in the finite element model, symmetry is utilized and a sufficiently large portion of the quarter-plane is loaded from below and pressed onto half of the rigid punch which is held fixed. The actual region modeled is shown shaded in Fig. 6. The elastic properties for the half-plane are the same as those in example 2.

The numerical results are in good agreement with theory of elasticity solution; the latter are easily derived from a general result given in [1]. The exact half-length of contact is found to be 0.6990 (L) while the computed value after internode interpolation is 0.6989 (L). Incredibly the error is nil. The normalized pressure distribution under the punch, also shown in Fig. 5, is seen to closely follow the exact distribution.

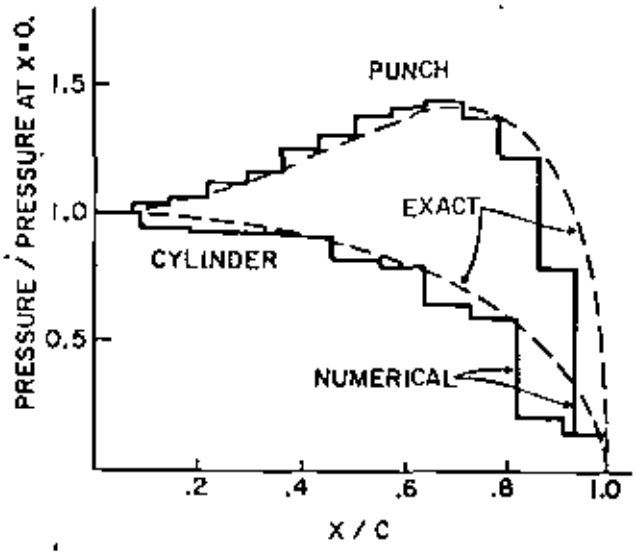

Fig. 5 Pressure in the region of contact

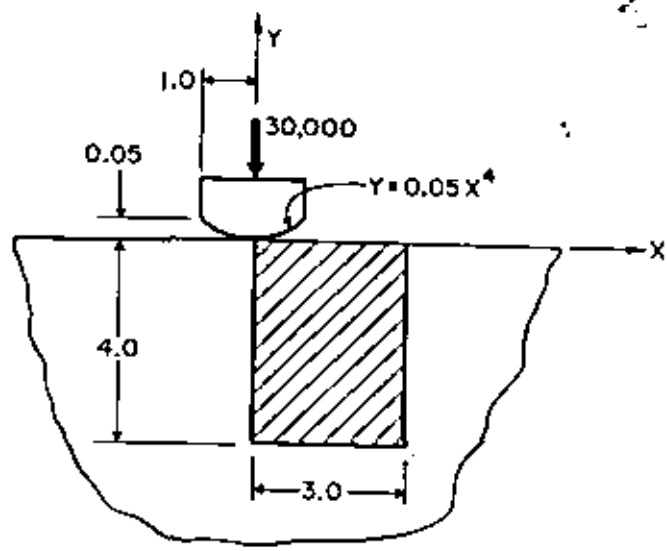

Fig. 6 Rigid punch on an elastic half-plane

Computation Details

Certain parameters useful in evaluating the efficiency of the program are given in Table 2. It is noted that despite the use of fewer degrees of freedom for the beam problem than for the other problems, the total number of iterations necessary to achieve convergence is higher. This may be attributed to a large difference in stiffness between the beam and spring elements which tends to ill-condition the global stiffness matrix. Nevertheless, the solution times for computer computation of all problems are reasonable.

Table 2 Computation details (CDC-175 computer)

	Beam	Cylinder	Punch
C.P. seconds for minimization	0.781	3.042	13.660
C.P. seconds for total job	0.994	1.740	15.209
Number of degrees of freedom	47	106	226
Stiffness matrix bandwidth	5	23	42
NSREL	9	9	9
Number of iterations	197	119	148
Contact node pairs; total	16	16	21
number in contact	11	11	14

CONCLUSION

The solution technique for frictionless static contact problems presented in this paper has been demonstrated to be accurate and reliably convergent. While extensive benchmarking against other solution techniques would be required to evaluate the relative efficiency of the modified conjugate gradient method, reasonably small amounts of central processor time have been required for the iterative minimization of potential energy in the numerical examples of this paper.

The modified conjugate gradient method is distinguished by its simplicity and compatibility with conventional finite element programs. In particular, the 'minimization' coding can be easily appended as a subroutine to any program which is based upon the

stiffness method to enable the solution of contact problems. This enhancement requires little additional computer storage. The extra subroutine would be used to solve for the equilibrium displacements of contact problems while a linear algebraic equation solver would remain for linear static problems.

Certain disadvantages inherent in other solution techniques are absent in the modified conjugate gradient method. For example, one popular technique utilizes bilinear elements with finite stiffness that often have no physical basis in the contact of elastic bodies. Another method requires the creation of a flexibility matrix, the introduction of additional unknowns including rigid body approaches and slack variables, and the solution of a modified linear programming problem.

Implemented in a comprehensive finite element program for static analysis of linear structures, the modified conjugate gradient method should provide an effective means for analyzing cams, gears, roller bearings, etc. The capability for substructuring found in many programs would improve solution economy by reducing the problem size during the iterative process.

ACKNOWLEDGEMENTS

The authors gratefully acknowledge the support of the Nordberg Machinery Group of Rexnord Inc. and the University of Wisconsin-Milwaukee.

REFERENCES

1 DeSalvo, G.J. and Swanson, J.A., "ASSYS Engineering Analysis System User's Manual," Rev. 3, Swanson Analysis Systems, Inc., Houston, PA, 1978.

2 Conry, T.F. and Seireg, A., "A Mathematical Programming Method for Design of Elastic Bodies in Contact," ASME Applied Mechanics Division Paper 70-WA/APM-52, Winter Annual Meeting, New York, N.Y., Dec. 1970.

3 Chand, R., Haug, E.J., and Rim, K., "Analysis of Unbonded Contact Problems by Means of Quadratic Programming," Journal of Optimization Theory and Applications, Vol. 20, No. 2, Oct. 1976, pp. 171-189.

4 Kalker, J.J. and Van Randen, Y., "A Minimum Principle for Frictionless Elastic Contact with Application to Non-Hertzian Half Space Contact Problems," Journal of Engineering Mathematics, Vol. 6, No. 2, 1972, pp. 193-206.

5 Paul, B. and Hashemi, J., "An Improved Numerical Method and Computer Program for Conforming Contact Stress Problems," In "Computational Techniques for Interface Problems" presented at The Winter Annual Meeting of the ASME, San Francisco, California, 10-15 Dec. 1978, Park, K.C. and Gartling, D.K., eds., The ASME, New York, 1978.

6 Wismer, D.A. and Chattergy, R., Introduction to Nonlinear Optimization: A Problem Solving Approach, Elsevier North-Holland, New York, 1978.

7 Fried, I. and Metzler, J., SOR vs. Conjugate Gradients in a Finite Element Discretization," International Journal for Numerical Methods in Engineering, Vol. 12, 1978, pp. 1329-1342.

8 Ko, P.Y. and Street, R.L., "Conjugate Gradient for Finite Element Equations," Proceedings of the Seventh Conference on Electronic Computation, ASCE, St. Louis, Mo., August 6-8, 1979, pp. 446-454.

9 Cook, R.D., Concepts and Applications of Finite Element Analysis, John Wiley & Sons, N.Y., 1974.

10 Marks, W.R., "Solution of Frictionless Contact Problems by a Conjugate Gradient Technique," M.S. thesis, The University of Wisconsin-Milwaukee, Milwaukee, WI, 1979.

11 Hetenyi, M., Beams on Elastic Foundation, University of Michigan Press, Ann Arbor, Michigan, 1967.

12 Seely, F.B. and Smith, J.O., Advanced Mechanics of Materials, John Wiley & Sons, New York, 1963.

13 Muskhelishvili, N.I., Some Basic Problems of the Mathematical Theory of Elasticity, Noordhoff International Publishing, Leyden, The Netherlands, 1975, pp. 497, 498.

reprinted from
Reliability, Stress Analysis and Failure Prevention Methods in Mechanical Design
Edited by W. D. Milestone

published by
THE AMERICAN SOCIETY OF MECHANICAL ENGINEERS
345 East 47th Street, New York, N.Y. 10017
Printed in U.S.A.

Direct Method

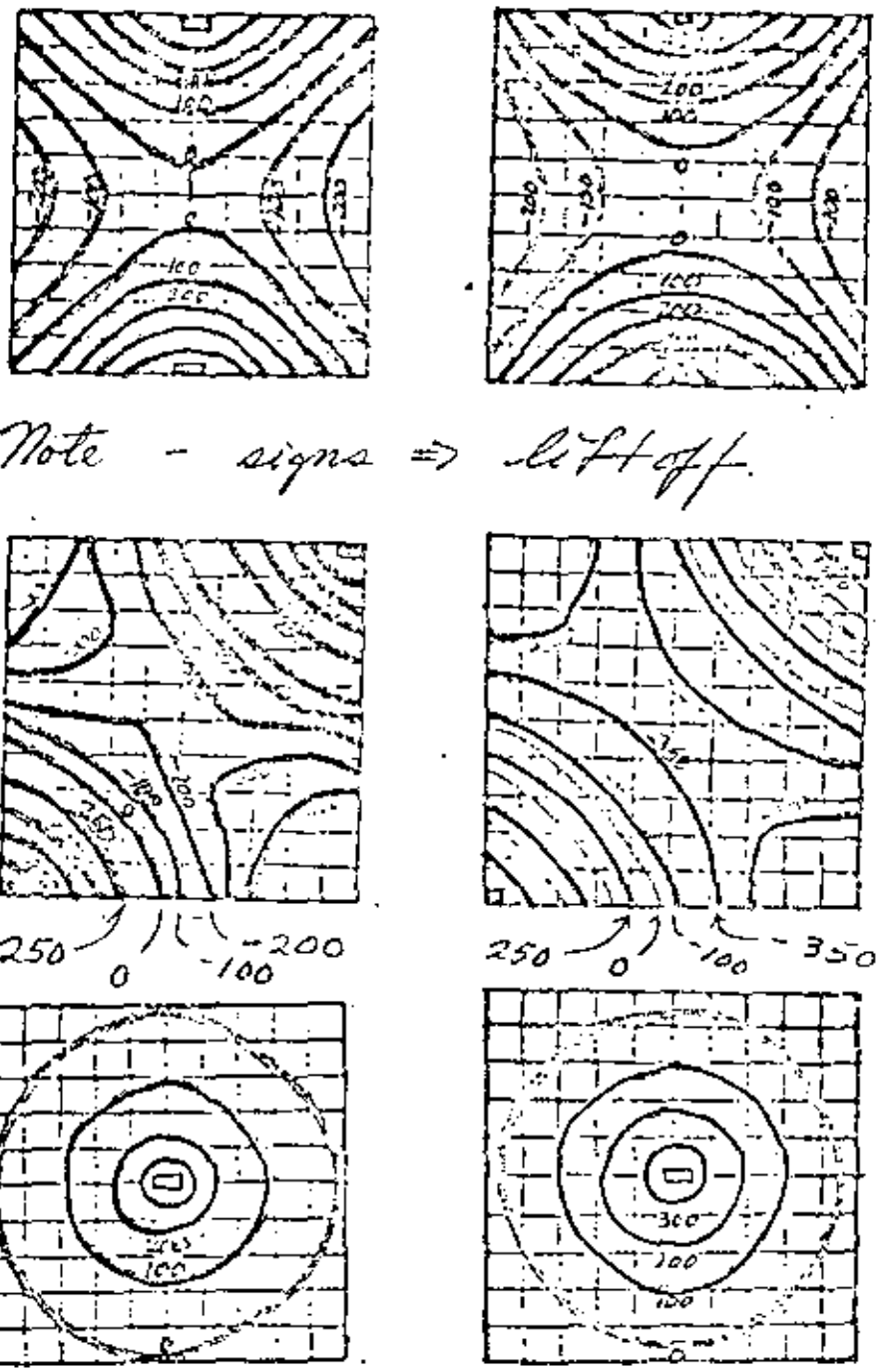

Note - signs ⇒ liftoff.

Load

(a) Measured, Ref. (28)

Load

(b) Computed

Deflection contours for different position of loads

from: Wang, Yi-Syin, Master Thesis, U. of Wisconsin – Milwaukee, 1981.

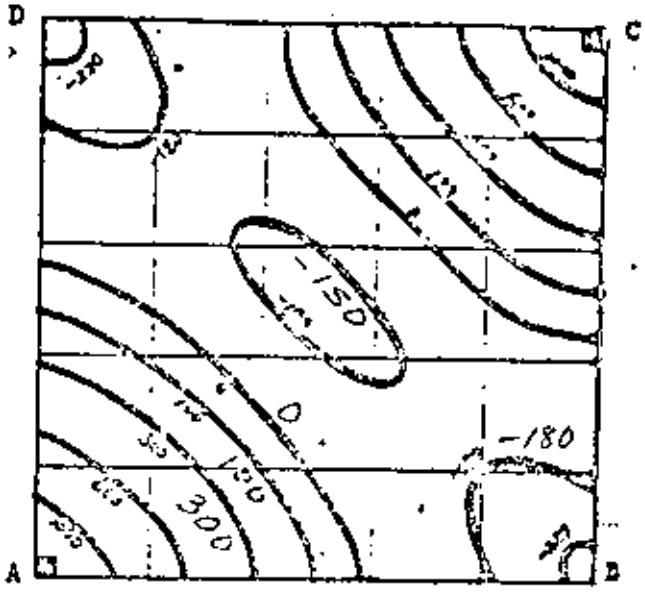

t = 6 inch

(a) Computed

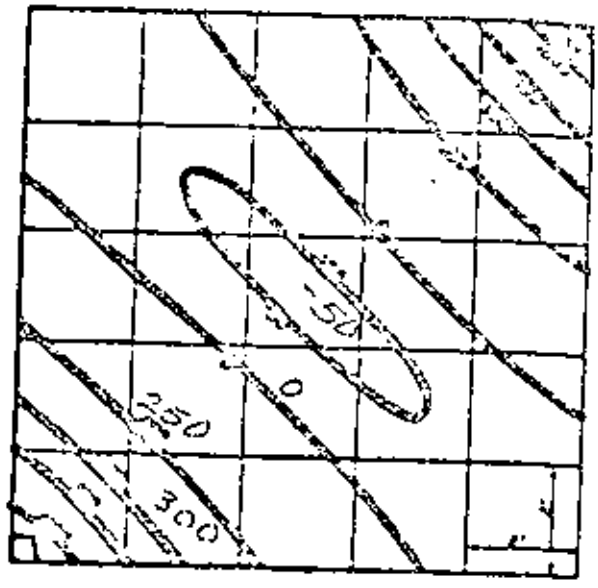

(b) Measured, Ref. (25)

Deflection contour with concentrated load (P=10,000 lb, thickness=6 in.) at corners A,C. Deflections are in ten thousandths of an inch.

ENRICHED FINITE ELEMENTS

Presented at the International Symposium on Engineering Sciences and Mechanics, Taiwan, Taiwan, 29-31 Dec 1981.

PECULIARITIES IN STRESS SOLUTIONS IN LAMINATED COMPOSITES*

Nicholas J. Salamon†

Computation of interlaminar stresses in laminated composites require precision for reliable failure prediction as well as laminate characterization. Numerical solutions to the problem are examined with the focus upon peculiarities in the results near interface/free edge junctions. These solutions include those to classical problems, to the more popular ideal interface model and to a model which features a finite interface. Through this examination, the problem is clearly defined and suggestions for its solution are offered. In particular the notion of a nonsymmetric stress tensor is discussed.

INTRODUCTION

Stress analysis at bimaterial interfaces has received considerable attention. Problems concerned with isotropic materials are now classic, but the contemporary development of layered, anisotropic composites has rekindled interest. An assessment and review of the problem has been reported by Salamon[1].

The analytical nature of such a problem is complicated. Not only do material properties change in crossing an interface, but the elastic behavior encountered in making such a crossing may lead to a rather perilous journey, albeit an exciting one. The analyst must not only contend with singular fields[2], but also a nonsymmetric stress tensor[3,4]. Yet putting these matters aside, the very untractability of such problems compels a numerical solution of some sort and it is in making the

---

*Prepared for a technical paper that may later be published in the Proceedings of the American Astronautical Society.

†Associate Professor, Department of Mechanical and Aerospace Engineering, West Virginia University, Morgantown, West Virginia 26506, USA. Phone: 304/293-3026.

transition from infinitesimal to discrete mathematics that causes trouble.

Through comparisons with known solutions to classical problems, Raju, et al.[3] illustrated certain difficulties in a perspicuous manner; they reminded the scientific community that the stress tensor need not by symmetric at boundaries and used this argument to explain differences between finite element and finite difference solutions.

In a related study, Evans and Salamon[5] showed that in using conventional finite elements, required continuity and boundary solutions at the interface/free edge junctions of a composite cannot be met in general. Furthermore they exposed interesting behavior in a finite interface which is not revealed by ideal interfaces having no thickness.

In the paper at hand, some difficulties encountered by conventional numerical solutions, particularly finite element displacement formulations, are illustrated. Then having made the point, theories to improve the solution are suggested.

THE STRESS FIELDS

For the problems of interest, there is no difficulty in computing accurate stress states away from regions of elastic discontinuity. Hence, the focus here is primarily on the neighborhood of elastic discontinuities.

A Classical Problem

Timoshenko (problem 16, p. 146)[6] provides the solution in the neighborhood of load discontinuity to the problem of a constant vertical "step" pressure applied to a horizontal half-plane. He leads the student to understand the lack of symmetry between the shear stress (which is nonzero) and its surface traction (which is). The difference between the closed-form solution and a conventional finite element solution for the shear quantities is illustrated in Figs. 1 and 2. Clearly the numerical solution cannot decide whether it is a stress or a surface traction.

Notably the stress state is finite everywhere, however the derivative of the stress field is singular at the load discontinuity. Although the numerical solution deviates from the stress solution, Raju, et al.[3] report (1) correct numerical force distributions, and (2) the aberration in the stress distribution is confined to two elements neighboring the load discontinuity regardless of the mesh size.

The Orthotropic (0-90) Laminate

Evans and Salamon[5] studied the effect of epoxy resin interlayers sandwiched between the four plies of a symmetrically stacked, 0°/90° graphite -reinforced, epoxy laminate using the conventional finite element method. The displacement fields u, v, w were taken as

$$u = \bar{u}(x), \quad v = V(y,z), \quad w = W(y,z) \tag{1}$$

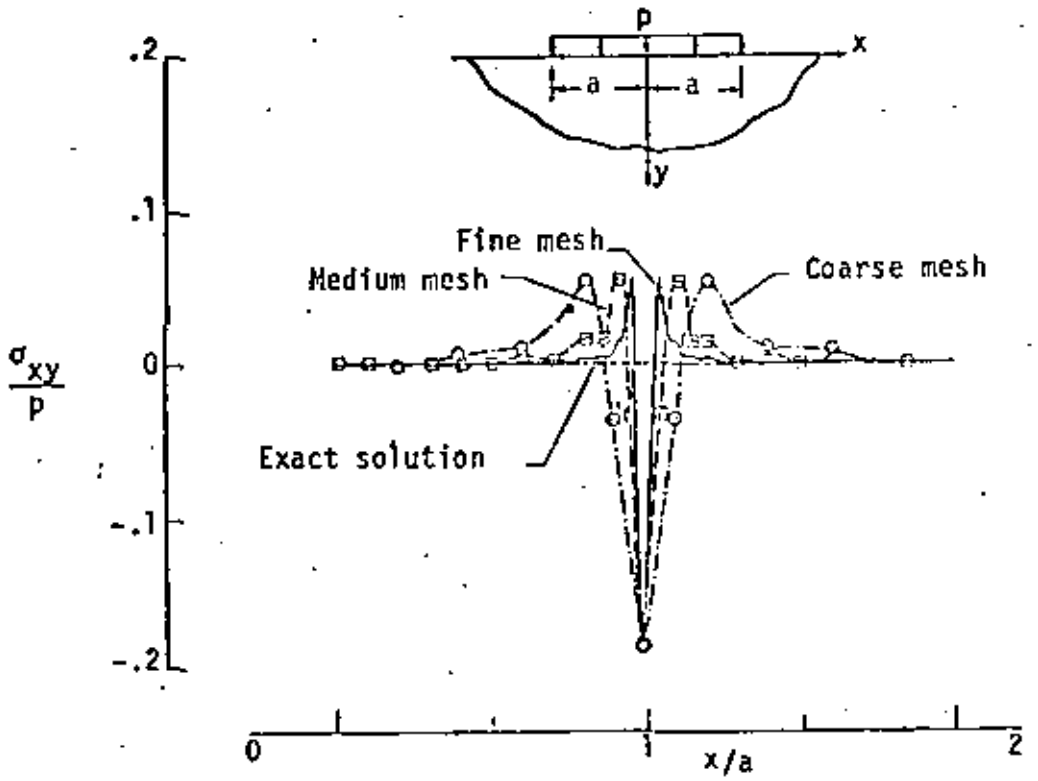

Fig. 1 Shear Traction on the Surface y = 0 (from ref. 3)

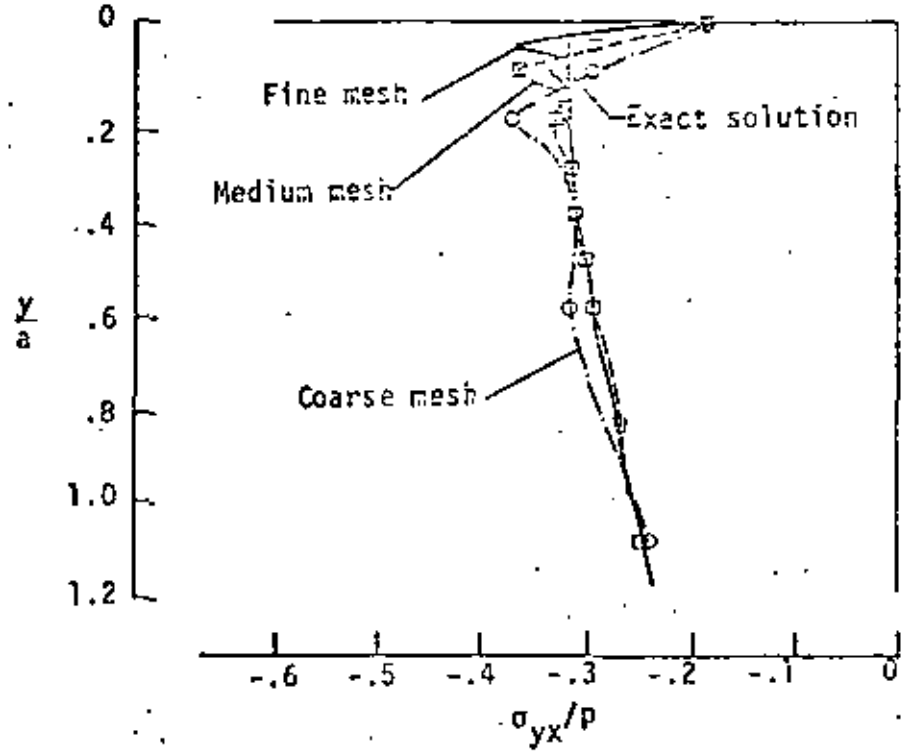

Fig. 2. Shear Stress Along x = a (from ref. 3)

where $\bar{u}$ is the known axial displacement resulting from a prescribed axial strain $\bar{e}$ and V, W are unknown displacement functions determined from finite element analysis. This equation together with the symmetry conditions

$$V(0,z) = W(y,0) = 0 \qquad (2)$$

permits a two-dimensional numerical treatment of only the shaded quarter section shown in Fig. 3.

Distributions along the 0°/90° interface of the stresses σ_z and τ_{yz} are shown in Fig. 4. Clearly σ_z appears to have converged except near the free edge (y/b = 1). On the other hand, τ_{yz} is not so well behaved. Indeed τ_{yz} fails to vanish along the free edge (Fig. 5).

Inclusion of a resin interlayer of thicknesses up to 10% of a single ply thickness h leads to some interesting results. When compared to the ideal interface model, (1) the interlaminar stresses (σ_z and τ_{yz}) approximately retain their peak magnitudes and display very similar distributions; yet (2) the disturbance at the interface/free edge junction is reduced and shifts to the resin/90° interface while the resin/0° interface exhibits no ill effects. The typical influence of the resin is comparatively illustrated in Fig. 6. But the peculiar influence of the interface/free edge junction is revealed by Fig. 7. The stress σ_y in the plane just above the 90° material for both cases (ideal and finite interfaces) undergoes an oscillatory divergence upon approach to the free edge, though somewhat mollified for the resin interlayer.

Notably the aberration in the results is confined to two elements, independent of mesh size, on either side of the interface. Moreover the stress state is most certainly singular. Inclusion of a finite resin interlayer does not alter the interlaminar stress distributions, but shifts them toward the critical interface; hence the more critical interface is exposed.

The Anisotropic (±45)-Laminate

This laminate configuration is similar to that of the previous section except that the 0° layers are replaced by +45° layers and the 90° layers by -45° layers. Raju, et al.[3] drew upon their experience with numerical solution of classical problems to interpret conventional finite element results for the (± 45) laminate. Clearly the free-edge (y = b) tractions σ_y, τ_{xy}, τ_{zy} must vanish over the entire surface. But as shown in Fig. 8, severe oscillations appear in the distribution for σ_y along the edge near the interface junction. Very similar results were presented[3] for τ_{xy} and τ_{zy}.

Notably the aberration is confined to two elements on either side of the interface and the stress state is most certainly singular. Furthermore, studies of this laminate[3,7] reveal that peak values of σ_z along the ± 45° interface are positive for certain pointwise formulations of the problem (e.g., finite difference methods) and negative for finite element formulations. Raju, et al.[3] argue that imposition of a symmetric stress

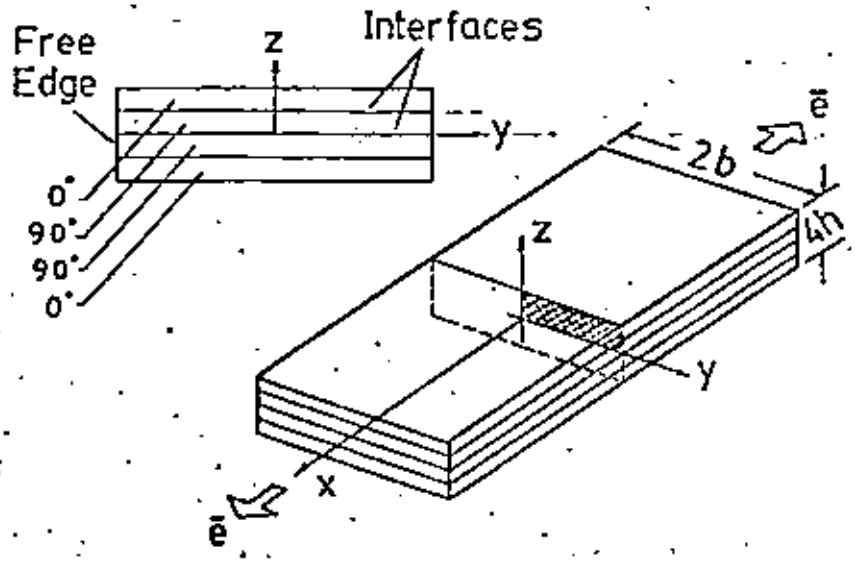

Fig. 3. Laminate Geometry

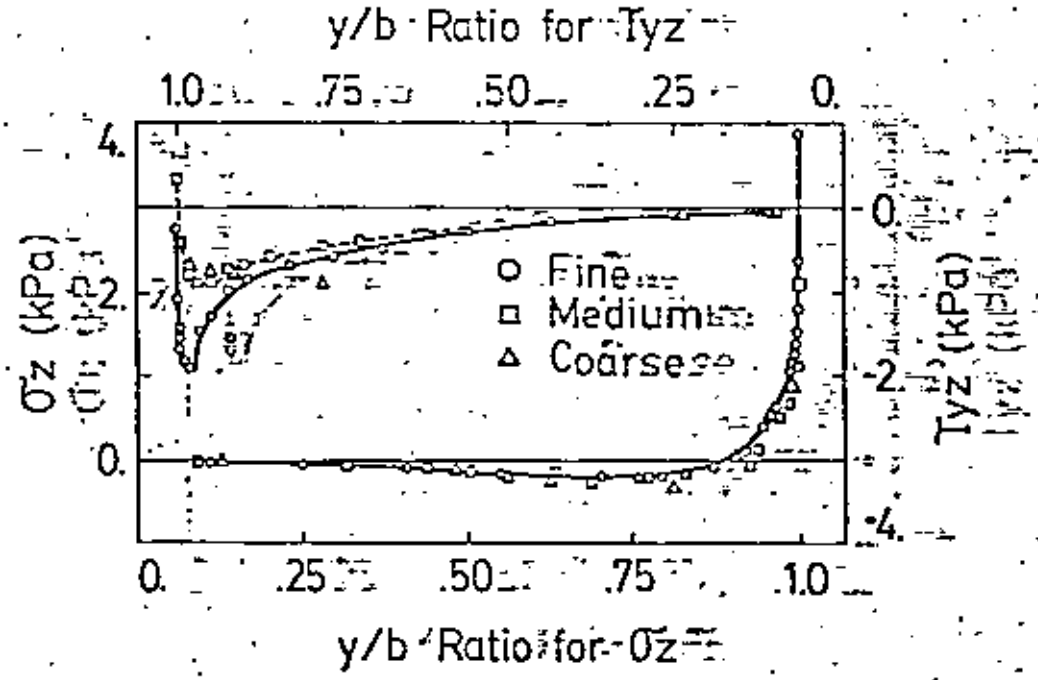

Fig. 4. Distributions of σ_z (lower curve) and τ_{yz} (upper curve). (from ref. 5)

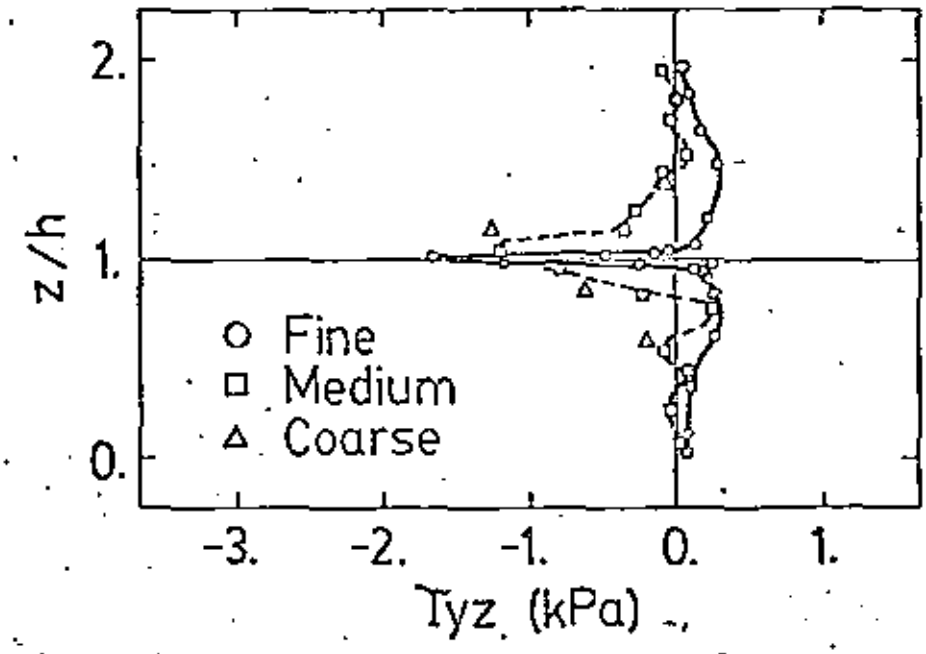

Fig. 5. Shear Traction Along y = b (from ref. 5)

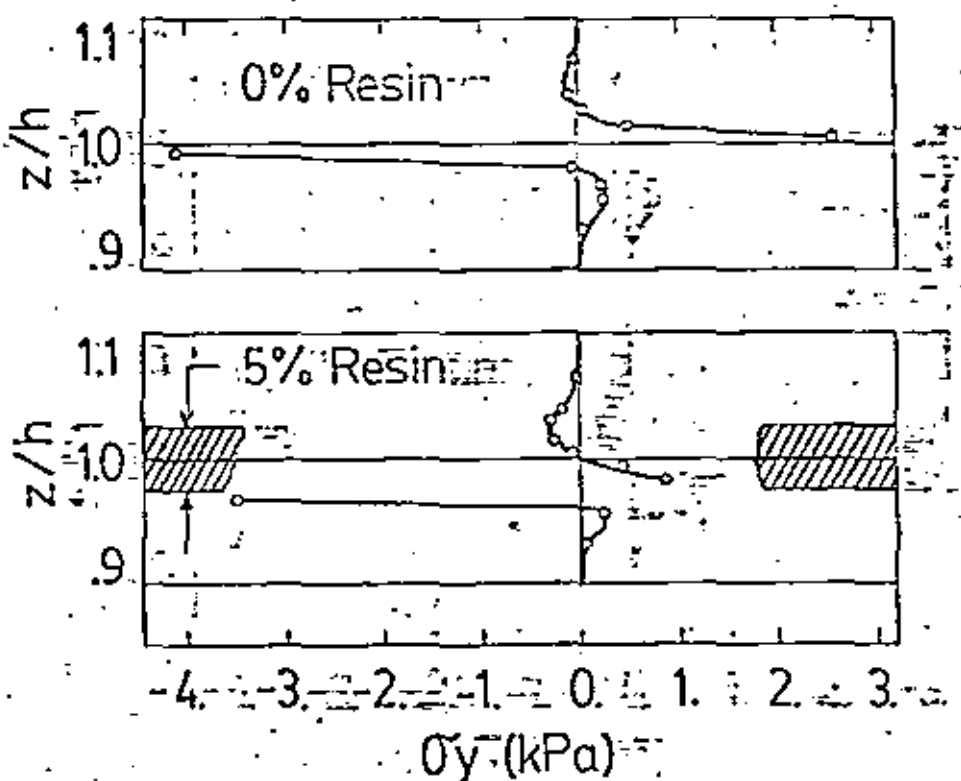

Fig. 6. Normal Traction Along y = b (from ref. 5)

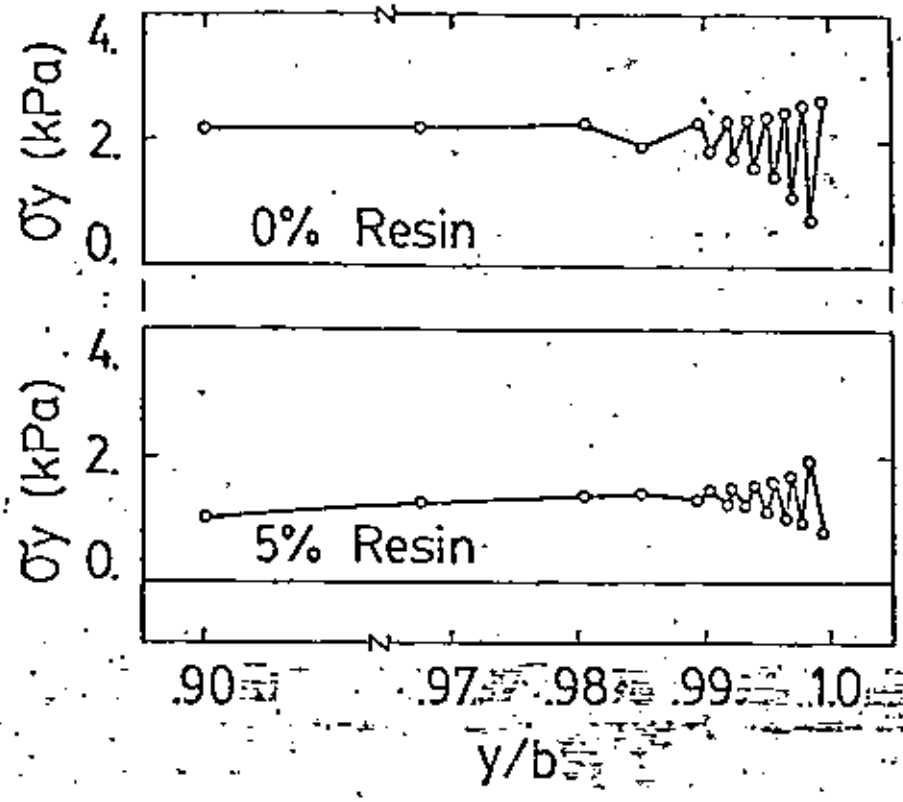

Fig. 7. Oscillatory Divergence in σ_y (from ref. 5)

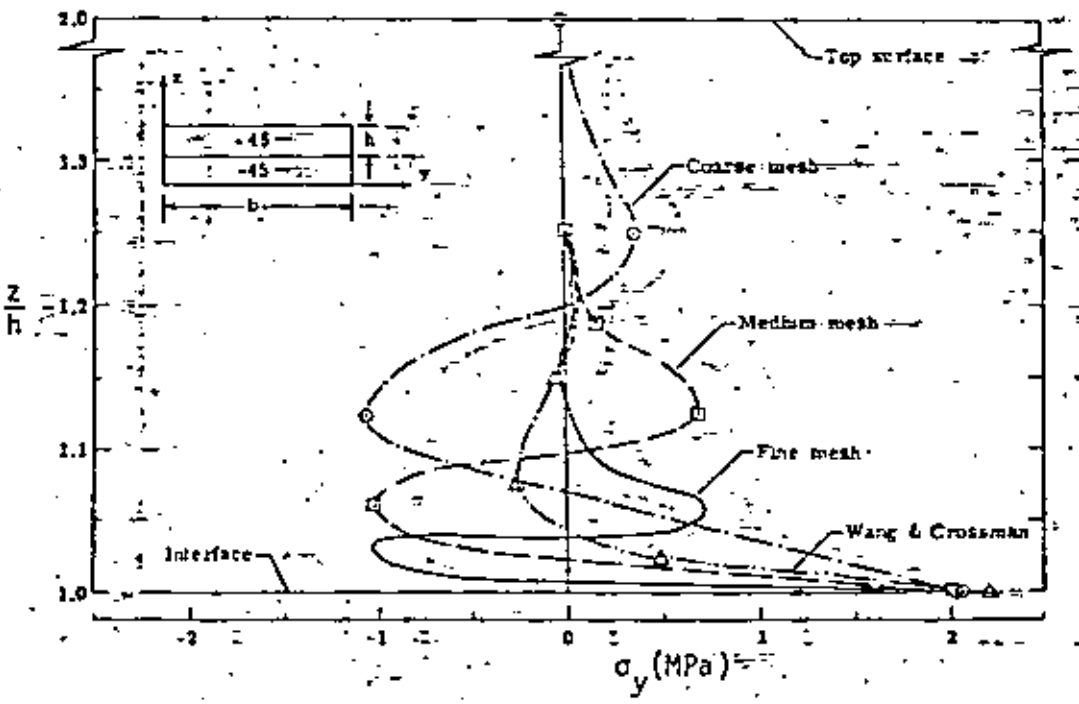

Fig. 8. Normal Traction Along y = b (from ref. 3)

tensor together with stress (traction) boundary conditions pre-determines a tensile σ_z in pointwise formulations while prescription of force boundary conditions in finite element formulations relieves this restriction.

CONCLUSION

It is apparent that aberrations in conventional numerical solutions are the result of discontinuities in elastic properties and/or load. At such discontinuities the interface shear traction is not symmetric with respect to its companion free surface traction. Moreover the stress fields in the neighborhood need not be singular, although in that case their derivatives are.

Yet not all elastic discontinuities cause difficulties. For instance the interface between the 0° reinforced orthotropic layer and a resin interlayer displays no apparent aberrations. Hence stress concentrations (or singularities) are intimately related to the degree of mismatch (or to their spatial rates of change) between material properties.

Momentarily ignoring any singular behavior, one can say that the solution tends to converge. For as the discretized model is scaled finer, the aberration remains bounded within two elements on either side of the interface at the free edge. But this may be of little consolation - the interface/free edge junction is critically important.

What is perhaps most disconcerting is the anomalous disagreement between solutions found from generally accepted numerical methods. It is serious to be uncertain of computations in the neighborhood of the interface/free edge junction; it is absolutely unacceptable to be uncertain of even the nature of solutions found from usually reliable methods. The disagreement between finite difference and finite element results must be rectified.

CORRECTIVE THEORIES

Several approaches to overcome the problem come to mind. Their applicability depends upon the physical situation and the inclination of the investigator. Nonetheless it would seem most approaches will ultimately depend upon numerical computations.

Couple Stress Theory

Perhaps one can argue that the stress tensor is not symmetric at the boundary. Then the natural course of action is to apply couple stress theory or asymmetric elasticity. In this case one admits body moments (in addition to body forces) on an element of material and the stress tensor is no longer symmetric. But are body moments appropriate only for boundary elements and not for interior elements? Furthermore one must set a value for an additional elastic constant which appears in the formulation. What value would one choose? The interested reader is referred to a wealth of literature on the subject, for instance refs. 8,9.

The Transition Element

The idea here is to permit material properties to vary in a smooth fashion across an interface, thereby eliminating the elastic discontinuity. This theory is not realistic for interfaces formed by abutting two materials together, but apparently would apply to reinforced, continuous matrix composites in which interfaces are not sharply defined[5]. First one must decide which properties to vary and the form of the varying function, then one should select an order of numerical discretization sufficiently high in order to appropriately match that function. The problem, of course, is that it will be difficult to model the high gradients involved.

Enriched Finite Elements

The term "enriched" simply means that the conventional nodal interpolation functions used to describe the elastic fields of a finite element are augmented by additional functions. Whereas the interpolation functions are connected to nodal degrees of freedom, the enriched functions are connected to nodeless degrees of freedom. For hybrid finite elements, one would augment the assumed stress fields; for displacement-based elements, one would augment the assumed displacement fields. The idea is known. A good example is an application to fracture mechanics problems[10].

In the present context, the idea is to include in the assumed field a singularity term $r^{\alpha} f(s,t)$ as well as a discontinuity term $g(s,t)$, where α is the power of the singularity, s,t the element coordinates and $r^2 = s^2 + t^2$. The value of α and the functions f, g might best be chosen from elasticity theory[1,2,11]. An example of the use of the singularity term is given in ref. 10 and in further references cited there.

For a discontinuity term, one may propose the following: consider a rectangular element whose lower left corner defines the origin of Cartesian coordinates s,t. Then choose for the augmented displacement functions

$$u = a\, t\, (\ln r + 1) \qquad (3)$$

$$v = -a\, t \ln r \qquad (4)$$

where a is an arbitrary constant (the nodeless degree of freedom). The linear strains are

$$\epsilon_s = -\epsilon_t = a\, st/r^2 \qquad (5)$$

$$\gamma_{st} = a\, t^2/(s^2 + t^2) \qquad (6)$$

If the origin of coordinates is placed such that t runs along a bimaterial interface and s along a free surface, then for an isotropic material, (1) with $s \neq 0$, $t = 0$, all stresses vanish and the free surface is free of traction, and (2) with $s = 0$, $t \neq 0$, the normal stresses vanish, but the

shear stress σ_{st} does not. Thus the only discontinuity appears in shear wherein $\sigma_{st} \neq \sigma_{ts}$. These results can be seen directly through (5) and (6).

In application of the above, a correct functional relationship is built into the finite element, but the investigator may have to tinker to arrive at correct computation of stress and traction. It should be noted that implementation follows the same procedure outlined in ref. 10. However the nodeless variables may be condensed out in the numerical scheme.

CLOSURE

The problem has been defined and some suggestions made on how to solve it. Yet a parting comment must be made on the notion of a nonsymmetric stress tensor.

For the class of problems considered, the stress tensor is symmetric. What is nonsymmetric (or discontinuous) is the traction vectors acting upon adjacent surfaces. The continuum mechanics relation $t_i = \sigma_{ij} n_j$ (t the traction, n the normal to the surface) holds deeper meaning than its simplicity makes apparent. In discrete analysis, it reminds one to be very careful in how the tractions are computed. There is more than semantics here, but imprecise usage (and this writer pleads guilty) over time leads one to forget the deeper meaning.

ACKNOWLEDGMENT

The author is grateful to William D. Evans and to I. S. Raju, J. D. Whitcomb and J. G. Goree whose works were made available to support the present thesis.

REFERENCES

1. Nicholas J. Salamon, "An Assessment of the Interlaminar Stress Problem in Laminated Composites," J. of Composite Materials, Vol. 14 (Supplement), 1980, pp. 177-194.

2. S. S. Wang, "Edge Delamination in Angle-Ply Composite Laminates," American Inst. of Aeronautics and Astronautics Paper No. 81-0578, 1981.

3. I. S. Raju, J. D. Whitcomb, and J. G. Goree, A New Look at Numerical Analyses of Free Edge Stresses in Composite Laminates, NASA Technical Paper 1751, December 1980.

4. Eric Reissner, "Note on the Theorem of the Symmetry of the Stress Tensor," J. of Mathematics and Physics, Vol. 23, 1944, pp. 192-194.

5. William D. Evans and Nicholas J. Salamon, "The Effect of a Resin Interlayer on Composites with Free Edges," ~~submitted for publication~~, 1981, Composites Technology Review, vol 3, pp. 148-151.

6. S. P. Timoshenko, Theory of Elasticity, McGraw-Hill Book Co., New York, 3rd Edition, 1970.

7. Nicholas J. Salamon, Unpublished studies of numerical solutions of composite laminates in bending and extension, 1977.

8. Giuseppi Grioli, Mathematical Theory of Elastic Equilibrium (Recent Results), Springer-Verlag, Berlin, 1962.

9. R. D. Mindlin and H. F. Tiersten, "Effects of Couple-Stresses in Linear Elasticity," Arch. for Rational Mechanics and Analysis, Vol. 11, 1962, pp. 415-448.

10. Glenn Heppler and Jorn S. Hansen, "Mixed Mode Fracture Analysis of Rectilinear, Anisotropic Plates by High Order Finite Elements," Int. J. for Numerical Methods in Engineering, Vol. 17, 1981, pp. 445-464.

11. I. S. Raju and John H. Crews, Jr., Interlaminar Stress Singularities at a Straight Free Edge in Composite Laminates, NASA Technical Memorandum 81876, August 1980.

17. APPLICATION OF THE FINITE ELEMENT METHOD TO SOME FREE SURFACE FLUID PROBLEMS*

K.Washizu, T.Nakayama

Department of Aeronautics, University of Tokyo, Tokyo, JAPAN

and H.Ikegawa

Hitachi Mechanical Engineering Research Laboratory, Hitachi Co., Ltd., Ibaragi, JAPAN

SUMMARY

The present paper deals with two applications of the finite element method to the motion of a fluid with free surface and under gravity. The first application is made to analysis of flow over a spillway crest, while the second application is made to analysis of sloshing in a container subjected to a forced sinusoidal vertical oscillation. The power of the finite element method in analysing these problems is demonstrated.

INTRODUCTION

The motion of a fluid with free surface presents important engineering as well as academic problems. Especially, the motion of a fluid with free surface and under gravity is one of the greatest engineering concerns as exemplified by water waves and their impacts on a wall along the shore. A great number of papers have been published on these problems and finite element techniques have been successfully applied to their numerical analyses [Refs. 3,8,10,12 and 19, for example].

We confine our interest of the present paper to applications of the finite element method (abridged FEM) to two-dimensional, steady and unsteady motions of an inviscid, irrotational and incompressible fluid with free surface and under gravity. As is wellknown, the conventional way of deriving a finite element formulation begins with deriving a

---

* This paper is to be presented to the International Conference on Finite Elements in Water Resources held at Princeton University, July 12-16, 1976.

variational principle which provides, as its stationary conditions, the equations which govern the problem. The variational principles developed by Whitham [Ref.21] and Luke [Ref.9] have played a guiding role in finite element formulations for problems of a fluid with free surface and under gravity.

In the present paper, FEM are applied to two problems on the motion of a fluid with free surface and under gravity. Modified versions of Luke's variational principle are established to begin with, and used in subsequent finite element formulations.

ANALYSIS OF FLOW OVER A SPILLWAY CREST

The first and third named authors applied FEM to analysis of flow over a spillway crest and obtained encouraging results [Ref.5]. The present paper is an extension of our previous work. The problem of convergence behavior of successive approximations is discussed and a method for estimating the actual rate of flow is proposed. A brief remark is made, referring to References 13-16, of the variational principle developed in Reference 5, and its relation with Luke's principle.

Governing equations

We consider a problem of a flow over a spillway crest defined in Reference 5. The parts denoted by S_1, S_2, S_3 and S_4 in Figure 1 are the free stream boundary, the station of the far-upstream boundary, the channel bottom and the station of the far-downstream boundary, respectively. The x-axis is taken horizontally in coincidence with the datum surface, while the y-axis is taken vertically upward. Assuming the flow to be two-dimensional, steady, inviscid, irrotational

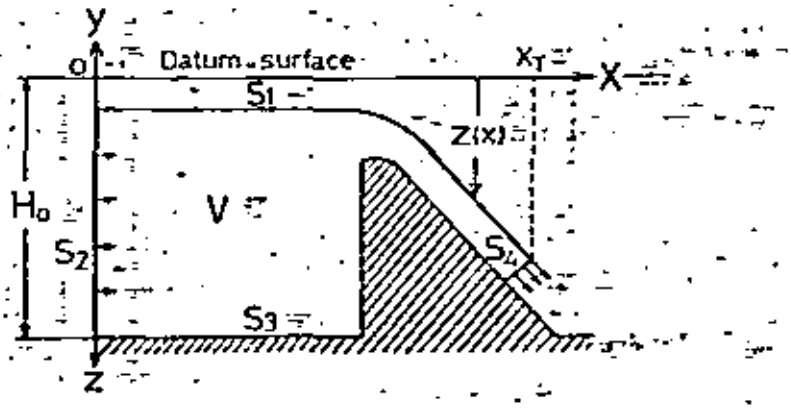

Figure 1. Flow over a spillway

and incompressible, our problem is to determine the profile of the free surface S_1, and the actual flow rate, denoted by Q_{exact}, as well as the flow field, when the total head H_t is specified. The governing equation is as follows:

$$\frac{\partial^2\Psi}{\partial x^2} + \frac{\partial^2\Psi}{\partial y^2} = 0 \quad \text{in } V, \tag{1}$$

where $\Psi(x,y)$ is the stream function, and V is the flow region bounded by the four boundaries. The boundary conditions are as follows :

$$\text{(i)} \quad \Psi = 0 \quad \text{on } S_1, \tag{2}$$

$$\text{(ii)} \quad \partial\Psi/\partial n = -\sqrt{2gz} \quad \text{on } S_1, \tag{3}$$

where n is the normal drawn outwards on the boundary, z(x) is the distance of the free surface measured from the datum surface and g is the gravitational acceleration.

$$\text{(iii)} \quad \Psi = Q_{exact} \quad \text{on } S_3, \tag{4}$$

$$\text{(iv) \& (v)} \quad \text{the flow is uniform on } S_2 \text{ and } S_4. \tag{5}$$

As mentioned in References 5 and 18, this is a difficult mathematical problem, because the problem is non-linear, and the free surface as well as Q_{exact} is unknown.

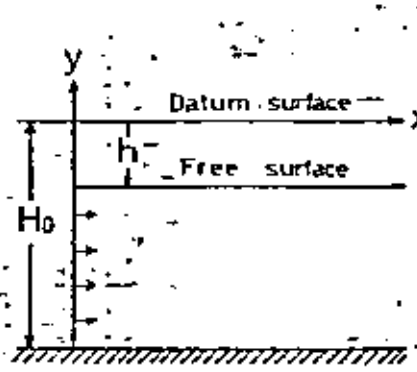

Figure 2 Uniform flow

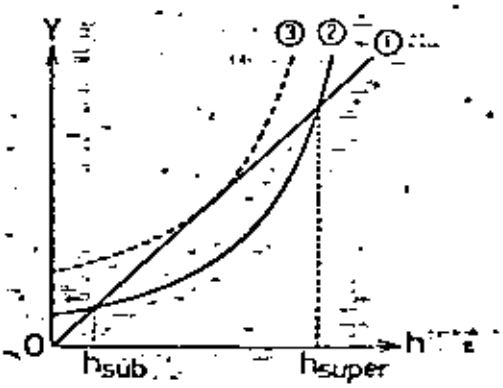

Figure 3 — Graphical solution

beforehand. Moreover, the flow is subcritical in the upstream portion of the crest, while it is supercritical in the downstream portion, and there exists near the crest a transition region, of which the location is also unknown beforehand.

A mention is made here of the subcritical and supercritical flows. We consider an uniform flow in a channel, of which the bottom is horizontal as shown in Figure 2, and assume that the total head H_0 and the flow rate Q are specified. Then, Equation (3) reduces to

$$Q^2/(H_0 - h)^2 = 2gh, \tag{6}$$

where h is the distance of the free surface measured from the datum surface. Equation (6) can be solved graphically as shown in Figure 3, where the two curves labelled with ① and ② represent

$$Y = 2gh, \qquad Y = Q^2/(H_0 - h)^2, \tag{7}$$

respectively, and the two roots, denoted by h_{sub} and h_{super}, provide values of h for the subcritical and supercritical flows, respectively, for the specified values of H_0 and Q. It is seen that as Q becomes greater, the two roots approach to each other, and there exists a critical flow rate, denoted by Q_{cr}, beyond which an uniform steady flow ceases to occur for the specified value of H_0, as shown by a dotted curve labelled with ③ in Figure 3.

Returning to Figure 1, our problem is to obtain a smooth free surface profile together with Q_{exact} by solving Equation (1) under the boundary conditions : (2), (3), (4) and (5), with a further specified condition that the flow is subcritical on S_2 and supercritical on S_4.

A variational principle

Ikegawa derived the following variational principle for the present problem :

$$\chi = \frac{1}{2}\iint_{V(z)} \{(\frac{\partial \psi}{\partial x})^2 + (\frac{\partial \psi}{\partial y})^2\} dxdy + \frac{1}{2}\int_0^{x_T} g z^2 dx, \tag{8}$$

where the flow region bounded by S_1, S_2, S_3 and S_4 is denoted by V(z), emphasizing that it is dependent on z(x), and where x_T denotes the x-coordinate of the point of intersec-

tion of the two boundaries S_1 and S_4, as shown in Figure 1. In the functional (8), the boundary conditions (2), (4) and (5) are taken as subsidiary conditions, while Equations (1) and (3) are obtained as stationary conditions if the variation is taken following the formulation introduced in Reference 5. By the use of the functional (8) and a finite element formulation, the convergence difficulty encountered in Reference 18 can be avoided as stated in the Reference 5.

Finite element formulation

For our finite element formulation, the flow region is divided into a large number of triangular elements as shown in Figure 4. For an arbitrary triangular element as shown in Figure 5, we assume Ψ to be a linear function of x and y, namely

$$\Psi(x,y) = a + bx + cy, \tag{9}$$

where a, b and c are constants, values of which are determined in terms of the values of Ψ at the three vertices and we obtain

$$\partial\Psi/\partial x = A^T\Psi, \tag{10-a}$$

$$\partial\Psi/\partial y = B^T\Psi, \tag{10-b}$$

where

$$A^T = (1/2\Delta)[y_j - y_k,\ y_k - y_i,\ y_i - y_j], \tag{11-a}$$

$$B^T = (1/2\Delta)[x_k - x_j,\ x_i - x_k,\ x_j - x_i], \tag{11-b}$$

$$\Psi^T = [\Psi_i,\ \Psi_j,\ \Psi_k], \tag{12}$$

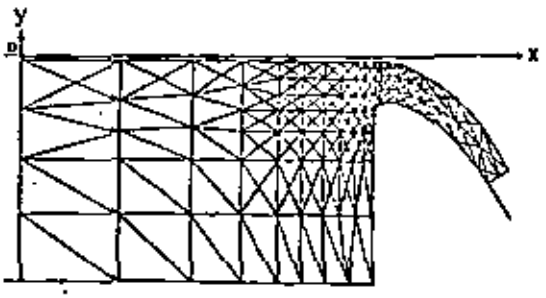

Figure 4 Mesh pattern

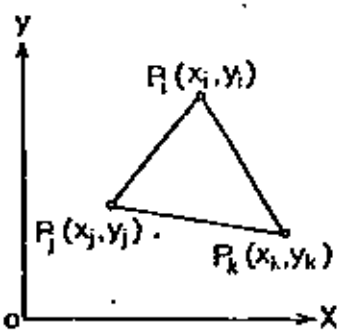

Figure 5 A triangular element

and where

$$2\Delta = \begin{vmatrix} 1 & x_i & y_i \\ 1 & x_j & y_j \\ 1 & x_k & y_k \end{vmatrix} \qquad (13)$$

The profile of the free surface between two neighbouring nodal points on S_1 is approximated by a straight element.

Since the problem is nonlinear, an iterative method, which may be taken as a kind of Newton-Raphson method, is introduced. We assume that the n-th approximate values of $\Psi(x,y)$ at all the nodal points as well as values of $z(x)$ at all the nodal points on S_1 have been obtained, and denote them by Ψ_0 and z_0, respectively. Then, we proceed to obtaining the (n+1)-th approximate values of these functions, which are denoted by Ψ and z, respectively, setting

$$\Psi = \Psi_0 + d\Psi, \quad z = z_0 + dz. \qquad (14)$$

Substituting the above relations into the functional (8), we obtain stationary conditions with respect to $d\Psi$ and dz as follows [Ref.5]:

$$\begin{bmatrix} G_{11} & G_{12} \\ G_{21} & G_{22} \end{bmatrix} \begin{Bmatrix} dz \\ d\Psi \end{Bmatrix} = \begin{Bmatrix} R_1 \\ R_2 \end{Bmatrix} \qquad (15)$$

By solving Equations (15), and substituting the values of $d\Psi$ and dz thus determined into Equation (14), we obtain the (n+1)-th approximation for Ψ and z.

Iteration procedure

Our iteration proceeds by assuming the first approximate values of Q_{exact} and denoting it by $Q^{(1)}$, and then choosing the first approximate profile of the free surface properly in such a way that it coincides with that of the uniform subcritical flow at S_2 and with that of the uniform supercritical flow at S_4, both belonging to $Q^{(1)}$. Then, keeping $Q^{(1)}$ unchanged, and by the use of the iteration based on Equation (15), the profile of the free surface corresponding to $Q^{(1)}$ is obtained.

By changing the value of the assumed flow rate successively, say $Q^{(1)}$, $Q^{(2)}$, $Q^{(3)}$, ..., we obtain profiles of

the free surface corresponding to these rates of flows. Figure 6 shows the profiles of the free surface thus obtained for the following flow rates :

$$Q = 5.25,\ 5.40,\ 5.56,\ 5.75 \quad m^2/sec.$$

This figure shows how the profile of the free surface behaves as the value of Q approaches to Q_{exact}. The zig-zag shape of the profile near the crest seems to be a character-

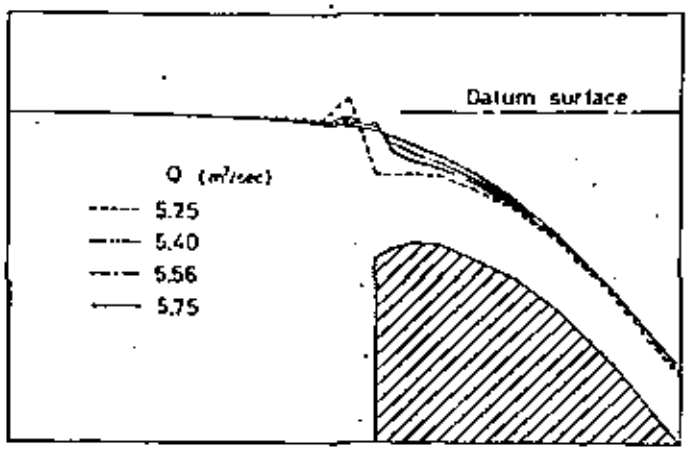

Figure 6 Shapes of the free surface profile

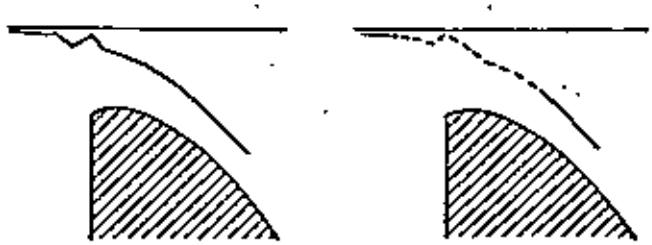

(a) $Q < Q_{exact}$ (b) $Q > Q_{exact}$

Figure 7 Convergence characteristics of the profile

istic which indicates that the specified value of Q is less than Q_{exact}, as shown in Figure 7-(a). If $Q > Q_{exact}$, on the other hand, the iteration for obtaining the profile of the free surface shows a divergent behavior near the crest, as shown in Figure 7-(b).

A method of estimating Q_{exact}

After an extensive numerical computations, Nakayama has found a method for estimating Q_{exact} from a series of the profile shapes obtained for flow rates $Q^{(m)}$; m = 1,2,3, ... He listed up all the values of z for a specified value of Q and denoted them by z_i; i = 1,2,3,..... , n, where n is the number of the nodal points on S_1. On the other hand, he denoted by $z_{i,exact}$; i = 1,2,..... , n, the values of z at all the nodal points on S_1 for Q_{exact}, where Q_{exact} was taken as the flow rate which provides the most smooth profile. Then, the following quantity was computed:

$$\varepsilon = \sum_{n} |z_i - z_{i,exact}|, \qquad (16)$$

where summation is taken with respect to all the nodal points on S_1.

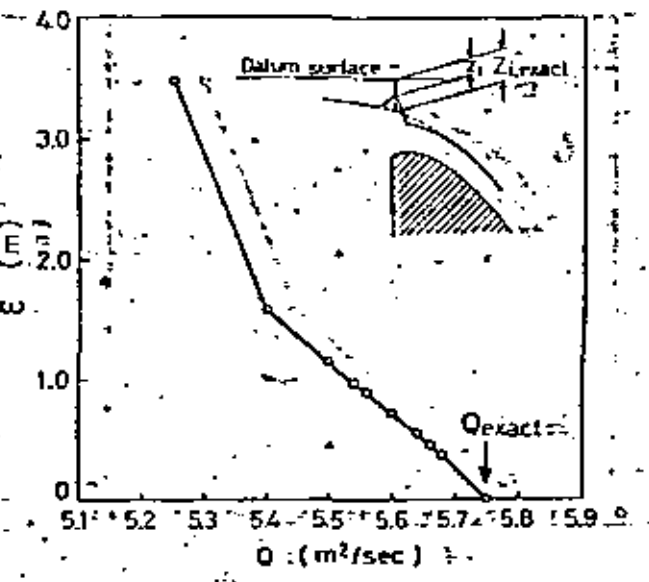

Figure 8 : ε vs. Q

Having obtained values of ε for $Q^{(m)}$; $m = 1,2,3,\ldots$, he plotted these values as shown in Figure 8, where the abscissa is Q and the ordinate is ε, and found that a monotonous convergence characteristic exists in the region where Q is close to Q_{exact}.

He has found also that even if the value of Q changes slightly, only very few changes occur in the values of z_i as far as the far-upstream and far-downstream portions are concerned, although a strong zig-zag in the vicinity of the crest may be subject to a severe change, and that a good estimate of $z_{i,exact}$ can be obtained by the use of the far-upstream and far-downstream portions of the free surface profile obtained for a value of Q, which is close to Q_{exact}, and by connecting these two portions by a smooth curve which is drawn as similarly as possible to the profile of $z_{i,exact}$. The profile thus obtained approximately by the smoothing will be denoted by $z_{i,smoothed}$.

Nakayama's method of estimating Q_{exact} is as follows : Firstly, a profile of $z_{i,smoothed}$ is obtained by the smoothing procedure above mentioned, and is substituted into Equation (16) to replace $z_{i,exact}$. Then, the figure of ε vs. Q is plotted as shown in Figure 8, and the value of Q_{exact} can be estimated by extrapolation. This has proved to be a method of practical use.

It is noted here that the computing time for obtaining Q_{exact} and the profile of its free surface is of the order of 300 seconds by HITAC 8800/8700. It should be noted also that the remarks mentioned about the convergence characteristics in Reference 5 have been found erroneous and should be corrected as mentioned in the above.

Some remarks on variational principles

Recently, O'Carroll published a series of papers concerning variational principles for steady ideal flow with free surface [Refs.13-16]. In these papers, he presented two functionals for the problem of flow over a spillway crest. The first functional, denoted by J_1, is expressed in terms of the velocity potential $\phi(x,y)$ and can be interpreted as a special case of Luke's variational principle. The second variational principle, denoted by J_2, is expressed in terms of the stream function $\Psi(x,y)$ and is complementary to J_1.

He states in Reference 13 that the functionals J_1 and J_2 are appropriate functionals for unrestricted variations, while the functional χ defined by Equation (8) is equivalent to neither of these two functionals, and is subject to some restricted variation. He concludes that the finite element interpretation introduced in Reference 5 is in fact valid,

because the finite element formulation in the paper has been made under restricted variation.

The first and second named authors have tried to develop finite element formulations based on the two functionals proposed by O'Carroll, and conducted extensive computational work. However, their limited experience seems to suggest that their finite element formulations based on J_1 and J_2 have convergence difficulty and that further study is necessary for obtaining finite element formulations of practical use.

LIQUID SLOSHING IN A RIGID CONTAINER SUBJECTED TO FORCED SINUSOIDAL VERTICAL OSCILLATION

Sloshing is an unsteady motion of a liquid with free surface in a container subjected to forced oscillation. This phenomenon is known as to make serious effects on the strength and stability of the large liquid propellant rocket or airplane carrying a great deal of fuel. This also presents important engineering problems as exemplified by the reservoir or fuel storage tank under the earthquake, or by the large tanker running on the rough sea. The problem of sloshing has been investigated extensively [Refs. 2,4,11 and 17, for example] and an excellent paper such as Reference 1 has been published.

The third named author applied FEM to the analysis of an unsteady linear and nonlinear motions of a liquid with free surface and under gravity, where the container was subjected to a forced sinusoidal horizontal oscillation [Refs. 6,7]. The liquid was assumed to be two-dimensional, inviscid, incompressible and irrotational, while the container was assumed rigid.

The present paper deals with an unsteady nonlinear motion of the same liquid in the same container which, however, is subjected to a forced sinusoidal vertical oscillation. A finite element formulation is made in a manner similar to that in the horizontal oscillation. Needless to say, finite element formulations for linear motions and the free oscillation of the liquid in the container can be derived as special cases of the subsequent finite element formulation.

Governing equations

We consider a container as shown in Figure 9, where the x- and y-axes are fixed to the container and taken in coincidence with the horizontal and vertical directions, respectively. The governing equations are given as follows [Refs. 1,2]:

$$\frac{\partial^2\phi}{\partial x^2} + \frac{\partial^2\phi}{\partial y^2} = 0 \quad \text{in } V, \tag{17}$$

$$\frac{\partial\phi}{\partial t} + \frac{1}{2}\{(\frac{\partial\phi}{\partial x})^2 + (\frac{\partial\phi}{\partial y})^2\} + (a(t) + g)\eta = 0 \quad \text{on } S_1, \tag{18}$$

$$\frac{\partial\eta}{\partial t} = \frac{\partial\phi}{\partial y} - \frac{\partial\phi}{\partial x}\cdot\frac{\partial\eta}{\partial x} \quad \text{on } S_1, \tag{19}$$

$$\frac{\partial\phi}{\partial n} = 0 \quad \text{on } S_2, \tag{20}$$

where $a(t)$ is the vertical acceleration (positive upward) of the container, and where V, S_1 and S_2 denote the fluid region, the free surface and the part of the liquid which is in contact with the wall of the container. The velocity potential $\phi(x,y,t)$ is related with the relative velocity V of the liquid with respect to the container by

$$V = \text{grad } \phi. \tag{21}$$

In Equations (18) & (19), $\eta(x,t)$ denotes the profile of the free surface measured from the free surface of the stationary state, while n in Equation (20) denotes the normal drawn outwards on S_2.

Variational principle

For our numerical example, we consider a two-dimensional rectangular container as shown in Figure 10, where h denotes the depth of the liquid in the stationary state. It

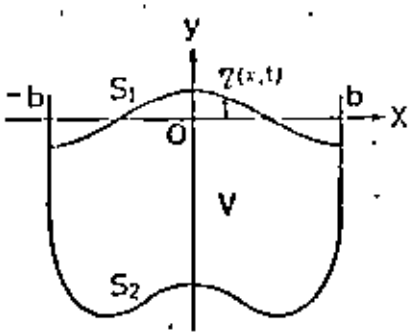

Figure 9 A container

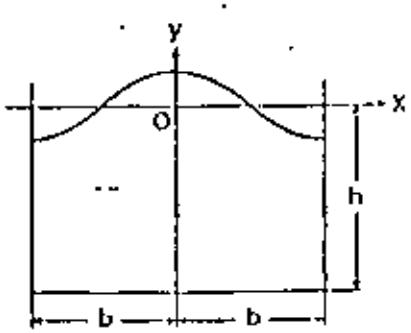

Figure 10 A two-dimensional rectangular container

is shown that the governing equations for the present problem are given by the stationary conditions of a functional defined by

$$\chi(t) = \frac{1}{2}\iint_{V(\eta)} \{(\frac{\partial\phi}{\partial x})^2 + (\frac{\partial\phi}{\partial y})^2\}dxdy + \frac{1}{2}(a(t) + g)\int_{-b}^{b}\eta^2 dx + \int_{-b}^{b}\frac{\partial\phi}{\partial t}\eta dx - \int_{-b}^{b}\frac{\partial\eta}{\partial t}\phi dx, \qquad (22)$$

where the flow region bounded by S_1 and S_2 are denoted by $V(\eta)$, emphasizing that it is dependent on $\eta(x,t)$. In the functional χ, the independent functions subject to variation are ϕ and η with no subsidiary conditions. It should be noted, however, that in Equation (22), the variation is taken at a certain definite time t, and $\partial\phi/\partial t$ and $\partial\eta/\partial t$ are treated as parameters not subject to variation. The functional (22) may be taken as an extension of Luke's variational principle.

Finite element formulation

For our finite element formulation, the fluid region is divided into a large number of triangular elements as shown in Figure 11. For an arbitrary triangular element such as shown in Figure 5, we assume ϕ to be a linear function of x and y, namely

$$\phi(x,y,t) = a + bx + cy, \qquad (23)$$

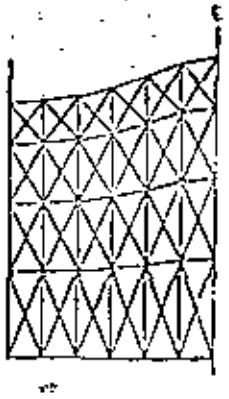

Figure 11 Mesh pattern

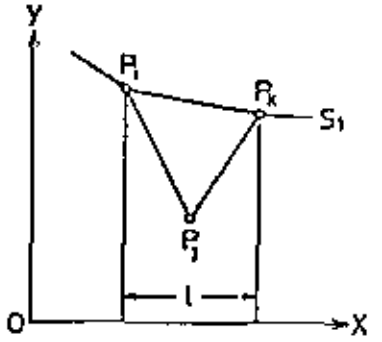

Figure 12 A triangular element with two nodal point on S_1

where a, b and c are time-dependent constants, values of which are determined in terms of the values of ϕ at the three vertices and we obtain

$$\partial\phi/\partial x = A^T\Phi, \tag{24-a}$$

$$\partial\phi/\partial y = B^T\Phi, \tag{24-b}$$

where A and B are the same as given by Eqs.(11-a) and (11-b), respectively, and where

$$\Phi^T = [\phi_1, \phi_2, \phi_3]. \tag{25}$$

The profile of the free boundary between two neighboring nodal points on S_1 is approximated by a straight element as shown in Figure 1?.

Since the problem is non-linear and time-dependent, we employ a step-by-step integration with respect to time. Denoting values of ϕ and η at the time of t_0 and $t_0+\Delta t$ by ϕ_0, η_0 and ϕ, η respectively, where Δt is time increment, we define increments $d\phi$ and $d\eta$ as follows :

$$\phi = \phi_0 + d\phi, \quad \eta = \eta_0 + d\eta. \tag{26}$$

We assume throughout following formulations that

$$d\phi << \phi_0, \qquad d\eta << \eta_0,$$

and that higher order terms can be neglected to obtain linearized equations with respect to $d\phi$ and $d\eta$, in a manner similar to the formulation developed in Reference 5.

A special care should be taken for an element which has nodal points on S_1. For example, for a triangular element which has two nodal points on S_1, we have

$$A = A_0 + C^T d\eta, \tag{27}$$

$$\partial\phi/\partial x = [A_0^T - d\eta^T A_1^T][\Phi_0 + d\Phi], \tag{28-a}$$

$$\partial\phi/\partial y = [B_0^T - d\eta^T B_1^T][\Phi_0 + d\Phi], \tag{28-b}$$

where Δ, Δ_0, A_0, A_1, B_0 and B_1 are defined in the same manner as in Reference 5, and where

$$C^T = (1/2)[x_k - x_j,\ 0,\ x_j - x_i], \tag{29}$$

$$d\eta^T = [d\eta_i,\ 0,\ d\eta_k]. \tag{30}$$

It is noted here concerning Equations (28-a) and (28-b) that ϕ_0 and $\phi_0+d\phi$ are matrices of the values of ϕ at the three vertices of the triangles (P_i^0, P_j, P_k^0) and (P_i, P_j, P_k) shown in Figure 13, respectively.

The functions $\phi(x,y,t)$ and $\eta(x,t)$ expressed by the use of these shape functions are substituted into the functional (22). By taking variations with respect to $d\phi$ and $d\eta$, and through linearization, we obtain following two equations as stationary conditions :

$$\sum_e (A_0A_0^T + B_0B_0^T)\Delta_0 d\phi + \sum_e [(A_1A_0^T + B_1B_0^T)\phi_0 C^T$$

$$- \{(A_0^T\phi_0 I + A_1\phi_0^T)A_1 + (B_0^T\phi_0 I + B_1\phi_0^T)B_1\}\Delta_0 d\eta$$

$$+ \sum_e (A_0A_0^T + B_0B_0^T)\phi_0\Delta_1 - \sum_e \Gamma\frac{\partial\eta}{\partial t} = 0 \tag{31}$$

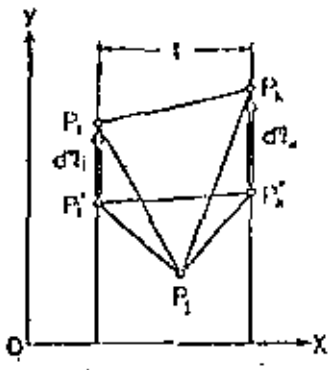

Figure 13 Triangular elements at t_0 and $t_0+\Delta t$

$$\sum_e C\Phi_0^T(A_0A_0^T + B_0B_0^T)d\Phi + [-\sum_e C\Phi_0^T(A_0\Phi_0A_1 + B_0\Phi_0^TB_1)$$

$$+ (a(t) + g)\sum_{S_e} F]d\eta + \frac{1}{2}\sum_e C\Phi_0^T(A_0A_0^T + B_0B_0^T)\Phi_0$$

$$+ \sum_{S_e} F[(a(t) + g)\eta_0 + \frac{\partial\phi}{\partial t}] = 0, \qquad (32)$$

where Σ_e and Σ_{S_e} denote summation with respect to all the elements and with respect to all the elements which have two nodal points on S_1, respectively, while I denotes unit matrix and

$$F = \begin{bmatrix} \ell/3 & \ell/6 \\ \ell/6 & \ell/3 \end{bmatrix} \qquad (33)$$

ℓ being the projected length of the straight element on S_1 onto the x-axis as shown in Figure 12.

By introducing the relations

$$\frac{\partial\phi}{\partial t} = \frac{2}{\Delta t}d\phi - (\frac{\partial\phi}{\partial t})_0, \quad \frac{\partial\eta}{\partial t} = \frac{2}{\Delta t}d\eta - (\frac{\partial\eta}{\partial t})_0 \qquad (34)$$

into Equations (31) and (32), we finally obtain the following equations for the determination of $d\phi$ and $d\eta$:

$$\left[\begin{array}{c:c} K_{11} & K_{12} \\ \hdashline K_{21} & K_{22} \end{array}\right] \left\{\begin{array}{c} d\phi \\ \hdashline d\eta \end{array}\right\} = \left\{\begin{array}{c} R_1 \\ \hdashline R_2 \end{array}\right\} \qquad (35)$$

where

$$K_{11} = \sum_e(A_0A_0^T + B_0B_0^T)\Delta_0 ;$$

$$K_{12} = \sum_e[(A_0A_0^T + B_0B_0^T)\Phi_0C^T - [(A_0^T\Phi_0I + A_0\Phi_0^T)A_1$$

$$+ (B_0^T\Phi_0I + B_0\Sigma_0^T B_1)\Delta_0] - \frac{2}{\Delta t}\sum_{S_e} F,$$

$$K_{21} = \sum_e C\Phi_0^T(A_0A_0^T + B_0B_0^T) + \frac{2}{\Delta t}\sum_{S_e} F.$$

$$K_{12} = -\sum_e C\phi_0^T(A_0\phi_0^T A_1 + B_0\phi_0^T B_1) + (a(t) + g)\sum_e F,$$

$$R_1 = -\sum_e (A_0A_0^T + B_0B_0^T)\phi_0 A_0 - \sum_e F\left(\frac{\partial\eta}{\partial t}\right)_0$$

$$R_2 = -\sum_e \frac{1}{2} C\phi_0^T(A_0A_0^T + B_0B_0^T)\phi_0$$

$$-\sum_e F[(a(t) + g)\eta_0 - \left(\frac{\partial\phi}{\partial t}\right)_0]. \qquad (36\text{-a,b,c,d,e,f})$$

By solving Equations (35), and substituting the values of $d\phi$ and $d\eta$ thus determined into Equations (26) we obtain ϕ and η at $t=t_0+\Delta t$.

For the start of the above procedure, values of ϕ, η, $\partial\phi/\partial t$ and $\partial\eta/\partial t$ at $t=0$ should be given. For this purpose, we assume that the liquid is stationary at $t=0$ and given a small rise of η such that

$$\phi = 0, \qquad \eta = d, \qquad (37)$$

where d is an initial rise vector properly chosen. Then, as suggested from Equations (18) and (19), we have

$$\frac{\partial\phi}{\partial t} = -(a(0) + g)d, \quad \frac{\partial\eta}{\partial t} = 0 \qquad \text{on } S_1, \qquad (38)$$

which are used as initial conditions.

It is noted that in order to reduce accumulation of time integration errors as small as possible, it is desirable to use a time integration scheme which has higher accuracy than Equations (34).

It is also noted that the mesh division is made at every time increment : when the profile of the free surface is obtained at $t=t_0+\Delta t$ as shown in Figure 11, the liquid region is divided into a new mesh pattern and the values of ϕ at newly defined nodal points are obtained by interpolation.

Numerical example

We take the two-dimensional container as shown in Figure 10 for a numerical example. Its dimension is :

2b=90 cm and h=60 cm. Then flow region is divided into a number of elements as shown in Figure 11. The container is assumed to be subjected to the following forced sinusoidal vertical displacement :

$$-a_0 \cos \omega t \qquad \text{for } t \geq 0 \tag{39}$$

where a_0 and ω are the amplitude and frequency of the forced oscillation respectively, and are given for the present numerical example as follows :

$$a_0 = 2.0 \text{ cm}, \quad \omega = 17.0 \text{ rad/sec.} \tag{40}$$

Some of the computed results are shown in the following.

Figure 14 shows timewise behaviors of $\eta(0,t)$ and $\eta(\pm b,t)$, where the wellknown nonlinear behavior is clearly observed : the upward amplitude is greater than the downward amplitude. Figure 15 shows the profile of the free surface at t=1.80 seconds and t=2.18 seconds. This profile is very similar to that of the standing waves observed in Taylor's experiment [Ref.20]. Figure 16 shows the pressure distribution acting on the wall of the container at t=1.63 seconds. In this figure, the dotted lines indicate static pressure. Figure 17 shows the velocity distribution of the liquid at t=0.5 second.

The frequency of the free oscillation of the liquid in the container was computed as a special case of the present finite element formulation, and was found to be 8.5 rad/sec. Consequently, Figure 14 shows time history of the so-called 1/2-subharmonic response.

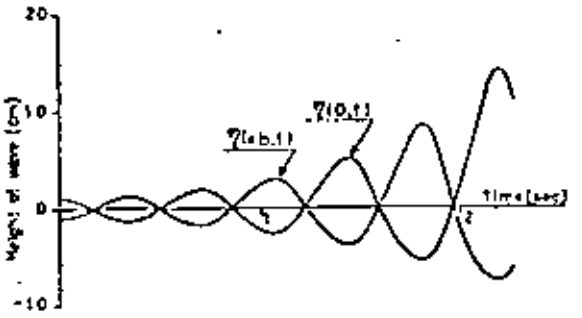

Figure 14 Time histories of $\eta(x,t)$

It is added that the time increment Δt for the above computation was taken to be 0.02 second, and that the initial profile d of the free surface was taken to be equal to the shape of the free surface in the first symmetrical mode of the free oscillation of the liquid and its amplitude was taken as 1 cm. It is finally added that the computing time for obtaining Figure 14 was of the order of 250 seconds by HITAC 8800/8700.

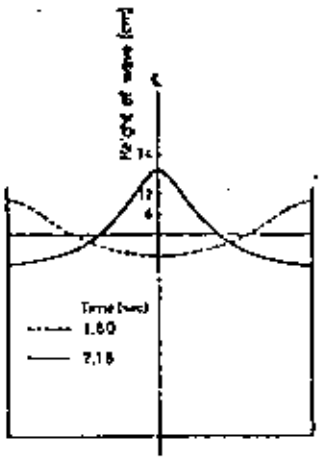

Figure 15 $\eta(x,t)$

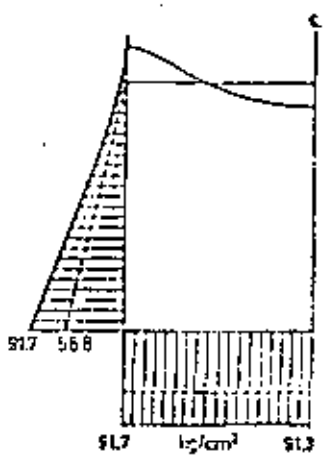

Figure 16 Pressure distribution

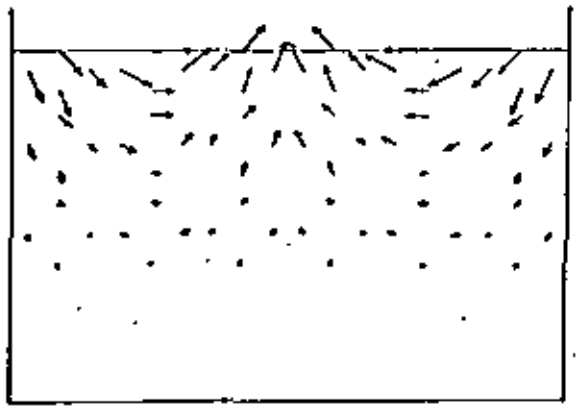

Figure 17 Flow field

FINAL REMARKS

It has been shown in the present paper that two nonlinear free surface problems under gravity are numerically solvable by the finite element method. These problems may be considered as typical examples which demonstrate the power of the finite element method in application to free surface problems under gravity.

REFERENCES

1. Abramson,H.N., "The Dynamic Behavior of Liquids in Moving Containers". NASA SP-106, 1966.

2. Benjamin,T.B. and Ursell,F., "The Stability of the Plane Free Surface of a Liquid in Vertical Periodic Motion". Proc. Roy. Soc. London, Series A, 225, pp.505-515, 1954.

3. Brebbia,C.A. and Connor,J.J., Editors, "Numerical Methods in Fluid Dynamics". Proceedings of the International Conference held at the University of Southampton, England, September 1973, Pentech Press, London, 1974.

4. Hutton,R.E., "An Investigation of Resonant, Nonlinear, Nonplanar Free Surface Oscillation of a Fluid". NASA TN D-1870, 1963.

5. Ikegawa,M. and Washizu,K., "Finite Element Method Applied to Analysis of Flow over a Spillway Crest". International Journal for Numerical Methods in Engineering, 6, pp.179-189, 1973.

6. Ikegawa,M., "Analysis of Unsteady Motion of a Liquid in a Container by the Finite Element Method (in Japanese)". Proceedings of National Symposium on Matrix Method of Structural Analysis and Design, pp.621-628, Society of Steel Construction of Japan, 1973.

7. Ikegawa,M., "Finite Element Analysis of Fluid Motion in a Container". Finite Element Methods in Flow Problems, edited by J.T.Oden et al., pp.737-738, UAH Press, 1974.

8. Kawai,T. and Watanabe,M., "Analysis of a Solitary Water Wave Problem by the Method of Weighted Residuals". Proceedings of the 2nd International Symposium on Finite Element Method in Flow Problems, Rapallo Italy, June 1976.

9. Luke,J.C., "A Variational Principle for a Fluid with a Free Surface". J. Fluid. Mech., 27, Part 2, pp.395-397, 1967.

10. McCorquodale,J.A. and Li,C.Y., "Finite Element Analysis of Sluice Gate Flow". Trans. Eng. Inst. Can., 14, 1971.

11. Moiseyev,N.N., "On the Theory of Nonlinear Vibrations of a Liquid of Finite Volume". Applied Mathematics and Mechanics (PMM), 22,5, pp.850-872, 1958.

12. Neuman,S.P. and Witherspoon,P.A., "Analysis of Non-steady Flow with a Free Surface Using the Finite Element Method". Water Resources Research, 7, 3, pp.611-623, 1971.

13. O'Carroll,M.J., "A Variational Principle for Ideal Flow over a Spillway" submitted to International Journal for Numerical Methods in Engineering, 1975.

14. O'Carroll,M.J., "Variational Principles for 2-dimensional Open Channel Flows". Proceedings of the Second International Symposium on Finite Element Methods in Flow Problems, Rappallo, Italy, June 1976.

15. O'Carroll,M.J. and Harrison,E.T., "A Variational Method for Free Boundary Problems" to appear in the Proceedings of IMA Conference on the Mathematics of Finite Elements and Applications, Brunel University, 1975.

16. O'Carroll,M.J., "Complementary Variational Principles for Steady Ideal Flows with Free Surfaces". Manchester Polytechnic Report, 1975.

17. Penney,W.G. and Price,A.T., "Finite Periodic Stationary Gravity Waves in a Perfect Liquid". Phil. Trans. Roy. Soc. London, Series A, 244, pp.254-284, 1952.

18. Southwell,R.V. and Vaisey,G., "Relaxation Methods Applied to Engineering Problems XII. Fluid Motions Characterized by 'Free' Stream-lines". Phil. Trans. Roy. Soc. London, Series A, 240, pp.117-160, 1946.

19. Taylor,C. and Davis, J., "Tidal and Long Wave Propagation — A Finite Element Approach". Computers & Fluids, 3, 2/3, pp.125-148, 1975.

20. Taylor,G.I., "An Experimental Study of Standing Waves". Proc. Roy. Soc. London, Series A, 218, pp.44-59, 1954.

21. Whitham,G.B., "Variational Methods and Applications to Water Waves". Proc. Roy. Soc. London, Series A, 299, pp.6-25, 1967.

INTERNATIONAL JOURNAL FOR NUMERICAL METHODS IN ENGINEERING, VOL. 6, 179-189 (1973)

FINITE ELEMENT METHOD APPLIED TO ANALYSIS OF FLOW OVER A SPILLWAY CREST

M. IKEGAWA* AND K. WASHIZU†
Department of Aeronautics, University of Tokyo, Tokyo, Japan

SUMMARY

Numerical analysis of fluid flow over a spillway is treated in the present paper. A variational principle is introduced for a flow with a free surface boundary under gravity, where the stream function and the profile of the free boundary are independent quantities subjected to variation. A new iteration method is formulated by the combined use of the variational principle and the finite element method. A numerical example based on the iterative method is illustrated. Results thus obtained show good agreement with those obtained from an empirical formula.

INTRODUCTION

Analysis of water flow over a spillway is an important engineering problem as pointed out by Theodore von Kármán in 1940.[1] As is well known, this is a difficult mathematical problem because it is nonlinear and the free water surface is unknown beforehand. Moreover, the flow is subcritical in the upstream portion of the crest of the spillway, while it is supercritical in the downstream portion. Also, there exists a transition region (the so-called control section) near the crest, and this adds another mathematical difficulty as stated below.

Southwell and Vaisey[2-4] treated fluid motions characterized by free stream lines by the use of the relaxation method. They introduced two iterative methods, named Method A and Method B, respectively, for the determination of the free stream lines. They applied these methods to several problems and found the existence of convergence difficulty in the determination of the free stream boundary, depending on whether the flow is subcritical or supercritical. The additional difficulty is that neither Method A alone nor Method B alone seems applicable for the determination of the free boundary surface of a flow over a spillway where there exists the transition region near the crest.

In the present paper, a variational principle is introduced for a flow with a free surface to begin with, and an iterative formulation by the use of the finite element method is made for the determination of the profile of the free boundary together with the field of flow over a spillway crest.

It is noted here that several problems of a flow with a free surface under gravity have been treated by a combined use of variational principles and the finite element method. For example, a sluice gate flow was treated by McCorquodale and Li,[5] while a non-steady flow of ground water was treated by Neuman and Witherspoon.[6]

GOVERNING EQUATIONS

A problem which will be treated in the present paper is as shown in Figure 1, where S_1, S_2, S_3 and S_4 denote the free stream boundary, the station of the far-upstream boundary, the channel bottom and the station of the far-downstream boundary, respectively. The x- and y-axes are taken in the horizontal and vertical directions, respectively. Assuming the flow to be two-dimensional, steady, incompressible, non-viscous and

* Graduate Student.
† Professor of Aeronautics and Astronautics.

Received 14 March 1972
Revised 24 April 1972

irrotational, the governing equation is found to be given by

$$\frac{\partial^2\psi}{\partial x^2}+\frac{\partial^2\psi}{\partial y^2}=0; \quad \text{in } V \tag{1}$$

where $\psi(x, y)$ is the stream function and V is the region bounded by the four boundaries.[3] The boundary conditions are given as follows.

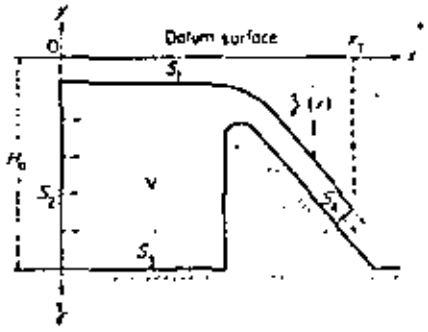

Figure 1. Flow over a spillway

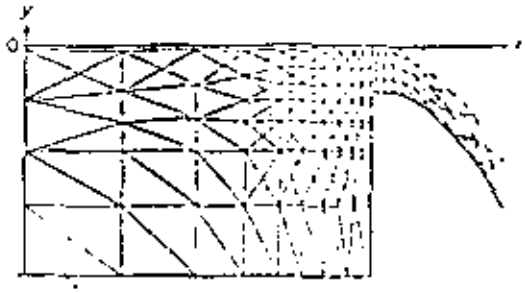

Figure 2. Mesh pattern

On the free boundary surface S_1 we have

$$\psi = 0 \tag{2}$$

$$\partial\psi/\partial n = -\sqrt{(2gz)} \tag{3}$$

where n is the normal drawn outwards on the boundary, $z(x)$ is the distance of the free surface measured from the datum surface of 'stagnation level' or 'asymptotic level' and g is the gravitational acceleration.[3,4]

On the channel bottom, S_3, we have

$$\psi = Q \tag{4}$$

where Q is the total rate of flow passing over the spillway per unit time. The value of Q is unknown beforehand.

On the far-upstream boundary S_2 and far-downstream boundary S_4, we assume

$$\text{the flow to be uniform;} \tag{5}$$

namely, the values of ψ are assumed to vary linearly along the boundaries S_2 and S_4, respectively.

Our problem is to obtain a smooth free boundary surface, together with the corresponding total rate of flow and flow field, by solving equation (1) under the boundary conditions, equations (2)–(5), with a further prescribed condition that the flow is subcritical in the upstream portion, while it is supercritical in the downstream portion. We shall treat this problem numerically by the use of the finite element method, where the field of interest is divided into a large number of triangular elements as shown in Figure 2.

DETERMINATION OF THE PROFILE OF THE FREE SURFACE BOUNDARY WHEN THE VALUE OF Q IS PRESCRIBED

Our initial interest will be focused on finding an interative procedure for the determination of the free boundary surface when the value of Q is prescribed, following the iterative methods proposed by Southwell and Vaisey.[4] We denote the prescribed value of Q by $\bar{Q}$, and assume a first approximate profile of the free boundary $z(x)$. The procedure of deriving a finite element formulation corresponding to equation (1) is well known,[1] and values of ψ at nodal points in the flow region of interest are determined by the finite element method. Then, values of $\partial\psi/\partial n$ on the free boundary are calculated numerically by the use of values of ψ thus obtained, and are substituted into equation (3) to yield an iterated value of $z(x)$, which provides a second

approximation for the free boundary. Again, the finite element method is applied to obtain values of ϕ in the region with the iterated boundary. This iteration procedure, called Method I hereafter, is repeated as shown in Table I, until the profile of the free boundary surface is found to have converged. This is a method for obtaining the profile of a subcritical flow.[3]

Table I. Flow chart of Method I

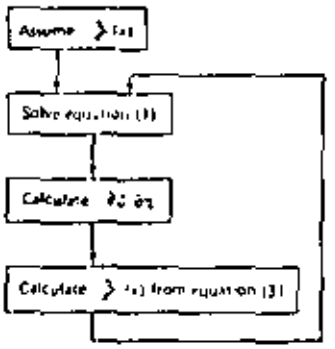

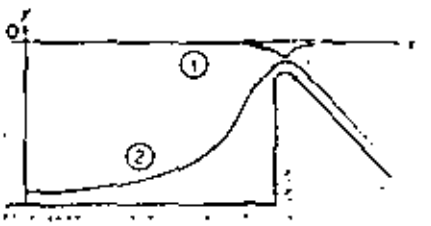

Figure 3. Numerical examples of subcritical and supercritical flow; 1, subcritical flow; 2, supercritical flow

Another method, called Method II hereafter, assumes a first approximate profile of the free boundary $z(x)$ to begin with, and values of ϕ at nodal points are determined by the finite element method. Then, the profile of the free boundary is varied, as outlined in Appendix A, until values of $\partial\phi/\partial n$ on the free boundary calculated by the use of ϕ thus obtained become equal to values of $\partial\bar{\phi}/\partial n$ obtained from equation (3) by the use of the first approximate value of $z(x)$, while values of ϕ at all nodes are kept unchanged. Again, the finite element method is applied to obtain values of ϕ in the region with the iterated boundary. This iteration procedure is repeated as shown in Table II, until the profile of the free boundary surface is found to have converged. This is a method for obtaining the profile of a supercritical flow.[3] Examples of free boundary surfaces thus determined by Methods I and II are illustrated in Figure 3.

Table II. Flow chart for Method II

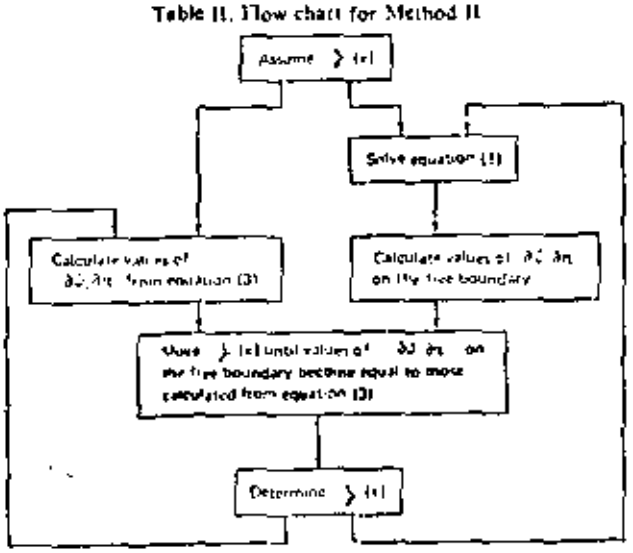

A VARIATIONAL FORMULATION FOR THE FLOW CHARACTERIZED BY THE FREE SURFACE

As mentioned in the Introduction, the flow over a spillway crest is characterized such that the flow in the upstream portion is subcritical, while the flow in the downstream portion is supercritical, and neither Method I alone nor Method II alone is applicable for the determination of the free stream boundary. Consequently, a new iteration process should be derived.

The first-named author proposed an iteration procedure based on a variational principle in which not only equation (1) but also equation (3) is given as stationary conditions. The functional of the principle is given as follows

$$\chi = \frac{1}{2}\iint_{V(z)}\left\{\left(\frac{\partial\psi}{\partial x}\right)^2+\left(\frac{\partial\psi}{\partial y}\right)^2\right\}dx\,dy+\frac{1}{2}\int_0^{x_1} g z^2\,dx \tag{6}$$

where we denote the region of the flow bounded by the four boundaries S_1, S_2, S_3 and S_4 by $V(z)$, emphasizing that it is dependent on $z(x)$. As shown in Figure 1, x_1 denotes the x-co-ordinate of the point of intersection of the two boundaries S_1 and S_4. In the functional (6), the independent quantities subjected to variation are $\psi(x, y)$ and $z(x)$, while conditions (2), (4) and (5) are taken as subsidiary conditions. This variational principle has been found to be a special case of the principle derived by Luke.[4] However, the proof of the above statement will be given here since a reference is found later in the present work.

For the proof, we see that the first variation of χ is given by the first-order quantity of the following expression

$$\frac{1}{2}\iint_{V(z)+\delta V(z)}\left\{\left(\frac{\partial\psi}{\partial x}+\frac{\partial\delta\psi}{\partial x}\right)^2+\left(\frac{\partial\psi}{\partial y}+\frac{\partial\delta\psi}{\partial y}\right)^2\right\}dx\,dy+\frac{1}{2}\int_0^{x_1+\delta x_1} g(z+\delta z)^2\,dx$$
$$-\frac{1}{2}\iint_{V(z)}\left\{\left(\frac{\partial\psi}{\partial x}\right)^2+\left(\frac{\partial\psi}{\partial y}\right)^2\right\}dx\,dy-\frac{1}{2}\int_0^{x_1} g z^2\,dx \tag{7}$$

or

$$\frac{1}{2}\iint_{V(z)}\left\{\left(\frac{\partial\psi}{\partial x}+\frac{\partial\delta\psi}{\partial x}\right)^2+\left(\frac{\partial\psi}{\partial y}+\frac{\partial\delta\psi}{\partial y}\right)^2\right\}dx\,dy-\frac{1}{2}\iint_{V(z)}\left\{\left(\frac{\partial\psi}{\partial x}\right)^2+\left(\frac{\partial\psi}{\partial y}\right)^2\right\}dx\,dy$$
$$+\frac{1}{2}\int_0^{x_1} g(z+\delta z)^2\,dx-\frac{1}{2}\int_0^{x_1} g z^2\,dx+\frac{1}{2}\iint_{\delta V(z)}\left\{\left(\frac{\partial\psi}{\partial x}+\frac{\partial\delta\psi}{\partial x}\right)^2+\left(\frac{\partial\psi}{\partial y}+\frac{\partial\delta\psi}{\partial y}\right)^2\right\}dx\,dy \tag{8}$$

where $\delta V(z)$ is an increment of $V(z)$ due to the variation of $z(x)$ and we have

$$dx\,dy = -dx\,\delta z \quad \text{in } \delta V(z) \tag{9}$$

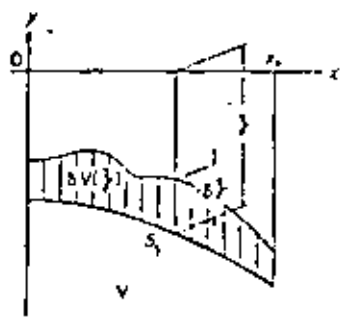

Figure 4. $\delta V(z)$ and δz

as shown in Figure 4. Thus, equation (8) provides

$$\delta\chi = \iint_{R(n)} \left(\frac{\partial\psi}{\partial x}\frac{\partial\delta\phi}{\partial x} + \frac{\partial\phi}{\partial y}\frac{\partial\delta\psi}{\partial y} \right) dx\,dy + \int_0^{x_n} g_2 \delta z\,dx - \frac{1}{2}\int_0^{x_n} \left\{ \left(\frac{\partial\psi}{\partial x}\right)^2 - \left(\frac{\partial\psi}{\partial y}\right)^2 \right\} \delta z\,dx \tag{10}$$

or

$$\delta\chi = -\iint_{R(n)} \left(\frac{\partial^2\psi}{\partial x^2} + \frac{\partial^2\psi}{\partial y^2} \right) \delta\phi\,dx\,dy + \int_0^{x_n} \left\{ g_2 - \frac{1}{2}\left(\frac{\partial\psi}{\partial n}\right)^2 \right\} \delta z\,dx \tag{11}$$

Consequently, equations (1) and (3) are found to be the stationary conditions of the functional χ.

TRIANGULAR ELEMENTS

For a finite element formulation, the domain of interest is divided into a large number of triangular elements as shown in Figure 2. For a triangular element of Figure 5, we assume ψ to be a linear function of x and y, namely

$$\psi = a + bx + cy \tag{12}$$

where a, b and c are constants, values of which are determined in terms of values of ψ at the three vertices as follows

$$\left.\begin{aligned} \psi_i &= a + bx_i + cy_i \\ \psi_j &= a + bx_j + cy_j \\ \psi_k &= a + bx_k + cy_k \end{aligned}\right\} \tag{13}$$

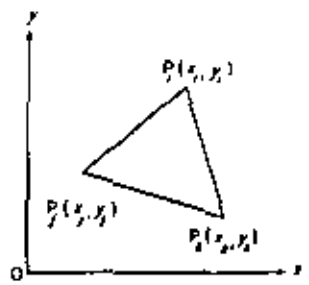

Figure 5. A triangular element $P_iP_jP_k$

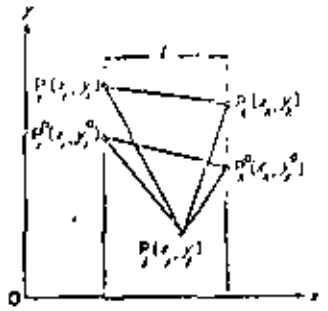

Figure 6. Displacement of a triangular element $P_i^0P_jP_k^0$ to $P_iP_jP_k$

By the use of equations (12) and (13), we have

$$\partial\psi/\partial x = \mathbf{A}^{\mathrm{T}}\boldsymbol{\psi} \tag{14a}$$

$$\partial\psi/\partial y = \mathbf{B}^{\mathrm{T}}\boldsymbol{\psi} \tag{14b}$$

where

$$\mathbf{A}^{\mathrm{T}} = \frac{1}{2\Delta}[y_j - y_k, y_k - y_i, y_i - y_j] \tag{15a}$$

$$\mathbf{B}^{\mathrm{T}} = \frac{1}{2\Delta}[x_k - x_j, x_i - x_k, x_j - x_i] \tag{15b}$$

$$\boldsymbol{\psi}^{\mathrm{T}} = [\psi_i, \psi_j, \psi_k] \tag{15c}$$

and where

$$2\Delta = \begin{vmatrix} 1 & x_i & y_i \\ 1 & x_j & y_j \\ 1 & x_k & y_k \end{vmatrix} \tag{16}$$

Next, some relations will be derived for a triangular element belonging to the free boundary S_1 as shown in Figure 6. The profile of the free boundary between two neighbouring nodal points on S_1 is approximated by a straight segment in the present formulation based on the finite element method. We assume the side $P_i^0P_j^0$ lies on the free boundary and increase the ordinates of P_i^0 and P_j^0 by dy_i and dy_j, respectively, to obtain another triangle $P_iP_jP_k$, where

$$y_i = y_i^0 + dy_i, \quad y_k = y_k^0 + dy_k \tag{17}$$

We shall express the area, $\partial\psi/\partial x$ and $\partial\psi/\partial y$ of the triangular element $P_iP_jP_k$ in terms of dy_i, dy_j and the co-ordinates of the original triangle $P_i^0P_j^0P_k^0$, assuming that

$$dy_i, dy_k \ll y_i^0, y_k^0$$

and denoting values of ψ at the vertices of the triangle $P_iP_jP_k$ by ψ_i, ψ_j and ψ_k. After some algebraic manipulation, we have for the area of the triangle

$$\Delta = \Delta_0 + \mathbf{P}^{\mathrm{T}}\mathbf{dy} \tag{18}$$

where

$$\mathbf{P}^{\mathrm{T}} = \tfrac{1}{2}[x_k - x_j, x_i - x_k, x_j - x_i] \tag{19a}$$

$$\mathbf{dy}^{\mathrm{T}} = [dy_i, 0, dy_k] \tag{19b}$$

and

$$2\Delta = \begin{vmatrix} 1 & x_i & y_i \\ 1 & x_j & y_j \\ 1 & x_k & y_k \end{vmatrix}, \quad 2\Delta_0 = \begin{vmatrix} 1 & x_i & y_i^0 \\ 1 & x_j & y_j \\ 1 & x_k & y_k^0 \end{vmatrix} \tag{19c}$$

On the other hand, we have for $\partial\psi/\partial x$ and $\partial\psi/\partial y$

$$\frac{\partial\psi}{\partial x} = \mathbf{A}_0^{\mathrm{T}}\boldsymbol{\psi} - \mathbf{dy}^{\mathrm{T}}\mathbf{A}_1^{\mathrm{T}}\boldsymbol{\psi} \tag{20a}$$

$$\frac{\partial\psi}{\partial y} = \mathbf{B}_0^{\mathrm{T}}\boldsymbol{\psi} - \mathbf{dy}^{\mathrm{T}}\mathbf{B}_1^{\mathrm{T}}\boldsymbol{\psi} \tag{20b}$$

where

$$\mathbf{A}_0^{\mathrm{T}} = \frac{1}{2\Delta_0}[y_j - y_k^0, y_k^0 - y_i^0, y_i^0 - y_j] \tag{21a}$$

$$\mathbf{A}_1 = \frac{1}{2\Delta_0}\begin{bmatrix} \dfrac{(y_j - y_k^0)(x_k - x_j)}{2\Delta_0}, & 0, & 1 + \dfrac{(y_j - y_k^0)(x_j - x_i)}{2\Delta_0} \\ 1 + \dfrac{(y_k^0 - y_i^0)(x_k - x_j)}{2\Delta_0}, & 0, & -1 + \dfrac{(y_k^0 - y_i^0)(x_j - x_i)}{2\Delta_0} \\ -1 + \dfrac{(y_i^0 - y_j)(x_k - x_j)}{2\Delta_0}, & 0, & \dfrac{(y_i^0 - y_j)(x_j - x_i)}{2\Delta_0} \end{bmatrix} \tag{22a}$$

and

$$\mathbf{B}_0^{\mathrm{T}} = \frac{1}{2\Delta_0}[x_k - x_j, x_i - x_k, x_j - x_i] \tag{21b}$$

$$\mathbf{B}_1 = \frac{1}{2\Delta_0}\begin{bmatrix} \dfrac{(x_k - x_j)(x_k - x_j)}{2\Delta_0}, & 0, & \dfrac{(x_k - x_j)(x_j - x_i)}{2\Delta_0} \\ \dfrac{(x_i - x_k)(x_k - x_j)}{2\Delta_0}, & 0, & \dfrac{(x_i - x_k)(x_j - x_i)}{2\Delta_0} \\ \dfrac{(x_j - x_i)(x_k - x_j)}{2\Delta_0}, & 0, & \dfrac{(x_j - x_i)(x_j - x_i)}{2\Delta_0} \end{bmatrix} \tag{22b}$$

Finally, we consider a triangle belonging to the free boundary S_1 as shown in Figure 7. We assume the vertex P_1^0 lies on the free boundary and increase the ordinate of P_1^0 by dy_1 to obtain another triangle $P_1P_2P_3$. Geometrical relations similar to the triangle shown in Figure 6 are derivable for the triangle shown in

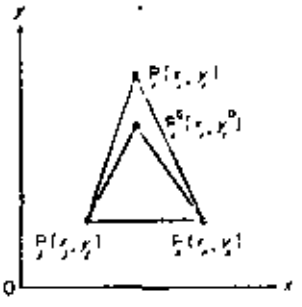

Figure 7. Displacement of a triangular element $P_1^0P_2P_3$ to $P_1P_2P_3$

Figure 7, by putting dy_2 equal to zero in equations (18), (20a) and (20b). Needless to say, equations (18), (20a) and (20b) reduce to equations (16), (14a) and (14b), when dy_1 and dy_2 are taken equal to zero.

A NEW ITERATION METHOD

Here we introduce a new iteration method which may be taken as a kind of Newton–Raphson method. We assume that the nth approximate values of the stream function at all the nodal points as well as the coordinates of the free surface boundary have been obtained, and we denote these values by ψ_0 and z_0, respectively. We shall proceed to obtain the $(n+1)$th approximate values, which are denoted by ψ and z, respectively, setting

$$\psi = \psi_0 + d\psi, \quad z = z_0 + dz \tag{23}$$

Then, the functional χ for the $(n+1)$th approximation is given by

$$\begin{aligned}\chi = \frac{1}{2}\sum_e &(\psi_0 + d\psi)^T([A_0 - A_1\,dy][A_0^T - dy^T A_1^T] \\ &+ [B_0 - B_1\,dy][B_0^T - dy^T B_1^T])(\psi_0 - d\psi)(\Delta_0 + F^T dy) \\ &+ \frac{1}{2}g\sum_{S_1}(z_0 + dz)^T F(z_0 + dz)\end{aligned} \tag{24}$$

where $\sum_e$ and $\sum_{S_1}$ denote summations with respect to elements and with respect to nodal points on S_1, respectively, and

$$F = \begin{bmatrix} l/3 & l/6 \\ l/6 & l/3 \end{bmatrix} \tag{25}$$

l being the projected length of the straight segment on S_1 onto the x-axis as shown in Figure 6. Remembering the subsidiary conditions (2), (4) and (5) together with equation (8) and noticing that

$$\delta dy = -\delta dz \quad \text{on } S_1 \tag{26}$$

we take the first variation of equation (24) to obtain

$$\begin{aligned}\delta\chi = \sum_e \delta\, d\psi^T\{&(A_0 A_0^T + B_0 B_0^T)\psi_0 \Delta_0 \\ &+ \int[(A_0^T\psi_0 I + A_1\psi_0^T)A_1 + (B_0^T\psi_0 I + B_0\psi_0^T)B_1]\,dz\,\Delta_0 \\ &+ (A_0 A_0^T + B_0 B_0^T)\,d\psi\,\Delta_0 \\ &- (A_0 A_0^T + B_0 B_0^T)\psi_0 P^T\,dz\} \\ &- \frac{1}{2}\sum_e \delta\, dz^T P\{\psi_0^T(A_0 A_0^T + B_0 B_0^T)\psi_0 \\ &+ 2\psi_0^T(A_0\psi_0^T A_1 + B_0\psi_0^T B_1)\,dz \\ &+ 2\psi_0^T(A_0 A_0^T + B_0 B_0^T)\,d\psi\} \\ &+ g\sum_{S_2} \delta\, dz^T(Fz_0 + \Gamma\,dz)\end{aligned} \tag{27}$$

where the first and second Σ_e mean summations with respect to all the nodes within $P(z)$ and on S_2, respectively and where I denotes unit matrix. The stationary conditions obtained from equation (27) are summarized as follows

$$\left[\begin{array}{c|c} G_{11} & G_{12} \\ \hline G_{21} & G_{22} \end{array}\right]\left\{\begin{array}{c} dz \\ \hline d\psi \end{array}\right\} = \left\{\begin{array}{c} R_1 \\ \hline R_2 \end{array}\right\} \tag{28}$$

where

$$G_{11} = P\psi_0^T(A_0\psi_0^T A_1 + B_0\psi_0^T B_1) - gP \tag{29a}$$

$$G_{12} = P\psi_0^T(A_0 A_0^T + B_0 B_0^T) \tag{29b}$$

$$G_{21} = [(A_0^T\psi_0 I + A_0\psi_0^T)A_1 + (B_0^T\psi_0 I + B_0\psi_0^T)B_1]\Delta_0 - (A_0 A_0^T + B_0 B_0^T)\psi_0 P^T \tag{29c}$$

$$G_{22} = (A_0 A_0^T + B_0 B_0^T)\Delta_0 \tag{29d}$$

$$R_1 = gFz_0 - \int P\psi_0^T(A_0 A_0^T + B_0 B_0^T)\psi_0 \tag{29e}$$

$$R_2 = -(A_0 A_0^T + B_0 B_0^T)\psi_0\Delta_0 \tag{29f}$$

and where matrix notations in equation (28) are defined with respect to all the related nodes. By solving equation (28), and substituting the values of dz and $d\psi$ thus determined into equation (23), we can obtain the $(n+1)$th approximation for z and ψ.

A NUMERICAL EXAMPLE

We take the spillway crest as shown in Figure 2 as an example, and divide the flow region of interest into a number of triangular elements. Main dimensions of the spillway are listed in Appendix B. Our iteration proceeds by first assuming an approximate value of Q and denote it by Q_1, and choosing the first approximate profile of the free boundary surface in such a way that it coincides with that of the uniform subcritical flow at S_2, and with that of the uniform supercritical flow at S_4, both belonging to Q_1. Then, keeping the value of Q_1 unchanged, and by the use of iteration based on equation (28), the profile of the free boundary corresponding to Q_1 is to be found. As far as our experience in numerical computation shows, it seems that if $Q_1 > Q_{exact}$, where Q_{exact} is the exact value of Q, the free surface boundary converges to a profile which, as shown in Figure 8(a), has broken segments near the crest of the spillway. On the other hand, if $Q_1 < Q_{exact}$, the profile of the free surface does not seem to converge to a definite form, but seems to show a divergent behaviour near the crest of the spillway, as shown in Figure 8(b). Consequently, we may vary a guessed value of Q step by step, until we find a most appropriate value of Q for assuring a smooth free surface. Needless to say, it is advisable to choose the first approximation of Q with the aid of empirical formulae such as given by Reference 9 and briefly stated in Appendix B.

Figure 9 shows a free boundary surface we thusly obtained numerically. The value of Q obtained by the present method is 5·75 m²/sec, while the value of Q obtained from an empirical formula in Appendix B is found to be 5·90 m²/sec. This seems to be an encouraging result.

Figures 10 and 11 show positions of four vertical sections A, B, C and D near the crest of the spillway, and pressure distribution along these sections. In each of Figures 11, the abscissa is the pressure P in ton m²,

Figure 8. Convergence characteristics of the profile

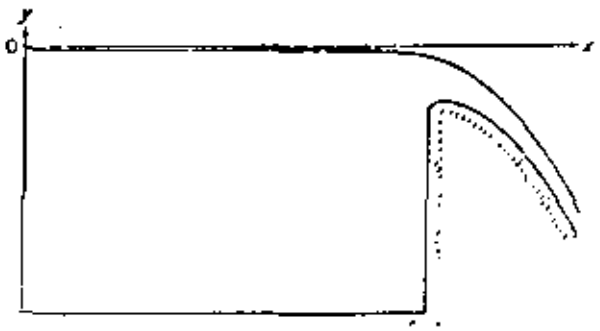

Figure 9. Free boundary surface

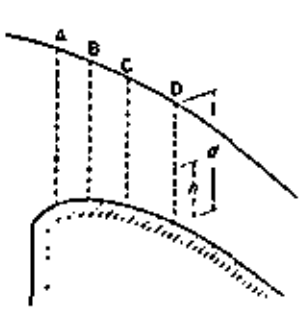

Figure 10. Station A, B, C and D

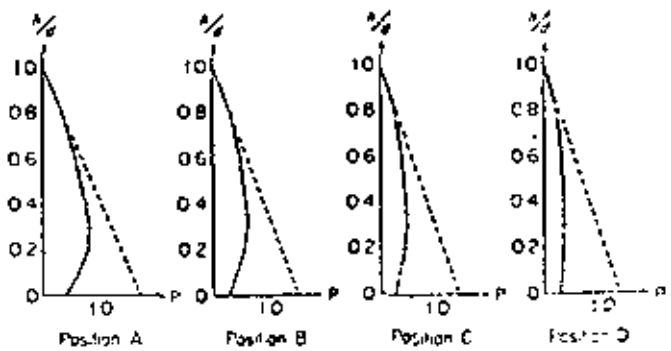

Figure 11. Pressure distributions along the station A, B, C and D

while the ordinate is h/d, where h is the distance of a point on the section from the boundary S_1 and d is the depth of water at the section as indicated in Figure 10. In Figure 11, solid broken lines show actual pressure, while dotted lines show static pressure due to the gravity only. It is added that for the calculation of pressure, the so-called 'zooming technique' was employed to provide finer meshes around the crest than those shown in Figure 2.

Finally, some of our experience in the computation of this particular example are briefly stated here. Figure 2 shows the subdivision before the zooming proceeds, and the total number of elements used in the

figure are 304. After zooming, the number of triangular elements in the region of interest are nearly tripled. The number of iterations and computation time cannot be given exactly mainly due to our limited experience. However, the computation time for obtaining a free stream line as shown in Figure 9 was of the order of 700 sec using a HITAC 5020-E computer at the University of Tokyo.

CONCLUDING REMARKS

The non-linear problem of analysing the flow over the spillway has been shown to be solved numerically by the finite element method. The convergence difficulty reported in References 2–4 has been overcome by the introduction of a variational principle. The present problem may be considered as a typical example of a combination of the variational method and the finite element method.

ACKNOWLEDGEMENT

The authors would like to express their sincere thanks to Professor K. Horikawa, Department of Civil Engineering, University of Tokyo, for his advice and comments given to the authors during the preparation of this paper. They also wish to express their gratitude to the referee for some of the cited references.

APPENDIX A

Variation of the profile of the free boundary in Method II

We consider a triangular element $P_iP_jP_k$ as shown in Figure 5, and assume that the vertex P_i is on the free surface. Referring to equations (14a) and (14b), the velocity at the vertex P_i is given as follows

$$\left(\frac{\partial\psi}{\partial n}\right)_i^2 = \left(\frac{\partial\psi}{\partial x}\right)_i^2 + \left(\frac{\partial\psi}{\partial y}\right)_i^2 = \psi^{\mathrm{T}}(AA^{\mathrm{T}} + BB^{\mathrm{T}})\psi \tag{A-1}$$

On the other hand, we obtain from equation (3)

$$\left(\frac{\partial\psi}{\partial n}\right)_i^2 = 2gz \tag{A-2}$$

By the use of equations (A-1) and (A-2), we have

$$\psi^{\mathrm{T}}(AA^{\mathrm{T}} + BB^{\mathrm{T}})\psi = F^2 \tag{A-3}$$

where

$$F^2 = 2gz$$

The ordinate of P_i is varied until equation (A-2) is satisfied, while values of ψ at the three vertices as well as the value of F^2 are kept unchanged. Thus the only unknown quantity to be determined is y_i. After some algebraic manipulation, equation (A-3) is reduced to a quadratic equation with respect to y_i. Namely

$$ay_i^2 + by_i + c = 0 \tag{A-4}$$

where

$$\begin{aligned} a &= (\psi_j - \psi_k)^2 - (x_k - x_j)^2 F^2 \\ b &= -2[(\psi_j - \psi_k)\{(\psi_i - \psi_k)y_j - (\psi_i - \psi_j)y_k\} \\ &\quad + (x_k - x_j)(x_j y_k - x_k y_j + x_i y_j - x_i y_k) F^2] \\ c &= \{(\psi_i - \psi_k)y_j - (\psi_i - \psi_j)y_k\}^2 \\ &\quad - (x_j y_k - x_k y_j + x_i y_j - x_i y_k)^2 F^2 + \psi^{\mathrm{T}} BB^{\mathrm{T}} \psi \end{aligned}$$

Solving equation (A-4), and choosing an appropriate one of two roots of y_i, we can obtain an iterated profile of the free boundary surface. Then, the finite element method is applied to obtain values of ψ in the region with the iterated boundary. Thus, the iteration proceeds as shown in Table II.

APPENDIX B

Geometry of a spillway and an empirical formula

The profile of the spillway taken in our example is the so-called 'Creager profile' as shown in Figure 12. Two geometrical quantities a and ξH_d determine the profile, where H_d is the design head given by

$$H_d = \frac{a}{0{\cdot}282} \tag{B-1}$$

An empirical formula for the total rate of flow over the spillway crest is given as follows[9]

$$Q = cBH^{\frac{3}{2}} \tag{B-2}$$

where Q is the total rate of flow, B is the width of the flow, H is the distance between the datum surface and spillway crest and

$$c = 1{\cdot}58\frac{1 + A(H/H_d)}{1 + 0{\cdot}646(H/H_d)}$$

$$A = \frac{c_d - 1{\cdot}6}{1{\cdot}60 - 0{\cdot}5c_d}$$

$$c_d = 1{\cdot}971 + 0{\cdot}498\xi + 6{\cdot}63\xi^2$$

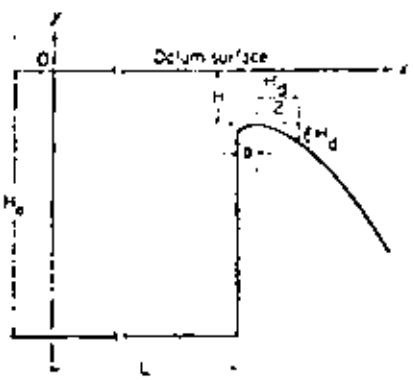

Figure 12. Geometry of the spillway

Main dimensions of the spillway used in our example are as follows

$$a = 0{\cdot}6\text{ m}, \quad \xi = 0{\cdot}151$$

$$H_d = 2{\cdot}127\text{ m}, \quad H = 2\text{ m}$$

$$H_0 = 10\text{ m}, \quad L = 15\text{ m}, \quad B = 1\text{ m}$$

REFERENCES

1. T. von Kármán, 'The engineer grapples with non-linear problems', *Bull. Math. Soc.* **46**, 615–683 (1940).
2. R. V. Southwell and G. Vaisey, 'Relaxation methods applied to engineering problems. VIII. Plane-potential problems involving specified normal gradients', *Proc. Roy. Soc. A* **182**, 129–151 (1943).
3. R. V. Southwell and G. Vaisey, 'Relaxation methods applied to engineering problems. XII. Fluid motions characterized by 'free stream-lines'', *Phil. Trans. Roy. Soc. Lond.* **240A**, 117–161 (1946).
4. R. V. Southwell and G. Vaisey, *Relaxation Methods in Theoretical Physics*, Oxford University Press, London, 1946.
5. J. A. McCorquodale and C. Y. Li, 'Finite element analysis of sluice gate flow', *Trans. Eng. Inst. Can.* **14** (1971). (Published in *Engineering Journal*.)
6. S. P. Neuman and P. A. Witherspoon, 'Analysis of non-steady flow with a free surface using the finite element method', *Water Resources Research*, **7**, 611–623 (1971).
7. O. C. Zienkiewicz, *The Finite Element Method in Engineering Science*, McGraw-Hill, London, 1971.
8. J. C. Luke, 'A variational principle for a fluid with a free surface', *J. Fluid Mech.* **27**, 395–397 (1967).
9. M. Homma and K. Aki, *Monomobe Suirigaku* (in Japanese), Iwanami Book Publishing Company, Tokyo, 1962.

WATER RESOURCES RESEARCH, VOL. 17, NO. 5, PAGES 1360-1366, OCTOBER 1981

Two-Phase Flow Simulation of Air Storage in an Aquifer

DAVID MEIRI

NUS Corporation, Rockville, Maryland 20850

A two-phase flow model is presented for simulating air storage in an aquifer used for a compressed air storage system. The governing equations describing the flow of air and water are coupled nonlinear partial differential equations and are solved by a Galerkin finite element method. The resulting computer model is used to simulate the air-water displacement in a one-dimensional storage reservoir during daily air cycling. The corresponding saturation and pressure variations and the effects of reservoir permeability on the system are presented. The results obtained realistically describe a variable volume storage system with only a small change in pressure.

INTRODUCTION

Compressed air storage systems have recently received considerable attention as an economically and technically attractive means of storing off-peak surplus energy for subsequent use during peak periods. Air is compressed during low demand periods by motor-driven compressors and is stored in an underground reservoir. When power is required, the compressed air is withdrawn from the reservoir, heated in combustion chambers by burning fuel, and then expanded through the turbines to drive electric generators. Four types of underground storage space are available: mined caverns, salt cavities, depleted oil and gas fields, and porous aquifers. However, only the latter mode of storage is considered in this paper.

Earlier studies of the performance of storage reservoirs [*Ayers and Hoover*, 1974; *Smith et al.*, 1979] assumed that the storage reservoir has a constant volume with only a single-phase flow of air. While this assumption appears to be reasonable for cavern storage, it is questionable whether it leads to acceptable results if an aquifer is selected for underground storage. A more realistic approach to aquifer performance may involve the analysis of the two-phase flow of air and water in which the volume of the reservoir will vary during air cycling. Many publications are available on the analysis of multiphase flow in porous media; most of them employ finite difference methods almost exclusively [*Douglas et al.*, 1959; *Blair and Weinaug*, 1969; *Nolen and Berry*, 1972; *Settari and Aziz*, 1975]. An alternative approach, based on the finite element techniques, was advanced by several investigators using various types of basis functions in order to obtain higher accuracy [*Lewis et al.*, 1975; *Dolen*, 1976; *Spivak et al.*, 1977; *Hasakorn and Pinder*, 1978].

The objective of this paper is to introduce the application of two-phase flow analysis to simulate air storage in an aquifer. The nonlinear partial differential equations describing two-phase flow of air and water through porous media are solved by a Galerkin finite element method. The time integration is carried out by a finite difference scheme, and the resulting system of equations is solved simultaneously for the air and water phase. The validity of the proposed model has been verified by *Meiri* [1979] by comparing the numerical results with the solutions of oil-water and gas-oil displacement problems. The model is employed here to simulate the performance of a storage aquifer during a daily air cycle. The air-water displacement and the effects of variations of reservoir permeability on the system have been investigated.

Paper number 1W1118
0043-1397/81/001W-01118$01.00

TWO-PHASE FLOW EQUATIONS

The governing equations for multiphase flow are obtained by combining Darcy's law and the conservation of mass equation for each fluid phase. Thus, the simultaneous flow of air and water phases in an anisotropic porous medium is described by the following differential equations [*Peaceman*, 1977]:

$$\frac{\partial}{\partial x_i}\left[k_w \frac{k_{rw}}{\mu_w B_w}\left(\frac{\partial p_w}{\partial x_j} + \rho_w g \frac{\partial x_3}{\partial x_j}\right)\right] = \frac{\partial}{\partial t}\left(\phi S_w / B_w\right) \tag{1}$$

$$\frac{\partial}{\partial x_i}\left[k_a \frac{k_{ra}}{\mu_a B_a}\left(\frac{\partial p_a}{\partial x_j} + \rho_a g \frac{\partial x_3}{\partial x_j}\right)\right] = \frac{\partial}{\partial t}\left(\phi S_a / B_a\right) \tag{2}$$

$$i, j = 1, 2, 3$$

where k_w is the intrinsic permeability tensor, k_{rw} and k_{ra} are the relative permeabilities of air and water, respectively; p_a and p_w are the pressures in air and water, respectively; S_a and S_w are the saturation of air and water, respectively; ϕ is the porosity of the porous medium; B_a and B_w are the formation volume factors of air and water, respectively defined as the ratio of the volume of the fluid phase at reservoir pressure and temperature to its volume at standard conditions; ρ_a and ρ_w are the densities of air and water, respectively; μ_a and μ_w are the viscosities of air and water, respectively; g is the acceleration of gravity; and x_i are the Cartesian coordinates (x_3 being the vertical coordinate oriented positive upward).

There are two additional equations involving capillary pressure and degree of saturation:

$$p_a - p_w = p_c \tag{3}$$

$$S_a + S_w = 1 \tag{4}$$

where p_c is the capillary pressure. This set of four equations can be further rearranged into two coupled equations with two dependent variables, p_a and p_w.

The time derivative of the saturations and the formation volume factors in (1) and (2) can be expressed in terms of the dependent variables if it is assumed that (1) capillary pressure is uniquely related to saturation, and (2) formation factors are functions of pressure only. In addition, the medium is assumed nondeformable so that the porosity is constant. With these assumptions, the flow equations are transformed to

$$\frac{\partial}{\partial x_i}\left[k_a \lambda_a \left(\frac{\partial p_a}{\partial x_i} + \rho_a g \frac{\partial x_3}{\partial x_i}\right)\right] = \phi\left[-(1/B_a)\frac{dS_w}{dp_c}\left(\frac{\partial p_a}{\partial t} - \frac{\partial p_w}{\partial t}\right)\right.$$

$$+ S_- \frac{d}{dp_-}(1/\beta_-)\frac{\partial p_-}{\partial t} \qquad (5)$$

$$\frac{\partial}{\partial x_i}\left[k_r\lambda_-\left(\frac{\partial p_-}{\partial x_i} + \rho_- g\frac{\partial x_3}{\partial x_i}\right)\right] = \phi\left[(1/\beta_-)\frac{dS_-}{dp_-}\left(\frac{\partial p_-}{\partial t} - \frac{\partial p_-}{\partial t}\right) + S_- \frac{d}{dp_-}(1/\beta_-)\frac{\partial p_-}{\partial t}\right] \qquad (6)$$

where $\lambda_+ = k_{r+}/(\mu_+\beta_+)$ and $\lambda_- = k_{r-}/(\mu_-\beta_-)$. The solution of these equations for the two unknowns p_+ and p_- requires appropriate initial and boundary conditions. Note that all other variables can be obtained from tables and empirical equations.

At initial time, it is common to assume a static state of equilibrium at which the water saturation is known; hence

$$S_-(x_i, 0) = S_0(x_i) \qquad i = 1, 2, 3 \qquad (7)$$

In addition to this there are, in general, two types of boundary conditions, prescribed pressure and prescribed flux normal to the boundary. Let the boundary of the flow region, Γ, consist of two types of segments, Γ_1 and Γ_2. Then the prescribed pressure or Dirichlet boundary condition can be written as

$$p = P \quad \text{on} \quad \Gamma_1 \qquad (8)$$

and the prescribed flux or Neumann boundary condition is given by

$$k_r\frac{k_r}{\mu}\left(\frac{\partial p}{\partial x_j} + \rho g\frac{\partial x_3}{\partial x_j}\right)l_i = -U \quad \text{on} \quad \Gamma_2 \qquad i, j = 1, 2, 3 \qquad (9)$$

where P and U are prescribed functions, which might also be dependent on time, and l_i are the direction cosines of the unit outward normal on Γ. Note that the boundary conditions have to be specified for each of the phases participating in the flow.

Finite Element Formulation

Applying the finite element method [e.g., *Zienkiewicz*, 1977], the flow region R is divided into a network of elements. These elements are connected at common nodes and collectively approximate the shape of the region. For each element the two dependent variables p_+ and p_- are being approximated, respectively, by

$$p_+ = [N]\{P_+\}^e \qquad (10a)$$

$$p_- = [N]\{P_-\}^e \qquad (10b)$$

where $[N]$ is a row matrix denoting a set of linearly independent basis (shape) functions, and $\{P_+\}^e$ and $\{P_-\}^e$ are column vectors representing undetermined time-dependent pressure values at element nodes.

According to the Galerkin method, the error between the approximate solution and the true solution is required to be orthogonal to the basis functions. Applying these orthogonality conditions to the flow equations (5) and (6) and application of Green's theorem to those integrals containing second-order space derivatives yield

$$\int_{R^e}\frac{\partial[N]^T}{\partial x_i}k_r\lambda_+\frac{\partial[N]}{\partial x_j}\{P_+\}^e\,dR + \int_{R^e}\frac{\partial[N]^T}{\partial x_i}k_r\lambda_+\rho_+ g\,dR + \int_{\Gamma^e}[N]^T(U_+/\beta_+)\,d\Gamma + \int_{R^e}[N]^T\phi S_+\frac{d}{dp_+}(1/\beta_+)[N]\frac{\partial}{\partial t}\{P_+\}^e\,dR - \int_{R^e}[N]^T\phi(1/\beta_+)\frac{dS_+}{dp_+}[N]\left\{\frac{\partial}{\partial t}\{P_+\}^e - \frac{\partial}{\partial t}\{P_+\}^e\right\}dR = 0 \qquad (11)$$

$$\int_{R^e}\frac{\partial[N]^T}{\partial x_i}k_r\lambda_-\frac{\partial[N]}{\partial x_j}\{P_-\}^e\,dR + \int_{R^e}\frac{\partial[N]^T}{\partial x_i}k_r\lambda_-\rho_- g\,dR + \int_{\Gamma^e}[N]^T(U_-/\beta_-)\,d\Gamma + \int_{R^e}[N]^T\phi S_-\frac{d}{dp_-}(1/\beta_-)[N]\frac{\partial}{\partial t}\{P_-\}^e\,dR + \int_{R^e}[N]^T\phi(1/\beta_-)\frac{dS_-}{dp_-}[N]\left\{\frac{\partial}{\partial t}\{P_+\}^e - \frac{\partial}{\partial t}\{P_-\}^e\right\}dR = 0 \qquad (12)$$

$$i, j = 1, 2, 3$$

where U_+ and U_- are the (normal) fluxes of air and water phases, respectively. It may be noted that the surface integrals in (11) and (12) apply only to external boundary points. In addition, it is assumed that k_r and ϕ are constant at each element, while the other variables are defined at the element nodes similar to (10).

Rearranging the terms in (11) and (12), the following element matrix equations for air and water are obtained:

$$[B_+]^e\{P_+\}^e + [C_+]^e\frac{\partial}{\partial t}\{P_+\}^e + [D_+]^e\frac{\partial}{\partial t}\{P_+\}^e = \{Q_+\}^e - \{G_+\}^e \qquad (13)$$

$$[B_-]^e\{P_-\}^e + [C_-]^e\frac{\partial}{\partial t}\{P_-\}^e + [D_-]^e\frac{\partial}{\partial t}\{P_-\}^e = \{Q_-\}^e - \{G_-\}^e \qquad (14)$$

A complete description of the element coefficient matrices is given by *Meiri* [1979].

Combining (13) and (14) in a suitable order and assembling the element matrices into the global matrices yield the following system of equations:

$$[B]\{P\} + [C]\frac{\partial}{\partial t}\{P\} = \{Q\} - \{G\} \qquad (15)$$

where $[B]$ is the conductance matrix, $[C]$ is the capacitance matrix, $\{Q\}$ is the flux vector, $\{G\}$ is the gravity vector, and $\{P\}$ is the dependent pressure vector. Note that $\{Q\}$ is zero for all internal nodal points that do not act as sources or sinks and $\{G\}$ is equal to zero for horizontal flow. Generally, $[B]$ and $[C]$ are sparse banded and nonsymmetric matrices.

Replacing the time derivative in (15) by a finite difference approximation and expressing $\{P\}$ as the weighted average of its values at the beginning and end of each time step yield:

$$\left(\gamma[B] + \frac{1}{\Delta t}[C]\right)\{P\}_{t+\Delta t} = \{Q\} - \{G\} - \left((1-\gamma)[B] - \frac{1}{\Delta t}[C]\right)\{P\}_t \qquad (16)$$

where γ is the time integration factor. If $\gamma = 0$, the scheme is explicit or forward difference approximation; when $\gamma = 1$, the scheme becomes a fully implicit or backward difference approximation; $\gamma = 0.5$ corresponds to a central difference or Crank-Nicholson scheme, which is also implicit.

Due to the nonlinear nature of (16) an implicit scheme is employed ($\gamma \geq 0$) which requires some iterations in order to obtain a satisfactory solution. First, (16) is solved by a direct

method, such as Gaussian elimination, for the unknown $\{P\}$ at time $t + \Delta t$, using initial conditions to evaluate its coefficients. Next, the coefficients are reevaluated at half the time step, and then (16) is again solved by Gaussian elimination to yield improved values of $\{P\}_{t+\Delta t}$. This iterative procedure continues until the difference between successive iterations is within a specific tolerance. Note that $\{P\}_t$ remains unchanged during the iterative process. Since the coefficients are evaluated at half the time step, the values of $\{P\}$ are required at this point. At the beginning of each time step, these values are estimated by linear extrapolation from two previous time steps, while in subsequent iterations they are improved by taking an average of the most recent values of $\{P\}_{t+\Delta t}$ and $\{P\}_t$.

Numerical Results

The computer model presented was tested by *Meiri* [1979] on two displacement-type problems involving an incompressible oil-water system and compressible gas-oil system. The numerical results compared favorably with the known solutions of these problems. In this paper the model is employed to simulate the air-water displacement in a storage aquifer during air cycling. The calculations are performed for a one-dimensional vertical column aquifer, and the effects of fluid densities and viscosities as well as capillary and gravitational forces are included in the analysis.

Description of Model Reservoir

The model reservoir to be analyzed is of cylindrical geometry where the air-water displacement takes place only along the vertical axis. The dimensions and parameters describing the reservoir are similar to the Media Galesville Aquifer [*Katz and Lady*, 1976]. The reservoir diameter is 110 m and the height is 20 m. The porous medium is considered homogeneous with (reference) permeability of 500 mdarcy (5×10^{-13} m^2) and porosity of 0.2. The system is assumed to be under isothermal conditions of 300°F (149°C), and the aquifer discovery (initial) pressure is 50 atm (5066 kPa). The air viscosity is selected as 0.024 cP (2.4×10^{-7} kg/m s), and the water viscosity as 0.3 cP (3×10^{-4} kg/m s). The densities of air and water at standard conditions (i.e., in English units a pressure of 14.7 psia and a temperature of 60°F) are 1.22 and 10^3 kg/m^3, respectively.

Assuming ideal gas behavior for the air, the formation volume factor of air at reservoir temperature can be expressed as [*Meiri*, 1979]

$$B_a = 1.46/p_a \tag{17}$$

where p_a is calculated in atm. If the water is assumed to be only slightly compressible, then the formation volume factor of water is expressed as [*Meiri*, 1979]

$$B_w = 1/(1 + c_w p_w) \tag{18}$$

where the compressibility of water c_w is 5.14×10^{-5} atm^{-1} (52 Pa), and p_w is calculated in atm.

The relative permeabilities of water and air as functions of water saturation and the capillary pressure as a function of saturation are obtained from relationships proposed by *Brooks and Corey* [1966]:

$$k_{rw} = S_e^{(2+3\lambda)/\lambda} \tag{19a}$$

$$k_{ra} = (1 - S_e)^2 (1 - S_e^{(2+\lambda)/\lambda}) \tag{19b}$$

$$p_c = p_d / (S_e)^{1/\lambda} \tag{19c}$$

where $S_e = (S_w - S_{wr})/(1 - S_{wr})$ is the effective saturation, S_{wr} is the irreducible saturation, ξ is the pore size distribution index, and p_d is the bubbling pressure. The values for ξ, S_{wr}, and p_d are given as 3.0, 0.2, and 0.0166 atm (1.65 kPa), respectively, corresponding to sand with permeability of 500 mdarcy (5×10^{-13} m^2).

Reservoir Simulation

The reservoir simulation is carried out in two stages. In the first (initiation stage), air is injected into the aquifer reservoir at pressure exceeding the hydrostatic pore pressure. The injected air displaces the water in the aquifer, which is initially fully saturated. The water continues to be displaced and also compressed until the air zone accounts for a sizeable volume, two thirds of the reservoir pore volume, for example, as depicted in Figure 1. During this stage, the water pressure at the bottom of the reservoir is maintained at its initial value of 50 atm (5066 kPa). A significant amount of water not displaced remains in the pores of the air zone. The residual water occupies from 20% (the irreducible water saturation) at the top of the reservoir to almost 60% at the bottom of the air zone.

In the second stage (operation stage), air is injected into and withdrawn from the reservoir according to the daily air cycle. During this stage, further enlargements of the air zone may be accomplished. Since the air mass flow rate required is approximately proportional to the power produced, a constant flow boundary condition is chosen to approximate constant power production. At the top of the column reservoir, the air mass flow is set equal to 2.44×10^{-4} kg s^{-1} m^{-2}, and no water is assumed to cross this boundary. At the bottom there is no flow of air, and the water pressure is specified at 50 atm (5066 kPa).

The reservoir height was subdivided into 24 one-dimensional linear elements. Each element was of cylindrical shape with variable length but constant circular cross section. A finer mesh was used along the air-water transition zone in order to improve the accuracy of the numerical solution. This, however, required the use of smaller time steps in order to avoid convergence problems. Relative permeabilities were weighted upstream in the direction of the flow, and the capacitance matrix was lumped at the nodes. For detailed discussion of upstream weighting and lumping matrix see, for example, *Meiri* [1979].

Integration with respect to time was executed for a value of $\gamma = 0.5$ (Crank-Nicholson scheme). Time steps were restricted such that the maximum saturation change for each time step was 5%. This results in an average time step of 0.5 hour. Iterations in each time step were continued until the maximum change in pressure was less than 0.005 atm. Approximately three iterations were required to meet this criterion. For convergence criterion of 0.005 atm, only two iterations were needed. This conservative criterion for convergence was necessary since the capillary pressure (the pressure difference between air and water phases) was very small in comparison to each phase pressure.

To simulate a daily air storage cycle, air was injected into the reservoir for a 10-hour period at a constant mass rate. After a 2-hour idle period, air was withdrawn from the reservoir for 10 hours at the same mass rate, which was again followed by a 2-hour idle period. The magnitude of the air flow was selected in such a way that 12% of the total stored air mass was cycling. The simulation continued until no significant difference was observed between two successive cycles. Hence, the

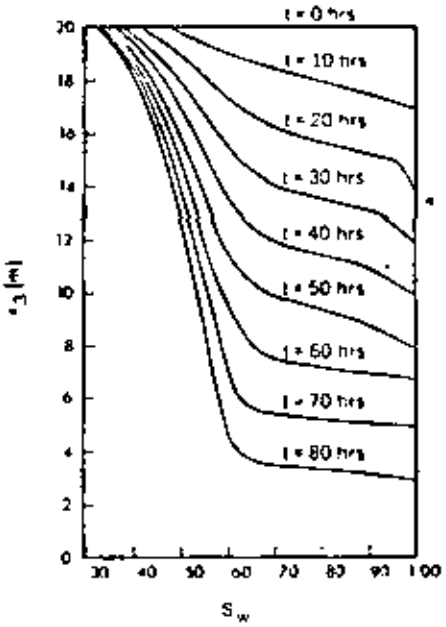

Fig. 1. Calculated water saturation profiles during the air zone initiation stage

following results describe the reservoir behavior after cyclic response is fully developed.

Water saturation profiles calculated after equal injection and withdrawal times of 10 hours for the reference permeability of 500 mdarcy (5×10^{-13} m^2) are shown in Figure 2. As expected, when air is injected into the aquifer, the displacement front moves downward, increasing the volume of air and decreasing the volume of water in the pores. When air is removed from storage, the front moves back (upward) with a corresponding shrinkage of the air zone. The saturation distribution in the transition zone after withdrawal clearly shows that the thickness of the transition zone is reduced.

While there is a significant change in the volume of air stored after injection and withdrawal periods, there is only slight change in the air pressure, as shown in Figure 3. The discharging pressure is obviously lower than the charging pressure, but the difference is very small, less than 1 atm. For a similar reservoir geometry and parameters, assuming only a single-phase of air (dry aquifer) with radial flow, air pressure calculations have shown an increase of slightly more than 3 atm during a 10-hour injection period [*Smith et al.*, 1979]. It can be also observed from Figure 3 that air pressure curves after injection and withdrawal are not the same. This is in contrast to the case of single-phase flow where the pressure curves would be approximately mirror images of each other.

The displacement process described above is strongly influenced by the permeability of the porous medium. For this paper, three different permeabilities were selected, using the same relative permeability-saturation relationship but different capillary pressure curves. There are several formulas in the literature describing the relationship between the (intrinsic) permeability k and various properties of the soil. Many of these formulas have the general form [*Harleman et al.*, 1963]

$$k = C_1 d^2 \tag{20}$$

where d is either the effective or the mean grain diameter and C_1 is a coefficient, depending on the geometry of the pore system. The bubbling pressure can also be related to the effective grain diameter by the following relationship [*Polubarinova-Kochina*, 1962]:

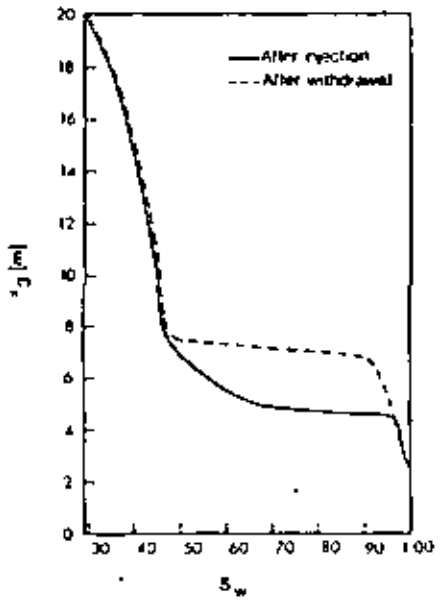

Fig. 2. Calculated water saturation profiles after equal injection and withdrawal times of 10 hours each.

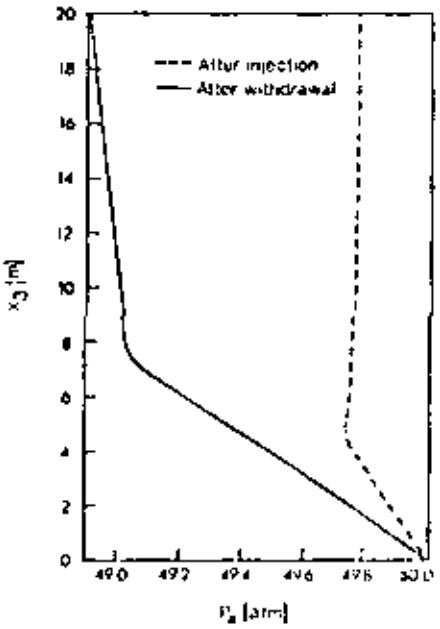

Fig. 3. Calculated air pressure profiles after equal injection and withdrawal times of 10 hours each.

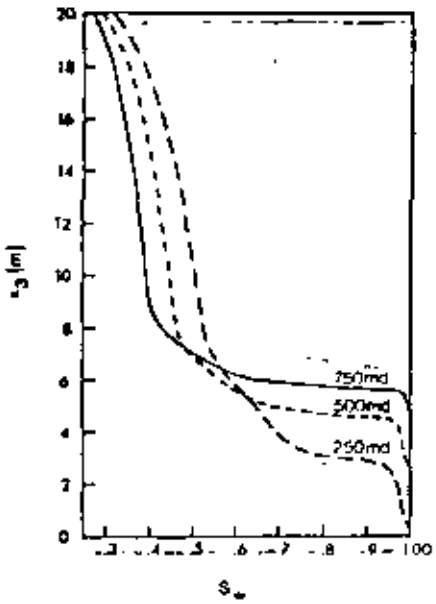

Fig 4. Calculated water saturation profiles for various permeabilities after 10 hours of injection

$$p_b = \frac{C_1}{d}\left(\frac{1-\phi}{\phi}\right) \tag{21}$$

where ϕ is the porosity and C_1 is a coefficient that depends on the type of soil. Combining (20) and (21) yields the following relationship:

$$p_b = C_1\left(\frac{1-\phi}{\phi}\right)k^{1/2} \tag{22}$$

The coefficient C_1 can be determined now for the reference permeability and the corresponding bubbling pressure. If the same porosity and irreducible saturation are assumed for all permeability values, then the corresponding bubbling pressure values and capillary pressure curves can be determined.

In Figures 4 and 5, the calculated water saturation profiles for various values of permeability after 10 hours of injection and 10 hours of withdrawal of air at the same constant mass rate are shown, respectively. It can be seen that the saturation curves are considerably different from each other. As the reservoir permeability increases, the amount of residual interstitial water remaining in the air zone significantly decreases in both cycles. This leads to a more desirable air storage characteristic. With decreasing permeability, the saturation front moves downward, and the thickness of the transition zone widens. Although not shown in these figures, flow calculations clearly indicate that as reservoir permeability increases water migrates faster out of the reservoir during injection and into the reservoir during withdrawal.

The calculated air pressure profiles for various values of permeability after 10 hours of injection and 10 hours of withdrawal of air at the same constant mass rate are shown in Figures 6 and 7, respectively. It can be seen from these curves that a decrease in reservoir permeability raises the required injection pressure (compressor outlet pressure), while increase in permeability lowers the required injection pressure. This phenomena has been also closely observed for the single-phase flow calculations presented by *Smith et al.* [1939]. When air is being withdrawn instead of injected, decrease in reservoir permeability lowers the resultant withdrawal pressure (turbine inlet pressure). Increasing permeability, however,

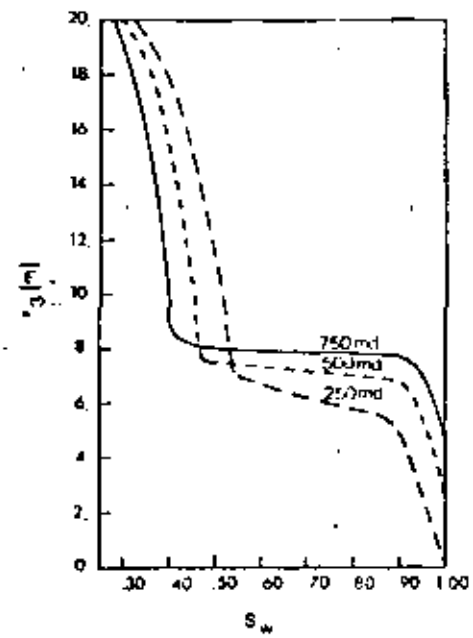

Fig 5. Calculated water saturation profiles for various permeabilities after 10 hours of withdrawal.

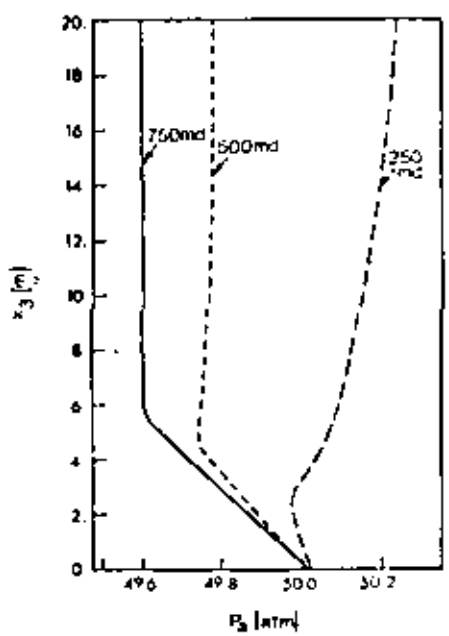

Fig 6. Calculated air pressure profiles for various permeabilities after 10 hours of injection

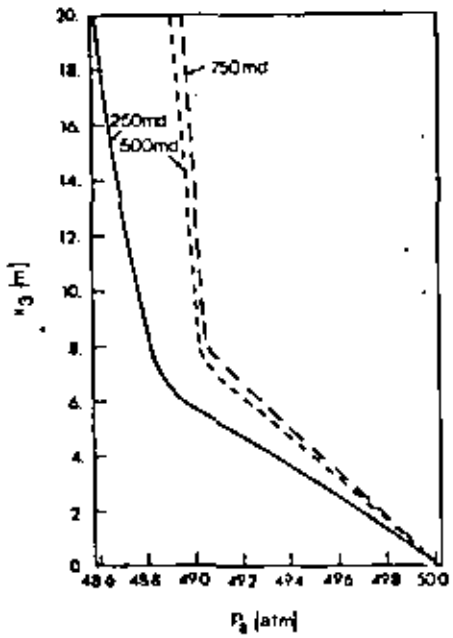

Fig. 7. Calculated air pressure profiles for various permeabilities after 10 hours of withdrawal

raises the resultant withdrawal pressure. In both cases, increasing permeability leads to a more stable pressure distribution in the reservoir, and the pressure swings during air cycles are very small. This is a very desirable situation which will bring to even more closely constant power production. Decrease in permeability brings an increase in pressure gradient in the reservoir, and the difference in pressure between injection and withdrawal increases.

Conclusions

The two-phase flow model based on a Galerkin finite element technique successfully simulates the performance of a storage aquifer during air cycling. Although no other numerical or experimental results are available for comparison purposes, results obtained herein appear to be realistic. Based on these results which are preliminary in their nature, the following conclusions pertinent to the design and operation of compressed air storage system can be advanced:

1. The porous aquifer selected as an underground storage reservoir for a compressed air storage system acts like a large elastic container in which volume, and to a lesser extent, pressure changes during injection and withdrawal cycles. This resembles closely the variable volume, constant pressure storage system.

2. After air storage development and during operation, approximately 20 to 50% residual interstitial water remains in the air zone. This results in reduction of air storage capacity and air deliverability. The presence of mobile water in the air zone can cause adverse impacts on well casing material and surface facilities.

3. Reservoir permeability appears to be a very important characteristic in determining the rate of water displacement and air deliverability. With increasing permeability, the rate of water migration increases, the thickness of the transition zone narrows, and the amount of interstitial water remaining in the air zone decreases.

4. Under the condition of constant mass flow rate of air during injection and withdrawal periods, variations in reservoir permeability show significant effect on the pressure distribution. Decreasing permeability increases the pressure gradient, while increasing permeability leads to a more stable pressure distribution in the reservoir.

Notation

- A cross-sectional area.
- c compressibility.
- C soil coefficient.
- d effective grain diameter.
- g acceleration of gravity.
- k_r relative permeability.
- k_{ij} intrinsic permeability tensor.
- l_i directional cosines.
- L length.
- N_i shape functions.
- p pressure.
- p_b bubbling pressure.
- p_c capillary pressure.
- P prescribed pressure.
- R flow region.
- S saturation.
- S_e effective saturation.
- S_{wr} irreducible water saturation.
- t time.
- U prescribed flux.
- x_i cartesian coordinates.
- x_3 vertical coordinate positive upward.
- Γ boundary of flow region.
- β formation volume factor.
- γ time integration factor.
- Δ difference.
- Δt time step.
- λ mobility coefficient, $k_r/(\mu\beta)$.
- μ viscosity.
- ξ pore size distribution index.
- ρ density.
- ϕ porosity.

Subscripts

- a air.
- i, j indexes.
- w water.

Superscripts

- e element
- T transpose.
- $\sim$ numerical approximation.

Acknowledgment. The work described in this paper is based on the author's doctoral thesis at the University of Wisconsin-Milwaukee. The author wishes to thank G. M. Karadi, H. J. Pincus, and N. J. Salamon for their support and guidance and J. W. Mercer for the critical review. Acknowledgment is also extended to NUS Corporation for technical assistance.

References

Avery, D. L., and D. Q. Hoover, Gas turbine systems using underground air storage, *Proc. Am. Power Conf.*, 36, 379–386, 1974.

Blair, P. M., and C. F. Weinaug, Solution of two-phase flow problems using implicit difference equations, *Soc. Pet. Eng. J.*, 9, 417–424, 1969.

Brooks, R. H., and A. T. Corey, Properties of porous media affecting fluid flow, *J. Irrig. Drain. Div. Am. Soc. Civ. Eng.*, 92(IR2), 61–68, 1966.

Dalen, V., Immiscible flow by finite element, in *Proceedings of the First International Conference on Finite Elements in Water Resources, Princeton University*, pp. 3.69–3.90, Pentech, London, 1976.

Douglas, J., Jr., D. W. Peaceman, and H. S. Rachford, Jr., A method for calculating multi-dimensional immiscible displacement, *Trans. AIME*, 216, 297–308, 1959.

Hardeman, D. R. E., P. F. Mehlhorn, and R. R. Rumer, Dispersion-permeability correlation in porous media, *J. Hydraul. Div. Am. Soc. Civ. Eng.*, 89(HY2), 67–85, 1963.

Huyakorn, P. S., and G. F. Pinder, Solution of two-phase flow using a new finite element technique, in *Proceedings of the International Conference on Applied Numerical Modeling, University of Southampton*, pp. 375–390, John Wiley, New York, 1977.

Katz, D. L., and E. R. Lady, *Compressed Air Storage for Electric Power Generation*, Ulrichs, Ann Arbor, Mich., 1976.

Lewis, R. W., E. A. Verner, and O. C. Zienkiewicz, A finite element approach to two-phase flow in porous media, in *Finite Elements in Fluids*, vol. 1, edited by R. H. Gallagher et al., pp. 183–199, John Wiley, New York, 1975.

Meus, D., Analysis of compressed air aquifer storage by finite element method, Doctoral thesis, Univ. of Wisc.-Milwaukee, Milwaukee, 1979.

Nolen, J. S., and D. W. Berry, Tests of the stability and time-step sensitivity of semi-implicit reservoir simulation techniques, *Soc. Pet. Eng. J.*, 12, 253–266, 1972.

Peaceman, D. W., *Fundamentals of Numerical Reservoir Simulation*, Elsevier, New York, 1977.

Polubarinova-Kochina, P. Ya., *Theory of Ground Water Movement*, Engl. transl. by R. J. M. DeWiest, Princeton University Press, Princeton, N. J., 1962.

Settari, A., and K. Aziz, Treatment of nonlinear terms in the numerical solution of partial differential equations for multiphase flow in porous media, *Int. J. Multiphase Flow*, 1, 817–844, 1975.

Smith, G. C., L. E. Wiles, and W. V. Losciutoff, Numerical analysis of temperature and flow effects in a dry, one-dimensional aquifer used for compressed air energy storage, *Rep. PNL-2546*, Pac. Northwest Lab., Richland, Wash., Feb. 1979.

Spivak, A., H. S. Price, and A. Settari, Solution of the equations for multidimensional two-phase immiscible flow by variational methods, *Soc. Pet. Eng. J.*, 17, 27–41, 1977.

Zienkiewicz, O. C., *The Finite Element Method in Engineering Science*, McGraw-Hill, New York, 1971.

(Received January 2, 1981;
revised June 23, 1981;
accepted July 8, 1981.)

DIVISION DE EDUCACION CONTINUA
FACULTAD DE INGENIERIA U.N.A.M.

EL METODO DEL ELEMENTO FINITO EN LA INGENIERIA MECANICA

A N E X O S

DR. NICHOLAS JOHN SALAMON

ABRIL, 1982

SECTION I. - HEADING CARD

IDENTIFICATION "HED"

cols 1-72

FORMAT: ALPHANUMERIC

SECTION II. - "MASTER CONTROL CARD"

ANALYSIS							
NUMNP	NELTYP	LL	NP	NDYN	MODEX	NAD	KEQB
cols 1-5	6-10	11-15	16-20	21-25	26-30	31-35	36-40

FORMAT(8I5)

NUMNP - No. of nodes (if Eq. 0 use two blank cards)

NELTYP - No. of types of elements

LL - No. of structural load cases (Eq. 0 for dynamic analysis)

NP - Frequencies to be found in the eigenvalue solution (applies for LL = 0)

NDYN - Analysis type:
Enter 0 for static analysis
1 eigenvalue/vector sol
2 forced dynamic response by mode superposition
3 response espectrum analysis
4 direct step by step integration

MODEX - Execution mode:
Enter 0 for problem solution
1 for data check only

NAD - No. of vectors applies only for NDYN = 1

KEQB - No. of D. O. F. Eq. 0 for automatic calculation

SAP INPUT DATA SHEET

Sheet _____

SECTION III - "NODAL POINT DATA"

NODES DEFINITION												
Coordinate System	Node Number	Translation Boundary Condition Code (X,Y,Z)			Rotation Boundary Condition Code (X,Y,Z)			Coordinates for Cylindrical (X=R,Z=θ)			Node No. Increment	Nodal Temperature
CT	N	IX(N,1)	IX(N,2)	IX(N,3)	IX(N,4)	IX(N,5)	IX(N,6)	X(N)	Y(N)	Z(N)	k(N)*	T(N)
cols 1	2-5	6-10	11-15	16-20	21-25	26-30	31-35	36-45	46-55	56-65	66-70	71-80

*Use for node generation with Node No. increment = k(N)

FORMAT(A1,I4,6I5,3F10.0,I5,F10.0)

SECTION III - "NODAL POINT DATA"

NODES DEFINITION												
Coordinate System	Node Number	Translation Boundary Condition Code (X,Y,Z)			Rotation Boundary Condition Code (X,Y,Z)			Coordinates for Cylindrical (X=R,Z=θ)			Node No. Increment	Nodal Temperature
CT	N	IX(N,1)	IX(N,2)	IX(N,3)	IX(N,4)	IX(N,5)	IX(N,6)	X(N)	Y(N)	Z(N)	k(N)*	T(N)
cols 1	2-5	6-10	11-15	16-20	21-25	26-30	31-35	36-45	46-55	56-65	66-70	71-80

*Use for node generation with Node No. increment = k(N)

FORMAT(A1,I4,6I5,3F10.0,I5,F10.0)

SECTION IV - "ELEMENT DATA"

TYPE 1 TRUSS ELEMENT

A. Control Card		
TYPE	NUMEL	NMAT
1		

cols 1-5 6-10 11-15

FORMAT(3I5)

TYPE - SAP Element Code

NUMEL- No. of Elements of Type 1

NMAT - No. of Material Property Cards

B. Material Properties (*)					
IMAT	E	α	ρ	A	W

cols 1-5 6-15 16-25 26-35 36-45 46-55

*as many cards as NMAT

FORMAT(I5,5F10.0)

IMAT - Material Identification Number

E - Young's Modulus

α - Coefficient of Thermal Expansion

ρ - Mass Density

A - Cross Section Area

W - Weight Density

C. Element Load Factors Cards			
Element Load Case A	Element Load Case B	Element Load Case C	Element Load Case D

cols 1-10 11-20 21-30 31-40

FORMAT(4F10.0)

NOTE: Four cards are required even if values are zero

For Gravity in the X Direction

For Gravity in the Y Direction

For Gravity in the Z Direction

Fraction of Thermal Load for Each Case ABCD

SECTION - "ELEMENT DATA"

TYPE 1 TRUSS ELEMENTS (cont.)

D. ELEMENT DATA CARDS					
ELNUM	NODE I	NODE J	IMAT	REFTEMP	K
cols 1-5	6-10	11-15	16-20	21-30	31-35

FORMAT(4I5,F10.0,I5)

ELNUM - Element Number

IMAT - Material Property Code

REFTEMP - Reference Temperatur for Zero Stress

K - Node Increment for Data Generation

SECTION IV - "ELEMENT DATA"

Type 2 BEAM ELEMENTS

A. CONTROL CARD

TYPE	NUMEL	NELP	NSETS	NMAT
2				
cols 1-5	6-10	11-15	16-20	21-25

FORMAT(5I5)

TYPE - SAP Element Code

NUMEL - Total No. of Elements Type 2

NELP - No. of Element Property Cards

NSETS - No. of Fixed End Force Sets

NMAT - No. of Material Property Cards

B. MATERIAL PROPERTIES(*)

IMAT	E	NU	ρ	W
cols 1-5	6-15	16-25	26-35	36-45

(*) As Many Cards as NMAT

FORMAT(I5,4F10.0)

IMAT - Material Identification Number

E - Young's Modulus

NU - Poisson's Coefficient

ρ - Mass Density

W - Weight Density

C. ELEMENT PROPERTY CARDS (*)

IGEOM	AXA	SHEAR2(†)	SHEAR3(†)	TOR	FLEXU2	FLEXU3
cols 1-5	6-15	16-25	26-35	36-45	46-55	56-65

(*) As Many Cards as NELP (†) Specify Only If Shear Deformation is Included

IEGOM - Geometric Property Number

AXA - Axial Area

SHEAR2 - Shear Area in Local 2 - Direction

SHEAR3 - Shear Area in Local 3 - Direction

TOR - Torsional Inertia

FLEXU2 - Flexural Inertia 2 - Axis

FLEXU3 - Flexural Inertia 3 - Axis

FORMAT(I5,6F10.0)

SECTION IV - "ELEMENT DATA"

Type 2 BEAM ELEMENTS (CONT.)

D. ELEMENT LOAD FACTORS			
Element Load Case A	Element Load Case B	Element Load Case C	Element Load Case D
cols 1-10	11-20	21-30	31-40

FORMAT(4F10.0)

NOTE: Three Cards are Required Even if Values are Zero

FOR GRAVITY IN THE X DIRECTION

FOR GRAVITY IN THE Y DIRECTION

FOR GRAVITY IN THE Z DIRECTION

E. FIXED END FORCES (*)							
FEFN	FEF1I	FEF2I	FEF3I	FEM1I	FEM2I	FEM3I	First Card
BLANK	FEF1J	FEF2J	FEF3J	FEM1J	FEM2J	FEM3J	Second Card
cols 1-5	6-15	16-25	26-35	36-45	46-55	56-65	

(*) Two Cards Required for Each Set

FORMAT(I5,6F10.0)

S ON IV - "ELEMENT DATA"

Type 2 BEAM ELEMENTS (CONT.)

F. ELEMENT DATA CARDS												
ELNUM	NODEI	NODEJ	NODEK	IMAT	NELP	FEFA	FEFB	FEFC	FEFD	RELI	RELJ	K
cols 1-5	6-10	11-15	16-20	21-25	26-30	31-35	36-40	41-45	46-50	51-56	57-62	63-70

FORMAT(1015,216,I8)

SECTION IV - "ELEMENT DATA"

Type 3 PLANE STRESS MEMBRANE ELEMENTS

	4.- CONTROL CARD			
TYPE	NUMEL	NMAT	MTEMP	*
3				

cols 1-5 6-10 11-15 16-20 30

FORMAT(6I5)

TYPE - SAP Element Code
NUMEL - Total No. of Elements
NMAT - No. of Material Property Cards
MTEMP - Max. No. of Temp. Points for Any One Mat.
* - Non-zero Character to Suppress the Introduction of Incompatible Displacement Modes

	8.1 MATERIAL PROPERTY CARDS			
IMAT	NTEMP	W	ρ	β

cols 1-5 6-10 11-20 21-30 31-40

IMAT - Material Identification Number
NTEMP - Nol of Diff. Temperatures
W - Weight Density
ρ - Mass Density
β - Angle, Counterclockwise

	8.2 MATERIAL PROPERTIES FOR NTEMP (2 CARD FOR EACH)						
T	E_n	E_s	E_t	ν_{ns}	ν_{nt}	ν_{st}	σ_{ns}

cols 1-10 11-20 21-30 31-40 41-50 51-60 61-70 71-80

FORMAT(8F10.0)

E - Young's Modulus
ν - Strain Ratio
σ - Shear Modulus
α - Thermal Expansion Coefficient

8.3

α_n	α_s	α_t

cols 1-10 11-20 21-30

FORMAT(3F10.0)

SAP INPUT DATA SHEET

SECTION IV - "ELEMENT DATA"

Type 4 TWO DIMENSIONAL FINITE ELEMENTS

A CONTROL CARD					
TYPE	NUMEL	NMAT	MTEMP	ANALYZ	*
4					
cols 1-5	6-10	11-15	16-20	25	30

TYPE - SAP Element Code
NUMEL - Total No. of Elements
NMAT - No. of Material Property Cards
MTEMP - Maximum No. of Temp. Cards for Any Mat.
ANALYZ- ENTER 0 for Axisymmetric
1 for Plane Strain
2 for Plane Stress
* - Non-zero punch will suppress incompatible Displacement Modes

B.1 MATERIAL PROPERTY CARDS				
IMAT	NTEMP	W	ρ	β
cols 1-5	6-10	11-20	21-30	31-40

FORMAT(2I5,3F10.0)

IMAT - Material Identification Number
NTEMP - No. of Diff. Temperatures
W - Weight Density
ρ - Mass Density
β - Angle Counterclockwise

B.2 MATERIAL PROPERTIES FOR NTEMP (2 CARDS FOR EACH)							
T	E_n	E_s	E_t	ν_{ns}	ν_{nt}	ν_{st}	σ_{ns}
cols 1-10	11-20	21-30	31-40	41-50	51-60	61-70	71-80

FORMAT(8F10.0)

E - Young's Modulus
ν - Strain Ratio
σ - Shear Modulus
α - Thermal Expansion Coefficient

B.3

α_n	α_s	α_t
cols 1-10	11-20	21-30

SECTION IV - "ELEMENT DATA"

Type 3 & 4 PLANE STRESS MEMBRANE ELEMENTS (CONT.)
TWO DIMENSIONAL FINITE ELEMENTS

C. ELEMENT LOAD FACTORS				
THERMAL LOAD FRAC.	PRESSURE LOAD FRAC.	GRAVITY IN X DIRECTION	GRAVITY IN Y DIRECTION	GRAVITY IN Z DIRECTION
cols 1-10	11-20	21-30	31-40	41-50

FORMAT(5F10.0)

Element Load Case A

Element Load Case B

Element Load Case C

Element Load Case D

(Four Cards Required Even If Not Used)

SECTION *** - "ELEMENT DATA"

Type 3 . . PLANE STRESS MEMBRANE (CONT)
TWO DIMENSIONAL FINITE ELEMENTS

D- ELEMENT CARDS										
ELEMENT NO. N	NODE I	NODE J	NODE K	NODE L	IMAT	REFTEMP	PRESSURE I-J SIDE	EVALUATION OPTION n	MESH GENE-RATOR k	THICKNESS T
cols 1-5	6-10	11-15	16-20	21-25	26-30	31-40	41-50	51-55	56-60	61-70

FORMAT(615,2F10.0,215,F10.0)

TYPE 5 THREE DIMENSIONAL SOLID ELEMENTS (8 NODES)

A. CONTROL CARD

TYPE	NUMEL	NMAT	LSETS
5			
COL. 1-5	6-10	11-15	16-20

FORMAT (4I5)

B. MATERIAL PROPERTY CARDS
(ONE CARD FOR EACH MATERIAL)

IMAT	E	NU	W	α
COL. 1-5	6-15	16-25	26-35	36-45

FORMAT (I5, 4F10.0)

C. DISTRIBUTED SURFACE LOADS

ISET	LT	P	Y	FACE
COL. 1-5	6-10	11-20	21-30	31-35

FORMAT (2I5, 2F10.2, I5)

D. ACCELERATION DUE TO GRAVITY

G
COL 1-10

FORMAT (F10.2)

TYPE	SAP ELEMENT TYPE 5
NUMEL	Nº OF ELEMENTS TYPE 5
NMAT	Nº OF DIFFERENT MATERIALS
LSETS	Nº OF LOAD SETS
IMAT	MATERIA IDENTIFICATION NUMBER
E	MODULUS OF ELASTICITY
NU	POISSON'S RATIO
W	WEIGHT DENSITY
α	COEFFICIENT OF THERMAL EXPANSION
ISET	LOAD SET ID NUMBER
LT	LOAD TYPE =1 UNIFORM PRESSURE =2 HYDROSTATICALLY VARYING
P	MAGNITUDE OF PRESSURE IF LT=1 WEIGHT DENSITY OF FLUID IF LT=2
Y	BLANK IF LT=1 Y AXIS IF LT=2
FACE	FACE OF ELEMENT ON WHICH PRESSURE ACTS

TYPE 5, THREE DIMENSIONAL SOLID ELEMENT (8 NODES)
(CONT. 1)

C. ELEMENT LOAD CASE MULTIPLIERS

PRESSURE			
PA	PB	PC	PD
THERMAL			
TA	TB	TC	TD
GRAVITY + X			
GXA	GXB	GXC	GXD
GRAVITY + Y			
GYA	GYB	GYC	GYD
GRAVITY + Z			
GZA	GZB	GZC	GZD

COL. 1-10 11-20 21-30 31-40

FORMAT (4F10.2)

TYPE 5. THREE DIMENSIONAL SOLID ELEMENTS (8 NODES)
(CONT. 2)

F. ELEMENT CARDS

NEL	I	J	K	L	M	N	O	P	INT	MN	INC	LSA	LSB	LSC	LSD	FACE	SFACE
1-5	6-10	11-15	16-20	21-25	26-30	31-35	36-40	41-45	46-50	51-55	56-60	61-62	63-64	65-66	67-68	69-70	71-80

FORMAT (12I5, 4I2, 2I1, F10.2)

SAP INPUT DATA SHEET

TYP- 6. PLATE AND SHELL ELEMENTS (QUADRILATERAL)

A. CONTROL CARD		
TYPE	NUMEL	NMAT
6		
COL 1-5	6-10	11-15

FORMAT (3I5)

B. MATERIAL PROPERTY INFORMATION (TWO CARDS FOR EACH MATERIAL)						
INAT	—	—	RO	α_x	α_y	α_{xy}
C_{xx}	α_y	C_{xs}	C_{yy}	C_{ys}	C_{xy}	
COL 1-10	11-20	21-30	31-40	41-50	51-60	61-70

FORMAT (I10, 20X, 4F10.0)
FORMAT (6F10.0)

WHERE:

$$\begin{Bmatrix} \sigma_{xx} \\ \sigma_{yy} \\ \sigma_{xs} \end{Bmatrix} = \begin{bmatrix} C_{xx} & C_{xy} & C_{xs} \\ C_{xy} & C_{yy} & C_{ys} \\ C_{xs} & C_{ys} & C_{ss} \end{bmatrix} \begin{Bmatrix} \varepsilon_{xx} \\ \varepsilon_{yy} \\ \gamma_{xy} \end{Bmatrix}$$

C. ELEMENT LOAD MULTIPLIERS (FIVE CARDS)				
LLM (A)	LLM (B)	LLM (C)	LLM (D)	DISTRIBUTED LOAD
TM (A)	TM (B)	TM (C)	TM (D)	TEMPERATURE
GRX (A)	GRX (B)	GRX (C)	GRX (D)	GRAVITY IN X
GRY (A)	GRY (B)	GRY (C)	GRY (D)	GRAVITY IN Y
GRZ (A)	GRZ (B)	GRZ (C)	GRZ (D)	GRAVITY IN Z
COL 1-10	11-20	21-30	31-40	

FORMAT (4F10.10)

SAP INPUT DATA SHEET

SHEET [redacted] OF ___

TY. 6. PLATE AND SHELL ELEMENTS (QUADRILATERAL)
(CONT. 1)

D. ELEMENT CARDS

ELNUM	NODE I	NODE J	NODE K	NODE L	NODE O	IMAT	Kn	THK	DLLP	MT	TGR
COL 1-5	6-10	11-15	16-20	21-25	26-30	31-35	36-40	41-50	51-60	61-70	71-80

FORMAT (8I5, 4F10.0)

SAP INPUT DA SHEET

SECTION IV - "ELEMENT DATA"

Type 7 BOUNDARY ELEMENTS

CONTROL CARD		
TYPE	NUMEL	

cols 1-5 6-10

FORMAT(2I5)

ELEMENT LOAD FACTORS			
ELEMENT LOAD CASE A	ELEMENT LOAD CASE B	ELEMENT LOAD CASE C	ELEMENT LOAD CASE D

cols 1-10 11-20 21-30 31-40

FORMAT(4F10.0)

NOTE: At least one card for element load factor is required.

Combinations of conditions for element load cases ABC&D can be done with the Structure Load Multipliers (Section VI)

SECTION - "ELEMENT DATA"

Type 7 BOUNDARY ELEMENTS (CONT.)

ELEMENT CARDS										
NODEN	NODEI	NODEJ	NODEK	NODEL	CDISP	CROT	K	DEAX	REAX	SSTF

cols 1-5 6-10 11-15 16-20 21-25 26-30 31-35 36-40 41-50 51-60 61-70

FORMAT(8I5,3F10.0)

SECTION "CONCENTRATED LOAD/MASS DATA"

LOADS MOMENTS/MASS							
N	L	FX(N,L)	FY(N,L)	FZ(N,L)	MX(N,L)	MY(N,L)	MZ(N,L)
*							
cols 1-5	6-10	11-20	21-30	31-40	41-50	51-60	61-70

(*) Terminate with a Blank Card

N - Node Number (Ascending Number)

L - Structure Load Case No. Eq. 0 for Dynamic Analysis

FX(N,L)
FY(N,L) } Force Components
FZ(N,L)

MX(N,L)
MY(N,L) } Moment Components
MZ(N,L)

SECTION - ELEMENT LOAD MULTIPLIERS

EM(1)	EM(2)	EM(3)	EM(4)

cols 1-10 11-20 21-30 31-40

EM(1) - Multiplier for Element Load Case A

EM(2) - Multiplier for Element Load Case B

EM(3) - Multiplier for Element Load Case C

EM(4) - Multiplier for Element Load Case D

NOTE: Each Card Represents a Structure Load Case

PROBLEM 1.1 PLANE TRUSS

Problem Definition

Ref: Timoshenko, S. P. and Young, D. H., Theory of Structures, 2nd ed., McGraw-Hill, New York, 1965, pp. 266-267.

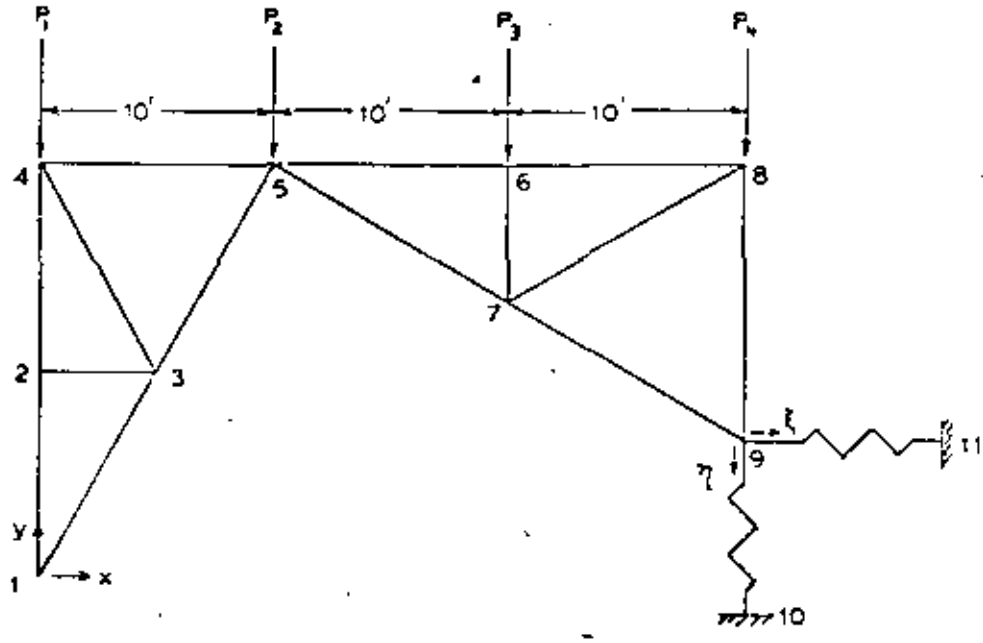

Each truss member has A = 2 in^2, E = 30 × 10^6 psi, α = 6.5 × 10^6 in/in/°F

This problem has two structure load cases:

1) Uniform temp. increase of 70°F; $P_1=P_2=P_3=P_4=0$; η = ξ = 0.

2) Uniform temp. decrease of 40°F; $P_1=P_2=P_3=P_4=10{,}000$ lb; η = ξ = .01 ft.

Problem Formulation

Since two different temperature cases are used, it is best to specify the nodal temperatures as 0°F and alter the zero stress reference temperature for each structure load case. The SAP IV manual, page IV.1.2, gives the temperature increase as

$$\Delta T = (T_i + T_j)/2.0 - T_r$$

where T_i and T_j are the nodal temperatures. Thus the zero stress reference temperature for each member is specified as -1°F, and the thermal load multipliers are +70.0 and -40.0 for element load cases A and B. To understand the signs, note that the element load case A the zero stress reference temperature is (+70.0)(-1.0) = -70°F. Since the nodal temperatures are 0°F, each member of the truss has experienced a rise of 70°F above the stress-free temperature, as required.

Problem 1.1 (cont.)

The settlement of the foundation is produced by using the boundary element (type 7). The default stiffness of 10^{10} is used, and the displacement specified is 0.12". For the first structural load case zero displacement is required, so the element load case multiplier for load case A is zero. For element load case B the multiplier is 1.0 to give the desired displacements.

The concentrated forces (section V) are all for structural load case 2, as required. The element load multipliers are such that structural load case 1 consists of element load case A, and structural load case 2 consists of element load case B.

Note that since no nodal generation is done, the printing of the generated nodal data is suppressed by coding "A" in column 6 of the first nodal card. This feature is not documented in the manual, but is incorporated in the program. (Other options available are B, which suppresses the printing of the ID array, and C, which combines the effect of A and B.)

Another feature not documented in the manual, but useful, is the coding of -1 for the boundary condition code where a series of nodes have a DOF suppressed. This is very useful for the elements with only translational DOF allowed.

Discussion of Results

Timoshenko gives only the y displacement of node 5:

	Timoshenko	SAP IV
load case 1	+0.158"	+0.15762"
load case 2	-0.223"	-0.22280"

PROBLEM 1.1 -- PLANE TRUSS

```
                1         2         3         4         5         6         7         8
CARD    12345678901234567890123456789012345678901234567890123456789012345678901234567890

    1   PROBLEM 1.1 -- PLANE TRUSS
    2        11    2     2
    3         1A   1     1    -1    -1    -1    -1
    4         2                                      103.923048
    5         3                                 60.  103.923048
    6         4                                      207.846097
    7         5                                120.  207.846097
    8         6                                240.  207.846097
    9         7                                240.  138.564065
   10         8                                360.  207.846097
   11         9                                360.   69.282032
   12        10    1     1                     360.     -100.
   13        11    1     1     1     1     1     1  460.   69.282032
   14         1   14     1
   15         1   30.0E+6     6.5E-6                2.
   16
   17
   18
   19        70.         -40.
   20         1    1     2     1    -1.
   21         2    1     3     1    -1.
   22         3    2     3     1    -1.
   23         4    2     4     1    -1.
   24         5    3     4     1    -1.
   25         6    4     5     1    -1.
   26         7    3     5     1    -1.
   27         8    5     7     1    -1.
   28         9    5     6     1    -1.
   29        10    6     7     1    -1.
   30        11    6     8     1    -1.
   31        12    7     8     1    -1.
   32        13    8     9     1    -1.
   33        14    7     9     1    -1.
   34         7    2
   35                    1.
   36         9   10                      1          .12
   37         9   11                      1          .12
   38         4    2          -10000.
   39         5    2          -10000.
   40         6    2          -10000.

                1         2         3         4         5         6         7         8
    12345678901234567890123456789012345678901234567890123456789012345678901234567890
```

```
CARD      1234567890123456789012345678901234567890123456789012345678901234567890
   41         6    2              -10000.
   42
   43         1.
   44                   1.

          1         2         3         4         5         6         7         8
12345678901234567890123456789012345678901234567890123456789012345678901234567890
```

PROBLEM . -- PLANE TRUSS

C O N T R O L I N F O R M A T I O N

NUMBER OF NODAL POINTS	=	11
NUMBER OF ELEMENT TYPES	=	2
NUMBER OF LOAD CASES	=	2
NUMBER OF EIGENVALUES	=	0
ANALYSIS CODE (NDYN)	=	0

EQ.0, STATIC
EQ.1, MODAL EXTRACTION
EQ.2, FORCED RESPONSE
EQ.3, RESPONSE SPECTRUM
EQ.4, DIRECT INTEGRATION

SOLUTION MODE (MODEX)	=	0

EQ.0, EXECUTION
EQ.1, DATA CHECK

NUMBER OF SUBSPACE ITERATION VECTORS (NAD)	=	0
EQUATIONS PER BLOCK	=	0
TAPE10 SAVE FLAG (NIOSV)	=	0

NODAL POINT INPUT DATA

NODE NUMBER	BOUNDARY CONDITION CODES. X	Y	Z	XX	YY	ZZ	NODAL POINT COORDINATES X	Y	Z	T
1	1	1	-1	-1	-1	-1	0.0	0.0	0.0	0.0
2	0	0	0	0	0	0	0.0	103.923	0.0	0.0
3	0	0	0	0	0	0	60.000	103.923	0.0	0.0
4	0	0	0	0	0	0	0.0	207.846	0.0	0.0
5	0	0	0	0	0	0	120.000	207.846	0.0	0.0
6	0	0	0	0	0	0	240.000	207.846	0.0	0.0
7	0	0	0	0	0	0	240.000	-138.564	0.0	0.0
8	0	0	0	0	0	0	360.000	207.846	0.0	0.0
9	0	0	0	0	0	0	360.000	69.282	0.0	0.0
10	1	1	0	0	0	0	360.000	-100.000	0.0	0.0
11	1	1	1	-1	1	1	460.000	69.282	0.0	0.0

EQUATION NCRS

N	X	Y	Z	XX	YY	ZZ
1	0	0	0	0	0	0
2	1	2	0	0	0	0
3	3	4	0	0	0	0
4	5	6	0	0	0	0
5	7	8	0	0	0	0
6	9	10	0	0	0	0
7	11	12	0	0	0	0
8	13	14	0	0	0	0
9	15	16	0	0	0	0
10	0	0	0	0	0	0
11	0	0	0	0	0	0

NUMBER OF 3S MEMBERS= 13
NUMBER OF 4 MEMBERS= 1

TYPE	E	ALPHA	DEN	AREA	WT
1	0.30000000 08	0.6500000D-05 0.0		0.2000000D 01	0.0

ELEMENT LOAD MULTIPLIERS

	A	B	C	D
X-DIR	0.0	0.0	0.0	0.0
Y-DIR	0.0	0.0	0.0	0.0
Z-DIR	0.0	0.0	0.0	0.0
TEMP	0.7000000D 02	-0.4000000D 02	0.0	0.0

N	I	J	TYPE	TEMP	BAND
1	1	2	1	-1.00	2
2	1	3	1	-1.00	2
3	2	3	1	-1.00	4
4	2	4	1	-1.00	6
5	3	4	1	-1.00	4
6	4	5	1	-1.00	4
7	3	5	1	-1.00	6
8	5	7	1	-1.00	6
9	5	6	1	-1.00	4
10	6	7	1	-1.00	4
11	6	8	1	-1.00	6
12	7	8	1	-1.00	4
13	8	9	1	-1.00	4
14	7	9	1	-1.00	6

N O U N D V E L E M E N T S

ELEMENT TYPE = 7
NUMBER OF ELEMENTS = 2

ELEMENT LOAD CASE MULTIPLIERS

CASE(A)	CASE(B)	CASE(C)	CASE(D)
0.0	1.0000	0.0	0.0

ELEMENT NUMBER	NODE (N)	NODES DEFINING CONSTRAINT DIRECTION (NI)	(NJ)	(NK)	(NL)	CODE KQ	CODE KR	GENERATION CODE (KN)	SPECIFIED DISPLACEMENT	SPECIFIED ROTATION	SPRING RATE
1	9	10	0	0	0	1	0	0	0.12000 00	0.0	0.10000 11
2	9	11	0	0	0	1	0	0	0.12000 00	0.0	0.10000 11

E Q U A T I O N P A R A M E T E R S

TOTAL NUMBER OF EQUATIONS = 16
BANDWIDTH = 6
NUMBER OF EQUATIONS IN A BLOCK = 16
NUMBER OF BLOCKS = 1

NODAL LOADS (STATIC OR QUASI DYNAMIC)

NODE NUMBER	LOAD CASE	X-AXIS FORCE	Y-AXIS FORCE	Z-AXIS FORCE	X-AXIS MOMENT	Y-AXIS MOMENT	Z-AXIS MOMENT
4	2	0.0	-0.100000 05	0.0	0.0	0.0	0.0
5	2	0.0	-0.100000 05	0.0	0.0	0.0	0.0
6	2	0.0	-0.100000 05	0.0	0.0	0.0	0.0
8	2	0.0	-0.100000 05	0.0	0.0	0.0	0.0

STRUCTURE LOAD CASE	ELEMENT LOAD MULTIPLIERS A	B	C	D
1	1.000	0.0	0.0	0.0
2	0.0	1.000	0.0	0.0

NODE DISPLACEMENTS/ROTATIONS

NODE NUMBER	LOAD CASE	X-TRANSLATION	Y-TRANSLATION	Z-TRANSLATION	X-ROTATION	Y-ROTATION	Z-ROTATION
11	1	0.0	0.0	0.0	0.0	0.0	0.0
	2	0.0	0.0	0.0	0.0	0.0	0.0
10	1	0.0	0.0	0.0	0.0	0.0	0.0
	2	0.0	0.0	0.0	0.0	0.0	0.0
9	1	0.272850-21	-0.818550-21	0.0	0.0	0.0	0.0
	2	0.120300 00	-0.120009 00	0.0	0.0	0.0	0.0
8	1	0.546000-01	0.630470-01	0.0	0.0	0.0	0.0
	2	0.601410-01	-0.190670 00	0.0	0.0	0.0	0.0
7	1	-0.27300D-01	0.788080-01	0.0	0.0	0.0	0.0
	2	0.10794D 00	-0.247590 00	0.0	0.0	0.0	0.0
6	1	0.448860-10	0.110130 00	0.0	0.0	0.0	0.0
	2	0.108660 00	-0.27715D 00	0.0	0.0	0.0	0.0
5	1	-0.546000-01	0.157620 00	0.0	0.0	0.0	0.0
	2	0.157180 00	-0.222800 00	0.0	0.0	0.0	0.0
4	1	-0.10920D 00	0.945700-01	0.0	0.0	0.0	0.0
	2	0.188380 00	-0.886810-01	0.0	0.0	0.0	0.0
3	1	-0.27300D-01	0.788080-01	0.0	0.0	0.0	0.0
	2	0.826100-01	-0.113720 00	0.0	0.0	0.0	0.0
2	1	-0.546000-01	0.472850-01	0.0	0.0	0.0	0.0
	2	0.982100-01	-0.443410-01	0.0	0.0	0.0	0.0
1	1	0.0	0.0	0.0	0.0	0.0	0.0
	2	0.0	0.0	0.0	0.0	0.0	0.0

TRUSS MEMBER ACTIONS

MEMBER	LOAD	STRESS	FORCE
1	1	0.00000	0.000
1	2	-5000.00003	-10000.000
2	1	-0.00000	-0.000
2	2	-6495.19050	-12990.381
3	1	-0.00000	-0.000
3	2	0.00000	0.0
4	1	0.00000	0.000
4	2	-5000.00003	-10000.000
5	1	-0.00000	-0.000
5	2	0.00003	0.000
6	1	-0.00000	-0.000
6	2	-0.00002	-0.000
7	1	0.00000	0.0
7	2	-6495.19052	-12990.381
8	1	0.00000	0.000
8	2	-1250.00000	-2600.000
9	1	-0.00000	-0.000
9	2	-4330.12701	-8660.254
10	1	-0.00000	0.0
10	2	-5000.00000	-10000.000
11	1	-0.00000	-0.000
11	2	-4330.12701	-8660.254
12	1	0.00000	0.000
12	2	4999.99999	10000.000
13	1	-0.00000	-0.000
13	2	-7499.99999	-15000.000
14	1	-0.00000	-0.000
14	2	-3750.00001	-7500.000

G R O U N D Y E L E M E N T F O R C E S / M E N T S

ELEMENT NUMBER	LOAD CASE	FORCE	MOMENT
1	1	0.018550-11	0.0
1	2	0.120000 10	0.0
2	1	0.272850-11	0.0
2	2	0.120000 10	0.0

S T A T I C S O L U T I O N T I M E L O G

EQUATION SOLUTION	=	0.30
DISPLACEMENT OUTPUT	=	0.21
STRESS RECOVERY	=	0.32

O V E R A L L T I M E L O G

NODAL POINT INPUT	=	0.25
ELEMENT STIFFNESS FORMATION	=	0.39
NODAL LOAD INPUT	=	0.09
TOTAL STIFFNESS FORMATION	=	0.35
STATIC ANALYSIS	=	0.85
EIGENVALUE EXTRACTION	=	0.0
FORCED RESPONSE ANALYSIS	=	0.0
RESPONSE SPECTRUM ANALYSIS	=	0.0
STEP-BY-STEP INTEGRATION	=	0.0
TOTAL SOLUTION TIME	=	1.92

PROBLEM 12.1 PIPE NETWORK STATIC ANALYSIS

Problem Definition

Ref: SAP IV Manual, problem 1

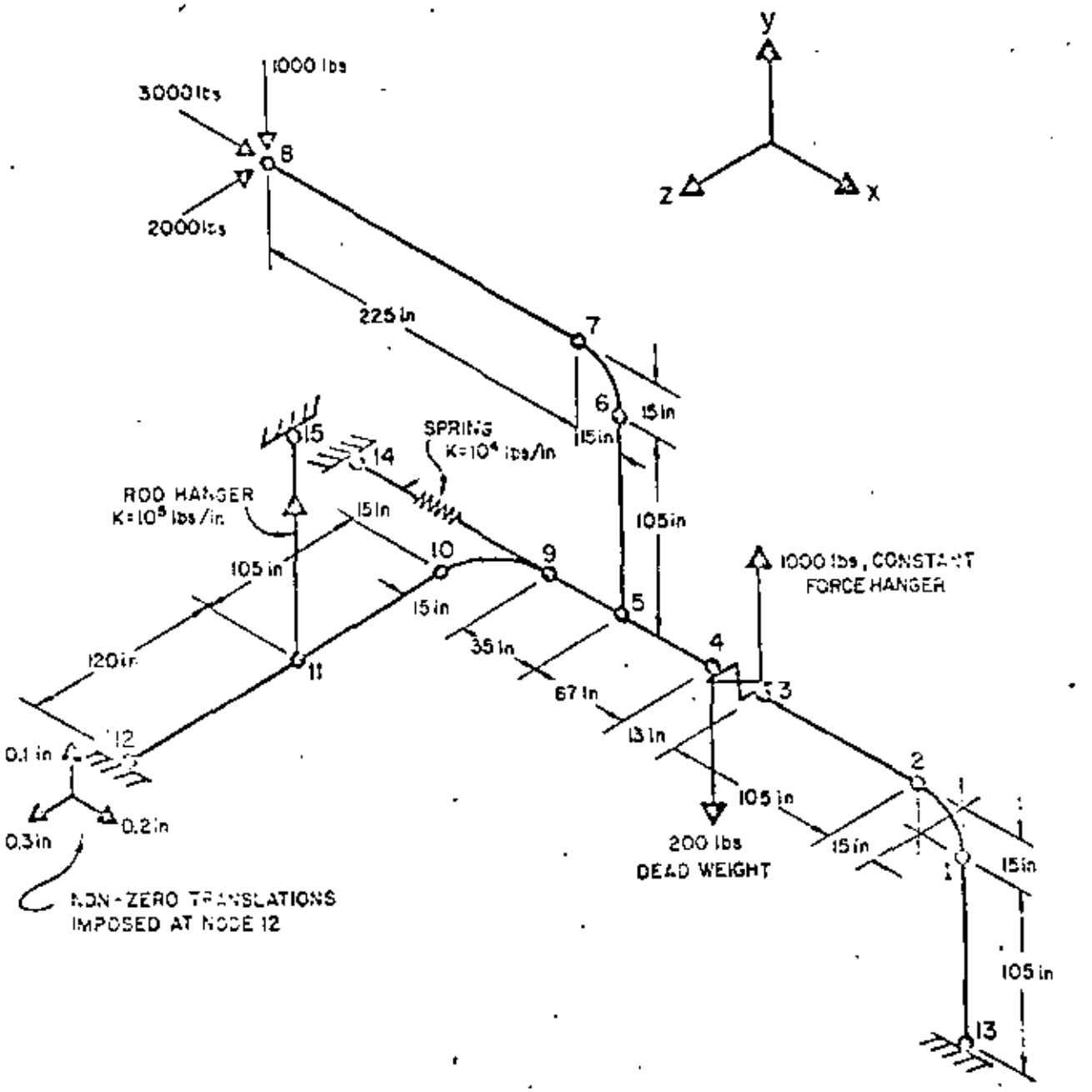

Problem Formulation

The non-zero displacements at node 12 are created by using boundary elements connected to added nodes 16, 17 and 18.

Problem 12.1 (cont.)

Discussion of Results

The results as given in the SAP IV Manual are:

REACTIONS:

Node	SAP FX	SAP FY	SAP FZ	ADLPIPE FX	ADLPIPE FY	ADLPIPE FZ
9	5643.51	--	--	5659.	--	--
11	--	-4044.59	--	--	-4052.	--
12	2350.08	4023.01	-4960.70	2361.	4026.	-4966.
13	-10993.59	4595.61	2960.70	-11021.	4509.	2966.
Total	-3000.00	4484.03	-2000.00	-3001.	4483.	-2000.

APPLIED LOADS:

Loading Type	Direction X	Y	Z
Concentrated:			
at node 3	-	1000.00	-
at node 4	-	-200.00	-
at node 8	3000.	1000.00	2000.
Distributed Weight		-6284.03	
TOTAL	3000.	-4484.03	2000.

```
CARD        1        2        3        4        5        6        7        8
    12345678901234567890123456789012345678901234567890123456789012345678901234567890

    1       PROBLEM 12.1 -- PIPE NETWORK STATIC ANLYSIS
    2         18       2        1        0        0        0              40
    3          1       0        0        0        0        0        0.0         105.0          0.0        0        740.0
    4          2       0        0        0        0        0        0       -15.0          120.0          0.0        0        740.0
    5          3       0        0        0        0        0        0      -120.0          120.0          0.0        0        740.0
    6          4       0        0        0        0        0        0      -135.0          120.0          0.0        0        740.0
    7          5       0        0        0        0        0        0      -200.0          120.0          0.0        0        740.0
    8          6       0        0        0        0        0        0      -200.0          225.0          0.0        0        740.0
    9          7       0        0        0        0        0        0      -215.0          240.0          0.0        0        740.0
   10          8       0        0        0        0        0        0      -230.0          240.0          0.0        0        740.0
   11          9       0        0        0        0        0        0      -245.0          120.0          0.0        0        740.0
   12         10       0        0        0        0        0        0      -250.0          120.0         15.0        0        740.0
   13         11       0        0        0        0        0        0      -250.0          120.0        120.0        0        710.0
   14         12       0        0        0        1        1        1      -250.0          120.0        240.0        0        740.0
   15         13       1        1        1        1        1        1         0.0            0.0          0.0        0        740.0
   16         14       1        1        1        1        1        1      -240.0          120.0          0.0        0          0.0
   17         15       1        1        1        1        1        1      -250.0          130.0        120.0        0          0.0
   18         16       1        1        1        1        1        1      -240.0          120.0        240.0        0          0.0
   19         17       1        1        1        1        1        1      -250.0          130.0        240.0        0          0.0
   20         18       1        1        1        1        1        1      -250.0          120.0        250.0        0          0.0
   21          7       5
   22                1.0              0.0              0.0              0.0
   23          9      14        0        0        0        1        0        0              0.0                    1.0  4
   24         11      15        0        0        0        1        0        0              0.0                    1.0  5
   25         12      16        0        0        0        1        0        0              0.2                 1.0E13
   26         12      17        0        0        0        1        0        0              0.1                 1.0E13
   27         12      18        0        0        0        1        0        0              0.3                 1.0E13
   28         12      12        1        1        2        2        2        0        0        0        0
   29          1       1CARBON STEEL
   30                0.0             27.9E6            0.333           6.81E-6
   31          1             10.74             0.50             0.0             6.61                    NORMAL PIPE
   32          2             10.74             2.00             0.0             6.61                    VALVE
   33                0.0              0.0              0.0              0.0        X-GRAVITY
   34               -1.0              0.0              0.0              0.0        Y-GRAVITY
   35                0.0              0.0              0.0              0.0        Z-GRAVITY
   36                1.0              0.0              0.0              0.0        THERMAL
   37                0.0              0.0              0.0              0.0        PRESSURE
   38         17      13        1        1        1
   39         20       1        2        1        1
   40              -15.0       CC       -15.0            105.0            0.0

    12345678901234567890123456789012345678901234567890123456789012345678901234567890
```

```
(A1)     1...+....2....+....3....+....4....+....5....+....6....+....7....+....8
  41       3T       2       3       1       1
  42       4T       3       4       1       2
  43       5T       4       5       1       1
  44       6T       5       6       1       1
  45       7D       6       7       1       1
  46              15.0      CC    -215.0          225.0           0.0
  47       8T       7       9       1       1
  48       9T       5       9       1       1
  49      10B       9      10       1       1
  50              15.0      CC    -235.0          120.0          15.0
  51      11T      10      11       1       1
  52      12T      11      12       1       1
  53         3       1                       1000.0
  54         4       1                       -200.0
  55         8       1      3000.0           1000.0          2000.0
  56
  57               1.0         0.0             0.0             0.0                  BLANK
                                                                                    LAST
```

```
     1....+....2....+....3....+....4....+....5....+....6....+....7....+....8
1234567890123456789012345678901234567890123456789012345678901234567890123456789012345678901234567890
```

PROBLEM 12 -- PIPE NETWORK STATIC ANLYSIS

C O N T R O I N F O R M A T I O N

NUMBER OF NODAL POINTS	=	18
NUMBER OF ELEMENT TYPES	=	2
NUMBER OF LOAD CASES	=	1
NUMBER OF FREQUENCIES	=	0
ANALYSIS CODE (NDYN)	=	0
EQ.0, STATIC		
EQ.1, MODAL EXTRACTION		
EQ.2, FORCED RESPONSE		
EQ.3, RESPONSE SPECTRUM		
EQ.4, DIRECT INTEGRATION		
SOLUTION MODE (MODEX)	=	0
EQ.0, EXECUTION		
EQ.1, DATA CHECK		
NUMBER OF SUBSPACE ITERATION VECTORS (NAD)	=	0
EQUATIONS PER BLOCK	=	40
TAPE10 SAVE FLAG (N10SV)	=	0

NODAL POINT INPUT DATA

NODE NUMBER	BOUNDARY CONDITION CODES X	Y	Z	XX	YY	ZZ	NODAL POINT COORDINATES X	Y	Z		T
1	0	0	0	0	0	0	0.0	105.000	0.0	0	740.000
2	0	0	0	0	0	0	-15.000	120.000	0.0	0	740.000
3	0	0	0	0	0	0	-120.000	120.000	0.0	0	740.000
4	0	0	0	0	0	0	-133.000	120.000	0.0	0	740.000
5	0	0	0	0	0	0	-200.000	120.000	0.0	0	740.000
6	0	0	0	0	0	0	-200.000	225.000	0.0	0	740.000
7	0	0	0	0	0	0	-215.000	240.000	0.0	0	740.000
8	0	0	0	0	0	0	-440.000	240.000	0.0	0	740.000
9	0	0	0	0	0	0	-235.000	120.000	0.0	0	740.000
10	0	0	0	0	0	0	-250.000	120.000	15.000	0	740.000
11	0	0	0	0	0	0	-250.000	120.000	120.000	0	740.000
12	0	0	0	1	1	1	-250.000	120.000	240.000	0	740.000
13	1	1	1	1	1	1	0.0	0.0	0.0	0	740.000
14	1	1	1	1	1	1	-245.000	120.000	0.0	0	0.0
15	1	1	1	1	1	1	-250.000	130.000	120.000	0	0.0
16	1	1	1	1	1	1	-240.000	120.000	240.000	0	0.0
17	1	1	1	1	1	1	-250.000	130.000	240.000	0	0.0
18	1	1	1	1	1	1	-250.000	120.000	250.000	0	0.0

NODAL DATA

NODE NUMBER	BOUNDARY CONDITION CODES X	Y	Z	XX	YY	ZZ	NODAL POINT COORDINATES X	Y	Z	T
1	0	0	0	0	0	0	0.0	105.000	0.0	740.000
2	0	0	0	0	0	0	-15.000	120.000	0.0	740.000
3	0	0	0	0	0	0	-120.000	120.000	0.0	740.000
4	0	0	0	0	0	0	-133.000	120.000	0.0	740.000
5	0	0	0	0	0	0	-200.000	120.000	0.0	740.000
6	0	0	0	0	0	0	-200.000	225.000	0.0	740.000
7	0	0	0	0	0	0	-215.000	240.000	0.0	740.000
8	0	0	0	0	0	0	-440.000	240.000	0.0	740.000
9	0	0	0	0	0	0	-235.000	120.000	0.0	740.000
10	0	0	0	0	0	0	-250.000	120.000	15.000	740.000
11	0	0	0	0	0	0	-250.000	120.000	120.000	740.000
12	0	0	0	1	1	1	-250.000	120.000	240.000	740.000
13	1	1	1	1	1	1	0.0	0.0	0.0	740.000
14	1	1	1	1	1	1	-245.000	120.000	0.0	0.0
15	1	1	1	1	1	1	-250.000	130.000	120.000	0.0
16	1	1	1	1	1	1	-240.000	120.000	240.000	0.0
17	1	1	1	1	1	1	-250.000	130.000	240.000	0.0
18	1	1	1	1	1	1	-250.000	120.000	250.000	0.0

EQUATIONS OF MOTION

N	X	Y	Z	XX	YY	ZZ
1	1	2	3	4	5	6
2	7	8	9	10	11	12
3	13	14	15	16	17	18
4	19	20	21	22	23	24
5	25	26	27	28	29	30
6	31	32	33	34	35	36
7	37	38	39	40	41	42
8	43	44	45	46	47	48
9	49	50	51	52	53	54
10	55	56	57	58	59	60
11	61	62	63	64	65	66
12	67	68	69	0	0	0
13	0	0	0	0	0	0
14	0	0	0	0	0	0
15	0	0	0	0	0	0
16	0	0	0	0	0	0
17	0	0	0	0	0	0
18	0	0	0	0	0	0

BOUNDARY ELEMENTS

ELEMENT TY
NUMBER OF UNITS = 5

ELEMENT LOAD CASE MULTIPLIERS

CASE(A)	CASE(B)	CASE(C)	CASE(D)
1.0300	0.0	0.0	0.0

ELEMENT NUMBER	NODE (N)	NODES DEFINING (NI)	(NJ)	CONSTRAINT DIRECTION (NK)	(NL)	CODE KD	CODE KR	GENERATION CODE (KN)	SPECIFIED DISPLACEMENT	SPECIFIED ROTATION	SPRING RATE
1	9	14	3	0	0	1	0	0	0.0	0.0	0.13040 01
2	11	15	0	0	0	1	0	0	0.0	0.0	0.13050 01
3	12	16	0	0	0	1	0	0	0.20003 00	0.0	0.10000 14
4	12	17	0	0	0	1	0	0	0.10000 00	0.0	0.10000 14
5	12	18	0	0	0	1	0	0	0.30000 00	0.0	0.10000 14

P I P E E L E M E N T I N P U T D A T A

C O N T R O L I N F O R M A T I O N

NUMBER OF PIPE ELEMENTS	=	12
NUMBER OF MATERIAL SETS	=	1
MAXIMUM NUMBER OF MATERIAL TEMPERATURE INPUT POINTS	=	1
NUMBER OF SECTION PROPERTY SETS	=	2
NUMBER OF BRANCH POINT NODES	=	0
MAXIMUM NUMBER OF TANGENTS COMMON TO A BRANCH POINT	=	4
FLAG FOR NEGLECTING AXIAL DEFORMATIONS IN BEND ELEMENTS (EQ.1, NEGLECT)	=	0

M A T E R I A L P R O P E R T Y T A B L E S

MATERIAL NUMBER = (1)
NUMBER OF TEMPERATURE POINTS = (1)
IDENTIFICATION = (CARBON STEEL)

POINT NUMBER	TEMPERATURE	YOUNG'S MODULUS	POISSON'S RATIO	THERMAL EXPANSION
1	0.0	27900000.0	0.333	0.6810-05

S E C T I O N P R O P E R T Y T A B L E

SECTION NUMBER	SIDE DIAMETER	WALL THICKNESS	SHAPE FACTOR FOR SHEAR	GMT/ UNIT LENGTH	MASS/ UNIT LENGTH	D E S C R I P T I O N
1	10.740	0.5000	0.0	0.66100 01	0.1711D-01	NORMAL PIPE
2	10.740	2.3000	0.0	0.66100 01	0.1711D-01	VALVE

E L E M E N T L O A D C A S E M U L T I P L I E R S

	CASE A	CASE B	CASE C	CASE D
X-DIRECTION GRAVITY	0.0	0.0	0.0	0.0
Y-DIRECTION GRAVITY	-1.000	0.0	0.0	0.0
Z-DIRECTION GRAVITY	0.0	0.0	0.0	0.0
THERMAL DISTORTION	1.000	0.0	0.0	0.0
PRESSURE DISTORTION	0.0	0.0	0.0	0.0

M E M B E R I N P U T D A T A

ELEMENT NUMBER	TYPE	NODE -I	NODE -J	MATERIAL NUMBER	SECTION NUMBER	REFERENCE TEMPERATURE (ZERO RADIANS)	EXPANSION COEFF (ALPHA)	DIRECTION COSINES A(YX) (X3-ORDINATE)	A(YY) (Y3-ORDINATE)	A(YZ) (Z3-ORDINATE)	NODE INCREMENT (ZERO DEGREES)	TAG
1	TANGENT	13	1	1	1	0.0	0.0	0.0	0.0	0.0	1	IL
2	BEND	1	2	1	1	0.0	0.0					IC
						(15.000)	(CC)	(-15.0000)(	180.000)(	0.0) (	0.1000)	
3	TANGENT	2	3	1	1	0.0	0.0	0.0	0.0	0.0	1	IL
4	TANGENT	3	4	1	2	0.0	0.0	0.0	0.0	0.0	1	IL
5	TANGENT	4	5	1	1	0.0	0.0	0.0	0.0	0.0	1	IL
6	TANGENT	5	6	1	1	0.0	0.0	0.0	0.0	0.0	1	IL
7	BEND	6	7	1	1	0.0	0.0					IC
						(15.000)	(CC)	(-215.0000)(	225.000)(	0.0) (	0.1000)	
8	TANGENT	7	8	1	1	0.0	0.0	0.0	0.0	0.0	1	IL
9	TANGENT	8	9	1	1	0.0	0.0	0.0	0.0	0.0	1	IL
10	BEND	9	10	1	1	0.0	0.0					IC
						(15.000)	(CC)	(-235.0000)(	120.000)(	15.000) (	0.1000)	
11	TANGENT	10	11	1	1	0.0	0.0	0.0	0.0	0.0	1	IL
12	TANGENT	11	12	1	1	0.0	0.0	0.0	0.0	0.0	1	IL

E Q U A T I O N P A R A M E T E R S

TOTAL NO. OF EQUATIONS	=	[illegible]
BANDWIDTH	=	30
NUMBER OF EQUATIONS IN A BLOCK	=	40
NUMBER OF BLOCKS	=	2

N O D A L L O A D S (S T A T I C) O R M A S S E S (D Y N A M I C)

NODE NUMBER	LOAD CASE	X-AXIS FORCE	Y-AXIS FORCE	Z-AXIS FORCE	X-AXIS MOMENT	Y-AXIS MOMENT	Z-AXIS MOMENT
3	1	0.0	0.100000 04	0.0	0.0	0.0	0.0
5	1	0.0	-0.200000 04	0.0	0.0	0.0	0.0
6	1	0.300000 04	0.100000 04	0.200000 04	0.0	0.0	0.0

STRUCTURE LOAD CASE	ELEMENT LOAD MULTIPLIERS A	B	C	D
1	1.000	0.0	0.0	0.0

N O D E   D I S P L A C E M E N T S / R O T A T I O N S

NODE NUMBER	LOAD CASE	X-TRANSLATION	Y-TRANSLATION	Z-TRANSLATION	X-ROTATION	Y-ROTATION	Z-ROTATION
18	1	0.0	0.0	0.0	0.0	0.0	0.0
17	1	0.0	0.0	0.0	0.0	0.0	0.0
16	1	0.0	0.0	0.0	0.0	0.0	0.0
15	1	0.0	0.0	0.0	0.0	0.0	0.0
14	1	0.0	0.0	0.0	0.0	0.0	0.0
13	1	0.0	0.0	0.0	0.0	0.0	0.0
12	1	0.20000D 00	0.10000D 00	0.30000D 00	0.0	0.0	0.0
11	1	-0.23701D 00	0.24036D 00	-0.30334D 00	0.24913D-02	0.59867D-02	-0.98374D-03
10	1	-0.87692D 00	0.62212D 00	-0.83127D 00	0.46491D-02	0.51914D-02	-0.18445D-02
9	1	-0.85293D 00	0.67357D 00	-0.93816D 00	0.56803D-02	0.50548D-03	-0.19557D-02
8	1	-0.12371D 01	0.35037D 01	0.56155D 01	0.11600D-01	0.26668D-01	-0.10589D-01
7	1	-0.10469D 00	0.13227D 01	0.25396D 00	0.11600D-01	0.18081D-01	-0.94242D-02
6	1	-0.14196D 00	0.11282D 01	-0.11576D 00	0.87383D-02	0.11426D-01	-0.68345D-02
5	1	-0.67678D 00	0.59932D 00	-0.94228D 00	0.63342D-02	0.32005D-04	-0.23464D-02
4	1	-0.34004D 00	0.54623D 00	-0.79028D 00	0.39505D-02	-0.40911D-02	0.35735D-03
3	1	-0.27458D 00	0.55174D 00	-0.73563D 00	0.37734D-02	-0.42902D-02	0.46305D-03
2	1	0.25315D 00	0.62396D 00	-0.18389D 00	0.37026D-04	-0.51543D-02	0.61334D-04
1	1	0.29269D 00	0.52834D 00	-0.10914D 00	-0.10141D-02	-0.39355D-02	-0.35586D-02

BOUNDARY ELEMENT FORCES/MOMENTS

ELEMENT NUMBER	LOAD CASE	FORCE	MOMENT
1	1	0.856340 00	0.0
2	1	0.241570 00	0.0
3	1	0.200000 13	0.0
4	1	0.100000 13	0.0
5	1	0.300000 13	0.0

ELEMENT NUMBER	ELEMENT TYPE	LOAD CASE	STATION	AXIAL FORCE	Y-AXIS SHEAR	Z-AXIS SHEAR	TORSIONAL MOMENT	Y-AXIS MOMENT	Z-AXIS MOMENT
1	TANGENT	1	END-I	-3735.024	-3174.927	6012.520	-165790.17	-515405.41	-2[illegible]
			END-J	-3040.974	-3174.927	6012.520	-165790.17	115825.22	19[illegible]
2	BEND	1	END-I	-3040.974	-3012.520	-3174.927	-165790.17	-19[illegible]	[illegible]
			CENTER	-6346.724	-2100.254	-3174.927	-204774.67	5[illegible]	[illegible]
			END-J	-6012.520	2005.230	-3174.927	-157364.25	118161.27	161[illegible]
3	TANGENT	1	END-I	-6012.520	-2005.230	3174.927	-157364.25	-118161.27	-161[illegible]
			END-J	-6012.520	-2191.189	3174.927	-157364.25	215206.04	104524.85
4	TANGENT	1	END-I	-6012.520	-3191.189	3174.927	-157364.25	215206.04	104524.85
			END-J	-6012.520	-3189.250	3174.927	-157364.25	299330.08	149591.65
5	TANGENT	1	END-I	-6012.520	-2589.250	3174.927	-157364.25	299330.08	149591.65
			END-J	-6012.520	-2592.389	3174.927	-157364.25	467205.17	325347.24
6	TANGENT	1	END-I	-1337.044	2000.000	3000.000	480000.00	-409526.71	240000.00
			END-J	-642.994	2000.000	3000.000	480000.00	-94526.71	30000.00
7	BEND	1	END-I	-642.994	-3000.000	2000.000	480000.00	-30000.00	-94526.71
			CENTER	-2520.927	-1721.719	2000.000	326974.85	-339411.25	-45364.15
			END-J	-3000.000	497.250	2000.000	-0.00	-450000.00	-57688.37
8	TANGENT	1	END-I	-3000.000	-497.250	-2000.000	0.00	450000.00	57681.34
			END-J	-3000.000	1000.000	-2000.000	0.00	-0.00	-0.00
9	TANGENT	1	END-I	-3012.520	-1125.335	5174.927	82635.75	-19[illegible]	-88159.46
			END-J	-3012.520	-893.995	5174.927	82635.75	170322.61	-48971.39
10	BEND	1	END-I	-3011.664	-5174.927	-491.085	82635.75	48971.39	170322.61
			CENTER	-5708.794	-1509.658	-810.113	49143.01	-37936.94	211279.55
			END-J	-5174.927	3011.664	-738.241	36260.48	-94553.29	202771.55
11	TANGENT	1	END-I	-5174.927	-738.241	-3011.664	36260.48	202771.55	94558.29
			END-J	-5174.927	-44.191	-3011.664	36260.48	-113453.17	135535.96
12	TANGENT	1	END-I	-5174.927	-42.040	-3011.664	36260.48	-113453.17	135535.96
			END-J	-5174.927	749.251	-3011.664	36260.48	-474052.96	91317.89

STATIC SOLUTION TIME LOG

EQUATION SOLUTION	=	0.73
DISPLACEMENT OUTPUT	=	0.27
STRESS RECOVERY	=	0.60

OVERALL TIME LOG

NODAL POINT INPUT	=	0.42
ELEMENT STIFFNESS FORMATION	=	1.92
NODAL LOAD INPUT	=	0.13
TOTAL STIFFNESS FORMATION	=	0.77
STATIC ANALYSIS	=	1.61
EIGENVALUE EXTRACTION	=	0.0
FORCED RESPONSE ANALYSIS	=	0.0
RESPONSE SPECTRUM ANALYSIS	=	0.0
STEP-BY-STEP INTEGRATION	=	0.0
TOTAL SOLUTION TIME	=	4.75

PROBLEM 3.2 PLANE STRESS CANTILEVER BEAM EIGENVALUES

Problem Definition

Ref: Carnegie, W. and Thomas, J., "The Effects of Shear Deformation and Rotary Inertia on the Lateral Frequencies of Cantilever Beams in Bending", ASME Journal of Engineering for Industry, February 1972, pp. 267-278.

See also problems 5.2 and 8.2.

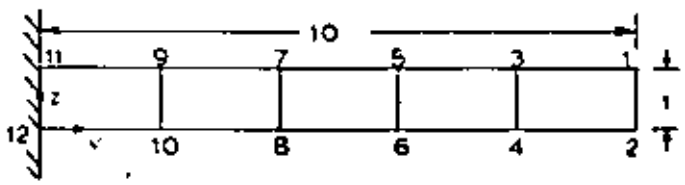

$E = 10^6$ psi

$y = 0.3$

$\gamma = .386$ lb/in^3

$t = 1.2$"

Problem Formulation

Note that by placing the first two nodes at the tip only four nodal cards are required. Since the boundary condition code for the generated nodes are set equal to the values on the first care of a series, the nodal numbering should be such that the nodes with unique boundary condition codes occur last in a series.

Discussion of Results

The frequencies for the flexural vibrations of a cantiler beam are

$$f_i = \frac{\lambda_i^2}{2\pi}\sqrt{\frac{EI}{\mu \ell^4}}$$

while the extensional vibration frequencies are

$$f_i' = \frac{i}{4\ell}\sqrt{\frac{E}{\mu}}$$

However, the flexural frequencies are too high because of neglecting shear and rotary inertia. This effort is more pronounced for the higher modes. The results for a Timoshenko beam were obtained by multiplying the Euler beam frequencies by a factor obtained from figure 1 in the article by Carnegie and Thomas.

Mode Number	Type	Euler Beam	Timoshenko Beam	SAP IV
1	flexural	55.96	55.6	50.01
2	flexural	350.7	332.	295.9
3	flexural	982.0	876.	788.5
4	extensional	790.6	--	791.5
5	flexural	1924.	1590.	1485.

GENERATED MODAL DATA

MODE NUMBER	FREQUENCY	XX	YY	ZZ
1	0.0	0.0	0.0	0.0
2	0.0	0.0	0.0	0.0
3	0.0	0.0	0.0	0.0
4	0.0	0.0	0.0	0.0
5	0.0	0.0	0.0	0.0
6	0.0	0.0	0.0	0.0
7	0.0	0.0	0.0	0.0
8	0.0	0.0	0.0	0.0
9	0.0	0.0	0.0	0.0
10	0.0	0.0	0.0	0.0
11	0.0	0.0	0.0	0.0
12	0.0	0.0	0.0	0.0

MODAL PARTICIPATION FACTORS

	X	Y	Z
	0.0	0.0	0.0
	0.0	0.0	0.0
	0.0	0.0	0.0
	0.0	0.0	0.0
	0.0	0.0	0.0
	0.0	0.0	0.0
	0.0	0.0	0.0
	0.0	0.0	0.0
	0.0	0.0	0.0
	0.0	0.0	0.0
	0.0	0.0	0.0
	0.0	0.0	0.0

EQUATION NUMBERS

	X	Y	Z
	0	0	0
	0	0	0
	0	0	0
	0	0	0
	0	0	0
	0	0	0
	0	0	0
	0	0	0
	0	0	0
	0	0	0
	0	0	0
	0	0	0

MESH STRESS ANALYSIS
REFERENCE [illegible] 1975

NUMBER OF POINTS	=	5
NUMBER OF MATERIALS	=	1
MAXIMUM TEMPERATURES PER MATERIAL	=	1
ANALYSIS CODE	=	2
CODE FOR INCLUSION OF BENDING MODES EQ.0. INCLUDE GT.0. SUPPRESS	=	0

MATERIAL I.D. NUMBER	=	1
NUMBER OF TEMPERATURES	=	1
WEIGHT DENSITY	=	0.1AACD C0
MASS DENSITY	=	0.10000-02
BETA ANGLE	=	0.0

TEMPERATURE	E(N)	E(S)	E(T)	NU(NS)	NU(NT)	NU(ST)	G(NS)	ALPHA(N)	ALPHA(S)	ALPHA(T)
0.0	0.10000 07	0.10000 07	0.10000 07	0.3000	0.3000	0.3000	0.384CD 06	0.0	0.0	0.0

ELEMENT LOAD MULTIPLIERS

LOAD CASE	TEMPERATURE	PRESSURE	X-GRAVITY	Y-GRAVITY	Z-GRAVITY
A	0.0	0.0	0.0	0.0	0.0
B	0.0	0.0	0.0	0.0	0.0
C	0.0	0.0	0.0	0.0	0.0
D	0.0	0.0	0.0	0.0	0.0

E I G E N   V A L U E   A N A L Y S I S

DETERMINANT SEARCH SOLUTION IS CARRIED OUT

CONTROL INFORMATION

FLAG FOR ADDITIONAL PRINTING (EQ.0, SUPPRESS; EQ.1, PRINT)	=	0
STURM SEQUENCE CHECK FLAG (*) (EQ.0, PERFORM CHECK; EQ.1, PASS)	=	0
MAXIMUM ITERATION CYCLES (*)	=	16
CONVERGENCE TOLERANCE (*)	=	0.10000-04
CUT-OFF FREQUENCY (CPS)	=	0.10000 09
NUMBER OF STARTING ITERATION VECTORS TO BE READ FROM TAPE10 (*)	=	0

(*) APPLICABLE TO SUBSPACE ITERATION SOLUTIONS ONLY

SOLUTION IS SOUGHT FOR FOLLOWING EIGENPROBLEM

NUMBER OF EQUATIONS	=	20
HALF BANDWIDTH OF STIFFNESS MATRIX	=	8
NUMBER OF EQUATION BLOCKS	=	1
NUMBER OF EQUATIONS PER BLOCK	=	20
NUMBER OF EIGENVALUES REQUIRED	=	5

WE SOLVED FOR THE FOLLOWING EIGENVALUES

0.987332583216D 05 0.345657494089D 07 0.245437047195D 08 0.247324605108D 08 0.870709345901D 08

3.2.7
pg 7

PRINT OF FREQUENCIES

MODE NUMBER	CIRCULAR FREQUENCY (RAD/SEC)	FREQUENCY (CYCLES/SEC)	PERIOD (SEC)
1	0.31420 03	0.50010 02	0.20000-01
2	0.18590 04	0.29590 03	0.33800-02
3	0.41540 04	0.73550 03	0.12680-02
4	0.49730 04	0.79150 03	0.12630-02
5	0.93310 04	0.14850 04	0.67340-03

PRINT OF EIGENVECTORS

[illegible]	[illegible]	[illegible]	[illegible]	[illegible]	[illegible]	[illegible]	[illegible]
	[illegible]	[illegible]	[illegible]	[illegible]	[illegible]	[illegible]	[illegible]
	[illegible]	[illegible]	[illegible]	[illegible]	[illegible]	[illegible]	[illegible]
	[illegible]	[illegible]	[illegible]	[illegible]	[illegible]	[illegible]	[illegible]
	[illegible]	[illegible]	[illegible]	[illegible]	[illegible]	[illegible]	[illegible]
[illegible]	[illegible]	[illegible]	[illegible]	[illegible]	[illegible]	[illegible]	[illegible]
	[illegible]	[illegible]	[illegible]	[illegible]	[illegible]	[illegible]	[illegible]
	[illegible]	[illegible]	[illegible]	[illegible]	[illegible]	[illegible]	[illegible]
	[illegible]	[illegible]	[illegible]	[illegible]	[illegible]	[illegible]	[illegible]
	[illegible]	[illegible]	[illegible]	[illegible]	[illegible]	[illegible]	[illegible]
[illegible]	[illegible]	[illegible]	[illegible]	[illegible]	[illegible]	[illegible]	[illegible]
	[illegible]	[illegible]	[illegible]	[illegible]	[illegible]	[illegible]	[illegible]
	[illegible]	[illegible]	[illegible]	[illegible]	[illegible]	[illegible]	[illegible]
	[illegible]	[illegible]	[illegible]	[illegible]	[illegible]	[illegible]	[illegible]
	[illegible]	[illegible]	[illegible]	[illegible]	[illegible]	[illegible]	[illegible]
[illegible]	[illegible]	[illegible]	[illegible]	[illegible]	[illegible]	[illegible]	[illegible]
	[illegible]	[illegible]	[illegible]	[illegible]	[illegible]	[illegible]	[illegible]
	[illegible]	[illegible]	[illegible]	[illegible]	[illegible]	[illegible]	[illegible]
	[illegible]	[illegible]	[illegible]	[illegible]	[illegible]	[illegible]	[illegible]
	[illegible]	[illegible]	[illegible]	[illegible]	[illegible]	[illegible]	[illegible]
[illegible]	[illegible]	[illegible]	[illegible]	[illegible]	[illegible]	[illegible]	[illegible]
	[illegible]	[illegible]	[illegible]	[illegible]	[illegible]	[illegible]	[illegible]
	[illegible]	[illegible]	[illegible]	[illegible]	[illegible]	[illegible]	[illegible]
	[illegible]	[illegible]	[illegible]	[illegible]	[illegible]	[illegible]	[illegible]
	[illegible]	[illegible]	[illegible]	[illegible]	[illegible]	[illegible]	[illegible]
[illegible]	[illegible]	[illegible]	[illegible]	[illegible]	[illegible]	[illegible]	[illegible]
	[illegible]	[illegible]	[illegible]	[illegible]	[illegible]	[illegible]	[illegible]
	[illegible]	[illegible]	[illegible]	[illegible]	[illegible]	[illegible]	[illegible]
	[illegible]	[illegible]	[illegible]	[illegible]	[illegible]	[illegible]	[illegible]
	[illegible]	[illegible]	[illegible]	[illegible]	[illegible]	[illegible]	[illegible]
[illegible]	[illegible]	[illegible]	[illegible]	[illegible]	[illegible]	[illegible]	[illegible]
	[illegible]	[illegible]	[illegible]	[illegible]	[illegible]	[illegible]	[illegible]
	[illegible]	[illegible]	[illegible]	[illegible]	[illegible]	[illegible]	[illegible]
	[illegible]	[illegible]	[illegible]	[illegible]	[illegible]	[illegible]	[illegible]
	5	[illegible]	[illegible]	[illegible]	[illegible]	[illegible]	[illegible]
10	1	[illegible]	[illegible]	[illegible]	[illegible]	[illegible]	[illegible]
	[illegible]	[illegible]	[illegible]	[illegible]	[illegible]	[illegible]	[illegible]
	[illegible]	[illegible]	[illegible]	[illegible]	[illegible]	[illegible]	[illegible]
	1	[illegible]	[illegible]	[illegible]	[illegible]	[illegible]	[illegible]
	[illegible]	[illegible]	[illegible]	[illegible]	[illegible]	[illegible]	[illegible]
11	[illegible]	[illegible]	[illegible]	[illegible]	[illegible]	[illegible]	[illegible]
	[illegible]	[illegible]	[illegible]	[illegible]	[illegible]	[illegible]	[illegible]
	[illegible]	[illegible]	[illegible]	[illegible]	[illegible]	[illegible]	[illegible]
	[illegible]	[illegible]	[illegible]	[illegible]	[illegible]	[illegible]	[illegible]
	[illegible]	[illegible]	[illegible]	[illegible]	[illegible]	[illegible]	[illegible]
[illegible]	[illegible]	[illegible]	[illegible]	[illegible]	[illegible]	[illegible]	[illegible]

N O D E D I S P L A C E M E N T S / R O T A T I O N S

NODE NUMBER	CONDITION VECTOR	X-TRANSLATION	Y-TRANSLATION	Z-TRANSLATION	X-ROTATION	Y-ROTATION	Z-ROTATION
12	1	0.0	0.0	0.0	0.0	0.0	0.0
	2	0.0	0.0	0.0	0.0	0.0	0.0
	3	0.0	0.0	0.0	0.0	0.0	0.0
	4	0.0	0.0	0.0	0.0	0.0	0.0
	5	0.0	0.0	0.0	0.0	0.0	0.0
11	1	0.0	0.0	0.0	0.0	0.0	0.0
	2	0.0	0.0	0.0	0.0	0.0	0.0
	3	0.0	0.0	0.0	0.0	0.0	0.0
	4	0.0	0.0	0.0	0.0	0.0	0.0
	5	0.0	0.0	0.0	0.0	0.0	0.0
10	1	0.0	-0.538960D 00	-0.111420 01	0.0	0.0	0.0
	2	0.0	0.200060 01	0.470530 01	0.0	0.0	0.0
	3	0.0	-0.305860 01	-0.896710 01	0.0	0.0	0.0
	4	0.0	-0.388740 01	0.377610 00	0.0	0.0	0.0
	5	0.0	0.211680 01	0.111970 02	0.0	0.0	0.0
9	1	0.0	0.538960 00	-0.11142D 01	0.0	0.0	0.0
	2	0.0	-0.200060 01	0.470530 01	0.0	0.0	0.0
	3	0.0	0.305860 01	-0.896710 01	0.0	0.0	0.0
	4	0.0	-0.388740 01	0.377610 00	0.0	0.0	0.0
	5	0.0	-0.211680 01	0.11197D 02	0.0	0.0	0.0
8	1	0.0	-0.912930 00	-0.405310 01	0.0	0.0	0.0
	2	0.0	-0.106420 01	0.113700 02	0.0	0.0	0.0
	3	0.0	0.263390 01	-0.103740 02	0.0	0.0	0.0
	4	0.0	-0.756130 01	-0.227350 00	0.0	0.0	0.0
	5	0.0	-0.666080 01	-0.109530 01	0.0	0.0	0.0
7	1	0.0	0.912940 00	-0.405310 01	0.0	0.0	0.0
	2	0.0	-0.106420 01	0.113700 02	0.0	0.0	0.0
	3	0.0	-0.263390 01	-0.103740 02	0.0	0.0	0.0
	4	0.0	-0.756130 01	0.227350 00	0.0	0.0	0.0
	5	0.0	0.666080 01	-0.109530 01	0.0	0.0	0.0
6	1	0.0	-0.113390 01	-0.817790 01	0.0	0.0	0.0
	2	0.0	-0.143690 01	0.107500 02	0.0	0.0	0.0
	3	0.0	0.400810 01	0.500500 01	0.0	0.0	0.0
	4	0.0	-0.104420 02	-0.190370 00	0.0	0.0	0.0
	5	0.0	0.393620 01	-0.875520 01	0.0	0.0	0.0
5	1	0.0	0.113390 01	-0.817780 01	0.0	0.0	0.0
	2	0.0	0.143690 01	0.107530 02	0.0	0.0	0.0
	3	0.0	-0.400810 01	0.500500 01	0.0	0.0	0.0
	4	0.0	-0.104420 02	0.190370 00	0.0	0.0	0.0
	5	0.0	-0.393620 01	-0.875520 01	0.0	0.0	0.0
4	1	0.0	-0.123030 01	-0.129290 02	0.0	0.0	0.0
	2	0.0	-0.356390 01	0.485510 00	0.0	0.0	0.0
	3	0.0	-0.250310 01	0.883030 01	0.0	0.0	0.0
	4	0.0	-0.122980 02	-0.864340-01	0.0	0.0	0.0
	5	0.0	0.226260 01	0.938450 01	0.0	0.0	0.0
3	1	0.0	0.123030 01	-0.129290 02	0.0	0.0	0.0

	2	0.0	0.356490 01	0.488510 00	0.0	0.0	0.0
	3	0.0	0.253410 01	0.863 01	0.0	0.0	0.0
	4	0.0	-0.122890 02	0.864 01	0.0	0.0	0.0
	5	0.0	-0.236260 01	0.938 01	0.0	0.0	0.0
2	1	0.0	-0.135230 01	-0.179030 02	0.0	0.0	0.0
	2	0.0	-0.429640 01	-0.156130 02	0.0	0.0	0.0
	3	0.0	-0.683240 01	-0.112630 02	0.0	0.0	0.0
	4	0.0	-0.129510 02	-0.291210-01	0.0	0.0	0.0
	5	0.0	-0.862370 01	-0.613720 01	0.0	0.0	0.0
1	1	0.0	0.135230 01	-0.179030 02	0.0	0.0	0.0
	2	0.0	0.429640 01	-0.156130 02	0.0	0.0	0.0
	3	0.0	0.683240 01	-0.112630 02	0.0	0.0	0.0
	4	0.0	-0.129510 02	0.291210-01	0.0	0.0	0.0
	5	0.0	0.862370 01	-0.613720 01	0.0	0.0	0.0

E I G E N S O L U T I O N T I M E L O G

EIGENSOLUTION	=	2.01
PRINTING	=	0.43

O V E R A L L T I M E L O G

NODAL POINT INPUT	=	0.23
ELEMENT STIFFNESS FORMATION	=	0.65
NODAL LOAD INPUT	=	0.10
TOTAL STIFFNESS FORMATION	=	0.41
STATIC ANALYSIS	=	0.0
EIGENVALUE EXTRACTION	=	2.51
FORCED RESPONSE ANALYSIS	=	0.0
RESPONSE SPECTRUM ANALYSIS	=	0.0
STEP-BY-STEP INTEGRATION	=	0.0
TOTAL SOLUTION TIME	=	3.90